



HAL
open science

Surface modifications of cellulose nanocrystals for biobased food packaging applications

Manon Le Gars

► **To cite this version:**

Manon Le Gars. Surface modifications of cellulose nanocrystals for biobased food packaging applications. Polymers. Université Grenoble Alpes [2020-..], 2020. English. NNT : 2020GRALI021 . tel-03170952v1

HAL Id: tel-03170952

<https://theses.hal.science/tel-03170952v1>

Submitted on 16 Mar 2021 (v1), last revised 17 Mar 2021 (v2)

HAL is a multi-disciplinary open access archive for the deposit and dissemination of scientific research documents, whether they are published or not. The documents may come from teaching and research institutions in France or abroad, or from public or private research centers.

L'archive ouverte pluridisciplinaire **HAL**, est destinée au dépôt et à la diffusion de documents scientifiques de niveau recherche, publiés ou non, émanant des établissements d'enseignement et de recherche français ou étrangers, des laboratoires publics ou privés.

THÈSE

Pour obtenir le grade de

DOCTEUR DE L'UNIVERSITE GRENOBLE ALPES

Spécialité : **Matériaux, Mécanique, Génie Civil, Electrochimie**

Arrêté ministériel : 25 mai 2016

Présentée par

Manon LE GARS

Thèse dirigée par **Julien BRAS**, Maître de Conférences, Grenoble INP, et codirigée par **Philippe ROGER**, Professeur, Université Paris-Sud et **Naceur BELGACEM**, Professeur, Grenoble INP

préparée au sein du **Laboratoire Génie des Procédés Papetiers** dans l'**École Doctorale I-MEP2 – Ingénierie – Matériaux, Mécanique, Environnement, Energétique, Procédés, Production**

Surface modifications of cellulose nanocrystals for biobased food packaging applications

Thèse soutenue publiquement le **05 Mars 2020**, devant le jury composé de :

Dr. Bénédicte LEPOITTEVIN

Maître de Conférences, ENSICAEN, Rapporteur

Pr. Jose-Maria LAGARON

Professeur, Spanish Council for Scientific Research, Rapporteur

Dr. Hélène ANGELLIER-COUSSY

Maître de Conférences, Université de Montpellier II, Examineur

Pr. Evelyne MAURET

Professeur, Grenoble INP, Présidente

Dr. Julien BRAS

Maître de Conférences, Grenoble INP, Directeur de thèse

Pr. Philippe ROGER

Professeur, Université Paris-Sud, Co-Directeur de thèse

Pr. Naceur BELGACEM

Professeur, Grenoble INP, Co-Directeur de thèse

Dr. Hanène SALMI-MANI

Maître de Conférences, Université Paris-Sud, Co-Encadrante de thèse

Dr. Sandra DOMENEK

Maître de Conférences, AgroParisTech, Membre Invité



Remerciements

I would like to address my first thanks to the jury of my PhD defense. Dr. Bénédicte Lepoittevin and Pr. José-Maria Lagaron, thank you for the time you spent on the evaluation of my manuscript, and for all your enriching and relevant questions and comments during the defense. Dr Hélène Angellier-Coussy, thank you for having examined this work and for your very constructive remarks. Evelyne, thank you for having chaired this jury and for your kindness over the past few months. Sandra, thank you for having attended my defense, and for all your availability and your help throughout this project. To all of you, thank you for being come all the way to Grenoble, and for having made this PhD thesis defense an enriching and interesting moment.

Je souhaiterais maintenant remercier mes directeurs et encadrants de thèse, sans qui l'aboutissement d'un tel projet n'aurait jamais pu se faire. Tout d'abord, Julien, merci de m'avoir toujours fait confiance, et ce, même avant le début de cette thèse. Merci pour ton optimisme, pour tes encouragements (tu as toujours su me remonter le moral quand j'en avais besoin), pour tes idées toujours plus nombreuses, ainsi que pour nos nombreux échanges et réunions. Merci également de m'avoir donné l'opportunité de voyager aux quatre coins du monde pour assister à des conférences (notamment notre séjour à la Nouvelle-Orléans). Philippe, merci à toi aussi de m'avoir fait confiance dès le début de cette thèse, de m'avoir intégrée à l'équipe d'Orsay, de m'avoir toujours poussée à aller plus loin dans ma réflexion, et de m'avoir soutenue jusqu'au bout de cette thèse. Hanène, merci de m'avoir beaucoup appris, que ce soit dans le laboratoire ou autour d'un café, tu as su me motiver et me donner confiance. Philippe et Hanène, merci à vous deux pour votre précieuse aide, j'ai énormément appris à vos côtés. Enfin, Naceur, merci pour ton soutien si bénéfique dans l'acheminement de cette thèse. Merci pour ta disponibilité et ton aide sans failles, pour tes relectures, tes conseils et avis qui m'ont été très précieux. Merci pour ta confiance, j'ai énormément apprécié travailler à tes côtés, et tout particulièrement lors des derniers mois de cette thèse. Julien, Naceur, Philippe et Hanène, vous avez été un quatuor encadrant très complémentaire, et vous m'avez permis, chacun à votre manière, d'évoluer tant professionnellement que personnellement au cours de ces trois années. Je vous remercie très sincèrement pour cela.

Cette thèse est non seulement le fruit d'un travail personnel, mais aussi celui d'un projet collaboratif dans lequel elle s'inscrit. Tout d'abord, merci à l'Agence Nationale de la Recherche d'avoir financé ce projet, et à Sandra de le coordonner. Merci pour tout ton investissement, et pour l'organisation des différents Copils aux quatre coins de la France. Je suis très heureuse de continuer à travailler à tes côtés dans les mois à venir. Je souhaiterais également remercier tous les membres du projet GASP. Eliane Espuche, Matthieu Gervais, Giana Perre, Antoine Cassel, Fabrice Gouanve, Alain Guinault, Laurent

Lebrun, Stéphane Marais, Cyrille Sollogoub, Matthieu Zinet, Nadège Follain et Vincent Huc, merci pour les discussions et présentations enrichissantes lors des Copils ou réunions téléphoniques. Bien qu'il ait parfois été délicat de s'accorder sur les attentes de chacun, je ressors grandie et je retire beaucoup de positif de tous ces échanges. Hajar, je suis heureuse de t'avoir rencontrée *via* ce projet et d'avoir pu y évoluer avec toi. Tu m'as beaucoup aidée, et j'ai énormément apprécié nos discussions, coups de téléphones et petites sorties dans Paris pour se motiver mutuellement. J'espère pouvoir t'aider sur la fin de ta thèse comme tu l'as fait pour moi, et te souhaite tout le meilleur. Un énorme merci à Karim et Benjamin avec qui j'ai également pu collaborer à travers ce projet. Karim, merci pour ta franchise, tes coups de gueule, ta disponibilité, ton aide et tes conseils. Benjamin, merci pour tout. J'ai rencontré un collègue génial, mais aussi un ami. Merci à vous deux pour les discussions et les soirées, j'en garde des souvenirs géniaux.

Je voudrais remercier les membres de mon comité de suivi de thèse, Aurore Denneulin, Isabelle Desloges et Alain Dufresne, pour leur écoute et leurs conseils. Ces réunions de comité ont à chaque fois été bénéfiques et motivantes.

Merci également à toutes les personnes qui m'ont apporté leurs connaissances techniques et scientifiques, et qui m'ont énormément aidée dans mes manipulations : Diana Drago (pour la XPS, à l'ICMMO), Thierry Encinas (pour la XRD, au CMTC), Jean-Luc Puteaux et Christine Lancelon-Pin (pour le TEM, au Cermav), Cécile Sillard (pour, entre autres, l'AFM, au LGP2), Marie-Christine Brochier-Salon (pour la RMN, au LGP2), Ludovic Costa (pour la SEC, à l'ICMMO), et Bertine Khelifi (pour le MEB, au LGP2). Merci à Laurine et Aurore que j'ai encadrées durant leur stage de fin d'étude, qui m'ont aidée sur ce projet de thèse, et à qui je souhaite tout le meilleur dans leurs parcours respectifs.

Ces travaux de recherche n'auraient pas été possibles sans la présence du personnel des deux laboratoires dans lesquels j'ai travaillé.

Au LGP2, merci au service technique (Chu, Charlotte, Olivier, Philippe, Momo) pour leur gentillesse, leur disponibilité et leur aide si précieuses. Merci à la direction du laboratoire, et tout particulièrement à Didier pour sa disponibilité et son écoute infaillibles. Merci au service administratif (le secrétariat, Stéphane V. et Laurence (qui m'a beaucoup vue passer...)), et tous les permanents (Stéphane D., Maxime T., et tous les autres) toujours prêts à aider. Un énorme merci à Cécile, non seulement pour son aide scientifique dans cette thèse, mais aussi pour son amitié, son écoute et sa gentillesse. Enfin, merci à tous les doctorants et post-doctorants que j'ai eu la chance de côtoyer dans les labos et/ou les bureaux, et qui ont rendu cette thèse bien plus agréable : Johanna, Claire, Gabriel, Lorelei, Estelle, Florian, Amina, Hugo, Axelle, Sudha, Saad, Enrique, Flavien, Fleur, Etienne G., Eva, Maxime W., Alhem, Malek, Bastien, Hippolyte, Erwan, Charlène, Lili, Clémentine, Elsa, Hélène, Fanny et tous les autres. Plus personnellement, merci à mes copines Johanna, Fleur, Fanny et Hélène, pour nos soirées, week-ends, deliveroo et j'en passe. J'ai rencontré des amies (et amis par la même occasion) formidables. Fleur,

merci pour ton aide, ton soutien, ton amitié, et pour tous nos commérages qui m'ont tellement manqué sur les derniers mois ! Une mention spéciale à Gabriel et Bastien, qui, malgré mes plaintes et mes doutes, ont toujours su trouver les mots, et avec qui j'ai vraiment passé de supers moments. Je vous souhaite tout le meilleur. Lorelei et Florian, vous m'avez supportée sur les derniers mois de ma thèse et avez toujours été là pour discuter et remonter le moral, merci pour tout. Enfin, merci à Estelle (copine de bureau, mais pas que) et Hugo pour tous les moments dans le labo et en dehors, merci d'avoir fait le déplacement pour assister à ma soutenance, ça m'a vraiment touchée.

Même si ils m'ont vue moins souvent, je tenais à remercier tous les membres de l'équipe SM2B à l'ICMMO, qui m'ont toujours bien accueillie : Philippe, Hanène, Nadine, Caroline, Ludo, Thu (pour m'avoir secourue à plusieurs reprises dans les labos), Mélanie, Mohamad et Nassim. Merci pour vos conseils, pour les cafés, et pour tous vos encouragements.

Les trois années de thèse ne sont pas toujours faciles, et j'ai eu la chance de pouvoir toujours compter sur le soutien et la bienveillance de mes collègues.

J'ai également la chance d'avoir, à l'extérieur, des amis en or, sans qui ces années auraient été bien différentes. Un énorme merci à mes copains de toujours (Eliot, Mylène, Aude, Romuald, Thibault, Jules, Adèle, Aymeric, Guillaume, Jolan, Titouan, et tous les +1 évidemment), pour leur amitié et soutien sans failles, et qui n'ont pas hésité une seule seconde à venir assister à ma soutenance. Vous n'imaginez pas à quel point votre présence le jour J m'a touchée et aidée. Héloïse, un énorme merci à toi aussi pour tout, j'ai été tellement déçue que tu ne puisses pas être là...

En plus d'avoir des amis en or, je suis entourée d'une famille exceptionnelle : mes parents et ma sœur qui m'ont toujours soutenue dans mes choix, ainsi que le reste de ma famille. Papa, Maman, Camille, merci d'avoir toujours su trouver les mots pour m'encourager, et merci de croire si fort en moi. C'est grâce à vous si j'en suis arrivée là aujourd'hui. Je vous aime.

Enfin, je souhaitais terminer en remerciant celui qui a rendu ces dernières années si belles. Jean-Marc, merci pour tout ce que tu fais pour moi au quotidien, pour ta joie de vivre, ton optimisme, tes solutions à tous problèmes (qui n'en sont donc plus), et pour tout ton amour. J'ai une chance inouïe de t'avoir à mes côtés, je t'aime.

This PhD project has been funded by Agence Nationale de la Recherche (ANR)

Project ANR-16-CE08-0040

General table of contents

Scientific contributions	11
Abbreviations	13
General introduction	15
I. Literature Review	25
Introduction to Chapter I	29
1. Biobased polymer materials for food packaging	31
2. Cellulose nanocrystals and functionalization	53
3. Use of nanocelluloses in polymeric systems for food packaging applications	83
Conclusions of Chapter I	99
References – Chapter I	101
II. Chemical modifications of cellulose nanocrystals	113
Introduction to Chapter II	117
<u>1.</u> Surface-initiated transfer radical polymerization from the surface of modified-cellulose nanocrystals	119
<u>2.</u> Grafting of fatty acids on cellulose nanocrystals via a novel procedure	145
<u>2.1.</u> Comparison between two different methods for the chemical modification of cellulose nanocrystals	145
<u>2.2.</u> Role of solvent exchange in dispersion of cellulose nanocrystals and their esterification using acids as solvents	157
<u>3.</u> Amidation of TEMPO-oxidized cellulose nanocrystals using aromatic aminated molecules	185
<u>4.</u> Adsorption of rosin nanoparticles from a nano-emulsion on both cellulose nanocrystals and nanofibrils	215
Conclusions of Chapter II	227
References - Chapter II	231
III. PLA-based materials including designed nanostructures	241
Introduction to Chapter III	245
<u>1.</u> Elaboration of poly(lactic acid)-based nanocomposites including different designed cellulose nanostructures: comparison of the interfaces	247
<u>2.</u> Two distinct methods for the elaboration of multi-layered materials based on poly(lactic acid) and active cellulosic nanostructures	271
Conclusions of Chapter III	299
References - Chapter III	301
General conclusion and perspectives	309
Extended French Abstract – Résumé en français	317

Scientific contributions (2017-2020)

Publications in scientific journals

1. **Le Gars M.**, Bras J., Salmi-Mani H., Ji M., Dragoe D., Faraj H., Domenek S., Belgacem M. N., Roger P. « Polymerization of glycidyl methacrylate from the surface of cellulose nanocrystals for the elaboration of PLA-based nanocomposites », *Carbohydrate Polymers*, 2020
2. **Le Gars M.**, Roger P., Belgacem M. N., Bras J. « Role of solvent exchange in dispersion of cellulose nanocrystals and their esterification using fatty acids as solvents », *Cellulose*, 2020
3. **Le Gars M.**, Delvart A., Roger P., Belgacem M. N., Bras J. « Amidation of TEMPO-oxidized cellulose nanocrystals using aromatic aminated molecules », *Colloid and Polymer Science*, 2020
4. **Le Gars M.**, Dhuiège B., Delvart A., Belgacem M. N., Missoum K., Bras J. « High barrier antioxidant PLA/nanocellulose multi-layered materials for packaging”, under revision, *ACS Omega*, 2020

Author's contributions:

1. Manon Le Gars, Naceur Belgacem, Julien Bras, Hanène Salmi-Mani and Philippe Roger were responsible for the experimental design and planning of the work. Marisol Ji performed preliminary work on the same topic. Manon Le Gars performed most of the experiments, analyzed the results and wrote the manuscript as principal author. Diana Dragoe carried out XPS experiments and helped for the interpretation of the corresponding results. Hajar Faraj and Sandra Domenek were involved in the nanocomposites part, and Hajar Faraj performed and provided nanocomposites samples to Manon Le Gars. Hanène Salmi-Mani, Philippe Roger and Julien Bras supervised the writing of the manuscript.
2. Manon Le Gars, Naceur Belgacem and Julien Bras were responsible for the experimental design and planning of the work. Manon Le Gars performed most of the experiments, analyzed the results and wrote the manuscript as principal author under the supervision of Julien Bras, Philippe Roger and Naceur Belgacem. Marie-Christine Brochier-Salon performed ¹³C-NMR analyses and helped for the interpretation of the NRM results. Diana Dragoe performed XPS analyses.
3. Manon Le Gars and Julien Bras were responsible for the experimental design and planning of the work. Manon Le Gars and Aurore Delvart were in charge of the experimental part. Cécile

Sillard performed the XPS analysis and helped for the corresponding part. Manon Le Gars wrote the manuscript as first author and all the authors helped for the corrections.

4. Manon Le Gars and Benjamin Dhuiège performed the experimental work related to the rosin adsorption and preparation of multi-layered films by lamination. Benjamin Dhuiège and Karim Missoum (from INOFIB startup) prepared the rosin nano-emulsion and performed the related characterizations. They supervised and designed the experimental work dealing with CNF. Manon Le Gars performed the work related to CNC. Manon Le Gars and Benjamin Dhuiège wrote the publication, supervised by Julien Bras, Naceur Belgacem and Karim Missoum.

Oral presentations in international conferences

Le Gars M., Salmi-Mani H., Ji M., Belgacem M. N., Roger P., Bras J. « Cellulose nanocrystals grafted with poly(glycidyl methacrylate) for their compatibilization in nanocomposites » in ACS, American Chemical Society – National Meeting & Exposition. New Orleans, USA (2018)

Le Gars M., Belgacem M. N., Roger P., Bras J. « Chemical modifications of cellulose nanocrystals for nanocomposites applications » in NRC-Grenoble INP International Conference. Cairo, Egypt (2019)

Le Gars M., Delvart A., Roger P., Belgacem M. N., Bras J. « Immobilization of active molecules on CNC for the preparation of hybrid multi-layered CNC-PLA based packaging materials » in EPNOE, International Polysaccharide Conference. Aveiro, Portugal (2019)

Poster presentation in scientific conference

Le Gars M., Belgacem M. N., Salmi-Mani H., Roger P., Bras J. « Role of cellulose nanocrystals dispersion on functionalization with fatty acids as solvent » in Scientific Day of Chemistry. Grenoble, France (2019)

Other contributions

Le Gars M., Douard L., Belgacem M. N., Bras J. « Cellulose Nanocrystals: From Classical Hydrolysis to the Use of Deep Eutectic Solvents », Chapter of the book «Nanosystems» (DOI:10.5772/intechopen.89878), IntechOpen (2019)

Abbreviations

▪ *Chemicals and Materials*

1-M-3-PP	1-methyl-3-phenylpropylamine
AGU	Anhydroglucose unit
BIB	α -bromoisobutyryl bromide
CNCs	Cellulose nanocrystals
CNC-1-M-3-PP	CNCs modified with 1-methyl-3-phenylpropylamine
CNC-Br	CNCs modified with α -bromoisobutyryl bromide
CNC-Lauric	CNCs modified with lauric acid
CNC-PGMA-Br	CNCs polymerized with poly(glycidyl methacrylate)
CNC-Rosin	CNCs modified with rosin mixture
CNC-Stearic	CNCs modified with stearic acid
CNFs	Cellulose nanofibrils
CNF-Rosin	CNFs modified with rosin mixture
DCM	Dichloromethane
DMF	Dimethylformamide
DPPH	2,2-diphenyl-1-picrylhydrazyl
EBIB	Ethyl α -bromoisobutyrate
EDC	N-(3-Dimethylaminopropyl)-N'-ethylcarbodiimide
EtOH	Ethanol
GMA	Glycidyl methacrylate
H₂SO₄	Sulfuric acid
HCl	Hydrochloric acid
NaBr	Sodium bromide
NaClO	Sodium hypochlorite
NaOH	Sodium hydroxide
NHS	N-Hydroxysuccinimide
PGMA	Poly(glycidyl methacrylate)
PLA	Poly(lactic acid)
TEMPO	2,2,6,6-Tetramethylpiperidine-1-oxyl
TEMPO-CNCs	TEMPO-oxidized cellulose nanocrystals

▪ *Characterization tools*

AFM	Atomic force microscopy
CI	Crystallinity index
¹³C-NMR	Carbon nuclear magnetic resonance
DLS	Dynamic light scattering
DMA	Dynamic mechanical analysis
DO	Degree of oxidation
DS	Degree of substitution
DSC	Differential Scanning Calorimetry
FTIR	Fourier transform infrared spectroscopy
¹H-NMR	Proton nuclear magnetic resonance
OTR	Oxygen transmission rate

QCM-d	Quartz crystal microbalance with dissipation monitoring
SEC	Size-exclusion chromatography
SEM	Scanning electron microscopy
SI-ATRP	Surface-initiated atom transfer radical polymerization
TEM	Transmission electron microscopy
TGA	Thermogravimetric analysis
WVTR	Water vapour transmission rate
XPS	X-ray photoelectron spectrometry
XRD	X-ray diffraction

General Introduction

General Introduction

In the current context, it is common to hear about pollution, sustainable development, recycling, and many other terms related to environmental issues. In addition, shocking images of beaches covered with plastic waste, or oceans of plastics, for example, are alarming. This pollution, both on land and in seas, is the logical result of an accumulation of plastic waste generated over the years. In fact, since the 1950s, the production of plastics has continuously increased, with an average increase by around 9% per year¹. Today, in Europe, the annual production of plastics represents 64.4 million tons (348 million tons all over the world), and is still on the rise, as presented in **Figure 1**. However, this evolution is not surprising, since it has followed the evolution of consumer society for decades, with an ever-increasing consumption of products, and thus, related packaging materials. Today, packaging is the sector representing the greatest demand for plastics².



Figure 1. Total demand and production of plastics in Europe in 2018 (Data extracted from ²)

However, with the society's awareness of the alarming state of environmental problems, this production and consumption of fossil-based plastics is now becoming increasingly controversial. In this environmental context, the interest in biobased polymers, especially for packaging materials, is particularly important, and these materials are intended to compete with traditional petro-based plastics. However, such a competition is ambitious, since the traditional plastics (PET, PE, PP, PVC, PS, etc.) exhibit exceptional characteristics, due to their low cost, lightness, transparency, mechanical properties and barriers, making them excellent materials to meet packaging — and especially food packaging — specifications³⁻⁵.

Among biobased polymers, poly(lactic acid), also known as PLA, is a transparent, biobased and biodegradable (in compost) polymer, and is currently one of the best alternatives to fossil-based polymers. PLA is polymerized from lactic acid monomer, which is extracted from agricultural products (mainly corn, sugar cane, and beet)^{6,7}. Although this point may be open to debate, as well as the lack of its recycling chain, PLA remains today one of the most interesting solutions. **Figure 2** illustrates its theoretical life cycle: after being produced from natural corn resources, PLA is processed for different applications, and the final products can then be recycled — although this recycling step is not always implemented —, and finally industrially composted, leading ideally to a closed loop. Since several decades, PLA has attracted academic and industrial research interests, especially because of its other promising properties, like its high stiffness, transparency, printability, and ease of processing⁸. However, certain aspects still limit its entry into the packaging market, in particular its low thermal and barrier properties which can be very restrictive for food packaging applications^{7,9}. Numerous research groups focused on the improvement of these thermal and barrier properties, especially through the introduction of nanometric fillers inside the polymer and so the development of nanocomposites. Various inorganic or organic nanofillers were thus introduced in PLA^{10,11}, including, more recently, the incorporation of nanocellulosic materials.

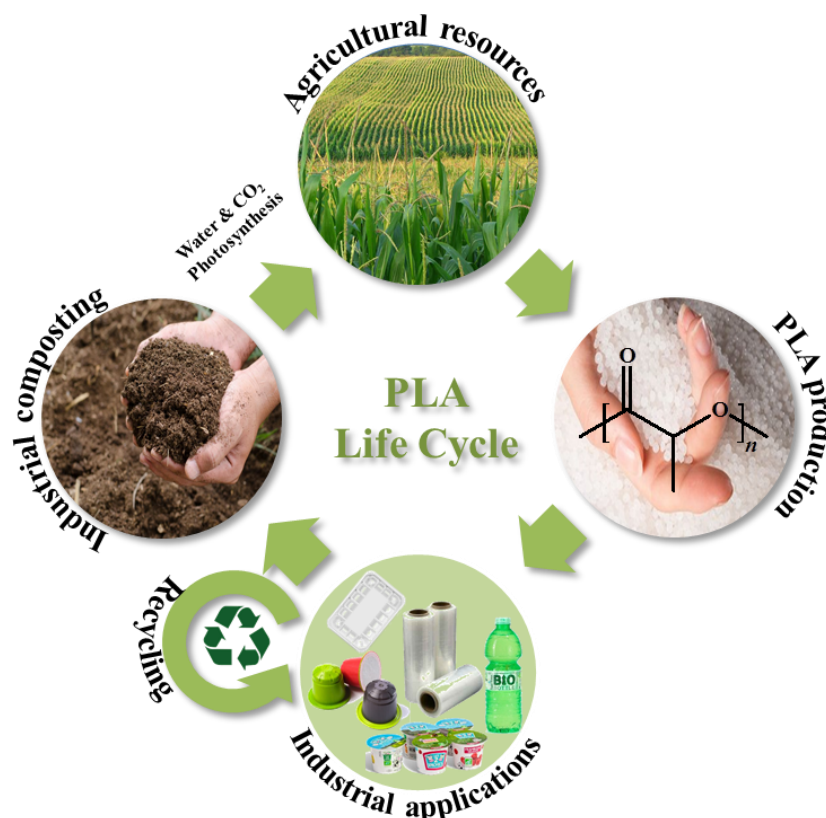


Figure 2. Theoretical life cycle of poly(lactic acid) (PLA)
 (Adapted from the website <https://www.total-corbion.com> (consulted in November 2019))

These nanomaterials — called nanocelluloses — are extracted from numerous cellulosic sources (wood, cotton, sisal, flax, tunicates, algae, bacteria, etc.) *via* different routes, leading to different types of nanocelluloses, namely cellulose nanofibrils (CNFs)^{12–14}, cellulose nanocrystals (CNCs)^{15–17}, and bacterial cellulose^{18,19}. **Figure 3** provides an example of TEM images of CNCs and CNFs materials. Both CNCs and CNFs exhibit outstanding properties — among other, a high crystallinity, a low density, a high specific surface area, a high surface reactivity, etc. — making them excellent candidates for a wide range of innovative applications, particularly for biobased and biodegradable materials^{20–22}.

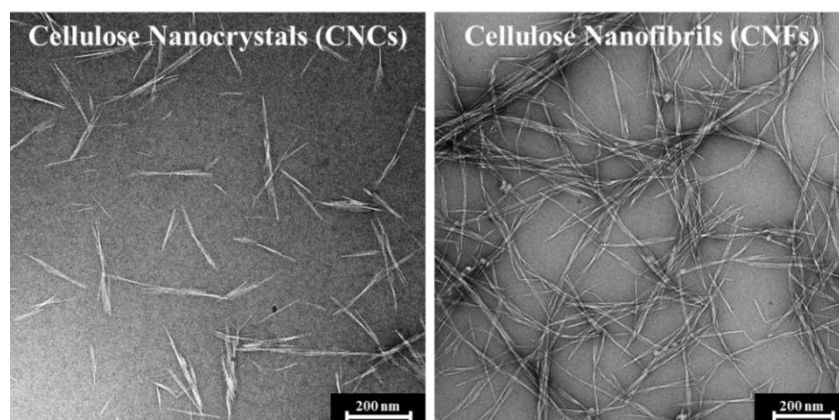


Figure 3. TEM images of cellulose nanocrystals (CNCs) and cellulose nanofibrils (CNFs)

Over the past decades, the interest in these cellulosic nanomaterials has significantly increased, in parallel with the environmental awareness. Moreover, as previously mentioned, the development and the optimization of PLA-based nanocomposites including cellulosic nanostructures have attracted a lot of researches^{23–25}. **Figure 4** represents the evolution of publications dealing with nanocelluloses and with PLA since the 1990s, confirming the previously mentioned trend.

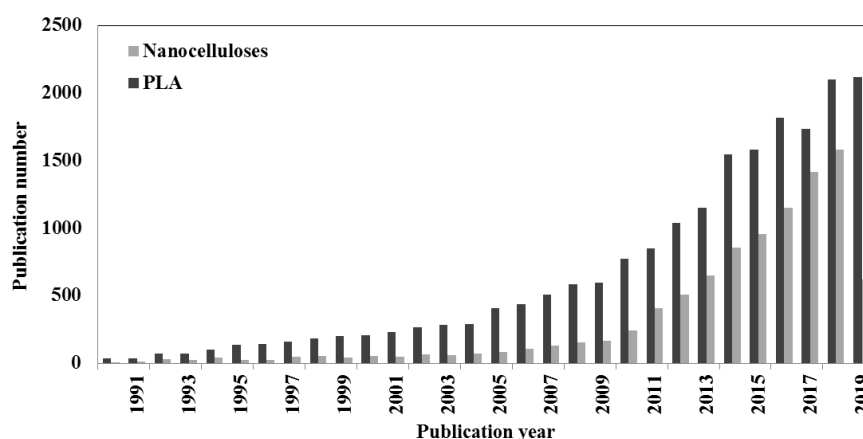


Figure 4. Non-cumulative evolution of the number of publications dealing with nanocelluloses and poly(lactic acid) (Source: SciFinder, November 2019 — Descriptors for “Nanocellulose”: cellulose nanocrystal, cellulose nanorod, rod-like cellulose, cellulose nanowire, cellulose crystallite, cellulose nanoparticle, cellulose whiskers, nanocrystalline cellulose, cellulose nanofibrils, cellulose microfibrils, nanofibrillated cellulose, microfibrillated cellulose, and descriptors for “PLA”: poly(lactic acid), PLA — Language: English)

In order to produce high performance PLA-based materials designed for their use as food packaging applications (i.e. with interesting mechanical and barrier properties), a consortium of industrial and

academic partners was established to include fillers, and especially chemically modified cellulosic nanostructures. This collaborative research was carried out through the GASP project, supported by the French National Research Agency (ANR-16-CE08-0040), which started in January 2017, for a total duration of 48 months. The PhD project presented in this manuscript took place within the framework of this GASP project, and more particularly between two partners (LGP2 and ICMMO). In addition, many collaborative stays and constructive exchanges were realized thanks to the wide and complementary fields of expertise of the different partners.



Figure 5. French National Research Agency (ANR, Agence Nationale de la Recherche) and GASP Project logos

The main objectives of this PhD are as follows:

1. Innovative chemical surface modifications of cellulose nanocrystals *via* grafting routes that are as environmentally friendly as possible
2. Study of the influence of the CNCs surface modification on their adhesion with a PLA-based matrix
3. Development of active biobased materials including both PLA and nanocellulosic structures for food packaging applications

Therefore, it is naturally that this thesis manuscript has been organized in three chapters, as presented in the general scheme (**Figure 6**).

The **Chapter I** provides a literature review of the general context of this study, with a more detailed state of the art of the nanocelluloses field — particularly that of cellulose nanocrystals (CNCs) and their functionalization —, as well as, that of multi-phasic materials including both poly(lactic acid) and nanocellulose materials, with a specific focus on food packaging applications.

In **Chapter II**, different surface modifications of CNCs are proposed. The chapter is divided into three main sections, each dealing with increasing possible grafted CNCs quantities. In fact, the sub-chapter **II.1** proposes a polymerization of a monomer bearing reactive epoxy functions from the surface of the CNCs. The sub-chapter **II.2** is divided in two parts. The short section **II.2.1** presents a comparison between a classical esterification procedure of long aliphatic chains on CNCs, and a novel esterification method with similar grafted compounds. This innovative esterification route is detailed in the section **II.2.2**, with the grafting of two fatty acids on the CNCs. The aim of the sub-chapter **II.3** is to introduce aromatic molecules at the surface of the CNCs *via* a two-step procedure. Finally, the

short sub-chapter **II.4** briefly introduces the preparation of a rosin-based nano-emulsion, which is then adsorbed on both CNCs and CNFs.

All these surface-modified CNCs are then used for the elaboration of PLA-based materials, whose two different strategies are presented in **Chapter III**. The sub-chapter **III.1** exhibits the preparation and the characterization of PLA-based nanocomposites including modified CNCs previously studied in the sub-chapters II.1 and II.2.2, in order to compare their interfaces with the PLA matrix. In the sub-chapter **III.2**, modified CNCs and CNFs presented in sections II.3 and II.4 are incorporated in PLA-based multi-layered materials, and their structural, barrier, and active properties are investigated.

The sub-chapters of this PhD project are based either on submitted scientific publications, or on additional parts structured as scientific publications. Some comments (*in grey italic*) are added and provide some complementary information about the PhD organization and/or guide the reader between the different sections of the manuscript.

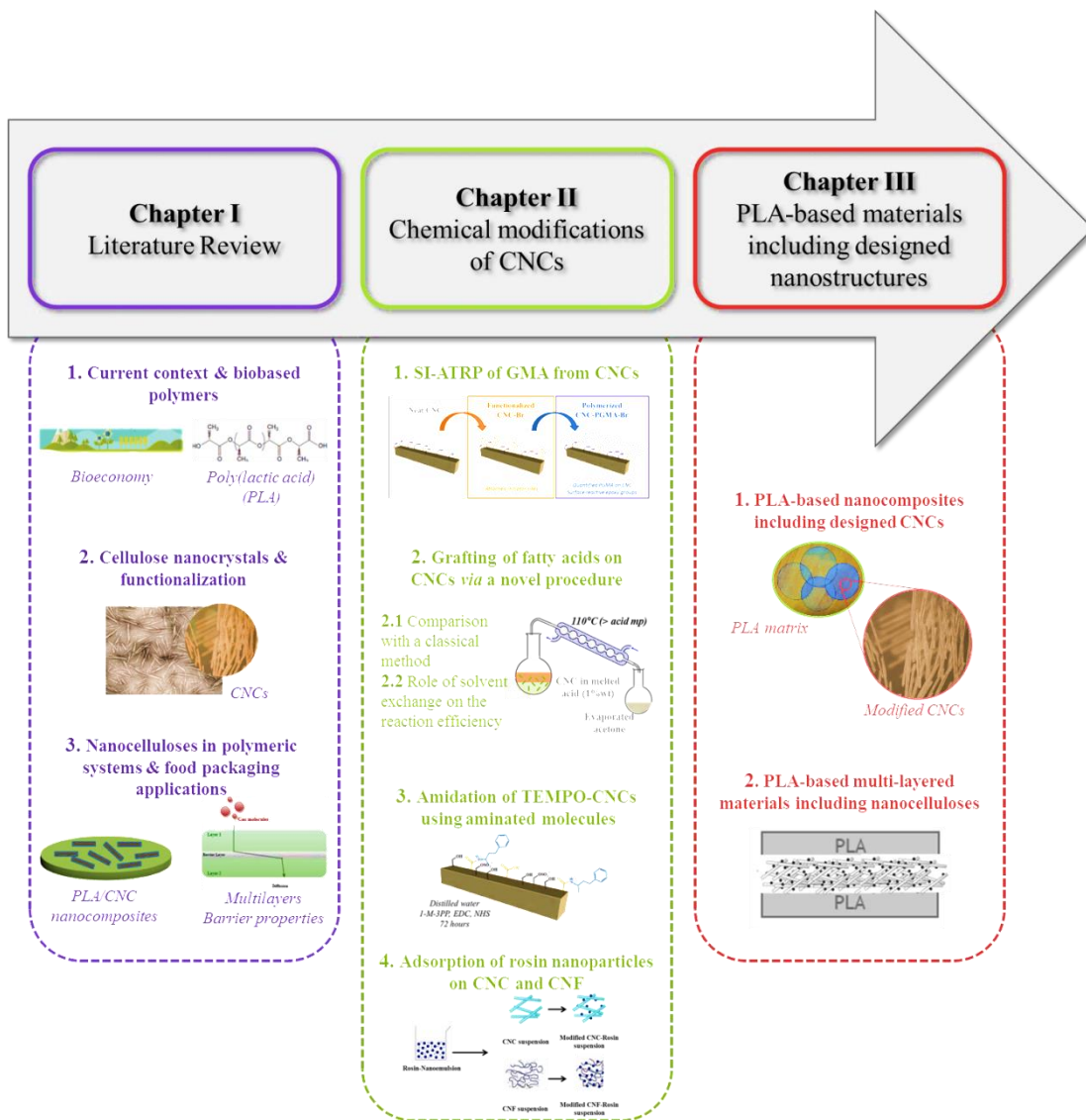


Figure 6. General organization of the PhD manuscript

The complete PhD study brings news understandings on cellulose nanocrystals surface modifications and their influence on PLA-based nanocomposites. Moreover, a proof a concept for the elaboration of food packaging materials is provided *via* the multi-layered materials produced from both PLA and modified –or not nanocelluloses.

References

1. Gourmelon, G. Global Plastic Production Rises, Recycling Lags. *WorldWatch Institute* (2015).
2. PlasticsEurope. Plastics - the Facts 2018 - An analysis of European plastics production, demand and waste data (2018).
3. PlasticsEurope. *PlasticsEurope Market Research Group (PEMRG)* (2016).
4. Crompton, T. R. *Mechanical Properties of Polymers* (2012).
5. Siracusa, V., Rocculi, P., Romani, S. & Rosa, M. D. Biodegradable polymers for food packaging: a review. *Trends in Food Science & Technology* **19**, 634–643 (2008).
6. Jiménez, A., Peltzer, M. & Ruseckaite, R. *Poly(lactic acid) science and technology: processing, properties, additives and applications* (Royal Society of Chemistry, 2015).
7. Castro-Aguirre, E., Iñiguez-Franco, F., Samsudin, H., Fang, X. & Auras, R. Poly(lactic acid)—Mass production, processing, industrial applications, and end of life. *Advanced Drug Delivery Reviews* **107**, 333–366 (2016).
8. Fiori, S. *Industrial Uses of PLA*. In: *Polymer Chemistry Series* (eds. Jiménez, A., Peltzer, M. & Ruseckaite, R.) (Royal Society of Chemistry, 2014).
9. Colomines, G., Ducruet, V., Courgneau, C., Guinault, A. & Domenek, S. Barrier properties of poly(lactic acid) and its morphological changes induced by aroma compound sorption. *Polymer International* **59**, 818–826 (2010).
10. Raquez, J.-M., Habibi, Y., Murariu, M. & Dubois, P. Polylactide (PLA)-based nanocomposites. *Progress in Polymer Science* **38**, 1504–1542 (2013).
11. Papageorgiou, G. Z., Achilias, D. S., Nanaki, S., Beslikas, T. & Bikiaris, D. PLA nanocomposites: Effect of filler type on non-isothermal crystallization. *Thermochimica Acta* **511**, 129–139 (2010).
12. Nechyporchuk, O., Belgacem, M. N. & Bras, J. Production of cellulose nanofibrils: A review of recent advances. *Industrial Crops and Product* **93**, 2–25 (2016).
13. Jonoobi, M. *et al.* Different preparation methods and properties of nanostructured cellulose from various natural resources and residues: a review. *Cellulose* **22**, 935–969 (2015).
14. Rol, F., Belgacem, M. N., Gandini, A. & Bras, J. Recent advances in surface-modified cellulose nanofibrils. *Progress in Polymer Science* **88**, 241–264 (2019).
15. Habibi, Y., Lucia, L. A. & Rojas, O. J. Cellulose Nanocrystals: Chemistry, Self-Assembly, and Applications. *Chemical Reviews* **110**, 3479–3500 (2010).
16. Natterodt, J. C., Petri-Fink, A., Weder, C. & Zoppe, J. O. Cellulose Nanocrystals: Surface Modification, Applications and Opportunities at Interfaces. *CHIMIA International Journal for Chemistry* **71**, 376–383 (2017).
17. Lin, N., Huang, J. & Dufresne, A. Preparation, properties and applications of polysaccharide nanocrystals in advanced functional nanomaterials: a review. *Nanoscale* **4**, 3274–3294 (2012).
18. Jozala, A. F. *et al.* Bacterial nanocellulose production and application: a 10-year overview. *Appl Microbiol Biotechnol* **100**, 2063–2072 (2016).
19. Fu, L., Zhang, J. & Yang, G. Present status and applications of bacterial cellulose-based materials for skin tissue repair. *Carbohydrate Polymers* **92**, 1432–1442 (2013).
20. Hubbe, M. A. *et al.* Nanocellulose in Thin Films, Coatings, and Plies for Packaging Applications: A Review. *BioResources* **12**, 2143–2233 (2017).
21. Ferrer, A., Pal, L. & Hubbe, M. Nanocellulose in packaging: Advances in barrier layer technologies. *Industrial Crops and Products* **95**, 574–582 (2017).
22. Kontturi, E. *et al.* Advanced Materials through Assembly of Nanocelluloses. *Advanced Materials* **30**, 1703779 (2018).

23. Bagheriasl, D., Safdari, F., Carreau, P. J., Dubois, C. & Riedl, B. Development of cellulose nanocrystal-reinforced polylactide: A comparative study on different preparation methods. *Polymer Composites* **40**, E342–E349 (2019).
24. Muiruri, J. K., Liu, S., Teo, W. S., Kong, J. & He, C. Highly Biodegradable and Tough Polylactic Acid–Cellulose Nanocrystal Composite. *ACS Sustainable Chem. Eng.* **5**, 3929–3937 (2017).
25. Spinella, S. *et al.* Polylactide/cellulose nanocrystal nanocomposites: Efficient routes for nanofiber modification and effects of nanofiber chemistry on PLA reinforcement. *Polymer* **65**, 9–17 (2015).

CHAPTER I

Literature Review

Table of contents – Chapter I

Introduction to Chapter I	29
1. Biobased polymer materials for food packaging	31
1.1. Polymers in packaging: generalities	31
1.1.1. Current context of packaging materials	32
1.1.2. Definitions of biopolymers	34
1.2. Requirements for food packaging	36
1.2.1. Barrier properties in food packaging	37
1.2.2. Mechanical properties of food packaging	39
1.2.3. Development of new active packaging	40
1.2.4. Biobased polymers in food packaging and sustainability approaches	41
1.2.5. Poly(lactic acid) : a relevant biopolymer	43
1.3. Packaging processing	46
1.3.1. Extrusion and composites materials	46
1.3.2. Coating strategy	48
1.3.3. Composites materials	50
2. Cellulose nanocrystals and functionalization	53
2.1. From cellulose to nanocelluloses	53
2.1.1. Structure of cellulose	53
2.1.2. Nanomaterials from cellulose: cellulose nanofibrils and nanocrystals	56
2.2. Cellulose nanocrystals: nanomaterials with interesting properties	59
2.2.1. Isolation of cellulose nanocrystals	59
2.2.2. Properties of cellulose nanocrystals	61
2.2.3. Various applications of cellulose nanocrystals and their industrialization	63
2.3. Functionalization of cellulose nanocrystals	65
2.3.1. TEMPO oxidation of cellulose nanocrystals	66
2.3.2. Covalent grafting on cellulose nanocrystals	67
2.3.3. Grafting of polymer chains at the surface of cellulose nanocrystals	73
2.3.4. Physical adsorption of various molecules on cellulose nanocrystals	79
3. Use of nanocelluloses in polymeric systems for food packaging applications	83
3.1. Nanocomposites and legislation	83
3.1.1. Interest of the introduction of nano-fillers in polymer matrices	83
3.1.2. Nanocomposites and legislation	84
3.2. Cellulose nanocrystals as fillers in nanocomposites	85
3.2.1. Effect of cellulose nanocrystals on nanocomposites mechanical and barrier properties	85
3.2.2. PLA-based / CNCs nanocomposites	87
3.3. Multi-layered CNC-based materials	94
3.3.1. Interest of nanocellulose-based multi-layered packaging materials	94
3.3.2. Absorbers and scavenging properties	96
Conclusion	99
References	101

Introduction to Chapter I

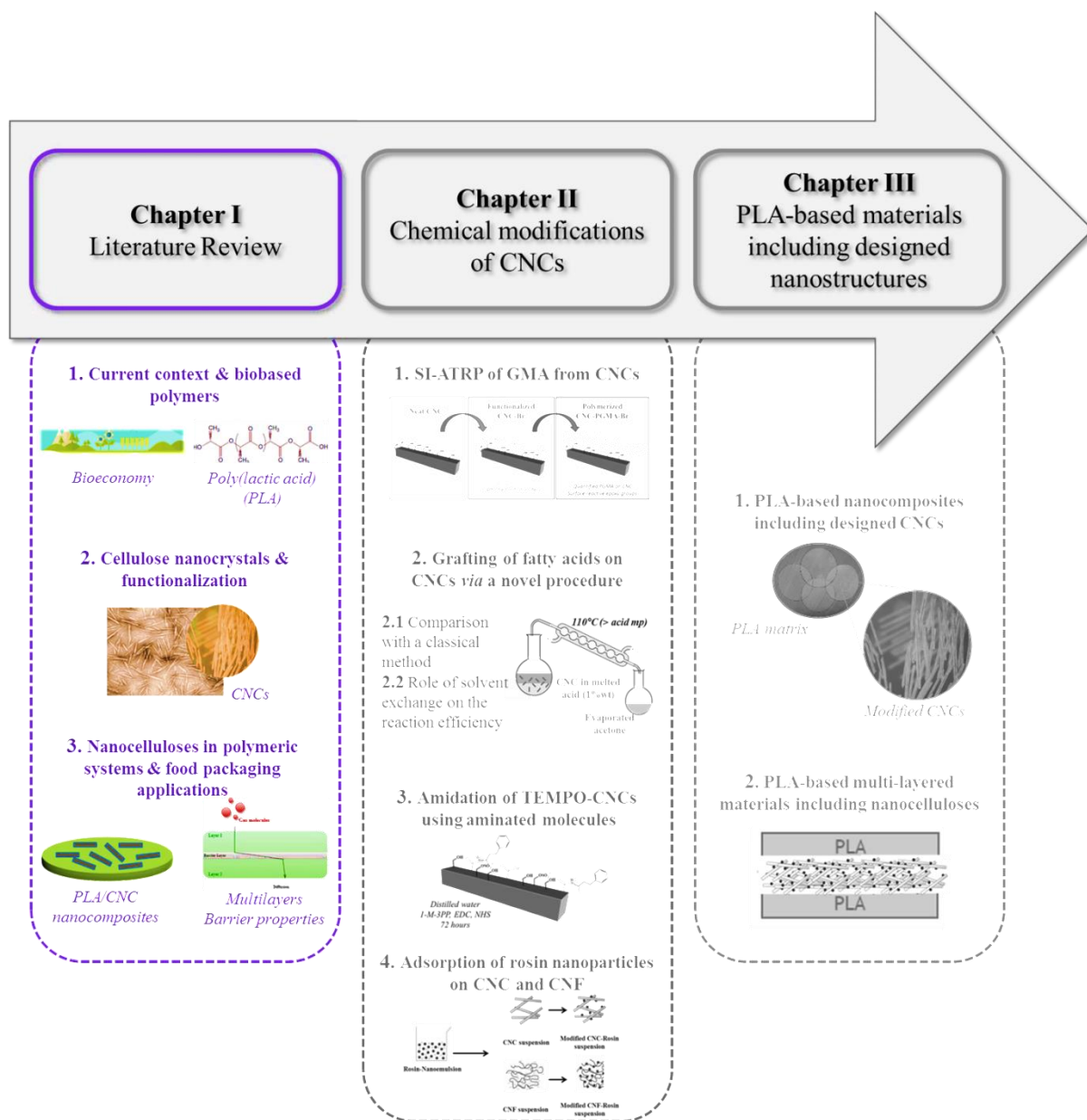
Through the literature review presented in this first chapter, the global context of this PhD project will be introduced. Indeed, this chapter attempts to give an overview of the context, by providing definitions and references (more than 200). Moreover, this chapter is intended for both “expert” and “non-experts” scientists. In this sense, general knowledge, as well as, more specific data will be presented in different forms (tables, schemes, figures). In order to link each section with the PhD project, some comments (*in grey and italic*) are added.

The first part of this chapter describes an overview of **biobased polymers for food packaging**. Generalities on current economic and environmental context will be provided. After having been defined, the place of biobased polymers in food packaging field, as well as, their requirements and main processing will be introduced. As poly(lactic acid) (PLA) is studied in this project, a part will be dedicated to this polymer.

In the second part, **nanocelluloses, and especially cellulose nanocrystals (CNCs)** – the main raw materials of this project – will be introduced. Their extraction, properties and applications will be detailed. Moreover, as CNC surface modification is one of the main challenges of this PhD, a part will provide an overview of the different ways of CNCs grafting described in the literature.

Finally, the third part will present the rising interest in combining CNCs with polymeric matrices, and especially with PLA. Thus, **CNC/PLA nanocomposites** will be the focus of this part. Their processing, properties and challenges will be detailed. A last part will describe multi-layered systems, which offer another way to produce polymeric systems by combining PLA and CNCs.

Thus, this literature review will highlight the main scientific advances and challenges closely associated to the objectives of the PhD project for an easier reading of the next chapters.



1. Biobased polymer materials for food packaging

This section aims to focus on current context of existing packaging materials and biopolymers, and on the requirements for the development of food packaging materials, as well as, their different processing routes. Moreover, one section will focus on poly(lactic acid) (PLA), the bio-based plastic used in this PhD project.

1.1. Polymers in packaging: generalities

Since the beginning of the 21st century, the current ecological situation is a priority in political and citizen spheres. Global warming, greenhouse gas emissions, ecosystem degradation, and plastic waste are the open-ended list of environmental challenges regularly referred in our society. All these issues, added to the global limited resources and the demographic growth, require -according to the European Commission- “new ways of producing and consuming that respect the ecological boundaries of our planet” and a “need to fit with sustainability”. It is part of the updated European Bioeconomy Strategy expressed in 2018, aiming at improving and innovating the way of production and consumption of food, products, and materials within healthy ecosystems through a sustainable bioeconomy, and implementing human and financial resources to reach their objectives, showing the large awareness on the part of the society. Fourteen actions are set out in this strategy, whose first is entitled “Strengthen and scale-up the bio-based sectors, unlock investments and markets”. Bio-based materials and products are described in order to substitute their fossil-based counterparts. One of the main sector concerned by the Bioeconomy strategy is plastic packaging material, which represents about 40 % of the total plastic demand (49.9 million of tons in 2016) in Europe¹. Among this plastic demand, fossil-based polypropylene (PP), polyethylene (PE), polyvinyl chloride (PVC), polyethylene terephthalate (PET), and polystyrene (PS) are widely and classically used in packaging industry¹. The interest of the development of new biobased polymers for packaging applications thus makes sense.

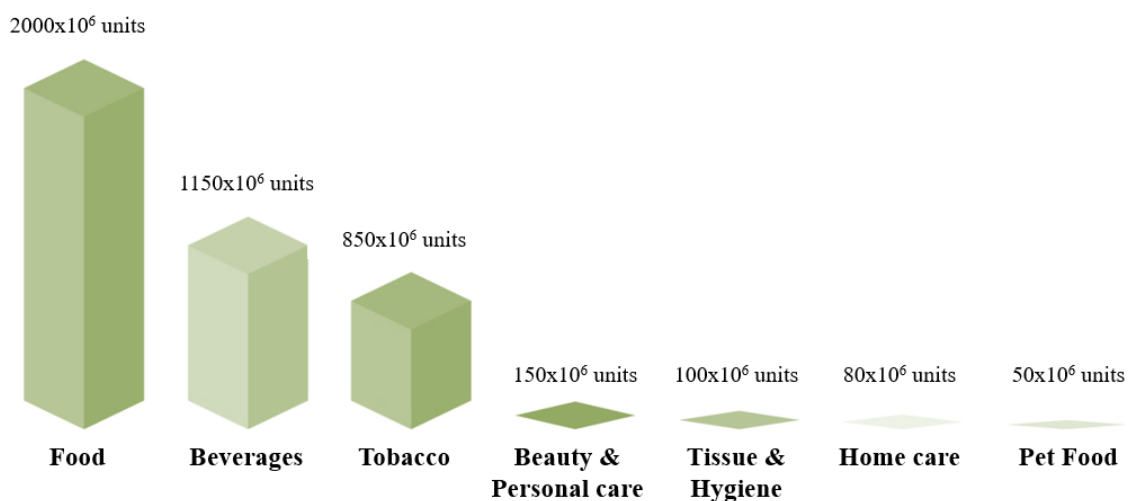


Figure I. 1. Packaging mondial market by sector, in 2015 (Adapted from Euromonitor International²)

1.1.1. Current context of packaging materials

By definition, a packaging is all the elements delivered with a product, and which is designed for its presentation, information, conservation, handling, and transporting. Food, beverages, and tobacco packaging are the most important sectors of the global packaging market, followed by beauty and personal care, tissue and hygiene, and home care packaging², as shown in **Figure I. 1**. Plastics are materials of choice in food packaging sector, representing over a quarter of the different materials used.³ Indeed, according to their outstanding mechanical and barrier properties, they allow a controlled and optimized distribution of products by preserving their aspect, shape, and, in the case of food packaging, the safety, taste, and shelf-life of the products. Currently, fossil-based plastics represent around 99% of the total plastic market⁴.

The production of such fully synthetic polymers dates back to the end of 19th century, with the 1st polymerization of PVC in 1938. The mondial plastic production increases over the years and grows from 50 million tons in 1977 to 335 million in 2016, with 50% of plastics produced in Asia, 19% in Europe and 18% in North America¹. Traditional plastic industry is based on the use of distilled crude oil, a limited resource extracted from oil reservoirs. Naphta, a mixture of hydrocarbons obtained from distilled crude oil, is essential for the further production of plastics, consisting in the polymerization of several monomers.

Today, a wide variety of fossil-based plastics exists with interesting properties, applications, and low prices. **Table I. 1** summarizes the main properties of produced plastics in European packaging field. At the end of their life, fossil-based synthetic plastics are left mostly as non degradable waste. Thermo-mechanical recycling is the most widely used treatment in Europe, representing around 99% of total recycling. It consists in two steps: first, the sorting (automatically or manually) of plastics to ensure the non presence of contaminants, and then, the melting of plastics into new pellets or granulates, without changing their chemical structure. The resulted recycled plastics can then be mixed with neat plastics, in order to reduce plastic consumption. Note that more and more companies are recycling internally their unused and cutting waste. In Europe, the collecting and recycling systems vary from a country to another, although all the countries seek to improve their system with innovative collect and society sensibilization. In 2016, in Europe, the total plastic packaging collected waste represented 16.7 million tons, and 41% were recycled, despite the huge effort in recycling loop regulations and waste management¹. These data clearly show the larger society consideration for recycling.

	Converter demand (million tons)	Properties	Applications	Unit price (€/kg) ⁵
Polypropylene (PP)	9.8	Low moisture vapor transmission / Inertness towards acids, alkalis and most solvents / Optical clarity in oriented films and molded containers	Containers for yogurts, takeout meals, butter / Medicine bottles	0.90
Low Density Polyethylene (LDPE)	8.8	Resistance to acids, bases and vegetable oils / Toughness / Flexibility / Transparency	Bags for frozen foods and fresh products / shrink wraps and stretch films / Coatings fro paper milk cartons and beverage cups	1.12
High Density Polyethylene (HDPE)	6.1	Resistance to solvents / High tensile strength / Stiffness	Bottles for beverages, cosmetics, detergents and household cleaners / Bags	1.21
Polyvinyl Chloride (PVC)	5			1.59
Polyethylene Teraphthalate (PET)	3.8	Clear and optically smooth surfaces / Oxygen, water and CO ₂ barrier / Resistance to solvents / Shatter resistance	Plastic bottles / Food jars / Ovenable films and microwavable food trays	1.05
Polyurethane (PUR)	3.8	Versatile chemistry : Strength / Rigidity / Flexibility / Good resistance to oil, hydrocarbons, oxygen	Versatile chemistry : Automotive industry(backs, armrests, door panels, bumpers) / Building / Refrigerators / Skateboards / Adhesives / Coatings / Sealants	3
Polystyrene (PS)	1.9	Moisture barrier / optical clarity / Stiffness / Low density and low thermal conductivity in foamed form	Food service items / Takeout containers / Meat trays / Rigid food containers	0.57

Table I. 1. Main synthetic polymers converter demand in Europe, in 2016, and their properties and applications (Data from PlasticsEurope Market Research Group¹)

In parallel, plastic pollution, especially of the oceans and seas, is increasing, and is a disaster for the aquatic flora and fauna. Geyer *et al.*⁶ conducted a study on the total production and waste of plastics within a period higher than 60 years over the world. According to this study, the total plastic waste was around 6300 Mt in 2015, taking into account primary and recycled plastic wastes, and only 9% of these resisudes have been already recycled. As shown in **Figure I. 2**, an accumulation of 4900 Mt of plastics produced between 1950 and 2015 are today accumulated in the nature. The projections concerning plastics waste are not optimistic. Indeed, considering similar production and use of plastics for the next decades, and validating the calculations done in the previously described study, 12000 Mt of plastic will be discarded in the nature⁶, and recent studies consider there will be more plastic than fish in the ocean in 2050. This alert was the main driver in the launching of the new bioeconomy and circular economy European directives.

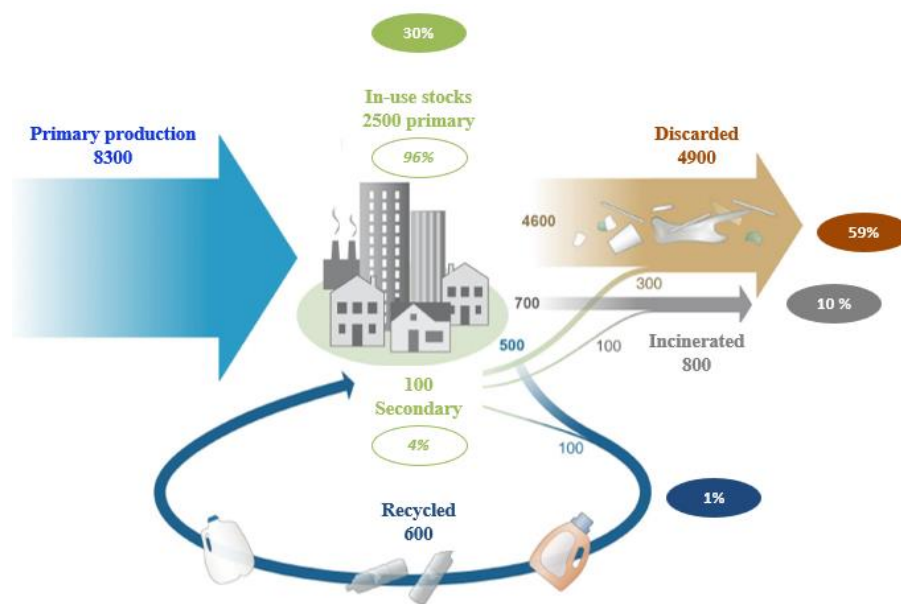


Figure I. 2. Accumulated amount (in million metric tons) of global production, stocks and waste of plastics between 1950 and 2015 (Extracted and completed from ⁶)

Packaging is a real need for a lot of applications, and fossil-based plastic polymers are today the best candidates in term of price and properties for the elaboration of such products. However, the awareness of the society about the environmental issues encourages research and development to focus on sustainable and bio-based materials for packaging. This last point is the purpose of the following section.

1.1.2. Definitions of biopolymers

First of all, it is essential to correctly define biopolymers, bio-based, biodegradable, and biocompostable (or compostable) terminologies. Indeed, in the current mass media and general discussions, generalisations are often carried out when it comes to sustainability and environmental issues. Note that a common confusion consists in the correlation between biodegradability and recyclability, the last term relating to the reintroduction of the materials in the production cycle at its end-of-life. Accordingly to the definition provided by IUPAC, a biopolymer is a macromolecule which is formed by living organisms. In 1999, Petersen *et al.*⁷ proposed the definition of biopolymers as biobased polymers. More recently, a bioplastic is defined as a family of polymeric materials comprising (i) bio-based, (ii) bio-based and biodegradable and (iii) fossil-based, and biodegradable plastics⁵. According to IUPAC (2012), a bio-based polymer is a polymer totally or partially composed or derived of biological products issued from biomass, such as plants, animals, marine or forestry materials. Bio-based polymers family is usually split into three groups: chemically synthesized from biomass monomers, produced by micro-organisms, or naturally occurring.

Note that bio-based polymers are not always biodegradable, biocompostable, biocompatible or environmentally-friendly. In short, bio-based character is opposed to fossil-based one. Both types of polymers can be biodegradable or biocompostable, and these terms need to be precisely defined. According to IUPAC definition, biodegradability is the capability of a material of being degraded by biological activity, by decreasing the polymer molar mass until bioassimilation, i.e. converting into H₂O, CO₂ or CH₄. This aerobic or anaerobic degradation results in a chemical process due to microorganisms activity producing biomass, carbon dioxide, water and/or methane from degraded polymer⁵, under different conditions of temperature, humidity, light, and environment, according to several standards. This large number of standards demonstrates how complex the biodegradation process is, since biodegradation can occur in different environments (industrial or individual compost, soil, water), and standards provide required parameterized conditions to argue biodegradability⁸. Speaking about biodegradability, it is essential to indicate in which environment the biodegradation takes place.

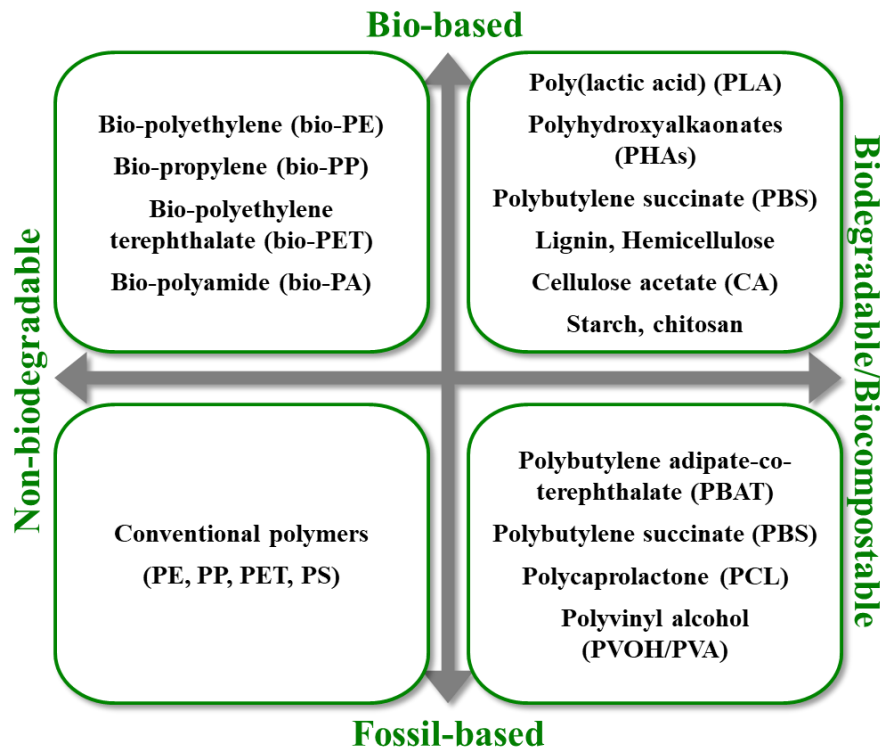


Table I. 2. Existing (bio-)polymers sorted according their properties (Extracted from ⁸)

Thus, the term biocompostability relates to biodegradability occurring in compost conditions (temperature around 70-80 °C, high humidity rate around 70%), with a decomposition of the material carried out in a specific environment and time without residues. In order to avoid misunderstanding and common confusion between these terms, the European Standard EN 13432 entitled “Requirements for packaging recoverable through composting and biodegradation – Test scheme and evaluation criteria for the final acceptance of packaging” defines the characteristics and properties of a

compostable packaging polymer, which, in addition to being biodegradable, must respond to other characteristics, like disintegrability (less than 10% of the initial mass of residues larger than 2 mm), ecotoxicity (low levels of heavy metals, absence of ecotoxicological effects on the plant growth), composition, and quality of final compost⁹. **Table I. 2** shows the properties of main (bio)-plastics currently used. Although the term fossil-based plastics (or petrochemical-based) suggests non-biodegradability, this is not always the case. In fact, as shown in **Table I. 2**, fossil-based plastics like PBAT, PBS, PCL, and PVOH are biodegradable in compost, even they are not produced from biomass resources.

Similarly, the term bio-based plastic leads to think about biodegradability, although these two properties are not necessarily linked. Moreover, as presented in **Table I. 2**, polylactide or poly(lactic acid) (PLA) is a bio-based and biodegradable polymer in industrial compost. Controversial place of PLA on current packaging market comes from this industrial compostability, needing specific conditions and infrastructures to be fully performed. This point is a current matter of controversy.

In this project, PLA is studied and used as a polymer matrix, especially in food packaging sector, and therefore it will be described more precisely afterwards (section 1.2.5).

1.2. Requirements for food packaging

Among all the packaging sectors, that of food and beverages is the most preponderant, regarding the production and demand (**Figure I. 1**). Indeed, food is a vital, valuable and perishable resource, whose more than one billion of tons are thrown away every year, leading to food waste (more than one third of the global production of food consumption), and induced environmental impact. This food waste is considered as the second reason of gas emission (especially CO₂) in the world, after transports. Innovation and research in packaging field has become one of the priorities of the European Commission since the beginning of the 2000s (Directive 2008/98/EC, Landfill Directive 1999/31/EC, Packaging and Packaging Waste Directive 94/62/EC). In parallel food plastic packaging generates a large amount of plastic waste. European Commission is releasing several calls aiming at finding new solutions to reduce the environmental footprint of packaging and ensure a better shelf life of food and specific indicators, less materials and energy use for packaging process, optimization of supply chain, better food safety and recyclability of materials. It is in this context that bio-based and biodegradable packaging, along with functional and active performance, has been at the centre of ongoing research on development of new food packaging systems.

Following part aims to describe the main barrier and mechanical properties required in food packaging area, then the current development of new active packaging, and finally the use of biobased polymers in food packaging.

1.2.1. Barrier properties in food packaging

A food packaging is produced and used in order to transport and protect the product against humidity, temperature, micro-organisms, to ensure its safety, and to inform the consumers. It correlates with the four basic functions of a packaging successively expressed by Paine¹⁰ and Robertson¹¹ in the 1990s, namely: protection, communication, convenience, and containment. Packaging ensures the conservation of the product and limit food waste by constantly improving its shelf life. Among these utilities, protection against external environment is the main challenge in the development of food packaging. Traditionally, food packaging acts as an inert wall between the product and oxygen or others gas and moisture from outside environment. Investigation on barrier properties of a packaging material is crucial and necessary when speaking about food packaging.

More precisely, oxygen and water vapor permeability are always studied. Indeed, these two permeants can largely influence and reduce the food conservation. **Figure I. 3** represents the interactions between outside and inside gas molecules. The movement of gas molecules can be described in three steps: first, external gas molecules at high concentration are in motion, and some of them sorb into the packaging material. Then, they diffuse through the material, and are finally desorbed from the material inside the packaging, at a lower concentration. Same principle acts from internal gas molecules to outside environment.

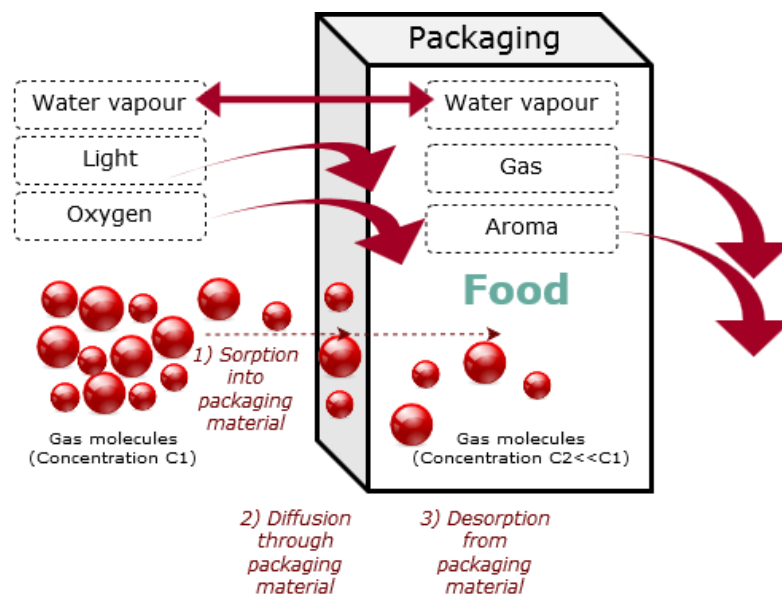


Figure I. 3. Schematic representation of gas permeant molecules through a packaging material

OTR (Oxygen transmission rate) is the most relevant characterization presented in the literature when investigating barrier properties. It allows the quantification of the oxygen amount permeating the material per unit of area and time, and is expressed in $\text{cc.m}^{-2}.\text{day}^{-1}$. Oxygen permeability (OP) is often expressed as a function of the thickness of the material, as well as, with respect to the oxygen partial pressure applied between the two sides of the sample material¹² (Standard ASTM F1927-14).

Generally speaking, lower the OTR value is, better the conservation of the product is, if oxidation process is neglected. WVTR (Water vapor transmission rate) is extremely important since the status of the food product is closely linked to its moisture content. As well as for oxygen, the water vapor amount is quantified by the water vapor permeability (WVP) indicating the amount of water vapor permeating the material per unit of area and time, normalized with the thickness of the material and the pressure difference between the two sides of the sample (Standard ISO 2528). The WVTR is then expressed in $\text{g}\cdot\text{m}^{-2}\cdot\text{day}^{-1}$ ¹². As well as for OTR, it is important for the majority of food products to have a low WVTR value, especially to avoid dehydration or moisturizing of the products. It is worth nothing that lot of different units can be found in the literature for OTR and WVTR, which may lead to some confusion. Moreover, for both oxygen and water vapor permeability, relative humidity (RH) at which the measure is carried out can affect the permeation of the gas, therefore this RH value is significant when speaking about barrier properties.

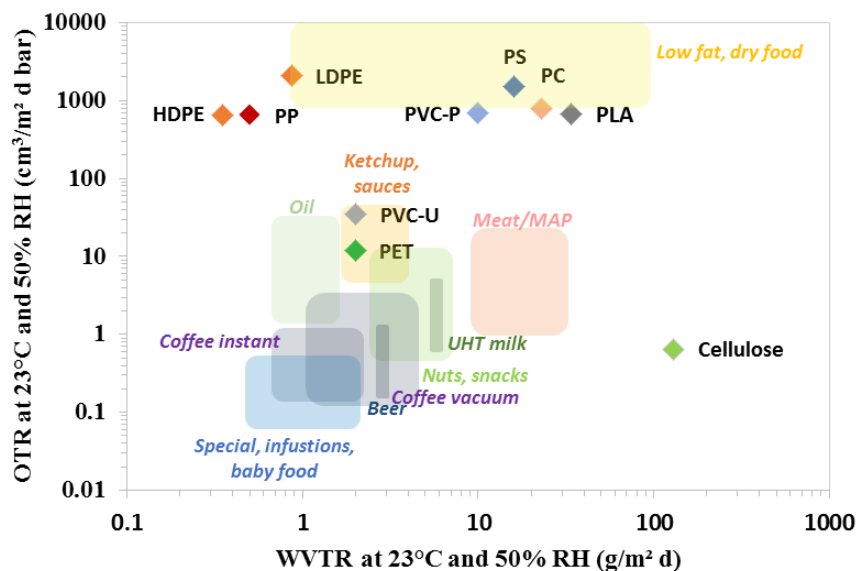


Figure I. 4. Water vapor transmission rate (WVTR) and Oxygen transmission rate (OTR) for polymers traditionally used for packaging materials and ranges of barrier properties required for specific food products (adapted from ¹³ and E. Espino Perez PhD, 2014)

Other gas permeability can be investigated, such as ethylene or carbon dioxide. Indeed, the importance of carbon dioxide relies in modified atmosphere packaging (MAP). A MAP consists in the change or replacement of initial gas inside the packaging by another (till the reaching of the equilibrium), including the use of a specifically chosen packaging material inducing the diffusion of gas through the material. Several techniques exist, with “passive” or “active” MAP, but they are all based of the previously described principle¹⁴. The gas inside the packaging and/or the material is chosen according to the product whose shelf life increases¹⁵. Carbon dioxide - produced by food products respiration - is one of the most common gases used in MAP, and equilibrium is established inside the packaging depending on its oxygen and carbon dioxide permeability¹⁶.

These barrier properties are crucial in the investigation of food packaging, since they largely influence the shelf life of the food products. **Figure I. 4** correlates barrier properties (WVTR and OTR) of classical polymers used in packaging with the required area of barrier properties of some food stuffs. According to **Figure I. 4**, the choice of a packaging material is highly dependent of its application. Moreover, as previously mentioned (**Figure I. 3**), the transportation and the safety of the product are also essential, and are closely linked to the mechanical properties of the packaging.

1.2.2. Mechanical properties of food packaging

The mechanical properties of polymers used for packaging are relevant, mainly for their processability, as well as, for the use of an adapted process, as described further in this section. Moreover, the storage conditions of filled packaging can vary, especially concerning temperature and humidity. Indeed, high or low temperature comparing to standard room temperature and high humidity can negatively influence the mechanical properties of the materials, like their tensile strength, Young's modulus, or elongation at break. These properties are also investigated under different conditions (temperature, humidity). Moreover, according to the targeted application (type of packaging, storage life and conditions, properties of the packaged product), required properties vary a lot. For example, meat or fish need to be stored between 0 and 5 °C, whereas pastas, spices or water can be stored at room temperature or even higher. According to the required gas composition and barrier properties, an adapted polymer has to be found. The following **Table I. 3** summarizes the main barrier and mechanical properties of synthetic polymers classically used in food packaging.

	Barrier properties		Mechanical properties		
	Oxygen permeability (cc.mm.m ⁻² .d ⁻¹ .atm ⁻¹) 23 °C, 50%-0% RH	WVTR (g.m ⁻² .d ⁻¹) 23 °C, 85% RH	Tensile strength (MPa)	Elongation at break (%)	Young's Modulus (GPa)
Polypropylene (PP)	50-100	0.2-0.4	26	80	2
Low Density Polyethylene (LDPE)	≈60	≈0.2	10	400	0.25
High Density Polyethylene (HDPE)	≈270	≈0.5	32	150	1.25
Plasticised Polyvinyl Chloride (PVC)	2-8	1-2	14-20	280-95	0.007-0.03
Polyethylene Teraphthalate (PET)	1-5	0.5-2	55	300	2.3
Polyurethane (PUR)	/	/	24	700	0.003
Polystyrene (PS)	100-150	1-4	34	1.6	3

Table I. 3. Barrier and mechanical properties of usual fossil-based polymers used in food packaging (data from ¹⁷)

These data correlate with the fact that fossil-based polymers are materials of choice for food packaging. Indeed, their properties largely satisfy the mechanical and barrier properties requirements, in addition to their large industrialization, and low price. Moreover, current research is focusing of the development of packaging with innovative properties, also called active packaging. This last point is the topic of the following part.

1.2.3. Development of new active packaging

In packaging field, the term “intelligent and active packaging” is increasingly used by researchers, as well as, by producers. Indeed, the development of such new kind of packaging has been naturally apprehended since the beginning of the 2000s, in order to follow the change in the consumer habits, and especially his wish for healthier eat with reduced additives, preservatives, and food waste.



Figure I. 5. Properties and examples of active and intelligent packaging : **a)** Respective functions of active and intelligent packaging (Extracted from ¹⁸), **Active packaging :** **b)** Oxygen absorbers and ethylene scavengers (EU Guidance to the Commission Regulation (EC) No 450/2009), **c)** Ethylene absorbers (Blueapple[®]), **d)** Antibacterial hand towels (Cascades[®]), **e)** Antimicrobial plasters (Hansaplast[®]), **f)** CO₂Pad for fish conservation (McAirlaid’s[®]), **Intelligent packaging :** **g)** & **h)** RFID readers for companies logistics and consumers (from StoraEnso www.storaenso.com), **i)** Time-temperature indicator (Fresh-Check[®] by Lifelines Technologies Inc. (extracted from ¹⁹), **j)** Freshness sensor (SensorQ[®]) (extracted from ²⁰), **k)** Time-temperature indicator (OnVu[®]) (extracted from ²⁰)

There is no official definition for active packaging, even if active packaging can be defined as an extension of protection function of a packaging. More precisely, according to Yam *et al.*¹⁸, active packaging can be considered as the second generation of packaging, following the primary passive generation, acting only as an inert protection barrier against oxygen and water vapor among others.

Miltz *et al.*²¹ have considered this new active protection as a system where the product, the packaging, and the environment are in interaction, in order to improve the shelf life of the product, or to provide interesting new properties, better food safety, and quality. Active packaging are often associated to intelligent or smart ones, which can be defined as an extension of communication and identification function of packaging, including for example RFID, NFC, QR codes, or time or temperature sensors technologies. Intelligent packaging does not change or improve the properties of the product, but it aims to enhance the logistic, stocks management, traceability, safety and marketing related to a product. Moreover, numerous active packaging exist today, like moisture scavengers, antimicrobial agents, ethylene absorbers or antimicrobial tissues. Some of intelligent and active packaging applications are summarized in **Figure I. 5**, taking into account the European definition for both active and intelligent packaging, respectively a packaging increasing products shelf life, and giving information about the product.

Today, the large majority of all active packaging are produced from fossil-based plastics. Indeed, the active packaging market is growing fast, and it still relies on the use of non-bio-based polymers.

The use of bio-based materials for barrier or active packaging processing appears to be a more sustainable solution as existing products.

1.2.4. Biobased polymers in food packaging and sustainability approaches

Through their properties, low price and processability, fossil-based plastics are largely used in traditional and in more innovative packaging sector. But the use of bio-based polymers is relevant and more and more investigated. Indeed, according to the results of a study carried out by the Institute for Bioplastics and Composites in 2016²², around 830.10³ tons of bio-based plastics for flexible packaging and 2230.10³ tons for rigid packaging will be produced in 2022, as presented in **Figure I. 6**. It's almost twice more that the data for the year 2017, highlighting the large impact of bio-based polymers in packaging field. Moreover, bioplastics will represent around 10% of the global plastics market in 2022, and most of them will be used in packaging industry.

Moreover, as shown in **Figure I. 6**, biodegradable polymers, and especially PLA, are of high interest in flexible packaging (bags, films for example), and less present – although relevant – in rigid packaging (food cups and trays, bottles for example). Although other bio-based plastics are under development and still commercialized - like among others bio-based PET (e.g. Johnson & Johnson with the commercialization of sunscreen bottles in Brazil since 2009) or bio-based HDPE (e.g. Procter and Gamble with the commercialization of shampoo and cosmetics packaging in USA since 2011)²³ - PLA presents interesting properties for food packaging applications. Indeed, despite its low thermal stability and brittleness which limits its access to a lot of applications, PLA presents interesting

mechanical properties, a controlled and easy processability²⁴, as well as, a low cost comparing to other bio-based plastics.

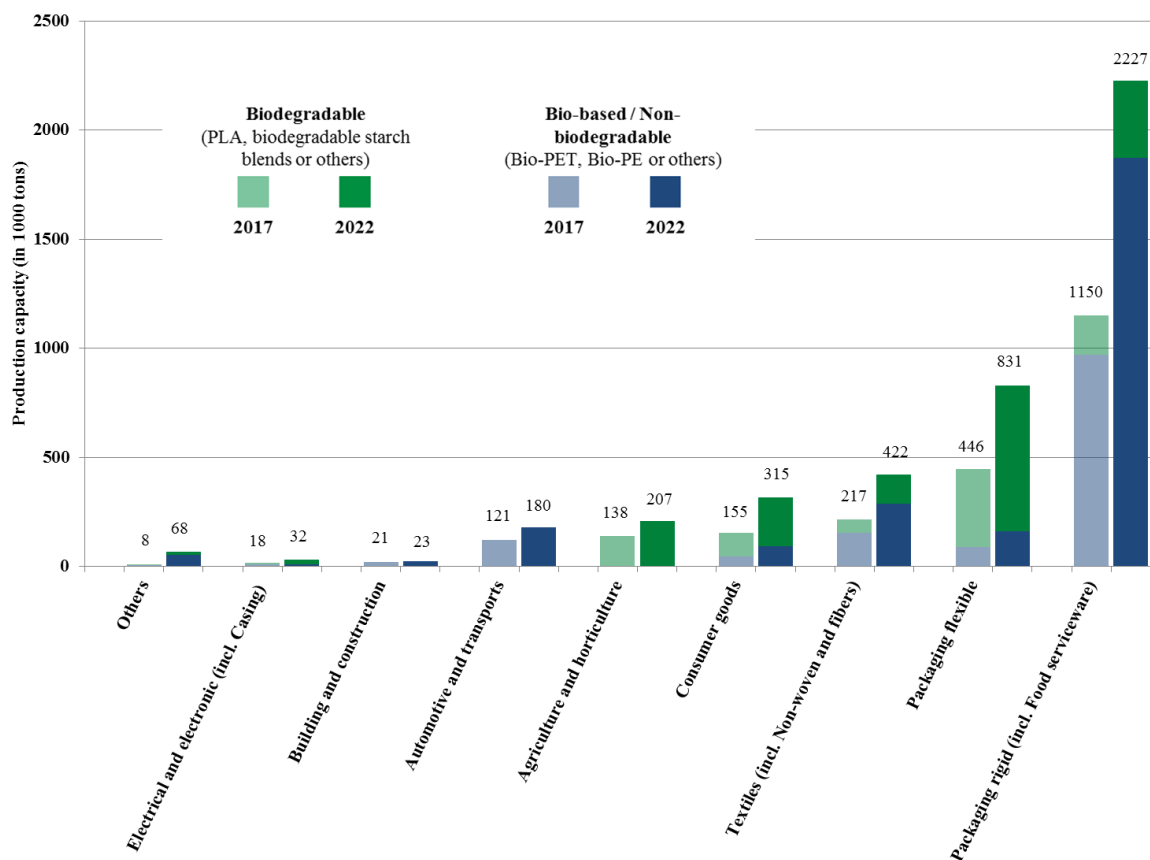


Figure I. 6. Bio-based plastics production capacities by market segment, in 2017, and projections for the year 2022 (Adapted from ²²)

A lot of researches are currently carried out in order to improve the poor thermal and mechanical properties (at temperatures higher than its glass transition temperature T_g) of PLA, as well as, its barrier properties. This point will be described later in this chapter. Moreover, as previously mentioned, interesting properties of PLA make it a promising and conceivable bio-based and biodegradable polymer for food packaging applications. Indeed, commercialized PLA packaging is currently accessible (bottles, cups, shopping bags etc.), as shown in **Figure I. 7**.

By definition, sustainable development is the development of products combining and satisfying social, economic, and environmental concerns. Economic and social issues were previously mentioned, and regarding the environmental aspect, Life Cycle Assessment (LCA) is the most popular sustainability assessment tool used to assess the environmental impacts in whole life cycle of selected subject matter. It can be used to rate and compare a product with another with similar functionality, and is based on two main standards (EN ISO 14040 and EN ISO 14044). Several researches were interested in the LCA of different bio-based polymers^{25–28}. Although all these studies are not using the same methods, criteria, assumptions, and boundaries for the LCA, all their conclusions are converging to the same

trend: the use of bio-based polymers has a more efficient sustainable impact than fossil-based ones, especially for what the non-renewable energy use and the global warming potential concerns²⁸. Moreover, several categories are investigated in LCA (e.g. climate change, ozone depletion, human toxicity, water depletion, freshwater ecotoxicity, etc.) and bio-based polymers present not always the lower impacts in other categories, leading to difficult conclusions. It can be attributed to the lack of data for these emerging polymers, and even they are not only environmental friendly compared to fossil-based homologues, they tend to improve this last point. Spierling *et al.*²⁶ concluded that an estimated 65.8% substitution of synthetic fossil-based polymers by bio-based counterparts can reduce the CO₂ emissions by almost 25%.



Figure I. 7. Examples of commercialized PLA-based food packaging : **a)** Sant'Anna water bottles (Italy), **b)** Carrefour grocery bags (Belgium, Romania), **c)** Noble Juice bottles (USA), and **d)** Activia (Danone) yogurt cups (Germany)

Despite not always favorable environmental LCA results, bio-based polymers, and especially PLA²⁷, seem to be environmentally relevant for what global warming potential and non-renewable energy use concerns. Nevertheless, industrial compostability and non-recyclability are once again negative points in the LCA of PLA. Indeed, in their critical review, Yates and Barlow²⁸ compared different LCA analyses undertaken with different assumptions and criteria. In all cases, industrial composting is not the best option, especially because of generated oxidized carbon-based gases from compost produced. Several studies conclude that incineration of PLA or landfills (leading to anaerobic digestion producing methane) are preferred waste management solutions. Moreover, it is difficult to conclude about recycling, since several limitations of the analysis (infrastructures availability and adaptability, competition with incineration and other waste treatments, low amount of studies) are important. However, this option would be the best from the environmental point of view, although PLA recycling is currently not totally proved and industrially possible, only at pilot scale. LCA of PLA is still a matter of debate about PLA industrial use.

1.2.5. Poly(lactic acid) : a relevant biopolymer

Poly(lactic acid) or polylactide, usually called PLA is, as previously mentioned, a bio-based and biocompostable polymer. It is a thermoplastic bio-polyester, polymerized from 2-hydroxy propionic acid monomer units of lactic acid. This monomer was isolated for the first time in 1780 from sour milk, by a Swedish chemist, and its production has been industrialized since the end of 19th century,

especially as additive in food, cosmetics and pharmaceutical products. Lactic acid can be obtained by chemical synthesis or by carbohydrate bacterial fermentation. The latter is classically used for its industrial production, with moderate costs and a better control of the synthesis, under mild reaction conditions (pH around 6, temperature around 40 °C, low oxygen concentration). Indeed, according to the type of bacterial fermentation, different yields of synthesis, as well as, different ratio of the two stereo isomers of lactic acid - the L-LA and D-LA (**Figure I. 8**) – can be reached, leading to different properties of the final polymer. Different sources of carbohydrates are extracted and used as raw materials, like corn, potatoes, cane, and beet sugar. The obtained lactic acid is purified in various ways, according to its application. The polymerization of PLA was first carried out in 1845, by the French chemist Pelouze, who performed the poly-condensation route, leading to low molecular weight polymer (800-5000 g.mol⁻¹). The polymerization of lactic acid into PLA has been then improved during the 20th century by Cargill Dow Company, leading to higher molecular weights *via* ring opening polymerization. **Figure I. 8** schematizes the different ways of PLA syntheses.

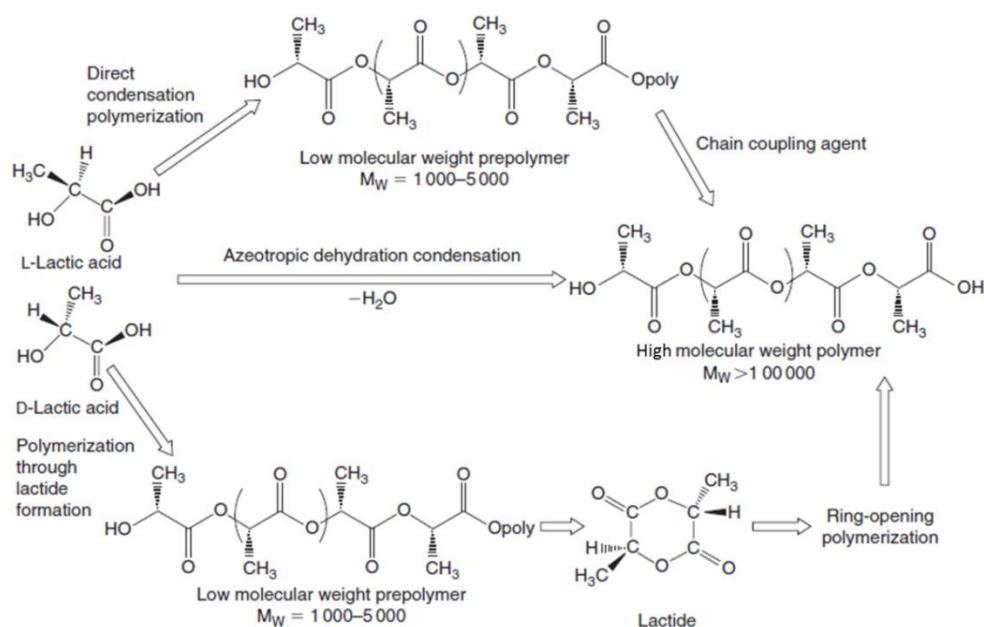


Figure I. 8. Three ways for the synthesis of high molecular weight PLA (extracted from ²⁹)

Another way of PLA synthesis consists in the dehydration-condensation of lactic acid monomer, leading to high molecular weight polymer, without any addition of chain extenders or additives. Actually, the main PLA production process is the intermediate formation of lactide, following by its ring-opening polymerization (ROP), and leading to high molecular weight PLA. At the industrial scale, PLA was first polymerized in the 1930s and patented twenty years later by DuPont industry.

Currently, a lot of companies all around the world are producing PLA in large volumes, as presented in the non-exhaustive **Table I. 4**. The largest producer is NatureWorks, producing the brand Ingeo, following by the joint-venture between Total and Corbion companies. Note that other numerous companies are plastic converters, supplying converted PLA materials like bags, food trays, or others.

Supplier	Product name / Brand	Country	Starting year of production	Annual production capacity (x10 ³ tons)
NatureWorks	Ingeo	USA	2003	150
Total Corbion (joint venture)	Luminy®	Netherlands	2018	75
Weforyou	/	Austria	2014	10
Synbra	BioFoam®	Netherlands	2011	/
Technology bv	Synterra®		2011	5
Radici Group	CornLeaf	Italy	/	/

Table I. 4. Main PLA producers with their starting year of production and their annual production capacity

If PLA generates all this interest, especially in food packaging field, it is especially because of its transparency, and some interesting properties. **Table I. 5** shows the main properties of PLA, as well as, those of PET and PP for the comparison. According to this non-exhaustive data table, it's possible to confirm about the interesting mechanical properties of PLA. Indeed, its high elastic modulus allows its use as rigid packaging, reducing the required thickness compared to other less rigid usual polymers (PET, PS). However, its low elongation at break limits its use as flexible packaging. Note that a high elastic modulus generally induces a high brittleness, which is the case for PLA in its pure form. Natural colorless, brightness of amorphous PLA (which is more opaque in its crystalline form due to the presence of relatively big-size crystals), as well as, its low interactions with passing light make it relevant for food packaging applications. Due to its high surface energy, the printability of PLA is suitable and relevant for packaging applications. Nevertheless, PLA is highly permeable to water vapor allowing applications for textile, fresh vegetables (reduced condensation inside the packaging), but limiting those for dried and perishable products.

	Properties	Unit	PLA	PET	PP
Thermal properties	T _g	°C	50-60	75	10
	T _m	°C	130-180	255-265	160
Mechanical properties	Elongation at break	%	3-30	50-300	10-600
	Modulus of elasticity	GPa	2-4	2-3	1-2
Barrier properties	Tensile strength	MPa	40-60	50-60	30-40
	Oxygen permeability	m ³ .m.m ⁻² .s ⁻¹ .Pa ⁻¹	1-4 10 ⁻¹⁸	6-8 10 ⁻¹⁹	2-4 10 ⁻¹⁸
	Water vapor permeability	kg.m.m ⁻² .s ⁻¹ .Pa ⁻¹	1-2 10 ⁻¹⁴	2-3 10 ⁻¹⁵	1-2 10 ⁻¹⁷

Table I. 5. Main properties of PLA and comparison with PET and PP properties (data from ^{27,30-35})

In addition, PLA is barrier to fatty substance and aroma and present a low toxicity. All these properties make the relevance of PLA in food packaging development^{27,31}. Nevertheless, controversies surrounding industrial use of PLA exist. Indeed, as previously mentioned, the first one deals with its biodegradability in industrial compost and its non-recyclability, which can negatively influence its use

for packaging for example. In fact, during their industrial composting requiring fossil energies especially for heating, greenhouse methane is produced. Moreover, the use of natural alimentary resources needed for its production is controversial in current economic health global context. Those aspects must be borne in mind when speaking about PLA interests, especially in this project.

1.3. Packaging processing

Polymers must be transformed and shaped into packaging materials, whether or not they are bio-based or fossil-based. Indeed, according to the type and the use of packaging and its required properties, different ways of shaping exist. The most common processing are moulding (blow, injection or compression), film casting, blown film extrusion, thermoforming, and spinning.

Since we are interested in PLA in this project, following part is focused on existing processing of PLA-based materials: composites and coating strategies are detailed, modifying bulk and surface properties of PLA, respectively.

1.3.1. Extrusion and composites materials

Extrusion processes are commonly used for PLA-based materials processing. Indeed, conventionally industrial extruders can be adapted for the PLA processing. The process temperature is generally set around 210 °C (40-50 °C above the PLA melting temperature), leading to an optimal controlled melt viscosity and homogeneity. According to the final desired material, different types of melt processing exist, and are briefly described in this section.

The **casting** of films and sheets leads to materials thickness from few micrometres to several millimetres, which can be co-extruded with other polymers or metallic films, in order to improve final properties.

Film blowing extrusion allows the production of bi-axially oriented films through efficient process, with large amount of production.

Injection stretch blow moulding is essentially used for bottles production, which is interesting in the case of PLA which has properties closed to those of PET, although parameters need to be adjusted.

Spinning processes *via* extrusion of PLA lead to polymer fibers generally used in textile of filter industry.

Another type of extrusion, called **reactive extrusion (REX)** is interesting in term of PLA synthesis and modification. Thus, REX uses existing extruders as continuous chemical reactors, and allows the production of highly viscous materials by reducing the heat and mass transfer issues generally involved. Moreover, additives can be easily added, like fillers and plasticizers. Modified produced PLA, with or without additives, is interested in term of properties for further applications³⁶.

All these processing methods (more precisely detailed in a recent review of Castro-Aguirre *et al.*²⁷) require the adjustments of conventional parameters. In particular, PLA extrusion is an essential and required step for any further processing, as those presented just before. Extrusion is an optimized process which was developed at the end of the 19th and has been widely used in plastic industry, especially for polymer processing, shaping or compounding, and more recently reactive extrusion as previously mentioned. Briefly, the solid polymer resin is transported, melted and mixed with control of the temperature, pressure and rotation of the screw (single or twin screw). **Figure I. 9** presents a general view of a twin-screw extruder. It is visible that the solid polymer is transported through rotating heated screw.

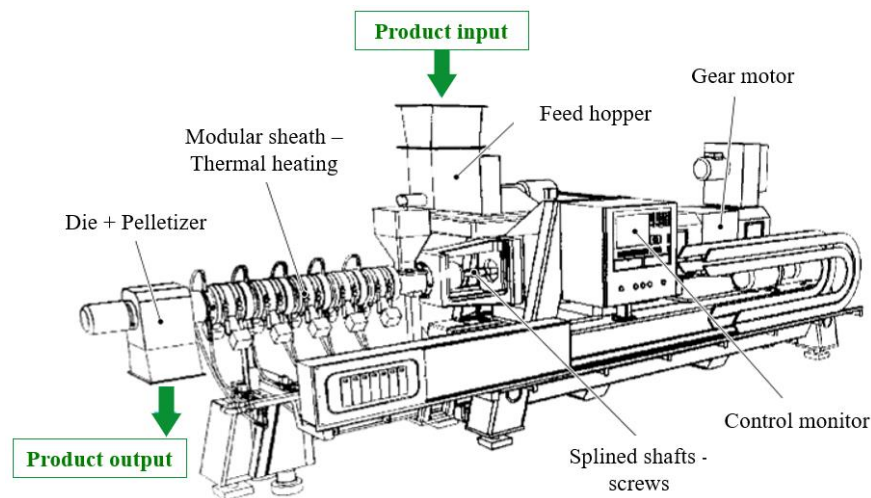


Figure I. 9. Twin-screw extruder general scheme (extracted from ³⁷)

Numerous parameters have to be set (e.g. temperature, pressure, dimensions of the screws (length/diameter)) in order to optimize extrusion of the polymer. Moreover, PLA extrusion can be carried out using same screw profiles, as those used for polyesters or PS, which is interesting for an industrial point of view, since it avoids wasting the production time. Indeed, although properties of PLA are closed of those of PET for what processing concerns, it's essential to modify some of them to ensure final mechanical and thermal properties of the materials.

The main challenge of PLA extrusion is the degradation of the polymer. By definition, the degradation of a polymer is an irreversible phenomenon, leading to polymer changes and losses of properties. In case of PLA, its degradation can be hydrolytic or thermal. In the first case, the presence of water in the solid PLA resin leads to the hydrolysis of ester bonds from polymer chains, conducting to the decrease of the molecular weight of the polymer, and thus to the presence of oligomers and monomers in the mixture. This reaction can be avoided with a previous drying step, in order to reach a water content lower than 0.01 wt% in the polymer²⁷. Moreover, the PLA thermal degradation can occur during the extrusion process. Indeed, it can be correlated with the presence of water leading to hydrolysis reaction, or to other reactions, like random main-chain scissions, intra- and intermolecular transesterifications. These mechanisms are complex, but they lead to a decrease of the polymer molecular weight, as well

as, to the presence of other degradation products (CO, CO₂, oligomers, acetaldehydes, methylketones) in the mixture. Optimization of extrusion processing parameters (e.g. polymer moisture, temperature, pressure, residence time in the extruder etc.) can reduce or avoid PLA degradation. Moreover, improving thermal properties of initial PLA has been a huge concern in literature since several years^{36,38}.

1.3.2. Coating strategy

Although extrusion is the main process for PLA shaping, coating strategy can be another solution to surface modify the PLA, and by thus providing additional properties to PLA-based materials. Indeed, coating process allows the deposition of a controlled thin layer on a substrate (a polymer film, textile, cardboard or paper for example), as shown in **Figure I. 10**. Industrially, different coating devices exist according to the substrate (thickness, porosity, etc.), coating colors (viscosity, composition, etc.), and application (targeted coating layer thickness, drying, etc.). As presented in **Figure I. 10**, knife coating, roll coating, deeping coating, spray coating, hot-melt coating, or powder coating are some coating methods usually used in industry. General principle always consists in the deposition of a thin material layer on a specific substrate, whatever the coating process. Moreover, other laboratory devices exist in order to carry out lab-scale experiment (e.g. bar-coater, pilot-scale roll, spin-coater).

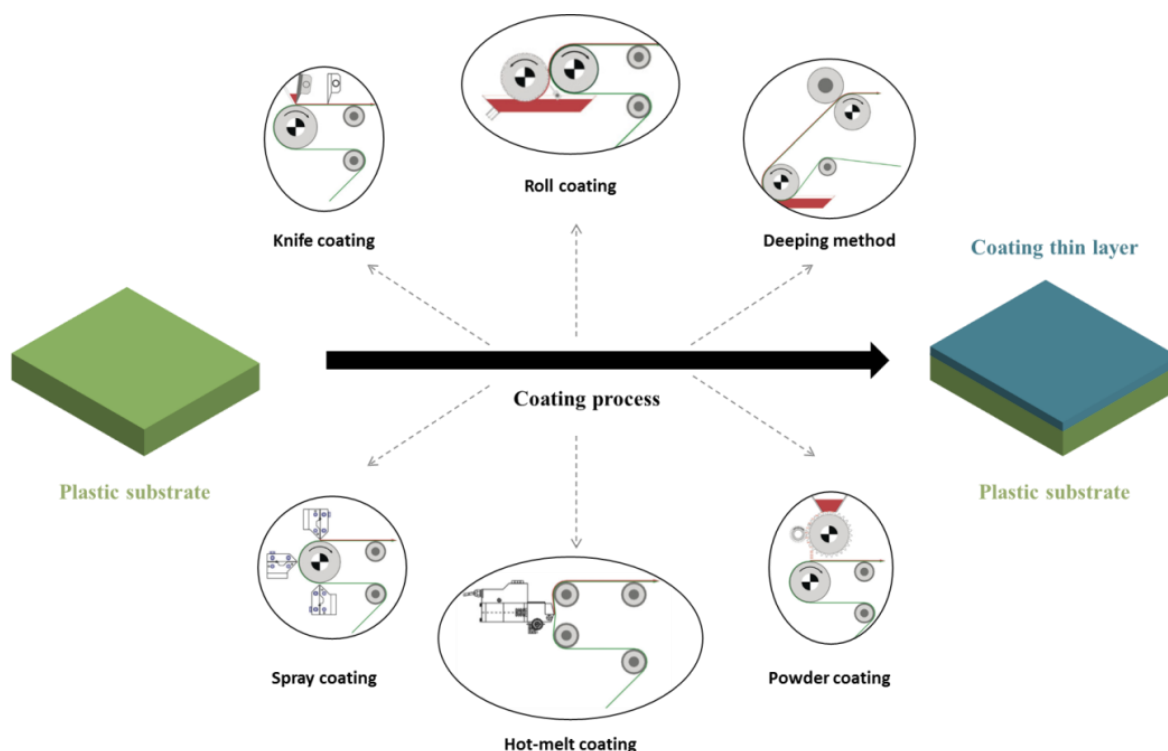


Figure I. 10. Schematized coating principle and main industrial coating processes (processes schemes extracted from ³⁹)

The coating strategy is particularly interesting in active packaging field, since it allows the increasing of barrier properties, or the deposition of active compounds (antioxidant, antibacterial for example) at the surface of a material, in order to confer enhanced properties to the final packaging. Although

regulations of food packaging are very strict, coating strategy is also often employed in “sandwich materials”, in which the coated layer is surrounded by another substrate and hot-pressed for example, so that the coated layer is encapsulated and does not enter directly in contact with the food, but can keep its activity. For example, Reis *et al.*⁴⁰ have recently shown that the coating of a natural wax emulsion on a tray made with a blend of PLA, and starch can improve the mechanical and barrier properties of the final product, which can be used as fresh fruits and vegetables packaging. In this case, coating layer is directly in contact with the food, but no release of any compound could occur. In another study of Pierleoni *et al.*⁴¹, it has been demonstrated that the incorporation of a graphene layer (0.25 g.m^{-2}) between two PLA films leads to enhanced gas barrier properties of final multi-layered materials. In a same way, Goh *et al.*⁴² have developed a similar multi-layered material in which a graphene oxide (GO) or reduced graphene oxide (rGO) layer is encapsulated between two PLA films by applying a polymer PVP solution as a binder, and by heat-compressing all the layers. **Figure I. 11** shows the morphology of these different composite films, as well as, their barrier properties.

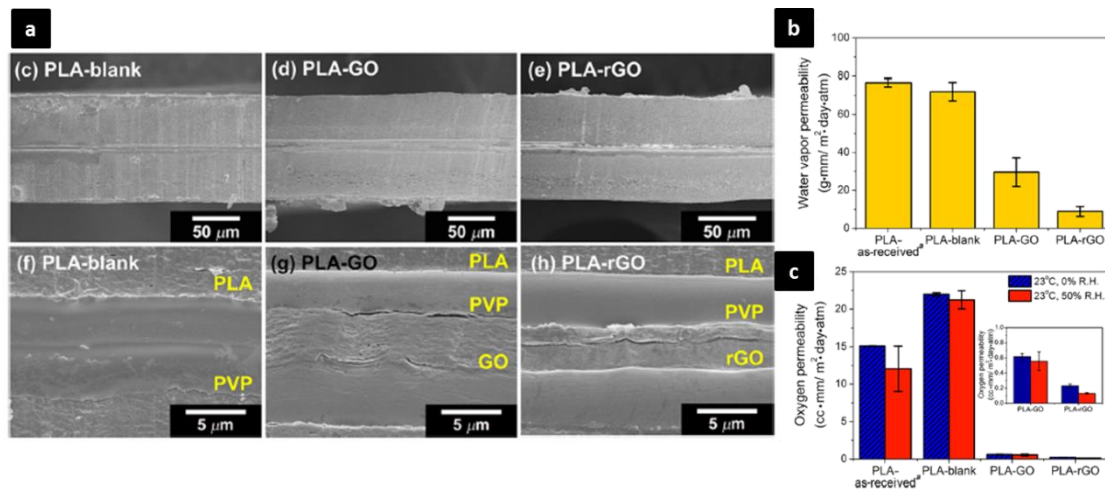


Figure I. 11. a) FE-SEM images of cross-sections of reference, PLA-GO and PLA-rGO multi-layered films, b) Water vapor permeability, and c) Oxygen permeability of composites films (extracted from ⁴²)

The main challenge of PLA coating relies on its hydrophobic nature, which makes difficult the deposition of an aqueous coating without a previous surface treatment of the PLA substrate, aiming at improving its wettability, and thus its adhesion with the deposited layer. Generally, corona or plasma treatments are carried out³⁹. In both cases, the surface energy of the substrate is modified once cold corona or plasma discharge has been applied, and induced partial ionization, leading to excited species oxidizing surface molecules of the polymer and creating new polar chemical groups. Such equipment is already widely used in printing and packaging industry⁴³. In a recent study, Rocca-Smith *et al.*⁴³ have investigated the effect of corona treatment on PLA properties.

a

Film surface	Elemental composition ^a (Atomic %)			Roughness ^b (nm)	Water contact angle ^c (°)	Surface tension ^d (mN·m ⁻¹)		
	C	O	O/C	R_{rms}	θ	γ_s^p	γ_s^d	γ_s
NCT-A	—	—	—	3.8 ± 0.4^a	79.7 ± 1.8^a	4.8	27.7	32.5
NCT-B	—	—	—	3.6 ± 1.1^a	81.2 ± 1.6^a	4.1	28.3	32.4
CT-untreated	73	27	0.37	2.3 ± 0.9^a	75.2 ± 2.1^b	6.0	28.6	34.6
CT-treated	68	32	0.47	7.4 ± 1.7^b	70.8 ± 0.5^c	7.0	32.2	39.2

^a Determined by XPS analysis.
^b Determined by AFM analysis.
^c Determined by goniometry analysis.
^d Determined using the Owens-Wendt method.

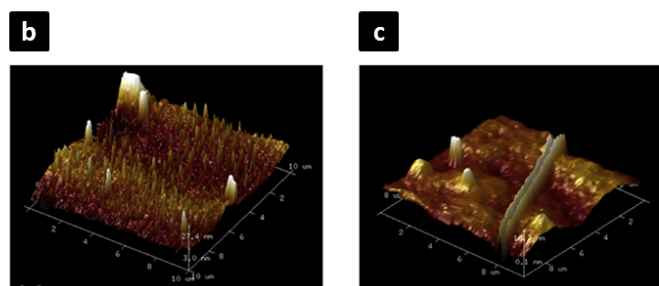


Figure I. 12. a) Surface properties of both faces of commercial untreated (NCT) and corona treated (CT) with (CT-treated) or without (CT-untreated) additional corona treatment (C=carbon, O=oxygen, R_{rms} =root mean squared roughness, γ_s =surface tension, γ_s^p =polar contribution, γ_s^d =dispersive contribution), surface topography of b) treated surface PLA film, and c) untreated surface PLA film obtained by AFM (extracted from ⁴³)

They concluded about the efficiency of the PLA surface modification at the nanometer scale, whether physically (topography and especially roughness) or chemically (increasing of oxygen content at the surface), as summarized in **Figure I. 12**. It confirms theoretical aspects of corona treatment: decreasing of water contact angle of the substrate and increasing of the polar contribution to the surface tension (even if this increase is quite slight in their study), in parallel to an unexpected lower increasing of dispersive contribution, which should not change, theoretically. Surprisingly, these authors claimed that corona treatment influenced the bulk of the material (by increasing its crystallinity and thus its mechanical properties) and improved barrier properties. Nevertheless, these conclusions only concern laboratory samples, but they are to be taken with care, when rationalizing the PLA surface modifications. Anyway, corona treatment has to be optimized and controlled to monitor PLA properties before any coating or any processing.

1.3.3. Composites materials

Melt processes are interesting, since they allow the shaping of PLA-based materials. But as previously mentioned, PLA properties -and especially thermal, mechanical and barrier ones- are not fully suitable for food packaging applications. Consequently, composites are produced, in order to improve these properties, by introducing reinforcements or other dispersed components in the PLA-based matrix. Different techniques are usually used to prepare composites, but melt-compounding is the widely used one. Melt-compounding can be performed using different devices, like internal mixers, single-screw or twin-screw extruders. Process conditions (temperature, time, shear etc.) have to be optimized in order to avoid any degradation of the polymer, as previously mentioned³⁸. Note that different fillers can be added, from cellulose, glass or carbon fibers, to mineral components (talc, kaolin etc.). Although melt-

compounding is the most used method, solvent-based methods are often used at lab-scale, although it does not always show the same final materials properties to compare with the previous method. Nevertheless, it's useful to simulate in the laboratory the behavior of composites and their properties. Finally, other methods are employed for the preparation of PLA-based composites, like physical blending of PLA with fibers, co-extrusion, hot pressing (film-stacking method) and others.

Table I. 6 summarizes the main PLA-based composites recently described in the literature, as well as, their production methods. It lists, in a non-exhaustive manner, some relevant examples, and shows the diversity of fillers introduced in PLA-based composites. Indeed, introduction of various natural or synthetic fibers (cellulose, glass, carbon, etc.), as well as, mineral fillers (clay, talc, hydroxyapatite, etc.) in PLA matrix allows the override of low properties of PLA for what food packaging applications concerns, particularly by improving the thermal and mechanical properties of final materials. Moreover, the barrier properties can be improved with the creation of tortuous pathways inside the materials to impede the passage of the gas molecules. Finally, it is important to bear in mind that biodegradation or biocompostability properties can be changed after addition of fillers inside the PLA, depending on the source and properties of the filler.

Fillers	Process	Filler wt%	Improved properties	Reference
Poly(urea-formaldehyde) (plasticizer) microcapsules	Solvent casting	5-20 %	Mechanical properties	(Meesorn <i>et al.</i> , 2019) ⁴⁴
Talc and biocarbon	Melt-compounding and compression-molding	10 %	Abrasive resistance, barrier properties and flammability	(Snowdon <i>et al.</i> , 2019) ⁴⁵
Talc and kaolinite	Twin-screw extruding	5-30%	Morphology and thermomechanical properties	(Ouchiar <i>et al.</i> , 2015) ⁴⁶
Basalt fibers	Dry-blending and single-screw extruding	5-20%	Mechanical properties and 3D printing feasibility	(Sang <i>et al.</i> , 2019) ⁴⁷
Cellulose fibers	Dry-blending, twin-screw extruding and injection molding	10%	Thermal and mechanical properties	(Kyutoku <i>et al.</i> , 2019) ⁴⁸
	Mixing, twin-screw extruding and injection molding	5-20%	Thermal and mechanical properties	(Aliotta <i>et al.</i> , 2019) ⁴⁹
Woven jute fabric	Hot pressing (film-stacking between two PLA films)	/	Mechanical properties	(Khan <i>et al.</i> , 2016) ⁵⁰

Table I. 6. Examples of recent PLA-based composites found in literature (Completed and adapted from ³⁸)

In this first part, bio-based materials were detailed. But another range of materials, called nanocomposites, have entered in the food packaging market. They aim to increase the properties of the materials by introducing nanometric materials in the packaging. Thus, the use of bio-based nanomaterials is interesting since it is consistent with the previously presented bioeconomy strategy. The following part focuses on a specific range of bio-based nanomaterials: the nanocelluloses.

2. Cellulose nanocrystals and functionalization

The sections 2.1 and 2.2 are adapted from « Le Gars M., Douard L., Belgacem M. N., Bras J. Cellulose Nanocrystals: From Classical Hydrolysis to the Use of Deep Eutectic Solvents », Chapter of the book « Nanosystems », published in IntechOpen (2019)

As renewable and biodegradable nanomaterials, nanocelluloses have raised a huge interest for the last decades. Indeed, their natural available and abundant sources – the biomass – as well as their interesting properties, make them materials of choice for new nanomaterials science, in a large panel of applications. As presented in **Figure I. 13**, the exponential evolution of the number of publications and patents dealing with nanocelluloses confirms the large interest generated by these nanomaterials. Only during this PhD project, about 2800 papers and 400 patents have been published on the topic.

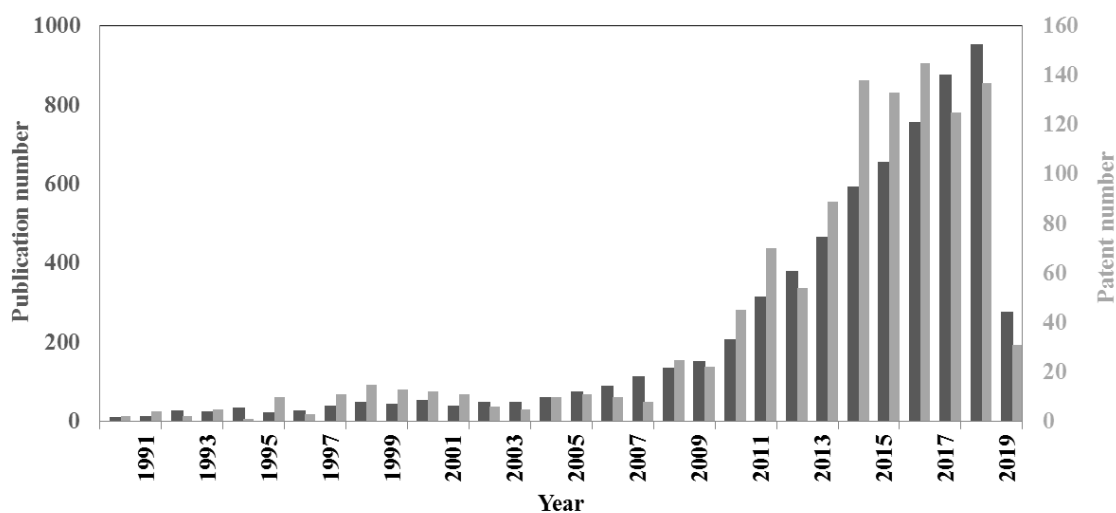


Figure I. 13. Non-cumulative evolution of the number of publications and patents dealing with nanocelluloses (CNC and CNF) (Source : SciFinder, April 2019 – Descriptors : cellulose nanocrystal, cellulose nanorod, rod-like cellulose, cellulose nanowire, cellulose crystallite, cellulose nanoparticle, cellulose whiskers, nanocrystalline cellulose, cellulose nanofibrils, cellulose microfibrils, nanofibrillated cellulose, microfibrillated cellulose – Language : English)

Two types of nanocelluloses exist: cellulose nanofibrils (CNFs) and cellulose nanocrystals (CNCs), differing from each other in their properties, as well as, in their isolation process. This part aims to describe their isolation from cellulose, properties, and applications. A third variety of nanocellulose is also available in the literature (bacterial cellulose)⁵¹.

2.1. From cellulose to nanocelluloses

2.1.1. Structure of cellulose

Cellulose can be extracted from a large variety of sources, like wood (the main source), seed fibers (cotton), bast fibers (flax, jute, ramie), some animal species (tunicates), fungi and fruits, with different cellulose contents⁵². With around 10^{11} - 10^{12} tons of cellulose produced through photosynthesis each year^{53,54}, whose less than 5% is extracted for applications, cellulose is the most abundant polymer on

our planet⁵⁵. Historically, cellulose was discovered after being extracted with nitric acid from several plants by the French researcher Anselme Payen, in 1838, who characterized the residual compound with chemical formula $C_6H_{10}O_5$ ^{55,56}. In 1939, the name cellulose was for the first time introduced in the scientific community. After almost 200 years of cellulose extraction, modification and industrial use, this sustainable and biodegradable polymer is currently used for several applications, from paper and cardboard to biomedical, building, textile, cosmetics, pharmacy and composites^{57,58}. Indeed, intrinsic properties of cellulose fibers – abundancy, renewability, availability – as well as, its fibrillary structure or mechanical properties (strength, flexibility), make them materials of choice for such applications. Indeed, in their natural form, cellulose fibers are included in hemicellulose- and lignin-based matrix like a natural composite, and act as the primary compound of plant cell walls, by providing high mechanical properties, and maintaining their structure.

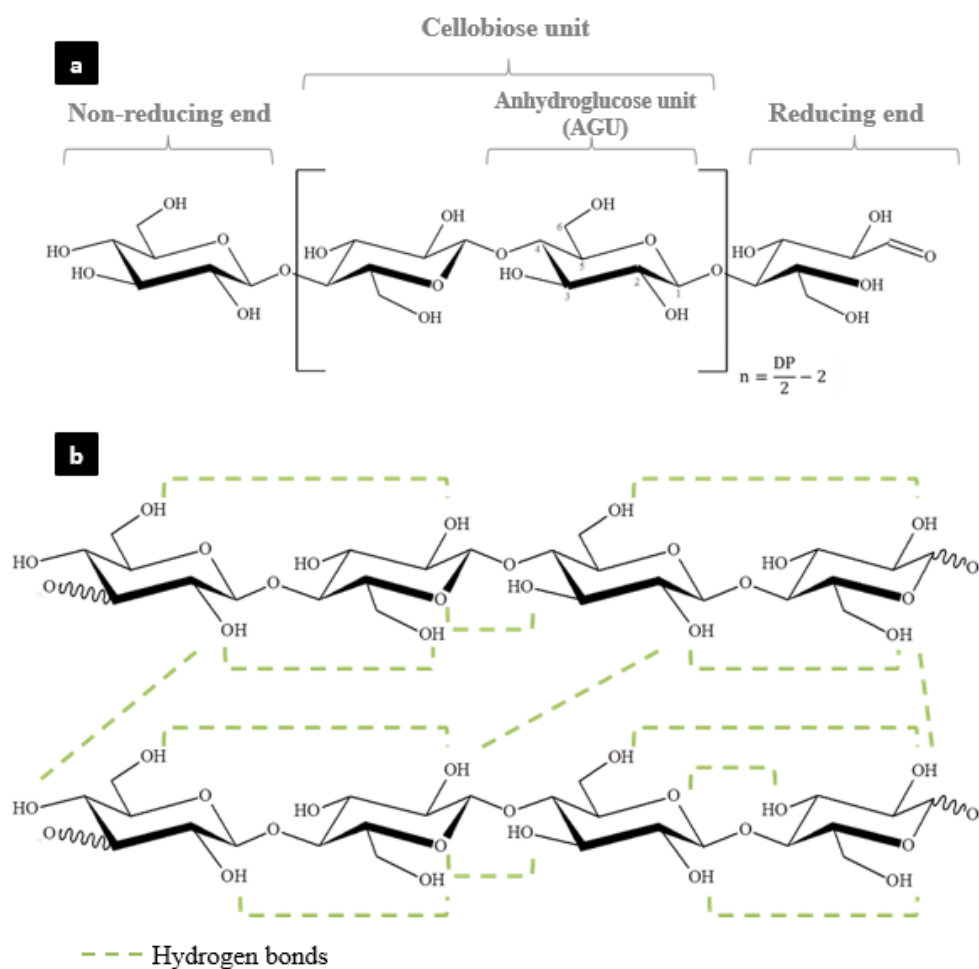


Figure I. 14. a) Chemical structure of cellulose chain and b) representation of some hydrogen bonds between two cellulose chains

Looking more precisely at the cellulose structure, it is a linear homopolymer of β -D-glucopyranose ($C_6H_{12}O_6$) units. These anhydro-D-glucose units (AGU) are linked by β (1-4)-glycosidic linkage, a covalent bonding between equatorial OH group in C4 and the C1 carbon atom of the next unit. Every unit is twisted at 180° in respect to its surrounding environment, and is in chair conformation, with the

three hydroxyl groups in equatorial position. Cellobiose ($C_{12}H_{22}O_{11}$) – the combination of two anhydroglucose units (AGU) – is the repeating unit of cellulose^{53,55}. The general formula of cellulose is represented in **Figure I. 14 a**).

End-groups of cellulose polymer are chemically different: one non-reducing end, and the other reducing bearing aldehyde group. Note that cellulose degree of polymerization (DP) is expressed as a function of the AGU unit number, and depends on the cellulose source and isolation process (DP between 300-1700 for wood pulp, 800-1000 for cotton for example)⁵⁵. The numerous hydroxyl groups – three per AGU – induce the possible functionalization of cellulose, as well as, intra- and intermolecular hydrogen bonds in and between the cellulose chains. These interactions form strong stabilized and flexible cellulose filaments: the cellulose microfibrils (**Figure I. 15 a**).

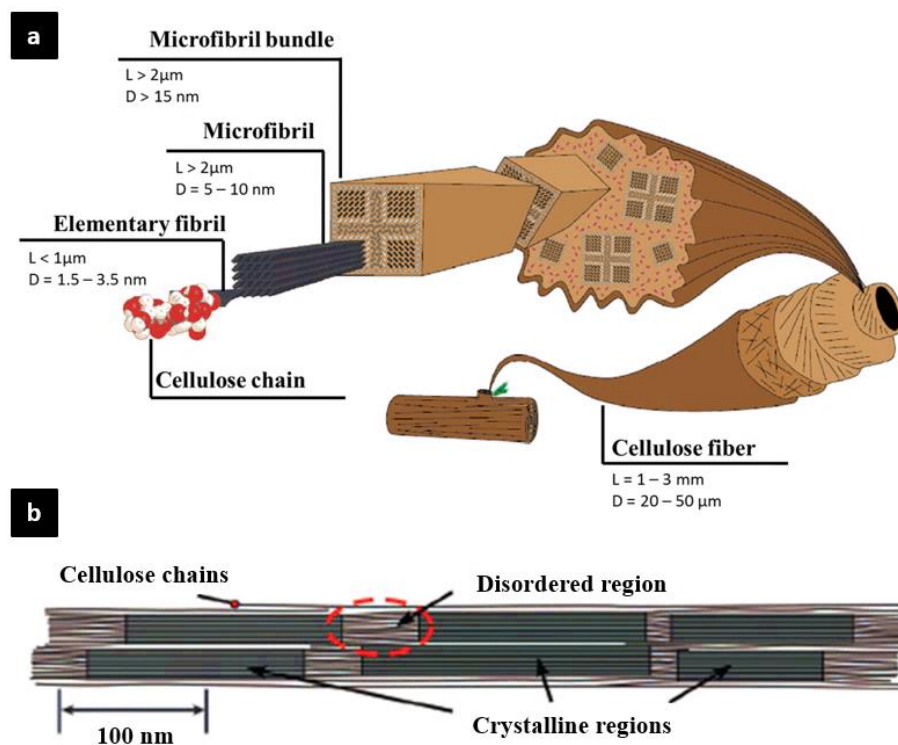


Figure I. 15. Schematization of a simplified **a**) composition of a cellulose fiber (extracted and adapted from ⁵⁹) and **b**) arrangements of crystalline and amorphous domains in cellulose chains (extracted from ⁶⁰)

Moreover, the cellulosic chains are rearranged into different regions: the ordered crystalline, and the disordered amorphous ones. Indeed, a cellulose chain can be represented as a crystalline wire connected by amorphous areas (**Figure I. 15 b**)). It explains the aggregation of cellulose chains, and thus, their arrangement into microfibrils. These last are assembled in bundles, themselves assembled in cellulose fibers, with a semi-crystalline structure. Cellulose crystals present four polymorphs: Cellulose I, II, III and IV. Cellulose I is the most abundant form in nature, and is present under cellulose I α and I β forms, whose ratio depends on the source. This ratio affects cellulose fibers properties^{55,56}. Crystallinity of the cellulose varies according to the source, and is in the large range of 40-80%⁵⁵, leading to highly cohesive fibers. Looking more precisely at the level of the microfibrils,

they are composed of elementary fibrils, with a diameter around 5 nm. This general structure provides visualization of the different scales inside the cellulose fiber. In addition to being environmentally relevant, cellulose fibers present interesting mechanical properties, an ability for further surface chemical modification, low toxicity, low cost, and others properties making them outstanding materials for lot of traditional, as well as, for innovative applications.

2.1.2. Nanomaterials from cellulose: cellulose nanofibrils and nanocrystals

The hierarchical structure of cellulose fibers is at the origin of cellulosic nanomaterials: the nanocelluloses, having at least one dimension of nanometric scale, as their name suggests. Indeed, from elementary fibrils, two types of nanocellulose can be obtained, differing by their isolation procedure, as well as, by their properties and applications. **Figure I. 16** shows their different morphologies.

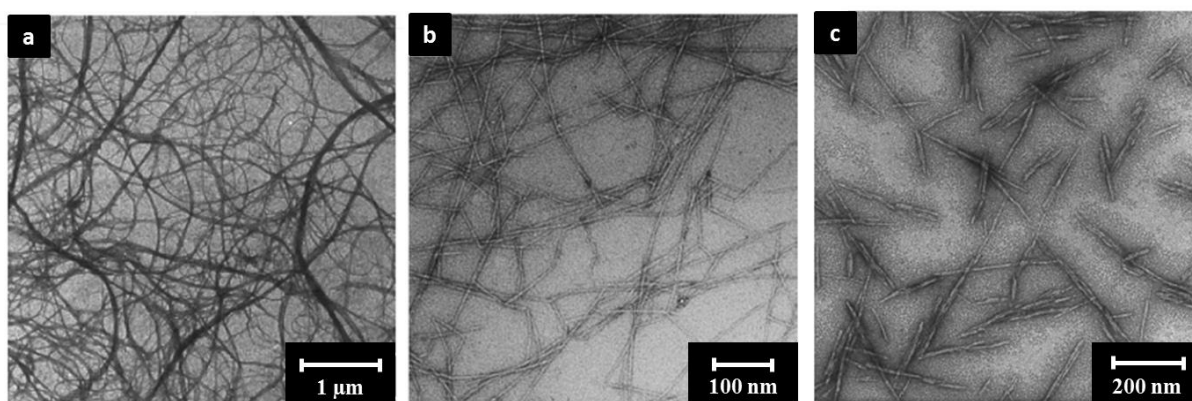


Figure I. 16. TEM images of **a)** Microfibrillated cellulose (MFC), **b)** TEMPO-oxidized nanofibrillated cellulose (CNF) and **c)** wood cellulose nanocrystals (CNCs) (extracted from ⁶⁰)

In the 1980s, two research groups, headed by Herrick⁶¹ and Turbak⁶², developed for the first time what they called microfibrillated cellulose (MFC), after applying repeated high-pressure homogenization to cellulose fibers. Resulting 2% suspension showed the presence of both fibrils and microfibrils, and presented a gel-like behavior. Rheological, morphological, and chemical reactivity properties of MFC (also called cellulose nanofibrils (CNFs) since new standards ISO/TC 6, ISO/TC 229 and TAPPI (2013) for nanocelluloses terminologies standardization) were extremely promising at the beginning and at the root of many further researches until today. Indeed, CNFs are interesting nanomaterials widely characterized and used in a large panel of applications. In accordance with the first results obtained by Herrick and Turbak, CNFs are obtained by applying a high shear mechanical treatment to a cellulose suspension. Most common mechanical processes are homogenization⁶³⁻⁶⁵, ultrafine grinding⁶⁶⁻⁶⁸, and microfluidizing⁶⁹, as broadly found in literature, and new innovative processes are presented since few years like extrusion^{70,71}, ultrasonication or steam explosion, for example. Due to the numerous strong hydrogen bonds between cellulose chains, obtaining nanofibrillated cellulose by these mechanical treatments required a lot of energy. In this context, during the last years, research

focused on the decrease of energy used, especially by chemical or biological pre-treatment of cellulose fibers facilitating the defibrillation. Main steps of CNFs extraction are represented in **Figure I. 17**.

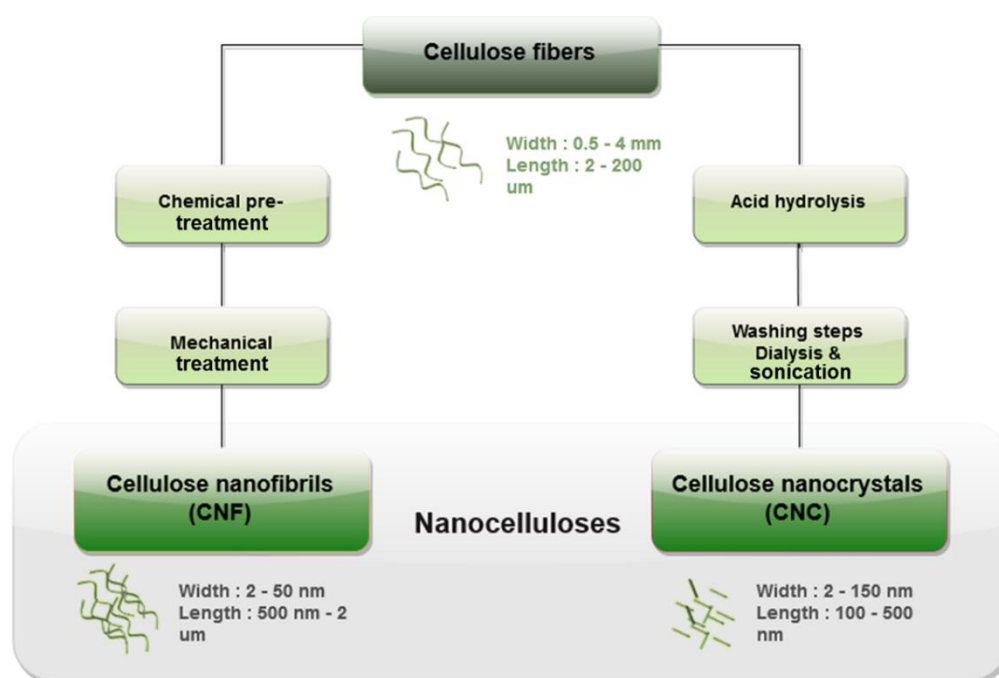


Figure I. 17. General schematized procedures for the production of both cellulose nanofibrils (CNFs) and cellulose nanocrystals (CNCs)

Numerous chemical pre-treatments have been reported in the literature, with among others some enzymatic pre-treatment⁷²⁻⁷⁵, cationization^{76,77} and oxidation using TEMPO⁷⁸⁻⁸⁰ or periodate^{81,82}. A recent review by Rol *et al.*⁸³ describes the recent advances in cellulose nanofibrils pre-treatments. As their name suggests, CNFs have at least one dimension of nanometric scale (i.e. <100nm). Their dimension vary, depending on the cellulose source and the extraction process, but their length is comprised between 500 nm and 10 μm , and their width between 5 and 50 nm⁶⁰ (see Figure I. 16). Note that chemical pre-treatments influence the morphology of CNFs by reducing their dimensions. Thus, CNFs composed of both crystalline and amorphous parts present a high aspect ratio which confers them, additionally to the hydrogen bonds between nanofibers, highly cohesive network properties. At low solid content, CNF water suspensions exhibit a gel-like properties⁷⁵. CNFs can also be assembled in flexible self-standing dried films (also called nanopapers), with interesting transparency in visible domain (80-90%) due to the nanometric size of CNFs and their dense arrangement⁵⁴. Their mechanical and thermal properties are also pretty high comparing to classical biopolymer. CNFs find application as rheological modifier, nanocomposites reinforcement, additives in paper, and cardboard industry, coating, barrier layer in packaging or biomedical applications⁸⁴⁻⁸⁶. Despite the high production energy costs, and the “nano risk” precautions industrialization of CNFs started in the 2010’s. Today, more than thirty CNFs producers can be listed all around the world, with production capacities up to 10000 tons per year, as shown in **Table I. 7**. To overcome their industrialization issues, the development and

optimization of pre-treatments, as well as, the search for advanced applications, aim to develop the CNFs industrial production.

Company	Country	Annual production capacity (tons)
FiberLean® Technologies	UK	12000
Borregaard	Norway	1000
Tuners Falls Paper	USA	700
Fibria	Brazil	700
Nippon Paper Group	Japan	500 (TEMPO)
Norske Skog	Norway	350 (Pilot)
University of Maine – Process Development Center	USA	350
Daio Paper Corp.	Japan	100 (Pilot)
American Process Inc.	USA	100
CelluComp	UK	50
DKS Co., Ltd	Japan	50
RISE Bioeconomy	Sweden	35 (Pilot)
Sappi	Netherlands	8 (Pilot)
Kruger Biomaterials Inc.	Canada	6
InTechFibres (CTP/FCBA)	France	4
University of Queensland	Australia	2 (Pilot)
University of Alberta / InnoTech Alberta	Canada	2 (Pilot)
Betulum Oy	Finland	Pilot
Forest Products Laboratory (FPL)	USA	Pilot
Stora Enso Ltd.	Sweden	Recent investment for ~6000t

Table I. 7. Non-exhaustive list of main CNFs producers and their country, as well as, their annual production capacity (data extracted from ⁸⁷)

Another class of nanocelluloses is cellulose nanocrystals (CNCs). Their first investigation was reported by Ranby *et al.* in 1950^{88,89} : after carrying out a sulfuric acid hydrolysis to wood cellulose fibers, they observed rod-like particles, with two nanoscale dimensions. Indeed, by hydrolyzing cellulose fibers, most of the amorphous parts of cellulose are disintegrated, and final nanomaterials are highly crystalline. Cellulose nanocrystals have a length between 100 and 500 nm, and a width varying from 2 to 15 nm, depending on the cellulose source and the chemical treatment applied. Indeed, even if the use of sulfuric acid for hydrolysis is the most common process, other research groups have investigated the use of other acids, leading to CNCs with different properties. In any case, washing steps are essential to remove chemicals and to well-disperse the isolated CNCs, as presented in **Figure I. 17.**

Regarding their industrialization, around thirteen CNCs producers can be recorded, with annual production capacity up to 400 tons per year. These productions are significantly lower than those of CNFs, but requirement of more chemicals and difficult industrial production steps (washing, dialysis, and sonication) can easily explain this difference. **Table I. 8** shows the non-exhaustive list of CNCs

producers, and their annual production capacity. Note that the leader and pioneer CelluForce® has recently announced a new strategy for efficient industrialization⁹⁰.

Company	Country	Annual production capacity (tons)
CelluForce Inc.	Canada	400
America Process Forest Industries Inc.	USA	200
Alberta Pacific Forest Industries Inc.	Canada	180 (expected in 2021)
Anomera Inc.	Canada	11
Forest Products Laboratory (FPL)	USA	5
University of Maine	USA	4
Blue Goose Biorefineries Inc.	Canada	4
Cellulose Lab	Canada	4
Advanced Cellulosic Material Inc.	Canada	1
FPIinnovations	Canada	0.5
InnoTech Alberta	Canada	0.3
Embrapa/National Nanotechnology Laboratory for Agriculture	Brazil	Pilot
Melodea	Israel	Pilot

Table I. 8. Main CNCs producers, their location, and their annual production capacity (data extracted from ^{87,91})

Although CNFs and CNCs are the two main types of nanocelluloses — and generally the only ones mentioned, another sort of nanocellulose exists — called bacterial cellulose. As its name suggests, bacterial cellulose is synthesized by some bacterial species forming characteristic nanofibrils, with ribbon shape with cross sections of 4-10 nm by 30-50 nm^{60,92}. As it is produced by bacteria, this type of cellulose is very pure and does not contain lignin or hemicelluloses, as it is the case for other cellulose sources. It makes bacterial cellulose highly interesting for high value-added applications, especially in biomedical field^{93,94}. This PhD is not focusing on bacterial nanocellulose, but some reviews provide more details on this nanomaterial^{51,95}.

As cellulose nanocrystals (CNCs) are the main materials investigated in this PhD, following sections are focused only on them. Their isolation, properties, and applications are more precisely detailed.

2.2. Cellulose nanocrystals: nanomaterials with interesting properties

2.2.1. Isolation of cellulose nanocrystals

Cellulose nanocrystals (CNCs) are obtained by applying a chemical treatment to biomass, *via* a strong acid hydrolysis. Typically employing strong sulfuric acid H₂SO₄ is going to penetrate into accessible amorphous domains of cellulosic chains, and dissolve them, to release crystalline parts. The amorphous domains are randomly oriented and arranged, inducing a lower density of these domains, which are thus more vulnerable to acid hydrolysis⁹⁶, and especially to the infiltration of hydronium

ions H_3O^+ , leading to hydrolytic cleavage of glycosidic bonds. In this sense, Ranby *et al.*^{88,89} were the first to prove the preparation and the presence of CNCs, the smallest cellulosic building blocks. **Figure I. 18** synthesises the different steps of CNCs isolation using sulfuric acid hydrolysis.

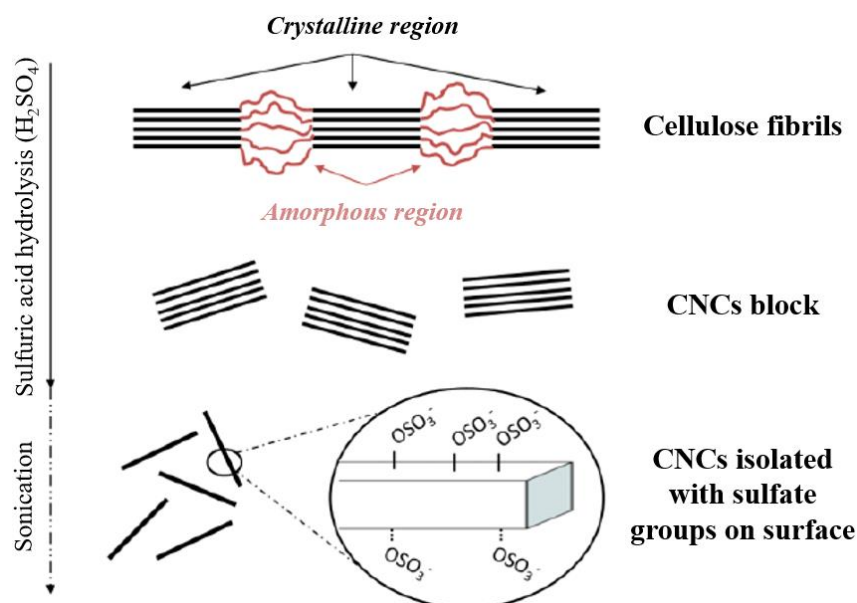


Figure I. 18. Schematic representation of sulfuric acid hydrolysis of cellulose fibers (extracted from E. Gicquel PhD, 2017)

As previously mentioned, the cellulose fibrils are exposed to a sulfuric acid hydrolysis, with a defined concentration, temperature, and reaction time. Once amorphous domains are dissolved, a sonication step allows the separation between intact crystalline domains, leading to isolated CNCs bearing half-sulfate ester groups on their surface. These charges come from the reaction between sulfuric acid and surface hydroxyl groups of cellulose, and induce repulsive forces between negatively charged CNCs, leading to colloidal stability and dispersion in water⁹⁷. While sulfuric acid is the most common acid used for the cellulose fibers hydrolysis, other researches have focused on the use of other organic or mineral acids, like phosphoric acid, hydrobromic acid, or hydrochloric acid^{98–101}, generally leading to less stable suspension, due to the lack of charges at the surface of the CNCs. Moreover, the use of deep eutectic solvents (DES) — a new class of green organic solvents — has been investigated too, and yielded cellulosic nanoparticles using less toxic and easier process^{102,103}.

When the cellulosic source is not totally pure, previous steps are required. Indeed, alkali treatment (generally NaOH) and bleaching steps (generally acetic acid, aqueous chlorite) are essential to remove impurities, especially lignin and hemicelluloses. Note that numerous studies have investigated the production of CNCs from less conventional sources like rice, soy, and others, in order to valorise food and organic waste^{104,105}.

Final yield and morphology of CNCs are highly dependent on the cellulosic botanic source and on the hydrolysis conditions. Indeed, optimization and control of the acid hydrolysis has been the subject of several publications. If common parameters are the hydrolysis with 64 wt% sulfuric acid at 40–45 °C during about 30 min, it has been proved that the variation of one of parameters can largely influence

the reaction yield, as well as, the final CNCs properties. For example, by increasing the time of hydrolysis by 10 min, it has been shown by Flauzino Neto *et al.*¹⁰⁴ that crystalline parts are destructed, inducing a significant decrease in CNCs length. Beck *et al.*¹⁰⁶ confirmed this point, admitting that too long times of reaction induce degradation of cellulose. In contrary, too short times induce only large and non-dispersible fibers and large aggregates. Only specific reaction times yield to a well-dispersed colloidal suspension of CNCs. Chen *et al.*⁹⁹ confirmed that the best yield and CNCs properties are obtained with previously mentioned standard conditions. Moreover, the importance of acid concentration relative to cellulose fibers is highlighted too, since a too high concentration could be too drastic, and a too low concentration insufficient for the hydrolysis efficiency.

At the end of the reaction, mixture media is first diluted with distilled water to quench the reaction, then submitted to several separation steps with centrifugation cycles and filtrations, and washed by dialysis against distilled water for several days, in order to remove unreacted compounds and chemicals. In some cases, NaOH is also used to neutralize pH, which can modify the crystallinity and the surface ions. After dialysis, a final centrifugation cycle or another filtration process aim to remove aggregates. CNC suspension is finally sonicated in order to well disperse the nanocrystals, and obtain a colloidal suspension thanks to dimensions and sulfate half ester groups bearing by CNCs.

In this PhD, a commercial batch of CNCs is used, and was obtained via sulfuric acid hydrolysis from wood. It was supplied by CelluForce (Canada). More details will be provided in corresponding results chapters.

2.2.2. Properties of cellulose nanocrystals

In addition to their nanometric size, CNCs are unique biodegradable and renewable nanomaterials. Moreover, they result from a previously described optimized acid hydrolysis applied on various sources of cellulose, and exhibit many other interesting properties. **Figure I. 19** summarizes the main CNCs properties, as well as, their potential applications. Regarding the surface properties of CNCs, they generally exhibit — in addition to –OH functions borne by cellulose macromolecules — half-sulfate ester groups ($-\text{SO}_3^-$) on their surface after being treated with sulfuric acid. Even if the amount of $-\text{SO}_3^-$ groups is pretty low (about 50-200 $\mu\text{mol.g}^{-1}$), these negative charges are sufficient to induce repulsive forces between nanomaterials, and thus ensure colloidal stability in aqueous media. Moreover, as presented in **Figure I. 19**, due to the isolation process, other charged groups can be present on CNC surface, like carboxyl groups ($-\text{COO}^-$), aldehyde groups ($-\text{CHO}$) and others¹⁰⁷, leading to different charge amount inducing different CNC properties. Moreover, numerous hydroxyl groups (3 groups in each AGU) are reactive surface sites for the introduction of new functional groups *via* hydroxyl groups' functionalization. Regarding the physical properties of CNCs, they have a low density (1.606 g.cm^{-3}) compared to other organic materials, a high aspect ratio length/width (varying between 10-30 for CNCs extracted from cotton and around 70 for those extracted from tunicate for

example⁹⁷), and a high surface area (between 150 and 800 m².g⁻¹). Note that all their morphological and surface properties are highly dependent on their source, as well as, on their isolation process and conditions^{60,108}. Moreover, CNCs exhibit highly interesting mechanical properties. In addition to their high crystallinity (between 54-88% according to the source¹⁰⁹), their high elastic modulus ($\approx 150 \pm 50$ GPa), and tensile strength ($\approx 7.5 \pm 0.5$ GPa)¹¹⁰ make them interesting materials as mechanical reinforcement in polymer matrices, for example. For comparison, their mechanical properties are similar to Kevlar[®] fibers¹¹¹ widely used in high-performance composites materials.

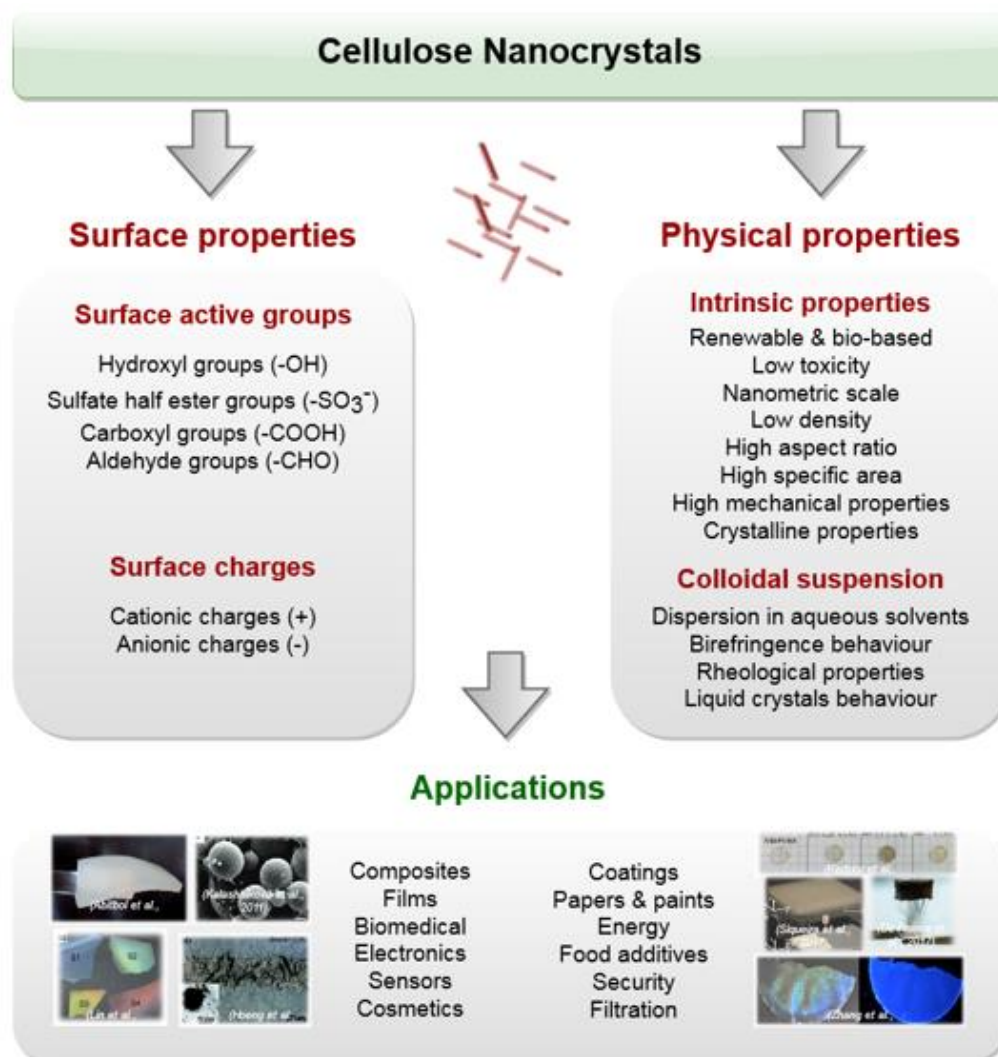


Figure I. 19. Main surface and physical properties of cellulose nanocrystals (CNCs) and inherent main applications

At low solid content (<3 wt%), due to hydrogen bonds between cellulose chains and thus between each nanocrystals, CNC water suspension is in the form of a translucent gel. Rheological properties of CNCs are outstanding and concentration dependent. Thus, at low concentration (<3 wt%), CNC suspension presents shear thinning behavior at high shear rate, and at higher concentration (>3 wt%), the suspension presents shear thinning behavior explained by the nanocrystals alignment in the flow direction at a critical shear rate¹¹². Source and isolation of CNCs influence these rheological properties

too. Besides all these properties, CNCs self-organize themselves in ordered structure, especially to form a nematic phase. Revol *et al.*¹¹³ described in the 1990s this self-organization of CNCs in water suspension into stable chiral nematic phases. The materials exhibit liquid crystalline properties, which added to intrinsic birefringence of CNCs, induce interesting optical properties. Moreover, when ordered CNC suspension is solvent evaporated, they yielded a self-standing film, conserving a chiral nematic structure (helicoidal structures), and an iridescent behavior of films is observed and monitored by CNC concentration and surface charge, as well as, the quality of suspension dispersion^{112,113}. **Figure I. 20** shows explicit pictures of these rheological and liquid crystalline properties.

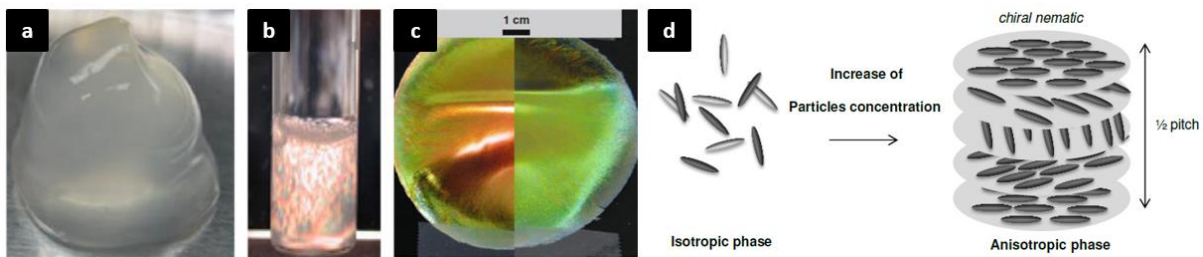


Figure I. 20. **a)** Translucent gel-like CNC suspension at 15 wt% in water (extracted from¹¹⁴), **b)** Birefringence with shear-inducing observed for an aqueous CNC suspension at 0.6 wt% in cross-polarized light (extracted from¹¹⁵), **c)** Solvent-casted CNC film in diffuse light, normal to the surface (on the left part) and oblique to the surface (on the right part) (extracted from¹¹⁶), and **d)** Schematic representation of CNCs orientation in isotropic and anisotropic phases (extracted from R. Bardet PhD, 2014)

All these outstanding surface and physical properties of CNCs confirm their high and increasing interest in research and industrial field during the last decades. Although their isolation and characterization are currently well-advanced and optimized, applications field are at the center of ongoing researches, as described in the following section.

2.2.3. Various applications of cellulose nanocrystals and their industrialization

As exposed in **Figure I. 19**, CNCs found applications in various fields thanks to their outstanding morphological, mechanical, and rheological properties, as well as, their colloidal stability and high surface reactivity. All these properties, added to their biodegradability and renewability, make them highly interesting and innovative materials with many potential applications. **Table I. 9** summarizes CNCs applications and the corresponding exploited properties, as well as, some literature references.

Nanocomposites field is an emerging research area which finds applications in several domains like food packaging, medical devices, and building. The renewable aspect of CNCs is particularly interesting, since it correlates with the development of bio-based and biodegradable polymers, as mentioned in the first part of this chapter. Moreover, these materials possess interesting properties, and could be potential candidates in new fields of applications, such as coatings, electronics, filtration, biomedical, energy, cosmetics, and security.

Market	Applications	Exploited CNC properties	References
Composites / Films	Nanocomposites	High mechanical properties	(Mariano <i>et al.</i> , 2014) ¹¹⁷
	Flexible packaging	Filmogenic properties	(Hube <i>et al.</i> , 2017) ⁸⁴
	Optical films	Morphology	
Coatings / Paints / Adhesives	Coatings for flexible packaging	Morphology	(Kaboarani <i>et al.</i> , 2012) ¹¹⁸
		Rheological properties	(Mascheroni <i>et al.</i> , 2016) ¹¹⁹
Electronics / Sensors	Flexible electronics	Electrical insulating	(Hoeng <i>et al.</i> , 2016) ¹²⁰
	E-paper	Piezoelectric properties	(Csoka <i>et al.</i> , 2012) ¹²¹
	Piezoelectric sensors	Surface area	(Gaspar <i>et al.</i> , 2014) ¹²²
Filtration	Mesoporous films and membranes	High specific surface area	
		High mechanical properties Hydrophilicity	(Karim <i>et al.</i> , 2014) ¹²³
Biomedical	Biocomposites for bone/tooth replacement	Low toxicity	
	Drug delivery	Colloidal stability	(Domingues <i>et al.</i> , 2014) ¹²⁴
	Protein immobilisation	High mechanical properties	(Lin <i>et al.</i> , 2014) ¹²⁵
	Wound dressings	Surface reactivity	
	Biosensors		
Energy	Supercapacitors	Strength	
	Flexible batteries	Large surface area	(Yang <i>et al.</i> , 2015) ¹²⁶
Cosmetics	Hydrogels & foams	Colloidal stability	(Kalashnikova <i>et al.</i> , 2013) ¹²⁷
		Emulsion interfacial stabilization	(Tasset <i>et al.</i> , 2014) ¹²⁸
Security	Security papers and inks	Iridescent properties	
		Morphology	(Zhang <i>et al.</i> , 2012) ¹²⁹

Table I. 9. Main market applications of CNCs with related properties, and some literature references

Note that for applications that may enter in contact with food or human body, and for any industrialization, toxicity of CNCs is a key challenge to investigate. Indeed, even if cellulose is known to be a non-toxic polymer, CNCs are nanomaterials — whose the “nano” prefix can be frightened for media and population — with specific morphology and surface properties. A recent review of Roman *et al.*¹³⁰ explored the CNCs toxicity. The results of this study correlate with previous results of Lin *et al.*¹²⁵ and Kovacs *et al.*¹³¹, who demonstrated that CNCs are not toxic by ingestion, or if a dermal contact is established. They were also considered as non-toxic for aquatic organisms. However, pulmonary diseases and cytotoxicity depend on CNCs properties and shapes (especially if they are in powder form, since they are more easily air-suspended). In any case, toxicity of CNCs is low, especially when they are in wet-state or in composites, films or coatings for example, not constraining the development of new CNC-based products.

The wide range of CNCs applications is subjected to numerous research projects and publications and is achieved, in most cases, thanks to the surface functionalization of CNCs. The following part aims to describe the potential surface modifications applied to CNCs.

2.3. Functionalization of cellulose nanocrystals

Through numerous hydroxyl groups on their surface and their high specific surface area, CNCs have been surface-modified through different techniques, in order to improve their properties and further potential applications. Recent reviews summarize the different ways of CNC surface functionalization, including those of Natterodt *et al.*¹³², Tang *et al.*¹⁰⁷, Wohlhauser *et al.*¹³³, Kedzior *et al.*¹³⁴ and less recently those of Eyley *et al.*¹³⁵ and Habibi *et al.*⁵⁷. Through their high reactivity, CNCs thus can be modified *via* different reactions. **Figure I. 21** shows the different possible ways for CNCs chemical modifications: by grafting or adsorbing single molecules or polymer chains at their surface. For each modification method, some examples are given, although the list is absolutely not exhaustive.

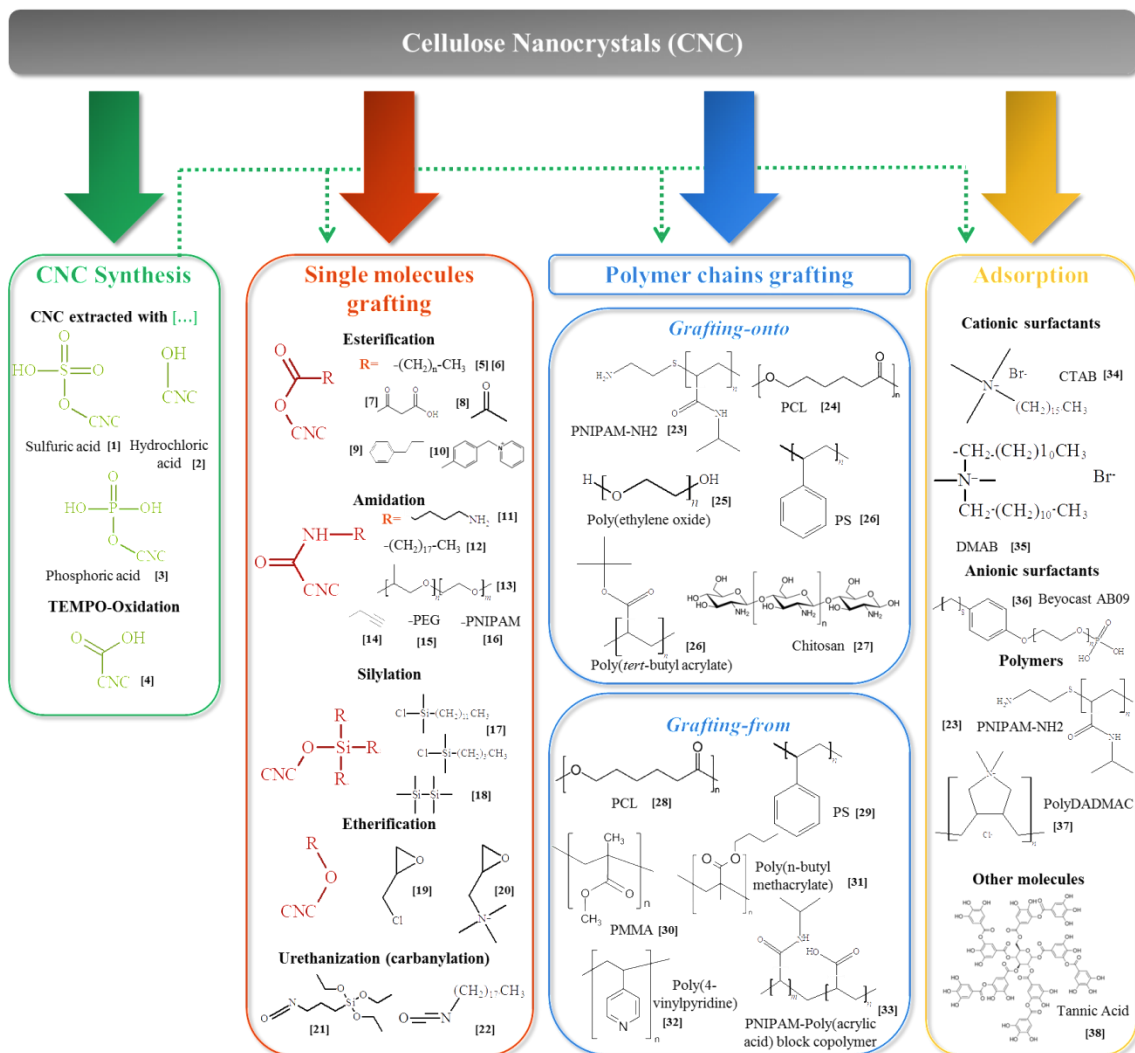


Figure I. 21. Different paths of chemically modifying cellulose nanocrystals with some examples for each method.

Synthesis: extraction with [1] sulfuric acid¹⁰⁶, [2] hydrochloric acid¹⁰¹ and [3] phosphoric acid⁹⁸, [4] TEMPO oxidized CNC¹³⁶ – **Single molecules grafting using:** [5] [6] long-chain aliphatic acid chlorides^{137,138}, [7] malonic acid¹³⁹, [8] acetic anhydride¹⁴⁰, [9] benzylacetic acid¹⁴¹, [10] 4-(bromomethyl)benzoic acid¹⁴², [11] 1,4-diaminobutane¹⁴³, [12] octadecyl amine¹³⁸, [13] Jeffamine¹⁴⁴, [14] propargylamine¹⁴⁵, [15] aminated-polyethylene oxide (PEO-NH₂)¹⁴⁶, [16] aminated-poly(*N*-isopropylacrylamide) (PNIPAM-NH₂)¹⁴⁷, [17] *n*-dodecyl and *n*-butyl dimethylchlorosilane¹⁴⁸, [18] hexamethyldisilane¹⁴⁹, [19] epichlorohydrin¹⁵⁰, [20] glycidyltrimethylammonium chloride (EPTMAC)¹⁵¹, [21] isocyanatepropyltriethoxysilane¹⁵² and [22] *n*-octadecyl isocyanate¹⁵³ – **Polymer chains : grafting-to :** [23] PNIPAM-NH₂¹⁴⁷, [24] polycaprolactone (PCL)¹⁵⁴, [25] poly(ethylene oxide) (PEO)¹⁵⁵, [26] polystyrene (PS) and poly(*tert*-butyl acetate)¹⁵⁶ and [27] chitosan¹⁵⁷ – **grafting-from :** [28] PCL¹⁵⁸, [29] ^{159,160} PS, [30] poly(methyl methacrylate) (PMMA)¹⁶¹, [31] poly(*n*-butyl methacrylate)¹⁶², [32] poly(4-

vinylpyridine)¹⁶³ and [33] block copolymer of PNIPAM and poly(acrylic acid)¹⁶⁴ – **Adsorption** : [34] cetyltrimethylammonium bromide (CTAB)¹⁶⁵, [35] didecyldimethylammonium bromide (DMAB)¹⁶⁶, [36] acid phosphate ester of ethoxylated nonylphenol (Beycostat A B09)¹⁶⁷, [23] PNIPAM-NH₂¹⁴⁷, [37] poly(diallyldimethylammonium chloride) (polyDADMAC)¹⁶⁸ and [38] tannic acid¹⁶⁹.

In this section, the different types of surface modification exploited in this PhD are described: TEMPO-oxidation, surface polymerization, covalent (especially esterification and amidation) and non-covalent bonding. These chemical surface modifications are carried out in order to compatibilize the CNCs with a polymer matrix, in the case of nanocomposites applications, as detailed in the next part (3) of this chapter.

2.3.1. TEMPO oxidation of cellulose nanocrystals

Among CNCs chemical modifications, oxidation – and especially TEMPO-mediated oxidation – of CNCs is one of the most common and optimized one. In fact, besides being well-known as pre-treatment of cellulose to facilitate the defibrillation in CNFs production¹⁷⁰, TEMPO radical oxidation allows the introduction of carboxylate groups –COO⁻ at the surface of CNC. These charges are highly reactive for further grafting or adsorption of molecules or polymers, and increase the stability of TEMPO-oxidized CNCs in water, leading to well dispersed nanosize particles, thus providing translucent suspension in water. This reaction was carried out on HCl hydrolyzed CNCs for the first time by Araki *et al.* in 2001¹⁴⁶, and was subsequently optimized by different research groups, including Habibi *et al.*¹³⁶, Montanari *et al.*¹⁷¹, and Fraschini *et al.*¹⁷², working with different types of CNC. **Figure I. 22** represents the oxidation mechanism generally presented in the literature with the system TEMPO/NaBr/NaClO, where RCH₂OH represents the CNC. Common chemicals used in TEMPO-assisted oxidation of cellulose are TEMPO radical (2,2,6,6-tetramethylpiperidin-1-yl)oxyl as oxidizing agent, sodium bromide (NaBr) and sodium hypochlorite (NaClO). The reaction is generally carried out in water, in basic conditions (pH=10), and follows different steps: a hypobromite ion BrO⁻ is formed *in situ* from the reaction between a hypochlorite ion ClO⁻ and NaBr. The BrO⁻ ion reacts with TEMPO radical ((1) in **Figure I. 22**) to form the nitrosonium salt (2), which is an active oxidizing agent in the reaction. Then, this nitrosonium salt is going to react with CNCs, and oxidize primary alcohol groups into sodium carboxylate. The oxidation occurs in two steps: first, the alcohol groups are oxidized into aldehyde groups. TEMPO radical being continuously regenerated (by reaction between (3) and (2)), a second oxidation can take place on aldehyde groups, leading to acid carboxyl groups. Thus, 2 mol of NaClO are required to oxidize one mole of primary alcohol, and the introduced initial amount of NaClO is determinative for the oxidation yield¹⁷².

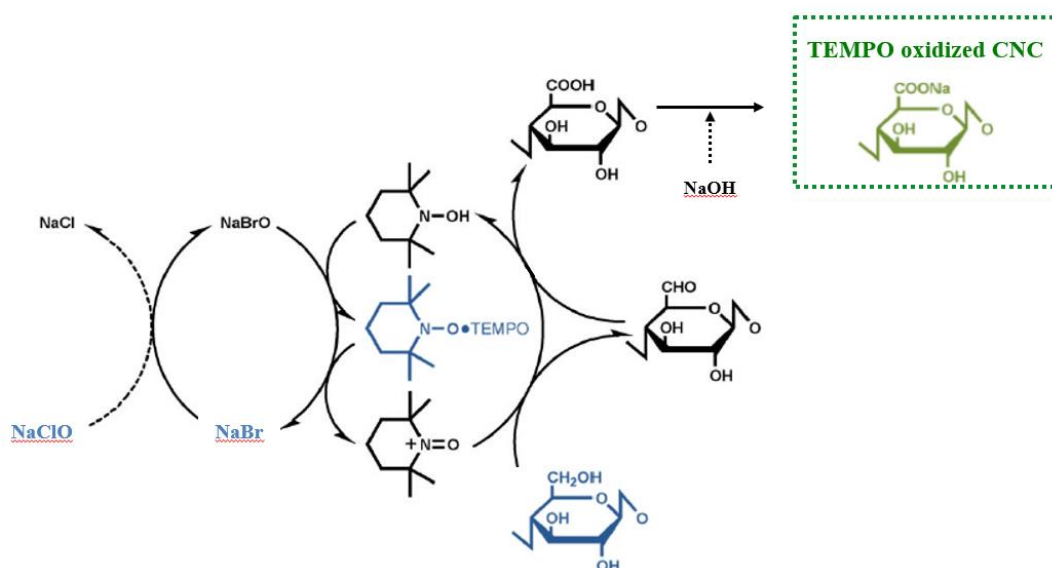


Figure I. 22. General reaction mechanism of TEMPO-mediated oxidation of CNC : regioselective oxidation of primary hydroxyl groups of cellulose using TEMPO/NaClO/NaBr system (in blue) and TEMPO oxidized CNC bearing carboxylate groups (in green) (extracted and adapted from ¹⁷³)

It has been proved that reaction occurs only on CNCs surface¹⁷¹, and on accessible primary alcohol carried by C₆ carbons. Some studies have shown that this selectivity is kept when the oxidation occurs in neutral conditions with NaClO₂¹⁷⁴. TEMPO-oxidized CNCs conserve their dimensions and crystallinity, and exhibit surface charge that may reach around 1600 $\mu\text{mol.g}^{-1}$ ¹³⁶. If TEMPO-mediated oxidation is the most optimized and used method to introduce carboxylate charges on the CNCs surface, other techniques, like the sodium periodate oxidation, have been published in the literature¹⁷⁵, leading to aldehyde groups on the surface.

In any case, introduction of carboxylate charges at the surface of CNCs is interesting in terms of suspension stability and in surface reactivity, expanding the grafting possibilities from this carboxylate groups, or the adsorption strategies.

2.3.2. Covalent grafting on cellulose nanocrystals

Thanks to the numerous hydroxyl groups present at the surface of CNC and to their high specific surface area, the availability of these reactive sites is a key point in the functionalization of CNCs. Indeed, the chemical modifications allow the introduction of various functional groups, aiming to confer them new functionalities, like active properties (antimicrobial, antioxidant etc.) or, in most cases, to enhance their compatibility with different hydrophobic polymeric matrices. These modifications are covalent, meaning that hydroxyl groups of CNCs are chemically bonded to another molecule with which they share electron pairs. In the literature, different covalent grafting processes are presented, with among others oxidation, esterification, amidation, etherification, silylation, and nucleophilic substitutions, as previously presented in **Figure I. 21**.

In an **amidation** reaction, reactive carboxyl groups $-\text{COOH}$ introduced on TEMPO-oxidized CNCs, can be activated by reacting with a primary amine *via* a peptidic linkage, meaning a covalent amide bond between a primary amine-terminated compound and carboxylate groups borne by CNCs. Commonly, EDC (1-ethyl-3-(3-dimethylaminopropyl) carbodiimide and NHS (N-hydroxysuccinimide) catalysts are used in amidation strategy as activators of the carboxyl groups. **Figure I. 23** schematizes this activation occurring during the amidation reaction. In a first time, EDC gives an unstable O-acyl urea compound to the carboxylic function. In a second time, NHS is reacting with this compound by stabilizing it in a stable N-acyl urea compound. Finally, aminated molecule is going to react with the activated CNC surface.¹³⁵

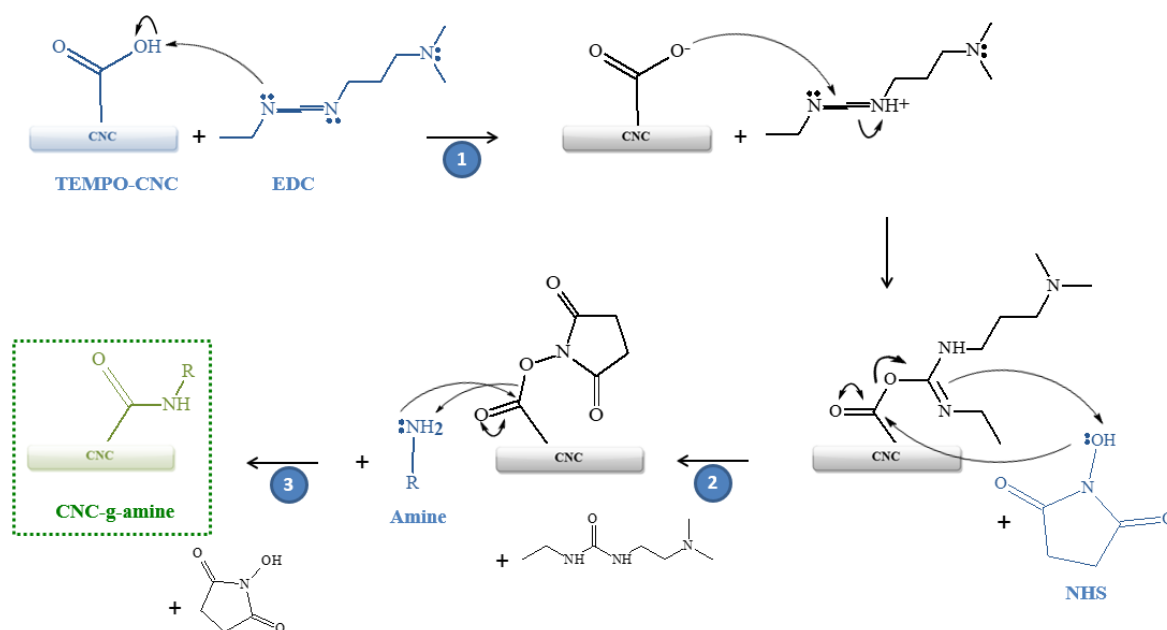


Figure I. 23. General mechanism of an amine-terminated molecule at the surface of TEMPO-oxidized CNCs in presence of EDC/NHS coupling agents ((1):activation of oxidized TEMPO-CNC with EDC, (2): stabilization with NHS, (3) reaction with aminated compound / reagents in blue – final grafted CNC (CNC-g-amine) in green)

Araki *et al.*¹⁴⁶ were the first who introduced this method, using EDC/NHS as catalyst system, to graft amine-terminated-poly(ethylene glycol) on TEMPO-oxidized CNCs, in order to sterically stabilized CNC water suspensions. Around 20-30% of the total amount of previously introduced carboxyl groups was converted into amide groups, which was sufficient for suspension stabilization and redispersion¹⁴⁶. Knowing that not all $-\text{COOH}$ groups (on C_6 carbons) are converted into amide groups during the amidation process and due to the previous low degree of oxidation of TEMPO-oxidized CNCs, the grafting density of an amidation is relatively low, generally lower than 0.2. The coupling reaction is pH dependent, and a pH between 7 and 10 has been reported to be efficient, in the case of CNC (R-NH₂ configuration)⁵⁷. In the literature, several studies used the EDC/NHS reagents to decorate the CNC surface with an amine. For example, Bendahou *et al.*¹³⁸ compared the efficiency of the amidation of aliphatic amine with that of the esterification of equivalent acid chloride molecules. Predictably, the esterification with highly reactive allyl chloride was highly efficient, although the amidation of

aliphatic amine was also proved, and selective at the level of C₆ carbons. Note that the pH, the time of reaction, and the introduction order of EDC/NHS compounds influence the yield of the reaction. Studies have been carried out to optimize this amidation reaction^{143,176}.

The amidation reaction is long, compared to classical reactions (several days for CNCs), and leads to low yields (around 10-30%). Nevertheless, the low amount of grafted aminated compounds is generally good enough to modify desired properties. For example, in a recent study, Guo *et al.*¹⁷⁶ investigated EDC/NHS monitored amidation reaction of functionalized aminated carbon quantum dots, in order to confer fluorescence properties to modified CNCs. The surface composition analysis was established using XPS, and allowed to conclude that about a 36% conversion of carboxyl groups into amide groups and fluorescence of final modified CNCs was performed, as shown in **Figure I. 24 a)** and **c)**. Moreover, although amidation reaction did not influence or damage CNCs morphology, grafted carbon quantum dots were visible by TEM imaging (**Figure I. 24 b)**).

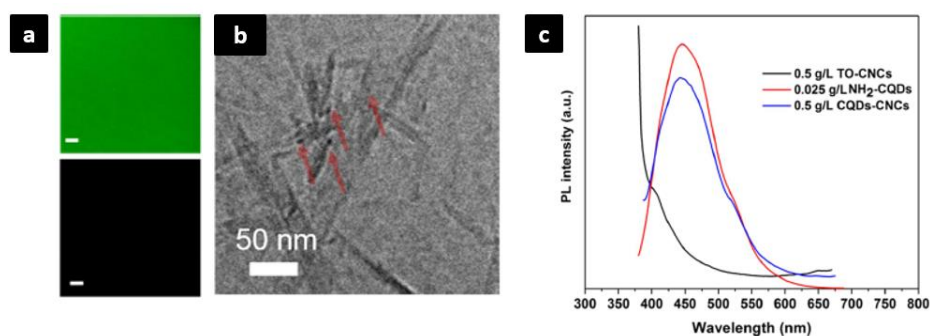


Figure I. 24. Evidence of fluorescent behavior of modified CNCs through EDC/NHS coupling amidation: **a)** Characterization of fluorescence by confocal microscopy : modified CNCs with carbon quantum dots on the top, unmodified TEMPO-CNCs at the bottom, **b)** TEM image of modified CNCs with carbon quantum dots (visible at the level of red arrows), and **c)** Fluorescence spectra of unmodified TEMPO-CNCs (TO-CNCs), aminated carbon quantum dots (NH₂-CQDs) and grafted TEMPO-CNCs with carbon quantum dots (CQDs-CNCs) (extracted from ¹⁷⁶)

Nevertheless, the advantages of an amidation catalysed by EDC/NHS compounds are its possible occurring in water, at room temperature, and without highly toxic chemicals, which is interesting in current ecological context, and in terms of green chemistry.

Esterification is another common CNCs grafting procedure. Different kind of esterification exist, with for example the sulfation and phosphorylation, occurring during the isolation of CNCs, according to the involved hydrolysis condition. Sulfate or phosphate half-ester groups are created on the surface of CNCs from secondary hydroxyl groups. Such *in situ* sulfation or phosphorylation allow colloidal stability of isolated CNCs. Several studies have taken advantage of the hydrolysis isolation process of CNCs by combining it with a Fischer esterification, in a one-step procedure, in order to obtain modified CNCs. Boujemaoui *et al.*¹⁷⁷ have produced functionalized CNCs by combining hydrochloric acid hydrolysis with Fischer esterification, using different functional carboxylic acids, as presented in **Figure I. 25 a)**.

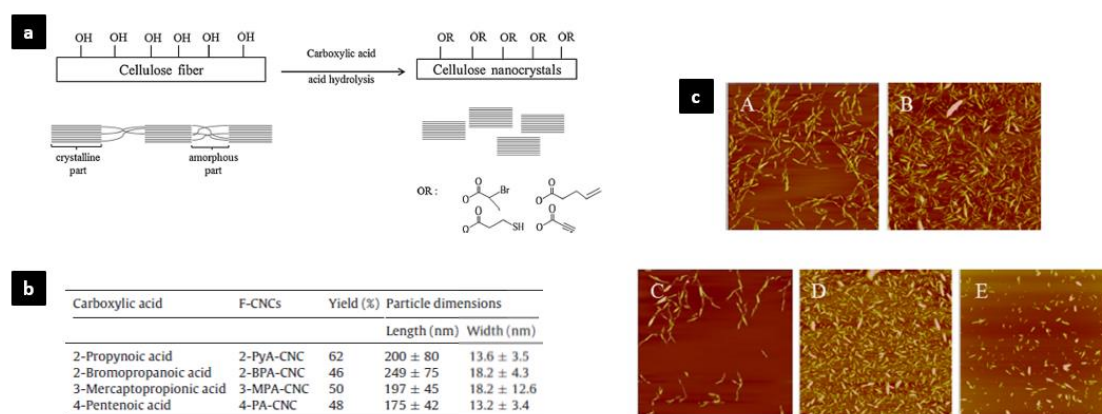


Figure I. 25. a) Principle of the one-step procedure combining acid hydrolysis and esterification of cellulose fibers using 2-bromopropionic acid / 3-mercaptopropionic acid / 4-pentenoic acid / 2-propynoic acid, **b)** Nomenclature of recovered CNCs with different acids, yield and dimensions, and **c)** obtained by AFM analyses, (A):HCl-CNC (unmodified), (B): 2-PyA-CNC, (C): 2-BPA-CNC, (D): 3-MPA-CNC and (E): 4-PA-CNC (extracted from ¹⁷⁷)

The modified CNCs were recovered with yield comprised between 48 and 62%, which was consistent with the values found in the literature for CNC produced from cotton sources¹⁷⁸. Functionalized CNCs with double and triple bonds, as well as with thiols and brominated groups, were also characterized. No significant differences in term of CNCs morphology were visible, with lengths between 170-200 nm and width between 13-18 nm, in agreement with the literature. In a same way, Spinella *et al.*¹³⁹ modified CNC in a similar one-step procedure with natural carboxylic acid (citric, malonic and malic acids). **Figure I. 26 a)** shows the schematized process for the isolation of modified-CNC. The grafting efficiency was highlighted by FTIR, among other techniques. First of all, all FTIR spectra showed the presence of intact cellulose (**Figure I. 26 c)**). Moreover, peaks related to ester groups (C=O stretches) and -CH₂ carbons evidenced the presence of the introduced ester bonds between cellulose and acids moieties. The TEM images of unmodified CNCs obtained *via* common hydrochloric acid hydrolysis and those associated to modified CNCs obtained *via* the one-step hydrolysis/Fischer esterification process showed no significant differences in terms of dimensions. Degrees of substitution between 0.16 and 0.22 were obtained, which was lower than those obtained with classical esterification (generally around 1 – 2)¹³⁵, but they still corroborated the literature values.

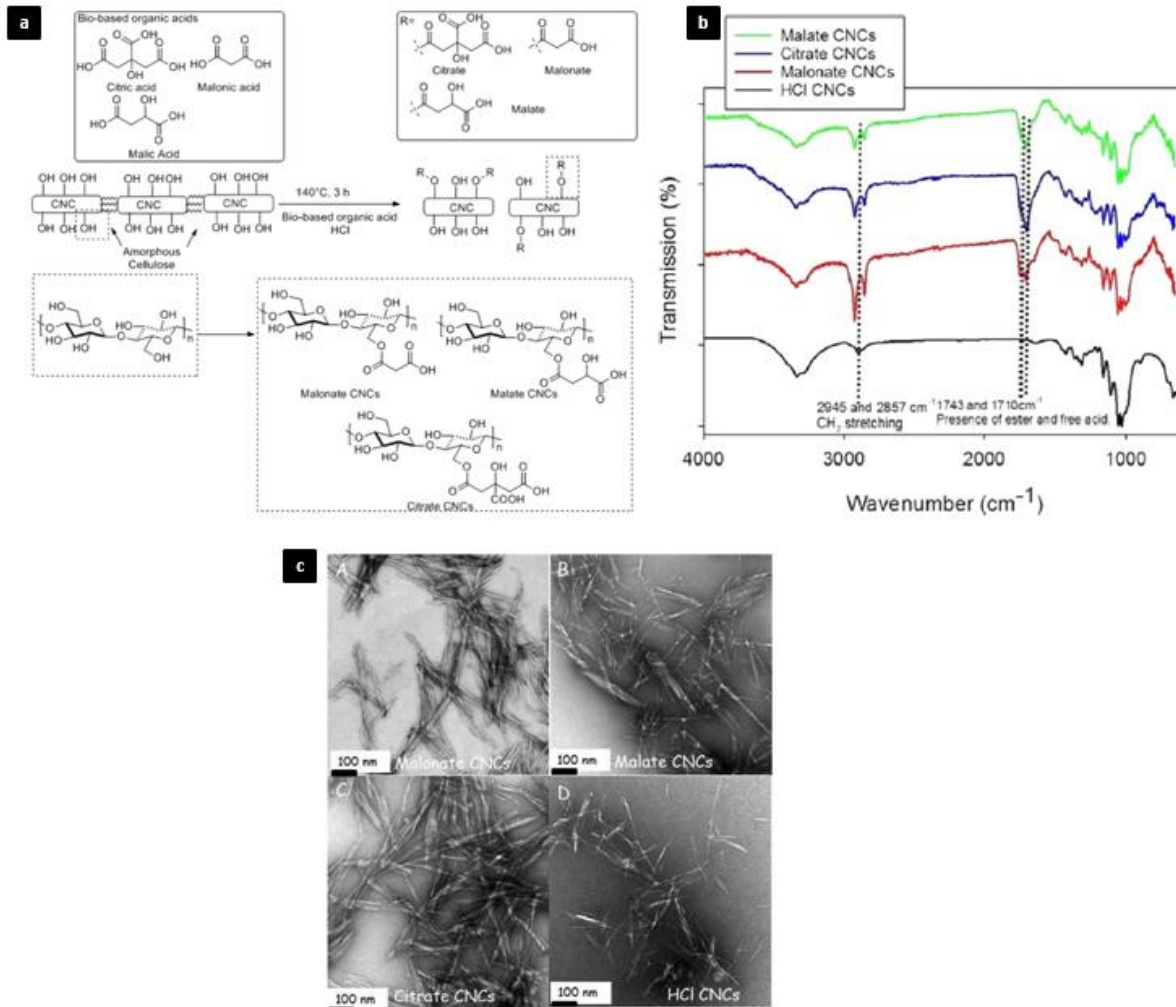


Figure I. 26. a) General procedure of the one-step isolation/modification process of CNCs with different bio-based carboxylic acids (citric, malic and malonic acids), b) FTIR spectra of unmodified HCl CNCs and modified malonate / citrated / malate CNCs, and c) TEM images of resulted unmodified (D) and modified (A, B, C) CNCs (extracted from ¹³⁹)

In their study, the compatibilization of modified CNCs with polymer was targeted, as it is often the case. In fact, several studies have investigated the grafting of long aliphatic chains on the surface of CNCs to increase their hydrophobic character, and thus their compatibility with hydrophobic polymers.

Other post-esterification of CNCs are widely presented in literature, including acetylation^{140,179}, transesterifications¹⁸⁰ or the use of acid halide reagents^{159,181}. The efficiency of these reactions was already proved in literature, with high degrees of substitution (generally higher than 0.4 and until 2-3)¹³⁵. Indeed, the surface high reactivity of the CNCs and the use of organic solvents are favourable conditions, and traditional method using fatty acid chlorides in organic solvents have been exposed in the literature^{135,153}. Another way of esterification is to modify directly CNC aerogels with a vapor phase of the chosen acid chloride. For example, Fumagalli *et al.*¹⁸² exposed that the modification of CNC aerogels, prepared in a mixture of water and tert-butanol, and then dried, could efficiently performed with palmitoyl chloride vapors. The redispersion of these modified CNCs in organic solvents was also a success. The efficiency of the esterification on CNCs was controlled and proved,

but the question of green chemistry and limitation of organic solvent remain a key point in current research. Indeed, in a spirit of green chemistry with limitation of toxic and organic solvent, esterification of CNCs remains a challenge, since the presence of water shifts the equilibrium in the undesired direction.

In the literature, more and more “solvent-free” or “green” methods are reported. Although these terms have to be understood properly, these methods have a common objective: the reduced use of toxic and organic solvents. Yoo and Youngblood¹⁸³ proposed a method in which aqueous lactic acid solution was used as reactive solvent in the esterification process of CNCs with long chains carboxylic acids. Thus, intermediate CNCs-grafted-PLA possessed a hydroxyl function at their end and acted as reactive species for the further esterification of carboxylic acids. Low degrees of substitution were calculated, although they were suitable for such innovative esterification. In a same way, Espino-Perez *et al.*^{141,184} presented a novel method for the esterification of CNCs. **Figure I. 27 a)** schematizes their protocol. Briefly, a CNC suspension in water was mixed with a water soluble acid, and heated above the acid melting point. After total evaporation of water, CNCs were in suspension in the melted acid and the reaction mixture was stirred for several hours, followed by washing steps. In this work, Espino-Perez *et al.* indirectly proved the enhanced dispersion of modified CNCs in organic solvents, like chloroform (**Figure I. 27 b)**), as well as, their increased hydrophobic character due to the introduction of hydrophobic groups at their surface, as suggested by the increasing of their water contact angle (**Figure I. 27 c)**). Generally speaking, chemical modifications of CNCs tend to turn to green and less toxic chemistry, although efficiency of such reaction is still lower than traditional reactions using organic and toxic chemicals.

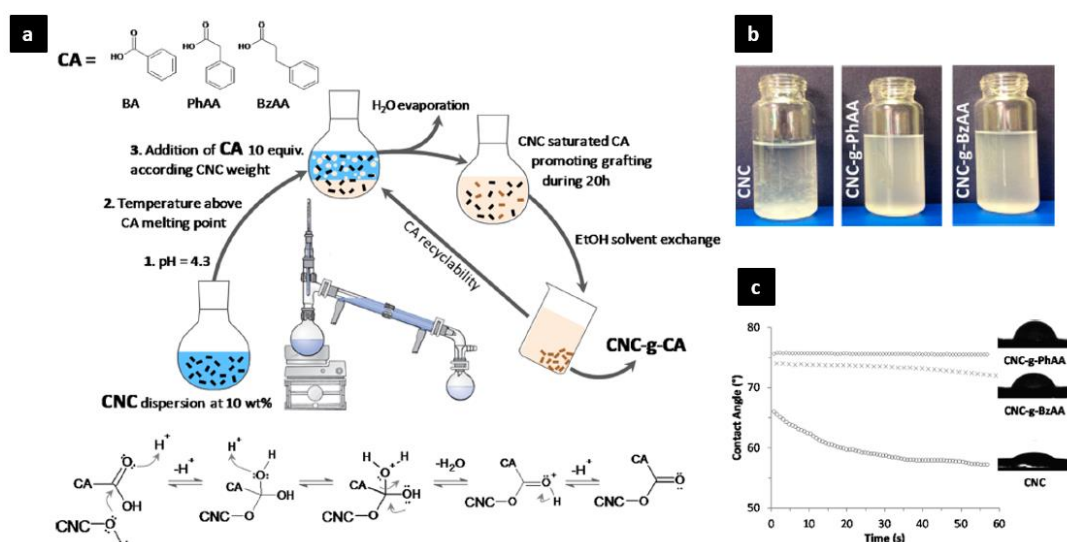


Figure I. 27. a) Solvent-free process ("SolReact") of the functionalization of CNCs with various carboxylic acids (benzoic acid (BA), phenylacetic acid (PhAA) and benzylacetic acid (BzAA)) and corresponding esterification mechanisms, b) Pictures of neat and esterified CNCs dispersed in chloroform at 0.5 wt%, and c) Contact angles of neat and modified CNCs (extracted from¹⁴¹)

2.3.3. Grafting of polymer chains at the surface of cellulose nanocrystals

For some applications, the modification of the CNC surface is required, in order to make them more compatible with apolar medium and polymeric matrix, or to confer them new interesting properties. The covalent grafting of polymer chains on the surface of CNCs can be performed, according to two different methods, respectively called *grafting-onto* and *grafting-from*. Recent reviews well described the polymer chains grafting on CNCs, with among others those of Natterodt *et al.*¹³², Kedzior *et al.*¹³⁴, and Wohlhauser *et al.*¹³³. They all put in parallel the two strategies.

The ***grafting-onto*** method is schematized in **Figure I. 28**. In this strategy, CNCs are used as such, or are pre-modified with functional groups. In the case of unmodified CNCs, the numerous reactive hydroxyl groups on their surface are used as functional groups. In the *grafting-onto* strategy, functional groups on the surface of the CNCs react with end-functionalized polymers (commercial grade or previously synthesized), generally in the presence of a coupling agent. Thus, the polymers are directly grafted onto the CNCs surface. Due to eventual steric repulsion between the grafted polymer chains — which can hindrance the polymer grafting — this method leads to quite low grafting densities. Nevertheless, it also presents benefits, since the grafted polymers, and especially its molecular weight, can previously be characterized, and the grafted surface of modified CNCs can thus be better controlled and modelled.

According to Kedzior *et al.*¹³⁴, the most common reactions generally used in the *grafting-onto* strategy are the carbodiimide coupling, the opening of epoxy groups and the grafting of isocyanate groups. In these cases, functional groups on the surface of CNCs are carboxylic acid –COOH (previously introduced by TEMPO-oxidation), deprotonated hydroxyl groups –O⁻ and hydroxyl groups –OH, respectively. These reactive groups thus react with amine-terminated polymers, epoxy-terminated polymers, and various polymers like poly(caprolactone) or poly(urethane), respectively. Although most of these reactions occur in organic solvent with any trace of water due to the hydrophobic character of grafted polymers, some of them can take place in aqueous conditions. It's the purpose, for example, of the research conducted by Araki *et al.*¹⁵⁵, who grafted aminated-poly(ethylene glycol) in water onto TEMPO-CNCs surface¹⁴⁶. Another example is the grafting of epoxy-terminated-poly(ethyleneoxide) on deprotonated CNCs, leading steric stabilization of grafted CNCs which are not ionic sensitive. Colloidal stability and compatibilization in apolar polymeric matrices are generally targeted, as well as, the development of new functional materials, like thermoresponsive behavior of amine-terminated PNIPAM (poly(N-Isopropylacrylamide)) grafted on CNCs surface in aqueous medium, as presented by Gicquel *et al.*¹⁴⁷ As previously mentioned, the main drawback of the “grafting-onto” strategy lies in the low grafting densities, mainly due to steric hindrance between the polymer chains.

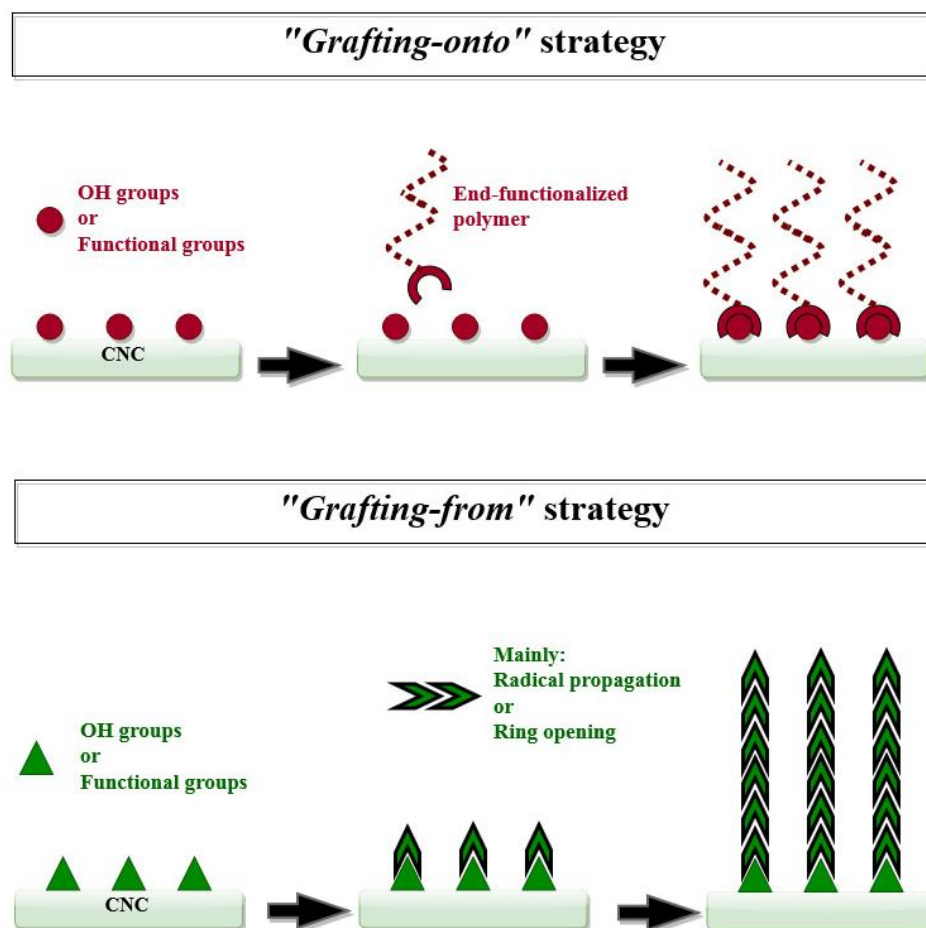


Figure I. 28. Schematized principles of *Grafting-onto* and *Grafting-from* strategies

The ***grafting-from*** method is a two-steps strategy, in which neat or previously grafted CNCs (with an initiator of the further reaction) are involved. The hydroxyl groups on the neat CNCs surface, or the grafted functional groups on the modified CNCs surface act, most of the time, as initiator of the polymerization. As its name suggests, the *grafting-from* strategy consists in the polymerization from the CNCs surface, by the addition of the monomer and potential coupling agents in the reaction mixture, as presented in **Figure I. 28**. This method allows higher grafting densities (between 100 and 1000 polymer chains per CNC), since the steric hindrance between the polymer chains are generally limited, because of their living polymerization, and a better control of the grafting density and polymeric chains length.

Several *grafting-from* strategies are known in the literature, where three main types are reported: the ring-opening polymerizations (ROP) of monomers bearing rings, the free radical polymerizations, and the controlled radical polymerizations.

ROP is currently a well-known procedure to graft cyclic monomers (ϵ -Caprolactone, lactide, ethers) from hydroxyl groups acting as initiator groups at the surface of CNCs, and most of these polymerizations are highly water sensitive. Habibi *et al.*¹⁵⁸ were the first to perform the ROP of ϵ -

Caprolactone *via* ring-opening polymerization (ROP) from the surface of CNC, in toluene, and using Tin(II) ethylhexanoate ($\text{Sn}(\text{Oct})_2$) as catalyst. In their review, Kedzior *et al.*¹³⁴ presented recent advances and publications dealing with ROP on CNCs. The polymerization of lactic acid from the CNCs surface by ROP was proposed several times in the literature. Peltzer *et al.*¹⁸⁵ performed the ROP of L-lactide in toluene, with a catalytic amount of $\text{Sn}(\text{Oct})_2$, and with different initial monomer/CNC weight ratios. More recently, Miao and Hamad¹⁸⁶ carried out a similar *in situ* ROP with $\text{Sn}(\text{Oct})_2$ and zinc oxide as catalyst and initiator, respectively. In both studies, the efficiency of the polymerization was highlighted.

Free radical polymerizations are generally performed in water and do not require the presence of attached surface initiators. In fact, these polymerizations involve water soluble radical initiators (for example, ceric ammonium nitrate (CAN), ammonium persulfate (APS), potassium persulfate (KPS), etc.) which mainly react with hydroxyl groups from CNC surface, allowing the chain growth of polymer from water soluble monomers. In 2013, Kan *et al.*¹⁸⁷ were among the first to carry out a free radical polymerization of poly(4-vinylpyridine) from the CNCs surface, using CAN as initiator. In the literature, numerous publications deal with the free radical polymerization from CNCs surface, like Kedzior *et al.*¹⁶¹ who polymerized poly(methyl methacrylate) from CNCs surface in water with CAN, or Zubik *et al.*¹⁸⁸ who performed the free radical polymerization of N-isopropylacrylamide monomer from CNCs surface, in the presence of APS as initiator and 1,2-di-(dimethylamino)ethane, in water. Each time, the efficiency of the polymerization was highlighted, as well as the benefits of the such free radical polymerizations (i.e. aqueous media and one-step reaction). In a same way of green chemistry, Espino-Pérez *et al.*¹⁶⁰ first activated the CNCs surface by ozonolysis, to create $-\text{O}\cdot$ radicals at their surface, and then performed the free radical polymerization of styrene from these radicals in the presence of APS. During free radical polymerizations, it is generally difficult to well control the polymer growth, which leads to heterogeneous chains lengths. Moreover, a significant amount of homopolymer — polymerized from the reaction media — is generally produced, and it is difficult to totally remove this free polymer.

Various **controlled radical polymerizations** exist, like among others, the atom-transfer radical polymerization (ATRP), the reversible addition-fragmentation chain-transfer polymerization (RAFT), single electron transfer-living radical polymerization (SET-LRP), or the nitroxide-mediated polymerization (NMP). These polymerizations are reversible-deactivation radical polymerizations (RDRP).

The atom transfer radical polymerization, referred to as the **ATRP**, was developed by Matyjaszewski *et al.*¹⁸⁹ and Sawamoto *et al.*⁹¹ at the end of the 1990s. ATRP is defined as equilibrium between propagating radicals and dormant species. **Figure I. 29** represents the ATRP principle.

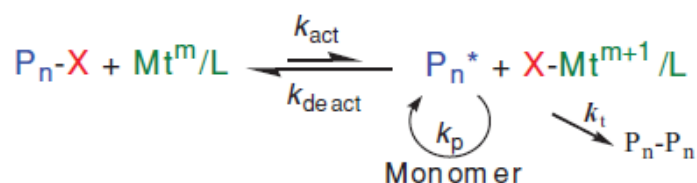


Figure I. 29. General representation of the ATRP equilibrium with ($\text{P}_n\text{-X}$) the initiating alkyl halides/macromolecular dormant species and (Mt^m/L) the transition metal complex, (P_n^*) the propagating radicals and ($\text{X-Mt}^{m+1}/\text{L}$) the metal complex in the higher oxidation state (extracted from ¹⁹⁰)

Briefly, the initiating dormant species ($\text{P}_n\text{-X}$) react with a transition metal complex in their lower oxidation state (Mt^m/L , generally $\text{Cu}^{\text{I}}/\text{L}$ or $\text{X-Cu}^{\text{II}}/\text{L}$, with m the oxidation state and L the ligand) with a rate constant of activation k_{act} . Thus, the growing radicals P_n^* are formed, leading to the addition of monomers, and thus the growth polymer chains, with k_p the rate constant of propagation. In parallel, the radicals react in a deactivation reaction with oxidized metal complex ($\text{X-Mt}^{m+1}/\text{L}$) to recreate dormant species and transition metal complex in their lower oxidation state, and thus recreating the activator with the rate constant of deactivation k_{deact} . The rate constant of termination k_t governs the termination of the polymerization. Several parameters influence the rate and yield of the polymerization : ligand and monomer/dormant species structure, reaction conditions like solvent, temperature, reaction time and reactive proportions^{190,191}. In the case of a grafting at the surface of CNC, surface-initiating ATRP (called SI-ATRP) is carried out. In a two-step procedure, CNC are first modified with an initiator of the polymerization, commonly the brominated initiator α -bromoisobutyryl bromide (BIBB), whose grafting occurs generally in DMF in presence of trimethylamine and 4-(dimethylamino)pyridine. In 2008, Yi *et al.*¹⁹² were the first to report the SI-ATRP of polystyrene of functionalized CNC and performed acidic cleavage of grafted chains in a way of characterization. Since that date, numerous publications have presented SI-ATRP on CNC with different kind of polymers, especially hydrophobic polymers, in a way of CNCs compatibilization with hydrophobic polymeric matrices. Grafting-from polystyrene on CNCs has been optimized in the literature, especially by Morandi *et al.*¹⁵⁹. In their study, they polymerized polystyrene by ATRP from brominated initiator sites, and proved that the substitution degree of these initiator sites influenced the polymerization efficiency. The principle of their grafting-from strategy is presented in **Figure I. 30**. The homopolymer produced from sacrificial initiator in solution was recovered after each polymerizations carried out with different conditions (initial brominated sites content, initial monomer/sacrificial initiator ratio, polymerization time), and in each case, the control of the polymerization was proved at short reaction times.

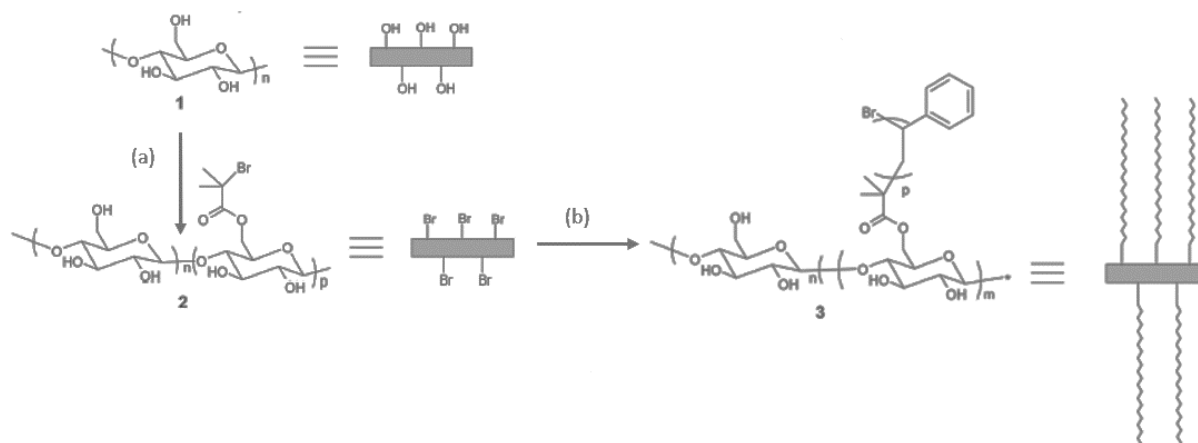


Figure I. 30. Principle of the grafting-from of polystyrene on pre-functionalized CNC-Br proposed by Morandi et al. (1 = unmodified CNCs, 2= CNCs modified with BIB and 3=CNCs grafted with polystyrene / Reaction conditions : (a) = 2-bromoisobutyrylbromide (BIB), Et₃N (trimethylamine), DMF, 24h, 70 °C and (b) = [styrene]:[EBiB]:[CuBr]:[PMDETA] = 100:1:0.5:0.5, anisole (50% v/v), 100 °C) (extracted and adapted from ¹⁵⁹)

The novel **ARGET-ATRP** method (Surface-Initiated Activator Re-Generated by Electron Transfer ATRP) is highly interesting, since it aims to reduce the amount of catalyst in the media, and can be performed with a better oxygen tolerance (presence of air). It clearly reduces the reaction time and the number of steps, especially for what the removal of metal salts concerns. Recently, Zhang *et al.*¹⁹³ polymerized styrene from the surface of CNCs (previously modified with BIB) by ARGET-ATRP, with CuBr₂ and tris(2-(dimethylamino)ethyl)amine as catalyst system. Briefly, ARGET-ATRP involves an excess of reducing agent which regenerates the active species (Cu(I)) from the deactivate species (Cu(II)). These species are thus continuously formed. The authors compared the ARGET-ATRP with the SI-ATRP procedure, and concluded that ARGET-ATRP allows the grafting of longer polymeric chains with a lower grafting density, with a reduced amount of catalysts and a reduced time of polymerization. In a recent publication, Lepoittevin *et al.*¹⁹⁴ performed surface-initiated ARGET-ATRP of 2-hydroxyethyl methacrylate (HEMA) on previously prepared chitosan-based polysaccharide films, in order to make them more hydrophobic. After having modified the films with the BIB as initiator, the reaction was performed at room temperature, using CuBr₂ and tris(2-pyridylmethyl)amine (TPMA) as catalyst system, and ascorbic acid as reducing agent. The authors confirmed that the presence of air in the reaction media didn't influence the efficiency of the polymerization, which is also controlled. The polymerized chitosan films were then fluorinated using heptafluorobutyryl chloride, in order to enhance their hydrophobic behavior. In addition to the direct characterization of the simple ARGET-ATRP polymerization limiting the use of metallic salts, the hydrophobicity of the modified chitosan films was evidenced by the significant increase in the value of the water contact angle (from 87° to 101° after fluorination). Photo-induced ATRP is another kind of ATRP using less initiator and thus leading less washing steps¹⁹⁵. In the review of Kedzior *et al.*¹³⁴, a complete Table I summarizes all the different polymers grafted on CNCs *via* SI-ATRP, with the same pre-functionalization with BIBB in all cases. Among others, hydrophobic polymers like polystyrene^{159,192}, poly(methacrylate)¹⁹⁶, poly(butyl methacrylate)¹⁹⁷, N-isopropylacrylamide¹⁹⁸ were

efficiently grafted on CNCs. Most of the time, targeted properties is hydrophobicity and compatibility of CNC with hydrophobic systems.

In the literature, in addition to the ATRP, other reversible-deactivation radical polymerizations (RDRP), like *SET (or SARA ATRP)* and **RAFT** are proposed. SET is carried out under the same conditions as the ATRP. Zoppe *et al.*¹⁸¹ were the first to use SET living radical polymerization for the grafting of poly(N-isopropylacrylamide) on CNCs, using Cu(I)Br copper salt as catalyst. Wang *et al.*¹⁹⁶ also reported a SET polymerization, and grafted poly(methacrylate) on CNC by using Cu(O) copper wire as catalyst. Both of their studied aimed to simplify the washing procedure of grafted CNCs. On the other hand, the RAFT technique is more recent, and its use in the *grafting-from* strategy is much less reported in the literature. RAFT can be used with numerous monomers and reactions conditions, and ensure a well-controlled polymerization. The techniques requires first the attachment of chains transfer agents (mainly xanthates, trithiocarbonates, and dithioesters)^{134,199} on the surface of the materials²⁰⁰, leading to fast exchanges with the monomers. The initiation and termination steps are similar to those of classical radical polymerizations, and termination reactions are limited, due to the low amount of radicals in the media. In 2014, Zeinali *et al.*²⁰¹ were the first to perform RAFT polymerization of N-isopropylacrylamide and acrylic acid copolymers from the CNCs surface previously modified with thiocarbonates (2-(dodecylthiocarbonothioylthio)-2-methylpropionic acid, DDMAT) as chain transfer agents. More recently, Boujemaoui *et al.*²⁰² immobilized a similar chain transfer agent (2-(ethoxycarbonothioylthio)-propanoic acid) on CNCs surface to perform the RAFT polymerization of vinyl acetate, as presented in **Figure I. 31**.

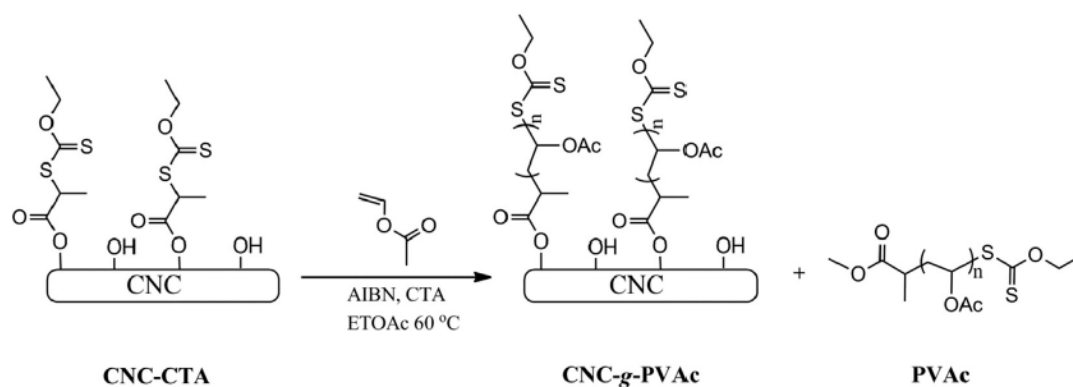


Figure I. 31. Principle of the grafting-from of poly(vinyl acetate) (PVAc) using the RAFT polymerization from the CNCs surface modified with (2-ethoxycarbonothioylthio)-propanoic acid) as chain transfer agent (extracted from ²⁰²)

Few other studies deal with the RAFT polymerization of various monomers from the surface of CNCs. For example, Liu *et al.*²⁰³ synthesized macro-agents, which were then covalently attached on the CNCs surface, and from which the RAFT polymerization of acrylamide was performed, in the presence of CAN and nitric acid.

Another controlled radical polymerization is the *NMP*, which involves nitroxide compounds as control agents and thus, reversible termination equilibrium between these nitroxide moieties and the growing

propagating radicals. In 2016, Roeder *et al.*²⁰⁴ were the first to perform NMP from the surface of CNCs. They polymerized poly(methyl acrylate) and poly(methyl methacrylate) from the CNCs surface previously modified with N-(2-methylpropyl)-N-(1-diethylphosphono-2,2-dimethylpropyl)-O-(2-carboxylprop-2-yl)hydroxylamine (BlocBuilder®) initiators, and they highlighted the efficiency of the polymerization. Only few publications deal with this technique in the *grafting-from* CNCs strategy.

More generally, the main *grafting-from* method's difficulty lies in the fact that the determination of the molecular weight of the grafted polymer is challenging. It is commonly assumed that the homopolymer growth from sacrificial initiator in the media is very similar to that of the polymer from initiator sites at the CNCs surface, leading to very close values of molecular weight of grafted and free homopolymers²⁰⁵. Cleavage of grafted polymeric chains could be a solution, but this process is drastic and could certainly damage both CNCs and polymer, leading to distorted results. In a recent publication, Zhang *et al.*²⁰⁶ proposed different characterizations (DLS, DSC, TGA) to determine precisely the grafted polymer characteristics. However, they concluded that the commonly done assumption is coherent: free homopolymer and grafted polymer are very similar in term of molecular weight. Noteworthy, the main advantage of the “grafting-from” technique relies in the control of the chains grafting density and length.

2.3.4. Physical adsorption of various molecules on cellulose nanocrystals

The stronger type of non-covalent bond relies on an electrostatic phenomenon. Indeed, negative surface charges at the surface of CNCs, and positive charge on molecules thus establish ionic bonds. Other types of interactions can occur, such as hydrogen bonds, or Van der Waals forces, but these phenomena are even weaker than charge-charge interactions ones. Thus, the surface charges of CNCs can be exploited in order to simply attach moieties at their surface, without using harsh chemistry. Although adsorption mechanisms are not easy to model (as studied by Villares *et al.*²⁰⁷) and not sufficient for all applications, the adsorption strategy has been widely studied in the literature.

In the case of surfactants acting as stabilizing compounds, their hydrophilic part can be adsorbed at the surface of hydrophilic CNCs, while their hydrophobic part aim to create a hydrophobic surface around the CNCs. Generally, the stabilization and dispersion of such decorated CNCs in organic solvents are targeted. Heux *et al.*²⁰⁸ were among the first to investigate the use of surfactant (in their case, a phosphoric ester of polyoxyethylene nonylphenyl ether anionic surfactant) in order to obtain a well-dispersed suspension of coated CNC in non-polar solvents, such cyclohexane, *via* a simple procedure. More generally, CNCs and oxidized TEMPO-CNCs bear surface anionic groups, providing from residual components from fibers, or naturally oxidized or ionized hydroxyl groups. The adsorption of anionic surfactants is thus interesting.²⁰⁹

Abitbol *et al.*¹⁶⁵ used cationic surfactant cetyltrimethylammonium bromide (CTAB) to adsorb *via* electrostatic interactions at the surface of CNCs, precisely on negatively charged half-sulfate ester

groups. According to their results, between 50% and 100% of surface charges were recovered by the CTAB, and this efficiency was mainly dependent on ionic strength, and to a lesser degree, on the surfactant concentration, and surfactants/anionic sulfur charges molar ratio. Indeed, by increasing the ionic strength of the reaction media, electrostatic interactions were screened, leading to a decrease in the adsorption efficiency. **Figure I. 32** schematizes the different reaction conditions exposed by Abitbol *et al.*¹⁶⁵ in their work. In case a), the pH was adjusted with NaOH, and electrostatic interactions between cationic surfactant and negative surface charges of CNC were more hindered than in case b), where pH was equal to 4. The concentration of CTAB varied between cases a) and b) (higher or equal to the critical micellar concentration).

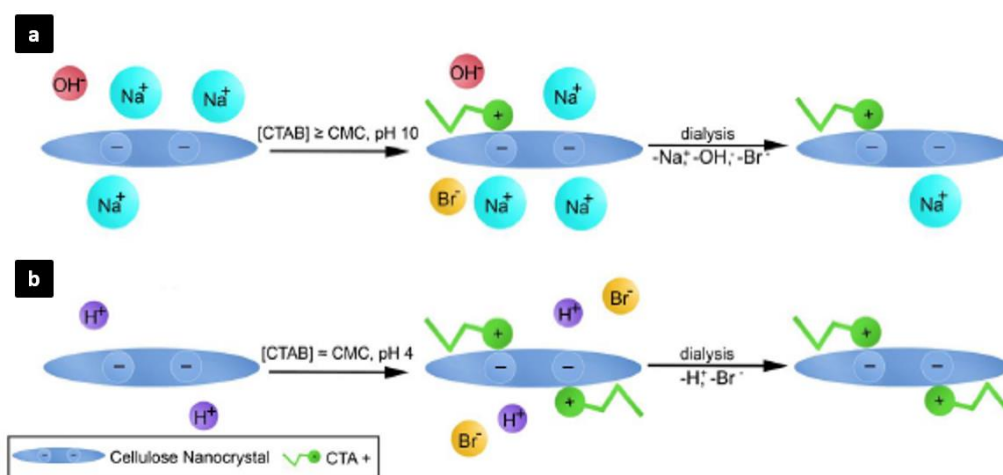


Figure I. 32. Scheme of the two adsorption reactions proposed by Abitbol *et al.* with **a)** a concentration of surfactant higher than the critical micelle concentration (CMC) and pH=10, and **b)** a concentration of surfactant equal to the CMC and pH=4 (extracted from ¹⁶⁵)

Note that CTAB is commonly used as surfactant for the adsorption on CNCs, since it is not expensive, widely available and efficient, although other cationic surfactants have also been studied, like hexadecyltrimethylammonium bromide (HDTMA). More recently, Kaboorani and Riedl.²¹⁰ have investigated the adsorption of HDTMA in a similar procedure as that previously proposed, varying the ratio HDTMA/CNC and the reaction time. The stability in water and THF of recovered modified CNCs at different conditions was studied, as shown in **Figure I. 33**. The AFM images clearly showed that by increasing the amount of HDTMA at the surface of CNCs, coated CNCs were more aggregated, which could be explained by the absence of repulsive negative charges which play a role in the stability of water suspensions. It was confirmed by the stability of water suspensions, as presented in **Figure I. 33 a)**: modified CNCs were not stable in water and precipitated, whereas they were stable in THF (**Figure I. 33 b)**), depending on the initial surfactant concentration. It highlighted the hydrophobic behavior of CNCs once they have adsorbed long aliphatic chains surfactants. More generally, negatively charged groups at the surface of CNCs result from residual fibers components and/or chemical modifications like TEMPO oxidation or acid hydrolysis, and are interesting sites for adsorption of cationic surfactants.

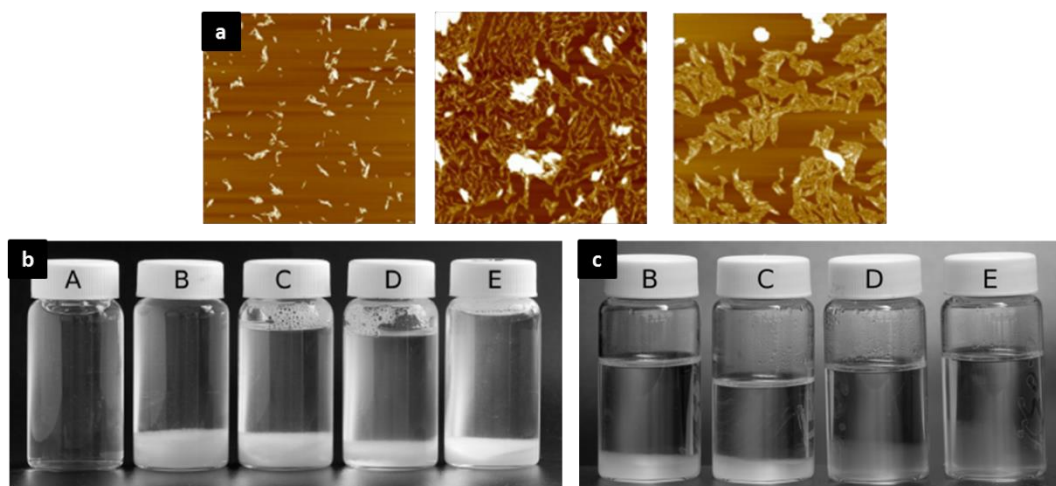


Figure I. 33. a) AFM images in high (from left to right) of unmodified CNCs, modified CNC at 0.35mmol/g HDTMA for 2 h and modified CNC at 1.4mmol/g for 4 h, b) Water suspensions, and c) THF suspensions of A) unmodified CNCs, B) modified CNCs at 0.35mmol/g for 2 h, C) modified CNCs at 0.35mmol/g for 4 h, D) modified CNCs at 1.4mmol/g for 2 h and E) modified CNCs at 1.4mmol/g for 4 h (extracted from ²¹⁰)

The use of non-ionic surfactants was also described in the literature. For example, Rojas *et al.*²¹¹ used non-ionic sorbitan monostearate surfactant to adsorb CNCs in order to introduce and disperse such modified CNC in a polystyrene matrix. Efficiency of the adsorption of anionic surfactant on CNCs was proved by the reduction of bead during the electrospinning process, because of the charges decreasing in the CNC/Polystyrene system. Another goal of the adsorption at the CNCs surface is the stabilization of emulsions. Capron *et al.*⁵⁹ highlighted the stabilization effect of CNCs on oil-water interfaces, in order to create strongly stabilized emulsions. Kedzior *et al.*²¹² built their work on the emulsion stabilization properties of CNCs, by adsorbing different types of surfactants (anionic or cationic) on the CNCs. The polymerization in emulsion was the aim of their study, and it was controlled and tailored by the presence of adsorbed CNCs. More generally, CNCs can act as stabilizer in Pickering emulsions (particle-stabilized emulsions), in which they can adsorb at the droplets interfaces. These Pickering emulsions have been widely studied in the literature, in particular with the use of surfactants to enhance their stabilization^{127,166,213}.

In the case of molecules or polymers adsorption, a similar principle is considered. Indeed, adsorbed molecule or polymer has to contain both hydrophilic and hydrophobic parts. The aim of macromolecules or polymer adsorption on CNCs is generally the enhancement of their compatibilization and dispersion in polymeric systems. In a recent publication of Boujemaoui *et al.*¹⁹⁷ the physisorption of the poly(n-butyl methacrylate) was carried out and compared with a covalent grafting strategy. Even if the covalent bonding was more efficient than the adsorption route, the final nanocomposites of modified-CNC in polycaprolactone matrix showed interesting properties. Cheng *et al.*²¹⁴ have performed the adsorption of polyethylene oxide (PEO) with different molar masses on CNCs in order to improve their re-dispersion after drying. They proved that the presence of adsorbed PEO allowed the CNCs re-dispersion in water. They also assumed that the presence of adsorbed PEO

on CNCs induced steric hindrance, and thus led to the re-dispersion. Pereda *et al.*²¹⁵ have mixed PEO solution with a CNC suspension, and investigated the evolution of the viscosity. They concluded, according to the trend of the viscosity curve function of the CNC content (decreasing of the viscosity when CNCs were added), that an optimum of CNCs amount, called “critical concentration”, existed and corresponded to the amount of CNCs needed for adsorbed all the PEO chains. Once CNCs have adsorbed PEO, the viscosity of the system increased. Final freeze-dried CNCs coated with PEO were then extruded with polyethylene and recovered films were more homogeneous than those prepared with unmodified CNCs, and more thermally stable. Thus, the PEO adsorption allows surface modification of CNCs *via* simple routes in water, with a wide range of possibilities. Nevertheless, since molecules are not covalently linked to CNCs, release or leaching phenomena have to be considered.

In this second part, nanocelluloses were introduced, and especially cellulose nanocrystals (CNCs). Their isolation, properties, applications, and some of their chemical surface modifications were detailed. As presented in the first part, composites — and especially those using bio-based polymers — are interesting materials in terms of barrier and mechanical properties. With the emergence of innovative nanomaterials such nanocelluloses, the research is focusing on outstanding nanocomposites materials. The following part focuses on the introduction of nanocelluloses in polymeric matrices, for food packaging applications.

3. Use of nanocelluloses in polymeric systems for food packaging applications

Cellulose nanocrystals are of great interest in composites field, and especially for food packaging applications. The number of publications and patents dealing with cellulose nanocrystals in nanocomposites field increased over the years, and followed the same trend as the evolution of cellulose nanocrystals alone. Although CNCs present a wide range of applications and applied researches, composites field — and especially that of nanocomposites — is the most important targeted application area of CNCs. As schematized in **Figure I. 34**, around 450 papers have been published on the topic just since the beginning of this project (2017), and innovative aspect of CNC-based nanocomposites is also highlighted. Recent reviews reported the use of cellulose nanocrystals in nanocomposites field^{117,216–218}.

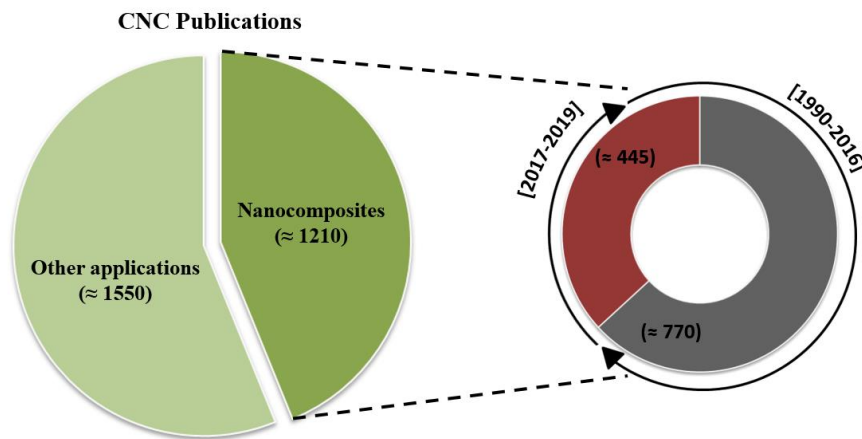


Figure I. 34. Schematic representation of number of publications dealing with CNCs and nanocomposite applications especially and number repartition before and after the starting year of this project (Source : SciFinder, April 2019 – Descriptors : cellulose nanocrystal, cellulose nanorod, rod-like cellulose, cellulose nanowire, cellulose crystallite, cellulose nanoparticle, cellulose whiskers, nanocrystalline cellulose combined with nanocomposites – Language : English)

Although both CNFs and CNCs can be introduced in polymeric matrix and enhance the final properties of the materials, CNCs are in the center of this PhD project, and their use in composite field is described in this last section. Several reviews detailed the use of CNFs for composites applications^{86,217,219,220}. Nanocomposites for food packaging applications will be first described, following by the interest of the CNCs introduction, and finally the properties of resulting CNC-based nanocomposites.

3.1. Nanocomposites and legislation

3.1.1. Interest of the introduction of nano-fillers in polymer matrices

By definition, a nanocomposite is a multiphasic material, in which one of the phases present one or several nanometric scale, meaning less than 100 nm¹¹⁷. Okada *et al.*²²¹ were the first to introduce

nanomaterials in a polymeric matrix. Indeed, by incorporating silicate in polyamide, they exhibited high mechanical properties and high temperature resistance of the final nanocomposites. Since this date, numerous studies have been investigated, and the incorporation of nanomaterials (especially inorganic ones) in polymer matrices for packaging applications has shown interesting results. Indeed, due to their nanometric size, nanomaterials allow to reach unique properties, when compared to properties of traditional composites, and this unique effect visible even at low filler content (few weight percentages)¹¹⁷. Safety, low cost, and enhanced barrier and mechanical properties, as well as antimicrobial activity, have stimulated the development of such nanocomposites, with among others the use of metal-based, oxide, carbon-based, or clay-based nanoparticles²²². Numerous examples of industrialized and commercialized nanocomposites in food packaging sector with inorganic fillers can be provided: nanoclays in nylon or starch for beer bottles (Aegis® OXCE, USA) and thermoformed trays for chocolate (Plantic® Plastic Tray, Australia), silver nanoparticles in polypropylene or polyethylene for food containers (FinePolymer, Inc., South Korea or Cixi Mingxin Plastic & Rubber Factory, China), and other examples. In each case, the properties of the final products are improved, especially their barrier, mechanical, or antimicrobial (with silver) properties.

As mentioned in the first part of this chapter, in the current economic and environmental context, development of innovative bio-based, biodegradable, active and intelligent food packaging is in the centre of researches in this field, especially with the use of renewable materials. Since the 1990s, the incorporation of bio-based nanomaterials into polymers has been of great interest.

3.1.2. Nanocomposites and legislation

When speaking about nanomaterials and nanocomposites, one spontaneous question is the health risk related to the presence of “nano”. Indeed, in consumers and media mind, the term “nano” refers to dangerous materials. Several studies have been carried out in order to get rid of this risk and this poor perception. European Union — the main European organization for nanotechnology and nanomaterials — has published in January 2011 a Commission Regulation on plastic materials and articles intended to come into contact with food²²³. The regulations and specifications were given, with limit values of compounds migrations. In this legislation, the European Union aims to limit the amount of additives used in food packaging and results of migration studies have to be provided before any industrialization. Bumbudsanpharoke *et al.*²²⁴ published a recent review on the nano-food packaging market. According to their study, the nanoparticles presented in nanocomposites possibly migrate from the packaging, but it has been proved that the amount of migrated nanoparticles is lower than the legislated limitations. Nevertheless, consumers and media perception is still suspicious. As previously mentioned, low toxicity of CNCs has been demonstrated but question of potential migration of the nanocelluloses into the food products is still under question for what CNC-based nanocomposites concerns. However, taking into account the bio-based and renewable character of CNCs, as well as,

that of bio-based polymer used as template matrix, the strategy of the elaboration of bio-nanocomposites is an innovative and promising strategy in food packaging science.

3.2. Cellulose nanocrystals as fillers in nanocomposites

After the first introduction of nanocelluloses in polymer in the beginning of the 1990s, lot of researches have been carried out to optimize and characterize the preparation of nanocellulose-based nanocomposites. Through their nanometric size and their high specific surface area, CNC exhibit outstanding properties when incorporated in a polymeric matrix. Moreover, use of renewable and bio-based polymeric matrices is currently leading the research.

3.2.1. Effect of cellulose nanocrystals on nanocomposites mechanical and barrier properties

The presence of nanometric fillers, like CNCs, in a polymer matrix exhibit enhanced properties comparing to the presence of micrometric fillers, even at low content of nanofiller. Thus, in the case of CNCs, due to their high specific area, their interphase with the polymer is large, especially for well-dispersed nanofillers. In fact, the molecular mobility of the polymer matrix is modified, leading to a relaxation behavior with improved thermal and mechanical properties²²⁵. In 1995, Favier *et al.*²²⁶ were the first to introduce CNCs in a copolymer of polystyrene/poly(butyl acrylate) and poly(acrylic acid). The study highlighted the improvement in mechanical and thermal properties when 6 wt% of CNCs are introduced into the matrix.

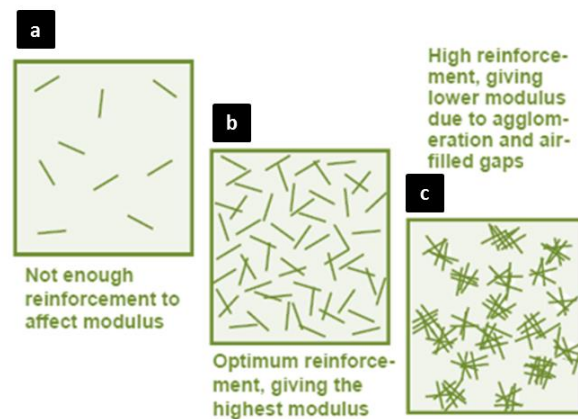


Figure I. 35. Schematization of nanocomposites with various amounts of nanofillers in the matrix: **a)** low amount, **b)** percolation threshold, and **c)** higher amount than the percolation threshold (extracted from ⁸⁴)

Since this date, several studies have modelled the behavior of such nanocomposites. Intrinsic tensile properties of CNCs lead to the continuous network formed by the percolation mechanism. Indeed, above a critical CNCs concentration, called the percolation threshold, a large increasing of mechanical properties of nanocomposite is observed. This formalism allows predicting mechanical behavior of nanocomposites, considering that CNCs are organized into a rigid network inducing their reinforcing

effect¹⁷⁸, and the optimum CNCs concentration in a polymer matrix for improvement of mechanical and thermal properties has been widely studied in the literature. This concentration does generally not exceed 10 wt%, in the case of rod-like particle shapes, and depends on the CNCs source and isolation process, as well as, on the polymer matrix. If CNCs are introduced in a too high concentration, dispersion and aggregation issues can occur, leading to a loss of mechanical properties. **Figure I. 35** schematizes this behavior.

Furthermore, CNCs act as nucleating agent, and can thus enhance the crystallization kinetics of the polymer, improving the thermal properties of the final nanocomposites. Well-dispersed nanofillers — particularly disk-like particle shapes — in a polymeric host matrix can also improve the barrier properties of the final material. Indeed, as presented in **Figure I. 36**, gas molecules diffuse through the nanocomposite material with a certain diffusion coefficient. In the case of a simple polymer, the gas molecules diffuse with a diffusion coefficient D . In the case of a nanocomposite, they diffuse following a tortuous pathway, with a diffusion coefficient D_m . Theoretically, D and D_m are linked by the following equation²²⁷ :

$$D = D_m / \tau.$$

Thus, one of the preponderant theories relies on the fact that the diffusion of gas molecules through a nanocomposite is slowed by the presence of nanofillers. In this sense, the enhancement of barrier properties of CNC-based nanocomposites is targeted, as a key property for food packaging application, as previously mentioned.

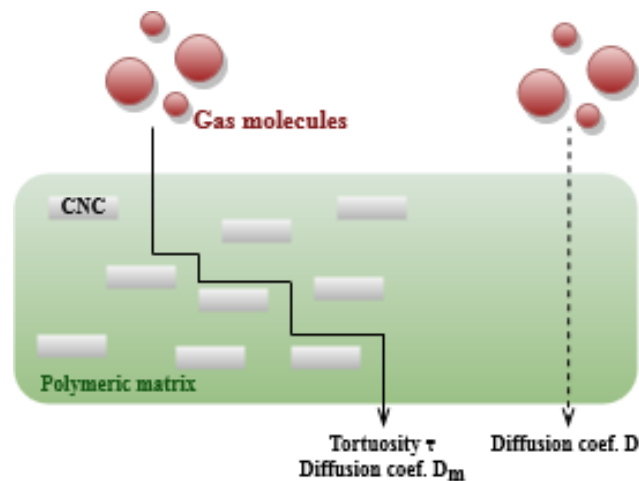


Figure I. 36. Schematized representation of tortuous pathway of gas molecules inducing by the presence of fillers (CNCs) through a polymeric matrix

However, all these assumptions are highly dependent on the properties of the introduced fillers (especially CNCs), and on their dispersion state. This dispersion of CNCs in a polymeric matrix is an important issue, which gives rise to a lot of studies. In fact, due to the inherent hydrophilic character of the CNCs, their introduction in hydrophobic polymer matrices is challenging, and requires generally

the surface modification of CNCs, as detailed in the previous part of this chapter. Due to the numerous hydroxyl groups at the surface of CNCs, their interfacial adhesion with hydrophobic polymers is too weak, and makes their dispersion difficult, which is cause for the limitation of their use in nanocomposites.

Since PLA is the selected biobased polymer in this PhD project, the rest of this section will focus on PLA-based / CNCs nanocomposites.

3.2.2. PLA-based / CNCs nanocomposites

The production of PLA-based / CNCs nanocomposites is interesting, especially because of the advantageous properties of both CNCs and PLA, as previously mentioned. Different processing can lead to the elaboration of such nanocomposites, grouped into three main types: melt-processing, electrospinning, and casting / evaporation, as presented in **Figure I 37**.

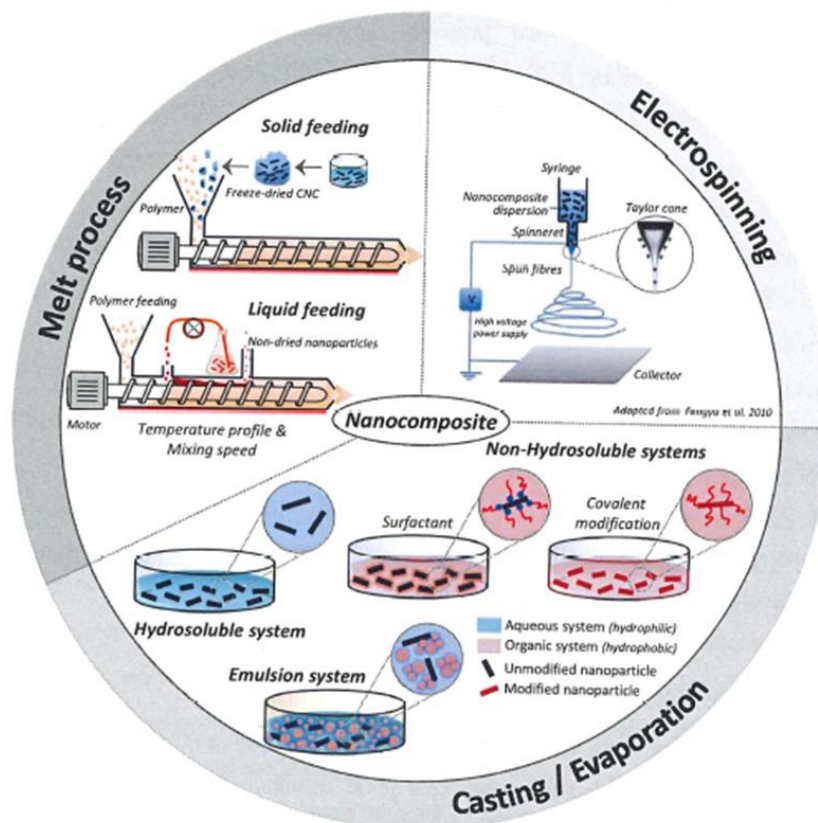


Figure I 37. Strategies for the elaboration of nanocomposites (Extracted from Espino-Perez E. PhD, 2014)

The **melt-processing** methods include extrusion and injection molding, and are commonly used to process and shape thermoplastic polymers. Industrial equipment used for common polymers can also be used for PLA nanocomposites processing, which is interesting from an industrial point of view. CNC fillers can be classically introduced in dried form (solid feeding), or in suspension (liquid feeding). In the liquid feeding strategy, a well-dispersed suspension of CNCs is directly pumped, improving the final CNCs dispersion in the extruded material. Oksman *et al.*²²⁸ were the first to

prepare CNC/PLA nanocomposites by compounding extrusion, with 5 wt% of CNCs. A gravimetric feeding system was used to introduce the CNC suspension, whose solvent phase was removed by evaporation under vacuum. This method allowed a better dispersion of CNCs in final nanocomposites. They added poly(ethylene glycol) to improve the CNCs dispersion and, as a consequence, the mechanical properties were also significantly improved (increase of 800% of elongation at break). One year later, Bondeson and Oksman¹⁶⁷ carried out the extrusion by introducing freeze-dried CNCs previously modified by adsorption with an anionic surfactant called Beycostat A B09 (**Figure I. 38 a**). The improvement of the nanofillers dispersion was highlighted, as well as, the nanocomposite mechanical properties. **Figure I. 38 a**) confirms this improvement of dispersion, as well as, tensile strength and elongation at break (**Figure I. 38 c**) when CNCs are introduced with the surfactant.

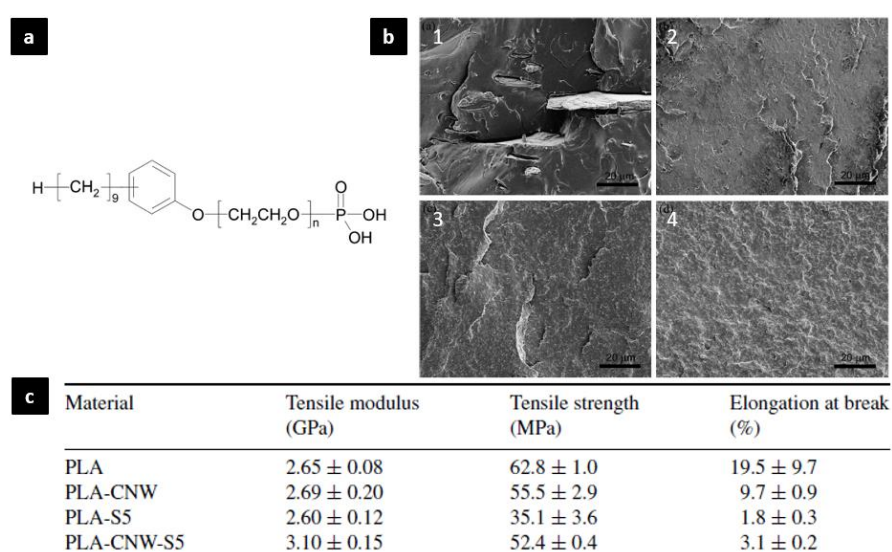


Figure I. 38. a) Acid phosphate ester of ethoxylated nonylphenol anionic surfactant (Beycostat A B09) adsorbed on CNCs, **b**) TEM images of nanocomposites fractured surfaces : 1) unmodified CNCs(5 wt%)/PLA, 2) CNCs (5 wt%) + Surfactant (5 wt%) / PLA, 3) CNCs (5 wt%) + Surfactant (10 wt%) / PLA and 4) CNCs (5 wt%) + Surfactant (20 wt%) / PLA, and **c**) Some mechanical properties of neat PLA, unmodified CNCs (5 wt%) /PLA (PLA-CNW), PLA with 5 wt% of surfactant (PLA-S5) and CNCs (5 wt%) + Surfactant (5 wt%) / PLA (PLA-CNW-S5) (extracted from¹⁶⁷)

The same research team investigated, the same year, the production of PLA/CNC nanocomposite by liquid feeding method²²⁹. First, they mixed CNCs and PVOH, and introduced the mixture directly during extrusion process. In order to prevent the challenging removal of water, they used different venting systems. Although CNCs were essentially located in the PVOH area, the improvement of CNCs dispersion and mechanical properties were highlighted. Nevertheless, PVOH reinforcement, at the cost of that of PLA, was proved.

More recently, Yang *et al.*²³⁰ performed reactive extrusion, in order to modify *in situ* the PLA with glycidyl methacrylate, following a masterbatch approach to produce CNC/PLA nanocomposites. Tensile strength and modulus increased by 22% and 19%, respectively, confirming the efficiency of the method. Dhar *et al.*²³¹ carried out reactive extrusion, by grafting CNCs onto PLA, using a crosslinking reagent (dicumyl peroxide, DCP). Briefly, dried PLA pellets were sprayed with DCP and

mixed with 3 wt% freeze-dried CNCs, and the mixture was extruded. The compatibilization between the PLA and the CNCs was enhanced, as well as, the ensuing mechanical properties, with an increasing in tensile strength and Young's modulus of 41 and 490%, respectively. Moreover, the crystallinity was also improved, probably because of the presence of amorphous PLA chains on crystalline CNCs, which also act as nucleating surface. In order to improve the CNCs dispersion, Arias *et al.*²³² have developed a two-step strategy, in which they first freeze-dried a poly(ethylene oxide) (PEO) solution containing CNCs, and then extruded the ensuing encapsulated CNCs into PEO with PLA. CNCs were well-dispersed in the nanocomposites, and the authors assumed that miscibility between PEO and PLA, in a certain composition, positively influenced this dispersion.

The **electrospinning** is usually performed to produce polymer nanofibers. Briefly, by the action of electrostatic forces, polymer filaments from a polymer solution are formed, principally due to the evaporation of the solvent. Xiang *et al.*²³³ were the first to use electrospinning to produce CNC/PLA nanocomposites, with amounts of CNCs equal to 1 or 10 wt%. After having proved the presence of CNCs on the surface of nanofibers, they assumed that the CNCs behaved as nucleation agent, inducing an increase in the fibers crystallinity. Nevertheless, they noted a poor adhesion between CNCs and PLA, correlated with the theory. Shi *et al.*²³⁴ investigated the electrospinning of CNC/PLA nanocomposites from a mixture of DMF and chloroform. Efficient processing was highlighted, as well as, the improvement of the mechanical properties of electrospun fibers. **Figure I. 39** shows SEM images of the fibers produced with different amount of nanofillers. Although thermal and mechanical properties of nanofibers were improved, they proved the presence of CNC aggregates too, leading to heterogeneity of morphology and properties of fibers.

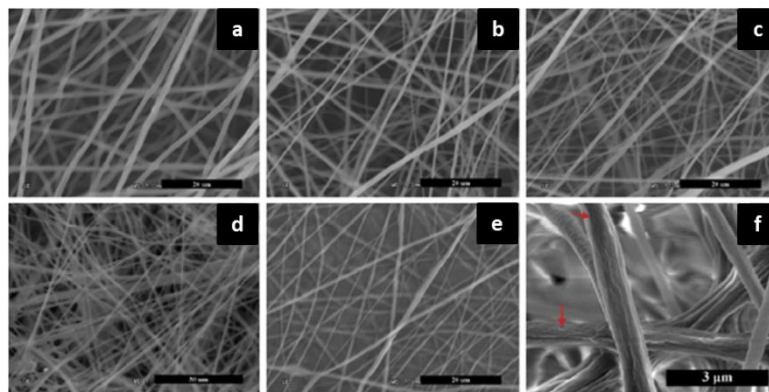


Figure I. 39. SEM images of electrospun nanocomposites fibers : PLA with **a)** 0 wt%, **b)** 1 wt%, **c)** 2 wt%, **d)** 5 wt%, **e)** 10 wt%, and **f)** 5 wt% (higher magnification) of CNCs (extracted from ²³⁴)

The **casting / evaporation** technique is commonly used at the laboratory level. A dispersed CNC suspension is introduced in a polymer solution, and the mixture is poured into a dish in order to evaporate the solvent. Thus, the dispersion of CNCs can be better conserved. It is important to have in mind that the prepared casted nanocomposite films are not fully representative of nanocomposites prepared at larger scale, by extrusion for example. Nevertheless, this efficient process is widely used

in the literature, especially to compare compatibilization between different kinds of CNCs. As schematized in **Figure I 37**, several systems exist, according to the matrix polymer: emulsion, hydrosoluble or non-hydrosoluble, and hydrodispersible and non-hydrodispersible systems. In hydrosoluble systems, the initial CNC aqueous suspension is well-dispersed, and CNCs are compatible with the host matrix which leads to well dispersed final systems, even if the water evaporation remains the main issue. In the case of CNC/PLA nanocomposite, the non-hydrosoluble system is a challenge which has to be overcome. Generally, previous surface modification is needed to enhance the compatibility and thus the adhesion between CNCs and PLA.

Various CNCs surface chemical modifications can be performed, as previously detailed in section 2.3. Adsorption and covalent grafting of molecules, macromolecules or polymers on CNCs for CNC/PLA nanocomposites have already been performed in the literature. The adsorption of surfactant, especially the Beycostat A B09, as previously described, can improve the CNCs dispersion after extrusion. The results obtained by Fortunati *et al.*²³⁵ showed that nanocomposites produced with same anionic surfactant adsorbed on CNCs, and performed by casting method, exhibited enhanced CNCs dispersion. The polymerization of PLA on CNCs surface by grafting-from method — especially by ring-opening polymerization — has been widely investigated. Recently, Miao and Hamad¹⁸⁶ have performed a similar polymerization of PLA on CNCs and produced CNC-g-PLA/PLA nanocomposites by both casting and extrusion methods. Free PLA used as matrix aimed to avoid the CNC-g-PLA aggregation and improved the interfacial adhesion between CNC-g-PLA and PLA homopolymer. **Figure I. 40 b**), **c**) and **d**) confirms the uniform dispersion of CNC in the PLA matrix. Moreover, the significant decrease of OTR values, presented in **Figure I. 40 a**), highlights the barrier effect induced by the presence of dispersed nanofillers in the PLA matrix.

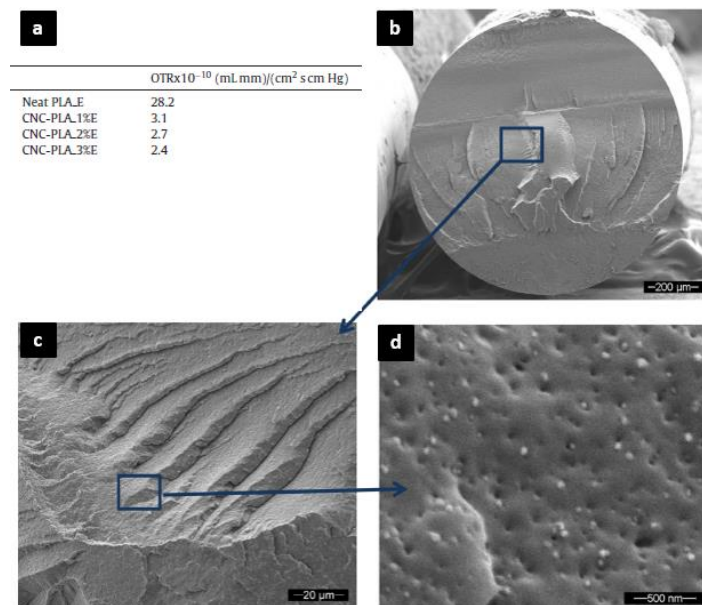


Figure I. 40. **a**) OTR (normalized with materials thickness) of unmodified PLA (neat PLA_E) and CNC/PLA with 1, 2 and 3 wt% of CNC-g-PLA (CNC-PLA_1%E, CNC-PLA_2%E and CNC-PLA_3%E), **b**) **c**) and **d**) SEM images of co-extruded CNC-g-PLA/PLA nanocomposites with 3 wt% CNC-g-PLA at different magnifications (extracted from ¹⁸⁶)

Similarly, the polymerization using same grafting-from procedure *via* the ROP of polycaprolactone (PCL) on CNCs was investigated by Lin *et al.*²³⁶ The polymerization was microwave assisted, and polymerized CNC-g-PCL was casted with a PLA solution. An optimal amount of 8 wt% of loaded CNCs was found, and the mechanical properties of the final nanocomposites were highly improved. According to this study, the grafted flexible PCL chains allow transferring a mechanical stress to the rigid reinforcing CNCs elements. Numerous other grafting of various compounds can be found in literature, as presented in **Table I. 10**. Indeed, acetylation, carbamylation, or other esterifications have been performed *via* classical methods, to enhance the compatibilization of CNCs with hydrophobic PLA. Generally, grafted molecules are composed of long aliphatic chains^{237,238} or other hydrophobic chemical groups.

	Surface modification type	Grafted compound	CNCs wt% in PLA matrix	Nanocompo -site processing	Improved properties	Reference
CNC Functionalization	Adsorption	Anionic surfactant (Beycostat A B09)	5	Extrusion	CNCs dispersion Tensile modulus and strength Elongation at break	(Bondeson and Oksman, 2007) ¹⁶⁷
			5 (+1 wt% silver nanoparticles)	Extrusion + film formation process	CNCs dispersion Thermal and mechanical properties	(Fortunati <i>et al.</i> , 2012) ²³⁹
			1 or 5	Casting/evaporation	CNCs dispersion Crystallinity OTR (decrease of 26% or 48%) WVTR (decrease of 34% for 1% wt CNC)	(Fortunati <i>et al.</i> , 2012) ²³⁵
			5- 10 - 20	Extrusion and injection-molding (masterbatch approach)	CNCs dispersion Rheological properties	(Mariano <i>et al.</i> , 2017) ²⁴⁰
	Polymerization "Grafting-from" (ROP microwave assisted)	Polycaprolactone (PCL)	8	Casting/evaporation	Miscibility PLC chains / PLA matrix : CNCs dispersion Tensile strength and elongation	(Lin <i>et al.</i> , 2009) ²³⁶
	Acetylation	Anhydride acetic	6	Casting/evaporation	CNCs dispersion Interfacial adhesion CNC/PLA Thermal properties Crystallization	(Lin <i>et al.</i> , 2001) ¹⁴⁰
			3	Casting/evaporation	Interface CNC/PLA adhesion Tensile strength (increase of 20%)	(Xu <i>et al.</i> , 2016) ²⁴¹
	Urethanization (carbonylation)	n-octadecyl isocyanate	10	Casting combined with extrusion	Crystallization	(Bitinis <i>et al.</i> , 2013) ²³⁷
		Toluene diisocyanate	1 - 9	Casting/evaporation	CNCs dispersion Tensile strength	
	Polymerization "Grafting-from" (ROP)	PLA	10	Casting combined with extrusion	Crystallization	(Bitinis <i>et al.</i> , 2013) ²³⁷
			2.5 / 5 / 10	Melt-blending (mini-extruder)	Mechanical properties	(Habibi <i>et al.</i> , 2013) ²⁴²
			1	Melt-spinning	Interfacial adhesion CNC/PLA Thermal stability Mechanical properties	(Mujica-Garcia <i>et al.</i> , 2016) ²⁴³

			1 / 3	Extrusion	Crystallization Mechanical properties	(Lizundia <i>et al.</i> , 2016) ²⁴⁴
			1	Casting evaporation or extrusion	CNCs dispersion Barrier properties (WVTR and OTR improvement of 81% and 87%) Mechanical properties	(Miao et Hamad., 2016) ¹⁸⁶
			1	Extrusion (PLA/PCL blend)	Blend compatibilization Mechanical properties	(Sessini <i>et al.</i> , 2018) ¹⁸⁴
		Maleic acid	5	Electrospinning	Fibers uniformity Thermal stability Mechanical properties	(Zhou <i>et al.</i> , 2013) ²⁴⁵
	Esterification	Dodecanoyl chloride	2	Extrusion	Interaction CNC/PLA Tensile strength (increase of 25%) Thermal properties	(Robles <i>et al.</i> , 2015) ²³⁸
		Hydrocinnamic and phenylacetic acid (In situ solvent exchange)	2 / 6	Casting/evaporation	Compatibility CNC/PLA Barrier properties	(Espino Perez <i>et al.</i> , 2018) ¹⁸⁴
	Radical grafting	Glycidyl methacrylate	1 / 6	Masterbatches / Extrusion	Thermal resistance Mechanical properties	(Pracella <i>et al.</i> , 2014) ²⁴⁶
	Acid hydrolysis/Fischer esterification	HCl / Lactic acid	3 / 5	Extrusion	CNC dispersion Thermal properties	(Spinella <i>et al.</i> , 2015) ²⁴⁷
PLA functionalization	Radical grafting	Glycidyl methacrylate	1 / 6	Masterbatches / Extrusion	Thermal resistance Mechanical properties	(Pracella <i>et al.</i> , 2014) ²⁴⁶
	Reactive extrusion	Glycidyl methacrylate	1 (+15 wt% grafted PLA)	Masterbatches / Extrusion	Crystallization Tensile strength and modulus (improvement of 22% and 19%)	(Yang <i>et al.</i> , 2015) ²³⁰

Table I. 10. Main surface modifications performed on CNCs to enhance their compatibilization with PLA matrix, inducing improved nanocomposites properties and corresponding literature references

As seen in **Table I. 10**, studies are generally focused on the improvement of mechanical and thermal properties of nanocomposites, and a lower amount of publications deal with the barrier properties, which are still required for numerous packaging applications. **Figure I. 41** summarizes the main advances in CNC/PLA nanocomposites processing, and highlights the huge interest for such materials in scientific community.

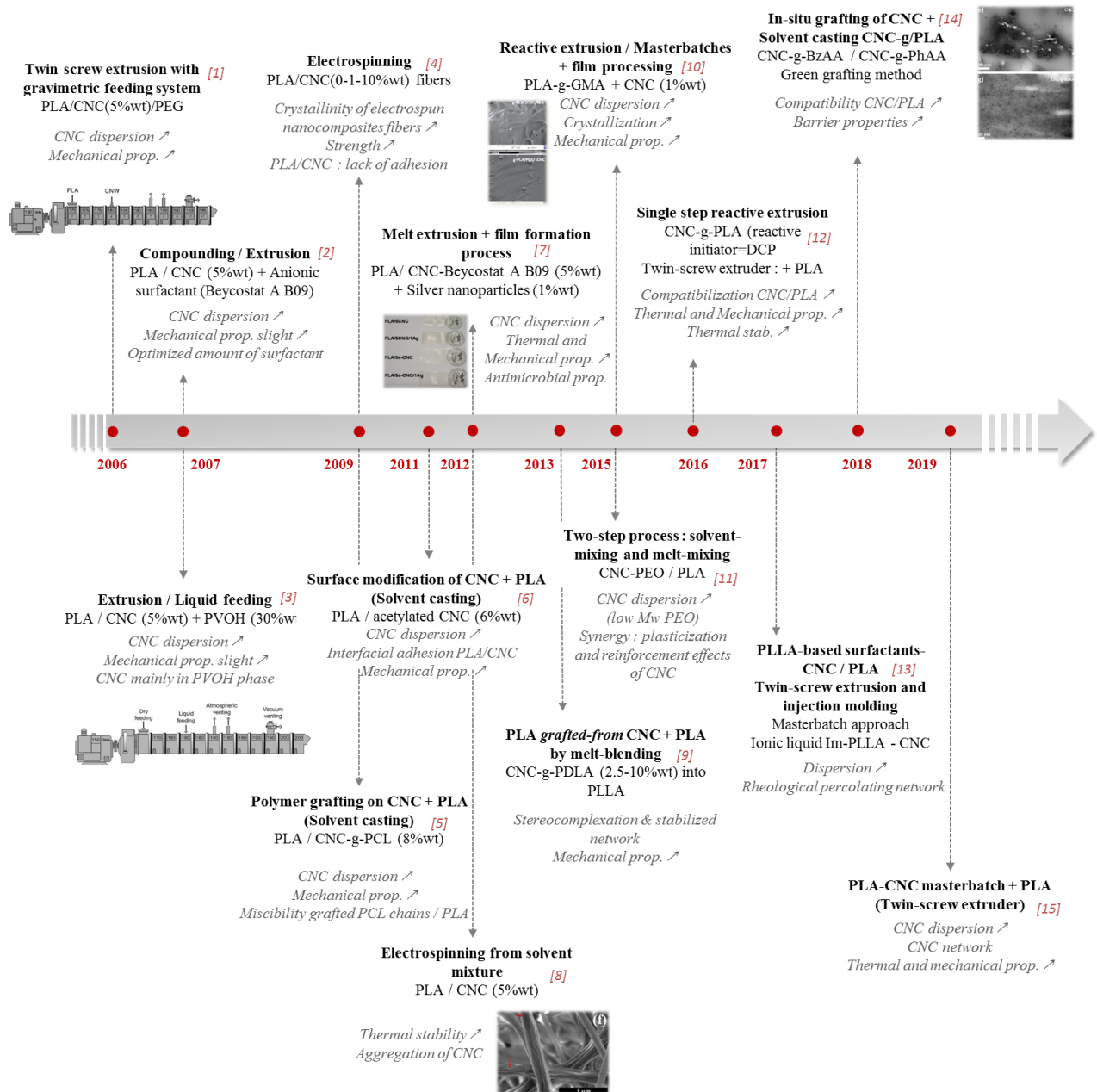


Figure I. 41. Some recent advances in CNC/PLA nanocomposites processing : [1] Twin-screw extrusion with gravimetric feeding system²²⁸, [2] Compounding / Extrusion¹⁶⁷, [3] Extrusion / Liquid feeding²²⁹, [4] Electrospinning²³³, [5] Polymer grafting on CNC + PLA (Solvent casting)²³⁶, [6] Surface modification of CNC + PLA (Solvent casting)¹⁴⁰, [7] Melt extrusion + film formation²³⁹, [8] Electrospinning from solvent mixture²³⁴, [9] PLA grafted-from CNC + PLA by melt-blending²⁴², [10] Reactive extrusion / Masterbatches + film processing²³⁰, [11] Two-step process : solvent-mixing and melt-mixing²³², [12] Single step reactive extrusion²³¹, [13] PLLA-based surfactants-CNC/PLA Twin-screw extrusion and injection molding²⁴⁰, [14] In-situ grafting of CNC + Solvent casting CNC-g/PLA¹⁸⁴, [15] PLA-CNC masterbatch + PLA (Twin-screw extruder)²⁴⁸

The elaboration of PLA/CNC nanocomposites with compatibilized CNCs is one of the main challenges of this PhD project. Although the casting/evaporation and extrusion methods are generally carried out, the development of multi-layered materials including CNCs and PLA structures is also investigated. The following part focuses on the state of the art associated to these multi-phase materials.

3.3. Multi-layered CNC-based materials

3.3.1. Interest of nanocellulose-based multi-layered packaging materials

In order to improve the polymer properties — especially for food packaging applications with required specific mechanical, thermal and, barrier properties — three main strategies are possible: i) the elaboration of (nano)composites, ii) the blending of different polymers, and iii) the elaboration of multi-layered materials. The first i) has been previously detailed (section 3.2). The second ii) is widely used in packaging industry, but is not described in this literature review. Here, we are concerned with the third iii) strategy, which has widely industrially increased over the past few years. This strategy consists in the incorporation of one or multiple layer(s) — generally more with enhance barrier properties when compared with those of the initial polymer — in order to improve final barrier and mechanical properties of the material. **Figure I. 42** schematizes the transport of gas molecules (O_2 , CO_2 etc.) through a material with an inner barrier layer.

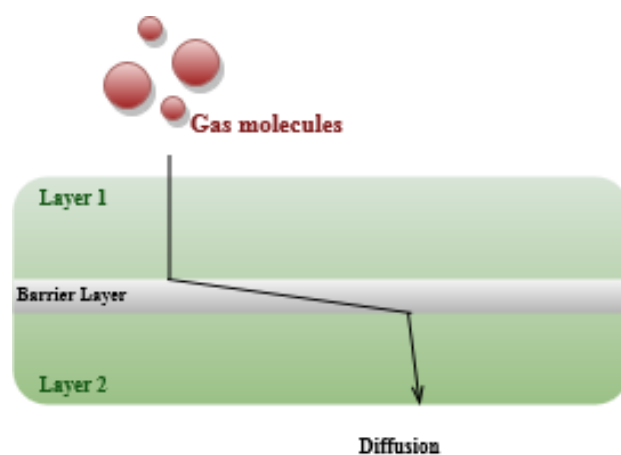


Figure I. 42. Schematized representation of gas molecules diffusion pathway through a simple multi-layered material

As shown in **Figure I. 42**, the transport of gas molecules is longer, since the barrier layer significantly slowed the molecules diffusion. By comparison with a nanocomposite material inducing a discontinuous barrier (**Figure I. 36**), barrier properties are improved by the presence of a continuous layer, in the present case²²². Furthermore, the mechanical properties can also be enhanced, according to the properties of the inner layer(s). The composition of layers has thus to be selected taking into account the required properties of the final packaging.

Different technologies allow processing of such multi-layered materials. The most developed techniques are layer-by-layer (LbL) deposition, electrohydrodynamic processing (EHDP), microlayer co-extrusion, and coating²²². In all cases, a thin layer of a selected material can be applied on a polymeric substrate, and another film can added in order to form a “sandwich” structure. Briefly, LbL is a promising technique, since it allows the deposition of a thin nanomaterials film on a substrate, by conserving a nanoscale organization. Podslidlo *et al.*¹⁶⁸ were among the first to deposit thin layers of

CNCs on poly(diallyldimethylammonium chloride) using the LbL technology. All these processing strategies have the same challenges, like the compatibility between all the materials, explaining the addition of adhesive layers in most cases. Moreover, the recycling issue is another challenge, since layers with different composition generally don't require the same recyclability processes.

Introduction of nanocelluloses-based layers is highly interesting. Indeed, due to the entrapped nanostructured network once nanocelluloses are dried, as well as, their outstanding mechanical properties, final properties of the multi-layered material can be significantly enhanced, and the use of adhesive is not always needed, since the adhesion of nanomaterials with surrounding layers can act as an adhesive. Note that for now, only micro-sized structures have been industrially developed (by extrusion coating or lamination). In this sense, the development of multi-layered materials including nanostructures is highly challenging. Moreover, the interest of such multi-layered materials including nanocellulosic materials and poly(lactic acid) makes sense, since the barrier and mechanical properties of PLA can thus be enhanced, and get close to those of traditional packaging polymers. Nevertheless, the incompatibility between hydrophobic PLA and hydrophilic CNCs is still a huge issue.

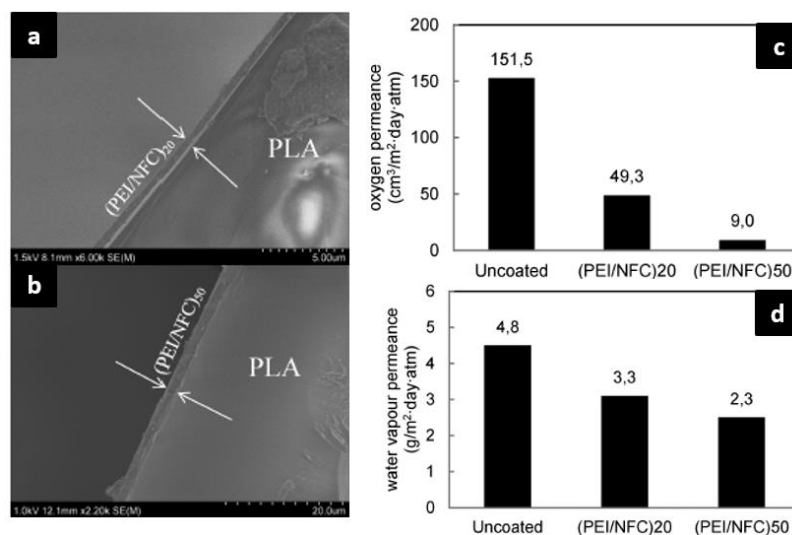


Figure I. 43. SEM images of cross-sections of LbL deposition of **a)** 20 layers and **b)** 50 layers of NFC/PEI, **c)** oxygen permeance and **d)** water vapor permeance of CNF/PEI coated on PLA (extracted from ²⁴⁹)

Regarding the literature, Aulin *et al.*²⁴⁹ performed layer-by-layer deposition of cellulose nanofibrils (CNFs) combined with a cationic polymer polyethyleneimine (PEI) on a PLA substrate. After having proved the efficient deposition of the PEI/CNF mixture onto PLA, they concluded about the improvement of the barrier properties (towards both oxygen and water vapor) of the final coated materials, as presented in **Figure I. 43**. In this case, even if CNFs were used, it is possible to draw a parallel with a possible behavior of CNCs. This promising study was confirmed by the work of Meriçer *et al.*²⁵⁰. Thus, the authors developed multi-layered PLA/MFC (microfibrillated cellulose) structures by casting evaporation of both layers, and concluded also about the improvement of the mechanical and barrier properties, as shown in **Figure I. 44**.

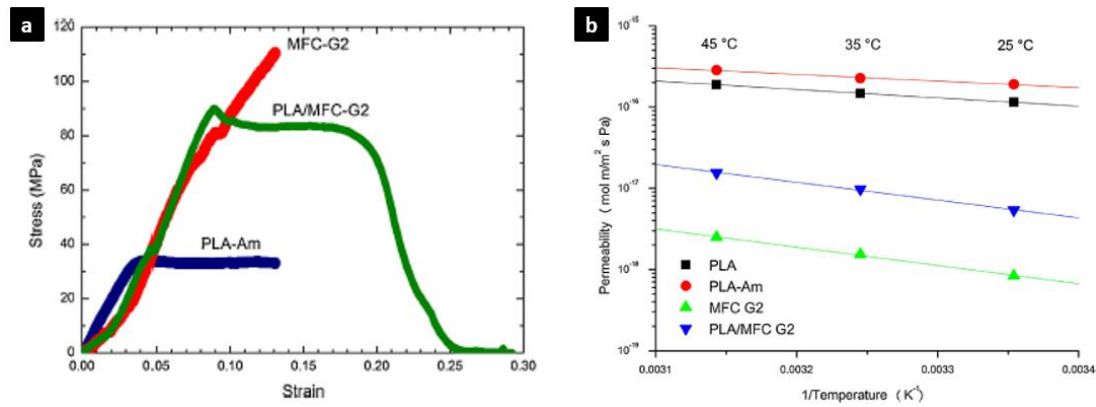


Figure I. 44. a) Stress-strain curves and b) oxygen permeability (different temperatures, RH=0%) of amorphous or crystalline PLA film (PLA-Am or PLA), MFC self-standing film (MFC G2) and PLA/MFC multi-layered film (PLA/MFC G2) (extracted from ²⁵⁰)

Thus, only few researches focused on multi-layered materials based on the introduction of nanocelluloses layers. However, they all concluded about the improvement of barrier and mechanical properties of the final materials.

The multi-layered strategy is encouraging for the development of new renewable food packaging materials, by potentially improving the properties of bio-based polymers. Moreover, active packaging materials can be produced through this strategy, as presented in the following part.

3.3.2. Absorbers and scavenging properties

Active packaging concept was described in previous section 1.2.3. Moisture or specific compound absorbers, as well as, antimicrobial or antioxidant agents are some examples of active compounds aiming to improve specificities of a food packaging. A recent and complete review reported by Yildirim *et al.*²⁵¹ summarizes the active compounds according to their properties for active food packaging. Other macromolecules exist, like calixarenes — modified or not — which present large cavities, able to entrap gas molecules like CO₂, and thus to slow their diffusion through a packaging. Such molecules have already been immobilized onto a cellulosic substrate surface, and the entrapment of nitrogen oxide molecules were proved²⁵².

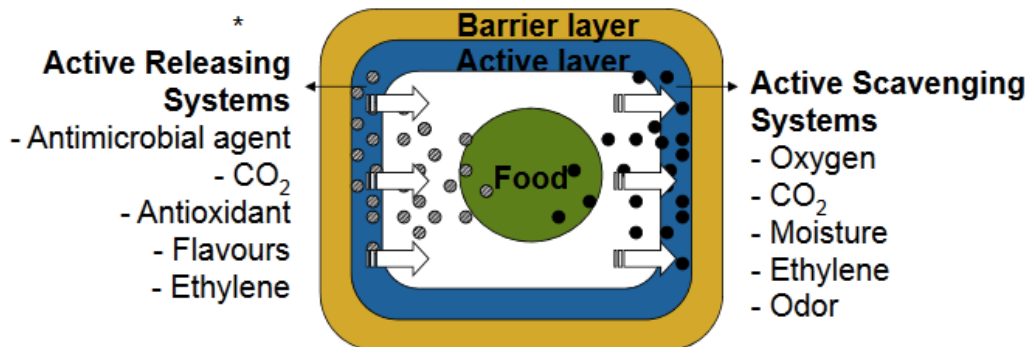


Figure I. 45. General principle of an active packaging (extracted from ²⁵³)

Distinctions between absorbers (scavenging systems) and emitter (releasing systems) are clear. **Figure I. 45** schematizes the behavior of an active packaging, with the two different systems, and the presence of an active layer is visible. Indeed, active compounds are generally introduced in multi-layered structure, in order to be released inside the packaging or to scavenge specific molecules from food products. In such a strategy, the presence of both nanocellulose and active compound in the active layer allow their entrapment or their possible release. In the literature, CNCs have been mixed with silver nanoparticles²³⁹ for antibacterial activity or with carvacrol²⁵⁴ for antioxidant for example. Even if nanocomposites were the aim of these studies, multi-layered strategies can also be considered.

In this third part, the introduction of cellulose nanocrystals in a polymeric matrix, and especially in PLA, was detailed. The outstanding final barrier and mechanical properties of the materials are encouraging and open the door to new composites or multi-layered systems including nanocelluloses, whose compatibilization with the matrix is still a challenge.

Conclusions of Chapter I

This chapter highlights the outstanding properties of cellulose nanocrystals (CNCs) for a wide range of applications. In particular, in current environmental context, in which bio-based materials are of high interest, cellulose nanocrystals can be combined with biobased poly(lactic acid) (PLA), in order to produce novel multi-component materials, especially for food packaging applications. Indeed, mechanical and barrier properties of PLA can thus be enhanced, and be competitive with those of traditional fossil-based polymers.

The main challenge emerging of this first chapter is the poor compatibility between hydrophilic CNCs and hydrophobic PLA. In this sense, CNCs have to be modified in order to improve their adhesion with the PLA.

This point is the main objective of this PhD project: the chemical modification of CNCs, in order to produce original PLA-based materials with improved barrier properties. Moreover, the use of toxic chemicals will be reduced as far as possible, in order to be consistent with environmental concerns.

References – Chapter I

1. PlasticsEurope. *PlasticsEurope Market Research Group (PEMRG) (2016)*.
2. Euromonitor International. *Euromonitor International Market Research (2015)*.
3. REXAM annual report. <https://www.companyreporting.com/sites/default/files/accounts/12.12-rexam-2011.pdf> (2011).
4. Alaerts, L., Augustinus, M. & Van Acker, K. Impact of Bio-Based Plastics on Current Recycling of Plastics. *Sustainability* **10**, 1487 (2018).
5. Karan, H., Funk, C., Grabert, M., Oey, M. & Hankamer, B. Green Bioplastics as Part of a Circular Bioeconomy. *Trends in Plant Science* **24**, 237–249 (2019).
6. Geyer, R., Jambeck, J. R. & Law, K. L. Production, use, and fate of all plastics ever made. *Science Advances* **3**, 1700782 (2017).
7. Petersen, K. *et al.* Potential of biobased materials for food packaging. *Trends in Food Science & Technology* **10**, 52–68 (1999).
8. Helanto, K., Matikainen, L., Talja, R. & Rojas, O. J. Bio-based Polymers for Sustainable Packaging and Biobarriers: A Critical Review. *BioResources* **14**, 1-50 (2019).
9. European Standard EN 13432. Requirements for packaging recoverable through composting and biodegradation – Test scheme and evaluation criteria for the final acceptance of packaging (2000).
10. Paine, F. A. *The packaging user's handbook*. (New York: AVI, 1991).
11. Robertson, G. L. *Food packaging: principles and practice*. (CRC press, 2005).
12. Siracusa, V., Rocculi, P., Romani, S. & Rosa, M. D. Biodegradable polymers for food packaging: a review. *Trends in Food Science & Technology* **19**, 634–643 (2008).
13. Schmid, M. *et al.* Properties of Whey-Protein-Coated Films and Laminates as Novel Recyclable Food Packaging Materials with Excellent Barrier Properties. *International Journal of Polymer Science* **2012**, 1–7 (2012).
14. Oliveira, M. *et al.* Application of modified atmosphere packaging as a safety approach to fresh-cut fruits and vegetables – A review. *Trends in Food Science & Technology* **46**, 13–26 (2015).
15. Lee, L., Arul, J., Lencki, R. & Castaigne, F. A review on modified atmosphere packaging and preservation of fresh fruits and vegetables: Physiological basis and practical aspects—part II. *Packaging Technology and Science* **9**, 1–17 (1996).
16. Sandhya. Modified atmosphere packaging of fresh produce: Current status and future needs. *LWT - Food Science and Technology* **43**, 381–392 (2010).
17. Crompton, T. R. *Physical testing of plastics* (Smithers Rapra, 2012).
18. Yam, K. L., Takhistov, P. T. & Miltz, J. Intelligent Packaging: Concepts and Applications. *Journal of Food Science* **70**, R1–R10 (2005).
19. Ghaani, M., Cozzolino, C. A., Castelli, G. & Farris, S. An overview of the intelligent packaging technologies in the food sector. *Trends in Food Science & Technology* **51**, 1–11 (2016).
20. Poyatos-Racionero, E., Ros-Lis, J. V., Vivancos, J.-L. & Martínez-Máñez, R. Recent advances on intelligent packaging as tools to reduce food waste. *Journal of Cleaner Production* **172**, 3398–3409 (2018).
21. Miltz, J., Passy, N. & Mannheim, C. Trends and applications of active packaging systems. *Special Publication-Royal Society of Chemistry* **162**, 201–201 (1995).
22. Institute for Bioplastics and Composites. *Biopolymers facts and statistics*. https://www.ifbb-hannover.de/files/IfBB/downloads/faltblaetter_broschueren/Biopolymers-Facts-Statistics-2018.pdf (2016).
23. Farmer, N. *Trends in packaging of food, beverages and other fast-moving consumer goods (FMCG): markets, materials and technologies*. (Elsevier, 2013).
24. Jiménez, A., Peltzer, M. & Ruseckaite, R. *Poly(lactic acid) science and technology processing, properties, additives and applications*. (Royal Society of Chemistry, 2015).
25. Hottle, T. A., Bilec, M. M. & Landis, A. E. Biopolymer production and end of life comparisons using life cycle assessment. *Resources, Conservation and Recycling* **122**, 295–306 (2017).
26. Spierling, S. *et al.* Bio-based plastics - A review of environmental, social and economic impact assessments. *Journal of Cleaner Production* **185**, 476–491 (2018).

27. Castro-Aguirre, E., Iñiguez-Franco, F., Samsudin, H., Fang, X. & Auras, R. Poly(lactic acid)—Mass production, processing, industrial applications, and end of life. *Advanced Drug Delivery Reviews* **107**, 333–366 (2016).
28. Yates, M. R. & Barlow, C. Y. Life cycle assessments of biodegradable, commercial biopolymers—A critical review. *Resources, Conservation and Recycling* **78**, 54–66 (2013).
29. Belgacem, M. N. & Gandini, A. *Monomers, polymers and composites from renewable resources*. (Elsevier, 2008).
30. Garlotta, D. A Literature Review of Poly(Lactic Acid). *Journal of Polymers and the Environment* **9**, 63-842 (2001).
31. Penu, C. & Helou, M. *Acide polylactique (PLA)*. (Techniques de l'Ingénieur, 2017).
32. Colomines, G., Ducruet, V., Courgneau, C., Guinault, A. & Domenek, S. Barrier properties of poly(lactic acid) and its morphological changes induced by aroma compound sorption. *Polymer International* **59**, 818-826 (2010).
33. Auras, R. A., Singh, S. P. & Singh, J. J. Evaluation of oriented poly(lactide) polymers vs. existing PET and oriented PS for fresh food service containers. *Packaging Technology and Science* **18**, 207–216 (2005).
34. Willige, R. W. G. van, Linssen, J. P. H., Meinders, M. B. J., Stege, H. J. van der & Vorage, A. G. J. Influence of flavour absorption on oxygen permeation through LDPE, PP, PC and PET plastics food packaging. *Food Additives & Contaminants* **19**, 303–313 (2002).
35. Dumont, M.-J., Reyna-Valencia, A., Emond, J.-P. & Bousmina, M. Barrier properties of polypropylene/organoclay nanocomposites. *Journal of Applied Polymer Science* **103**, 618–625 (2007).
36. Raquez, J.-M., Ramy-Ratiarison, R., Murariu, M. & Dubois, P. *Reactive Extrusion of PLA-based Materials: from Synthesis to Reactive Melt-blending*. In: *Poly(lactic acid) Science and Technology: Processing, Properties, Additives and Applications* (Royal Society of Chemistry, 2014).
37. Vergnes, B. & Chapet, M. *Extrusion - Procédés d'extrusion bisis*. (Techniques de l'Ingénieur, 2001).
38. Murariu, M. & Dubois, P. PLA composites: From production to properties. *Advanced Drug Delivery Reviews* **107**, 17–46 (2016).
39. Giessmann, A. *Coating Substrates and Textiles - A Practical Guide to Coating and Laminating Technologies*. (Springer Science & Business Media, 2012).
40. Reis, M. O. *et al.* Biodegradable trays of thermoplastic starch/poly (lactic acid) coated with beeswax. *Industrial Crops and Products* **112**, 481–487 (2018).
41. Pierleoni, D. *et al.* Graphene-based coatings on polymer films for gas barrier applications. *Carbon* **96**, 503–512 (2016).
42. Goh, K. *et al.* Sandwich-Architected Poly(lactic acid)–Graphene Composite Food Packaging Films. *ACS Applied Materials & Interfaces* **8**, 9994–10004 (2016).
43. Rocca-Smith, J. R. *et al.* Impact of corona treatment on PLA film properties. *Polymer Degradation and Stability* **132**, 109–116 (2016).
44. Meesorn, W., Calvino, C., Natterodt, J. C., Zoppe, J. O. & Weder, C. Bio-Inspired, Self-Toughening Polymers Enabled by Plasticizer-Releasing Microcapsules. *Advanced Materials* **31**, 1807212 (2019).
45. R. Snowdon, M., Wu, F., K. Mohanty, A. & Misra, M. Comparative study of the extrinsic properties of poly(lactic acid)-based biocomposites filled with talc versus sustainable biocarbon. *RSC Advances* **9**, 6752–6761 (2019).
46. Ouchiar, S. *et al.* Comparison of the influence of talc and kaolinite as inorganic fillers on morphology, structure and thermomechanical properties of polylactide based composites. *Applied Clay Science* **116–117**, 231–240 (2015).
47. Sang, L., Han, S., Li, Z., Yang, X. & Hou, W. Development of short basalt fiber reinforced polylactide composites and their feasible evaluation for 3D printing applications. *Composites Part B: Engineering* **164**, 629–639 (2019).
48. Kyutoku, H., Maeda, N., Sakamoto, H., Nishimura, H. & Yamada, K. Effect of surface treatment of cellulose fiber (CF) on durability of PLA/CF bio-composites. *Carbohydrate Polymers* **203**, 95–102 (2019).
49. Aliotta, L., Gigante, V., Coltelli, M. B., Cinelli, P. & Lazzeri, A. Evaluation of Mechanical and Interfacial Properties of Bio-Composites Based on Poly(Lactic Acid) with Natural Cellulose Fibers. *International Journal of Molecular Sciences* **20**, 960 (2019).

50. Khan, G. M. A., Terano, M., Gafur, M. A. & Alam, M. S. Studies on the mechanical properties of woven jute fabric reinforced poly(l-lactic acid) composites. *Journal of King Saud University - Engineering Sciences* **28**, 69–74 (2016).
51. Jozala, A. F. *et al.* Bacterial nanocellulose production and application: a 10-year overview. *Appl Microbiol Biotechnol* **100**, 2063–2072 (2016).
52. Varshney, V. K. & Naithani, S. *Chemical Functionalization of Cellulose Derived from Nonconventional Sources*. In: *Cellulose Fibers: Bio- and Nano-Polymer Composites* (Springer Berlin Heidelberg, 2011).
53. Suhas *et al.* Cellulose: A review as natural, modified and activated carbon adsorbent. *Bioresource Technology* **216**, 1066–1076 (2016).
54. Nechyporchuk, O., Belgacem, M. N. & Bras, J. Production of cellulose nanofibrils: A review of recent advances. *Industrial Crops and Products* **93**, 2–25 (2016).
55. Klemm, D., Heublein, B., Fink, H.-P. & Bohn, A. Cellulose: Fascinating Biopolymer and Sustainable Raw Material. *Angewandte Chemie International Edition* **44**, 3358–3393 (2005).
56. O’Sullivan, A. C. Cellulose: the structure slowly unravels. *Cellulose* **4**, 173–207 (1996).
57. Habibi, Y. Key advances in the chemical modification of nanocelluloses. *Chem. Soc. Rev.* **43**, 1519–1542 (2014).
58. Dufresne, A. *Nanocellulose: from nature to high performance tailored materials*. (Walter de Gruyter GmbH & Co KG, 2017).
59. Capron, I., Rojas, O. J. & Bordes, R. Behavior of nanocelluloses at interfaces. *Current Opinion in Colloid & Interface Science* **29**, 83–95 (2017).
60. Moon, R. J., Martini, A., Nairn, J., Simonsen, J. & Youngblood, J. Cellulose nanomaterials review: structure, properties and nanocomposites. *Chemical Society Reviews* **40**, 3941–3994 (2011).
61. Herrick, F. W., Casebier, R. L., Hamilton, J. K. & Sandberg, K. R. Microfibrillated cellulose: morphology and accessibility. *J. Appl. Polym. Sci.: Appl. Polym. Symp.; (United States)* **37**, (1983).
62. Turbak, A. F., Snyder, F. W. & Sandberg, K. R. Microfibrillated cellulose, a new cellulose product: properties, uses, and commercial potential. *J. Appl. Polym. Sci.: Appl. Polym. Symp.; (United States)* **37**, (1983).
63. Naderi, A., Lindström, T. & Sundström, J. Repeated homogenization, a route for decreasing the energy consumption in the manufacturing process of carboxymethylated microfibrillated cellulose? *Cellulose* **22**, 1147–1157 (2015).
64. Jonoobi, M. *et al.* Different preparation methods and properties of nanostructured cellulose from various natural resources and residues: a review. *Cellulose* **22**, 935–969 (2015).
65. Osong, S. H., Norgren, S. & Engstrand, P. Processing of wood-based microfibrillated cellulose and nanofibrillated cellulose, and applications relating to papermaking: a review. *Cellulose* **23**, 93–123 (2016).
66. Iwamoto, S., Nakagaito, A. N. & Yano, H. Nano-fibrillation of pulp fibers for the processing of transparent nanocomposites. *Appl. Phys. A* **89**, 461–466 (2007).
67. Josset, S. *et al.* Energy consumption of the nanofibrillation of bleached pulp, wheat straw and recycled newspaper through a grinding process. *Nordic Pulp & Paper Research Journal* **29**, 167–175 (2014).
68. Abdul Khalil, H. P. S. *et al.* Production and modification of microfibrillated cellulose using various mechanical processes: A review. *Carbohydrate Polymers* **99**, 649–665 (2014).
69. Taipale, T., Österberg, M., Nykänen, A., Ruokolainen, J. & Laine, J. Effect of microfibrillated cellulose and fines on the drainage of kraft pulp suspension and paper strength. *Cellulose* **17**, 1005–1020 (2010).
70. Baati, R., Magnin, A. & Boufi, S. High Solid Content Production of Nanofibrillar Cellulose via Continuous Extrusion. *ACS Sustainable Chem. Eng.* **5**, 2350–2359 (2017).
71. Rol, F. *et al.* Pilot-Scale Twin Screw Extrusion and Chemical Pretreatment as an Energy-Efficient Method for the Production of Nanofibrillated Cellulose at High Solid Content. *ACS Sustainable Chem. Eng.* **5**, 6524–6531 (2017).
72. Wang, W. *et al.* Production of cellulose nanofibrils from bleached eucalyptus fibers by hyperthermostable endoglucanase treatment and subsequent microfluidization. *Cellulose* **22**, 351–361 (2015).
73. Sehaqui, H., Zhou, Q., Ikkala, O. & Berglund, L. A. Strong and Tough Cellulose Nanopaper with High Specific Surface Area and Porosity. *Biomacromolecules* **12**, 3638–3644 (2011).

74. Henriksson, M., Henriksson, G., Berglund, L. A. & Lindström, T. An environmentally friendly method for enzyme-assisted preparation of microfibrillated cellulose (MFC) nanofibers. *European Polymer Journal* **43**, 3434–3441 (2007).
75. Pääkkö, M. *et al.* Enzymatic Hydrolysis Combined with Mechanical Shearing and High-Pressure Homogenization for Nanoscale Cellulose Fibrils and Strong Gels. *Biomacromolecules* **8**, 1934–1941 (2007).
76. Liimatainen, H., Suopajarvi, T., Sirviö, J., Hormi, O. & Niinimäki, J. Fabrication of cationic cellulosic nanofibrils through aqueous quaternization pretreatment and their use in colloid aggregation. *Carbohydrate Polymers* **103**, 187–192 (2014).
77. Saini, S., Yücel Falco, Ç., Belgacem, M. N. & Bras, J. Surface cationized cellulose nanofibrils for the production of contact active antimicrobial surfaces. *Carbohydrate Polymers* **135**, 239–247 (2016).
78. Fukuzumi, H., Saito, T. & Isogai, A. Influence of TEMPO-oxidized cellulose nanofibril length on film properties. *Carbohydrate Polymers* **93**, 172–177 (2013).
79. Shinoda, R., Saito, T., Okita, Y. & Isogai, A. Relationship between Length and Degree of Polymerization of TEMPO-Oxidized Cellulose Nanofibrils. *Biomacromolecules* **13**, 842–849 (2012).
80. Fujisawa, S., Okita, Y., Fukuzumi, H., Saito, T. & Isogai, A. Preparation and characterization of TEMPO-oxidized cellulose nanofibril films with free carboxyl groups. *Carbohydrate Polymers* **84**, 579–583 (2011).
81. Tejado, A., Alam, Md. N., Antal, M., Yang, H. & van de Ven, T. G. M. Energy requirements for the disintegration of cellulose fibers into cellulose nanofibers. *Cellulose* **19**, 831–842 (2012).
82. Liimatainen, H., Visanko, M., Sirviö, J. A., Hormi, O. E. O. & Niinimäki, J. Enhancement of the Nanofibrillation of Wood Cellulose through Sequential Periodate–Chlorite Oxidation. *Biomacromolecules* **13**, 1592–1597 (2012).
83. Rol, F., Belgacem, M. N., Gandini, A. & Bras, J. Recent advances in surface-modified cellulose nanofibrils. *Progress in Polymer Science* **88**, 241–264 (2019).
84. Hubbe, M. A. *et al.* Nanocellulose in Thin Films, Coatings, and Plies for Packaging Applications: A Review. *BioResources* **12**, 2143–2233 (2017).
85. Ferrer, A., Pal, L. & Hubbe, M. Nanocellulose in packaging: Advances in barrier layer technologies. *Industrial Crops and Products* **95**, 574–582 (2017).
86. Siró, I. & Plackett, D. Microfibrillated cellulose and new nanocomposite materials: a review. *Cellulose* **17**, 459–494 (2010).
87. ISO/TC 6/TG 1 - Cellulose Nanomaterials. *Summary of International Activities on Cellulose Nanomaterials*. (2017).
88. Ranby, B. G. Fibrous macromolecular systems. Cellulose and muscle. The colloidal properties of cellulose micelles. *Discuss. Faraday Soc.* **11**, 158–164 (1951).
89. Ranby, B. G. & Ribí, E. Über den feinaufbau der zellulose. *Experientia* **6**, 12–14 (1950).
90. CelluForce. *CelluForce* <https://www.celluforce.com/en/technology/> (2016).
91. Cranston, E. Overview of Canada. *TAPPI Nano Division Conference* (Chiba, Japan, 2019).
92. Stevanic, J. S. *et al.* Bacterial nanocellulose-reinforced arabinoxylan films. *Journal of Applied Polymer Science* **122**, 1030–1039 (2011).
93. Fu, L., Zhang, J. & Yang, G. Present status and applications of bacterial cellulose-based materials for skin tissue repair. *Carbohydrate Polymers* **92**, 1432–1442 (2013).
94. Svensson, A. *et al.* Bacterial cellulose as a potential scaffold for tissue engineering of cartilage. *Biomaterials* **26**, 419–431 (2005).
95. Gatenholm, P. & Klemm, D. Bacterial Nanocellulose as a Renewable Material for Biomedical Applications. *MRS Bull.* **35**, 208–213 (2010).
96. Lima, M. M. de S. & Borsali, R. Rodlike Cellulose Microcrystals: Structure, Properties, and Applications. *Macromolecular Rapid Communications* **25**, 771–787 (2004).
97. Habibi, Y., Lucia, L. A. & Rojas, O. J. Cellulose Nanocrystals: Chemistry, Self-Assembly, and Applications. *Chemical Reviews* **110**, 3479–3500 (2010).
98. Camarero Espinosa, S., Kuhnt, T., Foster, E. J. & Weder, C. Isolation of Thermally Stable Cellulose Nanocrystals by Phosphoric Acid Hydrolysis. *Biomacromolecules* **14**, 1223–1230 (2013).
99. Chen, L. *et al.* Tailoring the yield and characteristics of wood cellulose nanocrystals (CNC) using concentrated acid hydrolysis. *Cellulose* **22**, 1753–1762 (2015).

100. Sadeghifar, H., Filpponen, I., Clarke, S. P., Brougham, D. F. & Argyropoulos, D. S. Production of cellulose nanocrystals using hydrobromic acid and click reactions on their surface. *J Mater Sci* **46**, 7344–7355 (2011).
101. Yu, H. *et al.* Facile extraction of thermally stable cellulose nanocrystals with a high yield of 93% through hydrochloric acid hydrolysis under hydrothermal conditions. *Journal of Materials Chemistry A* **1**, 3938–3944 (2013).
102. Sirviö, J. A., Visanko, M. & Liimatainen, H. Acidic Deep Eutectic Solvents As Hydrolytic Media for Cellulose Nanocrystal Production. *Biomacromolecules* **17**, 3025–3032 (2016).
103. Liu, Y. *et al.* Efficient Cleavage of Strong Hydrogen Bonds in Cotton by Deep Eutectic Solvents and Facile Fabrication of Cellulose Nanocrystals in High Yields. *ACS Sustainable Chem. Eng.* **5**, 7623–7631 (2017).
104. Flauzino Neto, W. P., Silvério, H. A., Dantas, N. O. & Pasquini, D. Extraction and characterization of cellulose nanocrystals from agro-industrial residue – Soy hulls. *Industrial Crops and Products* **42**, 480–488 (2013).
105. Johar, N., Ahmad, I. & Dufresne, A. Extraction, preparation and characterization of cellulose fibres and nanocrystals from rice husk. *Industrial Crops and Products* **37**, 93–99 (2012).
106. Beck-Candanedo, S., Roman, M. & Gray, D. G. Effect of Reaction Conditions on the Properties and Behavior of Wood Cellulose Nanocrystal Suspensions. *Biomacromolecules* **6**, 1048–1054 (2005).
107. Tang, J., Sisler, J., Grishkewich, N. & Tam, K. C. Functionalization of cellulose nanocrystals for advanced applications. *Journal of Colloid and Interface Science* **494**, 397–409 (2017).
108. Beck-Candanedo, S., Roman, M. & Gray, D. G. Effect of Reaction Conditions on the Properties and Behavior of Wood Cellulose Nanocrystal Suspensions. *Biomacromolecules* **6**, 1048–1054 (2005).
109. Lin, N., Huang, J. & Dufresne, A. Preparation, properties and applications of polysaccharide nanocrystals in advanced functional nanomaterials: a review. *Nanoscale* **4**, 3274–3294 (2012).
110. Klemm, D. *et al.* Nanocelluloses: A New Family of Nature-Based Materials. *Angewandte Chemie International Edition* **50**, 5438–5466 (2011).
111. Cheng, M., Chen, W. & Weerasooriya, T. Mechanical Properties of Kevlar® KM2 Single Fiber. *Journal of Engineering Materials and Technology* **127**, 197–203 (2005).
112. George, J. & Sabapathi, S. Cellulose nanocrystals: synthesis, functional properties, and applications. *Nanotechnol Sci Appl* **8**, 45–54 (2015).
113. Revol, J.-F., Bradford, H., Giasson, J., Marchessault, R. H. & Gray, D. G. Helicoidal self-ordering of cellulose microfibrils in aqueous suspension. *International Journal of Biological Macromolecules* **14**, 170–172 (1992).
114. Foster, E. J. *et al.* Current characterization methods for cellulose nanomaterials. *Chemical Society Reviews* **47**, 2609–2679 (2018).
115. Viet, D., Beck-Candanedo, S. & Gray, D. G. Dispersion of cellulose nanocrystals in polar organic solvents. *Cellulose* **14**, 109–113 (2007).
116. Beck, S., Bouchard, J., Chauve, G. & Berry, R. Controlled production of patterns in iridescent solid films of cellulose nanocrystals. *Cellulose* **20**, 1401–1411 (2013).
117. Mariano, M., Kissi, N. E. & Dufresne, A. Cellulose nanocrystals and related nanocomposites: Review of some properties and challenges. *Journal of Polymer Science Part B: Polymer Physics* **52**, 791–806 (2014).
118. Kaboorani, A. *et al.* Nanocrystalline cellulose (NCC): A renewable nano-material for polyvinyl acetate (PVA) adhesive. *European Polymer Journal* **48**, 1829–1837 (2012).
119. Mascheroni, E. *et al.* Comparison of cellulose nanocrystals obtained by sulfuric acid hydrolysis and ammonium persulfate, to be used as coating on flexible food-packaging materials. *Cellulose* **23**, 779–793 (2016).
120. Hoeng, F., Denneulin, A. & Bras, J. Use of nanocellulose in printed electronics: a review. *Nanoscale* **8**, 13131–13154 (2016).
121. Csoka, L. *et al.* Piezoelectric Effect of Cellulose Nanocrystals Thin Films. *ACS Macro Lett.* **1**, 867–870 (2012).
122. Gaspar, D. *et al.* Nanocrystalline cellulose applied simultaneously as the gate dielectric and the substrate in flexible field effect transistors. *Nanotechnology* **25**, 094008 (2014).
123. Karim, Z., Mathew, A. P., Grahn, M., Mouzon, J. & Oksman, K. Nanoporous membranes with cellulose nanocrystals as functional entity in chitosan: Removal of dyes from water. *Carbohydrate Polymers* **112**, 668–676 (2014).

124. Domingues, R. M. A., Gomes, M. E. & Reis, R. L. The Potential of Cellulose Nanocrystals in Tissue Engineering Strategies. *Biomacromolecules* **15**, 2327–2346 (2014).
125. Lin, N. & Dufresne, A. Nanocellulose in biomedicine: Current status and future prospect. *European Polymer Journal* **59**, 302–325 (2014).
126. Yang, X., Shi, K., Zhitomirsky, I. & Cranston, E. D. Cellulose Nanocrystal Aerogels as Universal 3D Lightweight Substrates for Supercapacitor Materials. *Advanced Materials* **27**, 6104–6109 (2015).
127. Kalashnikova, I., Bizot, H., Bertoncini, P., Cathala, B. & Capron, I. Cellulosic nanorods of various aspect ratios for oil in water Pickering emulsions. *Soft Matter* **9**, 952–959 (2013).
128. Tasset, S., Cathala, B., Bizot, H. & Capron, I. Versatile cellular foams derived from CNC-stabilized Pickering emulsions. *RSC Adv.* **4**, 893–898 (2014).
129. Zhang, Y. P. Nanocrystalline cellulose for covert optical encryption. *Journal of Nanophotonics* **6**, 063516 (2012).
130. Roman, M. Toxicity of Cellulose ecotoxicological Nanocrystals: A Review. *Industrial Biotechnology* **11**, 25–33 (2015).
131. Kovacs, T. *et al.* An characterization of nanocrystalline cellulose (NCC). *Nanotoxicology* **4**, 255–270 (2010).
132. Natterodt, J. C., Petri-Fink, A., Weder, C. & Zoppe, J. O. Cellulose Nanocrystals: Surface Modification, Applications and Opportunities at Interfaces. *CHIMIA International Journal for Chemistry* **71**, 376–383 (2017).
133. Wohlhauser, S. *et al.* Grafting Polymers from Cellulose Nanocrystals: Synthesis, Properties, and Applications. *Macromolecules* **51**, 6157–6189 (2018).
134. Kedzior, S. A., Zoppe, J. O., Berry, R. M. & Cranston, E. D. Recent advances and an industrial perspective of cellulose nanocrystal functionalization through polymer grafting. *Current Opinion in Solid State and Materials Science* **23**, 74–91 (2018).
135. Eyley, S. & Thielemans, W. Surface modification of cellulose nanocrystals. *Nanoscale* **6**, 7764–7779 (2014).
136. Habibi, Y., Chanzy, H. & Vignon, M. R. TEMPO-mediated surface oxidation of cellulose whiskers. *Cellulose* **13**, 679–687 (2006).
137. Peng, S. X., Chang, H., Kumar, S., Moon, R. J. & Youngblood, J. P. A comparative guide to controlled hydrophobization of cellulose nanocrystals via surface esterification. *Cellulose* **23**, 1825–1846 (2016).
138. Bendahou, A., Hajlane, A., Dufresne, A., Boufi, S. & Kaddami, H. Esterification and amidation for grafting long aliphatic chains on to cellulose nanocrystals: a comparative study. *Research on Chemical Intermediates* **41**, 4293–4310 (2015).
139. Spinella, S. *et al.* Concurrent Cellulose Hydrolysis and Esterification to Prepare a Surface-Modified Cellulose Nanocrystal Decorated with Carboxylic Acid Moieties. *ACS Sustainable Chemistry & Engineering* **4**, 1538–1550 (2016).
140. Lin, N., Huang, J., Chang, P. R., Feng, J. & Yu, J. Surface acetylation of cellulose nanocrystal and its reinforcing function in poly(lactic acid). *Carbohydrate Polymers* **83**, 1834–1842 (2011).
141. Espino-Pérez, E., Domenek, S., Belgacem, N., Sillard, C. & Bras, J. Green Process for Chemical Functionalization of Nanocellulose with Carboxylic Acids. *Biomacromolecules* **15**, 4551–4560 (2014).
142. Jasmani, L., Eyley, S., Wallbridge, R. & Thielemans, W. A facile one-pot route to cationic cellulose nanocrystals. *Nanoscale* **5**, 10207–10211 (2013).
143. Hemraz, U. D., Boluk, Y. & Sunasee, R. Amine-decorated nanocrystalline cellulose surfaces: synthesis, characterization, and surface properties. *Canadian Journal of Chemistry* **91**, 974–981 (2013).
144. Azzam, F., Heux, L., Putaux, J.-L. & Jean, B. Preparation By Grafting Onto, Characterization, and Properties of Thermally Responsive Polymer-Decorated Cellulose Nanocrystals. *Biomacromolecules* **11**, 3652–3659 (2010).
145. Filpponen, I. & Argyropoulos, D. S. Regular Linking of Cellulose Nanocrystals via Click Chemistry: Synthesis and Formation of Cellulose Nanoplatelet Gels. *Biomacromolecules* **11**, 1060–1066 (2010).
146. Araki, J., Wada, M. & Kuga, S. Steric Stabilization of a Cellulose Microcrystal Suspension by Poly(ethylene glycol) Grafting. *Langmuir* **17**, 21–27 (2001).
147. Gicquel, E., Martin, C., Heux, L., Jean, B. & Bras, J. Adsorption versus grafting of poly(N-Isopropylacrylamide) in aqueous conditions on the surface of cellulose nanocrystals. *Carbohydrate Polymers* **210**, 100–109 (2019).

148. Gousse, C., Chanzy, H., Excoffier, G., Soubeyrand, L. & Fleury, E. Stable suspensions of partially silylated cellulose whiskers dispersed in organic solvents. **43**, 2645–2651 (2002).
149. Grunert, M. & Winter, W. T. Nanocomposites of Cellulose Acetate Butyrate Reinforced with Cellulose Nanocrystals. *Journal of Polymers and the Environment* **10**, 27–30 (2002).
150. Dong, S. & Roman, M. Fluorescently Labeled Cellulose Nanocrystals for Bioimaging Applications. *J. Am. Chem. Soc.* **129**, 13810–13811 (2007).
151. Zaman, M., Xiao, H., Chibante, F. & Ni, Y. Synthesis and characterization of cationically modified nanocrystalline cellulose. *Carbohydrate Polymers* **89**, 163–170 (2012).
152. de Oliveira Taipina, M., Ferrarezi, M. M. F., Yoshida, I. V. P. & Gonçalves, M. do C. Surface modification of cotton nanocrystals with a silane agent. *Cellulose* **20**, 217–226 (2013).
153. Siqueira, G., Bras, J. & Dufresne, A. New Process of Chemical Grafting of Cellulose Nanoparticles with a Long Chain Isocyanate. *Langmuir* **26**, 402–411 (2010).
154. Habibi, Y. & Dufresne, A. Highly Filled Bionanocomposites from Functionalized Polysaccharide Nanocrystals. *Biomacromolecules* **9**, 1974–1980 (2008).
155. Kloser, E. & Gray, D. G. Surface Grafting of Cellulose Nanocrystals with Poly(ethylene oxide) in Aqueous Media. *Langmuir* **26**, 13450–13456 (2010).
156. Harrisson, S., Drisko, G. L., Malmström, E., Hult, A. & Wooley, K. L. Hybrid Rigid/Soft and Biologic/Synthetic Materials: Polymers Grafted onto Cellulose Microcrystals. *Biomacromolecules* **12**, 1214–1223 (2011).
157. Akhlaghi, S. P., Berry, R. C. & Tam, K. C. Surface modification of cellulose nanocrystal with chitosan oligosaccharide for drug delivery applications. *Cellulose* **20**, 1747–1764 (2013).
158. Habibi, Y. *et al.* Bionanocomposites based on poly(ϵ -caprolactone)-grafted cellulose nanocrystals by ring-opening polymerization. *Journal of Materials Chemistry* **18**, 5002–5010 (2008).
159. Morandi, G., Heath, L. & Thielemans, W. Cellulose Nanocrystals Grafted with Polystyrene Chains through Surface-Initiated Atom Transfer Radical Polymerization (SI-ATRP). *Langmuir* **25**, 8280–8286 (2009).
160. Espino-Pérez, E. *et al.* Nanocomposites with functionalised polysaccharide nanocrystals through aqueous free radical polymerisation promoted by ozonolysis. *Carbohydrate Polymers* **135**, 256–266 (2016).
161. Kedzior, S. A., Graham, L., Moorlag, C., Dooley, B. M. & Cranston, E. D. Poly(methyl methacrylate)-grafted cellulose nanocrystals: One-step synthesis, nanocomposite preparation, and characterization. *The Canadian Journal of Chemical Engineering* **94**, 811–822 (2016).
162. Boujemaoui, A. *et al.* Polycaprolactone Nanocomposites Reinforced with Cellulose Nanocrystals Surface-Modified via Covalent Grafting or Physisorption: A Comparative Study. *ACS Applied Materials & Interfaces* **9**, 35305–35318 (2017).
163. Zhang, Z., Sèbe, G., Wang, X. & Tam, K. C. Gold nanoparticles stabilized by poly(4-vinylpyridine) grafted cellulose nanocrystals as efficient and recyclable catalysts. *Carbohydrate Polymers* **182**, 61–68 (2018).
164. Zeinali, E., Haddadi-Asl, V. & Roghani-Mamaqani, H. Synthesis of dual thermo- and pH-sensitive poly(N-isopropylacrylamide-co-acrylic acid)-grafted cellulose nanocrystals by reversible addition-fragmentation chain transfer polymerization. *Journal of Biomedical Materials Research Part A* **106**, 231–243 (2018).
165. Abitbol, T. Surface modification of cellulose nanocrystals with cetyltrimethylammonium bromide. *Nordic Pulp and Paper Research Journal* **29**, 046–057 (2014).
166. Hu, Z., Ballinger, S., Pelton, R. & Cranston, E. D. Surfactant-enhanced cellulose nanocrystal Pickering emulsions. *Journal of Colloid and Interface Science* **439**, 139–148 (2015).
167. Bondeson, D. & Oksman, K. Dispersion and characteristics of surfactant modified cellulose whiskers nanocomposites. *Composite Interfaces* **14**, 617–630 (2007).
168. Podsiadlo, P. *et al.* Molecularly Engineered Nanocomposites: Layer-by-Layer Assembly of Cellulose Nanocrystals. *Biomacromolecules* **6**, 2914–2918 (2005).
169. Hu, Z., Berry, R. M., Pelton, R. & Cranston, E. D. One-Pot Water-Based Hydrophobic Surface Modification of Cellulose Nanocrystals Using Plant Polyphenols. *ACS Sustainable Chem. Eng.* **5**, 5018–5026 (2017).
170. Isogai, A., Saito, T. & Fukuzumi, H. TEMPO-oxidized cellulose nanofibers. *Nanoscale* **3**, 71–85 (2011).
171. Montanari, S., Roumani, M., Heux, L. & Vignon, M. R. Topochemistry of Carboxylated Cellulose Nanocrystals Resulting from TEMPO-Mediated Oxidation. *Macromolecules* **38**, 1665–1671 (2005).

172. Frascchini, C., Chauve, G. & Bouchard, J. TEMPO-mediated surface oxidation of cellulose nanocrystals (CNCs). *Cellulose* **24**, 2775–2790 (2017).
173. Saito, T. & Isogai, A. Introduction of aldehyde groups on surfaces of native cellulose fibers by TEMPO-mediated oxidation. *Colloids and Surfaces A: Physicochemical and Engineering Aspects* **289**, 219–225 (2006).
174. Saito, T. *et al.* Individualization of Nano-Sized Plant Cellulose Fibrils by Direct Surface Carboxylation Using TEMPO Catalyst under Neutral Conditions. *Biomacromolecules* **10**, 1992–1996 (2009).
175. Sun, B., Hou, Q., Liu, Z. & Ni, Y. Sodium periodate oxidation of cellulose nanocrystal and its application as a paper wet strength additive. *Cellulose* **22**, 1135–1146 (2015).
176. Guo, J. *et al.* Photoluminescent Hybrids of Cellulose Nanocrystals and Carbon Quantum Dots as Cytocompatible Probes for in Vitro Bioimaging. *Biomacromolecules* **18**, 2045–2055 (2017).
177. Boujemaoui, A., Mongkhontreerat, S., Malmström, E. & Carlmark, A. Preparation and characterization of functionalized cellulose nanocrystals. *Carbohydrate Polymers* **115**, 457–464 (2015).
178. Dufresne, A. *Nanocellulose: from nature to high performance tailored materials*. (Walter de Gruyter GmbH & Co KG, 2017).
179. Çetin, N. S. *et al.* Acetylation of Cellulose Nanowhiskers with Vinyl Acetate under Moderate Conditions. *Macromolecular Bioscience* **9**, 997–1003 (2009).
180. Goffin, A.-L. *et al.* From Interfacial Ring-Opening Polymerization to Melt Processing of Cellulose Nanowhisker-Filled Polylactide-Based Nanocomposites. *Biomacromolecules* **12**, 2456–2465 (2011).
181. Zoppe, J. O. *et al.* Poly(*i*Ni -isopropylacrylamide) Brushes Grafted from Cellulose Nanocrystals via Surface-Initiated Single-Electron Transfer Living Radical Polymerization. *Biomacromolecules* **11**, 2683–2691 (2010).
182. Fumagalli, M., Sanchez, F., Molina Boisseau, S. & Heux, L. Gas-phase esterification of cellulose nanocrystal aerogels for colloidal dispersion in apolar solvents. *Soft Matter* **9**, 11309–11317 (2013).
183. Yoo, Y. & Youngblood, J. P. Green One-Pot Synthesis of Surface Hydrophobized Cellulose Nanocrystals in Aqueous Medium. *ACS Sustainable Chemistry & Engineering* **4**, 3927–3938 (2016).
184. Espino-Pérez, E. *et al.* Designed cellulose nanocrystal surface properties for improving barrier properties in polylactide nanocomposites. *Carbohydrate Polymers* **183**, 267–277 (2018).
185. Peltzer, M., Pei, A., Zhou, Q., Berglund, L. & Jiménez, A. Surface modification of cellulose nanocrystals by grafting with poly(lactic acid). *Polymer International* **63**, 1056–1062 (2014).
186. Miao, C. & Hamad, W. Y. In-situ polymerized cellulose nanocrystals (CNC)-poly(l-lactide) (PLLA) nanomaterials and applications in nanocomposite processing. *Carbohydr Polym* **153**, 549–558 (2016).
187. Kan, K. H. M., Li, J., Wijesekera, K. & Cranston, E. D. Polymer-Grafted Cellulose Nanocrystals as pH-Responsive Reversible Flocculants. *Biomacromolecules* **14**, 3130–3139 (2013).
188. Zubik, K., Singhsa, P., Wang, Y., Manuspiya, H. & Narain, R. Thermo-Responsive Poly(*N*-Isopropylacrylamide)-Cellulose Nanocrystals Hybrid Hydrogels for Wound Dressing. *Polymers* **9**, 119 (2017).
189. Matyjaszewski, K. & Xia, J. Atom Transfer Radical Polymerization. *Chemical Reviews* **101**, 2921–2990 (2001).
190. Matyjaszewski, K. Advanced Materials by Atom Transfer Radical Polymerization. *Advanced Materials* **30**, 1706441 (2018).
191. Matyjaszewski, K. Atom Transfer Radical Polymerization (ATRP): Current Status and Future Perspectives. *Macromolecules* **45**, 4015–4039 (2012).
192. Yi, J., Xu, Q., Zhang, X. & Zhang, H. Chiral-nematic self-ordering of rodlike cellulose nanocrystals grafted with poly(styrene) in both thermotropic and lyotropic states. *Polymer* **49**, 4406–4412 (2008).
193. Zhang, Z., Wang, X., Tam, K. C. & Sèbe, G. A comparative study on grafting polymers from cellulose nanocrystals via surface-initiated atom transfer radical polymerization (ATRP) and activator re-generated by electron transfer ATRP. *Carbohydrate Polymers* **205**, 322–329 (2019).
194. Lepoittevin, B. *et al.* Hydrophobization of chitosan films by surface grafting with fluorinated polymer brushes. *Carbohydrate Polymers* **205**, 437–446 (2019).
195. Hatton, F. L., Kedzior, S. A., Cranston, E. D. & Carlmark, A. Grafting-from cellulose nanocrystals via photoinduced Cu-mediated reversible-deactivation radical polymerization. *Carbohydrate Polymers* **157**, 1033–1040 (2017).

196. Wang, H.-D., Roeder, R. D., Whitney, R. A., Champagne, P. & Cunningham, M. F. Graft modification of crystalline nanocellulose by Cu(0)-mediated SET living radical polymerization. *Journal of Polymer Science Part A: Polymer Chemistry* **53**, 2800–2808 (2015).
197. Boujemaoui, A. *et al.* Polycaprolactone Nanocomposites Reinforced with Cellulose Nanocrystals Surface-Modified via Covalent Grafting or Physisorption: A Comparative Study. *ACS Appl. Mater. Interfaces* **9**, 35305–35318 (2017).
198. Hemraz, U. D., Lu, A., Sunasee, R. & Boluk, Y. Structure of poly(N-isopropylacrylamide) brushes and steric stability of their grafted cellulose nanocrystal dispersions. *Journal of Colloid and Interface Science* **430**, 157–165 (2014).
199. Braunecker, W. A. & Matyjaszewski, K. Controlled/living radical polymerization: Features, developments, and perspectives. *Progress in Polymer Science* **32**, 93–146 (2007).
200. Chiefari, J. *et al.* Living Free-Radical Polymerization by Reversible Addition–Fragmentation Chain Transfer: The RAFT Process. *Macromolecules* **31**, 5559–5562 (1998).
201. Zeinali, E., Haddadi-Asl, V. & Roghani-Mamaqani, H. Nanocrystalline cellulose grafted random copolymers of N -isopropylacrylamide and acrylic acid synthesized by RAFT polymerization: effect of different acrylic acid contents on LCST behavior. *RSC Advances* **4**, 31428–31442 (2014).
202. Boujemaoui, A., Mazières, S., Malmström, E., Destarac, M. & Carlmark, A. SI-RAFT/MADIX polymerization of vinyl acetate on cellulose nanocrystals for nanocomposite applications. *Polymer* **99**, 240–249 (2016).
203. Liu, T., Xue, F. & Ding, E. Cellulose nanocrystals grafted with polyacrylamide assisted by macromolecular RAFT agents. *Cellulose* **23**, 3717–3735 (2016).
204. D. Roeder, R., Garcia-Valdez, O., A. Whitney, R., Champagne, P. & F. Cunningham, M. Graft modification of cellulose nanocrystals via nitroxide-mediated polymerisation. *Polymer Chemistry* **7**, 6383–6390 (2016).
205. Hansson, S., Antoni, P., Bergenudd, H. & Malmström, E. Selective cleavage of polymer grafts from solid surfaces: assessment of initiator content and polymer characteristics. *Polymer Chemistry* **2**, 556–558 (2011).
206. Zhang, Z., Tam, K. C., Sèbe, G. & Wang, X. Convenient characterization of polymers grafted on cellulose nanocrystals via SI-ATRP without chain cleavage. *Carbohydrate Polymers* **199**, 603–609 (2018).
207. Villares, A., Moreau, C., Dammak, A., Capron, I. & Cathala, B. Kinetic aspects of the adsorption of xyloglucan onto cellulose nanocrystals. *Soft Matter* **11**, 6472–6481 (2015).
208. Heux, L., Chauve, G. & Bonini, C. Nonflocculating and Chiral-Nematic Self-ordering of Cellulose Microcrystals Suspensions in Nonpolar Solvents. *Langmuir* **16**, 8210–8212 (2000).
209. Tardy, B. L. *et al.* Nanocellulose–surfactant interactions. *Current Opinion in Colloid & Interface Science* **29**, 57–67 (2017).
210. Kaboorani, A. & Riedl, B. Surface modification of cellulose nanocrystals (CNC) by a cationic surfactant. *Industrial Crops and Products* **65**, 45–55 (2015).
211. Rojas, O. J., Montero, G. A. & Habibi, Y. Electrospun nanocomposites from polystyrene loaded with cellulose nanowhiskers. *Journal of Applied Polymer Science* **113**, 927–935 (2009).
212. Kedzior, S. A., Marway, H. S. & Cranston, E. D. Tailoring Cellulose Nanocrystal and Surfactant Behavior in Miniemulsion Polymerization. *Macromolecules* **50**, 2645–2655 (2017).
213. Hu, Z., Marway, H. S., Kasem, H., Pelton, R. & Cranston, E. D. Dried and Redispersible Cellulose Nanocrystal Pickering Emulsions. *ACS Macro Letters* **5**, 185–189 (2016).
214. Cheng, D. *et al.* Adsorption of polyethylene glycol (PEG) onto cellulose nano-crystals to improve its dispersity. *Carbohydrate Polymers* **123**, 157–163 (2015).
215. Pereda, M., Kissi, N. E. & Dufresne, A. Extrusion of Polysaccharide Nanocrystal Reinforced Polymer Nanocomposites through Compatibilization with Poly(ethylene oxide). *ACS Appl. Mater. Interfaces* **6**, 9365–9375 (2014).
216. Dufresne, A. Cellulose nanomaterials as green nanoreinforcements for polymer nanocomposites. *Philosophical Transactions of the Royal Society A: Mathematical, Physical and Engineering Sciences* **376**, 20170040 (2018).
217. Oksman, K. *et al.* Review of the recent developments in cellulose nanocomposite processing. *Composites Part A: Applied Science and Manufacturing* **83**, 2–18 (2016).
218. Ferreira, F. V. *et al.* How do cellulose nanocrystals affect the overall properties of biodegradable polymer nanocomposites: A comprehensive review. *European Polymer Journal* **108**, 274–285 (2018).

219. Abdul Khalil, H. P. S., Bhat, A. H. & Ireana Yusra, A. F. Green composites from sustainable cellulose nanofibrils: A review. *Carbohydrate Polymers* **87**, 963–979 (2012).
220. Eichhorn, S. J. *et al.* Review: current international research into cellulose nanofibres and nanocomposites. *J Mater Sci* **45**, 1–33 (2010).
221. Okada, A. *et al.* Composite material and process for manufacturing same. *U.S. Patent No 4,739,007* (1988).
222. Cerqueira, M. A. P. R., Lagaron, J. M., Castro, L. M. P., de Oliveira Soares Vincente A. A. M. *Nanomaterials for food packaging: materials, processing technologies and safety issues*. (Elsevier, 2018).
223. European Commission, Commission Regulation (EU) No 10/2011 of 14 January 2011 on plastic materials and articles intended to come into contact with food. *Off J Eur Union* **12**, 1-89 (2011).
224. Bumbudsanpharoke, N. & Ko, S. Nano-Food Packaging: An Overview of Market, Migration Research, and Safety Regulations. *Journal of Food Science* **80**, R910–R923 (2015).
225. Siqueira, G., Bras, J. & Dufresne, A. Cellulosic Bionanocomposites: A Review of Preparation, Properties and Applications. *Polymers* **2**, 728–765 (2010).
226. Favier, V. *et al.* Nanocomposite materials from latex and cellulose whiskers. *Polymers for Advanced Technologies* **6**, 351–355 (1995).
227. Nielsen, L. E. Models for the Permeability of Filled Polymer Systems. *Journal of Macromolecular Science: Part A - Chemistry* **1**, 929–942 (1967).
228. Oksman, K., Mathew, A. P., Bondeson, D. & Kvien, I. Manufacturing process of cellulose whiskers/poly(lactic acid) nanocomposites. *Composites Science and Technology* **66**, 2776–2784 (2006).
229. Bondeson, D. & Oksman, K. Poly(lactic acid)/cellulose whisker nanocomposites modified by poly(vinyl alcohol). *Composites Part A: Applied Science and Manufacturing* **38**, 2486–2492 (2007).
230. Yang, W., Dominici, F., Fortunati, E., M. Kenny, J. & Puglia, D. Melt free radical grafting of glycidyl methacrylate (GMA) onto fully biodegradable poly(lactic acid) films: effect of cellulose nanocrystals and a masterbatch process. *RSC Advances* **5**, 32350–32357 (2015).
231. Dhar, P., Tarafder, D., Kumar, A. & Katiyar, V. Thermally recyclable poly(lactic acid)/cellulose nanocrystal films through reactive extrusion process. *Polymer* **87**, 268–282 (2016).
232. Arias, A., Heuzey, M.-C., Huneault, M. A., Ausias, G. & Bendahou, A. Enhanced dispersion of cellulose nanocrystals in melt-processed poly(lactide)-based nanocomposites. *Cellulose* **22**, 483–498 (2015).
233. Xiang, C., Joo, Y. L. & Frey, M. W. Nanocomposite fibers electrospun from poly(lactic acid)/cellulose nanocrystals. *Journal of Biobased Materials and Bioenergy* **3**, 147–155 (2009).
234. Shi, Q. *et al.* Mechanical properties and in vitro degradation of electrospun bio-nanocomposite mats from PLA and cellulose nanocrystals. *Carbohydrate Polymers* **90**, 301–308 (2012).
235. Fortunati, E. *et al.* Effects of modified cellulose nanocrystals on the barrier and migration properties of PLA nano-biocomposites. *Carbohydrate Polymers* **90**, 948–956 (2012).
236. Lin, N., Chen, G., Huang, J., Dufresne, A. & Chang, P. R. Effects of polymer-grafted natural nanocrystals on the structure and mechanical properties of poly(lactic acid): A case of cellulose whisker-graft-poly(ε-caprolactone). *Journal of Applied Polymer Science* **113**, 3417–3425 (2009).
237. Bitinis, N. *et al.* Poly(lactic acid)/natural rubber/cellulose nanocrystal bionanocomposites. Part II: Properties evaluation. *Carbohydrate Polymers* **96**, 621–627 (2013).
238. Robles, E., Urruzola, I., Labidi, J. & Serrano, L. Surface-modified nano-cellulose as reinforcement in poly(lactic acid) to conform new composites. *Industrial Crops and Products* **71**, 44–53 (2015).
239. Fortunati, E. *et al.* Multifunctional bionanocomposite films of poly(lactic acid), cellulose nanocrystals and silver nanoparticles. *Carbohydrate Polymers* **87**, 1596–1605 (2012).
240. Mariano, M. *et al.* Preparation of Cellulose Nanocrystal-Reinforced Poly(lactic acid) Nanocomposites through Noncovalent Modification with PLLA-Based Surfactants. *ACS Omega* **2**, 2678–2688 (2017).
241. Xu, C. *et al.* Poly(lactide)/acetylated nanocrystalline cellulose composites prepared by a continuous route: A phase interface-property relation study. *Carbohydrate Polymers* **146**, 58–66 (2016).
242. Habibi, Y., Aouadi, S., Raquez, J.-M. & Dubois, P. Effects of interfacial stereocomplexation in cellulose nanocrystal-filled poly(lactide) nanocomposites. *Cellulose* **20**, 2877–2885 (2013).
243. Mujica-Garcia, A. *et al.* Poly(lactic acid) melt-spun fibers reinforced with functionalized cellulose nanocrystals. *RSC Adv.* **6**, 9221–9231 (2016).
244. Lizundia, E. *et al.* PLLA-grafted cellulose nanocrystals: Role of the CNC content and grafting on the PLA bionanocomposite film properties. *Carbohydrate Polymers* **142**, 105–113 (2016).

245. Zhou, C. *et al.* Electrospun Bio-Nanocomposite Scaffolds for Bone Tissue Engineering by Cellulose Nanocrystals Reinforcing Maleic Anhydride Grafted PLA. *ACS Appl. Mater. Interfaces* **5**, 3847–3854 (2013).
246. Pracella, M., Haque, Md. M.-U. & Puglia, D. Morphology and properties tuning of PLA/cellulose nanocrystals bio-nanocomposites by means of reactive functionalization and blending with PVAc. *Polymer* **55**, 3720–3728 (2014).
247. Spinella, S. *et al.* Polylactide/cellulose nanocrystal nanocomposites: Efficient routes for nanofiber modification and effects of nanofiber chemistry on PLA reinforcement. *Polymer* **65**, 9–17 (2015).
248. Bagheriasl, D., Safdari, F., Carreau, P. J., Dubois, C. & Riedl, B. Development of cellulose nanocrystal-reinforced polylactide: A comparative study on different preparation methods. *Polymer Composites* **40**, E342–E349 (2019).
249. Aulin, C., Karabulut, E., Tran, A., Wågberg, L. & Lindström, T. Transparent Nanocellulosic Multilayer Thin Films on Poly(lactic Acid) with Tunable Gas Barrier Properties. *ACS Appl. Mater. Interfaces* **5**, 7352–7359 (2013).
250. Meriçer, Ç. *et al.* Atmospheric plasma assisted PLA/microfibrillated cellulose (MFC) multilayer biocomposite for sustainable barrier application. *Industrial Crops and Products* **93**, 235–243 (2016).
251. Yildirim, S. *et al.* Active Packaging Applications for Food. *Comprehensive Reviews in Food Science and Food Safety* **17**, 165–199 (2018).
252. Hines, J. H., Wanigasekara, E., Rudkevich, D. M. & Rogers, R. D. Calix[4]arenes immobilized in a cellulose-based platform for entrapment and detection of NO_x gases. *Journal of Materials Chemistry* **18**, 4050–4055 (2008).
253. Yildirim, S. *Newsletter Transfer*. (Switzerland, 2010).
254. Luzi, F. *et al.* Cellulose nanocrystals from *Actinidia deliciosa* pruning residues combined with carvacrol in PVA-CH films with antioxidant/antimicrobial properties for packaging applications. *International Journal of Biological Macromolecules* **104**, 43–55 (2017).

CHAPTER II

Chemical modifications of cellulose nanocrystals

Table of contents – Chapter II

Introduction to Chapter II	117
1. Surface-initiated transfer radical polymerization from the surface of modified-cellulose nanocrystals	119
1. Introduction	121
2. Materials and methods	124
2.1. Materials	124
2.2. Functionalization of CNCs with α -Bromoisobutyryl Bromide	124
2.3. SI-ATRP of glycidyl methacrylate on functionalized CNC-Br	124
2.4. Polymerization of homopolymer PGMA	125
2.5. Characterization methods	125
3. Results and discussions	129
3.1. Characterization of cellulose nanomaterials	129
3.2. Preparation of initiator modified CNC	129
3.3. Kinetics of SI-ATRP of GMA	134
3.4. SI-ATRP of functionalized CNC-Br at different polymerization times	138
3.5. Efficiency of SI-ATRP on CNCs	139
4. Conclusion	143
2. Grafting of fatty acids on cellulose nanocrystals via a novel procedure	145
2.1. Comparison between two different methods for the chemical modification of cellulose nanocrystals	145
1. Introduction	147
2. Materials and methods	149
2.1. Materials	149
2.2. Classical esterification of CNCs using 10-undecenoyl chloride	149
2.3. Esterification of CNCs with 10-undecenoic acid <i>via</i> a novel method	149
2.4. Characterization methods	150
3. Results and discussions	152
3.1. Influence of the chemical modifications on the structure of the CNCs	152
3.2. Efficiency of the two surface modification methods	153
4. Conclusion	156
2.2. Role of solvent exchange in dispersion of cellulose nanocrystals and their esterification using acids as solvents	157
1. Introduction	159
2. Materials and methods	162
2.1. Materials	162
2.2. CNC suspensions preparation	162
2.3. Esterification of CNCs with fatty acids	163
2.4. Characterization methods	164
3. Results and discussions	167
3.1. Different ways for the dispersion of CNC in acetone	167
3.2. Influence of solvent exchange on the grafting efficiency	169
3.3. Influence of chain length on CNC grafting (Suspension 3)	176
3.4. Surface analyses of long chains onto CNC	179

4. Conclusion	183
3. Amidation of TEMPO-oxidized cellulose nanocrystals using aromatic aminated molecules	185
1. Introduction	187
2. Materials and methods	190
2.1. Materials	190
2.2. Oxidation of CNCs using TEMPO reagent	190
2.3. Amidation of TEMPO-CNC using 1-M-3-PP with EDC/NHS catalysis	190
2.4. Characterization methods	192
3. Results and discussions	199
3.1. Characterization of TEMPO-CNC prepared on a large scale	199
3.2. Grafting efficiency of 1-M-3-PP on TEMPO-CNC through amidation	205
3.3. Indirect proofs of grafting efficiency	207
3.4. Physico-chemical adsorption of 1-M-3-PP at the surface of TEMPO-CNC	209
4. Conclusion	213
4. Adsorption of rosin nanoparticles from a nano-emulsion on both cellulose nanocrystals and nanofibrils	215
1. Introduction	217
2. Materials and methods	219
2.1. Materials	219
2.2. Preparation of rosin nano-emulsion	219
2.3. Adsorption of rosin nano-emulsion on CNF	220
2.4. Adsorption of rosin nano-emulsion on CNC	220
2.5. Elaboration of neat and modified CNF-Rosin films by filtration	220
2.6. Elaboration of neat and modified CNC-Rosin films by solvent casting	220
2.7. Characterization methods	221
3. Results and discussions	222
3.1. Nanometric size of rosin particles	222
3.2. Efficiency of the rosin adsorption on both CNF and CNC	223
4. Conclusion	225
Conclusions of Chapter II	227
References - Chapter II	231

Introduction to Chapter II

As described in the **Chapter I**, surface chemical modifications of CNCs are made possible thanks to their high surface area and highly reactive surface. One of the main goals of this PhD project is the functionalization of the CNCs surface (objective **1**), in order to enhance their compatibilization with a hydrophobic PLA polymeric matrix. The global project — in which the PhD is part of — involved different partners, with different needs in terms of quantities of grafted CNCs. It explains the division of the following **Chapter II** in four different sections, whose respective chemical modifications can be performed on increasing amounts of CNCs.

More precisely, the **Chapter II** proposes four different new routes for the chemical modifications of CNCs, with related characterizations and discussions. The **Figure II. 1** represents the organization of this chapter.

- The section **II.1** relates the polymerization of the glycidyl methacrylate (GMA) from the surface of previously functionalized CNCs, as well as, the characterization of the kinetics of the polymerization. The chosen route for the polymerization is the SI-ATRP (Surface-Initiated Atom Transfer Polymerization), in order to control the surface polymerization. Moreover, the choice of GMA as monomer is explained by the presence of numerous highly reactive epoxy groups all along the polymer chain, which could be potentially help for the incorporation of polymerized CNC-PGMA-Br in a PLA matrix. This study was mainly performed in the laboratory ICMMO (Institut de Chimie Moléculaire et des Matériaux d'Orsay, in Orsay, France)

- The section **II.2** is divided in two sub-sections, and the first one (**II.2.1**) is a short additional part aiming to compare a classical esterification procedure using an acid chloride (10-Undecenoyl chloride) with that using a novel esterification using a similar carboxylic acid (10-Undecenoic acid). In the second sub-section (**II.2.2**), this new esterification procedure is more detailed, and its efficiency is investigated. Moreover, the preliminary study focusing on the role of the initial CNC dispersion state is also explained.

- The section **II.3** is dedicated to the modification of a large batch of previously oxidized TEMPO-CNC *via* an amidation reaction using an aromatic amine (1-methyl-3-phenylpropylamine). The efficiency of the two-step reaction is investigated, as well as, preliminary results of the parallel adsorption occurring in the reaction media.

Finally, the short section II.4 presents the preliminary results related to the preparation of rosin nano-emulsion, and their adsorption on both cellulose nanocrystals and nanofibrils surface. This study includes results produced by the start-up INOFIB (Grenoble, France), with whom collaboration was carried out during this PhD project.

All the modified nanomaterials described and characterized in this Chapter II will then be used for the preparation of PLA-based materials, whose results are described in the following Chapter III of this manuscript.

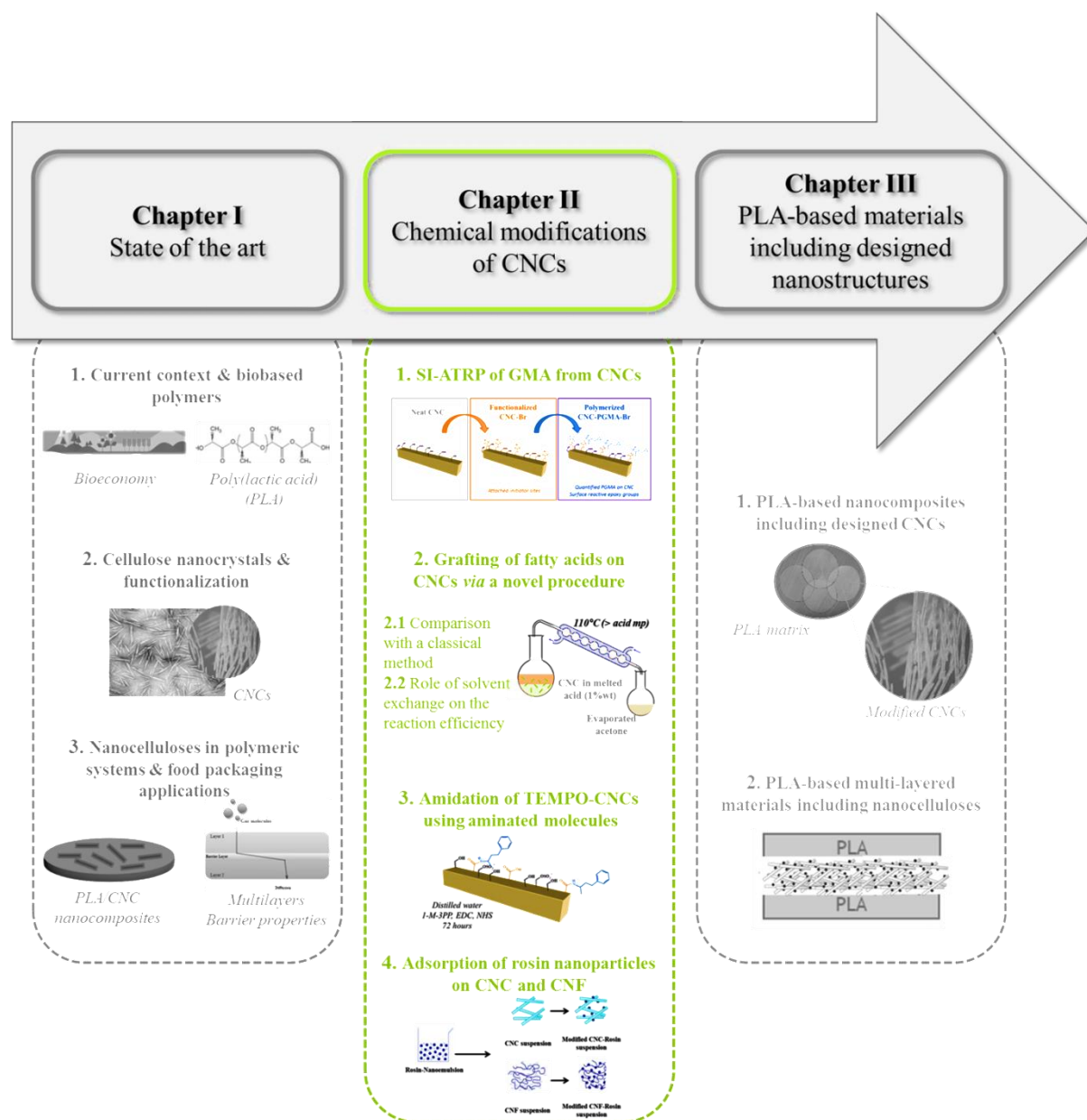
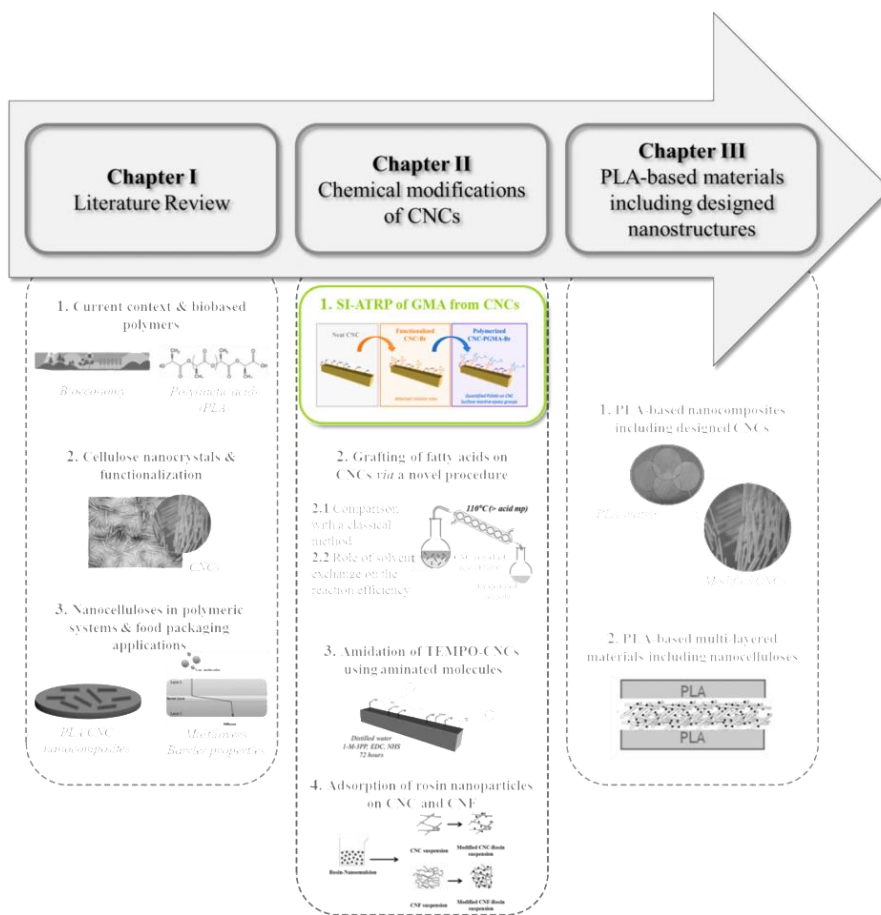


Figure II. 1. General organization of the PhD manuscript

1. Surface-initiated transfer radical polymerization of glycidyl methacrylate from the surface of modified-cellulose nanocrystals

This section is adapted from M. Le Gars, J. Bras, H. Salmi-Mani, M. Ji, D. Dragoe, H. Faraj, S. Domenek, M. N. Belgacem, P. Roger "Polymerization of glycidyl methacrylate from the surface of cellulose nanocrystals for the elaboration of PLA-based nanocomposites", *Carbohydrate Polymers*, 2020.



Abstract

Cellulose nanocrystals (CNCs) are used to design nanocomposites because of their high aspect ratio and their outstanding mechanical and barrier properties. However, the low compatibility of hydrophilic CNCs with hydrophobic polymers remains a barrier to their use in the nanocomposite field. To improve this compatibility, poly(glycidyl methacrylate) (PGMA) was grafted from CNCs containing α -bromoisobutyryl moieties *via* surface-initiated atom transfer radical polymerization. The novelty of this research is the use of a reactive epoxy-containing monomer that can serve as a new platform for further modifications or crosslinking. Polymer-grafted CNC-PGMA-Br prepared at different polymerization times were characterized by XRD, DLS, FTIR, XPS and elemental analysis. Approximately 40% of the polymer at the surface of the CNCs was quantified after only 1 h of polymerization.

Keywords:

Cellulose nanocrystals — Chemical grafting — Surface-initiated atom transfer radical polymerization — Poly(glycidyl methacrylate)

1. Introduction

Because of its abundance and availability from a wide variety of sources, cellulose is currently a polymer of choice in the field of bio-based materials. Recently, several novel nanomaterials have been extracted from this natural biopolymer. Indeed, cellulose nanofibrils (CNFs) have been classically obtained since the 1980s by applying a mechanical treatment to a cellulose suspension¹. Conversely, since the 1960s, CNCs are produced by performing an acid hydrolysis, meaning removing the amorphous part of cellulose^{2,3}. Such nanomaterials are relevant for a large number of research fields, like nanocomposites^{2,4-6}, coatings^{7,8}, packaging^{7,8} and biomedical applications⁹⁻¹¹. They exhibit interesting properties like biodegradability, renewability and mechanical and barrier properties that endow them with particular advantages. In the past decade, accelerated industrialization and commercialization of such cellulosic nanomaterials has occurred, in parallel with an ever-increasing demand from industry.

Among nanocelluloses, CNCs exhibit interesting properties. Acid hydrolysis of native cellulose from various sources (cotton, wood, natural fibers, etc.) using sulfuric acid H_2SO_4 leads to CNCs with different dimensions and aspect ratios. The resulting sulfuric-acid-hydrolyzed CNCs hold sulfate half ester groups ($-OSO_3^-$) on their surface^{12,13}, with a surface charge density generally in the range from 80 to 350 $\mu\text{mol.g}^{-1}$ ^{12,14}. These surface charges combined with their nanometric size — 150-500 nm in length (up to 1000 nm), 5-20 nm in width according to their source^{2,12} — induce colloidal stability of aqueous suspensions^{12,13}. In addition to their high aspect ratio, CNCs exhibit a high surface area^{12,15}, high crystallinity¹⁶ and a large availability of hydroxyl groups on their surface^{12,15}. Moreover, their rod-like shape, their high mechanical strength (Young's modulus between 120 and 200 GPa)^{17,18}, and their sustainability make them attractive materials as fillers in nanocomposites^{5,19-21}.

However, the hydrophilicity of CNCs, resulting from the three OH groups per anhydroglucose unit (AGU), limits their dispersion in several polymer matrices, especially non-polar matrices. Moreover, CNCs begin to degrade at approximately 200-300 °C²², depending on their morphology, crystallinity, and source. These two last points are challenging when such nanomaterials are used for nanocomposite processing, where high temperatures are reached with expected well-dispersed nanofillers^{23,24}. These challenges can be overcome through chemical or physico-chemical modifications of CNCs^{4,15,25}, by grafting single molecules^{19,20,25-28} or polymers chains^{21,29-32} at the surface of CNCs, or by adsorbing various molecules, involving ionic or low-energy bonding phenomena^{2,33-36}.

Chemical modifications are carried out by modifying multiple hydroxyl groups at the surface of CNCs to provide the nanomaterials with specific properties. To improve the compatibility of CNCs with a hydrophobic polymer matrix, grafting single molecules or polymer chains are classically described in the literature and in reviews. Focusing on the second strategy, two major approaches are commonly

used to introduce polymeric chains at the surface of CNCs. In the *grafting-onto* strategy, CNCs, either pre-functionalized or not, are directly grafted with previously polymerized and characterized polymer chains^{30,37–39}, leading to limited surface grafting density because of the steric hindrance between polymers. In the *grafted-from* approach — on which this study focuses — monomers are polymerized from pre-functionalized CNCs with initiator sites^{21,29,40,41}. This two-step strategy leads to an overall controlled structure and higher surface grafting density because of the facilitated access to the activated initiator sites on CNCs, although characterization of grafted polymer chains is more challenging⁴². Ring-opening polymerization (ROP)^{32,40} and atom transfer radical polymerization (ATRP)^{29,41,43} are the most common types of polymerization used in the *grafting-from* strategy. Controlled surface-initiated ATRP (SI-ATRP) from the surface of CNCs has been described in the literature^{29,41,43,44}. However, the major issues with SI-ATRP are the difficulty in characterizing grafted polymers and recovery of the free homopolymer. Control of the polymerization is generally studied using polymers obtained from a sacrificial initiator, from which the kinetics of the polymerization is considered similar to polymerization from the surface of CNCs. By recovering and characterizing the free homopolymer, information about the grafted chains can be acquired⁴⁵. It should be noted that this step of cleaning is challenging and crucial for characterizing both grafted CNCs and free polymers.

The aim of this study is to graft polymer brushes of various lengths on the surface of CNCs *via grafting-from* SI-ATRP. Numerous studies have focused on the polymerization of various polymers on CNCs, mostly in order to compatibilize these nanomaterials with various polymer matrices. Recently, Zoppe *et al.*⁴⁶ studied the synthesis of poly(N,N-dimethylacrylamide) chains at the surface of CNCs and carried out an alkaline hydrolysis to remove and analyze the polymerized chains. Sessini *et al.*³⁷ reported the polymerization *via grafting-from* of L-lactide and ϵ -caprolactone at the surface of CNCs and studied the morphological, thermal, and mechanical properties of such modified CNCs in various polymer matrices.

The objective of the present study is to graft the poly(glycidyl methacrylate) (PGMA) obtained from the polymerization of glycidyl methacrylate (GMA), an epoxy-functional and commercially available monomer⁴⁷ on CNCs. The traditional method of polymerizing GMA in a controlled manner is by atom transfer radical polymerization (ATRP), with the use of an initiator and a catalyst system⁴⁷. These methods aim to control the polymerization behavior. PGMA was selected for this study because of its hydrophobicity⁴⁸ and the presence of the highly reactive epoxy functions, which can be an active attachment point for further modifications. To our knowledge, such a strategy is new in the field of CNC modification and with respect to this reactive polymer at the surface of CNCs. Control of the polymerization is essential to quantify the polymer and is conducted through SI-ATRP, as mentioned previously. To the best of our knowledge, PGMA has never been polymerized at the surface of CNCs *via a grafting-from* SI-ATRP approach. Martinez-Sanz *et al.*⁴⁹ grafted PGMA *via* a non-controlled polymerization applied on bacterial cellulose nanowhiskers for PLA nanocomposites applications.

Hansson *et al.*⁵⁰ grafted various polymers, including PGMA from a cellulosic filter paper substrate, *via* activators regenerated by electron transfer (ARGET) ATRP to limit the use of reducing reagents and avoid the use of a totally inert atmosphere. Malmström *et al.*⁵¹ presented different ways of functionalizing cellulose papers by controlling the surface grafting and grafted PGMA *via* SI-ATRP but the grafting was done at the surface of cellulose fibers to introduce a large amount of oxirane groups. More recently, Cheng *et al.*⁵² performed a similar SI-ATRP of GMA from a nanoporous cellulose gel (NCG) followed by a hydrophobic modification of polymerized NCG to produce functional materials based on NCGs.

In the present paper, an efficient SI-ATRP polymerization of GMA from the surface of CNCs is described. The experiment method covers various steps. First, CNCs are functionalized with α -bromoisobutyryl bromide (BIB), a brominated initiator commonly used in ATRP^{47,53}. Then, GMA is polymerized from these initiator sites, with challenges like control and recovery of the homopolymer. Polymerized CNCs at different polymerization times are characterized using various techniques, from bulk characterization (FTIR, elemental analysis, TGA) to surface characterization (XPS).

2. Materials and methods

2.1. Materials

Cellulose nanocrystals (CNC) were produced from wood pulp and purchased from CelluForce (Quebec, Canada), in spray-dried form. 4-(dimethylamino)pyridine (DMAP), triethylamine (TEA), α -bromoisobutyryl bromide (BIB), ethyl α -bromoisobutyrate (EBIB), and N,N,N',N'',N'''-pentamethyldiethylenetriamine (PMDETA) were supplied from Sigma-Aldrich Chimie (Saint-Quentin-Fallavier, France) and were used as received. Copper (I) bromide (CuBr) was purchased from Sigma-Aldrich Chimie. CuBr was purified by washing in glacial acetic acid for 24 h at ambient temperature, filtered, rinsed extensively with ethanol and diethyl ether, dried under vacuum, and stored in an inert atmosphere before use⁵⁴. Glycidyl methacrylate (GMA) was purchased from Fisher Scientific (France) and purified through a basic alumina column to remove stabilizers before use. N,N-Dimethylformamide (DMF) was purchased from Sigma-Aldrich Chimie, stored, and used in anhydrous conditions. Dichloromethane (DCM) and ethanol (EtOH) were purchased from Sigma-Aldrich Chimie and used as received.

2.2. Functionalization of CNCs with α -Bromoisobutyryl Bromide

Functionalization of CNC with BIB was performed by esterification reaction according to the protocol adapted from Morandi *et al.*⁴¹. This protocol is as follows. First, 1.0 g of dry CNCs was dispersed in 100 mL of anhydrous DMF and an ultrasonic treatment was applied. Then, 125 mg of DMAP (1.02 mmol) was solubilized in 2 mL of anhydrous DMF and added to the CNC suspension. Thereafter, 2.1 mL of TEA (14.9 mmol) was added, followed by 1.9 mL of BIB (14.9 mmol). The reaction was performed at room temperature for 24 h, under argon flow. At the end of the reaction, the functionalized CNC-Br were washed by successive cycles of centrifugation (9000 rpm, 10', 5 °C): in DMF once, in DCM twice, in a mixture of DCM/EtOH (1/1, v/v) once, and in EtOH twice. CNC-Br were then dried under vacuum.

2.3. SI-ATRP of glycidyl methacrylate on functionalized CNC-Br

The method for SI-ATRP of GMA onto CNCs was adapted from classical ATRP of this monomer⁴⁷. First, 0.5 g of previously functionalized CNC-Br was redispersed in a Schlenk in 10 mL of anhydrous DMF and magnetically stirred under argon, before being treated with ultrasound. Then, 0.054 mL of EBIB, 0.076 mL of PMDETA, and 4.8 mL of purified GMA were successively added to the suspension ($[GMA]_0:[EBIB]_0:[PMDETA]_0:[CuBr]_0 = 100:1:1:1$). The sacrificial EBIB was added to react as a sacrificial initiator, assuming that the polymerization of GMA occurred from this initiator, in the same manner as from the surface of our CNC-Br. Next, 0.054 g of CuBr was introduced quickly and at the last moment, to avoid oxidation, noticeable by a color change. A flow of argon was set up in the closed Schlenk under magnetic stirring. A total of 7 freeze-thaw cycles were carried out to

completely remove oxygen from the suspension. The mixture was then magnetically stirred under argon at room temperature for 24 h. Study of the polymerization kinetics was performed by collecting aliquots of the reaction media with a purged argon syringe. At the end of the reaction, a small amount of DCM was added to recover all the mixture and a first centrifugation cycle (9000 rpm, 15', 5 °C) was carried out. The supernatant containing PGMA polymerized from the sacrificial initiator was recovered for characterization. The centrifuged part was further washed in DCM with five cycles of centrifugation (9000 rpm, 15', 5 °C) to eliminate all the free homopolymer and to only retrieve CNC-PGMA-Br. The solubilized PGMA homopolymer recovered in the DCM supernatant was purified on a basic alumina column, precipitated in cold methanol, filtered, and dried under vacuum.

2.4. Polymerization of homopolymer PGMA

The reference homopolymer PGMA was prepared by ATRP according to the previously described method. Indeed, the same protocol was used without CNC and a sacrificial initiator and with $[GMA]_0:[PMDETA]_0:[CuBr]_0 = 100:1:1$. After 7 freeze-thaw cycles, polymerization occurred at room temperature for 1 h. At the end of the reaction, solubilized PGMA was purified on a basic alumina column and precipitated in cold methanol. After filtration and drying, PGMA homopolymer was characterized by 1H -NMR, and a conversion rate of 52% and a theoretical molar mass of $7300 \text{ g}\cdot\text{mol}^{-1}$ was calculated. This homopolymer was used as reference PGMA in this study.

2.5. Characterization methods

2.5.1. Atomic Force Microscopy (AFM)

AFM images of CNC suspensions were recorded using a Dimension Icon Bruker equipped with a silicon-coated micro cantilever (O-TESPA) using tapping mode. Droplets of diluted CNC suspension (10^{-4} wt%) were deposited on clean mica plates, which were allowed to dry by evaporation overnight. Approximately ten scans of $10 \mu\text{m} \times 10 \mu\text{m}$ and $3 \mu\text{m} \times 3 \mu\text{m}$ were obtained for each sample to analyze the morphology of the nanoparticles by measuring the dimensions of at least 50 CNC samples using ImageJ software.

2.5.2. Transmission Electron Microscopy (TEM)

TEM copper grids with thin amorphous carbon films were submitted to glow discharge in an easiGlow station (Pelco). A 4- μL diluted CNC suspension droplet was deposited on the carbon film, followed by a droplet of uranyl acetate (2 wt%). Negative dye in excess was absorbed, and the remaining film was dried. The CNC suspension was observed through a transmission electron microscope FEI/Philips CM200 with the microscopy NanoBio-ICMG platform (Grenoble, France), under an acceleration voltage of 200 kV. Pictures were recorded with a digital camera TVIPS TemCam F216 (2040 x 2040 pixels). Representative images were selected for the analysis.

2.5.3. X-Ray Diffraction and Crystallinity Index (CI)

The crystallinity of CNCs was investigated with spectra obtained from wide-angle X-ray diffraction analyses. An X'Pert Pro MPD diffractometer supplied by PANalytical equipped with an X' accelerator detector and a copper anode ($K\alpha$ (Cu) = 1.5419 Å) was used for the symmetric scan of the reflection (theta/2theta in Bragg Brentano geometry) of the sample. Scans were performed from 5° to 60°. The crystallinity index of samples was determined according to the Segal height peak method⁵⁵⁻⁵⁷ (**Equation II. 1**).

$$CI = \frac{1 - I_{am}}{I_{002}} \times 100$$

Equation II. 1. Crystallinity index (CI) according to the Segal height peak method

where I_{am} corresponds to the intensity at the minimum (at $2\theta \simeq 18.3^\circ$) and I_{002} corresponds to the main crystalline peak (at $2\theta \simeq 22.5^\circ$). This method is the most widely used, although it slightly overestimates the value of the crystallinity and provides qualitative values of the crystallinity. The measures were duplicated.

2.5.4. Dynamic Light Scattering (DLS)

The hydrodynamic diameters of CNCs were measured using a Zeta Sizer NanoZS supplied by Malvern Instruments (Orsay, France), operated with DTS software. Suspensions of CNCs at 10⁻² wt% in DCM were freshly prepared before each measurement and treated in an ultrasonic bath. A total of 5 acquisitions with 15 measurements at 25 °C were performed and particle size average values are presented. These values correspond to the diameter of the sphere diffusing at the same rate as the measured particle. Moreover, the Brownian motion-induced particle speed is correlated to the size of the particle by the Stokes-Einstein equation. Boluk and Danumah⁵⁸ provided details of this principle applied to CNC analysis.

2.5.5. Thermogravimetric Analysis (TGA)

TGA thermograms were recorded using a thermal analyzer (NETZSCH STA 449 F3 Jupiter) from the LRMO team of the Commissariat à l'énergie atomique et aux énergies alternatives (CEA, Saclay, France). Dried samples were introduced in aluminum crucibles and were heated from 30 °C to 500 °C at 10 °C/min under helium flow at 60 mL/min. Data were at least duplicated and analyzed using Proteus software.

2.5.6. Fourier-Transform Infrared Spectroscopy (FTIR)

Infrared spectra of CNCs were performed on a Bruker IFS 66 spectrometer using an attenuated total reflectance (ATR) module composed of diamond crystals from Pike technologies. Absorbance spectra were registered between 600 and 4000 cm⁻¹, with a resolution of 4 cm⁻¹ and 300 scans. Spectra were visualized and normalized using OPUS software and were at least duplicated.

2.5.7. Elemental Analysis

Elemental analyses of CNCs were performed by the “Institut des Sciences Analytiques” (Villeurbanne, France), using an ISA-CNRS micro analyzer. Based on elemental organic microanalysis, the carbon, hydrogen, oxygen and sulfur contents of the samples were determined with a precision of $\pm 0.4\%$ by at least duplicates. The data can be used for the determination of the degree of substitution (DS) of the grafted CNCs, equivalent to the number of functionalized hydroxyl groups per anhydroglucose unit (AGU), in accordance with **Equation II. 2**²⁶:

$$DS = \frac{M(C)_{AGU} - \omega_C \times (M_{AGU} + DS_{SO_3} \times M_{SO_3})}{\omega_C \times M_{grafted} - M(C)_{grafted}}$$

Equation II. 2. Degree of substitution (DS)

where $M(C)_{AGU}$ is the carbon molar mass of an AGU, M_{AGU} is the molar mass of an AGU, ω_C is the carbon weight fraction (in %) obtained from elemental analysis, $M_{grafted}$ is the molar mass of the grafted moieties, and $M(C)_{grafted}$ is the carbon molar mass of the grafted moieties. DS_{SO_3} is the degree of substitution of sulfate half ester groups similarly calculated from the sulfur weight fraction ($S\%$), M_{SO_3} is the molar mass of $-OSO_3^-$ groups and M_S the sulfur molar mass of $-OSO_3^-$ groups, as shown in the **Equation II. 3**:

$$DS_{SO_3} = \frac{S\% \times M_{AGU}}{M_S - \%S \times M_{SO_3}}$$

Equation II. 3. Degree of substitution of half sulfate ester groups (DS_{SO_3})

Taking the presence of these groups into account allows the correction of the values of carbon and oxygen weight fractions by multiplying the experimental values by $1 + ((DS_{SO_3} \cdot M_{SO_3}) / M_{AGU})$. Other correction methods have also been proposed in the literature^{26,59}.

2.5.8. X-Ray Photoelectron Spectroscopy (XPS)

XPS measurements were carried out on a K-Alpha Thermo Fisher spectrometer, equipped with a monochromatic X-ray source (Al $K\alpha$, 1486.6 eV). A spot size of 400 μ m was used for all measurements, and a hemispherical analyzer was operated in constant analyzer energy mode with a pass energy of 200 eV and a step size of 1 eV (for survey spectra) and a pass energy of 50 eV and a step size of 0.1 eV (for high-resolution spectra). To neutralize the accumulation of charge, a dual-beam flood gun was used. Data treatment was carried out with Avantage software (Thermo Fisher). Background subtraction (Shirley type) and normalization of peak areas (using Scofield sensitivity factors) were performed before any calculation of elemental composition. Binding energies are referenced to the C1s neutral carbon peak at 285.4 eV.

2.5.9. ¹H-Liquid State Nuclear Magnetic Resonance (¹H-NMR)

¹H-NMR analyses were performed on a Bruker 360 MHz spectrometer in deuterated chloroform at room temperature, with a residual signal appearing at 7.24 ppm. Chemical shift values were calculated with TMS as the first reference. Spectra were analyzed using NMR Notebook software.

2.5.10. Size-Exclusion Chromatography (SEC)

Polymeric samples were dissolved in tetrahydrofuran (THF) at a concentration of 1 mg/mL. SEC analyses were carried out with a two-column ViscoGel mixed bed from Viscotek (7.8 x 300 mm, type GMHH r-H). This mixed bed was mounted on a device equipped with a refractive index detector (Waters 410). The injected volume of sample solution was equal to 50 µL. The calibration range corresponded to linear polystyrene standards. The process was duplicated.

3. Results and discussions

3.1. Characterization of cellulose nanomaterials

Commercial spray-dried cellulose nanocrystal powder was used in this study (**Figure II. 2 a**). These CNCs are produced from wood by sulfuric acid hydrolysis of bleached pulp¹⁴ and can easily be redispersed at low concentration in water and polar organic solvents (such as DMF or DMSO) using ultrasound treatment with an ultrasonic probe⁶⁰.

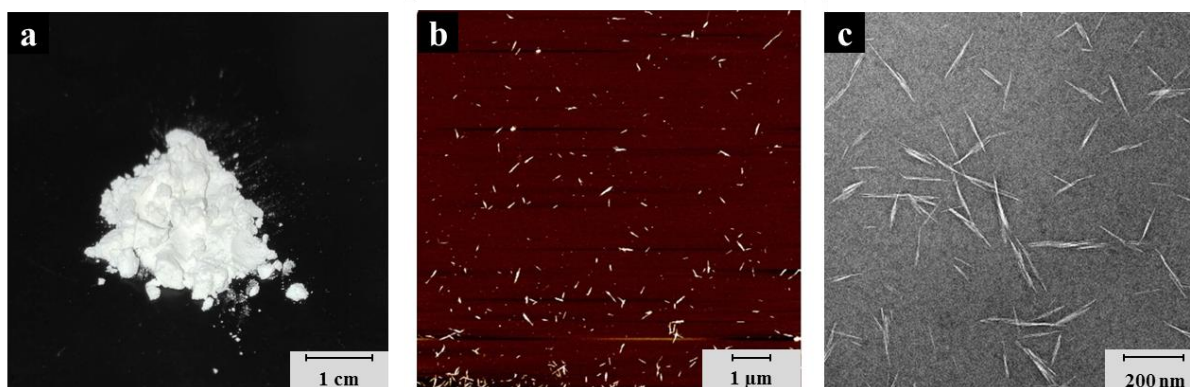
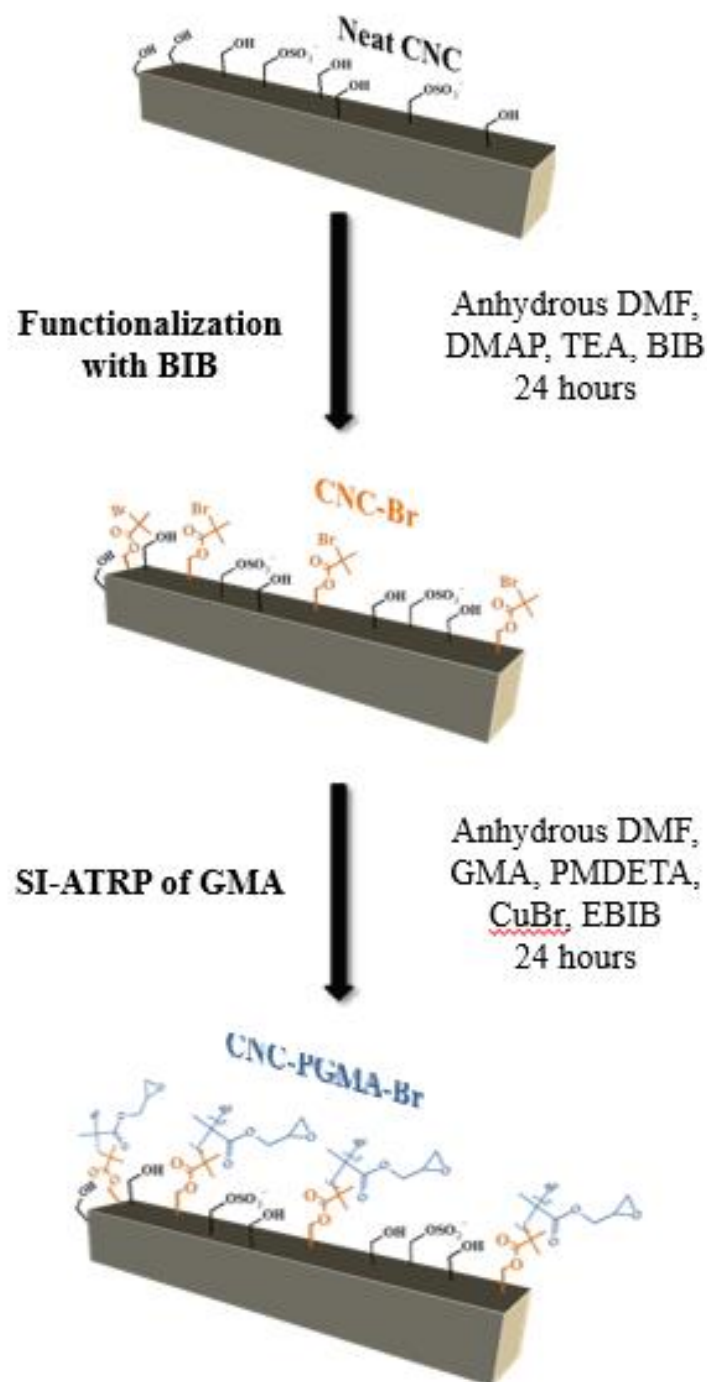


Figure II. 2. a) Spray-dried CNC from CelluForce, b) AFM height image of CNC, and c) TEM image of CNC

Using the AFM and TEM images (**Figure II. 2 b**) and **c**), morphology of the neat nanomaterials can be confirmed, and the average length is 108 ± 33 nm and average diameter is 4 ± 1 nm, confirming the values found in the literature^{12,14}. The X-Ray diffractograms (**Figure II. 3 a**) display three main peaks, at 16.2° (signal 110), 22.6° (signal 200), and 34.6° (signal 004), characteristic of the cellulose I crystalline form. Moreover, the *CI* calculated according to **Equation II. 1** has a value equal to 91%, consistent with the high crystallinity of CNC presented in the literature³.

3.2. Preparation of initiator modified CNC

BIB is a common reagent used in the CNC functionalization based on ATRP. As found in the literature^{41,44,48}, this grafting introduces highly reactive brominated functionality at the surface of nanomaterials. These functionalized sites can then be used as initiator sites for further controlled radical polymerization reactions. In the present study, the brominated functionalized site at the surface of the CNC-Br served as initiators for the SI-ATRP applied to the GMA monomer. The functionalization of CNCs with BIB, leading to CNC-Br, is illustrated in **Scheme II. 1**.



Scheme II. 1. Procedure for to the preparation of CNC-Br and CNC-PGMA-Br materials

Conservation of the structure of the CNCs after their functionalization is crucial and has been investigated by XRD analyses. **Figure II. 3 a)** shows wide-angle diffractogram of modified CNC-Br, whose spectra correspond to cellulose I *beta*. The calculated *CI* is equal to 86%, confirming the conservation of the crystalline structure of CNC-Br. Modified CNC-Br are well-dispersed in DCM, with a mean apparent diameter size of 122 nm, which is similar to that of neat CNC dispersed in DCM (**Figure II. 3 b)**). Even if the dispersion of CNC in DCM does not lead to conclusions regarding their dispersion in DMF, the dispersion state in DCM provides some insight about their dispersion in polar

DMF. This dispersion should theoretically be greater. Thus, it is likely that isolated CNC-Br in DMF would provide a large accessible surface for further polymerization.

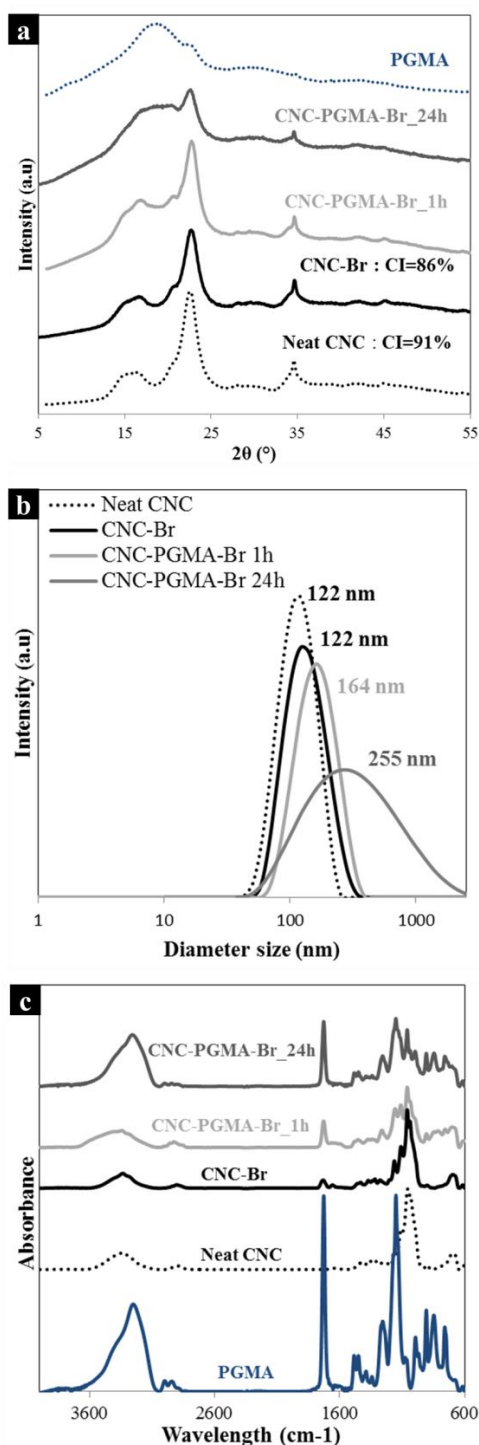


Figure II. 3. a) X-ray diffractograms of neat CNCs, pre-functionalized CNC-Br, CNC-PGMA-Br after 1 h and 24 h of polymerization and PGMA homopolymer, **b)** DLS curves of neat CNC, pre-functionalized CNC-Br and CNC-PGMA-Br after two different polymerization times in dichloromethane, and **c)** FTIR spectra of PGMA homopolymer, unmodified CNC, grafted CNC-Br, polymerized CNC-PGMA-Br-1h, and CNC-PGMA-Br_24h

FTIR analyses carried out on neat CNC and modified CNC-Br clearly show the efficiency of the grafting of BIB. Indeed, in addition to the characteristic peaks of cellulose (i.e., large peak between 3000 cm^{-1} and 3700 cm^{-1} corresponding to the stretching vibrations bands of the -OH bonds of

hydroxyl groups, as well as peaks at 1110 cm^{-1} , 1060 cm^{-1} and 1035 cm^{-1} corresponding to the vibration of the -C-O bonds of carbons from the repeating unit of cellulose), the peak at 1730 cm^{-1} is correlates to the -C=O vibration band resulting from ester functional units introduced at the surface of CNC (**Figure II. 3 c**).

Moreover, no peak near $1760\text{-}1800\text{ cm}^{-1}$ corresponding to the (-C=O)-Br bond from unreacted BIB is observed. This confirms the efficiency of the washing steps after the reaction. Elemental analyses were carried out on unmodified CNC and grafted CNC-Br to confirm this grafting (**Table II. 1**). Corrected values were obtained by considering the presence of half-sulfate ester groups at the surface of CNCs, and the DS of the grafts on the CNCs that were equal to 0.17 was calculated according to **Equation II. 2**. Differences between the corrected values for neat CNC and theoretical values for pure cellulose can be attributed to the presence of hemicelluloses and impurities in the raw materials. The calculations performed in this study are based on the values corrected according to the method proposed previously (**Equation II. 2**).

Sample	Experimental values				DS _{SO3}	Corrected values		Experimental O/C	Theoretical O/C	DS	%PGMA
	%C	%O	%H	%S		%C	%O				
Neat CNC	40.7	50.8	6.4	0.8	0.04	41.5	51.8	1.2	1.1	/	0
CNC-Br	42.0	45.3	6.0	0.8	0.04	42.8	46.2	1.1	0.8	0.17	0
CNC-PGMA-Br_1h	49.6	37.0	6.9	0.6	0.03	50.6	37.7	0.7	0.7	/	48
CNC-PGMA-Br_24h	53.2	36.7	6.9	0.2	0.01	54.2	37.4	0.7		/	70
PGMA (theoretical)	/	/	/	/	/	59.1	33.8	/	0.6	/	100

Table II. 1. Atomic composition of neat CNCs, CNC-Br, CNC-PGMA-Br_1h and CNC-PGMA-Br_24h obtained by elemental analysis

To further determine and quantify the grafting at the surface of CNC-Br, XPS measurements were taken allowing the characterization of the surface of the materials as being approximately 10 nm in depth⁴¹. **Figure II. 4 a)** shows the XPS sureys of neat CNC and grafted CNC-Br. Both spectra are composed of two main peaks at approximately 534 and 288 eV corresponding to the oxygen and carbon components, respectively. A peak at 71 eV correlated with a bromine component is visible in the CNC-Br survey, and quantification of the Br3d spectrum leads to an atomic percentage of bromine equal to 1.0% at the surface of CNC-Br. **Figure II. 4 b) and c)** show the decomposition spectra of the C1s signal for both neat and grafted CNC-Br.

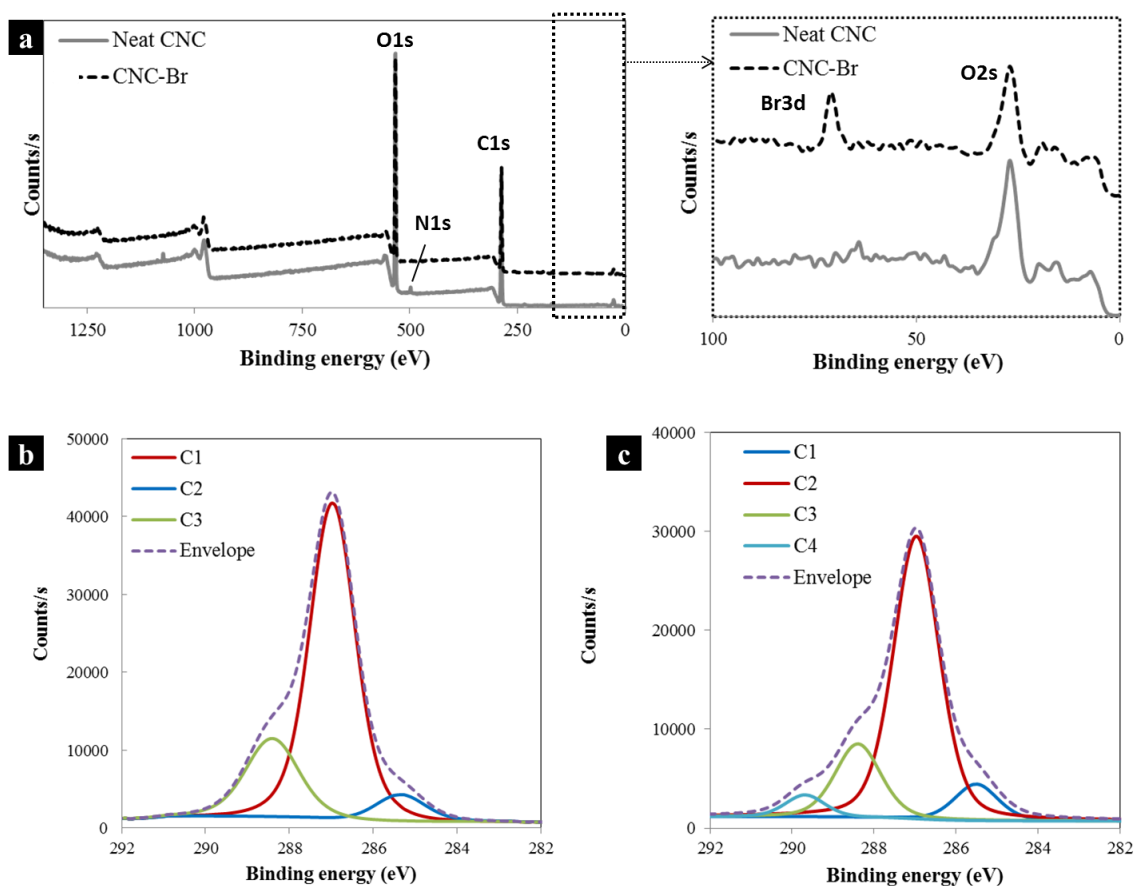


Figure II. 4. a) XPS survey of neat CNCs and grafted CNC-Br, and decomposition of the C1s peak of b) neat CNCs and c) CNC-Br spectra

The neat CNC spectrum displays three peaks, at 285.4 eV, 287.0 eV ($\Delta eV = 1.6$ eV), and 288.4 eV ($\Delta eV = 3$ eV), corresponding to C1 (C-C/C-H), C2 (C-O), and C3 (O-C-O/C=O) bonds respectively. The C1 signal is present in the neat CNC spectrum but is related to the contribution of non-oxidized alkane-type carbon atoms and impurities, residual lignin, or extractive compounds, justifying its presence. The C2 signal is related to the presence of ether groups from pure cellulose, as well as the hydroxyl groups of the unmodified CNCs and of the end of the cellulose chains, explaining its presence in both samples. The C3 signal corresponds to acetal moieties from AGU units and should not change significantly after chemical modification, because the corresponding carbon is not affected. Subsequent to α -bromoisobutyryl bromide grafting, a C4 contribution appears in the CNC-Br spectrum and is correlated to the introduction of (O-C=O) bonds on the material with a ratio of 5%, which confirms the success of the bromide derivative grafting, as previously described in the literature⁶¹ (Figure II. 4 b) and Table II. 2)

Sample	Experimental values			C1s decomposition					
	%C	%O	O/C	C-C / C-H	C-O	O-C-O / C-O	O-C=O	C*-C-O	C-O-C (epoxy ring)
Neat CNC	56	44	0.79	7	72	21	/	/	/
CNC-Br	57	41	0.72	8	69	18	5	/	/
CNC-PGMA-Br_1h	68	32	0.47	29	13	/	9	15	33
CNC-PGMA-Br_24h	70	30	0.43	21	17	/	16	18	28
PGMA homopolymer	72	28	0.39	30	31	/	13	13	13

Table II. 2. Elemental molar compositions and surface functional group compositions obtained by XPS analysis

In addition, the oxygen to carbon ratio (O/C) associated with the sample before and after modification changed from 0.79 (close to that of pure cellulose ≈ 0.83 ¹⁷) for the neat CNCs to 0.72 for the CNC-Br as a result of the α -bromoisobutyryl bromide moiety grafted at the surface of CNCs (**Table II. 2**). From these results, it is possible to conclude the efficient grafting of CNC-Br. Thus, the presence of initiator sites for the further polymerization of GMA on CNC-Br is clearly confirmed.

3.3. Kinetics of the SI-ATRP of GMA

Prior to any polymerization and characterization, it is essential to determine that no parallel reaction — especially adsorption — occurs between cellulose and the monomer. This point was investigated by applying a similar treatment to that of SI-ATRP, but without an initiator, catalyst, or ligand. Only neat CNCs dispersed in anhydrous DMF in the same proportions and the GMA monomer were magnetically stirred for 24 h. CNCs were then recovered after five centrifugation cycles in DCM, and FTIR spectra were obtained after evaporation of the solvent (**Figure II. 5 a**). There is no change in the FTIR spectra of neat CNC after being mixed with the monomer for 24 h; in particular, there is no peak related to a C=O bond from GMA at approximately 1720 cm^{-1} . At this stage, it can be assumed that further evidence of the presence of characteristic groups of GMA and PGMA do not come from possible adsorbed monomer on CNC.

After being grafted, CNC-Br were then polymerized at their brominated initiator sites with GMA, as illustrated in **Scheme II. 1**. Glycidyl methacrylate (GMA) is a monomer that has never been used as part of the polymerization from the surface of wood CNC, to the best of our knowledge. In the literature, only a few studies describe ATRP of GMA^{47,62} on cellulose, presented as a well-known and controlled polymerization. In our case, the difficulty of the polymerization lays in the high reactivity of the epoxy groups of PGMA which can rapidly open. Nevertheless, opening of these epoxy functional groups has been avoided by the reaction at room temperature, in anhydrous conditions, and with the absence of any reagents that can react with these groups. Moreover, it has been shown in the literature that a similar system for SI-ATRP of GMA on a substrate (CuBr/PMDTA) leads to the conservation of active epoxy groups on the polymer chains⁶³. Meanwhile, the presence of these epoxy groups at the surface of polymerized CNC is one objective of this polymerization and is precisely

investigated in this study. Kinetics is the key point in the understanding of a polymerization, and was investigated in this study. At different times during SI-ATRP of GMA initiated by CNC-Br materials, aliquots were withdrawn from the reaction media and analyzed by ^1H -liquid NMR to determine the polymerization conversion by following the disappearance of peaks related to vinyl protons from the monomer and the appearance of peaks related to protons from the methyl groups of the polymer (Figure II. 5 b)).

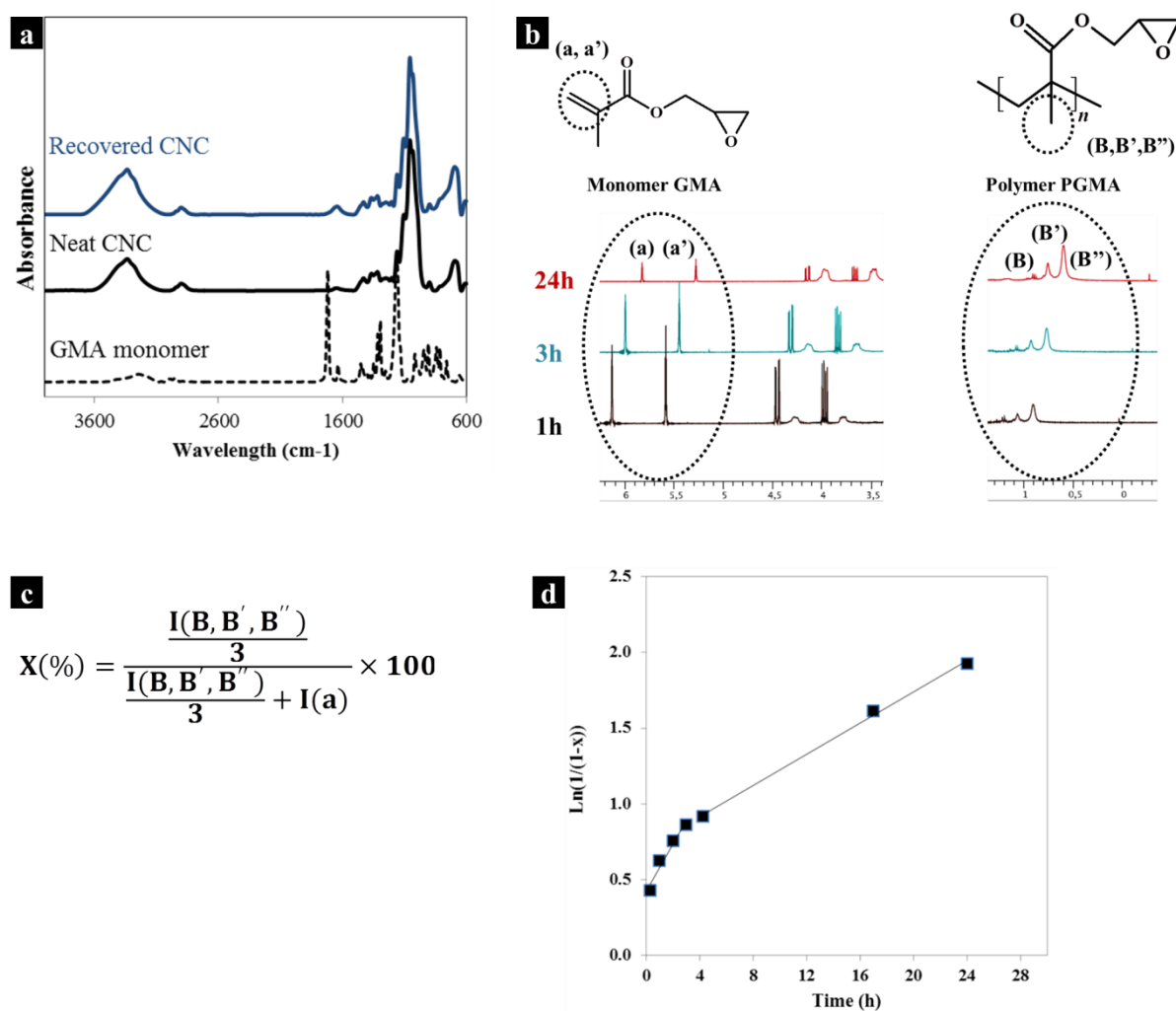


Figure II. 5. a) FTIR spectra of GMA, neat CNC and recovered CNC after mixing with GMA in conditions similar to polymerization, b) ^1H -liquid NMR spectra of the recovered reaction media after three different polymerization times, where (a) and (a') correspond to the protons of the end of the double-bond carbon-carbon of the monomer GMA and (B), (B'), and (B'') to the protons of the methyl groups of the polymer PGMA, c) equation of the conversion rate X calculation with I corresponding to the integral related to the area below the curve of the peak a ($I(a)$) or of the three peaks B, B' and B'' ($I(B, B', B'')$), and d) representation of the evolution of conversion as a function of polymerization time

The recorded NMR spectra show decreasing peak intensity at 5.6 and 6.1 ppm related to the vinyl protons of the monomer. In parallel, the intensity of the peaks between 0.9 and 1.2 ppm related to the protons from the methyl group from the growing polymer clearly increased. Conversion (p) of the GMA into PGMA can be calculated using the formula presented in Figure II. 5 c), where the value I corresponds to the integration of the peaks. The evolution of the conversion is represented by plotting the ratio $\ln(1/(1-p))$ as a function of time (Figure II. 5 d)), showing the two rates of polymerization

with a higher rate in a shorter time period (between 0 and 4 h) and a slower rate after a longer polymerization time period. From each collected aliquot the PGMA homopolymer was recovered after filtration on basic alumina and precipitated in cold methanol. Each homopolymer sample was subjected to SEC analysis to obtain the value of its molar mass (according to the equivalent polystyrene). Polydispersity index D was calculated as the ratio of weight average molar mass (M_w) to the number average molar mass (M_n). The results are presented in **Figure II. 6 a**).

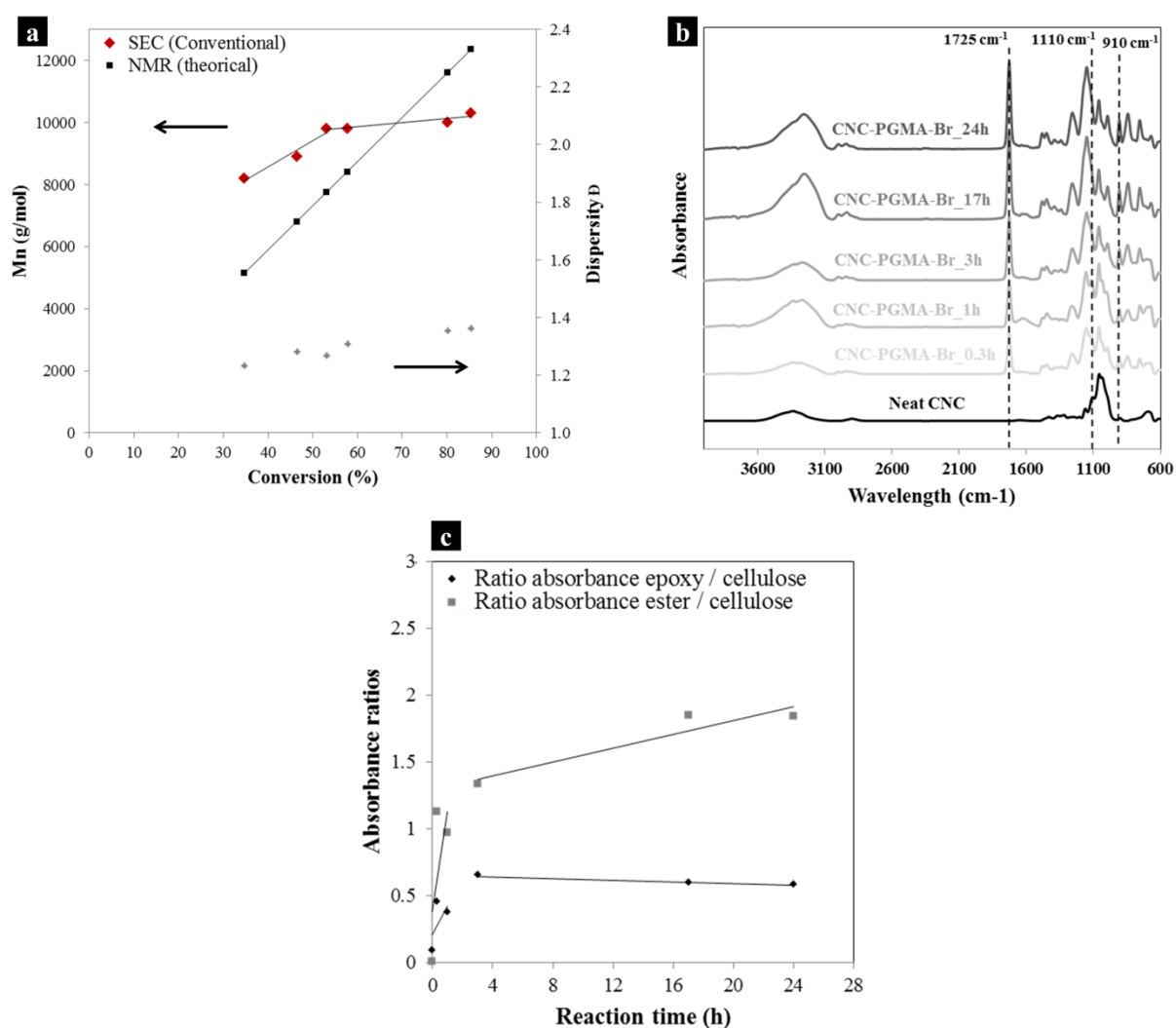


Figure II. 6. a) Molar masses of homopolymer and dispersities obtained by conventional SEC analyses, b) FTIR spectra of recovered CNC-PGMA-Br at different polymerization times, and c) ratios of peak intensities related to epoxy groups/cellulose and ester groups/cellulose

The evolution of the PGMA molar masses calculated by SEC analyses as a function of the conversion follows the same trend as previously mentioned with two different rates of polymerization. Indeed, in the first 3 h of polymerization, the molar masses increased from 8179 g.mol⁻¹ to 9791 g.mol⁻¹, followed by a slower rate of polymerization reaching molar masses equal to 10343 g.mol⁻¹ after 24 h of reaction (**Figure II. 6 d**). This behavior has been previously described for a similar system (GMA/CuBr/PMDETA) in the literature⁶⁴, where it was attributed to the heterogeneous character of the system inducing side-reactions at high conversion rates. Indeed, radical bromine elements from the

cellulose surface could be lost, inducing termination at the level of the CNCs. Nevertheless, polymerization would continue in the system solution. **Figure II. 6 b)** shows the FTIR spectra of CNC-PGMA-Br at different polymerization times, recovered from the aliquots after centrifugation in DCM. Qualitative analysis of these spectra confirms the polymerization on CNCs, with an increase in the peak at 1725 cm^{-1} related to the C=O stretching of ester groups and the presence of a peak at 910 cm^{-1} related to the C-O stretching from epoxy groups. It is interesting to note that ATRP polymerization applied on the GMA monomer, involving the present CuBr/PMEDETA catalytic system, ensures the preparation of an epoxy functional polymer. In fact, as shown in the literature⁶⁵, describing the grafting of multiwalled carbon nanotubes with PGMA polymer using the same ATRP polymerization procedure, a further post modification to introduce molecules of interest is possible by taking advantage of the epoxy functional groups.

Furthermore, to quantitatively analyze these spectra, the ratios of the absorbance values of both C=O and C-O peaks and cellulose (1110 cm^{-1}) were plotted as a function of time. The obtained curves (**Figure II. 6 c)**) follow the previously mentioned trend: with short polymerization time (1 to 3 h), there is an increase in the polymer chain length at the surface of cellulose, which becomes slower at longer times (4 to 24 h). Taking into account these results (summarized in **Table II. 3**), one hypothesis might be that the decreasing polymerization rate is due to the deactivation of brominated active sites grafted at the surface of CNC as well as those from the sacrificial initiator. A transfer reaction resulting from the hydroxyl -OH groups of CNC could be an explanation for this deactivation. In the remainder of this study, we will focus on the characterization of CNC-PGMA-Br polymerized at two different polymerization times (1 h and 24 h): CNC-PGMA-Br_1h and CNC-PGMA-Br_24h, respectively.

Time (h)	¹ H-liquid NMR		SEC (Conventional)		FTIR absorbance ratio	
	Conversion (%)	Mn _{theoretical} (g.mol ⁻¹)	Mn (g.mol ⁻¹)	Dispersity (Đ)	Epoxy (intensity at 910 cm ⁻¹) / Cellulose (intensity at 1110 cm ⁻¹)	Ester (intensity at 1725 cm ⁻¹) / Cellulose (intensity at 1110 cm ⁻¹)
0	0	/	/	/	0.08	0
0.3	35	4944	8200	1.2	0.45	1.13
1	46	6600	8900	1.3	0.37	1.0
2	53	7552	9800	1.3	0.65	1.33
3	58	8209	9800	1.3	0.54	1.60
17	80	11391	10000	1.4	0.59	1.85
24	85	12145	10300	1.4	0.58	1.84

Table II. 3. Summary of kinetics study data obtained from ¹H-liquid NMR, SEC (conventional), and FTIR (* Mn_{theoretical} = $p \cdot ([\text{GMA}] / [\text{EBIB}]) \cdot M_{\text{GMA}} + M_{\text{EBIB}}$ with p the conversion, [GMA] the initial concentration in monomer, [EBIB] the initial concentration in initiator, M_{GMA} the molar mass of GMA and M_{EBIB} the molar mass of EBIB (the calculation takes into account the polymer chain extremities))

3.4. SI-ATRP of functionalized CNC-Br at different polymerization times

CNC-PGMA-Br_1h and CNC-PGMA-Br_24h were polymerized in larger batches for characterization, according to the previously detailed protocol. *Grafting-from* of polymers at the surface of CNCs is a widely studied procedure that allows the grafting of a high density of polymer at the surface of CNCs. In the case of the PGMA grafted as an amorphous polymer, the morphology of the final materials was investigated. **Figure II. 3 a)** shows X-ray diffractograms of CNC-PGMA-Br_1h, CNC-PGMA-Br_24h, and PGMA homopolymer, which is not crystallized and whose XRD signature corresponds to consecutive large humps. The CNC-PGMA-Br_1h diffractogram is a combination of diffractograms of PGMA and cellulose I *beta*, with the presence of characteristic peaks at 22.6° and 34.6°. Similar to CNC-PGMA-Br_1h, CNC-PGMA-Br_24h diffractogram shows characteristic peaks of cellulose I *beta*, but the presence of the amorphous PGMA polymer is more highlighted here. These results confirm the growth of the PGMA on CNCs with increasing polymerization time.

Moreover, according to **Figure II. 3 b)**, the diameter of polymerized CNC-PGMA-Br in DCM increases with the polymerization duration. Indeed, after 1 h, apparent diameter size is equal to 164 nm (122 nm for neat CNC and functionalized CNC-Br), which is reasonable for dispersed CNC suspension. Nevertheless, after 24 h, CNC-PGMA-Br_24h show a higher mean apparent diameter equal to 255 nm and a larger peak, leading to a worse dispersion of grafted nanoparticles in the suspension. Inter-particle coupling reactions between CNC-PGMA-Br is a possible explanation.

The thermal properties of polymerized CNC were investigated through TGA analyses, whose thermograms and derivative thermogravimetry (DTG) curves are presented in **Figure II. 7**, showing that polymerization of PGMA at the surface of CNC enhances the thermal stability of the materials.

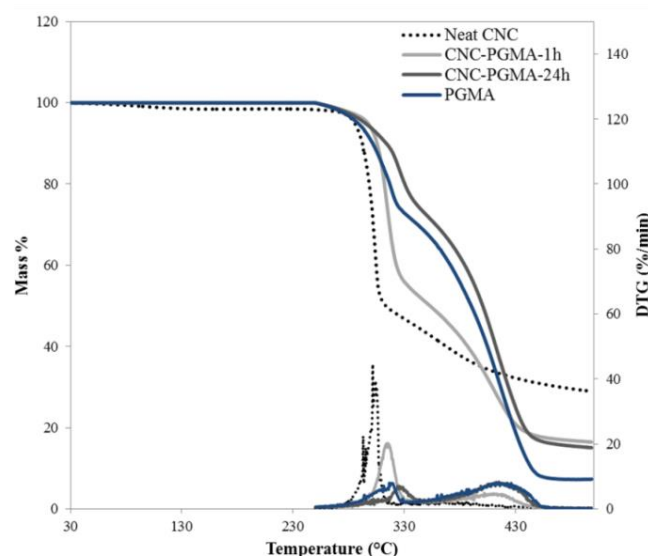


Figure II. 7. TGA thermograms and DTG curves of neat CNC, CNC-PGMA-Br_1h, CNC-PGMA-Br_24h, and homopolymer PGMA

Indeed, the primary onset of the degradation temperature of CNCs before and after 1 and 24 h of polymerization increases from 305 °C to 314 °C and 326 °C respectively. Moreover, the CNC thermogram shows one weight loss peak between 250 °C and 350 °C. In a recent study, Zhang *et al.*⁴² studied different ways to characterize grafted polymers on CNCs, including the use of TGA analysis. Their method appears to be not totally applicable in our case because of the presence of a weight loss peak of PGMA in the same temperature ranges as for cellulose. Moreover, the presence of a second weight loss peak for PGMA, polymerized CNC-PGMA-Br_1h, and CNC-PGMA-Br_24h between 350 °C and 480 °C allows an approximation of the amount of PGMA polymerized on CNC. Indeed, taking into account the slight weight loss of cellulose in this second temperature range for calculation, and considering that samples are only composed of cellulose and polymer, a weight percentage of PGMA equal to 38% and 83% respectively for CNC-PGMA-Br_1h and CNC-PGMA-Br_24h are calculated (**Table II. 4**). The large amount of grafted polymer after 24 h of polymerization is confirmed. Moreover, even after a short polymerization time, nearly 40% by mass of the sample is PGMA, corresponding to the previous kinetic study of this polymerization.

Sample	% weight loss (350 °C – 480 °C)	Thermal degradation onset T_{onset} (°C)	PGMA (wt%)
CNC	14	305	0
CNC-PGMA-Br_1h	30	314	38
CNC-PGMA-Br_24h	49	326	83
PGMA homopolymer	56	319	100

Table II. 4. Thermal degradation onset temperatures and calculated amount of PGMA in both CNC-PGMA-Br_1h and CNC-PGMA-Br_24h

By regarding only the morphology of polymerized CNC-PGMA-Br, 1 h of polymerization ensures the conservation of the crystallinity, which is critical for further applications, while introducing a significant amount of PGMA.

3.5. Efficiency of SI-ATRP on CNCs

The efficiency of the polymerization of GMA from brominated initiator sites previously grafted on CNC was first investigated by FTIR analysis, whose spectra are shown in **Figure II. 3 c**). Results confirm the conclusion drawn from **Figure II. 6 b**), proving the efficiency of the polymerization and the growth of the polymer over time. Indeed, peaks at 910 cm^{-1} , 906 cm^{-1} , 1728 cm^{-1} , and between 2840 cm^{-1} and 3000 cm^{-1} are respectively characteristic of the epoxy groups, terminal vinyl groups and ester bonds from carbonyl groups, and $-\text{CH}_2$ and $-\text{CH}_3$ carbons from the PGMA backbone polymer. The clear increase in those peaks for the CNC-PGMA-Br_1h and CNC-PGMA-Br_24h spectra demonstrates the polymerization of PGMA at the level of CNCs over time. These results are confirmed by elemental analyses (**Table II. 1**). Indeed, for both CNC-PGMA-Br_1h and CNC-PGMA-Br_24h, an increase in the %C values and a decrease in the %O values are notable and consistent with the introduction of the polymer PGMA $(\text{C}_7\text{H}_{10}\text{O}_3)_n$ on CNCs. This is reaffirmed by the

decrease in the O/C ratio for these polymerized CNCs, which is also similar to the corresponding theoretical calculated ratio and to those of pure PGMA. The slight difference between the O/C ratios of CNC-PGMA-Br and PGMA confirms the presence of cellulose in the sample. Note that values are corrected according to the previously described method by considering the presence of half-sulfate ester groups at the surface of CNCs, without however considering the presence of impurities like hemicelluloses in the samples, which could influence the values, so they must be interpreted comparatively. Moreover, considering that CNC-PGMA-Br_1h and CNC-PGMA-Br_24h are composed of cellulose and PGMA, an estimation of the weight percentage of PGMA may also be calculated in both cases, as presented in **Table II. 1**. Values are not totally equal to those previously calculated through TGA thermograms (**Figure II. 7 b**), but the trend is similar, keeping in mind that TGA and elemental analysis have different sensitivities and involve different approaches. The amount of PGMA with increasing polymerization time, and approximately 48% and 70% by mass of PGMA is attached to CNCs after 1 h and 24 h respectively.

One of the primary challenges to SI-ATRP on CNCs involves the characterization and quantification of the grafted polymer at the surface of the nanomaterials. Hansson *et al.*⁴⁵ investigated this point by proving that the kinetics of the polymerization at the surface of CNCs is similar to those in the media from a sacrificial initiator. Previous characterizations allow the proof of the polymerization as well as an estimate of the calculated amount of polymer. The surfaces of polymerized CNC-PGMA-Br_1h and CNC-PGMA-Br_24h were investigated by XPS analyses; the decompositions spectra of the C1s signal are presented in **Figure II. 8 c**) and **d**). In **Figure II. 8 b**), the decomposition spectra of the C1s peak of PGMA homopolymer shows the presence of characteristic peaks of the polymer: at 285.4 eV, 286.1 eV ($\Delta eV = 0.7$ eV), 287.1 eV ($\Delta eV = 1.7$ eV), 287.5 eV ($\Delta eV = 2.1$ eV), and 289.5 eV ($\Delta eV = 4.1$ eV) for respectively the C-C/C-H, C*-C=O-, C-O, C-O-C (epoxy ring), and O-C=O bonds. The CNC-PGMA-Br_1h and CNC-PGMA-Br_24h (**Figure II. 8 c**) and **d**)) decomposition spectra show the same characteristics, as well as a peak characteristic of cellulose at 288.2 eV ($\Delta eV = 3.3$ eV) related to the C3 signal (O-C-O or C=O) from the neat CNCs. It is important to note that the intense C2 signal from cellulose is also present but is superimposed over other C-O and C-O-C peaks. This result confirms the grafting of a PGMA polymer layer onto CNCs.

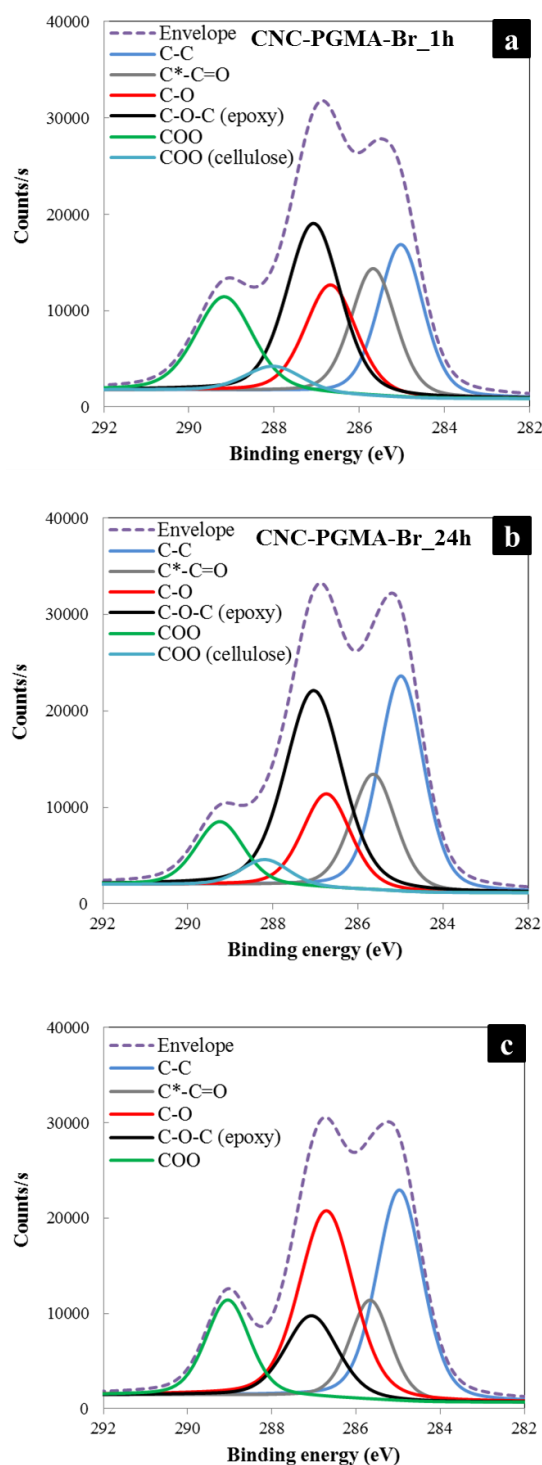


Figure II. 8. Decomposition of the C1s peak of **a)** CNC-PGMA-Br_1h, **b)** CNC-PGMA-Br_24h, and **c)** PGMA homopolymer obtained by XPS analyses

Moreover, the determination of the O/C ratio (**Table II. 2**) leads to a value of 0.47 for CNC-PGMA-Br_1h materials, whereas a ratio of 0.42 is observed for CNC-PGMA-Br_24h, which is similar to the theoretical value associated with pure PGMA polymer⁶⁶. This result could explain the increasing grafted polymer weight with time, as shown in **Figure II. 6 d)**. According to the XPS results, it is possible to make a conclusion about the presence of PGMA over the surface of CNC. Moreover, it is possible to observe in **Figure II. 8** that after 1 h of polymerization, the intensity of the peak associated

with the epoxy C-O-C bond is less intense than that of the homopolymer reference. After 24 h of polymerization, this intensity is closer to that of the homopolymer, confirming that the amount of polymerized PGMA is more important. Quantification of the polymer is not possible considering these results, but the presence of PGMA at the surface of CNCs is clearly highlighted. Moreover, highly reactive epoxy rings are conserved during the polymerization and are available at the surface of both CNC-PGMA-Br_1h and CNC-PGMA-Br_24h.

4. Conclusion

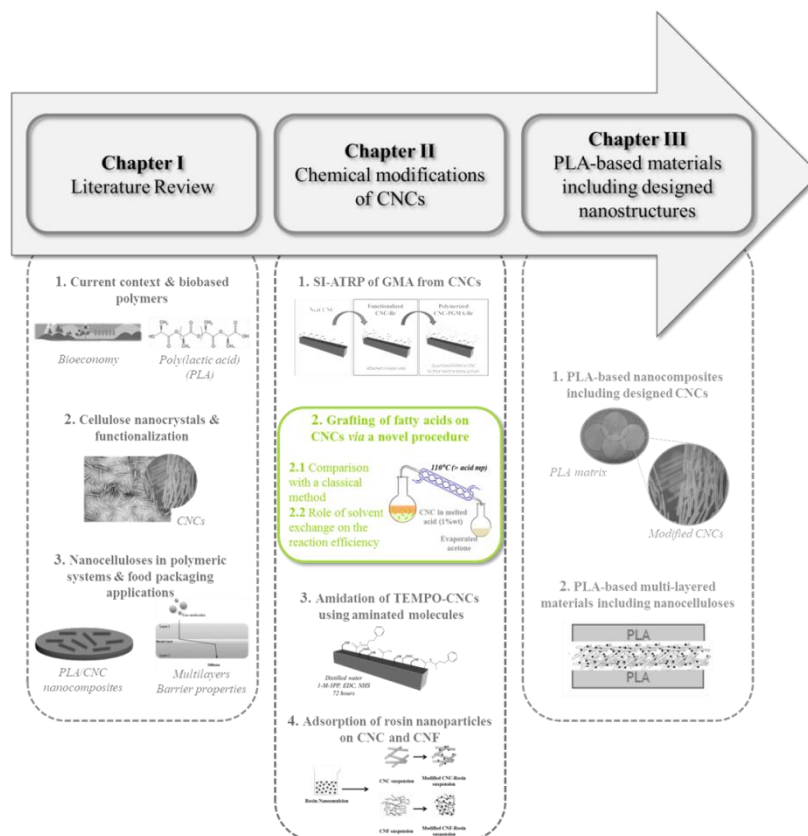
CNCs were initially modified with BIB as an initiator of SI-ATRP of PGMA; the efficiency of the functionalization was highlighted using bulk and surface characterization. After ensuring that only the polymerized monomer is present at the level of CNCs after washing, polymerized CNC at two different polymerization times were recovered and characterized using FTIR, XRD, TGA, XPS and elemental analysis. After only 1 h of polymerization, PGMA covers almost all the surface of CNCs, with a weight percentage of approximately 40% relative to CNC. After 24 h of polymerization, the weight proportion of PGMA represents almost 80% of the total weight, but the obtained polymerized CNCs are more aggregated in non-polar solvent. In both cases, the presence of characteristic bonds of the polymer, and especially carbonyl groups and epoxy rings are highlighted, although 1 h of polymerization seems to optimize the reaction conditions for the preparation of well-dispersed, polymerized, hydrophobized CNCs for further incorporation in hydrophobic polymer matrices or further chemical modification. The results presented in this study are encouraging, and further investigation of poly(lactic acid)-based nanocomposites including CNC-PGMA-Br as nanofillers would be interesting, in order to highlight the interest of the SI-ATRP of GMA at the surface of CNCs.

2. Grafting of fatty acids on cellulose nanocrystals *via* a novel procedure

2.1.

Comparison between two different methods for the chemical modification of cellulose nanocrystals

This short additional section aims to compare the efficiency of two CNC surface modification methods: a classically performed method involving an acid chloride and toxic solvents, and a novel procedure developed in this PhD using a carboxylic acid. This part intends to provide a first proof of concept of this new grafting method, which aims to limit the use of toxic chemicals and will be more detailed and described in the following section 2.2.



Abstract

In addition to their outstanding intrinsic properties making them excellent candidates for a wide range of applications, high surface reactivity of cellulose nanocrystals (CNCs) is highly interesting for potential diverse surface modifications. In fact, the presence of reactive hydroxyl groups at their surface allows many chemical grafting to be performed. Among these chemical modifications, esterification procedures have been widely described in the literature, with an incredible number of various (macro)molecules grafted. Moreover, in a spirit of greener and less toxic chemistry, a novel procedure for the esterification of CNCs using 10-undecenoic acid as carboxylic acid (CNC-10UndecenoicAcid) was developed in this work, and its efficiency was compared with that of a classical successful esterification method involving 10-undecenoyl chloride as acid halide (CNC-10UndecenoylChloride). Although the crystallinity of modified CNCs slightly decreased in both cases, the grafting efficiency was highlighted by Fourier-transform infrared (FTIR) spectroscopy and elemental analyses, with calculated degrees of substitution values equal to 0.1 and 0.4 for CNC-10UndecenoylChloride and CNC-10UndecenoicAcid, respectively. This study emphasizes the efficiency of such a novel greener procedure, as well as, its interest in the CNCs surface modification research field.

Keywords:

Cellulose nanocrystals — Esterification — Acid chloride — Carboxylic acid

1. Introduction

At a time of developing sustainable materials, nano-size cellulosic materials are highly attractive materials². In addition to being biobased and biodegradable, their crystallinity, density, high specific surface area, and high reactivity are outstanding properties which can be used for numerous and diverse applications^{2,7,8,22,67}. Focusing on cellulose nanocrystals (CNCs), they exhibit a highly reactive surface due to the presence of numerous hydroxyl groups, which are beneficial for a large panel of surface modifications. In fact, in the literature, a large amount of publications deal with the chemical modifications of the CNCs' surface^{4,15,18,68}, attending to graft molecules, macromolecules, or polymeric chains at their surface. These surface modifications have different objectives: For example, the grafting of single molecules can confer new active properties to the CNCs, like antibacterial^{27,69,70}, antioxidant⁷¹, or specific sorption properties⁷². On the other hand, the grafting of long aliphatic chains or hydrophobic polymer chains can lead to the CNCs hydrophobization, in order to enhance their compatibilization with an apolar polymeric matrix, for the purpose of nanocomposites preparation^{73–75}.

Among surface modifications of CNCs, esterification is commonly performed. In fact, numerous procedures are described in the literature, like the acetylation^{76,77}, transesterification³², or the use of acid halide reagents^{41,43}, and their efficiency was highlighted, with degrees of substitution generally comprise between 0.4 and 3⁶⁸. Furthermore, some authors performed a so-called “one-step” reaction, taking advantage of the hydrolysis isolation process of CNC by combining it with a Fischer esterification, in order to directly produce modified CNC. In this sense, Boujemaoui *et al.*⁴⁴ combined hydrochloric acid hydrolysis with a Fischer esterification using several carboxylic acids and determined degrees of substitution comprised between 0.06 and 0.27, depending on the carboxylic acid used. However, all these previously described esterification procedures are generally carried out in organic and toxic solvents and require numerous reagents and multi-step procedures.

In current environmental context, renewability and biodegradability of materials is a key point in the production and use of materials. The idea of green chemistry was born in the 2010s, and its principles were described by Anastas and Eghbali⁷⁸, aiming to make greener chemicals, processes and products, and by applying these principles, ensuring the efficiency of the chemical modifications and reactions. In the literature, more and more authors propose greener methods for the surface grafting of CNCs^{4,79,80}. Among these authors, Espino-Pérez *et al.*²⁶ developed a procedure — called *SolReact* process — in which an aromatic carboxylic acid was added to a water suspension of CNCs. By heating the system at a temperature higher than the acid melting point, and after water evaporation, CNCs were suspended in the melted acid, which became the solvent. Highly interesting results were shown by the authors, and degrees of substitution between 0.3 and 0.5 were calculated, accordingly to the acid grafted.

In this study, a novel method, adapted from that proposed by Espino-Pérez *et al.*²⁶, was carried out on CNCs, using the 10-undecenoic acid a long carbon chain molecule. In order to compare the efficiency of this developed method with that of a common esterification of CNCs surface, an esterification using the 10-undecenoyl chloride as acid chloride was performed, in parallel. Recovered modified CNCs, called CNC-10UndecanoicAcid and CNC-10UndecenoylChloride, respectively, were characterized by X-ray diffraction (XRD), Fourier-transform infrared (FTIR) spectroscopy and elemental analysis, in order to prove and compare their efficiency, and to give a proof of concept of the developed greener esterification procedure.

2. Materials and methods

2.1. Materials

Cellulose nanocrystals (CNCs) were supplied by CelluForce (Canada) in spray-dried form. 10-undecenoyl Chloride, 4-Dimethylaminopyridine (DMAP), 10-undecenoic Acid, and sulfuric acid (H_2SO_4 , 92 %) were supplied by Sigma-Aldrich Chimie (France), and used as received. Toluene was supplied by Sigma-Aldrich Chimie (France), and was stored and used in anhydrous conditions. Ethanol (95%) was purchased from Revol (France).

2.2. Classical esterification of CNCs using 10-undecenoyl chloride

An aqueous suspension of 10 g of CNCs in water at 1 wt% was prepared by introducing a proper amount of dried CNC in water, following by 1 h of magnetic stirring, and an ultrasonic treatment (2500 J/g) using a Sonifier S-250A (Branson, USA). The suspension was then solvent exchanged. Briefly, the water suspension was first subjected to a centrifugation cycle (10 000 rpm, 5 °C, 15 min), and the supernatant was removed. The recovered CNCs were re-dispersed in ethanol using an ultrasonic treatment, and the suspension was then submitted to another centrifugation step (10 000 rpm, 5 °C, 15 min). After recovery of the supernatant, the re-dispersion (this time in acetone) and centrifugation steps were carried out twice, following the same procedure as before. The two last centrifugations (10 000 rpm, 5 °C, 15 min) were similarly performed in toluene. The final concentration of the CNC suspension in toluene was adjusted to 1 wt%, sonicated (2500 J/g), and was then introduced into a three-neck flask. 2.26 g of DMAP (0.19 mol) were introduced in the flask, and the reaction mixture was left stirring at room temperature for 30 min. Thereafter, 3.75 g of 10-undecenoyl chloride (0.19 mol) were added dropwise, using a dropping funnel, and the reaction media was stirred under reflux at 110 °C for 4 h. At the end of the reaction, the mixture was cooled at room temperature, and submitted to 5 successive centrifugation cycles (10 000 rpm, 5 °C, 15 min) in ethanol. Recovered CNC-10UndecenoylChloride were stored in a hermetically sealed vial in the fridge.

2.3. Esterification of CNCs with 10-undecenoic acid *via* a novel method

An aqueous CNC suspension was prepared and solvent exchanged from water to ethanol, and then to acetone, as previously described in section 2.2. The concentration of the final suspension in acetone was adjusted to 1 wt%, and the suspension was poured into a round-bottomed flask equipped with a distillation system, and heated at 110 °C. The 10-undecenoic acid was then introduced into the flask in a ratio of 100:1 relatively to the dry mass of CNC, and a catalytic amount of sulfuric acid was also added. After the total acetone evaporation, the CNC suspension was dispersed in the melted 10-undecenoic acid (melting point ~ 25 °C) and was magnetically stirred for 8 h at 110 °C. At the end of the reaction, the CNCs were extensively washed by six successive centrifugation and re-dispersion

cycles (10 000 rpm, 25 °C, 15 min) in acetone. Recovered CNC-10UndecenoicAcid were stored in a hermetically sealed vial in the fridge.

2.4. Characterization methods

2.4.1. X-ray diffraction (XRD)

XRD analyses were performed on dried powder samples of neat CNC (commercially spray-dried), and modified CNC-10UndecenoylChloride and CNC-10UndecenoicAcid. Diffractogram patterns were obtained using a PANalytical X'Pert PRO MPD diffractometer, equipped with an X'accelerator detector. A copper anode ($K\alpha$ radiation of 1.5419 Å) allows a symmetric scan reflection ($\theta / 2\theta$, Bragg angle), in a range of 2θ between 5° and 60°. Using the Segal height peak method^{55,57}, the crystallinity indexes (CI) of each sample were calculated following the **Equation II. 4**:

$$CI = \left(1 - \frac{I_{am}}{I_{002}}\right) \times 100$$

Equation II. 4. Crystallinity index (*CI*) calculation according to the Segal height peak method

where I_{am} corresponds to the intensity at the minimum ($2\theta \approx 18.3^\circ$) and I_{002} is the intensity associated with the main crystalline region of cellulose ($2\theta \approx 22.5^\circ$). Measurements were repeated at least twice.

2.4.2. Fourier transform infrared (FTIR) spectroscopy

FTIR spectra of neat CNC, and modified CNC-10UndecenoylChloride and CNC-10UndecenoicAcid were performed on a Perkin Elmer Spectrum 65 spectrometer *via* the transmission method. By mixing and milling KBr and CNC powders (ratio 99:1 wt/wt), pellets were obtained by applying a 10 t/m² pressure for one min, and were left drying an oven (1 hour, 105 °C) before the analysis. The absorbance spectra were recorded between 600 and 4000 cm⁻¹, with a resolution of 4 cm⁻¹, and 32 scans. All the spectra were normalized at 1110 cm⁻¹ (characteristic peak of the pure cellulose). Measurements were at least duplicated for each sample.

2.4.3. Elemental analysis

Elemental analyses were performed by the Institut des Sciences Analytiques (Villeurbanne, France). The carbon, hydrogen, oxygen and sulfur contents were titrated by a micro analyzer (CNRS, France), and the relative error on the measurements was close to 0.4%. From the data, the degree of substitution (*DS*) of modified CNC — corresponding to the number of grafted hydroxyl groups per AGU — was calculated from the **Equation II. 5**, which was adapted from the previous work of Espino-Pérez *et al.*⁷²:

$$DS = \frac{M(C)_{AGU} - \omega_C \cdot (M_{AGU} + DS_{SO_3} \cdot M_{SO_3})}{\omega_C \cdot M_{grafted} - M(C)_{grafted}}$$

Equation II. 5. Degree of substitution (*DS*) calculation

where $M(C)_{AGU}$ corresponds to the carbon molar mass in an AGU (72.06 g.mol⁻¹), M_{AGU} is the total molar mass of an AGU (162.14 g.mol⁻¹), ω_C is the relative carbon content obtained from the analysis, $M_{grafted}$ the molar mass of the graft (154.1 g.mol⁻¹) and $M(C)_{grafted}$ the carbon molar mass of the grafted acid (120.1 g.mol⁻¹). Note that in the case of pure cellulose, weight fractions %C and %O are theoretically equal to 44.4% and 49.4%, with an O/C ratio equal to 1.11. In this study, experimental %C and %O values were corrected by taking the theoretical values for the neat CNC sample, as previously done in the literature^{26,59}. DS_{SO_3} corresponds to the degree of substitution linked to the presence of sulfate-half ester groups present the surface of CNC, and was calculated from the sulfur weight fraction %S obtained from the elemental analysis, accordingly to the **Equation II. 6**, where where M_{SO_3} is the molar mass of the substituted $-SO_3^-$ groups (80.1 g.mol⁻¹):

$$DS_{SO_3} = \frac{S\% \cdot M_{AGU}}{M_S - \%S \cdot M_{SO_3}}$$

Equation II. 6. Degree of substitution of half sulfate ester groups (DS_{SO_3}) calculation

3. Results and discussions

3.1. Influence of the chemical modifications on the structure of the CNCs

Chemical modifications carried out on CNCs can affect their crystallinity, mainly because of the reduction in hydrogen bonding or the change in polymorph to cellulose II⁶⁸. In the present study, the evolution of the crystalline structure of the CNCs after the two different surface modifications was investigated *via* XRD analyses performed on powder-form samples. The corresponding X-ray diffractograms are presented in **Figure II. 9**. As expected, the unmodified CNC sample exhibits a crystalline organization. At 16.5°, 22.6° and 34.6°, peaks related to the signals (101) / (10 $\bar{1}$), (002), and (040) are characteristic of the cellulose I β structure, and the crystallinity index (**Equation II. 4**) was determined to be equal to 86%, confirming the high crystalline behavior of neat CNCs.

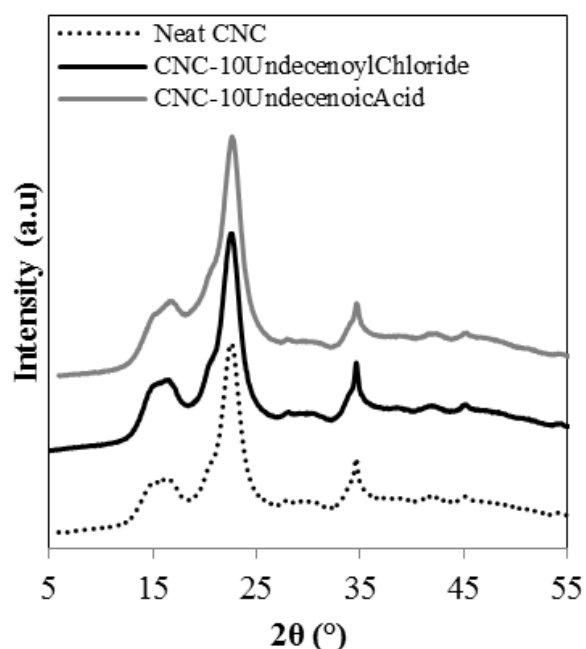


Figure II. 9. X-ray diffractograms of neat CNC, CNC-10UndecenoylChloride, and CNC-10UndecenoicAcid

The X-ray diffractograms of CNC-10UndecenoylChloride and CNC-10UndecenoicAcid samples present similar peaks at 16.5°, 22.6° and 34.6°, confirming the conservation of their cellulose I β structure. The calculated crystallinity indexes of modified CNC-10UndecenoylChloride and CNC-10UndecenoicAcid are equal to 81% and 78%, respectively. A slight decrease in crystallinity is thus observed in both cases, and can be assigned to the reactions conditions (time, temperature, etc.), as well as, to the manual grinding step. In fact, this step was particularly long, especially for the CNC-10UndecenoicAcid. Moreover, it is essential to point out that the peak height method should only be taken as an approximation¹⁴, and it is therefore difficult to quantitatively conclude about these results. Nevertheless, the two methods of functionalization do not heavily affect the crystallinity of the grafted materials. More generally, the conservation of the materials crystallinity is highly important,

especially for specific applications like composites, in which crystallinity of the nanomaterials is one of the main reasons for their use.

3.2. Efficiency of the two surface modification methods

The efficiency of the modifications, using a classical or a novel esterification procedure, was first investigated by FTIR, and the resulted spectra are presented in **Figure II. 10**. In both cases, the appearance of peaks related to the presence of ester bonds (O-C=O), aliphatic carbons (-CH₂), and double bonds (C=C) was expected. As seen in **Figure II. 10**, FTIR spectra of unmodified CNC exhibits typical peaks of pure cellulose, for example those at 1105 cm⁻¹ and 3000-3600 cm⁻¹, related to the vibrations of C-O bonds and hydroxyl groups (I and II), respectively.

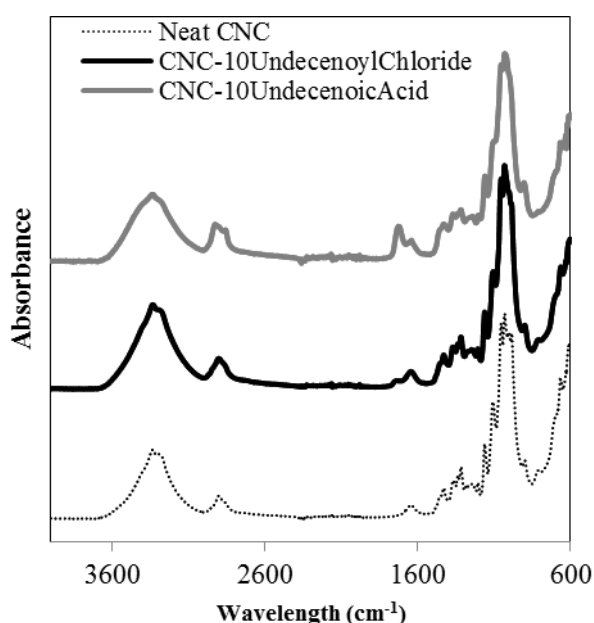


Figure II. 10. FTIR spectra of neat CNC, CNC-10UndecenoylChloride, and CNC-10UndecenoicAcid

Regarding the spectra of CNC-10UndecenoylChloride and CNC-10UndecenoicAcid samples, they exhibit a peak at 1735 and 1732 cm⁻¹, respectively. In both cases, this peak can be attributed to the C=O bond from the created ester groups at the surface of modified CNC. It is clearly noticeable that this peak is more intense in the spectra related to the CNC-10UndecenoicAcid sample. Moreover, around 2800-2900 cm⁻¹, the peak corresponding to the aliphatic -CH₂ and/or alkenes =CH₂ carbons is also visible in the CNC-10UndecenoicAcid spectra, and clearly evidences the presence of the long aliphatic chains (10 carbons) grafted at the surface of the CNCs. Although this peak cannot be clearly observed in the CNC-10UndecenoylChloride spectra, the presence of the peak related to the ester groups allows concluding about the presence of grafted chains at the CNCs surface. Thus, both CNC-10UndecenoylChloride and CNC-10UndecenoicAcid spectra evidenced the efficiency of the grafting of long chains at the surface of modified CNC, with a supposed higher grafting density in the case of CNC-10UndecenoicAcid. Moreover, no peaks related to the presence of unreacted products (10-

undecenoyl chloride or 10-undecenoic acid) are visible, confirming the efficiency of the washing steps at the end of each reaction.

In order to quantify the amount of grafted molecules, elemental analyses were performed on the modified CNC-10UndecenoylChloride and CNC-10UndecenoicAcid samples, as well as, on neat CNC sample as reference. Results of these analyses are summarized in **Table II. 5**. As previously mentioned, the values of %C and %O were corrected accordingly to the theoretical values of pure cellulose. Note that differences between experimental and theoretical values can be attributed to the presence of some impurities in the samples. It could also have been interesting to treat the unmodified CNCs in the same way as CNC-10UndecenoylChloride and CNC-10UndecenoicAcid (same reaction times, temperature, solvent and, washing steps) without reagents, in order to have a more representative reference. Moreover, the DS_{SO_3} was calculated for the three samples (**Equation II. 6**), and a decrease from 0.04 to 0.02 (50%) is observed for the CNC-10UndecenoicAcid sample, probably due to the desulphation of CNC occurring during the esterification reaction. On the other hand, the values of DS_{SO_3} are equal for both neat CNCs and modified CNC-10UndecenoylChloride, indicating that the acylation reaction conditions do not induce desulphation of the CNCs.

Sample	Experimental values				DS_{SO_3}	Corrected values		Experimental O/C	Theoretical O/C	DS
	%C	%O	%H	%S		%C	%O			
Neat CNC	40.7	50.8	6.4	0.8	0.04	44.4	49.4	-	1.11	-
CNC_10UndecenoylChloride	42.3	50.0	6.2	0.7	0.04	46.1	48.6	1.05	0.47	0.07
CNC_10UndecenoicAcid	49.0	43.2	7.3	0.4	0.02	53.5	42.0	0.79	0.47	0.36

Table II. 5. Atomic composition of neat CNC, CNC-10UndecenoylChloride and CNC-10UndecenoicAcid obtained by elemental analyses with corrected values, theoretical and calculated ratio O/C, and calculated degree of substitution (DS)

Regarding the calculated O/C ratios, that of CNC-10UndecenoylChloride only slightly decreased from 1.11 to 1.05, while CNC-10UndecenoicAcid sample exhibits a decrease around 0.79. It clearly highlights the efficient introduction of numerous carbons coming from the grafted long carbon chains. Note that in both cases, these experimental ratios were higher than the theoretical ones (equal to 0.47 in both cases), clearly indicating that not all hydroxyl groups have been modified during the two reactions, as expected. It was confirmed by the calculated degrees of substitution DS (**Equation II. 5**), whose values were equal to 0.07 and 0.36, for modified CNC-10UndecenoylChloride and CNC-10UndecenoicAcid, respectively. The low value obtained for CNC-10UndecenoylChloride was surprising, since high degree of substitution were reported in the literature for similar graftings using acid halide reagents^{68,81}. However, some publications^{74,82} showed that such a grafting using long aliphatic chains led to lower degrees of substitution, in the range 0.2-0.1. In our study, the low DS obtained for the grafting of 10-UndecenoylChloride can thus be attributed to the length of the grafted moieties, the possible presence of water traces, or the kinetics of the reaction which could have lasted longer. The DS calculated for the CNC-10UndecenoicAcid was equal to 0.36, which is very satisfied,

especially for such a novel esterification procedure involving no toxic reagents and milder conditions. Regarding the literature, the efficiency of this second esterification method is comparable with that of other classical efficient esterification methods^{4,68}.

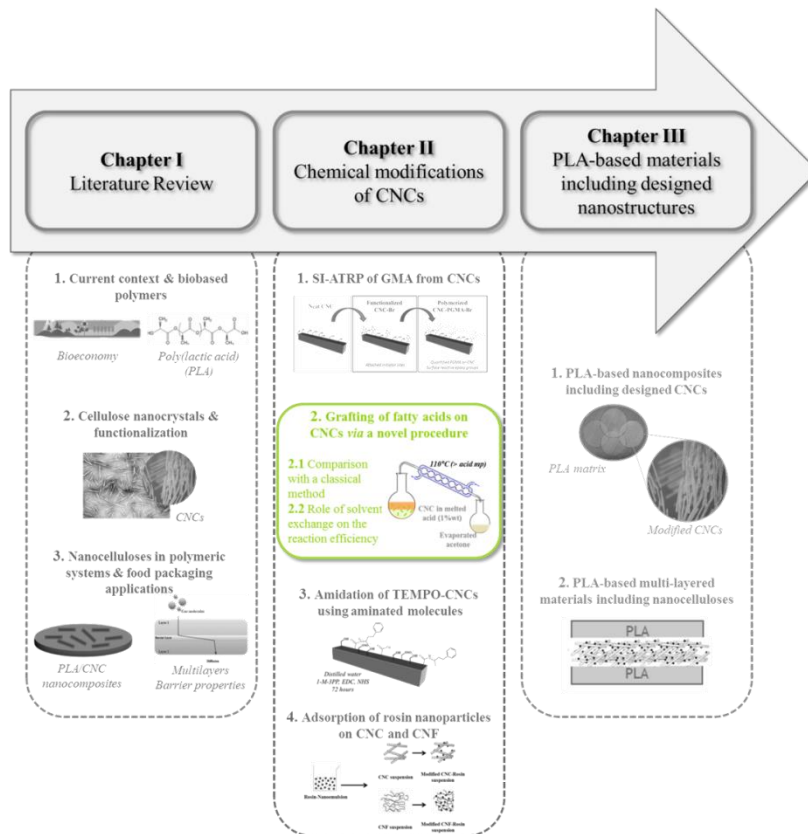
4. Conclusion

In the present short study, the efficiency of the two methods of esterification procedures was proved, and the presence of grafted 10-undecenoyl chloride and 10-undecenoic acid compounds on CNCs was highlighted by FTIR analysis. Moreover, their quantifications were performed *via* elemental analyses, and the calculated degree of substitutions values were consistent with those found in the literature, although the classical reaction involving an acid chloride was expected to be more efficient. Nevertheless, the satisfying degree of substitution of the 10-undecenoic acid compounds on the CNC *via* a novel esterification procedure aiming to reduce the use of toxic chemicals was highlighted. These results are encouraging as they allow the grafting of carboxylic acids on CNC, while limiting the use of organic toxic chemicals.

2.2.

Role of solvent exchange in dispersion of cellulose nanocrystals and their esterification using acids as solvents

This section is adapted from M. Le Gars, P. Roger, M. N. Belgacem, J. Bras “Role of solvent exchange in dispersion of cellulose nanocrystals and their esterification using fatty acids as solvents”, Cellulose, 2020.



Abstract

The recent emergence of bio-based nanocomposites makes perfect sense from a technical and environmental point of view. Cellulose nanocrystals (CNC) are novel bio-based nanomaterials with a wide range of beneficial properties. Their biodegradability, crystallinity, high surface area, and mechanical strength, as well as their highly reactive surface, make them ideal materials as nanofillers in polymeric matrices. However, most the bio-based polymers are hydrophobic, and the hydrophilicity of CNC is therefore a challenge to their incorporation in such matrices. In this study, a new procedure for surface modification of CNC with long aliphatic chains (lauric acid (12 carbons) and stearic acid (18 carbons)) was developed that limits the use of petro-chemicals and facilitates their potential recycling. A study of the dispersion state of CNC in acetone was performed first. Then, grafting efficiency was highlighted by several techniques and quantification of the amount of grafted fatty chains was investigated. Degrees of substitution on the bulk and on the surface of the CNC were calculated between 0.1 and 0.3, which provided enough grafted functions to confer hydrophobic behavior to modified CNCs, as highlighted by the increasing of contact angle from 65° for neat CNC to 80° after modification. Finally, conservation of CNC crystalline structure and morphology was proved by both X-ray diffraction and transmission electron microscopy analyses. Modified CNCs exhibit a crystallinity index close to 86% and length of approximately 350 nm. Thus, crystalline hydrophobic cellulosic nanomaterials were prepared using a more environmentally friendly procedure than those classically found in the literature.

Keywords:

Cellulose nanocrystals — Chemical surface modification — Esterification — Green chemistry

1. Introduction

Recently, novel nanomaterials extracted from cellulose sources have been developed and exponentially studied¹⁷. Two main types of nanocelluloses currently exist: cellulose nanofibrils (CNFs) and cellulose nanocrystals (CNCs). CNFs can be obtained by applying a mechanical treatment after biological or chemical pre-treatments on cellulose, resulting in nanofibrils with dimensional properties varying from 2 to 50 nm in width and 500 nm to 2 μm in length, depending on the isolation process and the source¹. By chemically treating biomass using acid hydrolysis, CNCs are extracted. Ranby *et al.*⁸³ were the first to discover that reacting cellulose with sulfuric acid leads to a disintegration of the amorphous parts of the cellulose polymer chains while keeping crystalline areas intact. Although several studies have demonstrated this method's success with several different acids, sulfuric acid hydrolysis remains the most common, controlled and optimized method for CNC extraction^{3,84-87}. CNCs classically present widths in the range of 2 to 15 nm and lengths between 100 and 500 nm, leading to high aspect ratios, depending mainly on their source — some CNCs from tunicate can even achieve lengths of approximately 1500 nm³. As their name and isolation process suggests, CNCs have high crystallinity (up to 95%) depending on their specific source and isolation process¹⁸. They exhibit other interesting intrinsic properties like low toxicity, low density, high specific area, and high intrinsic mechanical properties^{3,12,16}. Moreover, their isolation *via* sulfuric acid hydrolysis induces the presence of sulfate half ester groups (-OSO₃-) on their surfaces. CNCs are therefore highly stable in aqueous media, leading to stable colloidal suspensions with interesting rheological properties⁸⁸. This partly explains the enthusiasm for these novel nanocelluloses for use in the laboratory as well as on an industrial scale. Indeed, CNCs are studied for a wide range of applications, like biomedicine, cosmetics, paints, coatings, food additives, filtrations, and composites.

Nonetheless, CNCs also have some drawbacks. Due to the numerous hydroxyl groups of cellulose chains and the resulting hydrogen bonds, dispersion of CNCs in organic solvents, as well as their re-dispersion after drying is difficult^{60,89}. This point can be an issue when working in non-aqueous solvents or in dried form. CNCs are hydrophilic, and their dispersion in hydrophobic compounds — solvents or polymers — is challenging and is the main obstacle for their use in nanocomposites, although they are the materials of choice for this kind of application. Indeed, their nano-scale dimensions, high crystallinity, and stiffness, as well as high specific area are extremely relevant for their use as nanofillers in a polymeric matrix^{3,90}. Most polymeric systems used are hydrophobic (including polyethylene (PE), polypropylene (PP), and poly(lactic acid) (PLA), among others), and incorporation of CNCs as fillers requires a previous compatibilization step with the selected apolar matrix in order to render them hydrophobic. In literature, numerous publications deal with this compatibilization of CNC in order to enhance the mechanical and barrier properties of the final nanocomposites^{5,6,90,91}. The abundance of reactive hydroxyl groups (three per anhydroglucose unit (AGU)) on the surface of CNCs offers a wide range of possible functionalizations and three main

types of surface modifications are presented in literature: physical adsorption, the grafting of polymer chains, and the grafting of single (macro)molecules. These functionalizations aim to maintain other intrinsic properties of CNCs, like their morphology and crystallinity.

In this study, covalent grafting of long aliphatic chains *via* esterification on the surface of CNCs is investigated by the limited use of chemicals and organic solvents. Grafting fatty acids on nanocellulose for their hydrophobization has been a scientific challenge for several decades, and numerous strategies have been described in literature. Indeed, apart from surfactant adsorption^{92,93} or polymer adsorption⁹⁴, covalent grafting of fatty acids has been the subject of many publications. Acylation of cellulose fibers and cellulose nanocrystals with various fatty acyl chlorides^{95–97} or surface modification of cellulose nanofibers using octadecyl isocyanate⁵⁹ have been efficiently developed over the past several years. However, these surface modifications require the use of organic and often toxic solvents. Other modifications carried out in water have been described with the use of hydrophobic alkyl ketone dimer (AKD) molecule nano-emulsion to modify the surface of cellulose nanofibers^{98–100}. However, this simple and efficient procedure has never been performed on CNCs because they would play an undesirable role as a surfactant. Currently, surface hydrophobization of CNCs traditionally involves multi-step procedures and toxic organic solvents, and these aspects are limiting factors for any industrialization. However, other hydrophobization procedures have been proposed through the use of fatty acid chlorides directly onto dried cellulosic substrate *via* a chromatogeny procedure involving liquid-vapor equilibrium¹⁰¹, or *via* a gas procedure on CNC aerogels¹⁰². Both methods, however, require already-formed cellulosic materials and cannot be performed on CNC suspensions.

Though grafting of long aliphatic chains on CNC is a research topic that has already proposed several times in literature, it has always been performed with the use of organic solvents or on dried formed materials. In this work, we investigated a novel method of modification of suspended CNCs that makes limited use of toxic solvents. Recently, Espino-Pérez *et al.*^{20,26} described a novel method — called *SolReact* — for the surface functionalization of CNCs directly with carboxylic acids, using a “Green Process” for further incorporation of such modified CNCs in PLA matrices. In this method, a CNC-water suspension was briefly heated to a temperature greater than the melting point of the selected carboxylic acid, which was added in large excess. After complete water evaporation, the CNCs are dispersed in the melted acid, acting as the reaction solvent. Half sulfate ester groups on the surface of the CNC play the role of catalyst. After several hours of reaction, recovered washed CNCs were characterized, and the efficiency of the grafting was highlighted. This novel method was the starting point of our work. This technique is promising (limited solvent used) but cannot be used with fatty acids, as they are not soluble in water. Indeed, an emulsion is obtained and grafting would not be homogeneous on CNCs. Therefore we decided to investigate a possible pre-step to favor a good dispersion of CNC, and to avoid emulsification.

In this paper, a new and adapted method for the surface esterification of CNCs with aliphatic chains is described. Although the idea is still to use such natural fatty carboxylic acid as a solvent, it opens the door to the use of acids that are not soluble in water. The initial dispersion of CNCs is studied extensively, and its influence on grafting yield is analyzed. The efficiency of a novel esterification procedure in which a reagent acts as solvent and can be recycled is investigated. CNCs were modified with lauric or stearic acid — long aliphatic chains bearing 12 and 18 carbons respectively — and different characterization techniques were used to highlight the grafting efficiency in the bulk (Fourier-transform infrared spectroscopy (FTIR), ^{13}C -solid state nuclear magnetic resonance (NMR), elemental analysis), as well as on the surface (X-ray photoelectron spectroscopy (XPS)).

2. Materials and methods

2.1. Materials

Spray-dried cellulose nanocrystals supplied by CelluForce (Canada) were produced from bleached Kraft pulp by sulfuric acid hydrolysis. Sulfuric acid (H₂SO₄, 92%) was purchased from Revol (France). Lauric acid (≥98%) and stearic acid (Reagent grade 95%) were supplied by Sigma-Aldrich Chimie (France) and used as received. Acetone (95%) and ethanol (95%) were purchased from Revol (France) and used as received.

2.2. CNC suspensions preparation

In order to study the dispersion of CNC suspensions, different suspension preparations with a common concentration equal to 1 wt% were investigated. In *Suspension 1*, CNC powder was introduced into distilled water and magnetically stirred for one hour at room temperature. Next, an ultrasonic treatment (2500 J/g) was applied to the suspension, maintaining the temperature with the use of an external ice water bath. *Suspension 2* was prepared by following the same method, but water was replaced with acetone. After ultrasound treatment, the suspension was continuously stirred until further characterization occurred. *Suspension 3* was prepared by solvent-exchange. First, *suspension 1* was centrifuged (10 000 rpm, 5 °C, 15 min), and the supernatant was recovered. Recovered CNCs were re-dispersed in ethanol, and ultrasonic treatment was applied (2500 J/g). This step was repeated twice, and the suspension was submitted to another centrifugation step (10 000 rpm, 5 °C, 15 min). After recovery of the supernatant, the re-dispersion (this time in acetone) and centrifugation steps were carried out twice, following the same procedure as before. Recovered CNCs were then re-dispersed in acetone with ultrasonic treatment after adjusting the final concentration to 1 wt%. Finally, *suspension 4* was prepared by evaporating acetone from *suspension 3* at room temperature, re-dispersing the obtained dried CNCs in acetone following the described *suspension 2* protocol, and adjusting concentration to 1 wt%. All suspensions were stored in perfectly closed vials in a refrigerator before any reaction or characterization. **Figure II. 11 a)** schematizes the different procedures for CNC suspension preparation.

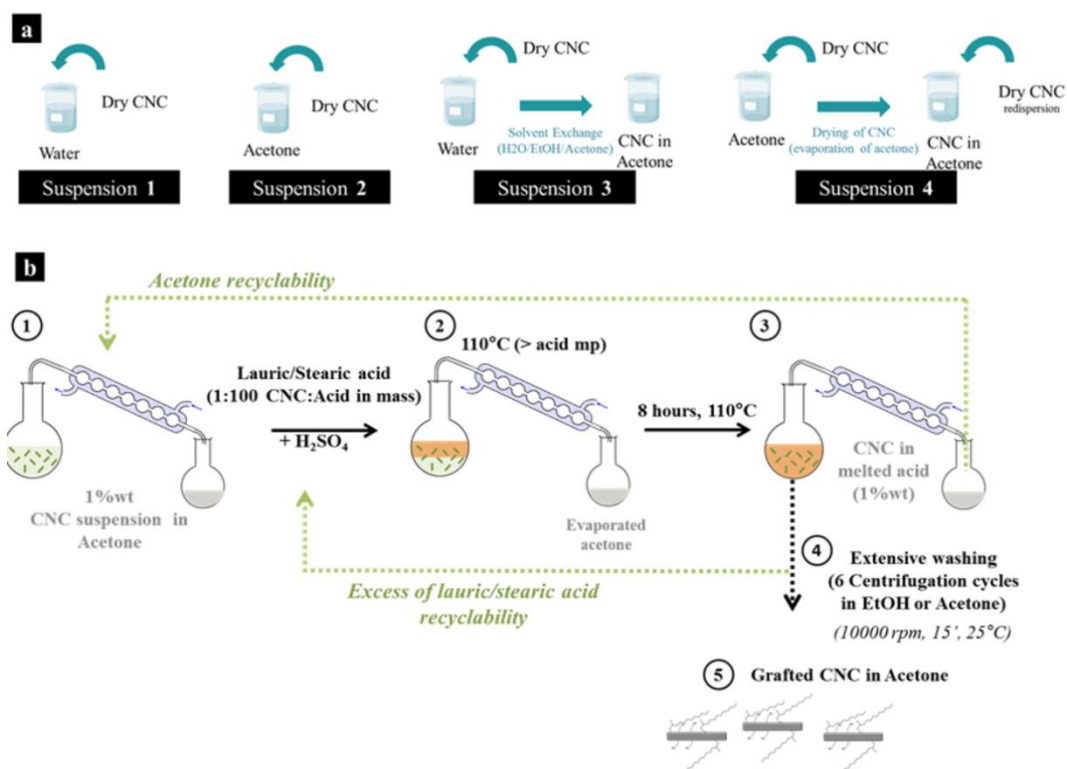


Figure II. 11. a) CNC suspension preparation methods for their dispersion study and **b)** General procedure of CNC esterification using fatty acid reagent as solvent : (1) CNC suspension in acetone obtained after solvent exchange, (2) heating of the reaction media at 110 °C and addition of fatty acid, (3) 8 h of reaction after complete acetone evaporation, (4) washing steps by centrifugation-redispersion cycles in ethanol or acetone according to the fatty acid used, (5) recovering of washed grafted CNC in acetone. Green dashed lines represent recyclability of both acetone and fatty acid after the process

2.3. Esterification of CNCs with fatty acids

The CNC esterification procedure was adapted from the protocol described by Espino-Pérez *et al.*²⁶ However, knowing that both lauric and stearic acid are not soluble in water, unlike the acids used in their work, this study's procedure has been modified and optimized. Firstly, a CNC suspension was prepared according to the protocol previously described for *suspensions 2* or *3*. The suspension was introduced into a round-bottomed flask equipped with a distillation system to allow evaporation of the solvent. An oil bath was heated to 110 °C. A fatty carboxylic acid — lauric or stearic — was introduced into the flask in a ratio of 100:1 relative to the mass of CNC. A catalytic amount of sulfuric acid was also added to catalyze the esterification. After total evaporation of acetone, the CNC suspension was then dispersed in melted lauric acid (melting point 44–46 °C) or stearic acid (melting point 67–72 °C) and was magnetically stirred for 8 h at 110 °C. At the end of the reaction, CNCs were extensively washed with a solvent of the fatty acid (ethanol or acetone in the case of lauric or stearic acid, respectively) by six centrifugation and re-dispersion cycles (10 000 rpm, 25 °C, 15 min). To ensure effective washing of CNC, the supernatant from the last centrifugation was recovered and analyzed by FTIR. No trace of unreacted acid was found. After the last washing step, the CNC

suspension in acetone or ethanol was subjected to an ultrasonic treatment and stored in a hermetically sealed vial in the fridge. A scheme of the reaction is presented in **Figure II. 11 b**).

2.4. Characterization methods

2.4.1. Dynamic light scattering (DLS)

DLS analysis was carried out to determine the apparent size of CNCs. A VASCO particle size analyzer (Cordouan Technologies, France) was used for particle size measurement from nano- to micro-scales in liquid. A diluted suspension of CNCs around 10^{-2} — 10^{-3} wt% in a chosen solvent was prepared and introduced to the device. Ten measurements at 15 second time steps and a limit noise ratio of 0.7 were carried out for each sample. To correlate the result with the theoretical model used, the polydispersity index (PDI) must be less than 0.2. Measurements, that were at least triplicated, were collected and analyzed using nanoQ™ software. The cumulative method allows for the calculation of the hydrodynamic diameter of particles.

2.4.2. Fourier-transform infrared (FTIR) spectroscopy

FTIR spectra of neat and modified CNCs were performed on a Perkin Elmer Spectrum 65 spectrometer *via* the transmission method. KBr pellets were prepared by mixing and milling a 99:1 ratio by mass of KBr:CNC, followed by 10 t/m^2 pressure for one min. Pellets were dried in an oven (1 hour, $105 \text{ }^\circ\text{C}$) before any analysis to limit the presence of water. Absorbance spectra were registered between 600 and 4000 cm^{-1} , with a resolution of 4 cm^{-1} and 32 scans. Spectra were normalized according to the characteristic peak of cellulose at 1110 cm^{-1} , and were at least triplicated. The most representative spectrum was used for the discussion.

2.4.3. Transmission electron microscopy (TEM)

Diluted suspensions of neat and modified CNCs were prepared in water and acetone, respectively. Suspension drops were deposited on copper grids covered with a thin amorphous carbon film, which had been previously plasma cleaned (easiGlow Pelco). After a few minutes, liquid excess was absorbed with filter paper. If necessary, the preparation was negatively colored by placing a drop of 2% uranyl acetate on the grid. After one min, the excess dye was absorbed with the filter paper. Samples were observed with a JEOL JEM 2100-Plus transmission electron microscope, operating at an acceleration voltage of 200 kV. Images were recorded using a Gatan Rio 16 digital camera.

2.4.4. Atomic force microscopy (AFM)

Diluted suspensions at approximately 10^{-3} — 10^{-4} wt% were prepared and dispersed using a sonication probe (2500 J/g). A suspension droplet was deposited on the surface of a cleaved mica plate which was left to dry overnight at ambient temperature. Images of dried CNC suspensions were analyzed using AFM and recorded using the tapping mode with a Dimension Icon Bruker equipped with a

silicon cantilever (O-TESPA, Bruker, USA). Scans of $10 \mu\text{m}^2$ and $3 \mu\text{m}^2$ were recorded and analyzed using Nanoscope Analysis and ImageJ software. Average dimensions with standard deviation were measured from at least 50 measurements of CNC for each sample, and the height was used to measure CNC width.

2.4.5. X-Ray diffraction (XRD)

XRD analysis was performed on dried powder samples obtained by drying neat or grafted CNC suspensions at room temperature, which were then gently ground with a mortar to obtain a very fine powder. Diffractogram patterns were obtained with a PANalytical X'Pert PRO MPD diffractometer, equipped with an X'accelerator detector. A copper anode ($K\alpha$ radiation of 1.5419 \AA) allows a symmetric scan reflection ($\theta / 2 \theta$, Bragg angle), in a range of 2θ between 5° and 60° . In accordance with the Segal height peak method^{55,57}, the crystallinity index (CI) of each sample can be calculated according to the **Equation II. 7**:

$$CI = \left(1 - \frac{I_{am}}{I_{002}}\right) \times 100$$

Equation II. 7. Crystallinity index (CI) calculation according to the Segal height peak method

where I_{am} is the intensity at the minimum ($2\theta \simeq 18.3^\circ$) and I_{002} is the intensity associated with the main crystalline region of cellulose ($2\theta \simeq 22.5^\circ$). Measurements were repeated at least twice.

2.4.6. Elemental analysis

Elemental analyses were carried out by Institut des Sciences Analytiques (Villeurbanne, France). Carbon, hydrogen, oxygen and sulfur contents were titrated with the use of a micro analyzer (CNRS, France). The relative error of our duplicated measurements was approximately 0.4%. Obtained data allowed the determination of the degree of substitution (DS) of modified CNC — corresponding to the number of grafted hydroxyl groups per AGU — according to **Equation II. 8** and adapted from a previous study²⁶.

$$DS = \frac{M(C)_{AGU} - \omega_C \cdot (M_{AGU} + DS_{SO_3} \cdot M_{SO_3})}{\omega_C \cdot M_{grafted} - M(C)_{grafted}}$$

Equation II. 8. Degree of substitution (DS) calculation

where $M(C)_{AGU}$ is the carbon molar mass in an AGU (72.06 g.mol^{-1}), M_{AGU} the total molar mass of an AGU ($162.14 \text{ g.mol}^{-1}$), ω_C the relative carbon content obtained from the analysis, $M_{grafted}$ the molar mass of the graft (173 g.mol^{-1} or 267 g.mol^{-1} respectively for lauric or stearic acid) and $M(C)_{grafted}$ the carbon molar mass of the grafted acid (144 g.mol^{-1} or 216 g.mol^{-1} respectively for lauric or stearic acid). DS_{SO_3} — the degree of substitution related to the presence of sulfate half ester groups on the surface of CNC — was introduced in the equation and calculated from the sulfur weight fraction $\%S$ obtained by the analysis following **Equation II. 9**:

$$DS_{SO_3} = \frac{S\% \cdot M_{AGU}}{M_S - \%S \cdot M_{SO_3}}$$

Equation II. 9. Degree of substitution of half sulfate ester groups (DS_{SO_3}) calculation

where M_{SO_3} corresponds to the molar mass of the substituted $-\text{SO}_3^-$ groups ($80.1 \text{ g}\cdot\text{mol}^{-1}$). Considering the presence of these sulfate half ester groups allows for the correction of the values of carbon and oxygen weight fractions, which has been determined by other methods in literature^{26,59}.

2.4.7. CP-MAS ^{13}C -solid state NMR

^{13}C -NMR analyses were performed at Institut Nanoscience and Cryogénie, which is attached to the French Alternative Energies and Atomic Energy Commission. ^{13}C -NMR spectra were obtained from a Bruker AVANCE 500 spectrometer. Dry CNC samples were placed in ZrO_2 rotors and cross-polarization, high power proton decoupling and magic angle spinning (CP/MAS) were applied. Spectra were provided at 298K, with a spinning speed equal to 12 kHz. For each sample, 40,000 scans with 300 ppm spectral width were recorded with relaxation and CP times equal to 2.0 seconds and 2.0 milliseconds, respectively. Chemical shift values were calculated with tetramethylsilane as the first reference, and with glycine as the second. The carboxyl signal was set to 176.03 ppm.

2.4.8. X-ray photoelectron spectroscopy (XPS)

XPS experiments were carried out on a K-Alpha Thermo Fischer spectrometer installed with a monochromatic source ($\text{Al K}\alpha$, 1486.6 eV). A spot size of 400 μm was used for all measurements, and the hemispherical analyzer operated in constant analyzer energy mode (CAE), with pass energy of 200 eV and a step of 1 eV for surveys spectra, and with pass energy of 50 eV and a step of 0.1 eV for high resolution spectra. To neutralize charge accumulation, a dual beam flood gun was used. Data treatment was carried out using Advantage software (Thermo Fischer). Background subtraction (Shirley type) and normalization of peak areas (using Scofield sensitivity factors) were performed before any calculation of elemental composition. Binding energies were referenced to C1s neutral carbon peak at 284.8 eV. Measurements were performed on at least two zones of 0.12 cm^2 of the sample.

2.4.9. Contact angle

Contact angle measurements were carried out using a contact angle meter OCA20 equipped with a CCD camera and SCA20 software. A 5 μL droplet of distilled water was deposited on casted films of neat CNC or on pellets of modified CNC. Experiments were performed at room temperature and acquisition of contact angle and droplet volume evolution was recorded during the first 30 seconds, just after droplet deposition until its stabilization. All measurements were at least repeated five times.

3. Results and discussions

3.1. Different ways for the dispersion of CNC in acetone

Although numerous methods have been described to functionalize CNC surfaces to favor their compatibilization with hydrophobic polymers, only a few of them were performed in non-toxic solvents. The *SolReact* method recently described by Espino-Pérez et al.²⁶ was a novel strategy limiting solvent use. However, our use of lauric or stearic fatty acids did not allow the use of aqueous conditions due to their insolubility in water. Indeed, the use of water-suspended CNCs would lead to an emulsion. For this reason, a different solvent was needed for CNC suspensions, acetone was chosen because of its solubility with both lauric and stearic acids, as well as its low boiling point. The dispersion of CNC in such an organic solvent, however, is not as efficient as in aqueous media. The presence of half sulfate ester groups on the surface of CNC induces electrostatic repulsions between the nanoparticles in a diluted aqueous system, leading to an extremely well-dispersed and stabilized CNC. However, in non-polar organic solvents, these electrostatic repulsions are not sufficient to stabilize the CNCs which will aggregate and decant relatively rapidly^{60,103}. Several studies have investigated the dispersion of CNCs in organic solvent by modifying their surface, particularly by the adsorption of surfactants¹⁰⁴, or after the covalent grafting of low molecular weight polymers⁹³ at the CNC surface. In our case, we aimed to avoid pre-functionalization or surfactants, and therefore dispersion of unmodified CNCs in acetone was required as the first step of the CNC esterification reaction. Thus, a study of the dispersion state of different CNC suspensions in both acetone and water (for the sake of comparison) was essential before any surface modification of CNCs could be done. Indeed, CNC dispersion is crucial for any chemical modification, because the larger their surface is, the more accessible the surface hydroxyl groups will be, and therefore the more efficient their modification will be. In this study, four different CNC suspensions were prepared, according to protocols previously described (**Figure II. 11 b**).

To determine the state of CNC dispersion in the different suspensions, dynamic light scattering (DLS) measurements were performed. It is important to bear in mind that dynamic light scattering only provides qualitative information, because it uses a model based on spherical particles, as opposed to the rod-like CNC particles. In our case, DLS analyses allow quantitative and comparative studies of our different samples, as same has already been performed in literature^{58,60,105,106}. As previously mentioned, CNCs are known to stabilize in an aqueous media, and therefore *Suspension 1* is our positive reference for dispersion. Each suspension was analyzed by DLS, and recovered curves are presented in **Figure II. 12 a**).

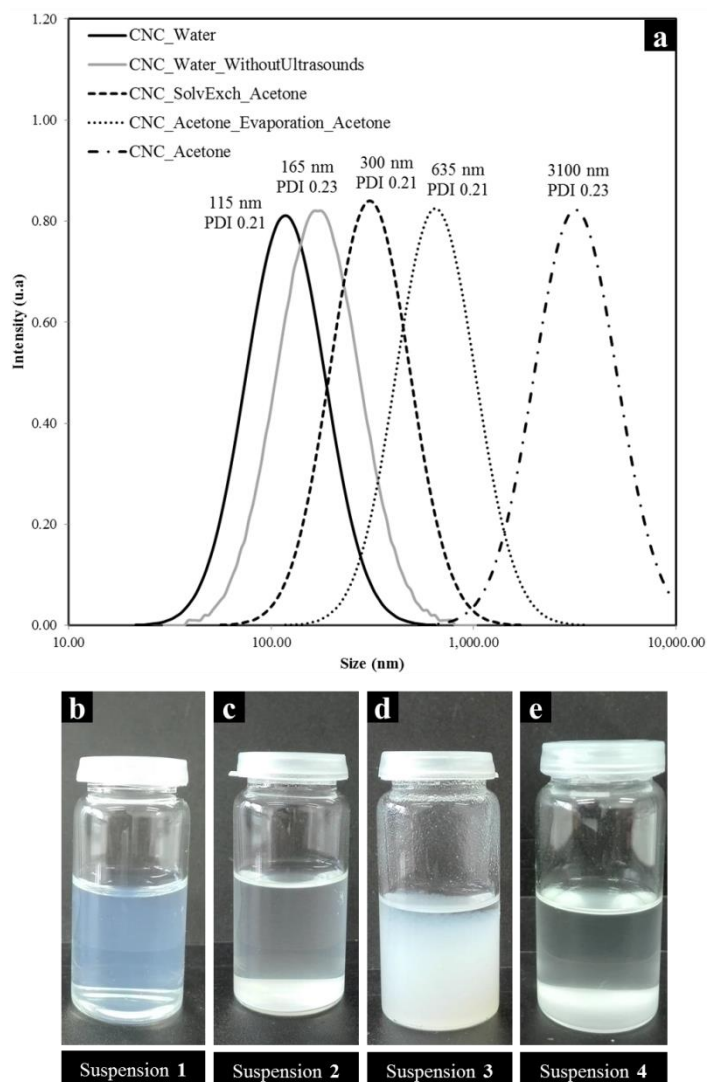


Figure II. 12. a) Dynamic light scattering (DLS) curves of CNC suspensions in water with and without ultrasonication (dark and grey solid lines), in acetone after solvent exchange (---- line), in acetone after redispersion of dried CNC from acetone suspension (..... line) and in acetone after direct incorporation of dried CNC (--- line), **b-e)** Pictures of CNC suspensions at 1 wt% after four hours of rest, **b)** CNC in water (Suspension 1), **c)** CNC in acetone (Suspension 2), **d)** CNC in acetone after solvent exchange (Suspension 3) and **e)** CNC in acetone after re-dispersion of dried CNC from suspension in acetone (Suspension 4)

As seen in **Figure II. 12 a)**, all polydispersity indexes (PDI) were close to 0.2, which allows for validation of the model used by the acquisition software. Moreover, CNCs dispersed in water and ultrasonically treated exhibited an apparent mean diameter of 115 nm, which correlates with values found in the literature¹². Note that without ultrasounds, this value increased to 165 nm, confirming the role of ultrasounds in CNC dispersion in water. By directly incorporating the dry powder of neat CNCs in acetone (**Suspension 2**), the apparent particle size reached 3100 nm, suggesting the presence of micrometric aggregates, and confirming the fact that CNCs are not stabilized by electrostatic repulsions in such an organic solvent. **Suspension 4**'s protocol was designed to avoid the solvent

exchange procedure, which is energy- and time-consuming on a larger scale. By firstly mixing CNCs in acetone, drying them, and finally re-dispersing them in acetone, an improvement of the dispersion due to a possible surface modification of CNC was expected. Although the apparent particle size was lower than that in *Suspension 2*, it was equal to 635 nm, suggesting the presence of large aggregates. On the other hand, by firstly dispersing CNCs in water and then performing a solvent exchange with ethanol and then acetone, the particle size observed by DLS was approximately equal to 300 nm. Even though this value was higher than those obtained for water-suspended CNCs, it was still in the range of nanometric particles, and we can speak about a dispersed nano-suspension. It could be explained by the fact that the electrostatic forces occurring in water between each CNC were not totally lost after the centrifugation cycles, leading to a more stable suspension in acetone than those obtained by direct mixing of CNC in acetone. Moreover, when CNCs in acetone were dried at ambient temperature and then re-dispersed in acetone, the mean diameter obtained by DLS was approximately 635 nm. This value was six times higher than for neat CNCs in water, but still lower than in *suspension 2*. This could be because acetone slightly modifies the surface layer of CNC, inducing a better compatibilization and dispersion with the solvent. These results are illustrated by **Figure II. 12 b-e)**, showing the different suspensions 1, 2, 3 and 4 at 1 wt% four hours after dispersion. In **Figure II. 12 b)**, it is clearly visible that water-suspended CNC was highly stable and transparent, confirming the stability of CNC in water. Moreover, in **Figure II. 12 c)**, it is observable that CNC sedimented at the bottom of the vial. This confirms the fact that CNCs directly introduced in acetone were not stabilized and dispersed, leading to their complete sedimentation. On the other hand, as observed in **Figure II. 12 d)**, the CNC suspension in acetone obtained after solvent exchange was much more stable. Indeed, even if a slight sedimentation is visible, a more homogeneous suspension is observed, although no transparency is reached. Finally, in **Figure II. 12 e)** corresponding to *suspension 4*, similar sedimentation to that of *suspension 2* is observed. All these results confirm the fact that CNCs were well-dispersed in aqueous systems but their dispersion was more difficult in an organic solvent. Without surface modification, the most effective method to obtain the most dispersed suspension in acetone is to perform solvent exchange from a well-dispersed suspension in water to ethanol and then to acetone (*suspension 3*). In the remainder of this study, the aforementioned method was chosen and performed.

3.2. Influence of solvent exchange on the grafting efficiency

In order to confirm the previous assertion (assuming that *suspension 3* would be the most suitable for our protocol) and to highlight the role of the dispersion state of CNC suspensions before chemical modification, esterification reactions using both lauric and stearic acid were performed on CNC directly dispersed in acetone (*suspension 2*) (on aggregated CNC). Esterification was carried out according to the previously described protocol. After the washing steps, recovered CNCs respectively

named CNC_Lauric and CNC_Stearic were analyzed by FTIR. The obtained spectra are presented in **Figure II. 13 a)**.

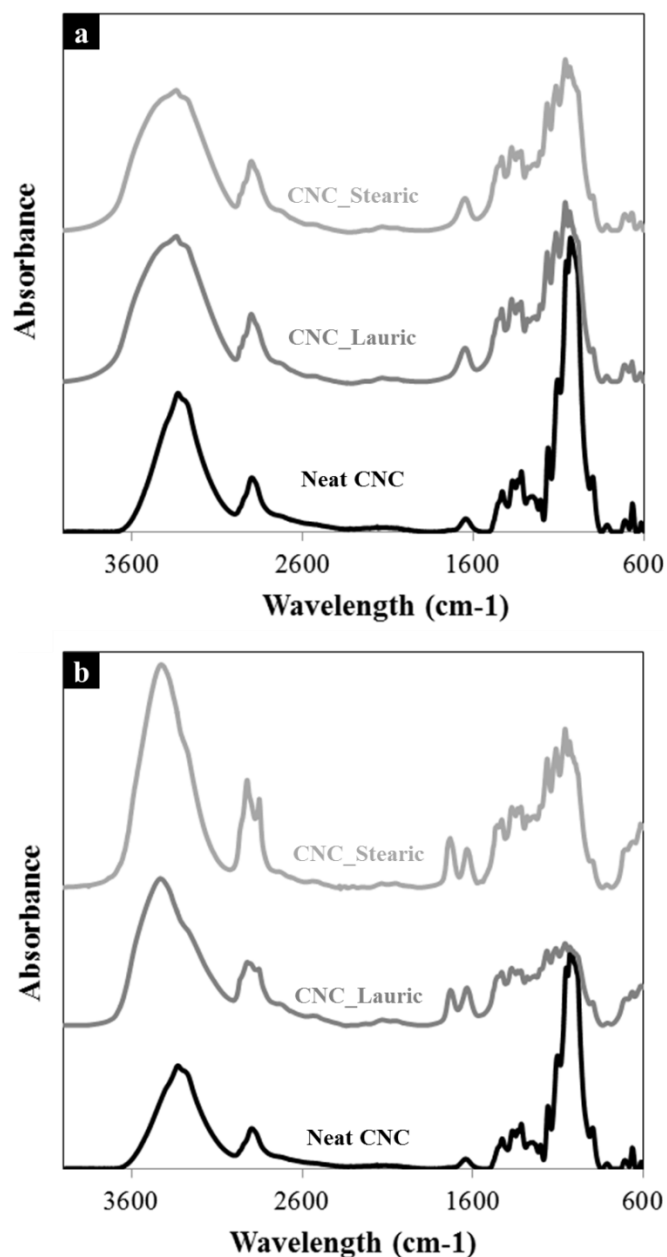


Figure II. 13. FTIR spectra of recovered CNCs after esterification performed with lauric or stearic acid carried out on **a)** aggregated CNCs in acetone (*suspension 2*) and **b)** dispersed CNCs in acetone (*suspension 3*)

According to these FTIR spectra (**Figure II. 13 a)**), no significant difference in peaks is visible. However, in both **Figure II. 13 a)** and **b)**, all spectra present peaks of pure cellulose, among others: the large peak between 3000 and 3600 cm⁻¹ is linked to stretching vibration bonds in hydroxyl groups (I and II), the peak at 1636 cm⁻¹ is related to the presence of adsorbed water, and peaks at 1105, 1059, and 1028 cm⁻¹ are linked to the vibrations of C-O bonds. The esterification reaction aims to create ester bonds with the hydroxyl groups of CNCs, and therefore the appearance of a peak related to the -C=O bond in an ester bond (at approximately 1720-1730 cm⁻¹) should be observed after reaction. Thus,

no evidence of grafting is seen here, which confirms the fact that grafting on poorly-dispersed CNC is not effective because of the limited available surface area of the nanoparticles. Furthermore, the peak at approximately 1700 cm^{-1} related to the -C=O bond from the acid is not visible on CNC_Lauric and CNC_Stearic spectra, which highlights the washing step's efficiency in totally removing unreacted acid. In the rest of this study, it is therefore accepted that the washing steps were optimized and allowed us to perfectly remove all the unreacted acid.

Thus, it has been proved that esterification carried out on aggregated CNC was not efficient. According to the preliminary study of CNC dispersion, a suspension of CNC in acetone obtained by solvent exchange (*suspension 3*) was prepared to achieve an esterification reaction. A kinetic follow-up of the esterification of CNC was investigated. An aliquot of the reaction media was collected at different reaction times and analyzed by FTIR. This kinetics study was carried out for an esterification performed with stearic acid. It was considered that the kinetics of esterification using lauric acid would be quite similar. Obtained FTIR spectra are represented on **Figure II. 14 a**).

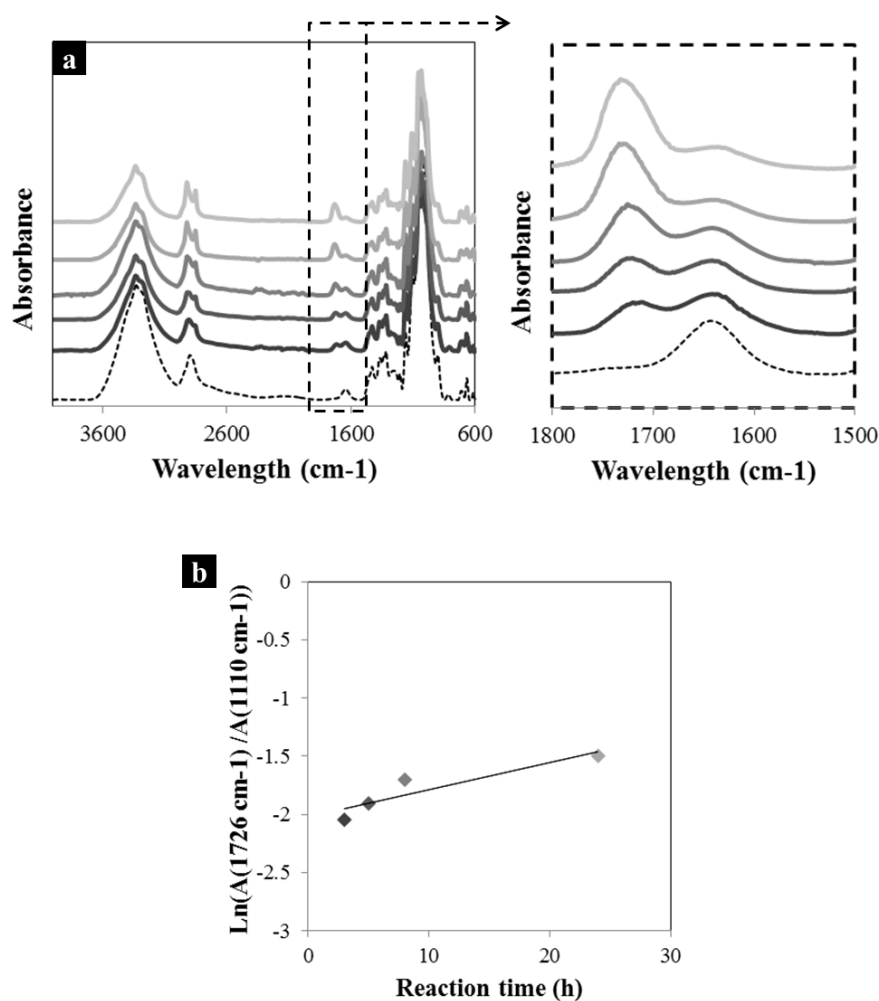


Figure II. 14. Kinetics study of esterification of CNC with stearic acid : **a**) FTIR spectra of different CNC_Stearic in the time and **b**) evolution of the logarithm \ln of the ratio of absorbance values related to the peak of -C=O bond from ester (1726 cm^{-1}) on the peak characteristic of cellulose (1110 cm^{-1})

The appearance and increase of the peak at 1728 cm^{-1} related to the $\text{C}=\text{O}$ bond from introduced ester groups is observed. In addition, the appearance of two intense peaks between 2900 and 2950 cm^{-1} related to the CH_2 and CH_3 carbons correlates with the introduction of long aliphatic chains on the surface of CNC. **Figure II. 14 b)** was plotted as function of the time. The resulting curve exhibits a linear evolution with respect to time and evidences the first order of the esterification reaction with a velocity constant k equal to $6.4 \times 10^{-6}\text{ s}^{-1}$. Because the esterification proposed in this work follows a first-order kinetic law, it is possible to assume that the reaction takes place as long as there is a limiting reagent, which is the surface hydroxyl group of CNC. These first-order esterification kinetics have already been demonstrated in literature in a heterogeneous system consisting of flax fibers¹⁰⁷. As part of our study, an 8-hour reaction time was chosen to be conscious of energy consumption. Moreover, in the spirit of greener, sustainable chemistry, washed unreacted acid was recovered and characterized. **Figure II. 15** shows the FTIR spectra of both unreacted lauric and stearic acids recovered after the reaction and compared with their commercial received forms. For each of the acids, the two FTIR spectra are perfectly identical and in both cases the peak at 1700 cm^{-1} related to the $\text{C}=\text{O}$ bond from the carboxylic groups remains unchanged. Thus, recycling and reuse of these acids after reaction is feasible and would be interesting from an economic and environmental point of view because it would reduce the cost and chemicals waste of this esterification reaction on CNC.

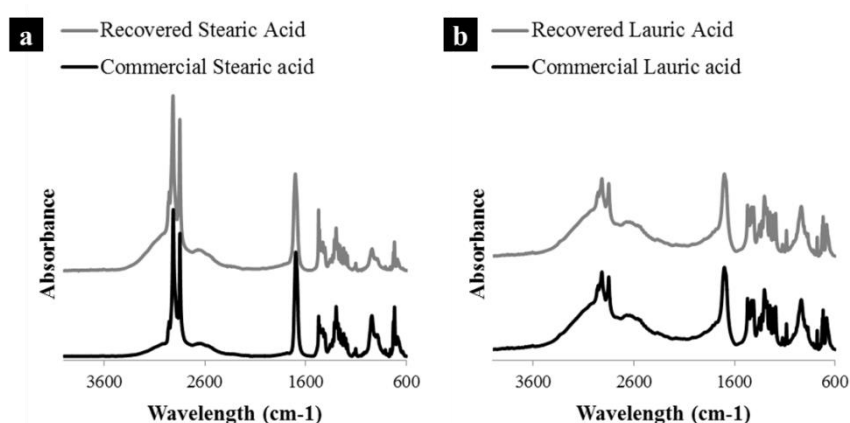


Figure II. 15. FTIR spectra of commercial and recovered unreacted **a)** stearic acid and **b)** lauric acid

The structure of modified CNC was investigated by TEM, AFM, and XRD analyses. TEM images were obtained with and without coloring in order to mitigate against possible artefacts, especially due to the presence of acetone. Nevertheless, coloring allows for a more accurate observation of the nanoparticles. Resulting images are presented in **Figure II. 16 a), b) and c)**. It is clearly visible that both modified CNC_Lauric and CNC_Stearic were slightly aggregated at the end of the reaction. Indeed, neat CNC size was determined to be equal to $110 \pm 30\text{ nm}$ in length and $4 \pm 1\text{ nm}$ in width, whereas CNC_Lauric and CNC_Stearic exhibited lengths equal to $347 \pm 106\text{ nm}$ and $350 \pm 60\text{ nm}$ and widths equal to $29 \pm 8\text{ nm}$ and $30 \pm 10\text{ nm}$ respectively. It can then be assumed that several modified CNCs have aggregated together.

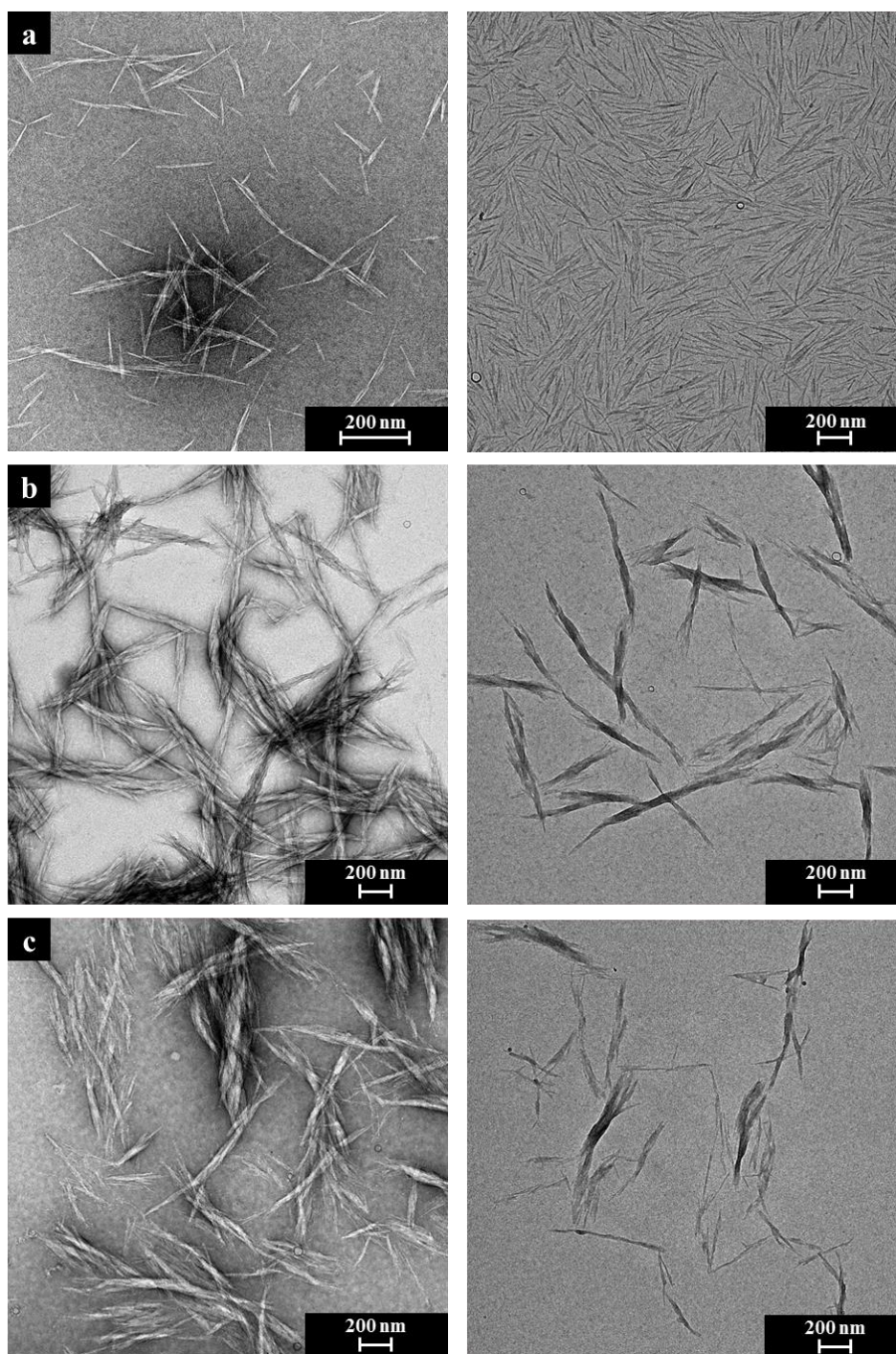


Figure II. 16. TEM images obtained with negative coloring using uranyl acetate (on the left) and without coloring (on the right) of **a)** unmodified CNC, modified **b)** CNC_Lauric and **c)** CNC_Stearic, **d)** XRD analyses of near CNC, CNC_Lauric and CNC_Stearic

AFM images of modified CNC_Lauric recovered in acetone after modification are presented in **Figure II. 17**. Length dimensions were determined equal to 470 ± 170 nm and are in adequacy with those measured from TEM.

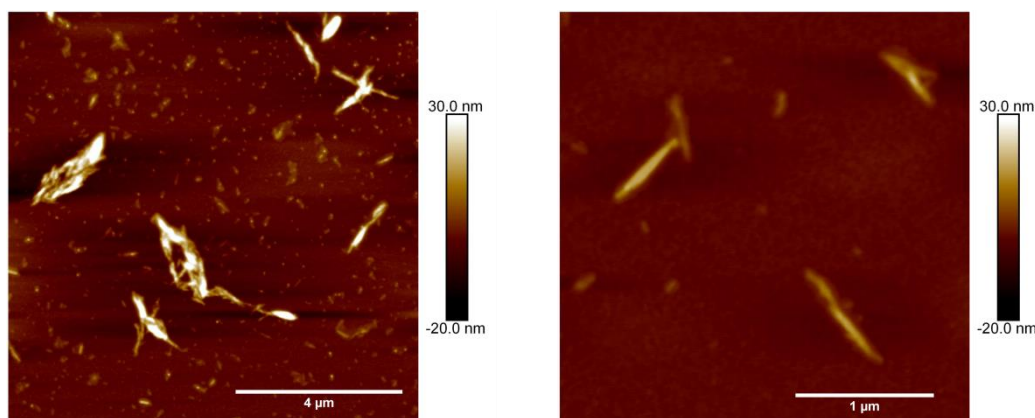


Figure II. 17. AFM height images of modified CNC_Lauric

Moreover, particle size of unmodified CNC in acetone determined by DLS (**Figure II. 12 a**) was close to 300 nm. This suggests that the particle size of CNC after reaction would not change, and that CNCs would keep their initial dispersion state. This point was confirmed by DLS analyses performed on CNC_Lauric and CNC_Stearic diluted suspensions in acetone, presented in **Figure II. 18**. Measured particle sizes were equal to 373 +/- 18 nm (PDI = 0.2) and 402 +/- 5 nm (PDI = 0.2) for CNC_Lauric and CNC_Stearic, respectively. No significant differences with value obtained for neat CNC in acetone after solvent exchange (*suspension 2*) was observed. It can be assumed that the dispersion state and size of the CNC nanoparticles after reaction was unchanged. Moreover, the particle sizes obtained by DLS correlated with data obtained from the TEM analyses. Aggregation of esterified CNCs was thus evidenced, but aggregated modified particles are still on the nanoscale, which was satisfying for the study, because modified nanoparticles were obtained at this stage of the study.

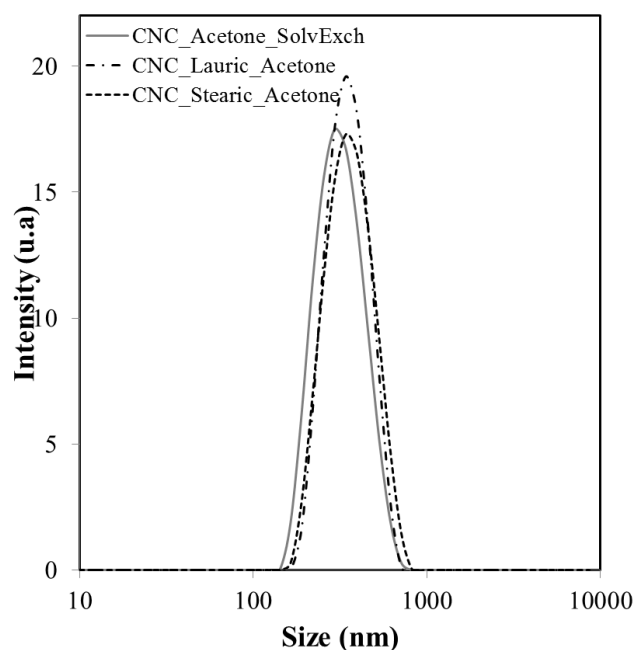


Figure II. 18. Dynamic light scattering (DLS) curves of CNC suspension in acetone after solvent exchange (grey line) and recovered CNC_Lauric (--- line) and CNC_Stearic (---- line) in acetone

The change in the crystalline structure of modified CNCs was investigated by XRD (**Figure II. 19**) and crystallinity indexes (CI) were determined according to **Equation II. 7**. Although this method provides overestimated values of crystallinity compared to other values like peak deconvolution or amorphous subtraction methods described by Park *et al.*⁵⁶, it was chosen in this study to provide a qualitative comparison of samples crystallinity. For both neat and modified CNCs, the presence of signals 110 and 200 respectively at 16.5° and 22.6° was characteristic of cellulose I β .

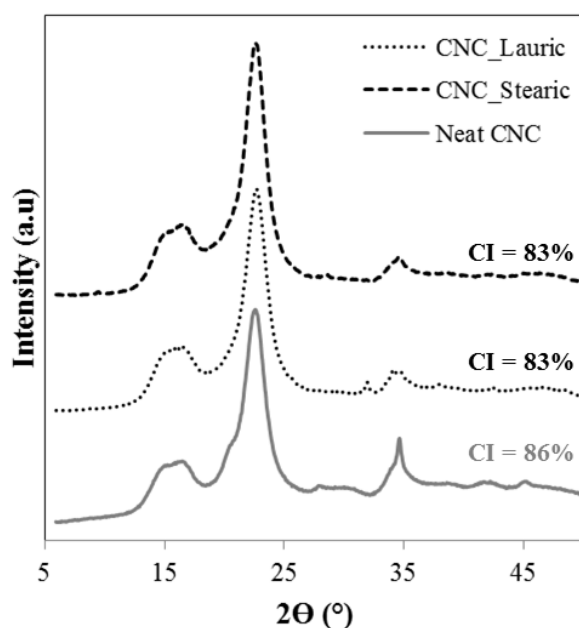


Figure II. 19. XRD analyses of neat CNC, CNC_Lauric and CNC_Stearic

Moreover, neat CNCs exhibit a CI equal to 86%, whereas both CNC_Lauric and CNC_Stearic have a CI equal to 83%. Considering the measurement error, the slight crystallinity decrease is not significant. Thus, cellulose I crystalline structure of CNC after esterification was conserved, which is critically important for further applications, especially for those of polymeric material reinforcement.

Other indirect or qualitative methods can also highlight the grafting. After reaction and washing steps, modified CNCs were stored in an acetone suspension. A small amount of this suspension was added to distilled water, and the final concentration was adjusted to 1 wt%. Pictures of resulting water suspensions are presented on the right side of **Figure II. 20**. In **Figure II. 20 a)**, a well-dispersed suspension of unmodified hydrophilic CNC in water was observed. In contrast, in **Figure II. 20 b) and c)**, flotation of modified CNCs on the surface of the aqueous system was clearly observed.

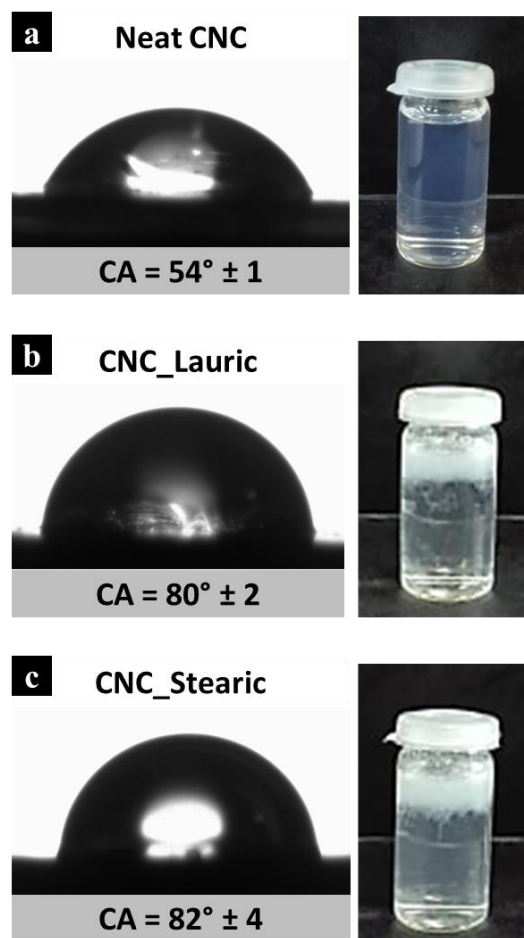


Figure II. 20. Water contact angle and pictures of water suspension at 1 wt% of **a)** neat CNC, modified **b)** CNC_Lauric, and **c)** CNC_Stearic

It qualitatively proves that CNCs recovered after esterification with both lauric and stearic acids are more hydrophobic than neat CNCs and are not dispersible in water. It was further confirmed by water contact angle measurements, presented on the left side of **Figure II. 20**. Indeed, the water contact angle measured after the deposition of a water droplet on a neat CNC casted film was equal to 54° ($\pm 1^\circ$), while those measured on both CNC_Lauric and CNC_Stearic pellets were respectively equal to 80° ($\pm 2^\circ$) and 82° ($\pm 4^\circ$), clearly indicating an hydrophobization of modified CNC.

3.3. Influence of chain length on CNC grafting (Suspension 3)

FTIR analyses were carried out on purified grafted CNCs recovered after 8 h of reaction with lauric and stearic acid, and spectra are presented in **Figure II. 13 b)**. Peaks at 1728 cm^{-1} , and between 2900 and 2950 cm^{-1} were observed and associated to the presence of $\text{C}=\text{O}$ bonds from ester groups and CH_2 and CH_3 aliphatic carbons respectively. Efficiency of the grafting of both lauric and stearic acid on initially-well-dispersed CNC in acetone was thus highlighted.

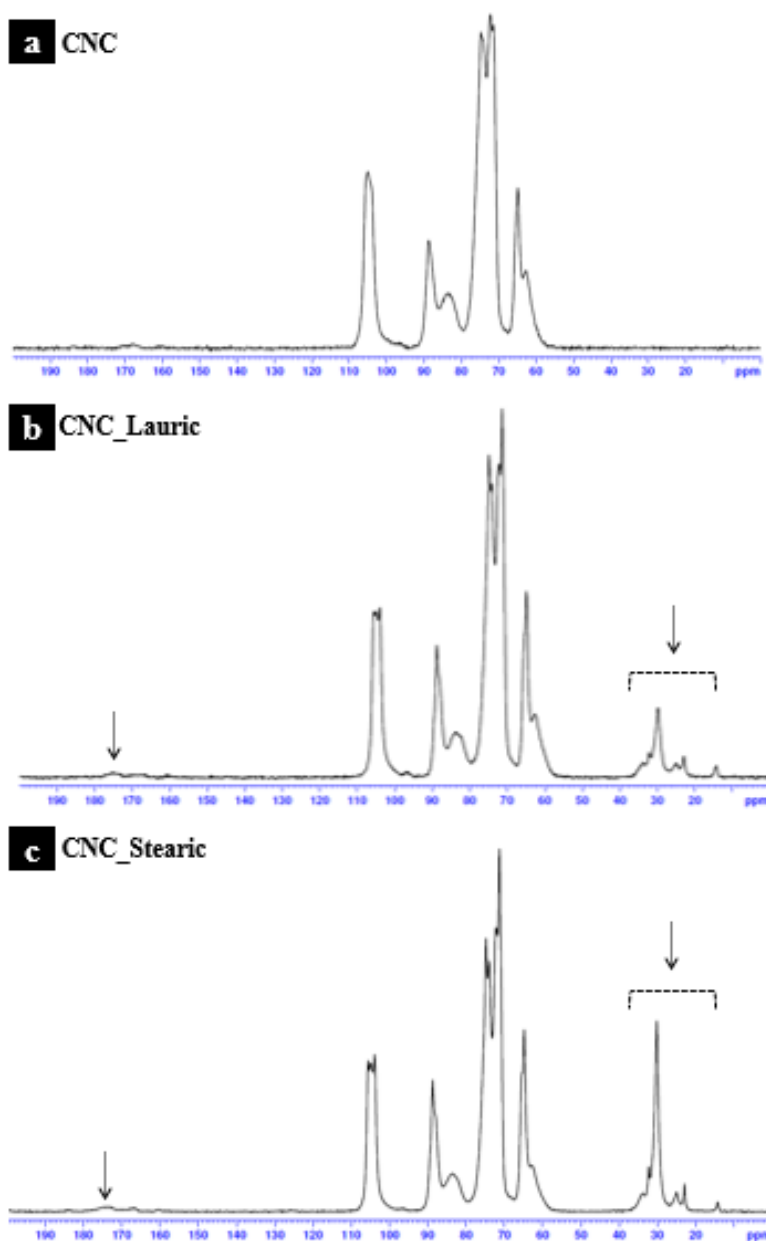


Figure II. 21. ^{13}C -Solid NMR spectra of a) unmodified CNC, modified b) CNC_Lauric and c) CNC_Stearic

Moreover, to more precisely investigate the grafting of these carboxylic acids on CNC, ^{13}C -solid state NMR was carried out on neat and modified CNC. Spectra related to neat CNC and both CNC_Lauric and CNC_Stearic are presented on **Figure II. 21**. Characteristic peaks of cellulose are observed in **Figure II. 21 a)**, with chemical shifts at 105 ppm, 88.7 ppm, and between 74.7 and 64.9 ppm for C1, C4 and C2, C3, and C5 carbons respectively, as summarized in a recent review¹².

In **Figure II. 21 b) and c)**, new peaks between 22.9 and 34 ppm, and a single peak at 14.4 ppm are present and can be related to $-\text{CH}_2$ and $-\text{CH}_3$ carbons, respectively. The intensity of the peaks at approximately 30 ppm is higher for CNC_Stearic than for CNC_Lauric, due to the greater number of carbons comprising the aliphatic chains. Moreover, at 174.8 ppm and 173.8 ppm (respectively for

CNC_Lauric and CNC_Stearic), low peaks can be observed and correlated to ester bonds. They clearly evidence the covalent grafting of acids on CNC, even if the intensity of these peaks is low which could be explained by the low grafting density of acids and by the chain lengths introduced on the surface, making the detection of these ester bonds difficult. However, it is possible to ensure that there was a covalent grafting of fatty acids on the CNC surface, although quantification of the amount of grafted acid was not possible according to FTIR and NMR results.

In order to investigate this point, elemental analyses were carried out on neat CNC and grafted CNC, and the results are presented in **Table II. 6**. For both CNC_Lauric and CNC_Stearic samples, the increase of %C values was significant, leading to a large decrease of experimentally calculated O/C ratio, and is explained by the introduction of long aliphatic chains. Values of %C and %O were corrected according to the previously described method taking into account the presence of sulfate half ester groups on the surface of CNCs and without considering the presence of other impurities which could influence the values. Note that the sulfur content %S decreased after esterification, which was probably due to the desulphation of CNC under the reaction conditions. Moreover, by comparing experimental and theoretical O/C ratios, experimental ratios are higher than theoretical ones, indicating that not all hydroxyl groups –OH of anhydroglucose units (AGU) are modified by the esterification, which was predictable.

Sample	Experimental values				DS _{SO3}	Corrected values		Experimental O/C	Theoretical O/C	DS
	%C	%O	%H	%S		%C	%O			
Neat CNC	40.7	50.8	6.4	0.8	0.04	42.4	52.9	1.2	1.1	-
CNC_Lauric	47.3	40.0	7.2	0.7	0.04	49.3	41.7	0.8	0.4	0.14
CNC_Stearic	55.4	28.8	9.0	0.4	0.02	57.7	30.0	0.5	0.3	0.35

Table II. 6. Atomic composition of neat CNC, CNC_Lauric and CNC_Stearic obtained by elemental analyses with corrected values, theoretical and calculated ratio O/C, and calculated degree of substitution (*DS*)

Degrees of substitution (*DS*) were calculated according to the previously described **Equation II. 5** for both CNC_Lauric and CNC_Stearic samples. These *DS* were equal to 0.13 and 0.31 for CNC_Lauric and CNC_Stearic respectively, which was in accordance with values generally found in literature for covalent grafting on a CNC surface^{12,20,108}. However, it is important to keep in mind that experimental measurement errors are large, and there was some amount of difficulty in determining slight differences between carbon element contents before and after modifications due to the large presence of the cellulosic background signal¹². Nevertheless, higher values of *DS* obtained for CNC_Stearic suggest better efficiency of the grafting using a longer fatty chain. One explanation for this could be the difference in viscosity between lauric and stearic acids in the molten state. However, rheological analyses were performed on both lauric and stearic acids to understand their rheological behavior as solvents during the esterification reaction. At the reaction temperature (110 °C), both of the acids

exhibited the same behavior of Newtonian fluids, because the evolution of the shear stress function of shear rate was linear in both cases, as presented **Figure II. 22 a)**. Moreover, their viscosities are close to zero at a low shear rate as well as at a high shear rate (**Figure II. 22 b)**). These results confirmed that their low viscosities at 110 °C made them good solvents for the reaction but did not provide a better understanding of why grafting density of stearic acid is higher than that of lauric acid on CNC.

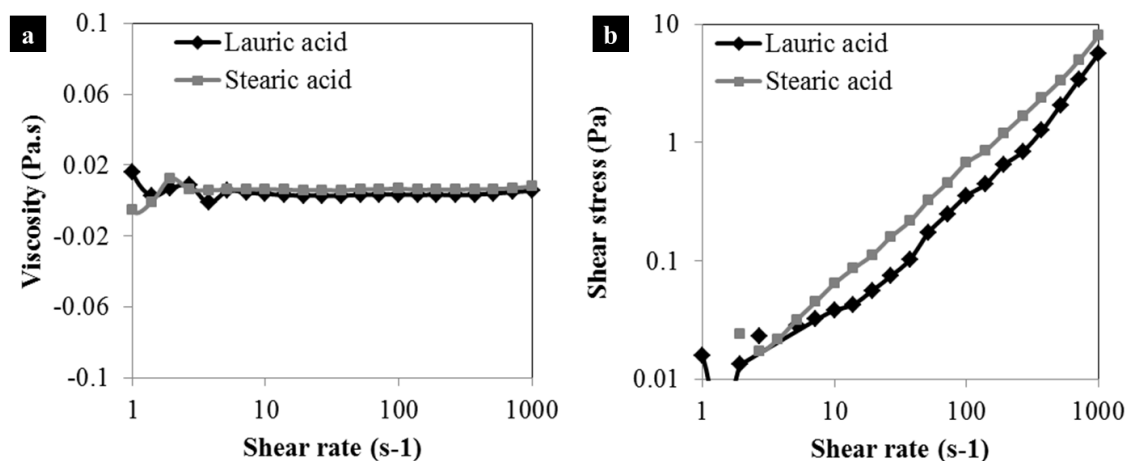


Figure II. 22. Shear Rheological analyses of both lauric and stearic acids at 110 °C, **a)** apparent viscosity function of shear rate, and **b)** shear stress function of shear rate

Another potential explanation is based on the difference in acidity between both acids. Indeed, the stronger an acid is, the smaller its pKa is. As found in literature¹⁰⁹, pKa in solution of lauric acid (pKa = 4.80) and stearic acid (pKa = 4.75) are similar. This difference is very slight, and therefore other more relevant explanations should be found, including the repetition of the experiments in order to draw a clear conclusion.

3.4. Surface analyses of long chains onto CNC

The efficiency of the grafting at the bulk level of both CNC_Lauric and CNC_Stearic has been previously studied and highlighted. It was interesting to investigate the grafting at the CNC surface level, because it is this modified interface that will influence further compatibilization of grafted CNC with a hydrophobic polymer matrix. Thus, to characterize just the surface of the materials with a penetration depth less than 5 nm, XPS analyses were carried out on the different samples. Decomposition spectra of the C1s signal are represented in **Figure II. 23 a) c) and d)**. Neat CNC spectra exhibits four peaks at 285.4 eV, 287.0 eV ($\Delta eV = 1.6$ eV), 288.4 eV ($\Delta eV = 3$ eV) and 289.5 eV ($\Delta eV = 4.1$ eV) corresponding to C1 (C-C/C-H), C2 (C-O), C3 (O-C-O/C=O) and C4 (O-C=O) bonds respectively. The C1 signal is related to the contribution of non-oxidized alkane-type carbon atoms and impurities, residual lignin or extractive compounds. The C2 signal is related to the presence of ether groups from pure cellulose, as well as the hydroxyl groups of the unmodified CNCs, and of the end of the cellulose chains. The C3 signal corresponds to acetal moieties from AGU units and should not change significantly after chemical modification because the corresponding carbon is not affected.

The C4 signal is present in low proportions in the neat CNC spectrum, and is attributed to presence of glucuronic acid from hemicelluloses residuals.

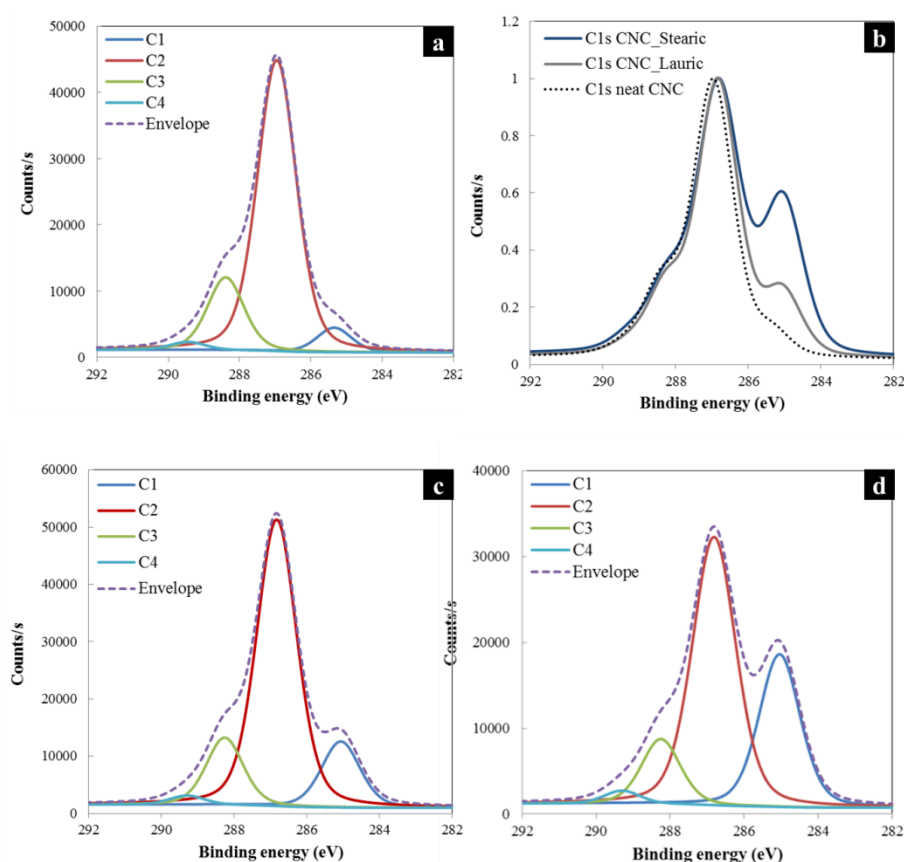


Figure II. 23. Decomposition of the C1s peaks of **a)** neat CNC, **c)** CNC_Lauric, and **d)** CNC_Stearic, and **b)** Superposition of the C1s spectra of the three samples

In the case of the grafting of long aliphatic chains inducing the introduction of a large number of carbons on the surface of CNC, the C1 peak was particularly interesting, because it was correlated to C-C and C-H bonds. Superposition of the C1s envelopes of neat CNC, CNC_Lauric, and CNC_Stearic was plotted on **Figure II. 23 b)**, and the main difference between the three curves is clearly visible at the C1 peaks. In **Table II. 7**, the percentages of carbon and oxygen (molar compositions) are expressed, as well as, the different percentages for each peak of the C1s decomposition.

Sample	Experimental values			C1s decomposition				Ratio C1/C3	DSS
	%C	%O	O/C	C1 C-C / C-H	C2 C-O	C3 O-C-O / C=O	C4 O-C=O		
Neat CNC	56	44	0.8	7	72	20	1	0.4	-
CNC_Lauric	59	41	0.7	15	68	15	2	1	0.1
CNC_Stearic	64	36	0.6	30	56	12	2	2.5	0.2

Table II. 7. Elemental molar compositions and surface functional groups compositions obtained by XPS analysis and C1s decomposition

First, a large increase in %C was observed, correlated with previous bulk characterizations like elemental analysis. It was interesting to follow the evolution of the calculated ratio C1/C3, because C3 carbons are normally not affected by the chemical grafting of cellulose. Therefore, this ratio reflected the increase of aliphatic carbons introduced on the surface of CNC. Indeed, the C1/C3 ratio was equal to 0.4 for neat CNC, and increased to 1 for CNC_Lauric, and finally to 2.5 for CNC_Stearic. The efficiency of the grafting on the surface of CNC was clearly seen here. Also, an increase in the percentage of the C4 carbon related to the ester bonds was also evidenced, although this evolution was less significant, possibly due to the steric hindrance on the surface of CNCs coated with long aliphatic chains. Nonetheless, the presence of a large number of aliphatic chains on the surface, as well as the covalent grafting of these compounds, was highlighted with these XPS spectra.

It is important to mention that in this study, commercial neat CNCs were used as a reference. It would have been preferable to subject them to the same reaction conditions without acid (time, temperature, centrifugations in acetone) but the rapid, total evaporation of acetone would have led to their degradation. Thus, the elemental molar compositions expressed in **Table II. 7** for neat CNCs probably would have been different from those of the neat CNCs after treatment, due to the potential removal of some sample impurities. In this sense, the results should be carefully analyzed. This also applies to the previous results of the elemental analyses. Despite errors in XPS values, surface degrees of substitution (*DSS*) were calculated for both CNC_Lauric and CNC_Stearic. This calculation was based on the evolution of the C1 ratio, which should increase significantly after the grafting of long aliphatic chains on CNC surface. However, because of the presence of impurities, the C1 signal is present in neat CNC sample. Calculation of the *DSS* has been adapted from the previous work of Espino-Pérez *et al.*²⁶. First, it is possible to express %C1 of modified CNC_Lauric or CNC_Stearic by following **Equation II. 10** :

$$\%C1 = \frac{\text{Number of C1 carbons}}{\text{Number of total carbons}} = \frac{DSS \times M(C1)_{\text{grafted}}}{M(C)_{AGU} + DSS \times M(C)_{\text{grafted}}}$$

Equation II. 10. General expression of the %C1 obtained from XPS analysis

where $M(C1)_{\text{grafted}}$ corresponds to the molar mass of C1 carbons of the grafted acid (respectively 132.1 g.mol⁻¹, 204.2 g.mol⁻¹ for lauric and stearic acid), $M(C)_{\text{grafted}}$ corresponds to the molar carbon mass of the grafted acid (respectively 144.1 g.mol⁻¹ and 216.2 g.mol⁻¹ for lauric and stearic acid), and $M(C)_{AGU}$ is related to the carbon molar mass of an anhydroglucose unit (AGU) (72.1 g.mol⁻¹). It is then possible to propose **Equation II. 11** for the calculation of the *DSS* from XPS data:

$$DSS = \frac{\%C1 \times M(C)_{AGU}}{M(C1)_{\text{grafted}} - \%C1 \times M(C)_{\text{grafted}}}$$

Equation II. 11. General equation for the calculation of the degree of surface substitution from XPS data

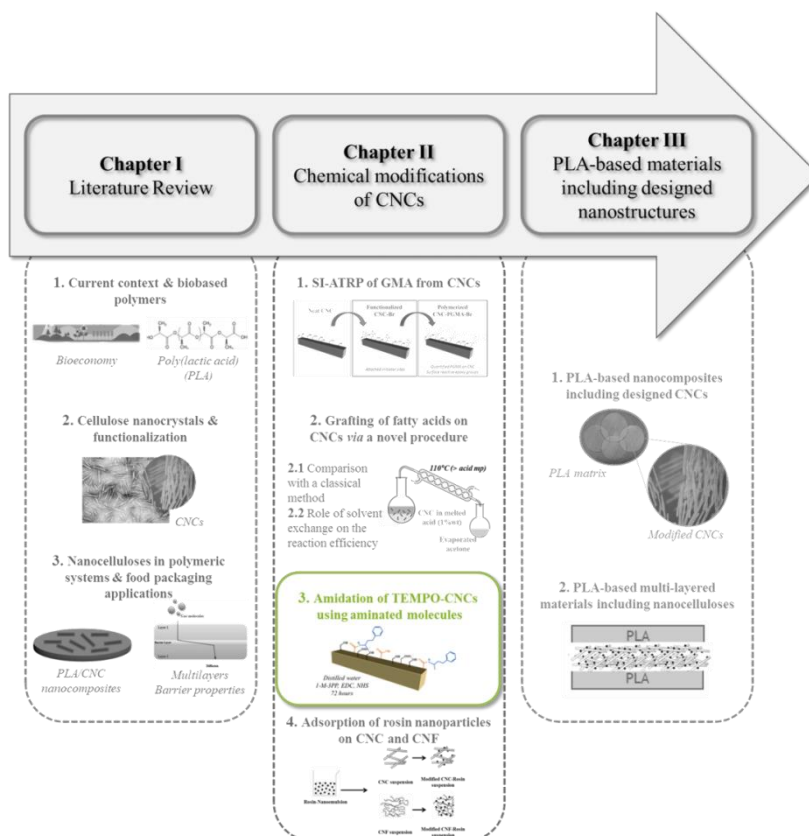
Calculated *DSS* are expressed in **Table II. 7** and are equal to 0.1 and 0.2 for CNC_Lauric and CNC_Stearic, respectively. To be consistent with the literature, it was expected that the values of *DSS* would be higher than those of the *DS*, because grafting normally takes place mainly on the CNC surface^{26,110}. In our case, values of *DS* and *DSS* were similar for CNC_Lauric and CNC_Stearic, respectively. This can be explained by the fact that the neat CNC taken as reference should have endured the same treatment as described for our sample, in order to take into account the reference value of C1 signals to correct our equation.

4. Conclusion

In this study, dried CNC powder was dispersed in acetone *via* different methods, and the dispersion state of each suspension was investigated. After accepting that the solvent exchange method was the most accurate procedure for the preparation of a well-dispersed CNC suspension in acetone, the aim of this study was to perform the esterification of neat CNC with natural fatty lauric or stearic acids following a *SolReact* procedure. The novelty of this grafting lies in the fact that the consumption of toxic solvents and chemicals is largely reduced, and that the fatty acids can be simply recycled and reused after the reaction. Esterification of the CNCs was characterized *via* FTIR, ¹³C-NMR, elemental analyses, and XPS, ensuring that a covalent grafting was performed. Quantification of the amount of aliphatic chains was completed, leading to a significant and satisfying degree of substitution results: between 0.1 and 0.3. Finally, structure conservation was assessed by TEM, AFM, and XRD techniques. These results are chemically and environmentally satisfying and open the way for further incorporation of modified CNCs in hydrophobic polymer matrices for nanocomposites applications.

3. Amidation of TEMPO-oxidized cellulose nanocrystals using aromatic aminated molecules

This section is adapted from M. Le Gars, A. Delvart, P. Roger, M. N. Belgacem, J. Bras “Amidation of TEMPO-oxidized cellulose nanocrystals using aromatic aminated molecules”, Colloid and Polymer Science, 2020.



Abstract

In this study, the grafting of 1-methyl-3-phenylpropylamine (1-M-3-PP) on cellulose nanocrystals (CNCs) *via* a two-step reaction route was investigated and compared with physico-chemical surface adsorption. The first step involved subjecting CNCs to a 2,2,6,6-Tetramethyl-1-piperidinyloxy (TEMPO)-mediated oxidation. The carboxylic groups present on recovered oxidized TEMPO-CNC were quantified by several characterization methods (conductometric titration, elemental analysis, and X-ray photoelectron spectroscopy) and a degree of oxidation close to 0.2 was found. The second step was an amidation reaction carried out in an aqueous medium under mild conditions and in the presence of N-(3-dimethylaminopropyl)-N'-ethylcarbodiimide (EDC)/N-hydroxysuccinimide (NHS) as catalyst. The recovered modified CNCs after amidation reaction with 1-M-3-PP (CNC-1-M-3-PP) were extensively washed and then characterized. The amount of grafted molecules was determined by several techniques like X-ray photoelectron spectroscopy, and the calculated degree of substitution was found to be close to 0.05 with respect to the bulk CNC. This low amount is sufficient to enhance the modified CNC dispersion and their colloidal stabilization in organic solvents, allowing the preparation of nanocomposites. Furthermore, such CNC-1-M-3-PP units with aromatic molecules attached to it can find applications in barrier materials in which the sorption of aromatic molecules can be very useful.

Keywords:

Cellulose nanocrystals (CNCs) — Amidation — Aromatic molecule — 1-methyl-3-phenylpropylamine — Adsorption

1. Introduction

Cellulose is one of the most abundant natural polymers, with 10^{11} - 10^{12} tons of cellulose produced through photosynthesis per year¹. Its large availability (wood, cotton, leaves, bacteria, algae, etc.) makes it a strong competitor against numerous traditional materials¹¹¹. Thus, cellulose is an attractive biodegradable, renewable and biocompatible material. With the emergence and the development of nanotechnology, interest in nanoscale cellulose has widely increased in the last two decades. These nanoscale cellulose materials – also called nanocellulose – are produced in different ways. Three main types can be described, of which two are cellulose nanofibrils (CNFs) and cellulose nanocrystals (CNCs). They differ in morphology, crystallinity, surface charges and intrinsic properties. The third variety deals with bacterial cellulose¹¹².

CNC extraction from various cellulose sources was introduced by Rånby et al. in the 1950s¹¹³, and is currently being optimized and even industrialized. Traditionally, it involves sulfuric acid hydrolysis (under specific conditions of time, temperature, and concentration) of biomass which leads to CNC formation followed by several sonication and washing steps¹¹⁴. Other preparation procedures are also described in literature^{85,86}. When prepared *via* sulfuric acid hydrolysis, the residual half-sulfate ester groups present on the surface of the recovered CNC allow for colloidal stability of the prepared nanomaterials in aqueous media¹⁰³. CNCs exhibit a wide range of other outstanding properties as well, such as high crystallinity (until 90%¹⁸), high aspect ratio (length between 100 nm and several μm and, width between 2 and 15 nm^{2,17,114}), high specific surface area ($150 - 800 \text{ m}^2 \cdot \text{g}^{-1}$)¹⁷, high viscosity even at low concentrations (liquid crystalline phase behavior, gelation properties⁹¹) and optical properties (iridescence capacity^{115,116}). Due to these intrinsic properties, CNCs are excellent candidates for a large range of applications (such as for cosmetics, coatings, papers, paints, food additives, films, biomedical, composites)^{8,67,117,118}. Furthermore, after having been prepared on a laboratory-scale for several years and with several studies aimed at the optimization and characterization of their production, CNCs are currently being produced on a larger scale and being industrialized, especially in North America (for example, CelluForce, Canada (yearly capacity of 365 tons)).

Surface modification of CNCs has been the aim of numerous studies over the past few years. In fact, with increasing interest in nanocelluloses and their applications, providing them with new properties (like sorption, antioxidant, antibacterial, or compatibilization with hydrophobic matrices improvement)^{19,20,27,68,72,119} has been made possible by grafting molecules or polymers onto their surface. Thus, their chemical structure — especially the three reactive hydroxyl groups present on each anhydroglucose unit (AGU) — allows efficient chemical modifications. There are numerous publications and reviews dealing with these surface graftings of CNC, which can be classified in two main groups: *grafting-from* and *grafting-onto* strategies¹²⁰. *Grafting-from* procedures consist of the functionalization of CNCs with initiator sites, followed by the polymerization of monomers from these

reactive sites. On the other hand, *grafting-onto* strategies aim to directly graft previously characterized molecules or polymers onto the surface of CNCs. These two approaches differ not only in their procedure, but also in the final grafting density and graft size, which makes the characterization of the grafted surfaces more or less easy. Moreover, contrary to the *grafting-from* procedure — in which organic and toxic solvents and reagents are generally needed — *grafting-onto* strategy opens the way to a more eco-friendly chemistry with limited use of polymerization coupling reagents and toxic chemicals.

In this work, we decide not to graft polymers, but to directly graft aromatic molecules on the surface of the CNCs. More precisely, CNCs are first oxidized *via* a 2,2,6,6-tetramethyl-1-piperidinyloxy (TEMPO)-mediated oxidation process, which introduces carboxylate groups ($-\text{COO}^-$) at their surface. TEMPO oxidation has been well described in the literature and its optimization leads to TEMPO-CNCs bearing controlled surface charges^{121–123}. Interest in the carboxylate groups' introduction is due to the further potential chemical modifications possible by these groups as well as guaranteeing the colloidal suspension of the CNC. Thereby, in the second step, an amidation was carried out between these carboxylate groups ($-\text{COO}^-$) and the amine functions ($-\text{NH}_2$) borne by a reactive molecule. This reaction is performed through peptidic linkages using N-(3-dimethylaminopropyl)-N'-ethylcarbodiimide (EDC)/N-hydroxysuccinimide (NHS) catalyst¹²⁴, as sketched in **Scheme II. 2**. In literature, several studies have proved the efficiency of EDC/NHS catalyzed amidation on oxidized TEMPO-CNC^{125,126}. Recently, Guo *et al.*¹²⁷ performed a similar amidation in for grafting previously amino-functionalized carbon quantum dots on TEMPO-CNC in order to enhance photoluminescent hybrid materials. It was followed by Gicquel *et al.*¹²⁴, who proved the efficiency of the peptidic linkage between amine terminated poly-N-isopropylacrylamide (PNIPAM) and oxidized TEMPO-CNC obtained through grafting compared to those obtained through its adsorption. The limited use of chemicals and the aqueous conditions are the advantages of employing the amidation *via* EDC/NHS coupling.

The purpose of this study was to investigate the grafting of 1-methyl-3-phenylpropylamine (1-M-3PP) on previously oxidized TEMPO-CNC. 1-M-3-PP is an amine-containing aromatic molecule, and the interest in it is due to the presence of aromatic rings, as already demonstrated by Espino-Pérez *et al.*, who showed that the presence of aromatic functions on the surface of CNCs significantly improved the aromatic-ring-bearing molecules' sorption, owing to the π - π interactions between the sorbent and the sorbate⁷². In their study, CNCs were modified *via* different procedures (esterification, silylation, and grafting using isocyanates), taking advantage of the presence of hydroxyl groups on the surface of CNCs. In short, amidation coupled with EDC/NHS was chosen to graft 1-M-3-PP on TEMPO-CNC because of the reaction's efficiency and low toxicity, combined with the aim to introduce aromatic rings on the surface of CNCs.

In this study, we aim to develop an efficient and green method for the introduction of aromatic molecules on the surface of CNCs, in order to enhance their physico-chemical affinity towards aromatic compounds and apolar polymers, which in turn will enhance their sorption capacity. Moreover, the hydrophobic character of aromatic compounds could be interesting for the elaboration of nanocomposites with apolar polymeric systems, which can also exhibit barrier properties. The degree of oxidation of TEMPO-oxidized CNC is generally between 1000 and 2000 $\mu\text{mol}\cdot\text{mg}^{-1}$, depending on the oxidation conditions¹²². It naturally leads to low degree of substitution after amidation reaction, and thus to low amount of aromatic groups on the surface of CNC, considering that all $-\text{COOH}$ groups will not be converted. However, it has been proved that even a low amount of hydrophobic grafts at the surface of nanocellulosic materials can induce positive effects on its barrier or compatibilization properties.

In this work, TEMPO-mediated oxidation of a large batch of CNCs will be first described. After characterization of these oxidized TEMPO-CNCs, their amidation with aromatic 1-M-3-PP will be described and characterized (Fourier-transform infrared spectroscopy, conductometric titration, elemental analysis, X-ray photoelectron spectrometry). The presence of peptidic amide bonds will be highlighted, as well as, the effects associated with the presence of aromatic rings.

2. Materials and methods

2.1. Materials

CNCs were supplied in spray-dried form by CelluForce[®] (Canada). Briefly, their extraction was processed *via* an acid hydrolysis process performed on wood pulp. 2,2,6,6-Tetramethyl-1-piperidinyloxy (TEMPO, 98%), sodium bromide (NaBr, BioXtra, >99.0%), sodium hydroxide (NaOH, BioXtra, >98%, pellets), hydrochloric acid (HCl, ACS reagent, 37%), N-(3-dimethylaminopropyl)-N'-ethylcarbodiimide (EDC, >97%), N-hydroxysuccinimide (NHS, 98%), 1-methyl-3-phenylpropylamine (98%) and polyethylenimine (PEI, average Mn 10,000 g.mol⁻¹) were supplied by Sigma-Aldrich Chimie (France) and used as received. Sodium hypochlorite solution (NaClO, 12% Cl) was provided by Carl Roth (France) and used as received. Ethanol (95%) was purchased from Revol (France) and used without further purification.

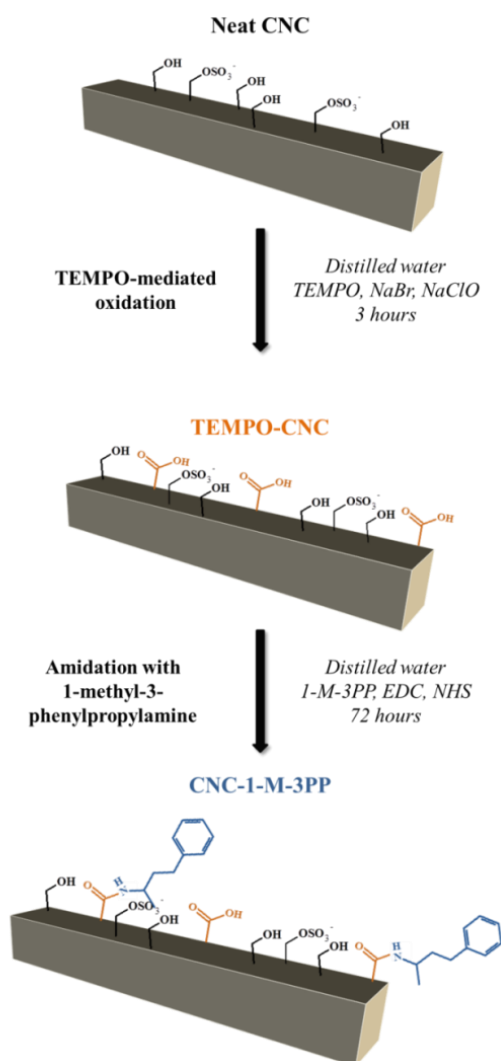
2.2. Oxidation of CNCs using TEMPO reagent

In order to oxidize a large amount of CNCs, the oxidation was performed in a 15 L reactor (Büchiglasuster, Switzerland). Firstly, 150 g of dried CNCs were dispersed in 10 L of distilled water following the dispersion procedure provided by the supplier, i.e., one hour of magnetic stirring followed by sonication (2.5 kJ per g of dried CNC). In order to avoid the temperature rise during the sonication process, the suspension was maintained in an ice bath. Well-dispersed CNC suspension was then introduced into the reactor under moderate mechanical stirring at ambient temperature. 4.43 g of TEMPO and 48.6 g of NaBr were dissolved in 150 mL of water, and the solution was then added dropwise to the CNC suspension. 900 g of NaClO was then slowly introduced into the reaction media. The pH was set and adjusted to 10-10.5 with freshly prepared 1 M NaOH solution. At this stage of the reaction, coloration of the reaction switched from whitish to yellowish. After 3 h of oxidation at room temperature, the reaction was quenched with 550 mL of ethanol. In order to extensively wash the oxidized CNCs, three centrifugation cycles (10000 rpm, 15 min, 5 °C) were performed after adjusting the pH of the suspension to 2-3 using 0.5 M HCl which would make the separation of CNCs from the supernatant easier. Oxidized CNCs were then put into a dialysis membrane (molecular weight cut-off 6-8 kD) against distilled water for one week with the water regularly changed until a neutral pH was attained. Recovered TEMPO-CNCs were dispersed in distilled water using a sonication probe (2.5 kJ per g of dried CNC) and were suitable for further characterizations and use. Scheme II. 2 presents the TEMPO-mediated oxidation.

2.3. Amidation of TEMPO-CNC 1-M-3-PP with EDC/NHS catalysis

Concentration of lab-made TEMPO-CNC suspension was adjusted to 1 wt% with distilled water and dispersed using a sonication probe (2.5 kJ per g of dried CNC). The pH of the suspension was adjusted

to 4.5 with 0.5 M HCl in order to be in acidic form (-COOH). The TEMPO-CNC suspension underwent a controlled magnetic stirring at room temperature. Solutions of dissolved EDC and NHS in water were freshly prepared with molar ratios $4N_{\text{COOH}}: N_{\text{EDC}}: N_{\text{NHS}}$, where N_{COOH} , N_{EDC} and N_{NHS} represent the molar amounts of carboxylic groups in TEMPO-CNC, EDC, and NHS, respectively. Firstly, EDC solution was added to the suspension, followed by the addition of NHS solution. After 30 min of stirring, the pH was adjusted to 8-8.5 using 0.5M NaOH solution. Then, 1-M-3-PP was added to the suspension with the molar ratio $4N_{\text{COOH}}: N_{\text{NH}_2}$, where N_{NH_2} corresponds to the molar amount of amino groups in 1-M-3-PP. The suspension was left magnetically stirring at room temperature with the pH controlled at 8-8.5 using 0.5 M NaOH or HCl solutions. After 72 h, the amidation reaction was quenched by decreasing the pH to 1-2 with 0.5 M HCl, followed by three centrifugation cycles (10000 rpm, 15 min, 5 °C) with distilled water. The suspension of the recovered modified CNC-1-M-3-PP was then put into dialysis (molecular weight cut-off 6-8 kD) against distilled water for at least one week to ensure a high quality washing step. Before stopping the dialysis, the water was characterized to prove there is no more 1-M-3-PP leaching. **Scheme II. 2** shows the amidation reaction.



Scheme II. 2. Procedure of the preparation of oxidized 2,2,6,6-tetramethyl-1-piperidinyloxy (TEMPO)-cellulose nanocrystals (CNC) and functionalized CNC-1-methyl-3-phenylpropylamine materials

2.4. Characterization methods

2.4.1. Atomic force microscopy (AFM)

AFM images were obtained from a Dimension Icon Bruker equipped with a silicon cantilever (O-TESPA, Bruker, USA). Well-dispersed CNC suspension was diluted to 10^{-3} or 10^{-4} wt%, and a drop was deposited on a cleaved mica plate, which was left drying overnight under a fume hood at ambient temperature until complete water evaporation. AFM analysis was performed in a tapping mode in air and scans of $10 \mu\text{m}^2$ and $3.3 \mu\text{m}^2$ were recorded. Image treatment and dimensional analyses were carried out by Nanoscope Analysis and ImageJ software, respectively. At least 40 measurements were needed to give representative dimensions with standard deviation values.

2.4.2. Transmission electron microscopy (TEM)

Diluted CNC suspension and uranyl acetate were deposited on a carbon film set on a TEM copper grid and were dried in ambient air. The suspension was observed using a transmission electron microscope FEI/Philips CM200 (acceleration voltage of 200 kV) of the microscopy platform from the NanoBio-ICMG platform (Grenoble, France). The most relevant pictures were selected for the discussion.

2.4.3. X-ray diffraction (XRD)

X-ray diffraction analyses were carried out on an X'Pert Pro MPD diffractometer, PANalytical with an X'accelerator detector. A copper-based anode was used with $K\alpha$ radiation of 1.5419 \AA in order to obtain $\Theta/2\Theta$ (Bragg angle) symmetric scan reflections between 5° and 60° . Crystallinity of dried powder samples was calculated using the Segal height peak method^{55,56}, where crystallinity index (CI) of a sample is evaluated according to **Equation II. 12**,

$$CI = \left(1 - \frac{I_{am}}{I_{002}}\right) \times 100$$

Equation II. 12. Crystallinity index calculation according to the height peak method (Segal et al.)

where I_{am} corresponds to the minimum value of intensity ($2\Theta \approx 18.3^\circ$) and I_{002} to the value of intensity of the main crystalline area ($2\Theta \approx 22.5^\circ$). The analyses were repeated twice for each sample.

2.4.4. Fourier transform infrared (FTIR) spectroscopy

A PerkinElmer spectrum was used to record FTIR spectra. Dried films of neat and modified CNCs were analyzed using Attenuated Total Reflectance (ATR) method. After performing background scans in air, absorbance spectra were recorded ($600\text{-}4000 \text{ cm}^{-1}$, 4 cm^{-1} resolution, 32 scans) and analyzed using Spectrum, PerkinElmer software. All spectra were normalized at 1110 cm^{-1} (characteristic peak of cellulose), and at least two spectra for each sample were recorded.

2.4.5. Conductometric titration

To determine the carboxyl content of oxidized TEMPO-CNC and modified CNC-1-M-3-PP, conductometric titrations were performed on 200 mL of 7.5×10^{-3} wt% diluted well-dispersed suspensions (~15 mg of CNCs). The pH of the suspension was adjusted to 3 with 0.1 M HCl solution before being titrated with 0.01 M freshly prepared and titrated NaOH solution. Volumes of NaOH added were adjusted during the titration process according to the slopes of the obtained curve, and were reduced around the equivalence points. Measured conductivity was corrected with the total mixture volume. The resulting titration curves, as shown in **Figure II. 24**, exhibited two equivalent volumes related to strong and weak acid equivalence points, and were named *V1* and *V2*, respectively.

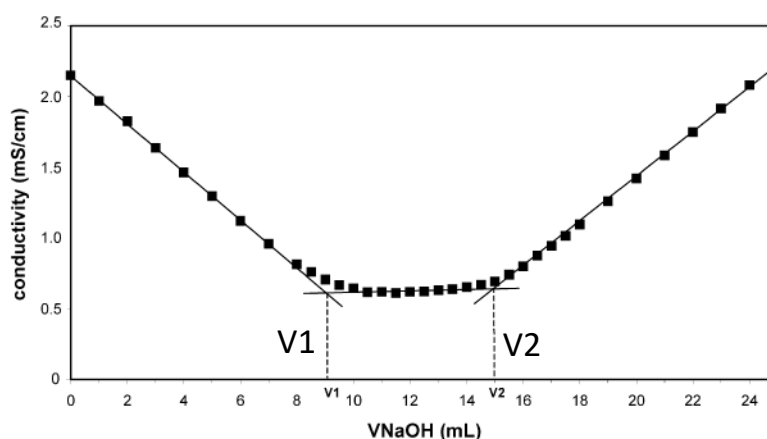


Figure II. 24. Schematized curve obtained from the titration of 2,2,6,6-tetramethyl-1-piperidinyloxy (TEMPO)-cellulose nanocrystal (CNC) using NaOH solution

Degree of oxidation (*DO*) — corresponding to the number of carboxylic groups per AGU — of oxidized CNC could be calculated from the titration curves according to **Equation II. 13**:

$$DO = \frac{M_{AGU} \times C \times (V2 - V1)}{w - 36 \times C \times (V2 - V1)}$$

Equation II. 13. General equation for the calculation of the degree of oxidation (*DO*) of oxidized or modified CNC

In **Equation II. 13**, *C* corresponds to the exact NaOH concentration (mol.L^{-1}), *V1* and *V2* are equivalent volumes added NaOH (L), *w* is the initial dry amount of CNC (g), $M_{AGU} = 162.14 \text{ g.mol}^{-1}$ is the molar mass of an AGU, and 36 g.mol^{-1} corresponds to the difference between the molar masses of an AGU and the sodium salt of a glucuronic acid moiety. Furthermore, the grafting rate or carboxyl group content, expressed in $\mu\text{mol.g}^{-1}$, could be calculated, according to **Equation II. 14**:

$$X = \frac{C \times (V2 - V1)}{w}$$

Equation II. 14. General equation for the calculation of the grafting rate (*X*) of oxidized or modified cellulose nanocrystals

In **Equation II. 14**, terms used are similar to those in **Equation II. 13**. The obtained grafting rate could be used to quantify residual carboxyl groups and was named X_{res} , where *V1* and *V2* represented

equivalent volumes of the titration performed on grafted CNC-1-M-3-PP. According to **Equation II. 15**, the difference between the grafting rates before and after amidation can lead to the percentage of carboxylic groups converted during this reaction ($\%COOH_{react}$):

$$\%COOH_{react} = \left(1 - \frac{X_{res}}{X}\right) \times 100$$

Equation II. 15. General equation for the calculation of the number of converted carboxylic groups during the amidation reaction

In order to ensure repeatability of the measure, each titration was performed at least three times.

2.4.6. Elemental analysis (EA)

Carbon, hydrogen, oxygen, nitrogen and sulfur contents of dried CNC samples were sent to “Institut des Sciences Analytiques” in Villeurbanne (France) and quantified by a micro analyzer with a precision of 0.4%. The experiments were conducted on each sample. Weight percent of different atoms can be used to quantify the $-COOH$ charges of oxidized TEMPO-CNC and the grafting degree of substitution of modified CNC. The degree of oxidation calculated from these data, $DO_{elemental\ analysis}$, can be also determined according to **Equation II. 16**:

$$DO_{elemental\ analysis} = \frac{M(C)_{AGU} - \%C \times M_{AGU}}{\%C \times (M_{AGU-COONa} - M_{AGU})}$$

Equation II. 16. General equation for the calculation of the degree of oxidation of TEMPO-CNC from elemental analysis results

In **Equation II. 16**, $M(C)_{AGU}$, $\%C$, M_{AGU} and $M_{AGU-COONa}$ correspond to the molecular mass of carbon in an AGU (72.04 g.mol^{-1}), the carbon content in CNC-TEMPO sample obtained by elemental analysis, the total molar mass of an AGU (162.14 g.mol^{-1}), and the molar mass of an oxidized AGU with sodium salt as counter ion (35.93 g.mol^{-1}), respectively. Moreover, a degree of substitution ($DS_{elemental\ analysis}$) can be calculated according to **Equation II. 17**:

$$DS_{elemental\ analysis} = \frac{\%N \times (M_{AGU} + DO \times (M_{AGU-COONa} - M_{AGU}))}{M(N)_{grafted} - \%N \times M_{grafted}}$$

Equation II. 17. General equation for the calculation of the degree of substitution of modified cellulose nanocrystals after amidation calculated from elemental analysis results

In **Equation II. 17**, the terms M_{AGU} and $M_{AGU-COONa}$ are similar to those used in **Equation II. 16**. Terms $\%N$, $M(N)_{grafted}$ and $M_{grafted}$ correspond to the nitrogen content in modified CNC sample obtained by elemental analysis, the nitrogen molar mass of grafted moieties (14.0 g.mol^{-1}), and the total molar mass of the grafted moieties (131.23 g.mol^{-1}), respectively. Degree of substitution corresponds to the number of amine compounds introduced in each AGU.

2.4.7. X-ray photoelectron spectrometry (XPS)

XPS measurements were carried out on a K-Alpha+ surface analysis spectrometer (Thermo Scientific), equipped with a monochromatic X-ray source (Al K α , 1487.5 eV). Spots of diameter 400 μm were used for all the measurements and a hemispherical analyzer was operating in constant analyzer energy mode under ultra-high vacuum. Data treatments were carried out using Avantage software (Thermo Fisher). Background subtraction (Smart type) and normalization of peak areas (using Scofield sensitivity factors) were performed before any elemental composition calculation. Calibration of binding energies was carried out with the C1s neutral carbon peak at 285 eV. O/C ratios were calculated according to **Equation II. 18**,

$$\frac{O}{C} = \frac{I_O}{S_O} \times \frac{S_C}{I_C}$$

Equation II. 18. General equation for the calculation of oxygen to carbon ratio from X-ray photoelectron spectrometry data where I_O and I_C are intensities of oxygen and carbon peaks, and S_O and S_C are the atomic Scofield sensitivity factors of oxygen and carbon equal to 0.00477 and 0.00170, respectively. From O/C ratios, it is possible to determine the degree of oxidation of TEMPO-CNC. By knowing the O/C ratios for both neat CNC ($(O/C)_{\text{neat}}$) and oxidized TEMPO-CNC ($(O/C)_{\text{TEMPO}}$), their values can be linked to the degree of oxidation, DO_{XPS} , as presented in **Equation II. 19**:

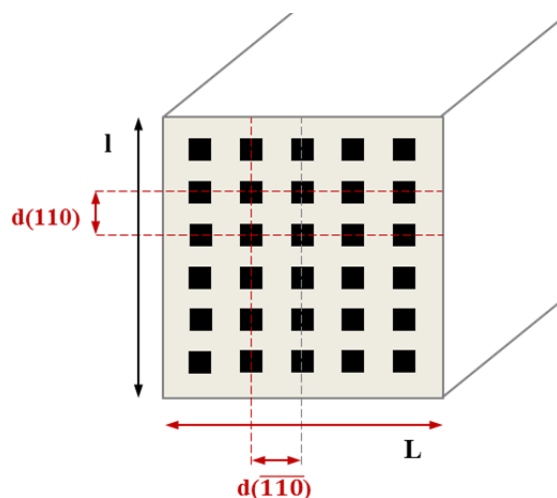
$$DO_{\text{XPS}} = \left(\left(\frac{O}{C} \right)_{\text{TEMPO}} - \left(\frac{O}{C} \right)_{\text{Neat}} \right) \times \frac{M(C)_{\text{AGU}}}{M(O)}$$

Equation II. 19. General equation for the calculation of the degree of oxidation from X-ray photoelectron spectrometry data. Moreover, from C1s spectra decompositions, it is possible to determine a degree of substitution at the surface (DS_{XPS}) of CNC-1-M-3-PP according to **Equation II. 20**:

$$DS_{\text{XPS}} = \frac{\%C - N \times M(C)_{\text{AGU}}}{M(C - N)_{\text{grafted}} - \%C - N \times M(C)_{\text{grafted}}}$$

Equation II. 20. General equation for the calculation of the degree of substitution from X-ray photoelectron spectrometry data

On the other hand, taking into account the geometry of CNC and the crystalline arrangement of their cellulosic chains, a ratio of the amount of surface chains to the total amount of chains has been proposed in literature. In fact, Eyley and Thielemans⁶⁸ — based on the previous work of Habibi et al.¹²⁸ — have determined the relation between the number of exposed cellulose chains on the surface of a CNC and its total number of cellulose chains, and named R_c . This relation takes into account the crystalline cellulose I_β structure of a nanocrystal in which (110) and $(\overline{1}\overline{1}0)$ planes are perpendicular to the crystal face, as presented in **Scheme II. 3**.



Scheme II. 3. Schematized section of an isolated cellulose nanocrystal, where black squares correspond to cellulose chains' ends, $d(110)$ and $d(\overline{110})$ the plane spacings of the crystal planes (Adapted from ^{68,128})

According to the values found in literature and especially those presented by Lin et Dufresne¹²⁹, mean values for $d(110)$ and $d(\overline{110})$ for CNC are on average equal to 0.66 and 0.53 nm, respectively. Moreover, the cross-section of an isolated CNC was supposed to be a square in our study, with $l = L = 6$ nm. In their study, Eyley and Thielemans⁶⁸ have proposed **Equation 21** for the calculation of the previously defined ratio, R_c .

$$R_c = \frac{\text{\#surface cellulose chains of the CNC}}{\text{\#cellulose chains of the CNC}} = \frac{2 \times \left(\frac{L}{d(\overline{110})}\right) + 2 \times \left(\frac{l}{d(110)}\right)}{\frac{L \times l}{d(\overline{110}) \times d(110)}}$$

Equation 21. General equation for the calculation of the ratio R_c , which represents the number of cellulose chains at the surface to the total number of cellulose chains of a cellulose nanocrystal

In our case, using our assumptions, R_c was equal to 0.39. Additionally, a simple relation links the degree of substitution with the degree of substitution (DS) at the surface (for example, calculated from XPS data), as presented by **Equation II. 22**:

$$DS = R_c \times DS_{\text{surface}}$$

Equation II. 22. Relation between the degree of substitution, DS , and the degree of the substitution at the surface, DS_{surface} , of a cellulose nanocrystal

It is important to keep in mind that only 1.5 OH groups are accessible for modification at the surface of an AGU. All these assumptions and calculations allow the modified groups to be quantified at the surface or in the bulk of CNCs.

2.4.8. Contact angle

Casted films of unmodified, oxidized and modified CNCs were prepared, and a droplet of 4 μL of distilled water was deposited for the determination of the angle between the substrate and the droplet at room temperature. A contact angle meter OCA20 combined with a camera charge-coupled device (CCD) was used. Acquisition of the angle was performed for one min after the droplet's deposition, and the collected data was processed on SCA20 software. All measurements were at least repeated five times.

2.4.9. Quartz crystal microbalance with dissipation (QCM-d)

Quartz crystals coated with gold (F-QSX-301) supplied by LOT-QuantumDesign (France) were washed in a piranha bath ($\text{H}_2\text{O}_2:\text{H}_2\text{SO}_4 = 1:3$) for 30 min, rinsed with deionized water, and dried with nitrogen steam. Spin-coating of the sensors with CNCs was performed just after cleaning. Sensors were introduced in a spin-coater (SPIN150i – POLOSTM) and a washing step (60 seconds off after drop deposition, acceleration of $360 \text{ rpm}\cdot\text{s}^{-1}$, and 3600 rpm for 60 seconds) was carried out with milliQ water. Sensors were then i) spin-coated with a $2.5 \text{ mg}\cdot\text{mL}^{-1}$ PEI solution (300 seconds off after drop deposition, acceleration of $360 \text{ rpm}\cdot\text{s}^{-1}$, and 3600 rpm for 60 seconds), ii) rinsed with milliQ water, iii) spin-coated with a 2 wt% CNC water suspension, and iv) finally rinsed with milliQ water. Sensors were then left in an oven for 2 h at $80 \text{ }^\circ\text{C}$ in order to ensure the stability of the created CNC film. AFM was used to observe the sensor surface before any analysis in order to ensure the formation of a homogeneous CNC film. Lastly, the sensors were put in milliQ water for 3 h before QCM-d analysis. Once the sensors were successfully prepared, they were mounted onto the QCM-d device (Biolin Scientific, Sweden) and exposed to a milliQ water flow ($0.07 \text{ }\mu\text{L}\cdot\text{min}^{-1}$) until baseline stabilization. Measurement temperature was set at $20 \text{ }^\circ\text{C}$. A 0.1 wt% 1-M-3-PP solution in milliQ water at pH 8 was passed through the device with a $100 \text{ }\mu\text{L}\cdot\text{min}^{-1}$ flow. After reaching a plateau, milliQ water was introduced ($100 \text{ }\mu\text{L}\cdot\text{min}^{-1}$) until another plateau was observed. QCM-d analysis can be used for the investigation of the mass change of the sensor, and Rodhal *et al.*¹³⁰ described the principle of the technique. They were among the first to relate the change in frequency to the mass added to the crystal and explained that the sensor vibration fluctuates with the adsorbed mass on its surface. Frequency and dissipation data were recorded and processed on QTools software (Biolin). Sauerbrey equation (**Equation II. 23**) was used for the calculation of the amount of molecules adsorbed on the CNC-coated gold sensor (Δm in mg per m^2 of CNC, or $\text{mg}\cdot\text{m}^{-2}_{\text{CNC}}$). This equation was proposed by Sauerbrey in 1959¹³¹ and required assumptions that have been proposed only more recently in literature. In order to ensure the validity of the equation, it has been clarified that the film created on the sensor should i) be rigid (dissipation change inferior to 10 times the frequency change), ii) be uniform, and iii) have a small mass compared to that of the crystal^{132,133}.

$$\Delta m = -C \times \frac{\Delta f}{n}$$

Equation II. 23. Sauerbrey equation for the calculation of the amount of adsorbed molecules from QCM-d analysis

where C is a constant related to the quartz crystal parameters (density and thickness) and equal to $17.7 \text{ ng.cm}^{-2}.\text{Hz}^{-1}$ (for a 5 MHz crystal), Δf the change in frequency, and n the overtone number. In this work, the third overtone number was used and the frequencies were normalized by the QTools software, so n was equal to 1. From Δm value, the amount (in mol) of molecules adsorbed per g of CNC was calculated, taking into consideration the theoretical specific surface area of a CNC which was equal to $500 \text{ m}^2.\text{g}^{-1}$ (value extracted from literature¹⁷).

3. Results and discussions

3.1. Characterization of TEMPO-CNC prepared on a large scale

As presented in **Scheme II. 2**, commercially dried CNCs were oxidized *via* a TEMPO-mediated oxidation after being well-dispersed in water. The presence of negatively charged sulfate half ester groups on their surface (around $250 \text{ mmol}_{\text{R-OSO}_3\text{H}}/\text{kg}_{\text{CNC}}$)¹⁴ induced the colloidal stability of the supplied unmodified CNCs in water. AFM and TEM images obtained from the unmodified CNC in water, presented in **Figure II. 25 a)** and **d)**, confirmed the well-dispersed behavior of the aqueous suspension. Isolated CNCs exhibited dimensions equal to $108 \pm 33 \text{ nm}$ in length and to $4 \pm 1 \text{ nm}$ in width, correlating to values commonly found in literature^{14,22}.

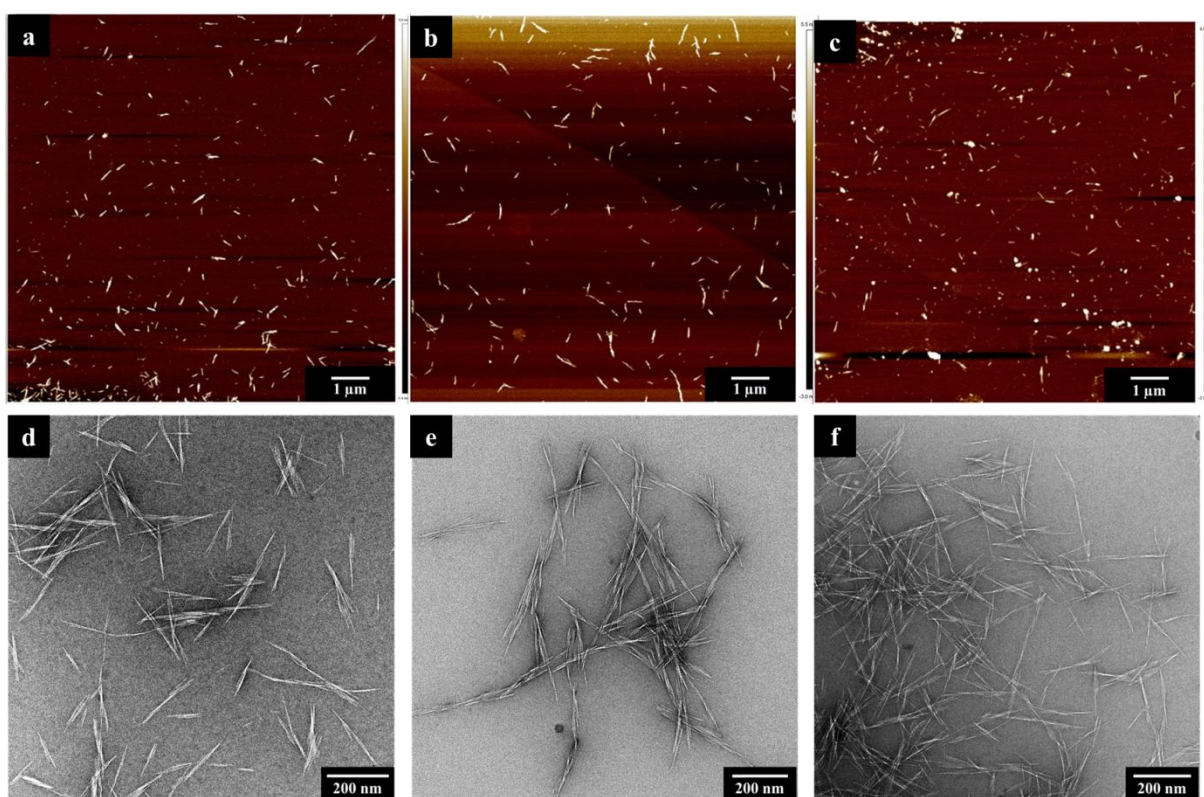


Figure II. 25. Atomic force microscopy (AFM) (height sensor) and transmission electron microscopy (TEM) images of neat cellulose nanocrystal CNC (**a** and **d**), TEMPO-CNC (**b** and **e**), and modified CNC-1-M-3-PP (**c** and **f**)

Figure II. 25 b) and **e)** represent AFM and TEM observations of oxidized TEMPO-CNC. AFM image allowed to conclude about the dispersion of TEMPO-CNC in water, even if they were more aggregated compared to TEM images, probably because of a lack of sonication treatment before analysis. Moreover, the dimensions of TEMPO-CNCs were close to those of neat CNCs, with $127 \pm 25 \text{ nm}$ in length and $5 \pm 1 \text{ nm}$ in width, meaning that TEMPO oxidation did not induce any significant change in terms of CNC dimensions. All the dimensions measured by TEM are summarized in **Table II. 8**.

		Neat CNC	TEMPO-CNC	CNC-1-M-3-PP
Length (nm)	Mean	108	127	111
	Std. dev.	33	25	19
Width (nm)	Mean	4	5	4
	Std. dev.	1	1	1

Table II. 8. Summarized lengths and widths of neat CNC, TEMPO-CNC and CNC-1-M-3-PP measured by TEM

In order to further investigate TEMPO oxidation's influence on CNC's morphology, XRD analyses were performed on both unmodified and oxidized CNCs. **Figure II. 26** shows diffractograms obtained from XRD analyses. The three spectra exhibited classical cellulose crystalline structure, with peaks at $2\theta \sim 15.2^\circ$ and $2\theta = 22.6^\circ$ related to the planes (101) / (10 $\bar{1}$), and (002), respectively¹². Additionally, a peak at $2\theta = 34.6^\circ$ was present only in the neat CNC sample, and can be related to the (040) crystalline cellulose contribution due to a textural effect of cellulose, as mentioned several times in the literature^{129,134,135}. Note that the determination of samples' crystallinity did not take into account this contribution. Crystallinity indexes (*CI*) calculated according to **Equation II. 12** demonstrated that oxidative treatment did not induce any significant change in the crystallinity of CNC since *CI* decreases from 91% to 89%. These values corroborate those found in literature^{4,22}, where it has been proved that an overly intensive oxidation can damage the crystallinity of CNC, contrary to the findings in another work¹³⁶. At this stage, it was possible to conclude about the structure conservation of CNC after their TEMPO oxidation, which was crucial for further chemical modifications and applications.

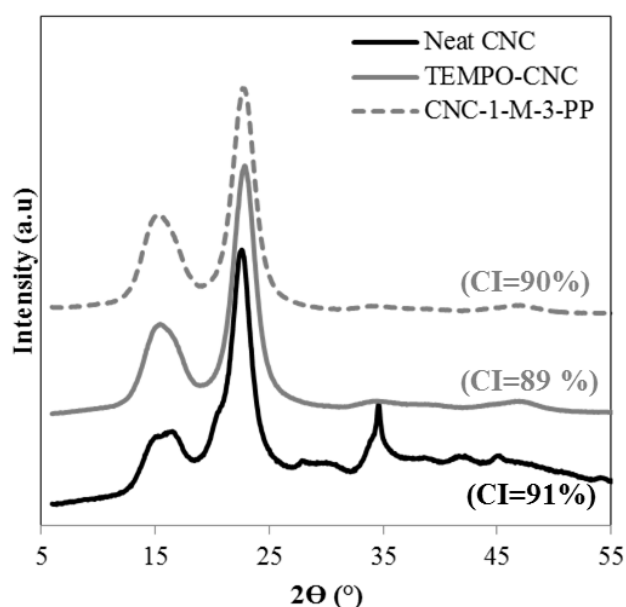


Figure II. 26. X-Ray diffractograms of neat cellulose nanocrystal (CNC), oxidized TEMPO-CNC, and modified CNC-1-M-3-PP

Further characterizations were performed in order to confirm and quantify oxidation efficiency. FTIR spectra were recorded for both unmodified and oxidized CNCs, as shown in **Figure II. 27**. After normalization at 1110 cm^{-1} for both spectra, a clear peak at 1730 cm^{-1} was visible and was correlated to

the presence of carboxylic $-\text{COOH}$ groups introduced through the oxidation process. This peak was related to the $\text{C}=\text{O}$ stretching vibrations from the acid form of carboxyl groups.

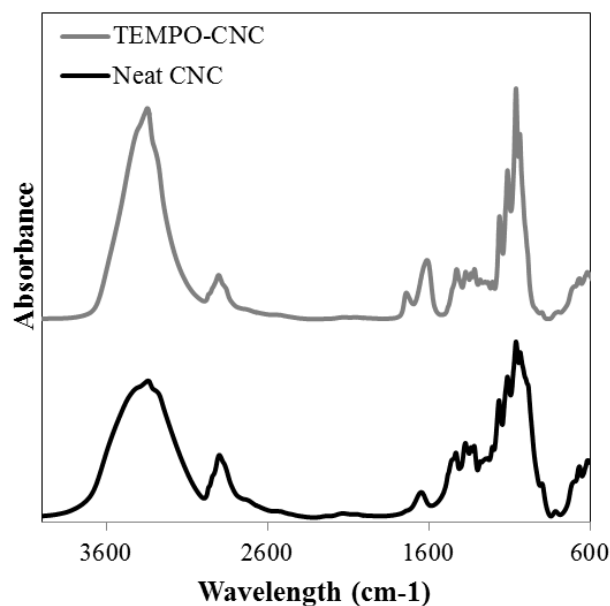


Figure II. 27. Fourier transform infrared normalized spectra of neat cellulose nanocrystal (CNC) and oxidized TEMPO-CNC. Thus, the efficiency of the grafting was proved by FTIR analysis, which in turn proved the presence of carboxyl groups in the TEMPO-CNC sample. To further modify these groups, their quantification was needed. In this sense, conductometric titrations were performed on TEMPO-CNC, and one of the titration curves is presented in **Figure II. 28** as example.

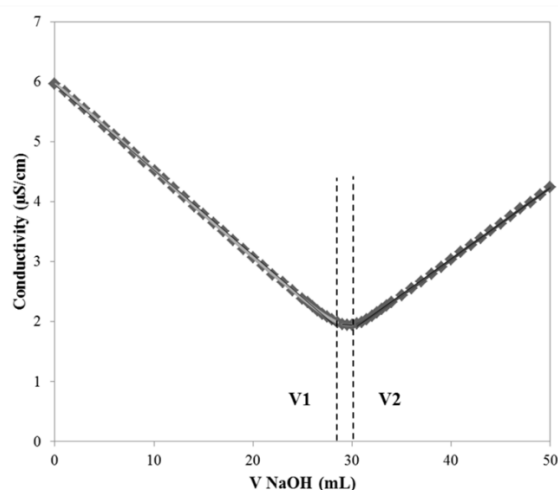


Figure II. 28. Conductometric titration curve of TEMPO-CNC with equivalent volumes V_1 and V_2

The calculated values of degree of oxidation (DO) (**Equation II. 13**) and grafting rate (X) (**Equation II. 14**) are presented in **Table II. 9**. Oxidized TEMPO-CNC exhibited a calculated degree of oxidation equal to 0.22 ± 0.03 and a grafting rate of 1295 ± 147 μmol of $-\text{COOH}$ group per g of dry TEMPO-CNC, which was in agreement with the literature data^{128,137}. However, although conductometric

titration is a simple and rapid method, it is highly dependent on the operator, especially during the titration. Thus, these results must be confirmed by other bulk or surface characterizations.

Sample	DO	X ($\mu\text{mol.g}^{-1}$)	%COOH _{react}
TEMPO-CNC	0.22 \pm 0.03	1295 \pm 147	/
CNC-1-M-3-PP	0.19 \pm 0.01	1138 \pm 28	12%

Table II. 9. Summarized values of the quantification of carboxylic groups on TEMPO-CNC and modified CNC-1-M-3-PP. Elemental analyses were performed on each sample, and the obtained results are presented in **Table II. 10**. Experimental values obtained from elemental analyses were corrected since presence of impurities or other species can largely influence the results. The experimental values were corrected with the degree of substitution of half-sulfate ester groups (DS_{SO_3}) calculated from the percentage of sulfur element in neat CNC sample. Several other methods to correct these values have been reported, by the likes of Siqueira et al.⁵⁹ and Espino-Pérez et al.²⁶, considering that the corrected value of %C for unmodified CNC sample was equal to the theoretical one (44.4%). In our study, calculated values of DS_{SO_3} (presented in **Table II. 10**) were equal to 0.04 for both CNC and TEMPO-CNC samples, showing that no release of sulfate groups occurred during TEMPO oxidation process, which was predictable from the mild conditions (temperature, pH, and reaction time) of TEMPO-mediated oxidation.

Sample	Experimental values					DS_{SO_3}	Corrected values		DO	DS	%COOH _{react}
	%C	%O	%H	%S	%N		%C	%O			
Neat CNC	40.7	50.8	6.4	0.8	<0.1	0.04	42.4	47.1	/	/	/
TEMPO-CNC	37.0	52.2	5.9	0.8	<0.1	0.04	38.6	48.4	0.68	/	/
CNC-1-M-3-PP	40.1	49.5	6.2	0.6	0.5	0.03	41.8	45.9	/	0.07	10

Table II. 10. Atomic composition of neat cellulose nanocrystals (CNCs), oxidized TEMPO-CNC and modified CNC-1-M-3-PP obtained by elemental analyses and calculations of $DO_{\text{elemental analysis}}$, $DS_{\text{elemental analysis}}$ and %COOH_{react} elemental analysis

From elemental analyses' data, it was possible to determine the degree of oxidation, $DO_{\text{elemental analysis}}$ (**Equation II. 16**). Calculated $DO_{\text{elemental analysis}}$ was equal to 0.68, which was higher than that obtained from conductometric titrations (**Table II. 9**). Nevertheless, if corrections to %C and %O were made according to the previously described method in literature (i.e., considering %C_{corrected} in neat CNC is equal to 44.4), a value of $DO = 0.45$ would have been obtained. It emphasizes the fact that data obtained from such analyses (elemental analyses or conductometric titrations) have to be handled with care, and that calculated values are highly dependent on corrections and formulas used. Therefore, comparative rather than purely quantitative analyses are preferred. However, when the correction of the values and the large errors in the values were taken into account, it was possible to conclude that the degree of oxidation values obtained from both conductometric titrations and elemental analyses were consistent.

In order to chemically investigate the surface of oxidized TEMPO-CNC, XPS analyses were carried out on both CNC and TEMPO-CNC. **Figure II. 29** shows survey spectra of neat CNC and oxidized TEMPO-CNC.

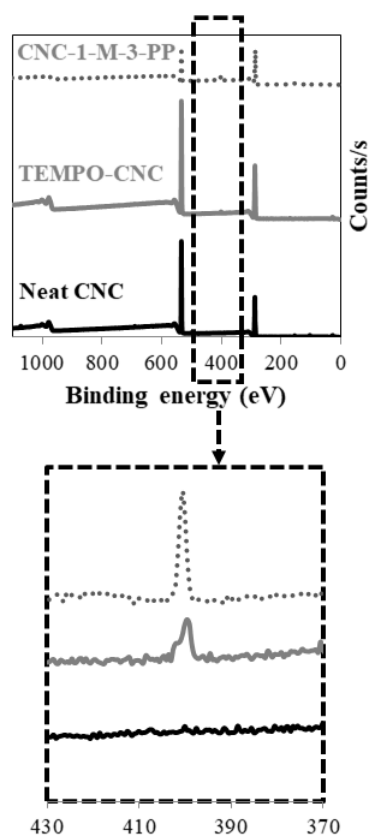


Figure II. 29. a) X-ray photoelectron spectroscopy (XPS) survey of neat cellulose nanocrystal (CNC), oxidized TEMPO-CNC and modified CNC-1-M-3-PP and b) Elemental molar compositions, surface functional groups compositions, DO_{XPS} and DS_{XPS} obtained by XPS analyses

On both spectra, peaks at 532 eV and 285 eV have been related to the O1s and C1s elements, respectively. In addition, a peak at 400 eV (assigned to nitrogen atoms) appeared on the TEMPO-CNC spectra and was consistent with the presence of residual TEMPO reagent. No significant change was observed between the survey spectra of neat and oxidized CNCs, although a slight increase in O1s peak could be monitored and related to the introduction of $-\text{COOH}$ groups.

	%C	%O	%N	O/C	C1s				N1s			DO	DS
					C1 (C-C/C-H)	C2 (C=O)	C3 (O-C-O/C=O)	C4 (O-C=O)	C-N	N-H/N-C	N-C=O		
Neat CNC	62.3	36.7	<0.1	0.58	16	66	15	2	/	/	/	/	/
TEMPO-CNC	62.4	37.4	0.3	0.60	18	61	17	4	/	/	/	0.23	/
CNC-1-M-3-PP	62.7	36.3	1	0.58	17	57	17	4	5	73	27	/	0.05

Table II. 11. Elemental molar compositions, surface functional groups compositions, DO_{XPS} and DS_{XPS} obtained by XPS analyses

Surface DO_{XPS} related to the amount of $-COOH$ groups on the surface of CNC was calculated according to **Equation II. 19** and found to be 0.09. Taking into account the relation expressed in **Equation II. 22**, the total degree of oxidation was found to be equal to 0.23, as presented in **Table II. 11**. This value was consistent with the DO determined by conductometric titration. Here again, XPS measurement errors have to be taken into consideration, especially in the case of such surface modifications that introduce a low amount of carbon or oxygen elements.

Figure II. 30 a) and **b)** present the decomposition spectra of C1s peaks of neat and oxidized CNCs, respectively. On the neat CNC C1s decomposition spectra, four peaks were displayed at 284.7 eV, 286.3 eV ($\Delta eV= 1.6$ eV), 287.8 eV ($\Delta eV= 3.1$ eV) and 289.1 eV ($\Delta eV= 4.4$ eV), and these correspond to C1 (C-C/C-H), C2 (C-O), C3 (O-C-O/C=O) and C4 (O-C=O) contributions, respectively.

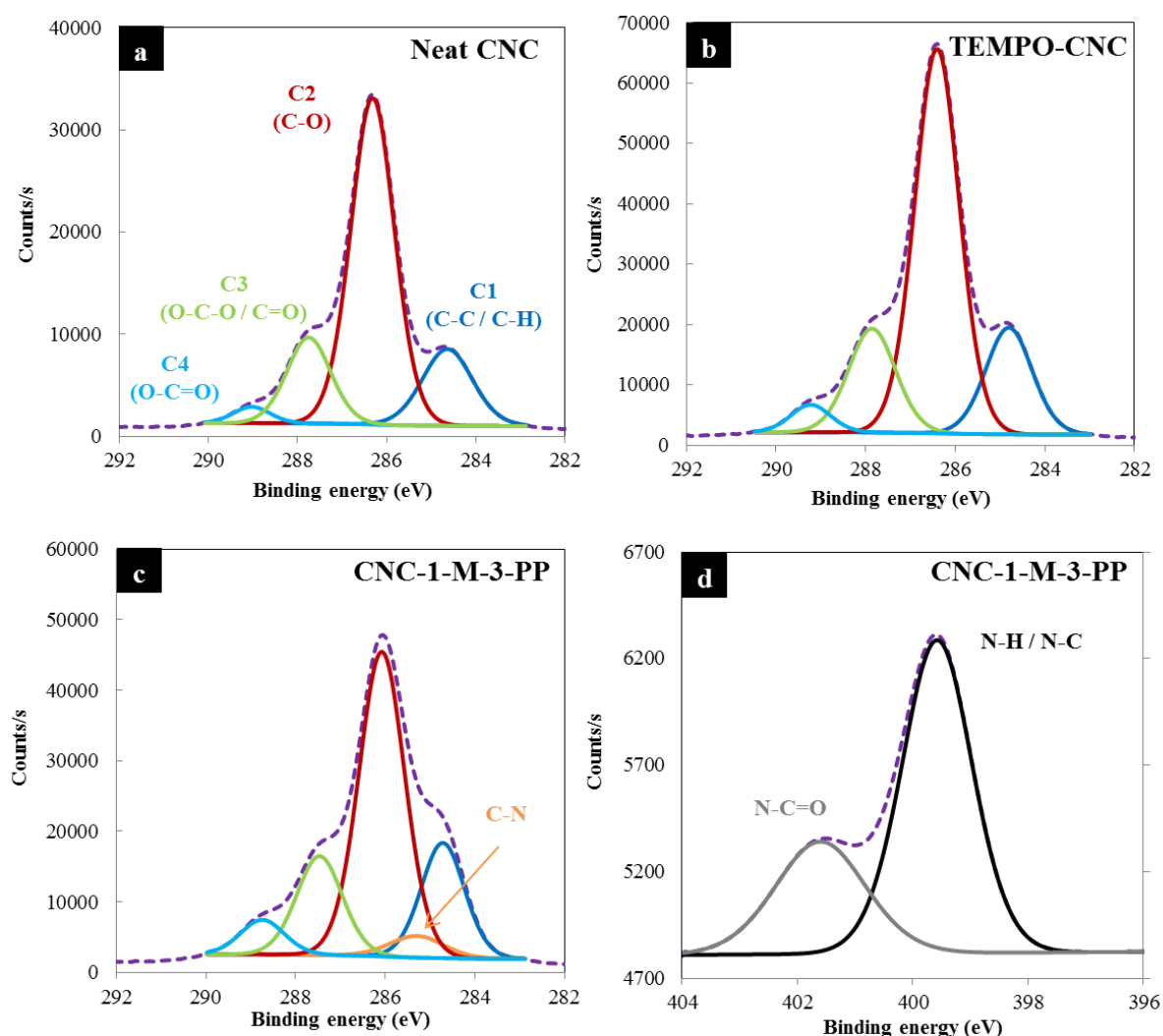


Figure II. 30. X-ray photoelectron spectroscopy decomposition of the C1s peak of **a)** unmodified cellulose nanocrystal (CNC), **b)** oxidized TEMPO-CNC, and **c)** modified CNC-1-M-3-PP, and **d)** decomposition of the N1s peak of modified CNC-1-M-3-PP

The C1 signal from neat CNC decomposition spectra was linked to the presence of non-oxidized alkane-type carbon atoms and some impurities like lignin residuals or other compounds. Therefore, its intensity should not increase after oxidation. The C2 signal was related to the ether groups or hydroxyl groups from pure cellulose as well as to the ends of cellulose chains. The C3 signal corresponded to the acetal entities present that bridged two AGUs. Its intensity should not increase after chemical modifications since the corresponding carbon will not be affected by chemical modifications. Finally, C4 signal was present in low proportions in the neat CNC spectra, and was attributed to the presence of glucuronic acid from hemicellulose residuals. Comparing **Figure II. 30 a)** and **b)**, an increase in this C4 peak was observed and was consistent with the oxidation performed on CNC. This observation was confirmed by values of C4 contribution (**Table II. 11**) which increased by a factor of 2.

Thus, the efficiency of TEMPO-mediated oxidation performed in a reactor on a large batch of CNCs was proved. The amount of -COOH groups on a CNC was quantified and confirmed *via* direct characterizations, and it was needed for further modifications for the groups with 1-M-3-PP molecule obtained through the amidation reaction.

3.2. Grafting efficiency of 1-M-3PP on TEMPO-CNC through amidation

Taking advantage of the carboxylic groups previously introduced at the surface of CNC *via* different chemical reactions has been already proposed in literature^{4,68}. In this study, efficiency and green aspects of amidation *via* EDC/NHS catalysis have been key elements for the choice of such an amidation procedure. 1-M-3-PP molecule has been widely used in the pharmaceutical industry for biotechnology, highlighting its potential for further applications, e.g. in barrier packaging with food contact. Moreover, as mentioned in literature, its possible interaction with aromatic compounds could be interesting in terms of organic compounds' sorption.

In a preliminary study, the kinetics of the EDC/NHS catalyzed amidation reaction was investigated. After the beginning of the reaction, aliquots of the system were collected at different times of reaction, washed by centrifugation cycles, and then dialyzed against water, as presented in the section 1.3. Aqueous suspensions of different modified CNC-1-M-3-PP were casted and dried films were analyzed by FTIR spectroscopy, whose spectra are presented in **Figure II. 31**. For each spectra of recovered CNC-1-M-3-PP at acidic pH, the presence of a peak at 1650 cm^{-1} was related to the presence of -N(H)-C=O amide bonds introduced during amidation reaction. When the pH was changed from an acidic pH to a basic pH, this peak shifted to 1745 cm^{-1} . Simultaneously, a peak at 1600 cm^{-1} appeared which was related to the presence of residual unreacted carboxylic groups. Moreover, between 2800 and 3000 cm^{-1} , peaks related to -CH_2 and -CH_3 groups from grafted 1-M-3-PP were observed and correlated with the same peaks present in the commercial molecule 1-M-3-PP. These peaks can also be attributed to the presence of =C-H and -C=C elongations from the aromatic rings of 1-M-3-PP

molecule, confirming the presence of 1-M-3-PP on the surface of CNC. Peaks related to amide bonds highlight the covalent grafting between TEMPO-CNC and 1-M-3-PP. After the kinetics study of the amidation performed on TEMPO-CNC, a reaction time of 72 h was selected for the reaction. Following this study, samples named “CNC-1-M-3-PP” were recovered after 72 h of reaction.

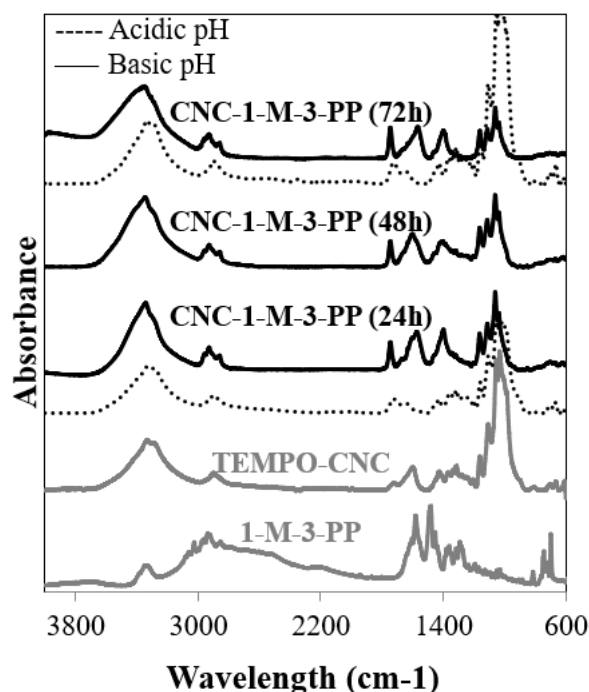


Figure II. 31. Fourier transform infrared (FTIR) spectra of 1-M-3-PP molecule, oxidized TEMPO-CNC, modified CNC-1-M-3-PP after 24h (at acid and basic pH, dashed and solid lines, respectively), 48h and 72h of amidation

Regarding the AFM image of CNC-1-M-3-PP in **Figure II. 25 c)**, a length of 150 ± 50 nm was obtained, showing that no significant change in size was induced after the amidation. Furthermore, their crystallinity index (CI = 90%) was substantially the same. Thus, the morphology of CNCs did not change after amidation with 1-M-3-PP, which was once again predictable due to the mild conditions (pH, temperature) of the amidation reaction. This result was interesting since crystallinity and dimensions of CNCs are required properties for most applications.

In order to quantify the amount of carboxylic groups converted into amide groups, conductometric titrations were performed on CNC-1-M-3-PP sample. Using both **Equation II. 13** and **Equation II. 14**, the degree of oxidation and the residual grafting rate of $-\text{COOH}$ were determined to be 0.19 ± 0.01 and 1138 ± 28 , respectively. The percentage of converted $-\text{COOH}$ groups were deduced from the results obtained for TEMPO-CNC using **Equation II. 15** and was equal to 12%, as presented in **Table II. 9**. The results of the elemental analysis performed on CNC-1-M-3-PP are presented in **Table II. 10**. The atomic percentage of nitrogen was found to be 0.5% (whereas, less than 0.1% was present in both neat and oxidized samples), confirming the presence of nitrogen compound in the CNC-1-M-3-PP sample. Moreover, a degree of substitution of 0.07 was obtained using **Equation II. 17**, corresponding to 10% of COOH groups converted into amide groups. This was in line with the values found through

the conductometric titrations. Finally, XPS analysis was performed on the amidated sample. Regarding the **Figure II. 29**, the survey spectra obtained from CNC-1-M-3-PP exhibited an intense peak at 400 eV, which clearly indicates the presence of nitrogen elements in the sample. From **Table II. 11**, it can be seen that the atomic percentage of nitrogen we found to be 1% the analysis, which was much higher than the percentage found in the TEMPO-CNC sample (0.3 %), correlating with the survey spectra. C1s decomposition spectrum of CNC-1-M-3-PP is presented in **Figure II. 30 c**. C1, C2, C3 and C4 peaks were clearly identified, and a new peak at 285.3 eV ($\Delta eV = 0.6$ eV) which is related to the C-N bond was also identified. Although the determination of this peak was difficult because of its overlapping with C1 peak, it was clearly assigned to the C-N bond, as previously shown in literature^{33,138}. However, at this stage, it was not possible to confirm the presence of any covalent amide linkage between nitrogen compound and oxidized TEMPO-CNC. In this sense, N1s decomposition spectrum of CNC-1-M-3-PP was performed as presented in **Figure II. 30 d**. The two peaks at 399.6 eV and 401.6 eV ($\Delta eV = 2$ eV) were related to N-H/N-C and N-C=O bonds, respectively. In literature, it has already been seen that the second peak was decomposed in two peaks³³. However, due to the close electronegativity of hydrogen and carbon elements, only one peak can be attributed to the two bonds N-H and N-C. According to the amidation reaction and as shown in **Scheme II. 2**, theoretical ratio between the peaks N-H/N-C and N-C=O should be equal to 2:1 if only amidation takes place. However, this ratio was higher in our case (2.7:1), suggesting that other nitrogen compounds were present in the sample. This opened the door to a possible case of adsorption of the 1-M-3-PP molecule at the surface of TEMPO-CNC. Nevertheless, a degree of substitution (DS_{XPS}) was calculated according to **Equation II. 20** and was equal to 0.6. This value was related to the -COOH groups present on the surface of TEMPO-CNC, and by taking into account the previously determined DO_{XPS} as well as the relation presented in **Equation II. 22**, a degree of substitution of 0.05 was obtained. It was consistent with the value previously found by conductometric titration and elemental analysis and in accordance — although lower — with values found in literature for such amidation procedures^{124,125}. It can be due to the heterogeneous reaction leading to lower grafting densities than those obtained in homogenous chemistry or the mild reaction conditions (i.e. aqueous system, ambient temperature) compared to traditionally performed organic chemistry reactions.

3.3. Indirect proofs of grafting efficiency

We proved the presence of covalently attached 1-M-3-PP molecules at the surface of CNCs. Although the degree of substitution was quite low, it has been proved in literature that even if that is the case, grafting can lead to significant changes in properties like barrier or compatibilization properties^{20,72}, and some indirect characterization can further confirm their grafting efficiency.

Dispersion of modified CNC-1-M-3-PP in different organic solvents was investigated. Indeed, as shown in **Figure II. 32**, suspensions of both oxidized TEMPO-CNC and modified CNC-1-M-3-PP

were prepared by solvent exchange in acetone or dichloromethane at the same concentration (0.3 wt%) through successive centrifugation cycles (10000 rpm, 5 °C, 15'). Pictures presented in **Figure II. 32** were taken after 4 h following a sonication step (2500 J.g_{CNC}⁻¹). As shown in **Figure II. 32 a**), TEMPO-CNC was less stable in acetone than in dichloromethane, and in both cases, sedimentation of CNC at the bottom of the vial was observed after 4 h of rest.

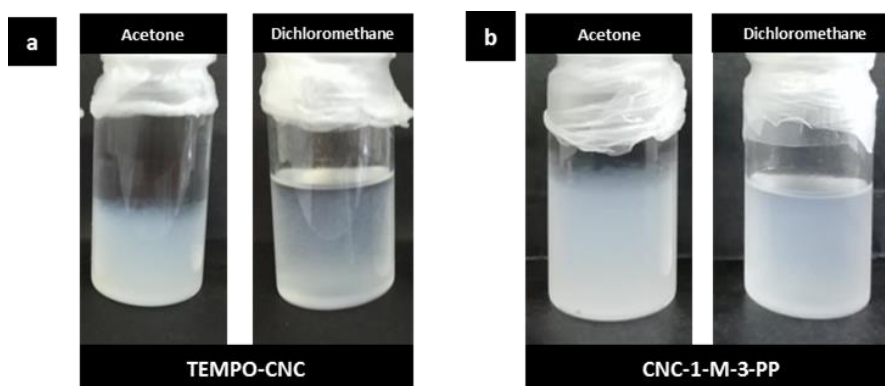


Figure II. 32. Pictures of **a)** TEMPO-CNC and **b)** CNC-1-M-3-PP suspensions (0.3 wt%) in acetone and dichloromethane after 4 h without stirring

In **Figure II. 32 b)**, modified CNC-1-M-3-PP in acetone was also subjected to sedimentation, but it was significantly less than TEMPO-CNC in acetone. On the other hand, the suspensions of CNC-1-M-3-PP in dichloromethane were stable after 4 h. Stabilization of CNCs in an organic solvent — acetone and dichloromethane in this study — after their modification with aromatic compounds highlighted the presence of the hydrophobic groups at their surface. Moreover, this dispersion in an organic solvent — especially in dichloromethane which is the solvent of numerous polymers — was encouraging in terms of application purposes, and especially for the preparation of nanocomposites, where the preparation of stable and well-dispersed CNC suspension in dichloromethane is generally the first step in the nanocomposites' elaboration. Furthermore, in order to confirm the hydrophobization of CNC-1-M-3-PP, contact angles of neat CNC, TEMPO-CNC, and modified CNC-1-M-3-PP were determined and the results are summarized in **Table II. 12**.

		Neat CNC	TEMPO-CNC	CNC-1-M-3-PP
Contact angle (°)	Mean value	53	52	43
	Std. Dev.	3	2	1

Table II. 12. Contact angles measured with a 4- μ L water drop on neat cellulose nanocrystals (CNCs), TEMPO-CNC and CNC-1-M-3-PP casted films

Measured contact angles of both unmodified CNC and oxidized TEMPO-CNC were close (53 +/- 3° and 52 +/- 2°, respectively). This result was predictable since oxidized hydroxyl groups were replaced by carboxyl groups after oxidation, which did not affect hydrophilicity of the TEMPO-CNC surface. After modification with 1-M-3-PP, surface behavior of CNC-1-M-3-PP was expected to change. As mentioned before, presence of aromatic hydrophobic groups would change polarity, and thus an

increase in the contact angle was expected. According to **Table II. 12**, contact angle measured for CNC-1-M-3-PP ($43 \pm 1^\circ$) did not follow this trend. The reason could be the bad surface quality of the casted film or the presence of more pores leading to the absorption of water inside the film, which was confirmed by the significant decrease in water droplet volume during the experiment.

All these characterizations helped determine the efficiency of the grafting of 1-M-3-PP molecules from carboxylic groups. Nevertheless, as deduced from quantitative analyses of the CNC-1-M-3-PP sample, parallel adsorption possibly occurred at the CNC surface. Several researchers have previously investigated the competition between covalent grafting and non-covalent phenomenon. Recently, Gicquel *et al.* reported that the adsorption of aminated PNIPAM-NH₂ competed with its amidation on the TEMPO-CNC surface¹²⁴. In the present study, this adsorption was also investigated, and QCM-d experiments were performed in a preliminary study, as presented in the remainder of this section.

3.4. Physico-chemical adsorption of 1-M-3-PP at the surface of TEMPO-CNC

The investigation of the adsorption of 1-M-3-PP occurring on oxidized TEMPO-CNC was firstly monitored by UV absorbance. In the first step, a calibration curve of the absorption of the molecule at 258 nm as a function of the concentration was plotted, as shown in **Figure II. 33 a**). Beer-Lambert law is valid for values of absorbance comprised between 0.1 and 1. For a defined ratio $N_{\text{COOH}}:N_{\text{NH}_2}$, a specific amount of 1-M-3-PP was added to an aqueous TEMPO-CNC suspension, and the reaction mixture was left under magnetic stirring. At different stirring times, an aliquot was recovered and two centrifugation cycles (10000 rpm, 5 °C, 20') were performed. Each recovered filtrate was then diluted in order to correlate with Beer-Lambert law and analyzed using an UV spectrophotometer. Concentration of 1-M-3-PP — corresponding to the non-adsorbed mass — was determined using its calibration curve presented in **Figure II. 33 a**). Finally, adsorbed mass of 1-M-3-PP was plotted as a function of the reaction time. In order to investigate the behavior of 1-M-3-PP molecules on TEMPO-CNC, the adsorption was monitored within the time. Taking into account the number of carboxylic groups –COOH at the surface of TEMPO-CNC, as previously determined, a precise amount of 1-M-3-PP was added to the TEMPO-CNC suspension with conservation of the molar ratio $N_{\text{COOH}}:N_{\text{NH}_2}$ (1:4) used in the amidation reaction. According to the previously described method, adsorbed mass of 1-M-3-PP per g of dry TEMPO-CNC was determined and plotted as a function of the time, as presented in **Figure II. 33 b**).

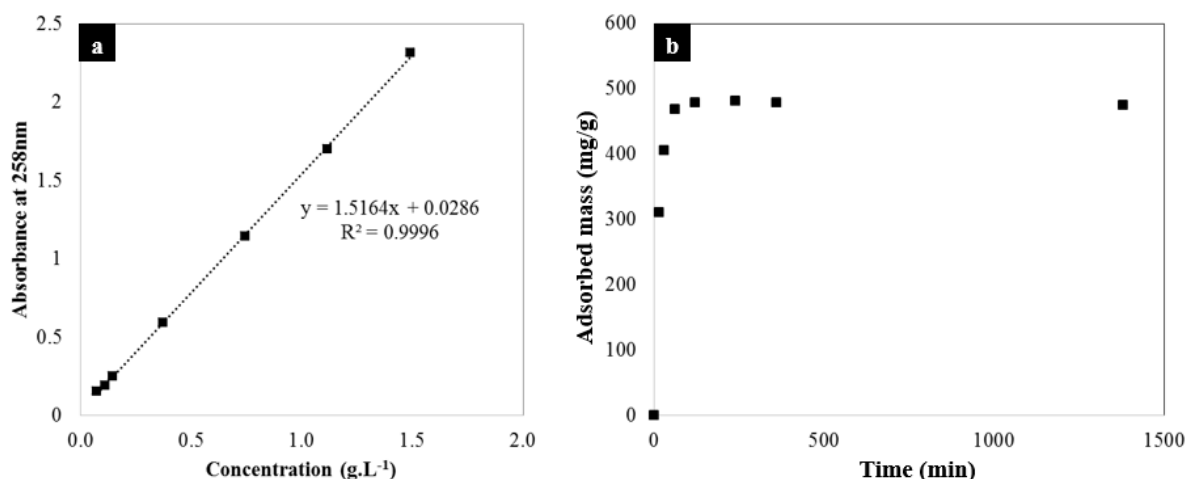


Figure II. 33. a) Calibration curve of 1-M-3-PP absorbance function of its concentration in a water solution and b) Mass of 1-M-3-PP adsorbed per gram of dry TEMPO-CNC function on the time (with molar ratio $4N_{COOH}=N_{NH_2}$)

Figure II. 33 b) shows clearly that the adsorbed mass reached a plateau after 2 h. In this sense, it was difficult to assume if the previously determined $\%COOH_{react}$ was related only to the amidation reaction or to the adsorption phenomenon also. This point was relevant: indeed, as soon as a chemical modification is performed, competing adsorptions or other parallel modifications must be considered. Since one objective of this study was to introduce aromatic ring at the surface of CNCs for further barrier properties, this parallel adsorption did not hinder our work.

In order to investigate more precisely the adsorption of 1-M-3-PP on TEMPO-CNC, QCM-d analyses were performed. **Figure II. 34** shows the QCM-d measurements obtained after 1-M-3-PP adsorption on both unmodified CNC and oxidized TEMPO-CNC at pH 8, in order to be in $-OSO_3^-$ (neat CNC) or $-COO^-$ (TEMPO-CNC) configuration. In both **Figure II. 34 a)** and **b)**, a long plateau can be observed at the beginning of the measurement recording, corresponding to the water flow, and thus the water swelling of cellulose. Just after 1-M-3-PP solution injection (indicated by arrows), a large increase in the frequency was observed which was related to the increase of the sensors' mass and thus the adsorption of the molecule (**Figure II. 34 a)**). Note that this increase was much greater for TEMPO-CNC than for unmodified CNC. In both cases, the rinsing (indicated by droplet symbols) and the subsequent increase in frequency followed by a stable plateau indicated a partial release of compounds from the CNC surface.

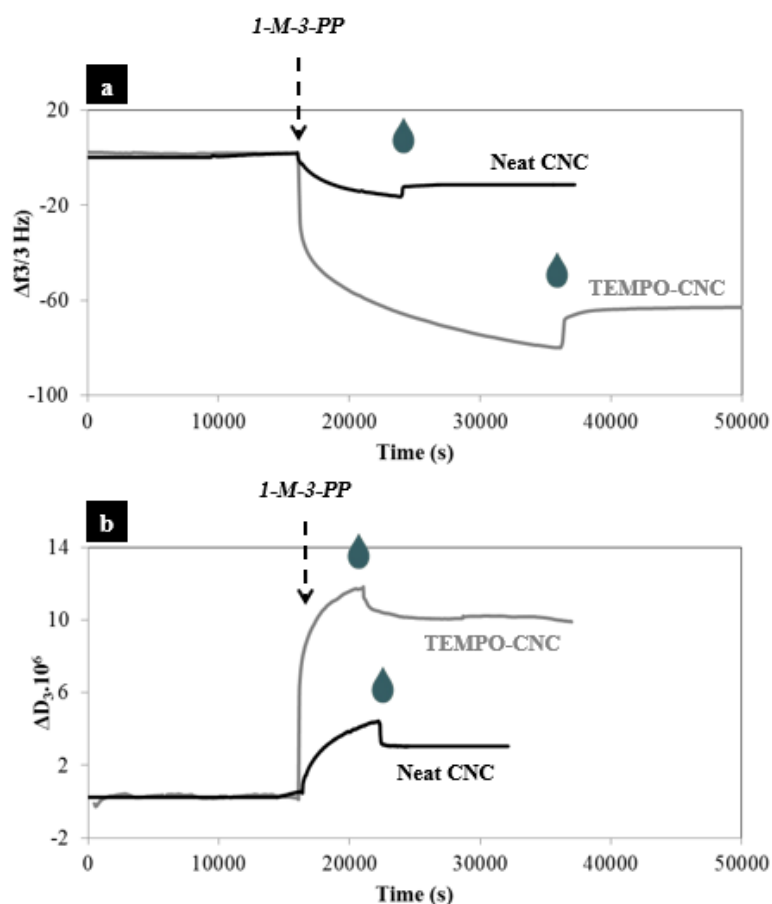


Figure II. 34. Shifts in **a)** frequency and **b)** dissipation plotted function of the time and obtained from the third overtone of QCM-d measurement data and normalized by $n=3$ (Arrows indicate when 1-M-3-PP solution was injected and droplet symbols correspond to the beginning of rinsing with milliQ water)

The final frequency changes are presented in **Table II. 13** and were equal to -11.6 Hz and -47.8 Hz for neat and oxidized CNC, respectively. In parallel, an increase in dissipation — much lower than frequency changes in both cases — was clearly observed and the final dissipation changes equal to $2.8 \cdot 10^6$ and $9.7 \cdot 10^6$ for CNC and TEMPO-CNC, respectively, are presented in **Table II. 13**. Note that in both cases, dissipation changes were largely lower than 10 times the corresponding frequency changes, which allowed the use of Sauerbrey equation (**Equation II. 23**) as previously detailed.

	Neat CNC	TEMPO-CNC
$\Delta f_3/3$ (Hz)	-11.6	-47.8
ΔD_3 (10^6)	2.8	9.7
Δm ($\text{mg}_{1\text{-M-3-PP}} \cdot \text{m}^{-2}_{\text{CNC}}$)	2.1	8.5
Δn ($\text{mol}_{1\text{-M-3-PP}} \cdot \text{g}^{-1}_{\text{CNC}}$)	7.0×10^{-3}	2.8×10^{-2}

Table II. 13. Frequency ($\Delta f/3$) and dissipation (ΔD_3) changes after 1-M-3-PP adsorption on both CNC and TEMPO-CNC with determined adsorbed amount (Δm and Δn)

Table II. 13 presents the amounts of 1-M-3-PP molecule adsorbed (in mass or in mol, Δm and Δn respectively) per surface or mass of CNC and calculated using Sauerbrey equation (**Equation II. 23**). According to QCM-d experiments, 2.1 and 8.5 mg of 1-M-3-PP were adsorbed per m^2 of neat CNC and TEMPO-CNC, respectively, corresponding to 7.0×10^{-3} and 2.8×10^{-2} moles of 1-M-3-PP adsorbed

per g of CNC and TEMPO-CNC. Thus, adsorption occurred in both cases and was four times more efficient when CNCs were previously oxidized, which was predictable due to the presence of a large number of negative charges ($-\text{COO}^-$) on their surface. Moreover, by comparing the value of DS_{XPS} (0.05, or 3.10^{-4} moles of 1-M-3-PP per g of TEMPO-CNC) with the value of Δn , it can be assumed that adsorption allows the introduction of about 90 times more 1-M-3-PP molecules on the surface of CNCs, than the amidation procedure. This value is very high and confirms that the washing step applied during the QCM-d experiment is not adapted, since the value after the grafting is much lower. It also proves that the value of adsorbed molecules obtained from QCM-d is related to irreversibly adsorbed molecules. Unfortunately, QCM-d cannot simulate the same extensive washing steps as those performed in the amidation procedure. In this sense, it is not possible to conclude about the proportion of grafted and/or adsorbed molecules on the CNCs.

Based on the literature and on the direct characterizations performed on the CNC-1-M-3-PP, it can be assumed that the washing steps performed in the grafting strategy is sufficient, and it is thus possible to assume that most of the quantified aminated molecules are covalently attached on the CNCs at the end of the reaction.

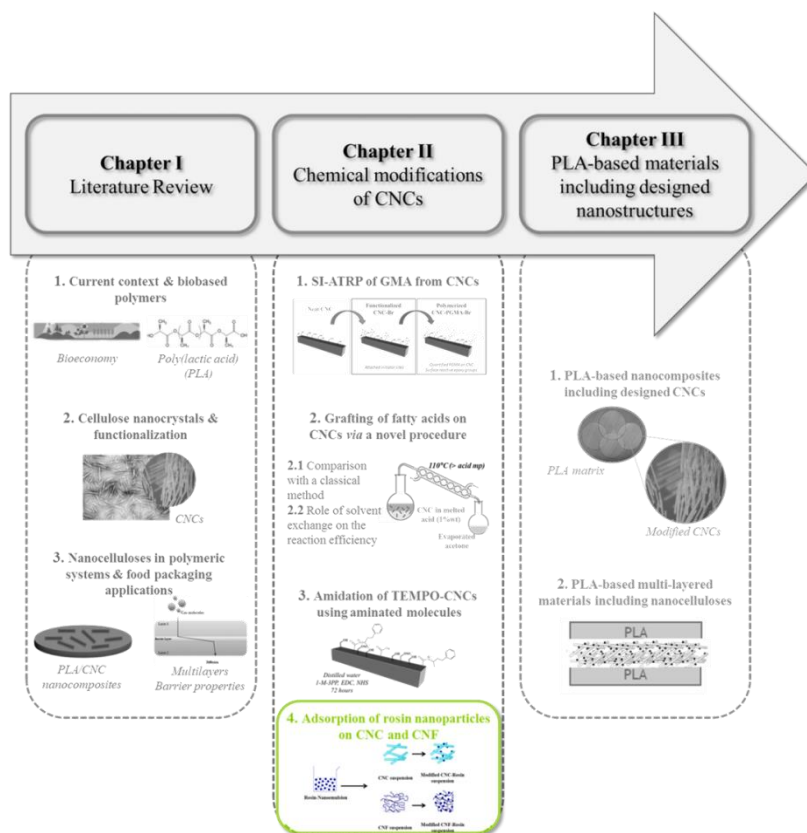
4. Conclusion

In this study, a TEMPO-mediated oxidation was performed on a large batch of CNCs. Although this oxidation has been widely detailed in the literature, performing it efficiently on such a large volume is interesting and challenging. Quantification of carboxyl groups introduced on TEMPO-CNC was carried out by classic conductometric titrations, and confirmed by elemental analyses and XPS methods. In the second step, TEMPO-CNCs were subjected to an amidation reaction using 1-M-3-PP which bears aromatic groups. These chemically modified CNCs have been characterized by direct methods (FTIR spectroscopy, elemental analysis, XPS) as well as, by indirect methods. Dispersion and stabilization in organic solvents, such as dichloromethane, is an interesting feature since it opens the door to further applications for nanocomposites. Furthermore, with the investigation of sorption and barrier properties, it opens the road to nanocomposites' applications in packaging materials.

4. Adsorption of rosin nanoparticles from a nano-emulsion on both cellulose nanocrystals and nanofibrils

This short section aims to briefly describe the preparation of modified nanocelluloses, whose application will be further discussed in Chapter III.2 of this manuscript.

Moreover, this part is the result of a close collaborative work with the startup INOFIB (K. Missoum and B. Dhuiège), and the presented results are the subject of a patent registered by the startup.



Abstract

Outstanding properties of nanocelluloses make them materials of choice for their use in nanocomposites or multi-layered materials. Indeed, besides their sources availability, renewability and, sustainability, their intrinsic properties (low density, morphology and, chemical reactivity) are of great interest for the enhancement of the final materials properties. In this short study, both cellulose nanofibrils (CNF) and cellulose nanocrystals (CNC) were modified by adsorption of rosin nanoparticles obtained from the preparation of a rosin-based nano-emulsion. The rosin mixture as a natural compound is of interest because of its low cost, renewability, hydrophobicity, as well as, its antimicrobial and antioxidant properties. Successfully prepared modified CNF-Rosin and CNC-Rosin aqueous suspensions can then be used for further applications, especially for the preparation of fully bio-based food packaging materials with improving active properties.

Keywords:

Cellulose nanofibrils — Cellulose nanocrystals — Rosins — Nano-emulsion — Adsorption

1. Introduction

Sustainability, biodegradability, renewability and abundancy are the main exceptional advantages of the novel category of cellulosic materials: the nanocelluloses. These nanoscale materials, whether cellulose nanofibrils (CNF) or nanocrystals (CNC), have been the focus of numerous researches in recent decades. In fact, their outstanding intrinsic properties (i.e., low density compared to other organic materials, high specific surface area, surface chemical reactivity, high tensile strength, barrier properties towards oxygen)^{1,2,15-17} make them materials of choice for many different applications (hydrogels, composites, conducting materials, piezoelectric materials, biosensors, pharmaceuticals, biomedical devices, etc.)^{2,67}. Among these applications, their use in the elaboration of multi-phasic materials (i.e. nanocomposites, multi-layers) is highly interesting and promising, especially for bio-based food packaging applications. Moreover, conferring them active functionalities, like antimicrobial or antioxidant properties, could increase their interest in such applications^{7,8}. In the literature, numerous publications focused on this topic, with the use of various active molecules and different procedures for their attachment on nanocelluloses^{27,139,140}.

Among exploitable and tunable natural materials, rosins are highly interesting because of their abundancy, sustainability and low cost. They are the main products from conifers, especially pine resin derived from pine trees, and more than 1 million metric tons of rosin are produced each year^{141,142}. Abietic- and primaric-type acids are the main components of a natural rosin mixture, whose structure is presented in **Figure II. 35**¹². These acids bear hydrophenanthrene ring structures, conferring them similar rigidity to that of fossil-based plastics, and Liu *et al.* took advantage of rosin rigidity to produce rosin-based thermosetting resins with properties comparable to synthetic materials¹⁴³. Moreover, rosins find applications in inks, adhesives, cosmetics, varnishes, paints, coatings, medicines, paper-sizing agents and, emulsions^{142,144,145}. It is worth to note that rosin is often used in growth polymerization in order to produce low molecular weight polymeric materials including rosin as natural compounds, and these polymerizations are generally performed *via* atom-transfer radical polymerization (ATRP)¹⁴⁴. For example, Wang *et al.*¹⁴¹ performed ATRP to polymerize rosin monomers on the surface of lignin for surface functionalization. Moreover, antimicrobial activity of rosin is a major advantage, which has been widely exploited, as found in the literature. Indeed, Moustafa *et al.*¹⁴² recently focused on the fact that rosin can be used as food products shelf-life extender in packaging materials, and performed esterification of rosin on organoclay and introduced these modified organoclays in a blend of poly(lactic acid)/poly(butylene adipate-co-terephthalate). They concluded about the antibacterial activity of produced nanocomposites and their interest in food packaging applications. De Castro *et al.*²⁷ performed an efficient green esterification of rosin on cellulose nanocrystals and highlighted the hydrophobic and antimicrobial behavior of the resulted grafted CNC. Note that insolubility of natural rosins in water may limit their use in numerous applications requiring water conditions, unless they are used in suspended form.

One main advantage of the preparation of emulsions is the solubility of compounds in a solvent with which they are not soluble. In fact, by definition, an emulsion lies in the mixing of two immiscible liquids by using both mechanical shear and surfactant¹⁴⁶. A nano-emulsion is defined as the dispersion of nano-sized particles (typically between 20 and 200 nm)¹⁴⁷ prepared by mechanical forces. More precisely, nano-emulsions are clear and thermodynamically stable and their main application is the drug-delivery in various systems, as widely described in the literature^{147,148}.

The combination of both nanocelluloses and natural rosins has only recently been proposed in literature. Indeed, as previously mentioned, de Castro *et al.*²⁷ performed a green esterification procedure, adapted from a previous study published by Espino-Pérez *et al.*²⁶, to covalently link rosins on the cellulose nanocrystals surface. More recently, Niu *et al.*¹⁴⁹ performed a similar protocol on cellulose nanofibers and introduced modified CNF in a poly(lactic acid)/chitosan polymeric matrix. Both studies highlighted antimicrobial activity brought by the presence of rosin in the prepared systems. Although these grafting methods aimed to limit the use of organic and toxic solvents, they required time-consuming multi-steps procedure. In this sense, adsorption of rosin on nanocellulose can be considered, thus decreasing the use of chemicals and reaction steps.

In this short part, a nano-emulsion of natural rosin was prepared and its stability and nano-size character were carefully investigated by Dynamic Light Scattering (DLS). In a second step, both CNF and CNC were modified by adsorption of rosin nano-particles from the nano-emulsion, leading to modified CNF-Rosin and CNC-Rosin. Films of the ensuing modified nanocelluloses were performed by filtration or solvent casting for CNF-Rosin and CNC-Rosin respectively, and the presence of rosins in each film was investigated by infrared spectroscopy and contact angle measurements.

2. Materials and methods

2.1. Materials

Tetradecyltrimethylammonium Bromide (TTAB), Gum rosin (natural resin) and, Chloroform (>99%) were supplied by Sigma Aldrich and used as received. Spray-dried powder of cellulose nanocrystals (CNC) was supplied by CelluForce[®] (Canada). Cellulose nanofibrils suspension (2 wt%) was provided by INOFIB (Saint-Martin d'Hères, France). **Figure II. 35** represents the main components found in commercial mixture of natural rosin.

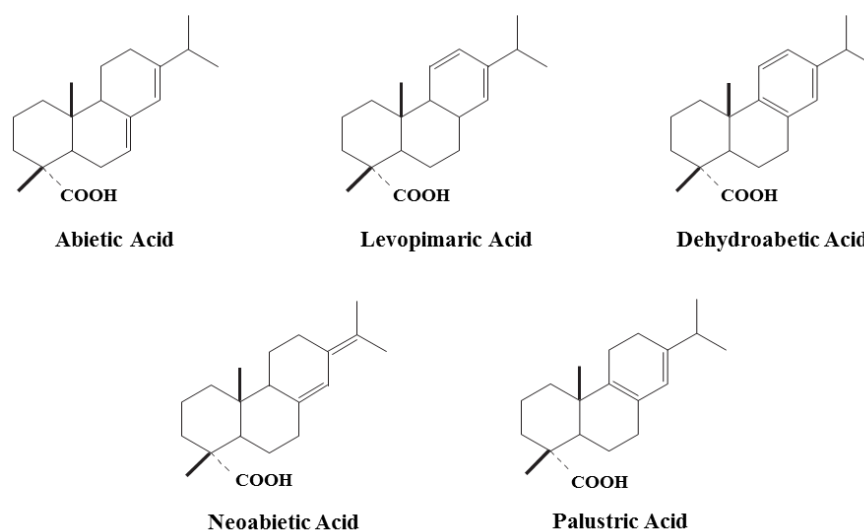


Figure II. 35. Main carboxylic acids found in rosin (extracted from ²⁷)

2.2. Preparation of rosin nano-emulsion

An aqueous and an oily phase were prepared according to the following protocols. Aqueous phase was prepared by total dissolving 0.606 g of TTAB in 50 mL of water, which corresponds to around 10 times the TTAB Critical Micellar Concentration. Concerning the oily phase preparation, a solution of rosins in chloroform was prepared at the concentration of 550 g/L. Thereafter, 14.8 g of the oily phase were slowly introduced into 49.5 g of the aqueous phase previously put in a beaker, and the mixture was emulsified by using an ultrasonic probe for 2 min with a 25 W power. The reaction media was then heated at 65 °C using an oil bath until total evaporation of the chloroform. Final nano-emulsion was then recovered in a perfectly hermetically closed vial and stored at 4 °C until used.

Preparation of rosin nano-emulsion was performed by the INOFIB startup (Karim Missoum and Benjamin Dhuiège).

2.3. Adsorption of rosin nanoparticles on CNF

A correct amount of previously prepared rosin nano-emulsion was added to a 2% (wt/wt) aqueous suspension of CNF in order to reach a rosin/CNF weight ratio equal to 0.11. The formulated suspension was then mixed under mechanical stirring for 30 min at room temperature to adsorb the nano-micelles of rosin onto the CNF surface. Final CNF-Rosin suspension was stored in a hermetically closed vial at 4 °C before being used.

Adsorption of rosin nanoparticles on CNF was performed by the INOFIB startup (Karim Missoum and Benjamin Dhuiège).

2.4. Adsorption of rosin nano-emulsion on CNC

Rosin nanoparticles were adsorbed on CNC, as previously described for CNF. Briefly, an aqueous suspension of CNC at 1% (wt/wt) was prepared by adding a correct amount of spray-dried CNC in water and by applying an ultrasonic treatment to the suspension (2.5 kJ/g of dried CNC). A precise amount of rosin nano-emulsion was then introduced in the suspension by keeping a rosin/CNC weight ratio equal to 0.11. After 30 min of magnetic stirring at room temperature, it was considered that rosin was adsorbed at the CNC surface. Recovered CNC-Rosin suspension was stored in a hermetically closed vial at 4 °C before use.

2.5. Elaboration of neat and modified CNF films by filtration

Appropriate amounts of both neat CNF and formulated CNF-Rosin suspensions were diluted to 0.5 wt%. and mixed for 10 min under magnetic stirring. The diluted suspensions were then filtered through a 1µm-cut-off Nylon web, dried at 90 °C for 12 min under vacuum to obtain the CNF and CNF-Rosin films. More precisely, 20 cm diameter sheets were prepared at 30 g/m², using a Rapid-Köthen hand sheet former.

Preparation of modified CNF-Rosin films was performed by the INOFIB startup (Karim Missoum and Benjamin Dhuiège).

2.6. Elaboration of neat and modified CNC-Rosin films by solvent casting

Both neat CNC and modified CNC-Rosin suspensions were diluted at 0.5 wt% and sonicated (2.5 kJ/g of dried CNC). Correct amounts of both suspensions were introduced in petri dishes keeping the basis weight of targeted films equal to 40 g/m². Casted suspensions were left under fume hood at room temperature for several days until total water evaporation, in order to prepare the CNC and CNC-Rosin films.

2.7. Characterization methods

2.7.1. Rosin nano-emulsion characterization by Dynamic Light Scattering (DLS)

The particle size of the rosin nanoparticles from the nano-emulsion was determined by DLS using a VASCO Cordouan nanosizer. More precisely, three droplets of the nano-emulsion were introduced in the device with the dual thickness controller (DTC) in up position, diluted with distilled water and roughly homogenized. The laser intensity and the correlator settings were adjusted at 5 μs as time interval, and 600 as the number of channels. Data were recorded using NanoQ software at 25 °C for 15 acquisitions of 30 s with a noise/signal ratio limit inferior to 0.5% (dual limits settings). Both the Pade-Laplace and the Cumulants method were used for data processing. At least triplicate measurements were performed.

2.7.2. CNC and CNF film characterization by Fourier-transform infrared spectroscopy (FTIR)

Fourier-transform infrared spectroscopy was performed on both unmodified and modified nanocellulose films using a Perkin-Elmer spectrum 65. Films were analyzed through 16 scans and with a resolution of 2 cm^{-1} . The baseline of the FTIR spectra was corrected and the data tuned up. Each spectrum containing CNC or CNF was normalized at 1110 cm^{-1} (related to pure cellulose). Each measurement was at least duplicated, and most representative spectra were plotted.

2.7.3. Contact angle measurements

Contact angle measurements were carried out on neat and modified nanocellulose films by depositing 5 μL -water droplets on the film surface at room temperature. An OCA20 DataPhysics (DataPhysics Instrument) system, equipped with a CCD camera, was used to record the angles between the solvent and the substrate. The acquisition of contact angle was collected for the first 60 s after deposition. At least five measurements were performed for each sample.

3. Results and discussions

3.1. Nanometric size of rosin particles

The preparation of rosin nano-emulsion was based on the alkyl ketene dimer (AKD)-based nano-emulsion production method patented by Missoum *et al.*⁹⁹. By definition, as previously mentioned, nano-emulsions are nano-sized stable colloidal emulsions¹⁵⁰. Rosin nano-emulsion was prepared following the protocol of mixing two immiscible liquids (water and chloroform) in the presence of a surfactant (TTAB), which resulted in a dispersed oil-in-water single phase. To avoid the aggregation and get the proper nanometric size of rosin particles in the prepared emulsion, DLS measurement was performed on a diluted sample. The size distribution of the intensity of rosin particles obtained with the cumulant method is presented in **Figure II. 36**. The size distribution of particles is Gaussian, with the particle diameter size equal to 186 nm measured by DLS, confirming the nanometric character of the rosin particles in the emulsion.

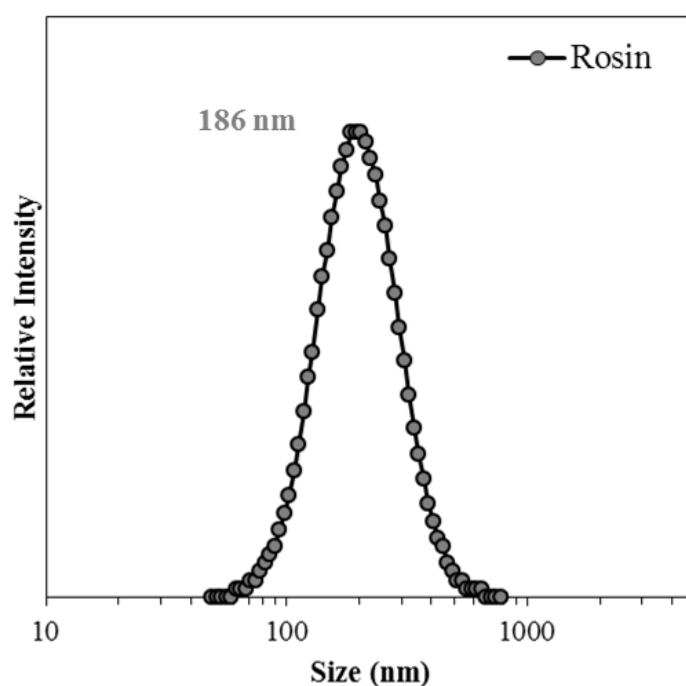


Figure II. 36. Size distribution of relative intensity obtained from DLS measurement performed on rosin nano-emulsion

The DLS measurement has been performed six months after the nano-emulsion preparation, which proves the stability of the nano-emulsions, that were used for further adsorption on both CNF and CNC.

3.2. Efficiency of the rosin adsorption on both CNF and CNC

Adsorption of rosin nano-emulsions on CNF and CNC was performed according to the previously described procedure. As discussed in the introduction, several acids are present in natural rosin mixture, the most predominant of which are shown in **Figure II. 35**. Both CNF and CNC contain many hydroxyl groups ($-OH$) at their surface, which can easily create hydrogen bonds with carboxyl groups in the acid mixture from rosin particles. In order to confirm the presence of rosin molecules on both CNF and CNC, FTIR analyses were performed on commercial rosin, as well as, neat CNF, CNF-Rosin, neat CNC, and CNC-Rosins films. The resulting spectra are presented in **Figure II. 37**.

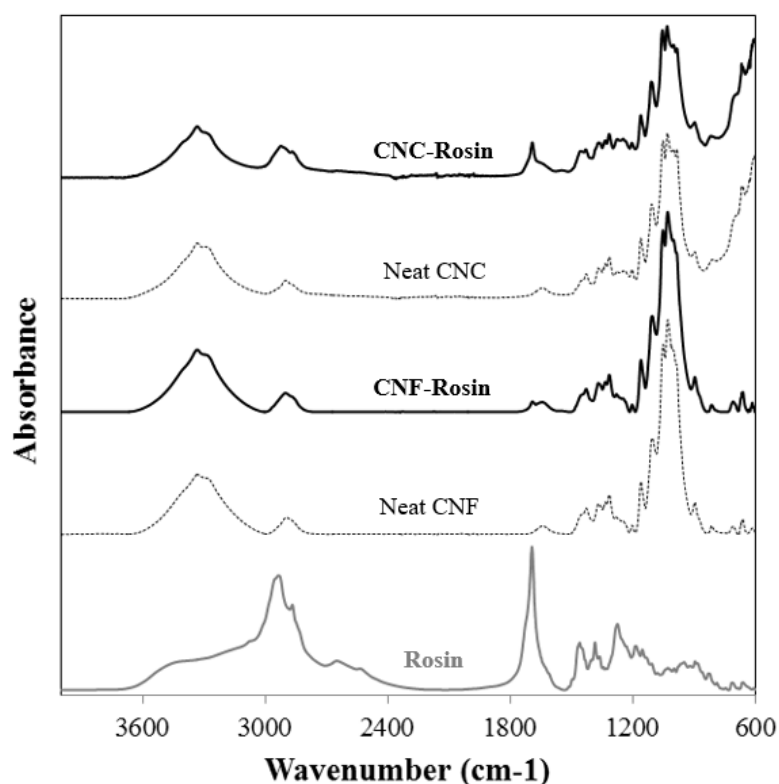


Figure II. 37. FTIR spectra of commercial rosin (powder), and, neat CNF, CNF-Rosin, neat CNC, and CNC-Rosin films

In the spectrum of the supplied neat rosin, an intense peak at 1695 cm^{-1} can be related to many carboxylic groups ($-COOH$) from the different acids composing the rosin mixture. Moreover, a large peak between 2900 and 3000 cm^{-1} can be attributed to the $-CH$ carbons from alkene bonds of different acids. The spectra related to neat CNF and CNC both exhibit peaks classically observed for cellulosic samples, with, among others, peaks at 1105 , 1059 and 1028 cm^{-1} linked to the vibrations of C-O bonds, and a large peak at approximately $3000 - 3600\text{ cm}^{-1}$ linked to stretching vibration of bonds of primary and secondary hydroxyl groups. In both CNF-Rosin and CNC-Rosin spectra, respectively, the peaks at 1692 cm^{-1} and 1691 cm^{-1} are attributed to the carboxylic groups from the rosin mixture present in the samples. Note that this peak is more intense in the case of CNC, which could be explained by the loss of the not adsorbed rosin nano-emulsion during the filtration process of CNF-based film preparation.

However, from the FTIR spectra, it is possible to qualitatively conclude about the presence of rosin in both CNF-Rosin and CNC-Rosin samples. Modified CNF-Rosin and CNC-Rosin were thus efficiently produced, with a weight ratio of rosin to CNC or CNF close to 0.11.

Water contact angle measurements were performed on both unmodified CNF and CNC films, as well as on modified CNF-Rosin and CNC-Rosin films. Neat CNC and CNF films exhibit water contact angle equal to $54^{\circ} \pm 1^{\circ}$ and $36^{\circ} \pm 6^{\circ}$, respectively, and these values are consistent with values found in the literature^{151,152}. After adsorption of rosin nanoparticles on CNC, CNC-Rosin casted film shows a visible decrease in the contact angle down to $32^{\circ} \pm 1.5^{\circ}$, probably due to the presence of hydrophilic properties of rosin molecules. The contact angle of the modified CNF-Rosin film is equal to $42^{\circ} \pm 5^{\circ}$. Taking into account the standard deviation of this value and the uncertainty of the neat CNF film contact angle, it is difficult to reach any conclusions about the evolution of the water contact angle, although a similar trend was observed for the CNC-Rosin sample.

4. Conclusion

A stable nano-emulsion of rosins was successfully prepared by the INOFIB Startup. In order to confer new active properties (antibacterial, antioxidant, etc.) to nanocelluloses, rosin nanoparticles from the nano-emulsion were adsorbed on the surface of both CNF and CNC by a simple, fast and, low chemical consumption route. Finally, prepared aqueous suspensions of modified CNF-Rosin and CNC-Rosin can then be used for further applications.

Conclusions of Chapter II

The aim of the **Chapter II** was to propose new routes for the CNCs surface chemical modification. Four different strategies were successfully performed on cellulose nanocrystals.

- In the first section **II.1**, the grafting-from *via* a surface-initiated radical transfer polymerization (SI-ATRP) of the glycidyl methacrylate (GMA) was successfully performed, accordingly to an optimized protocol. The initial surface modifications of CNCs with the BIB — a common initiator of the SI-ATRP method — was efficiently performed, in accordance with values found in the literature. Furthermore, the kinetics study of the SI-ATRP led to an optimization of the reaction time. In fact, after only one hour of polymerization, around 50% of the total mass of recovered nanomaterials was related to the PGMA polymer. The presence of reactive epoxy groups at the surface of recovered polymerized CNCs at the end of the reaction was also highlighted, and this point is highly encouraging, since it could favor further reactions with a polymeric matrix, or more simply the compatibility between the polymerized CNCs and a hydrophobic polymeric matrix, like the poly(lactic acid).

- The section **II.2** was introduced in a first part (**II.2.1**) evidencing the efficiency of a novel esterification procedure compared to a well-known esterification involving an acid chloride as reagent. The degree of substitution of CNCs modified *via* the new esterification method was five times higher than that of CNCs obtained through the classical method. In the second following part (**II.2.2**), the novel esterification procedure was described and performed on CNCs using both lauric and stearic acids as reagents. The efficiency of the reaction was highlighted — with degrees of substitution equal to 0.1 and 0.3 for lauric and stearic acids, respectively —, as well as, the hydrophobicity of the modified CNCs surface, and these results are encouraging for further use of the modified CNCs. Moreover, the possible recyclability of the chemicals, less toxic as usual, at the end of the proposed esterification method is an important matter, particularly in a spirit of more green chemistry.

- In the section **II.3**, the characterization of TEMPO-CNC oxidized on a larger scale than those reported in the literature (~ 100 g) proved the efficiency of the oxidation (with an oxidation degree around 0.2), in accordance with values found in the literature. Furthermore, the grafting of the 1-methyl-3-phenylpropylamine molecule — an aminated molecule bearing aromatic group — was performed on the TEMPO-CNCs through an amidation reaction, and the efficiency of the reaction was quantified, with a degree of substitution close to 0.1. Through multiple characterizations, it was assumed that another reaction — the adsorption — could take place at the surface of the TEMPO-CNCs. This adsorption phenomenon was thus investigated, and it was shown that it allowed the introduction of ninety times more aromatic molecules on the surface of the CNCs than the amidation reaction. This

result highlighted the potential bonding of numerous molecules on the TEMPO-CNC, in a simple and more environmentally friendly way.

▪ Finally, the additional section **II.4** was intended to briefly introduce the preparation of CNCs and CNFs adsorbed with rosin nanoparticles. The stable nanometric behavior of the prepared nano-emulsion containing rosin nanoparticles, and the presence of rosin in final dried films composed of CNCs or CNFs were proved. This adsorption procedure did not involve toxic chemicals, and is interesting because of its simplicity and short duration (no washing steps required).

The **Table II. 14** summarizes the different grafting methods described in the **Chapter II**, as well as, their required reaction time, their efficiency, and the limitation in terms of quantity of grafted CNCs. This highlights the fact that in order to be able to functionalize the CNCs on a large scale — which is often necessary for many applications, such as the elaboration of packaging materials —, it is necessary to move towards grafting or adsorption methods that consume less reaction steps, and thus less time and toxic chemicals.

Chapter	Grafted or adsorbed polymer/molecule	Grafting method	Reaction time	Efficiency	Maximum possible quantity of grafted CNCs at lab scale
II.1	Poly(glycidyl methacrylate) (PGMA)	Surface-initiated transfer radical polymerization (SI-ATRP)	1h	50 % (w/w) of PGMA	A few milligrams
II.2(.2)	Lauric & stearic acid	Esterification (novel procedure: the acid acts as the solvent)	8h	Degree of substitution 0.1-0.3	A few tens of grams
II.3	1-methyl-3-phenylpropylamine	Amidation on oxidized TEMPO-CNC or adsorption	72h	0.1	A few hundred grams
II.4	Rosin nanoparticles	Adsorption	30 min	/	A few hundred grams

Table II. 14. Summary of the different grafting methods presented in the Chapter II

By way of a detailed comparison between these different grafting methods, the **Table II. 15. Main advantages and drawbacks of the different grafting methods proposed in the Chapter II** presents the main advantages and main drawbacks of the latter, from the point of view of the reaction time, the cost of raw materials, the possible amount of modified material, and the industrial feasibility.

Procedure	Main advantages	Main drawbacks
SI-ATRP (PGMA)	<ul style="list-style-type: none"> ▪ Entire CNCs surface covered with polymer ▪ Quantified and controlled amount of grafted polymer ▪ Short time of polymerization (1h) 	<ul style="list-style-type: none"> ▪ Restricting amount of grafted CNCs (\approx 1g) ▪ Organic & toxic chemicals ▪ Oxygen free media required ▪ 2-step procedure (1st surface-initiation with active sites) ▪ Difficult industrial feasibility ▪ Considerable cost
Esterification (fatty acids)	<ul style="list-style-type: none"> ▪ Limiting use of toxic chemicals ▪ Satisfying grafting densities ▪ Possible recyclability of solvent/chemicals ▪ Low cost of chemicals ▪ Conceivable industrial feasibility 	<ul style="list-style-type: none"> ▪ Limited amount of grafted CNCs at lab-scale (\approx 10-20g) ▪ Large amount of solvent (acetone) required ▪ Multi-step procedure ▪ High energy consumption ▪ Time-consuming washing steps ▪ Long reaction times (solvent exchange + 8h)
Amidation (1-M-3-PP)	<ul style="list-style-type: none"> ▪ Mild and aqueous conditions ▪ Relative low cost and low energy consumption ▪ Possible reaction on a larger scale (TEMPO oxidation performed on \approx 100g) 	<ul style="list-style-type: none"> ▪ Low grafting densities ▪ Possible concurrent adsorption ▪ Mutli-step procedure ▪ Long reaction time (72h)
Adsorption (Rosins)	<ul style="list-style-type: none"> ▪ Simple efficient route, no washing-step ▪ Low energy consumption ▪ Possible large amount of modified CNCs (\approx kg) ▪ Short reaction time (\approx 30 min) 	<ul style="list-style-type: none"> ▪ No control of the adsorption (reversible / irreversible?) ▪ Preliminary step required for the preparation of the nano-emulsion

Table II. 15. Main advantages and drawbacks of the different grafting methods proposed in the Chapter II

As previously mentioned, all the modified nanocellulosic materials prepared and characterized were then used for the preparation of final materials based on a polymer matrix, whose results are presented in the following **Chapter III**.

References – Chapter II

1. Nechyporchuk, O., Belgacem, M. N. & Bras, J. Production of cellulose nanofibrils: A review of recent advances. *Industrial Crops and Products* **93**, 2–25 (2016).
2. Kargarzadeh, H. *et al.* Advances in cellulose nanomaterials. *Cellulose* **25**, 2151–2189 (2018).
3. Habibi, Y., Lucia, L. A. & Rojas, O. J. Cellulose Nanocrystals: Chemistry, Self-Assembly, and Applications. *Chemical Reviews* **110**, 3479–3500 (2010).
4. Habibi, Y. Key advances in the chemical modification of nanocelluloses. *Chem. Soc. Rev.* **43**, 1519–1542 (2014).
5. Oksman, K. *et al.* Review of the recent developments in cellulose nanocomposite processing. *Composites Part A: Applied Science and Manufacturing* **83**, 2–18 (2016).
6. Ferreira, F. V., Pinheiro, I. F., Gouveia, R. F., Thim, G. P. & Lona, L. M. F. Functionalized cellulose nanocrystals as reinforcement in biodegradable polymer nanocomposites. *Polymer Composites* **39**, E9–E29 (2017).
7. Ferrer, A., Pal, L. & Hubbe, M. Nanocellulose in packaging: Advances in barrier layer technologies. *Industrial Crops and Products* **95**, 574–582 (2017).
8. Hubbe, M. A. *et al.* Nanocellulose in Thin Films, Coatings, and Plies for Packaging Applications: A Review. *BioResources* **12**, 2143–2233 (2017).
9. Domingues, R. M. A., Gomes, M. E. & Reis, R. L. The Potential of Cellulose Nanocrystals in Tissue Engineering Strategies. *Biomacromolecules* **15**, 2327–2346 (2014).
10. Lin, N. & Dufresne, A. Nanocellulose in biomedicine: Current status and future prospect. *European Polymer Journal* **59**, 302–325 (2014).
11. Jorfi, M. & Foster, E. J. Recent advances in nanocellulose for biomedical applications. *Journal of Applied Polymer Science* **132**, 41719–41738 (2015).
12. Foster, E. J. *et al.* Current characterization methods for cellulose nanomaterials. *Chemical Society Reviews* **47**, 2609–2679 (2018).
13. Beck, S., Méthot, M. & Bouchard, J. General procedure for determining cellulose nanocrystal sulfate half-ester content by conductometric titration. *Cellulose* **22**, 101–116 (2015).
14. Reid, M. S., Villalobos, M. & Cranston, E. D. Benchmarking cellulose nanocrystals: from the laboratory to industrial production. *Langmuir* **33**, 1583–1598 (2016).
15. Natterodt, J. C., Petri-Fink, A., Weder, C. & Zoppe, J. O. Cellulose Nanocrystals: Surface Modification, Applications and Opportunities at Interfaces. *CHIMIA International Journal for Chemistry* **71**, 376–383 (2017).
16. Klemm, D. *et al.* Nanocelluloses: A New Family of Nature-Based Materials. *Angewandte Chemie International Edition* **50**, 5438–5466 (2011).
17. Dufresne, A. *Nanocellulose: from nature to high performance tailored materials*. (Walter de Gruyter GmbH & Co KG, 2017).
18. Lin, N., Huang, J. & Dufresne, A. Preparation, properties and applications of polysaccharide nanocrystals in advanced functional nanomaterials: a review. *Nanoscale* **4**, 3274–3294 (2012).
19. Espino-Pérez, E. *et al.* Nanocomposites with functionalised polysaccharide nanocrystals through aqueous free radical polymerisation promoted by ozonolysis. *Carbohydrate Polymers* **135**, 256–266 (2016).
20. Espino-Pérez, E. *et al.* Designed cellulose nanocrystal surface properties for improving barrier properties in polylactide nanocomposites. *Carbohydrate Polymers* **183**, 267–277 (2018).
21. Boujemaoui, A. *et al.* Polycaprolactone Nanocomposites Reinforced with Cellulose Nanocrystals Surface-Modified via Covalent Grafting or Physisorption: A Comparative Study. *ACS Applied Materials & Interfaces* **9**, 35305–35318 (2017).

22. Moon, R. J., Martini, A., Nairn, J., Simonsen, J. & Youngblood, J. Cellulose nanomaterials review: structure, properties and nanocomposites. *Chemical Society Reviews* **40**, 3941–3994 (2011).
23. Belgacem, M. N., Gandini, A. *Monomers, polymers and composites from renewable resources*. (Elsevier, 2008)
24. Siqueira, G., Bras, J. & Dufresne, A. Cellulosic Bionanocomposites: A Review of Preparation, Properties and Applications. *Polymers* **2**, 728–765 (2010).
25. Eyley, S. & Thielemans, W. Surface modification of cellulose nanocrystals. *Nanoscale* **6**, 7764–7779 (2014).
26. Espino-Pérez, E., Domenek, S., Belgacem, N., Sillard, C. & Bras, J. Green Process for Chemical Functionalization of Nanocellulose with Carboxylic Acids. *Biomacromolecules* **15**, 4551–4560 (2014).
27. de Castro, D. O., Bras, J., Gandini, A. & Belgacem, N. Surface grafting of cellulose nanocrystals with natural antimicrobial rosin mixture using a green process. *Carbohydrate Polymers* **137**, 1–8 (2016).
28. Fatona, A., Berry, R. M., Brook, M. A. & Moran-Mirabal, J. M. Versatile Surface Modification of Cellulose Fibers and Cellulose Nanocrystals through Modular Triazinyl Chemistry. *Chemistry of Materials* **30**, 2424–2435 (2018).
29. Kedzior, S. A., Graham, L., Moorlag, C., Dooley, B. M. & Cranston, E. D. Poly(methyl methacrylate)-grafted cellulose nanocrystals: One-step synthesis, nanocomposite preparation, and characterization. *The Canadian Journal of Chemical Engineering* **94**, 811–822 (2016).
30. Azzam, F., Heux, L., Putaux, J.-L. & Jean, B. Preparation By Grafting Onto, Characterization, and Properties of Thermally Responsive Polymer-Decorated Cellulose Nanocrystals. *Biomacromolecules* **11**, 3652–3659 (2010).
31. Hatton, F. L., Kedzior, S. A., Cranston, E. D. & Carlmark, A. Grafting-from cellulose nanocrystals via photoinduced Cu-mediated reversible-deactivation radical polymerization. *Carbohydrate Polymers* **157**, 1033–1040 (2017).
32. Goffin, A.-L. *et al.* From Interfacial Ring-Opening Polymerization to Melt Processing of Cellulose Nanowhisker-Filled Polylactide-Based Nanocomposites. *Biomacromolecules* **12**, 2456–2465 (2011).
33. Hu, Z., Berry, R. M., Pelton, R. & Cranston, E. D. One-Pot Water-Based Hydrophobic Surface Modification of Cellulose Nanocrystals Using Plant Polyphenols. *ACS Sustainable Chem. Eng.* **5**, 5018–5026 (2017).
34. Abitbol, T. Surface modification of cellulose nanocrystals with cetyltrimethylammonium bromide. *Nordic Pulp and Paper Research Journal* **29**, 046–057 (2014).
35. Kedzior, S. A., Marway, H. S. & Cranston, E. D. Tailoring Cellulose Nanocrystal and Surfactant Behavior in Miniemulsion Polymerization. *Macromolecules* **50**, 2645–2655 (2017).
36. Nagalakshmaiah, M., El Kissi, N. & Dufresne, A. Ionic Compatibilization of Cellulose Nanocrystals with Quaternary Ammonium Salt and Their Melt Extrusion with Polypropylene. *ACS Applied Materials & Interfaces* **8**, 8755–8764 (2016).
37. Sessini, V. *et al.* Effect of the addition of polyester-grafted-cellulose nanocrystals on the shape memory properties of biodegradable PLA/PCL nanocomposites. *Polymer Degradation and Stability* **152**, 126–138 (2018).
38. Kloser, E. & Gray, D. G. Surface Grafting of Cellulose Nanocrystals with Poly(ethylene oxide) in Aqueous Media. *Langmuir* **26**, 13450–13456 (2010).
39. Zhou, L. *et al.* Grafting polycaprolactone diol onto cellulose nanocrystals via click chemistry: Enhancing thermal stability and hydrophobic property. *Carbohydrate Polymers* **189**, 331–341 (2018).

40. Habibi, Y. *et al.* Bionanocomposites based on poly(ϵ -caprolactone)-grafted cellulose nanocrystals by ring-opening polymerization. *Journal of Materials Chemistry* **18**, 5002–5010 (2008).
41. Morandi, G., Heath, L. & Thielemans, W. Cellulose Nanocrystals Grafted with Polystyrene Chains through Surface-Initiated Atom Transfer Radical Polymerization (SI-ATRP). *Langmuir* **25**, 8280–8286 (2009).
42. Zhang, Z., Tam, K. C., Sèbe, G. & Wang, X. Convenient characterization of polymers grafted on cellulose nanocrystals via SI-ATRP without chain cleavage. *Carbohydrate Polymers* **199**, 603–609 (2018).
43. Zoppe, J. O. *et al.* Poly(N-isopropylacrylamide) Brushes Grafted from Cellulose Nanocrystals via Surface-Initiated Single-Electron Transfer Living Radical Polymerization. *Biomacromolecules* **11**, 2683–2691 (2010).
44. Boujemaoui, A., Mongkhontreerat, S., Malmström, E. & Carlmark, A. Preparation and characterization of functionalized cellulose nanocrystals. *Carbohydrate Polymers* **115**, 457–464 (2015).
45. Hansson, S., Antoni, P., Bergenudd, H. & Malmström, E. Selective cleavage of polymer grafts from solid surfaces: assessment of initiator content and polymer characteristics. *Polymer Chemistry* **2**, 556–558 (2011).
46. Zoppe, J. O. *et al.* Effect of Surface Charge on Surface-Initiated Atom Transfer Radical Polymerization from Cellulose Nanocrystals in Aqueous Media. *Biomacromolecules* **17**, 1404–1413 (2016).
47. Cañamero, P. F., de la Fuente, J. L., Madruga, E. L. & Fernández-García, M. Atom Transfer Radical Polymerization of Glycidyl Methacrylate: A Functional Monomer. *Macromol. Chem. Phys.* **205**, 2221–2228 (2004).
48. Nyström, D., Lindqvist, J., Östmark, E., Hult, A. & Malmström, E. Superhydrophobic bio-fibre surfaces via tailored grafting architecture. *Chem. Commun.* 3594–3596 (2006)
49. Martínez-Sanz, M. *et al.* Incorporation of poly(glycidylmethacrylate) grafted bacterial cellulose nanowhiskers in poly(lactic acid) nanocomposites: Improved barrier and mechanical properties. *European Polymer Journal* **49**, 2062–2072 (2013).
50. Hansson, S., Östmark, E., Carlmark, A. & Malmström, E. ARGET ATRP for Versatile Grafting of Cellulose Using Various Monomers. *ACS Appl. Mater. Interfaces* **1**, 2651–2659 (2009).
51. Malmström, E. & Carlmark, A. Controlled grafting of cellulose fibres – an outlook beyond paper and cardboard. *Polymer Chemistry* **3**, 1702–1713 (2012).
52. Cheng, D., Wei, P., Zhang, L. & Cai, J. Surface-initiated atom transfer radical polymerization grafting from nanoporous cellulose gels to create hydrophobic nanocomposites. *RSC Adv.* **8**, 27045–27053 (2018).
53. Morandi, G. *et al.* ATRP and ROMP: Modular chemical tools for advanced macromolecular engineering. *Materials Science and Engineering: C* **29**, 367–371 (2009).
54. McCaig, H. C., Myers, E., Lewis, N. S. & Roukes, M. L. Vapor Sensing Characteristics of Nanoelectromechanical Chemical Sensors Functionalized Using Surface-Initiated Polymerization. *Nano Letters* **14**, 3728–3732 (2014).
55. Segal, L., Creely, J. J., Martin, A. E. & Conrad, C. M. An Empirical Method for Estimating the Degree of Crystallinity of Native Cellulose Using the X-Ray Diffractometer. *Textile Research Journal* **29**, 786–794 (1959).
56. Park, S., Baker, J. O., Himmel, M. E., Parilla, P. A. & Johnson, D. K. Cellulose crystallinity index: measurement techniques and their impact on interpreting cellulase performance. *Biotechnology for Biofuels* **3**, 1–10 (2010).

57. Ahvenainen, P., Kontro, I. & Svedström, K. Comparison of sample crystallinity determination methods by X-ray diffraction for challenging cellulose I materials. *Cellulose* **23**, 1073–1086 (2016).
58. Boluk, Y. & Danumah, C. Analysis of cellulose nanocrystal rod lengths by dynamic light scattering and electron microscopy. *J Nanopart Res* **16**, 2174 (2014).
59. Siqueira, G., Bras, J. & Dufresne, A. New Process of Chemical Grafting of Cellulose Nanoparticles with a Long Chain Isocyanate. *Langmuir* **26**, 402–411 (2010).
60. Viet, D., Beck-Candanedo, S. & Gray, D. G. Dispersion of cellulose nanocrystals in polar organic solvents. *Cellulose* **14**, 109–113 (2007).
61. Tian, C., Fu, S., Habibi, Y. & Lucia, L. A. Polymerization Topochemistry of Cellulose Nanocrystals: A Function of Surface Dehydration Control. *Langmuir* **30**, 14670–14679 (2014).
62. Barbey, R., Laporte, V., Alnabulsi, S. & Klok, H.-A. Postpolymerization Modification of Poly(glycidyl methacrylate) Brushes: An XPS Depth-Profiling Study. *Macromolecules* **46**, 6151–6158 (2013).
63. Wang, X., Jing, S., Liu, Y., Qiu, X. & Tan, Y. Preparation of dithiocarbamate polymer brush grafted nanocomposites for rapid and enhanced capture of heavy metal ions. *RSC Advances* **7**, 13112–13122 (2017).
64. Xiao, M., Li, S., Chanklin, W., Zheng, A. & Xiao, H. Surface-initiated atom transfer radical polymerization of butyl acrylate on cellulose microfibrils. *Carbohydrate Polymers* **83**, 512–519 (2011).
65. Sabatini, D. M. *Leading Edge Nanotechnology Research Developments*. (Nova Publishers, 2007).
66. Beamson, G. & Briggs, D. High Resolution XPS of Organic Polymers: The Scienta ESCA300 Database. *J. Chem. Educ.* **70**, A25 (1993).
67. Kontturi, E. *et al.* Advanced Materials through Assembly of Nanocelluloses. *Advanced Materials* **30**, 1703779 (2018).
68. Eyley, S. & Thielemans, W. Surface modification of cellulose nanocrystals. *Nanoscale* **6**, 7764–7779 (2014).
69. Castro, D. O. *et al.* Effect of different carboxylic acids in cyclodextrin functionalization of cellulose nanocrystals for prolonged release of carvacrol. *Materials Science and Engineering: C* **69**, 1018–1025 (2016).
70. de Castro, D. O. *et al.* Controlled release of carvacrol and curcumin: bio-based food packaging by synergism action of TEMPO-oxidized cellulose nanocrystals and cyclodextrin. *Cellulose* **25**, 1249–1263 (2018).
71. Tang, J., Sisler, J., Grishkewich, N. & Tam, K. C. Functionalization of cellulose nanocrystals for advanced applications. *Journal of Colloid and Interface Science* **494**, 397–409 (2017).
72. Espino-Pérez, E. *et al.* Cellulose nanocrystal surface functionalization for the controlled sorption of water and organic vapours. *Cellulose* **23**, 2955–2970 (2016).
73. Wei, L. *et al.* Chemical modification of nanocellulose with canola oil fatty acid methyl ester. *Carbohydrate Polymers* **169**, 108–116 (2017).
74. Peng, S. X., Chang, H., Kumar, S., Moon, R. J. & Youngblood, J. P. A comparative guide to controlled hydrophobization of cellulose nanocrystals via surface esterification. *Cellulose* **23**, 1825–1846 (2016).
75. Bendahou, A., Hajlane, A., Dufresne, A., Boufi, S. & Kaddami, H. Esterification and amidation for grafting long aliphatic chains on to cellulose nanocrystals: a comparative study. *Research on Chemical Intermediates* **41**, 4293–4310 (2015).
76. Çetin, N. S. *et al.* Acetylation of Cellulose Nanowhiskers with Vinyl Acetate under Moderate Conditions. *Macromolecular Bioscience* **9**, 997–1003 (2009).

77. Lin, N., Huang, J., Chang, P. R., Feng, J. & Yu, J. Surface acetylation of cellulose nanocrystal and its reinforcing function in poly(lactic acid). *Carbohydrate Polymers* **83**, 1834–1842 (2011).
78. Anastas, P. & Eghbali, N. Green Chemistry: Principles and Practice. *Chemical Society Reviews* **39**, 301–312 (2010).
79. Shojaeiarani, J., Bajwa, D. S. & Stark, N. M. Green esterification: A new approach to improve thermal and mechanical properties of poly(lactic acid) composites reinforced by cellulose nanocrystals. *Journal of Applied Polymer Science* **135**, 46468 (2018).
80. Yoo, Y. & Youngblood, J. P. Green One-Pot Synthesis of Surface Hydrophobized Cellulose Nanocrystals in Aqueous Medium. *ACS Sustainable Chemistry & Engineering* **4**, 3927–3938 (2016).
81. Junior de Menezes, A., Siqueira, G., Curvelo, A. A. S. & Dufresne, A. Extrusion and characterization of functionalized cellulose whiskers reinforced polyethylene nanocomposites. *Polymer* **50**, 4552–4563 (2009).
82. de Mesquita, J. P., Donnici, C. L., Teixeira, I. F. & Pereira, F. V. Bio-based nanocomposites obtained through covalent linkage between chitosan and cellulose nanocrystals. *Carbohydrate Polymers* **90**, 210–217 (2012).
83. Ranby, B. G. & Ribi, E. Über den feinaufbau der zellulose. *Experientia* **6**, 12–14 (1950).
84. Sadeghifar, H., Filpponen, I., Clarke, S. P., Brougham, D. F. & Argyropoulos, D. S. Production of cellulose nanocrystals using hydrobromic acid and click reactions on their surface. *J Mater Sci* **46**, 7344–7355 (2011).
85. Camarero Espinosa, S., Kuhnt, T., Foster, E. J. & Weder, C. Isolation of Thermally Stable Cellulose Nanocrystals by Phosphoric Acid Hydrolysis. *Biomacromolecules* **14**, 1223–1230 (2013).
86. Yu, H. *et al.* Facile extraction of thermally stable cellulose nanocrystals with a high yield of 93% through hydrochloric acid hydrolysis under hydrothermal conditions. *Journal of Materials Chemistry A* **1**, 3938–3944 (2013).
87. Beck-Candanedo, S., Roman, M. & Gray, D. G. Effect of Reaction Conditions on the Properties and Behavior of Wood Cellulose Nanocrystal Suspensions. *Biomacromolecules* **6**, 1048–1054 (2005).
88. Roman, M. & Winter, W. Effect of Sulfate Groups from Sulfuric Acid Hydrolysis on the Thermal Degradation Behavior of Bacterial Cellulose. *Biomacromolecules* **5**, 1671–1677 (2004).
89. Liu, Y. *et al.* Nanoscale Assembly of Cellulose Nanocrystals during Drying and Redispersion. *ACS Macro Lett.* **7**, 172–177 (2018).
90. Ferreira, F. V. *et al.* How do cellulose nanocrystals affect the overall properties of biodegradable polymer nanocomposites: A comprehensive review. *European Polymer Journal* **108**, 274–285 (2018).
91. George, J. & Sabapathi, S. Cellulose nanocrystals: synthesis, functional properties, and applications. *Nanotechnol Sci Appl* **8**, 45–54 (2015).
92. Abitbol, T. Surface modification of cellulose nanocrystals with cetyltrimethylammonium bromide. *Nordic Pulp and Paper Research Journal* **29**, 046–057 (2014).
93. Heux, L., Chauve, G. & Bonini, C. Nonflocculating and Chiral-Nematic Self-ordering of Cellulose Microcrystals Suspensions in Nonpolar Solvents. *Langmuir* **16**, 8210–8212 (2000).
94. Nagalakshmaiah, M., Pignon, F., Kissi, N. E. & Dufresne, A. Surface adsorption of triblock copolymer (PEO–PPO–PEO) on cellulose nanocrystals and their melt extrusion with polyethylene. *RSC Advances* **6**, 66224–66232 (2016).
95. Freire, C. S. R., Silvestre, A. J. D., Neto, C. P., Belgacem, M. N. & Gandini, A. Controlled heterogeneous modification of cellulose fibers with fatty acids: Effect of reaction conditions on

- the extent of esterification and fiber properties. *Journal of Applied Polymer Science* **100**, 1093–1102 (2006).
96. Robles, E., Urruzola, I., Labidi, J. & Serrano, L. Surface-modified nano-cellulose as reinforcement in poly(lactic acid) to conform new composites. *Industrial Crops and Products* **71**, 44–53 (2015).
 97. Yuan, H., Nishiyama, Y., Wada, M. & Kuga, S. Surface Acylation of Cellulose Whiskers by Drying Aqueous Emulsion. *Biomacromolecules* **7**, 696–700 (2006).
 98. Boufi, S. *et al.* Nanofibrillated cellulose as an additive in papermaking process: A review. *Carbohydrate Polymers* **154**, 151–166 (2016).
 99. Missoum, K., Bras, J. & Belgacem, N. Method for forming a hydrophobic layer. *U.S. Patent Application No. 14/907, 326* (2016).
 100. Missoum, K., Martoia, F., Belgacem, M. N. & Bras, J. Effect of chemically modified nanofibrillated cellulose addition on the properties of fiber-based materials. *Industrial Crops and Products* **48**, 98–105 (2013).
 101. Martinez, P., Guerin, D., Jeong-Yong Ryu & Kwon, J. Y. Upscaling a new technology for the development of silicone free recyclable release paper. (2016) doi:10.13140/rg.2.1.2656.5526.
 102. Fumagalli, M., Sanchez, F., Molina Boisseau, S. & Heux, L. Gas-phase esterification of cellulose nanocrystal aerogels for colloidal dispersion in apolar solvents. *Soft Matter* **9**, 11309–11317 (2013).
 103. Zhong, L., Fu, S., Peng, X., Zhan, H. & Sun, R. Colloidal stability of negatively charged cellulose nanocrystalline in aqueous systems. *Carbohydrate Polymers* **90**, 644–649 (2012).
 104. Araki, J., Wada, M. & Kuga, S. Steric Stabilization of a Cellulose Microcrystal Suspension by Poly(ethylene glycol) Grafting. *Langmuir* **17**, 21–27 (2001).
 105. Brand, J., Pecastaings, G. & Sèbe, G. A versatile method for the surface tailoring of cellulose nanocrystal building blocks by acylation with functional vinyl esters. *Carbohydrate Polymers* **169**, 189–197 (2017).
 106. Chang, H. *et al.* Individually Dispersed Wood-Based Cellulose Nanocrystals. *ACS Appl. Mater. Interfaces* **8**, 5768–5771 (2016).
 107. Zini, E., Scandola, M. & Gatenholm, P. Heterogeneous Acylation of Flax Fibers. Reaction Kinetics and Surface Properties. *Biomacromolecules* **4**, 821–827 (2003).
 108. Spinella, S. *et al.* Concurrent Cellulose Hydrolysis and Esterification to Prepare a Surface-Modified Cellulose Nanocrystal Decorated with Carboxylic Acid Moieties. *ACS Sustainable Chemistry & Engineering* **4**, 1538–1550 (2016).
 109. Quast, K. Flotation of hematite using C6–C18 saturated fatty acids. *Minerals Engineering* **19**, 582–597 (2006).
 110. Missoum, K., Bras, J. & Belgacem, M. N. Organization of aliphatic chains grafted on nanofibrillated cellulose and influence on final properties. *Cellulose* **19**, 1957–1973 (2012).
 111. Ikram, S. & Ahmed, S. *Natural Polymers: Derivatives, Blends and Composites*. (Nova Publishers, 2016).
 112. Rol, F., Belgacem, M. N., Gandini, A. & Bras, J. Recent advances in surface-modified cellulose nanofibrils. *Progress in Polymer Science* **88**, 241–264 (2019).
 113. Ranby, B. G. Fibrous macromolecular systems. Cellulose and muscle. The colloidal properties of cellulose micelles. *Discuss. Faraday Soc.* **11**, 158–164 (1951).
 114. Beck-Candanedo, S., Roman, M. & Gray, D. G. Effect of Reaction Conditions on the Properties and Behavior of Wood Cellulose Nanocrystal Suspensions. *Biomacromolecules* **6**, 1048–1054 (2005).

115. Nguyen, T.-D., Y. Hamad, W. & J. MacLachlan, M. Tuning the iridescence of chiral nematic cellulose nanocrystals and mesoporous silica films by substrate variation. *Chemical Communications* **49**, 11296–11298 (2013).
116. Frka-Petesic, B., Radavidson, H., Jean, B. & Heux, L. Dynamically Controlled Iridescence of Cholesteric Cellulose Nanocrystal Suspensions Using Electric Fields. *Advanced Materials* **29**, 1606208 (2017).
117. Athukoralalage, S. S., Balu, R., Dutta, N. K. & Roy Choudhury, N. 3D Bioprinted Nanocellulose-Based Hydrogels for Tissue Engineering Applications: A Brief Review. *Polymers* **11**, 898 (2019).
118. Du, H. *et al.* Cellulose nanocrystals and cellulose nanofibrils based hydrogels for biomedical applications. *Carbohydrate Polymers* **209**, 130–144 (2019).
119. Mariano, M., Kissi, N. E. & Dufresne, A. Cellulose nanocrystals and related nanocomposites: Review of some properties and challenges. *Journal of Polymer Science Part B: Polymer Physics* **52**, 791–806 (2014).
120. Kedzior, S. A., Zoppe, J. O., Berry, R. M. & Cranston, E. D. Recent advances and an industrial perspective of cellulose nanocrystal functionalization through polymer grafting. *Current Opinion in Solid State and Materials Science* **23**, 79-91 (2018).
121. Hoeng, F., Denneulin, A., Neuman, C. & Bras, J. Charge density modification of carboxylated cellulose nanocrystals for stable silver nanoparticles suspension preparation. *Journal of Nanoparticle Research* **17**, 244 (2015).
122. Fraschini, C., Chauve, G. & Bouchard, J. TEMPO-mediated surface oxidation of cellulose nanocrystals (CNCs). *Cellulose* **24**, 2775–2790 (2017).
123. Saito, T. *et al.* Individualization of Nano-Sized Plant Cellulose Fibrils by Direct Surface Carboxylation Using TEMPO Catalyst under Neutral Conditions. *Biomacromolecules* **10**, 1992–1996 (2009).
124. Gicquel, E., Martin, C., Heux, L., Jean, B. & Bras, J. Adsorption versus grafting of poly(N-Isopropylacrylamide) in aqueous conditions on the surface of cellulose nanocrystals. *Carbohydrate Polymers* **210**, 100–109 (2019).
125. Hemraz, U. D., Boluk, Y. & Sunasee, R. Amine-decorated nanocrystalline cellulose surfaces: synthesis, characterization, and surface properties. *Canadian Journal of Chemistry* **91**, 974–981 (2013).
126. Arcot, L. R., Lundahl, M., Rojas, O. J. & Laine, J. Asymmetric cellulose nanocrystals: thiolation of reducing end groups via NHS–EDC coupling. *Cellulose* **21**, 4209–4218 (2014).
127. Guo, J. *et al.* Photoluminescent Hybrids of Cellulose Nanocrystals and Carbon Quantum Dots as Cytocompatible Probes for in Vitro Bioimaging. *Biomacromolecules* **18**, 2045–2055 (2017).
128. Habibi, Y., Chanzy, H. & Vignon, M. R. TEMPO-mediated surface oxidation of cellulose whiskers. *Cellulose* **13**, 679–687 (2006).
129. Lin, N. & Dufresne, A. Surface chemistry, morphological analysis and properties of cellulose nanocrystals with gradiented sulfation degrees. *Nanoscale* **6**, 5384–5393 (2014).
130. Rodahl, M., Höök, F., Krozer, A., Brzezinski, P. & Kasemo, B. Quartz crystal microbalance setup for frequency and Q -factor measurements in gaseous and liquid environments. *Review of Scientific Instruments* **66**, 3924–3930 (1995).
131. Sauerbrey, G. Z. The use of quartz oscillators for weighing thin layers on a microbalance. *J Phys* **155**, 206–212 (1959).
132. Vogt, B. D., Lin, E. K., Wu, W. & White, C. C. Effect of Film Thickness on the Validity of the Sauerbrey Equation for Hydrated Polyelectrolyte Films. *J. Phys. Chem. B* **108**, 12685–12690 (2004).

133. Slavin, S. *et al.* Adsorption behaviour of sulfur containing polymers to gold surfaces using QCM-D. *Soft Matter* **8**, 118–128 (2012).
134. Bardet, R. *et al.* Substitution of nanoclay in high gas barrier films of cellulose nanofibrils with cellulose nanocrystals and thermal treatment. *Cellulose* **22**, 1227–1241 (2015).
135. Trinh, B. M. & Mekonnen, T. Hydrophobic esterification of cellulose nanocrystals for epoxy reinforcement. *Polymer* **155**, 64–74 (2018).
136. Montanari, S., Roumani, M., Heux, L. & Vignon, M. R. Topochemistry of Carboxylated Cellulose Nanocrystals Resulting from TEMPO-Mediated Oxidation. *Macromolecules* **38**, 1665–1671 (2005).
137. Xu, Q., Li, W., Cheng, Z., Yang, G. & Qin, M. TEMPO/NaBr/NaClO-Mediated Surface Oxidation of Nanocrystalline Cellulose and Its Microparticulate Retention System with Cationic Polyacrylamide. *BioResources* **9**, 994–1006 (2013).
138. Morandi, G. & Thielemans, W. Synthesis of cellulose nanocrystals bearing photocleavable grafts by ATRP. *Polym. Chem.* **3**, 1402–1407 (2012).
139. Bideau, B., Bras, J., Saini, S., Daneault, C. & Loranger, E. Mechanical and antibacterial properties of a nanocellulose-polypyrrole multilayer composite. *Materials Science and Engineering: C* **69**, 977–984 (2016).
140. Missoum, K., Sadocco, P., Causio, J., Belgacem, M. N. & Bras, J. Antibacterial activity and biodegradability assessment of chemically grafted nanofibrillated cellulose. *Materials Science and Engineering: C* **45**, 477–483 (2014).
141. Wang, J. *et al.* Combining renewable gum rosin and lignin: Towards hydrophobic polymer composites by controlled polymerization. *Journal of Polymer Science Part A: Polymer Chemistry* **49**, 3728–3738 (2011).
142. Moustafa, H., El Kissi, N., Abou-Kandil, A. I., Abdel-Aziz, M. S. & Dufresne, A. PLA/PBAT Bionanocomposites with Antimicrobial Natural Rosin for Green Packaging. *ACS Appl. Mater. Interfaces* **9**, 20132–20141 (2017).
143. Liu, X. Q., Huang, W., Jiang, Y. H., Zhu, J. & Zhang, C. Z. Preparation of a bio-based epoxy with comparable properties to those of petroleum-based counterparts. *Express Polym. Lett.* **6**, 293–298 (2012).
144. Zheng, Y. *et al.* Well-Defined Renewable Polymers Derived from Gum Rosin. *Macromolecules* **43**, 5922–5924 (2010).
145. Arrieta, M. P., Samper, M. D., Jiménez-López, M., Aldas, M. & López, J. Combined effect of linseed oil and gum rosin as natural additives for PVC. *Industrial Crops and Products* **99**, 196–204 (2017).
146. Kale, S. N. & Deore, S. L. Emulsion Micro Emulsion and Nano Emulsion: A Review. *Systematic Reviews in Pharmacy* **8**, 39–47 (2016).
147. Fornaguera, C. *et al.* PLGA nanoparticles prepared by nano-emulsion templating using low-energy methods as efficient nanocarriers for drug delivery across the blood–brain barrier. *Journal of Controlled Release* **211**, 134–143 (2015).
148. Anton, N., Benoit, J.-P. & Saulnier, P. Design and production of nanoparticles formulated from nano-emulsion templates—A review. *Journal of Controlled Release* **128**, 185–199 (2008).
149. Niu, X., Liu, Y., Song, Y., Han, J. & Pan, H. Rosin modified cellulose nanofiber as a reinforcing and co-antimicrobial agents in polylactic acid /chitosan composite film for food packaging. *Carbohydrate Polymers* **183**, 102–109 (2018).
150. Jaiswal, M., Dudhe, R. & Sharma, P. K. Nanoemulsion: an advanced mode of drug delivery system. *3 Biotech* **5**, 123–127 (2015).

151. Xhanari, K., Syverud, K., Chinga-Carrasco, G., Paso, K. & Stenius, P. Reduction of water wettability of nanofibrillated cellulose by adsorption of cationic surfactants. *Cellulose* **18**, 257–270 (2011).
152. Dankovich, T. A. & Gray, D. G. Contact Angle Measurements on Smooth Nanocrystalline Cellulose (I) Thin Films. *Journal of Adhesion Science and Technology* **25**, 699–708 (2011).

CHAPTER III

PLA-based materials including designed nanostructures

Table of contents – Chapter III

Introduction to Chapter III	245
1. Elaboration of poly(lactic acid)-based nanocomposites including different designed cellulose nanostructures: comparison of the interfaces	247
1. Introduction	249
2. Materials and methods	252
2.1. Materials	252
2.2. SI-ATRP of glycidyl methacrylate on pre-functionalized CNCs	252
2.3. Surface esterification of CNCs with lauric acids	253
2.4. PLA-CNC nanocomposites preparation	253
2.5. Characterization methods	254
3. Results and discussions	257
3.1. Morphological analyses of PLA-based nanocomposites	257
3.2. Thermomechanical properties of PLA-based nanocomposites	263
3.3. Barrier properties of PLA-based nanocomposites	265
4. Conclusion	270
2. Two distinct methods for the elaboration of multi-layered materials based on poly(lactic acid) and active cellulosic nanostructures	271
1. Introduction	273
2. Materials and methods	276
2.1. Materials	276
2.2. Elaboration of multi-layered materials by the wet way	276
2.3. Elaboration of multi-layered materials by complexing	277
2.4. Characterization methods	277
3. Results and discussions	281
3.1. Coating of wet CNC suspension for the elaboration of PLA-based multi-layered materials	281
3.2. Multi-layered materials prepared by complexing	288
4. Conclusion	298
Conclusions of Chapter III	299
References - Chapter III	301

Introduction to Chapter III

As described in the **Chapter I**, surface modifications of CNCs are performed for two main reasons, in this PhD: (objective **2**) their compatibilization with a PLA-based matrix for the development of nanocomposites including CNCs as nanofillers, or (objective **3**) the preparation of final biobased materials (including both PLA and nanocelluloses) for food packaging applications. The global ANR project of this PhD is a collaborative project, and some of the results presented in the following **Chapter III** have been obtained after many collaborative exchanges between different partners (especially the partner AgroParisTech, INRA, in Massy, France).

The **Chapter III** is divided in two sections, each presenting the final PLA-based materials of this PhD project, prepared through different strategies. The **Figure III. 1** schematizes the organization of the **Chapter III**.

- The section **III.1** presents the results obtained from the preparation of PLA-based nanocomposites including the modified CNC-PGMA-Br and CNC-Lauric previously described in the sections II.1 and II.2.2 (Chapter II), respectively. The nanocomposites are performed by the solvent-casting method at the laboratory scale. The main goal of this section **III.1** is to compare the morphological behavior of the different nanocomposites, as well as, their barrier properties, in a spirit of food packaging applications. Moreover, this comparison aims to understand the role of each grafted moieties on the adhesion between the nanofillers and the matrix. The main difficulty encountered in this study (III.1) was the limited modified CNCs available for the sample's preparation, and therefore, the limited number of nanocomposites samples.

- In the section **III.2**, another strategy is adopted for the preparation of multi-phase materials. Indeed, in this part, multi-layered materials based on PLA are prepared. More precisely, a thin layer of modified CNC-1-M-3-PP (presented in Chapter II, section II.3) is coated on a PLA substrate, and another PLA sheet is heat-pressed on the coated materials, leading to a multi-layered material. Similarly, another protocol consists in the introduction in a modified CNF-Rosin or CNC-Rosin dried film (described in Chapter II, section II.4) between two PLA sheets, following by a similar heat-pressing step. The different "sandwich" PLA-nanocelluloses-PLA materials are compared in terms of processability, and barrier properties. This section **III.2** is therefore a proof of concept of the proposed multi-layered materials elaboration strategy.

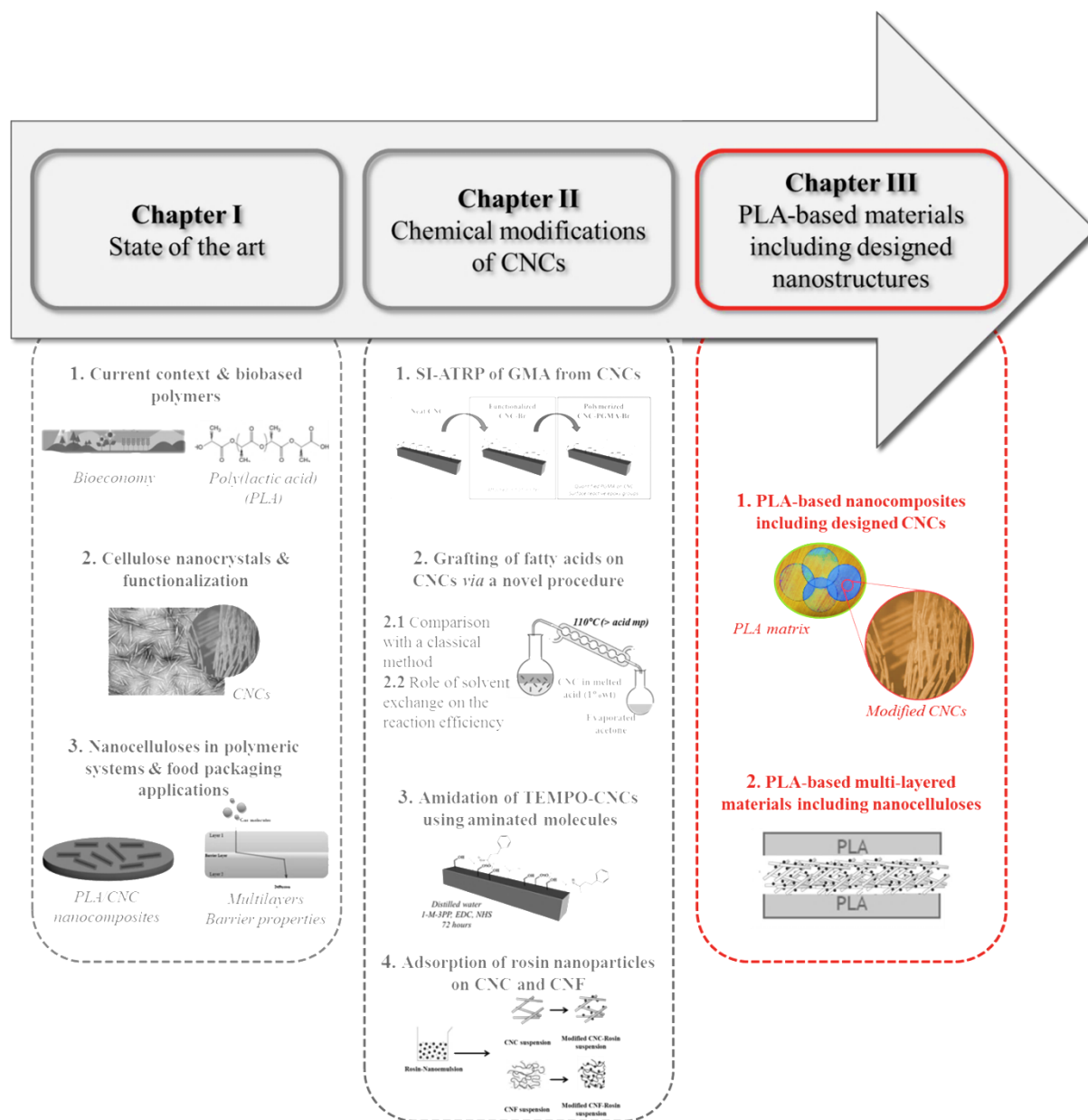
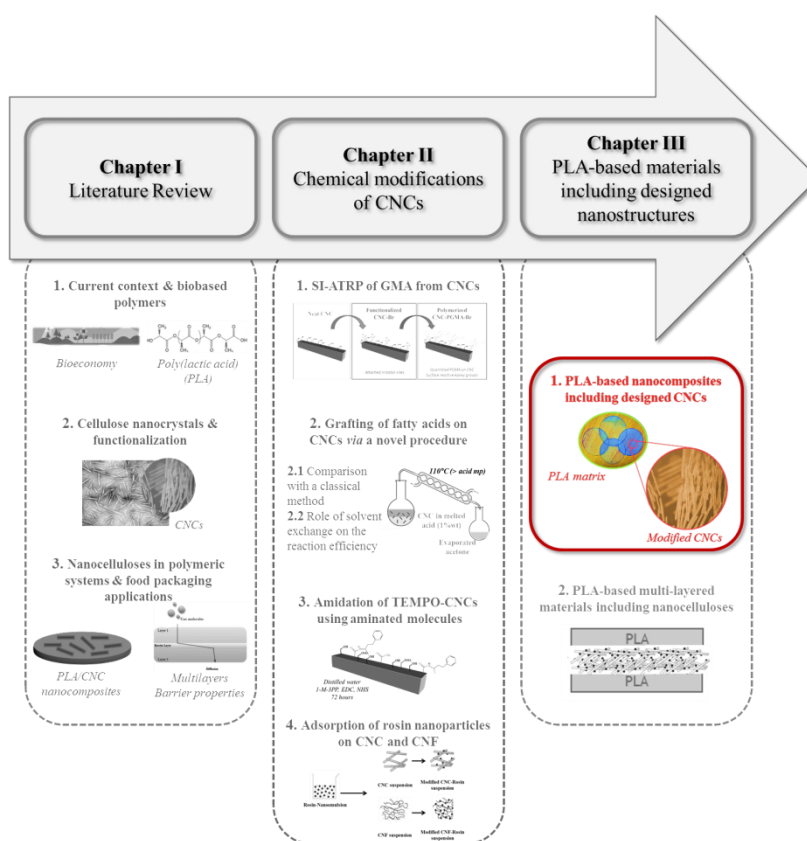


Figure III. 1. General organization of the PhD manuscript

1. Elaboration of poly(lactic acid)-based nanocomposites including different designed cellulose nanocrystals: comparison of the interfaces

This section is the result of a collaborative work with H. Faraj and S. Domenek (AgroParisTech, INRA, Massy, France). The nanocomposites samples were prepared by H. Faraj, and characterizations were performed by M. Le Gars and H. Faraj. This work will be subject of the writing of a common publication, after further characterization.



Abstract

Cellulose nanocrystals (CNC) were previously functionalized by different original methods, and both surface polymerized CNC with poly(glycidyl methacrylate) (PGMA) and surface esterified CNC with long fatty lauric acid, respectively named CNC-PGMA-Br and CNC-Lauric, were used in the present study. These two types of modified CNC were introduced in an amorphous poly(lactic acid) (PLA) matrix at different concentrations. Their dispersion in the PLA matrix has been observed by several microscopic methods like scanning electron microscopy (SEM), transmission electron microscopy (TEM), and optical microscopy under polarized light. After having assumed that both CNC modifications enhanced the interfacial effects between CNC and PLA, thermomechanical and barrier properties of nanocomposites have been investigated by dynamic mechanical analysis (DMA), differential scanning calorimetry (DSC), oxygen and water vapor permeability. After having shown the reinforcing effect of CNC-PGMA-Br in related PLA-based nanocomposites, the positive influence of CNCs modifications on oxygen permeability has been highlighted.

Keywords:

Cellulose Nanocrystals — Compatibilization — Poly(lactic acid) — Nanocomposites — Barrier properties

1. Introduction

In polymer composites science, the nanocomposites field has emerged since the late 1980s¹. Indeed, over the last few decades, the development of such promising multi-phase materials has attracted particular interest, in both academic and industrial research. The introduction of various nanofillers into polymeric systems – synthetic or not – has thus made it possible to achieve interesting properties, whether at the barrier, conductive or mechanical level. These nanofillers can then be of an inorganic or organic nature. In the literature, many complete reviews deal with the development of nanocomposites, such as those of Thostenson *et al.*² and Winey *et al.*³. Nanometric fillers (spheres, rods or plates) like among others carbon nanofibers, nanoclay or nano-TiO₂ have been widely used in nanocomposites in order to enhance strength and stiffness mechanical properties of initial polymeric materials, for various applications (packaging, automotive, paints, adhesives etc.).

However, current environmental context tends to limit the use of fossil-based synthetic plastics, and particularly for packaging applications. Thus, bio-based and biodegradable polymers have seen their interest increased significantly in recent years. Among these polymers, poly(lactic acid), known as PLA, has been at the centre of scientific discussions. Because of its bio-sourced and biodegradable nature, the PLA has long been chosen as a model for biobased plastic packaging. However, like many other bio-based polymers, this polymer exhibit poor barrier and thermal properties, although its mechanical properties are sufficient for most packaging applications. Indeed, PLA exhibit oxygen and water vapor permeability values respectively five and six times higher than traditionally used synthetic polyethylene terephthalate (PET)⁴⁻⁶, as well as, a low glass transition temperature (around 60 °C)⁴. The development of PLA-based – and more generally of bio-based polymers-based – nanocomposites then makes sense, and the elaboration of such materials makes it possible to comply with packaging – and especially food packaging – requirements. In the literature, numerous publications deal with the introduction of various fillers in PLA. Cabedo *et al.*⁷ have studied the introduction of modified kaolinite in a PLA/PCL (polycaprolactone) blend and concluded about the improvement of oxygen permeability of resulted nanocomposites. Thellen *et al.*⁸ investigated the presence of 5 wt% of montmorillonite layered silicate in PLA, and showed the increasing of resulted barrier properties. More recently, it was confirmed by Bouakaz *et al.*⁹ who studied the introduction of combined montmorillonite and graphene in PLA, and concluded about an improvement in both mechanical properties and water vapor permeability.

Nevertheless, although these nanofillers can enhance the properties of polymers, and especially those of PLA, their inorganic and non-biodegradable character is not consistent with current ecological trend and the use of fully biodegradable materials. In this way, the introduction of bio-based and biodegradable nanofillers in polymeric matrices, and especially nanometric cellulosic materials (cellulose nanofibrils CNFs and nanocrystals CNCs), has been widely studied in recent years. More

generally, the properties of nanocomposites rely on the interface between the nanofillers and the matrix, and thus on their compatibility. The presence of a well-dispersed nanofillers network in a polymeric matrix induces a tortuosity in gas molecules diffusive pathway, and thus an improvement of the gas barrier properties. It has been demonstrated that above a specific amount of nanofillers, the latter percolate and mechanically reinforce the system. Several studies provided theoretical modeling approaches of this percolation¹⁰. More broadly, the interface between the fillers and a matrix is the main element governing the final nanocomposites properties. This point is the main issue when working with nanocellulosic fillers, and especially with CNCs. Indeed, although the latter exhibit outstanding properties, like a high crystallinity and large specific surface area, their hydrophilic character remains the main issue for their compatibilization with generally hydrophobic polymeric matrices. According to the book of Dufresne¹⁰, it is crucial to promote CNC homogenous dispersion in the matrix and favorable interactions between the two phases, while ensuring interactions between the fillers themselves in order to allow the percolation network formation.

In order to ensure the dispersion of the CNC inside a hydrophobic matrix – especially the PLA – and to favour their interactions, a compatibilization step is generally required. Many research teams have worked on this point, and several literature reviews synthesize the elaboration of CNC/PLA-based nanocomposites^{11–13}, in which several routes are proposed for this compatibilization strategy. Most of the time, surface modification – specifically hydrophobization – of the CNCs is performed, although the polymeric PLA matrix can also be modified^{14,15}. The modification can be performed through surfactant adsorption^{16,17}, or by covalent grafting of single molecules^{18–23} or polymers, as previously summarized in the **Chapter I**. Focusing on the covalent grafting of single molecules, Robles *et al.*²¹ performed a similar protocol as that proposed by Freire *et al.*²⁴ to graft dodecanoyl chloride on the surface of the CNCs. After having prepared PLA-based nanocomposites by twin-screw extrusion, they highlighted an increase in both mechanical and thermal properties of the nanocomposites. Spinella *et al.*²³ have esterified CNCs with both lactic acid and acetic acid and produced PLA/CNC nanocomposites by melt-blending, and they also proved the increase in the mechanical properties. Focusing on the polymer grafting, the *Grafting-from* of lactic acid on the CNCs surface through ring-opening polymerization (ROP), as described by Habibi *et al.*²⁵ and more recently by Lizundia *et al.*²⁶ and Miao and Hamad²⁷. This strategy was highly efficient in terms of CNCs dispersion and barrier properties of produced CNC-PLA nanocomposites. For their part, Lin *et al.*²⁸ polymerized poly(ϵ -caprolactone) (PCL) chains on CNCs *via* a ROP microwave-assisted, and proved the enhancement in nanocomposites mechanical properties. Looking more precisely on the molecules grafted on the CNCs, those containing epoxy groups have been particularly appreciated. Pracella *et al.*¹⁴ have grafted glycidyl methacrylate (GMA) on cellulose nanofibers, and the enhancement of such modified fibers dispersion in the PLA has been highlighted.

In this study, on the one hand, the CNCs were surface modified with poly(glycidyl methacrylate) (PGMA) polymer chains containing such epoxy groups. This modification was performed through a SI-ATRP method previously described in the **Chapter II.1** of this manuscript, and CNC-PGMA-Br were recovered. On the second hand, the CNCs were surface grafted with long aliphatic lauric acid *via* a novel esterification procedure previously described in the **Chapter II.2.2**, and modified CNC-Lauric were recovered. Different amount of both CNC-PGMA-Br and CNC-Lauric were then introduced in PLA matrices by solvent casting method, in order to enhance barrier and/or thermomechanical properties of resulted nanocomposites. In the literature, it has already been proved that the presence of epoxy groups at the level of fillers could improve their compatibilization with a PLA matrix. Sun *et al.*²⁹ modified nanoparticles of acrylonitrile-butadiene-styrene (ABS) with GMA, and investigated the properties of PLA/ABS-GMA nanocomposites. According to the improved mechanical properties of the materials, they concluded about the probable cross-linking reaction between the epoxy groups from GMA on particles surface and carboxyl or hydroxyl groups at the end of the PLA polymeric chains. This cross-linking reaction was confirmed by Juntuek *et al.*³⁰ who used a copolymer composed of GMA as compatibilizing agent between poly(ethylene oxide) copolymers and PLA.

Therefore, in the present work, the compatibility between a PLA matrix and both epoxy-containing and long aliphatic chains-bearing CNCs was expected to be enhanced. In order to avoid the crystallisation of the polymer due to possible nucleating effect of CNCs, an amorphous PLA — composed of a high D-Lactic acid content — was selected for this study²². PLA_CNC-PGMA-Br and PLA_CNC-Lauric nanocomposites were then characterized by various microscopic characterization techniques (SEM, TEM, polarized light microscopy) and thermo-mechanical analyses (DMA and DSC). Moreover, in order to investigate the effect of the introduction of modified cellulosic nanofillers in the PLA matrix, oxygen and water vapor permeability was determined. These last characterizations were performed for food packaging applications purposes, for which these barrier properties aspects are particularly required.

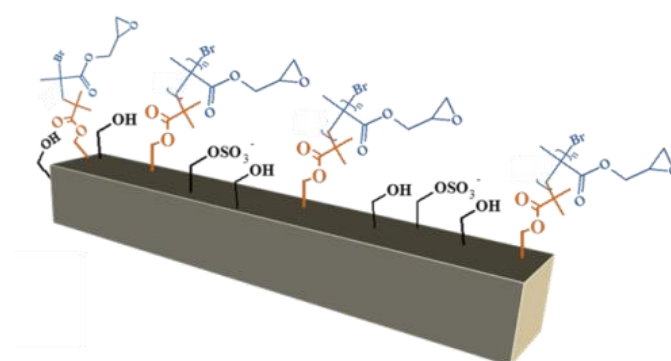
2. Materials and methods

2.1. Materials

Cellulose nanocrystals (CNCs) were supplied by CelluForce (Quebec, Canada), in spray-dried form. 4-(dimethylamino)pyridine (DMAP), triethylamine (TEA), α -bromoisobutyryl Bromide (BIB), ethyl α -bromoisobutyrate (EBIB), N,N,N',N'',N'''-pentamethyldiethylenetriamine (PMDETA) and Copper(I) bromide (CuBr) were purchased from Sigma-Aldrich Chimie (Saint-Quentin-Fallavier, France) and were used as received except CuBr which was purified. Glycidyl Methacrylate (GMA) was purchased from Fisher Scientific (France) and purified through a basic alumina column to remove stabilizers before use. N,N-Dimethylformamide (DMF) was purchased from Sigma-Aldrich Chimie and was stored and used in anhydrous conditions. Dichloromethane (DCM) and Ethanol (EtOH) were purchased from Sigma-Aldrich Chimie and used as received. Poly(lactic acid) INGENO pellets (4060D grade) were purchased from NatureWorks (France).

2.2. SI-ATRP of Glycidyl methacrylate on pre-functionalized CNCs

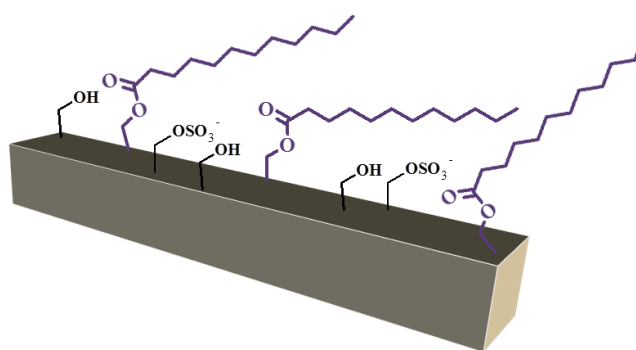
CNCs were modified by a surface-initiated radical polymerization (SI-ATRP) of glycidyl methacrylate (GMA), previously described in the **Chapter II.1**. Briefly, the CNCs were first modified with α -bromoisobutyryl bromide reagent (BIB), in order to introduce brominated initiator sites at their surface for further radical polymerization. Recovered CNC-Br were then subjected to several freeze-thaw cycles to remove oxygen, following by the SI-ATRP of GMA for one hour involving GMA/EBIB/PMDETA/CuBr reagents system with 100:1:1:1 composition ratio. At the end of the reaction, polymerized CNC-PGMA-Br were extensively washed by successive centrifugation cycles (9000 rpm, 15', 5 °C) in dichloromethane to remove all unreacted reagents and homopolymer PGMA polymerized from EBIB as sacrificial initiator. CNC-PGMA-Br were stored in dichloromethane until further use and characterizations. **Scheme III. 1** schematizes the recovered polymerized CNC-PGMA-Br.



Scheme III. 1. Schematic representation of polymerized CNC-PGMA-Br

2.3. Surface esterification of CNC with lauric acid

CNCs were modified according to the esterification procedure previously described in the **Chapter II.2.2**. Briefly, a CNC water suspension was solvent exchanged to acetone. This acetone suspension (1 wt%) was then introduced in a flask mounted with a distillation system, and heated at 110 °C. A catalytic amount of sulfuric acid H_2SO_4 , as well as, a large excess of lauric acid (weight ratio CNC: acid = 1: 100) were added to the reaction media. After total acetone evaporation, CNCs were dispersed in melted lauric acid, which thus acted as the reaction solvent, and the system was let under stirring for 8 h. At the end of the reaction, CNCs were extensively washed with ethanol by successive centrifugation cycles (10000 rpm, 25 °C, 15 min). The recovered modified CNC-Lauric in ethanol were then stored in a perfectly hermetically closed container until further use and characterizations. **Scheme III. 2** schematizes the recovered modified CNC-Lauric.



Scheme III. 2. Schematic representation of esterified CNC-Lauric

2.4. PLA-CNC nanocomposites preparation

First, a 10 wt% PLA solution was prepared by dissolving PLA pellets in dichloromethane under constant magnetic stirring overnight. Neat CNCs or polymerized CNC-PGMA-Br were solvent exchanged to dichloromethane, and introduced into the PLA solution. The mixture was then homogenized using an Ultra-Turrax homogenizer (IKA), following by an ultrasound treatment ($10 \text{ kJ.g}_{\text{CNC}}^{-1}$), and then poured into a Teflon petri dish. The latter was left to evaporate under a fume hood for 48 h. The recovered films were then hot pressed between two Teflon sheets with the use of a 150- μm -thick mould. Hot pressing was performed at 180 °C, first for 3 min without pressure, and then for 1 min under 150 bar pressure. After the compression, the samples were cooled down to room temperature. The films prepared with 10 wt% of neat CNCs, with 2 wt%, 5 wt% and 10 wt% of polymerized CNC-PGMA-Br, and with 5 wt% and 10 wt% of modified CNC-Lauric were respectively referenced as PLA_CNC10, PLA_CNC-PGMA-Br2, PLA_CNC-PGMA-Br5 and PLA_CNC-PGMA-Br10, and PLA_CNC-Lauric5 and PLA_CNC-Lauric10. Neat PLA reference was prepared following this protocol without any addition of CNCs.

2.5. Characterization methods

2.5.1. Scanning Electron Microscopy (SEM)

Samples cross-sections of PLA_CNC10, PLA_CNC-PGMA-Br10 and PLA_CNC-Lauric10 were prepared by cryofracture or at ambient temperature. Briefly, each sample was fractured in liquid nitrogen and was allowed to return at room temperature. Fractured samples of 3 nm thickness were then metallized with gold/palladium. On the other hand, 90 nm-thick sample cuts at room temperature were performed using an ultra-microtome UC6 (LEICA) equipped with a diamond knife, and were then metallized as previously described. For each sample, both cuts obtained by cryofracture or with the microtome at ambient temperature were analyzed using a Quanta 250 FEG (Thermofischer) device at a 2.5 kV voltage in high vacuum mode. Images were processed using ImageJ software.

2.5.2. Transmission Electron Microscopy (TEM)

Sample cuts of PLA_CNC10, PLA_CNC-PGMA-Br10 and PLA_CNC-Lauric10 were prepared at room temperature, using an ultra-microtome UC6 (LEICA) equipped with a diamond knife, and exhibit thicknesses of 90 nm. The cuts were then deposited on a copper grid covered with a carbon film and observed with a JEOL JEM 2100-Plus transmission electron microscope operating at an acceleration voltage of 200 kV. Images were recorded using a Gatan Rio 16 digital camera and were then processed using ImageJ software.

2.5.3. Polarized Light Microscopy

The surfaces of both PLA_CNC10 and PLA_CNC-PGMA-Br10 nanocomposites casted films were analyzed using an Axioplan 2 (ZEISS) microscope, operating under polarized light. Recorded images were processed using ImageJ software.

2.5.4. Dynamic Mechanical Analysis (DMA)

DMA analyses were performed on neat PLA, PLA_neatCNC10 and PLA_CNC-PGMA-Br nanocomposites casted films using a TA Instrument RSA 3 device. Samples of 10 mm length and 5 mm width were carefully prepared and analyses were performed from 30 °C to 120 °C at 1 Hz with a heating rate equal to 2 °C per minute. Data were recorded and processed using a TA Orchestra software. As far as possible (limited number of samples), each analysis was duplicated or triplicated and the most representative curve was plotted.

2.5.5. Differential Scanning Calorimetry (DSC)

DSC analyses were carried out with a MT-DSC Q1000 (TA Instruments) device. Samples of neat PLA and PLA_CNC-PGMA-Br were deposited in hermetically closed aluminum pans. Heating rate was set at 2 °C per minute and analyses were performed from -20 °C to 260 °C under nitrogen flow (50 mL

per minute). Around 5 mg of each sample was weighted, and each mass was exactly determined at the beginning of each analysis. TA Universal Analysis software was used to process data. For each sample, measurement was at least duplicated.

2.5.6. Oxygen Permeability

The oxygen permeability of neat PLA and PLA_CNC-PGMA-Br nanocomposites cased films was investigated at 23 °C and 0% RH, using a Systech Illinois (USA) M8001 Oxygen Permeation Analyzer. Data were processed according to the ASTM-F 1927 standard. For each sample, masks with a specific exchange surface of 1.5 cm² were prepared and placed in the device chamber. Pure oxygen was used for the measure. The final value of oxygen transmission rate (OTR) was determined at the level of the reached plateau of the curve. The oxygen permeability coefficient (OP) was obtained according to the **Equation III. 1**, where l is the average thickness of the sample, in mm.

$$OP = OTR \times l$$

Equation III. 1. General relation between oxygen permeability coefficient (OP) and oxygen transmission rate (OTR) according to ASTM-F 1927 standard

Another sample of neat PLA, as well as PLA_CNC-Lauric samples, were analyzed using a GDP-C device from Brugger (Germany). Samples were outgassed under vacuum for 15 h, and then an oxygen pressure gradient was applied at 1 bar, 0% RH and 23 °C. Control samples were used to ensure measurement accuracy among different devices. All experiments should be at least duplicated as much as possible (limited number of samples).

2.5.7. Water Vapor Permeability

The water vapor permeability of both neat PLA and PLA_CNC nanocomposites cased films was determined at 23 °C and 50% RH, according to T 448 om-09 TAPPI standard. For each sample, masks with a specific exchange surface of 1.5 cm² were prepared, and installed on specific test dishes filled with dried CaCl₂ as desiccant material. Regular weighing of the whole system was performed, and the water vapor transmission rate (WVTR), in g/m².day, was determined following the **Equation III. 2** :

$$WVTR = \frac{24x}{Ay}$$

Equation III. 2. General equation for the calculation of the water vapor transmission rate (WVTR) according to T 448 om-09 TAPPI standard

where x is the gain in grams for the period y in hours, and A the exposed area of the sample (1.5 cm² in our study). The water vapor permeability coefficient (WVP) was determined according to the **Equation III. 3**, where l is the average thickness of the sample, in mm.

$$WVP = WVTR \times l$$

Equation III. 3. General relation between water vapor permeability coefficient (WVP) and water vapor transmission rate ($WVTR$)

Elaboration of poly(lactic acid)-based nanocomposites including different designed cellulose nanocrystals: comparison of the interfaces

Taking into consideration the heterogeneity of the samples, each experiment should be at least duplicated as much as possible (limited number of samples).

3. Results and discussions

3.1. Morphological analyses of PLA-based nanocomposites

In this study, bio-based PLA has been selected as the host matrix for the elaboration of CNC/PLA-based nanocomposites. The surface-polymerized CNC-PGMA-Br were previously characterized in the **Chapter II.1**, and it was proved that their surface was covered with PGMA polymeric chains containing reactive epoxy functions. Although several methods exist to process CNC/PLA-based nanocomposites, as described in the literature review (**Chapter I**), the solvent casting method was selected in this study because of its lab-scale size and its adaptability to low amounts of material, as was the case for prepared CNC-PGMA-Br. Indeed, as presented in the **Chapter II.1**, only few grams of CNC-PGMA-Br were produced, limiting the quantity of produced nanocomposites films. Besides, even if the CNC_Lauric were produced at a larger scale (**Chapter II.2**), PLA_CNC-Lauric were also produced by the solvent casting method, in order to be able to compare their final properties. However, it is important to keep in mind that morphological properties can vary with the processing materials method, especially on a larger scale. These differences in the properties can result, for example, from the nanofillers orientation inducing by the process, or by the drying conditions. In their work, Yang *et al.*³¹ showed the differences in terms of mechanical properties of PLA-based nanocomposites prepared with lignin nanoparticles by both extrusion and solvent casting methods. In fact, they observed poor nanoparticles dispersion in PLA by solvent casting, whereas extruded nanocomposites samples exhibited a better fillers dispersion and adhesion, leading to better mechanical properties. Fortunati *et al.*³² confirmed these results, and observed better fillers dispersion in the nanocomposites prepared by extrusion, leading to a positive change in their elongation at break. A review of Oksman *et al.*³³ synthesizes and details the different cellulose/PLA-based nanocomposites processing techniques.

The **Figure III. 2 a)** shows a photograph of a neat PLA casted film of 155 μm thickness, as presented in the **Table III. 1**. The neat PLA film is highly transparent and homogenous, as expected, according to the literature³⁴. In fact, the transmittance of a PLA film is generally comprised around 95% at 700 nm wavelength³⁵, confirming its huge interest for food packaging applications.



Figure III. 2. Photographs of a) neat PLA casted film, b) PLA_neatCNC10 nanocomposite, PLA_CNC-PGMA-Br nanocomposites with c) 2 wt%, d) 5 wt%, and e) 10 wt% of polymerized CNC-PGMA-Br, and PLA_CNC-Lauric nanocomposites with f) 5 wt% and g) 10 wt% of modified CNC-Lauric

In the **Figure III. 2 b)**, the transparency of 153 μm -thick nanocomposite film prepared with 10 wt% of unmodified neat CNC decreased, and this opacity can be attributed to the presence of large CNCs aggregates in the matrix, resulted from the poor compatibility between neat hydrophilic CNCs and hydrophobic PLA. Such a transparency reduction has been already observed several times in the literature^{22,36} and is related to the presence of non-dispersed micrometric materials. In **Figure III. 2 c)**, **d)** and **e)**, it is clearly observed that by increasing filler content of CNC-PGMA-Br from 2 wt% to 10 wt%, the films coloration changed from light green to darker green. This color was attributed to the presence of copper salts residues from the SI-ATRP polymerization of GMA on CNC surface. However, the homogeneity of PLA_CNC-PGMA-Br nanocomposites films could be clearly confirmed from these photographs, as well as, their preserved transparency, suggesting a good dispersion of the cellulosic fillers inside the matrix. Moreover, relatively homogenous thicknesses were comprised between 120 and 130 μm (**Table III. 1**) and were ensured thanks to the use of normalized metal spacers during films heat-pressing. Note that this compression step is essential for the removal of residual solvent, as well as, for the erasing of the thermal history of each nanocomposite films, which was critical for further thermo-mechanical analyses of the materials. Nevertheless, the coloration of PLA_CNC-PGMA-Br films would be a major disadvantage for packaging applications, where perfect colorless transparency is a key requirement, especially with regard to consumers opinion^{37,38}.

The photographs of both PLA_CNC-Lauric5 and PLA_CNC-Lauric10 are presented in **Figure III. 2 f)** and **g)**, respectively. Both samples show a good transparency and any coloration, confirming also the well dispersion of modified CNC-Lauric in the PLA matrix. **Table III. 1** summarizes the thicknesses measured for each sample.

Ref	Sample	Thickness (μm)
a)	Neat PLA	155
b)	PLA_neatCNC10	153
c)	PLA_CNC-PGMA-Br2	130
d)	PLA_CNC-PGMA-Br5	130
e)	PLA_CNC-PGMA-Br10	120
f)	PLA_CNC-Lauric5	182
g)	PLA_CNC-Lauric10	230

Table III. 1. Measured thicknesses for each nanocomposite

In order to investigate the morphological behavior of PLA-based nanocomposites in more details, SEM analyses were performed on PLA_neatCNC10, PLA_CNC-PGMA-Br10 and PLA_CNC-Lauric10 samples. **Figure III. 3** shows SEM images of PLA_neatCNC10 cross-sections prepared at ambient temperature (**Figure III. 3 a**) and **b**) or by cryofracture (**Figure III. 3 c**) and **d**). In **Figure III. 3 a**) and **b**), large micrometric aggregates are clearly visible. These aggregates exhibit apparent size equal to $11 \mu\text{m} \pm 8 \mu\text{m}$, clearly confirming their micrometric size, as well as, their heterogeneous character. Moreover, regarding the repartition of these aggregates inside the PLA matrix, their sedimentation is observed, and is probably due to the deposition of the large and dense cellulosic aggregates at the bottom of the dish during solvent casting process. By regarding **Figure III. 3 c**) and **d**), the cryofractured CNC_neatPLA10 sample highlights the presence of very distinguishable large aggregates, as well as, the poor adhesion between cellulosic materials and the PLA matrix. Indeed, the interface between PLA and the aggregates exhibits any adhesion, and several cavities can be observed, resulting from remnants of removed aggregates during the cryofracture process. It demonstrates the lack of adhesion between micrometric fillers and the polymeric matrix. Similar expected SEM observations of PLA/unmodified CNC have been already shown in literature^{17,22,39}.

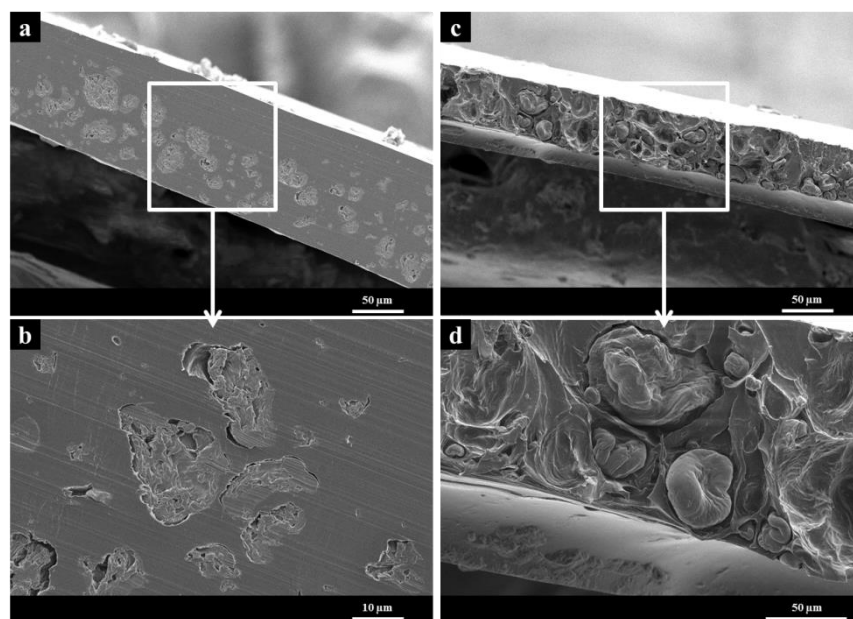


Figure III. 3. SEM images of PLA-neatCNC10 cross-sections prepared **a**), **b**) at ambient temperature, and **c**), **d**) by cryofracture at different magnifications

Figure III. 4 a) and b) represent SEM images of PLA-based nanocomposites prepared with 10 wt% of polymerized CNC-PGMA-Br, whose cross-sections were prepared at ambient temperature. A more homogenous surface is observed compared to that PLA_neatCNC10 sample, since no micrometric aggregates are visible. Moreover, the cryofractured sample (**Figure III. 4 c) and d)** also exhibits a homogeneous cross-section, as no micrometric particles or cavities are visible. This result emphasizes the enhancement of the fillers dispersion inside the matrix, and thus the improvement of the adhesion between the cellulosic nanofillers CNC-PGMA-Br and the PLA matrix. Such similar behavior between epoxy groups present on fillers and a PLA matrix has already been described in literature. In fact, Wang *et al.*⁴⁰ introduced an epoxidized natural rubber in a PLA matrix, and concluded about a possible cross-linking reaction between the epoxy functional groups and the end-chains of PLA, as well as, about the enhanced adhesion between rubber and PLA. Highly comparable SEM images were presented in their study.

Similar observations were made from cryofractured cross-sections of the PLA_CNC-Lauric10 sample presented in **Figure III. 4 e) and f)**. In fact, no micrometric aggregates are distinguished, and a similar smooth surface as in the case of PLA_CNC-PGMA-Br10 is observed. In **Figure III. 4 f)**, some spherical particles are observed and, although their interpretation is difficult, they probably result from residual unreacted lauric acid. However, cryofractured PLA_CNC-Lauric10 confirms the enhanced compatibilization between the modified CNC-Lauric and the PLA matrix.

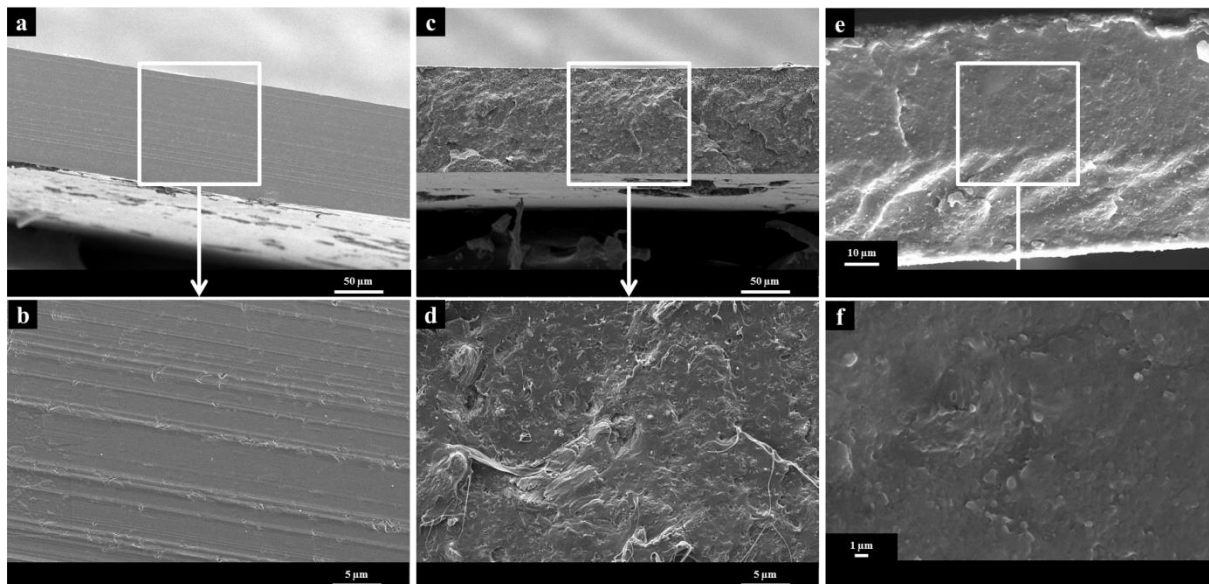


Figure III. 4. SEM images of nanocomposites cross-sections of PLA_CNC-PGMA-Br prepared **a), b)** at ambient temperature and **c), d)** by cryofracture; and **e), f)** of PLA_CNC-Lauric10 prepared by cryofracture at different magnifications

In a recent publication, Rigotti *et al.*⁴¹ modified CNCs with lauryl chloride (same carbon chains as lauric acid used in our study) *via* a classical acylation procedure (i.e., anhydrous conditions, organic toxic solvents) and introduced the recovered modified CNCs in a PLA matrix *via* a solvent casting

method. They observed micrometric aggregates at fillers concentration higher than 6.5 wt%, resulting in the observation of large pores on the nanocomposites SEM images. This difference is probably due to the grafting, which was possibly less homogenous or less dense at the surface of their CNCs. However, numerous studies have presented results correlated with our SEM images. For example, Dong *et al.*⁴² modified CNC with acetic anhydride and Shojaeiarani *et al.*⁴³ and Espino-Pérez *et al.*²² esterified the CNCs with benzoic and hydrocinnamic acid, respectively, and in both cases, similar PLA-based nanocomposites cross-sections were observed. Both PLA_CNC-PGMA-Br10 and PLA_CNC-Lauric10 samples exhibit more homogenous cryofractured surfaces than that of PLA_neatCNC10 sample, clearly confirming that the interfaces between CNC-PGMA-Br or CNC-Lauric and PLA were therefore improved.

In order to observe the samples cross-sections on a smaller scale, TEM observations were performed on PLA_neatCNC10 (**Figure III. 5 a**), PLA_CNC-PGMA-Br10 (**Figure III. 5 b**) and PLA_CNC-Lauric10 (**Figure III. 5 c**). The PLA_neatCNC10 TEM picture presented in **Figure III. 5 a** confirms the previous SEM observations, since large micrometric aggregates ($15 \mu\text{m} \pm 4 \mu\text{m}$) are clearly visible. Bagheriasl *et al.*⁴⁴ prepared PLA_neatCNC nanocomposites (with 4 wt% of nanofillers) by solvent casting, and observed similar large micrometric aggregates on TEM images, although their nanocomposites preparation method seemed to be more efficient since aggregates were in the range of 1-3 μm . These differences can result from the nanocomposites processing method, or from the CNCs source and preparation. In **Figure III. 5 b**), CNC-PGMA-Br are more dispersed in the matrix than the neat CNCs, although some CNC clusters are clearly observed, with heterogeneous nanometric size. It emphasizes the improved dispersion of CNC-PGMA-Br due to the presence of PGMA polymer at the CNCs surface, although nanometric aggregates are still present.

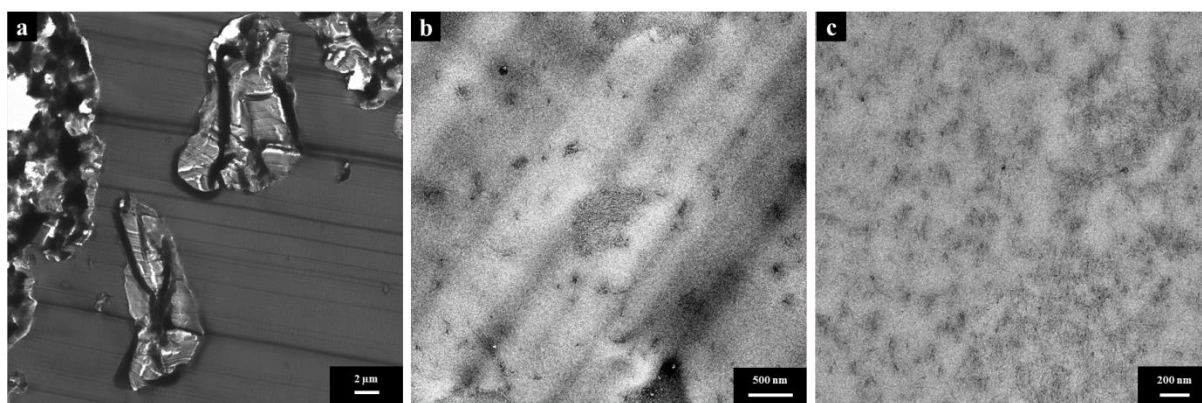


Figure III. 5. TEM images of nanocomposites cross-sections prepared at ambient temperature: **a)** PLA_neatCNC10, **b)** PLA_CNC-PGMA-Br10, and **c)** PLA_CNC-Lauric10

In **Figure III. 5 c**), CNC-Lauric seem to be more dispersed in the PLA matrix. Even if CNC-Lauric clusters are observed, they are smaller and more homogeneously distributed throughout the matrix than those of CNC-PGMA-Br. It highlights the enhanced compatibilization of CNC-Lauric with the PLA

matrix, similarly to CNC-PGMA-Br. Espino-Pérez *et al.*²² obtained close results after having similarly made CNC hydrophobic with hydrocinnamic acid and introduced them in a PLA matrix.

Another way to investigate the dispersion state of crystalline anisotropic CNCs inside an amorphous PLA matrix was the observation of nanocomposites surface by optical microscopy under polarized light. Briefly, as explained by Xu *et al.*⁴⁵, the polarized light can pass through the nanocomposite sample, and observed birefringent zones thus correspond to the presence of CNC particle or aggregates perpendicularly to the light path. Although this observation method does not provide precision at the nano-scale, it makes it possible to conclude whether or not micrometric CNC aggregates are present in the sample. Only PLA_neatCNC10 and PLA_CNC-PGMA-Br10 nanocomposites were observed under polarized light in this study, as presented in **Figure III. 6**.

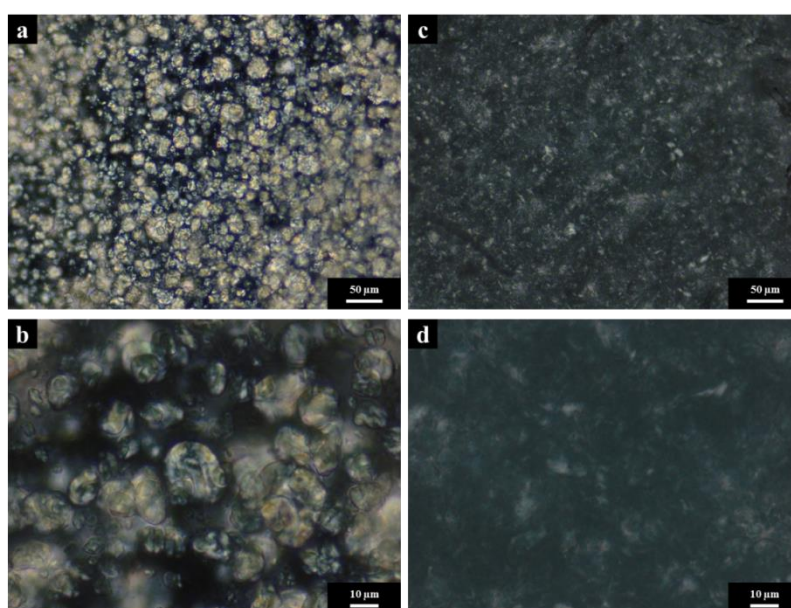


Figure III. 6. Images of a), b) PLA_neatCNC10 and c), d) PLA_CNC-PGMA-Br10 obtained from optical microscope with polarized light at different magnifications

In **Figure III. 6 a)** and **b)**, large micrometric aggregates ($12 \mu\text{m} \pm 4 \mu\text{m}$) are visible on PLA_neatCNC10 sample, correlated with previously SEM results. In the literature, it is confirmed by Xu *et al.*⁴⁵ who introduced CNC in an epoxy resin, and observed similar aggregation under polarized light. Kaboorani *et al.*⁴⁶ also performed microscopy analyses under polarized light in order to detect CNC aggregates in a wood coating system. In **Figure III. 6 c)** and **d)**, no large particles are visible, suggesting that CNC-PGMA-Br were more isolated and no clustered at micrometric scale, confirming the previous results obtained by SEM and TEM observations. Similar observations performed on PLA_CNC-Lauric10 would be interesting, in order to be able to compare the dispersion state and the clusters size of CNC-Lauric with that of CNC-PGMA-Br.

3.2. Thermomechanical properties of PLA-based nanocomposites

In order to investigate the potential reinforcing effect of nanofillers in a polymeric matrix, the DMA analysis is generally carried out on the nanocomposites samples. In our study, DMA tests were performed on neat PLA, PLA_neatCNC10 and PLA_CNC-PGMA-Br10 nanocomposites. The resulting evolution of the storage modulus E' and the mechanical loss factor $\tan \delta$ function of the temperature is presented in **Figure III. 7 a)** and **b,)** respectively. In **Figure III. 7 a)**, the typical response of a neat amorphous PLA is visible (curve in solid dark line), and it is observed that above the alpha relaxation temperature associated to the glass transition temperature (T_g), the storage modulus of the polymer clearly decreases, and PLA becomes softer. A similar behavior is observed for all PLA_CNC-PGMA-Br samples, where crystallization in the rubbery plateau is absent. This behavior was expected and consistent with the results presented in the literature⁴⁷. The curves were normalized in the glassy plateau at 30 °C, as proposed in the literature by Espino-Pérez *et al.*²² and Azizi Samir *et al.*⁴⁸. This normalization allows the comparison of the different storage modulus values in the rubbery plateau ($E'_{70\text{ °C}}$). The values of $E'_{70\text{ °C}}$ for each sample are presented in **Table III. 2**. For the neat PLA, $E'_{70\text{ °C}}$ is equal to 1.8 MPa, correlating with the values found in the literature for an amorphous PLA film⁴⁹. This modulus is equal to 2.1 MPa after the addition of 10 wt% of unmodified CNC. Thus, no significant difference between the $E'_{70\text{ °C}}$ is observed, confirming the fact that unmodified CNC do not provide significant mechanical reinforcement to the nanocomposite material, probably because of their poor dispersion and their lack of adhesion with the PLA matrix.

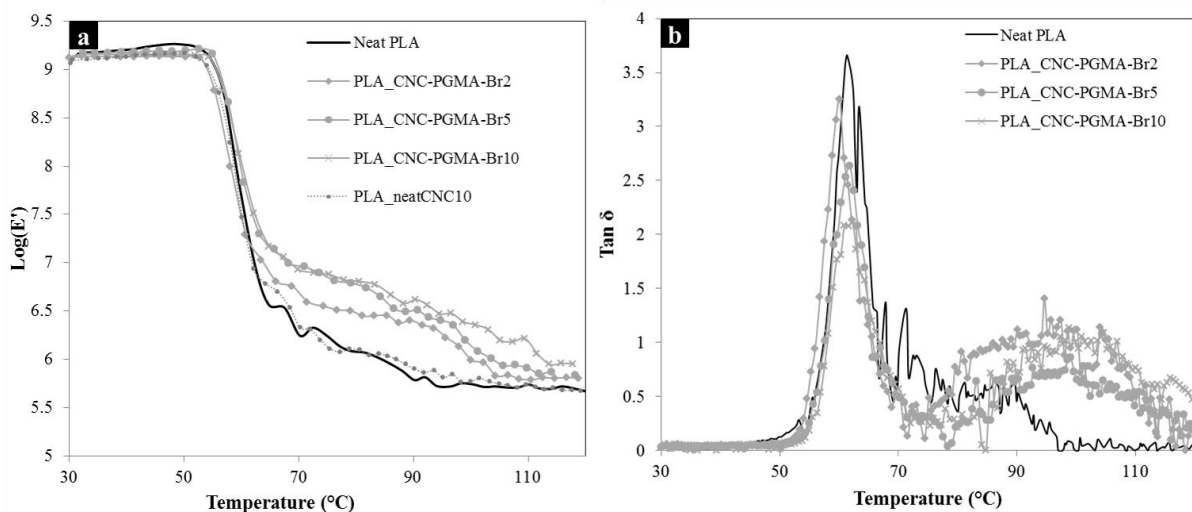


Figure III. 7. a) Storage tensile modulus (E') function of the temperature, and **b)** $\tan \delta$ function of the temperature for neat PLA, PLA_neatCNC10 and PLA_CNC-PGMA-Br samples obtained from DMA analyses

However, by increasing the amount of CNC-PGMA-Br in the PLA matrix from 2 wt% to 10 wt%, the value of $E'_{70\text{ °C}}$ significantly increased from 3.8 MPa to 9.5 MPa. According to Sullivan *et al.*³⁹, this increasing in storage modulus— attributed to the decreasing of polymeric chains mobility - can be related to the tightening of polymeric chains displacements and to the reinforcing effects of CNC-

PGMA-Br at a temperature higher than the T_g of the material. The presence of a percolated network of CNCs in the matrix could also be discussed, as presented by numerous authors^{10,17,50,51}. Moreover, in **Figure III. 7 b)**, it is observed that the values of the mechanical loss factor $\tan \delta$ decreased by increasing the amount of fillers, which is expected since there is less PLA that can relax.

In order to determine the glass transition temperatures T_g of neat PLA, PLA_CNC-PGMA-Br and PLA_CNC-Lauric nanocomposites samples, DSC analyses were performed. Note that a heat-pressing step was performed on each sample in same conditions before the analyses, in order to get rid of thermal history of the materials. Due to the amorphous grade of PLA, only the glass transition was analyzed in this study. T_g values are presented in **Table III. 2**.

Sample	$E'_{70\text{ °C}}$ (MPa)	Tan δ	T_g (°C) _{DSC}
Neat PLA	1.8	3.7	54.9
PLA_neatCNC10	2.1	3.5	/
PLA_CNC-PGMA-Br2	3.8	3.3	53.5
PLA_CNC-PGMA-Br5	6.7	2.6	51.6
PLA_CNC-PGMA-Br10	9.5	2.2	50.7
PLA_CNC-Lauric5	/	/	54.6
PLA_CNC-Lauric10	/	/	54.9

Table III. 2. Storage modulus E' in rubbery region at 70 °C and intensity of the $\tan \delta$ peak obtained from DMA results and glass transition temperature T_g obtained from DSC analyses for both neat PLA, PLA_neatCNC10, PLA_CNC-PGMA-Br and PLA_CNC-Lauric samples

In the case of PLA_CNC-PGMA-Br samples, the T_g decreased by increasing the amount of nanofillers in the PLA matrix. Moreover, the T_g measured for PLA_CNC-Lauric5 and PLA_CNC-Lauric10 samples do not show any significant change. This result has already been shown in the literature by, among others, Fortunati *et al.*^{35,52}, who explained it by the good adhesion between the CNCs and the polymeric matrix. Moreover, both low molecular residues plasticizing the PLA from CNC-PGMA-Br and CNC-Lauric surfaces are different, which could explain the different values of T_g obtained for nanocomposites prepared with same amount of CNCs.

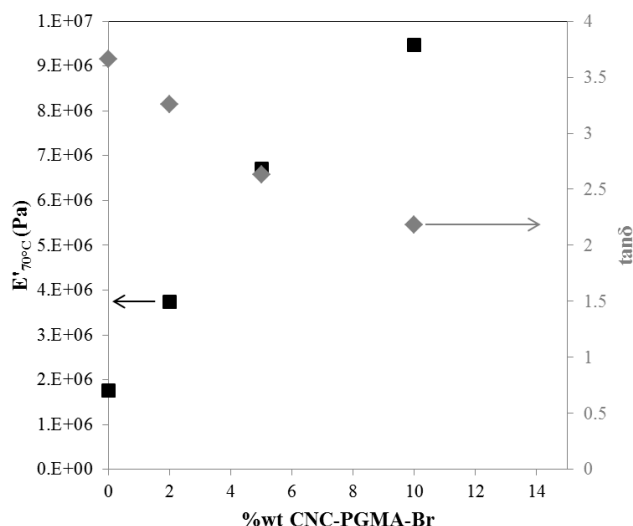


Figure III. 8. Evolution of the storage modulus (E') at 70 °C and the $\tan \delta$ value function of the weight fraction (wt%) of CNC-PGMA-Br from DMA analyses

Figure III. 8 graphically represents the values of $E'_{70^{\circ}\text{C}}$ and $\tan \delta$ (expressed in the **Table III. 2**) for neat PLA and PLA_CNC-PGMA-Br, function of the filler content, in wt%. According to the previous discussion and **Figure III. 8**, it is possible to do the assumption that PLA_CNC-PGMA-Br10 sample is the best candidate in term of thermo-mechanical properties, although its T_g slightly decreased compared to the neat PLA casted film. Moreover, even if DMA analyses have not been performed on PLA_CNC-Lauric sample, it would be interesting to compare their thermomechanical response, in order to be able to conclude about the different CNCs filler content influence, since first thermomechanical properties are encouraging. Indeed, thermomechanical nanocomposites properties are essential, especially when thinking about packaging applications, since they allow being aware of the mechanical behavior of a nanocomposite material in a specific range of temperatures.

3.3. Barrier properties of PLA-based nanocomposites

Besides the thermomechanical properties of the nanocomposites, their barrier properties are key points for their application as food packaging. Indeed, as previously mentioned in the **Chapter I**, the permeability towards oxygen and water vapor are main elements responsible for food products deterioration. In order to investigate this point, oxygen permeability measures were performed on neat PLA, PLA_neatCNC, PLA_CNC-PGMA-Br and PLA_CNC-Lauric nanocomposites, in order to understand the effect of the various CNC fillers and content. **Table III. 3** summarizes the values of oxygen permeability (in $\text{m}^3.\text{m}/\text{m}^2.\text{s}.\text{Pa}$) and water vapor permeability (in $\text{kg}.\text{m}/\text{m}^2.\text{s}.\text{Pa}$). Oxygen permeability of neat PLA is consistent with the values found in the literature^{4,53}, and the P/P_0 ratio has been calculated for each sample, in order to clearly understand the effect of each nanofillers on the nanocomposites.

Sample	Oxygen permeability (x10 ¹⁸) (m ³ .m/m ² .s.Pa) (23 °C, 0% RH)		P/P ₀	Water vapor permeability (x10 ¹⁴) (kg.m/m ² .s.Pa) (23 °C, 50% RH)	
	Mean value	Std. Dev.		Mean value	Std. Dev.
Neat PLA	5.60	1.0	1	1.8	0.02
PLA_CNC-PGMA-Br2	5.10	1.2	0.91	1.1	0.15
PLA_CNC-PGMA-Br5	5.13	/	0.92	0.9	/
PLA_CNC-PGMA-Br10	3.25	/	0.58	0.4	/
Neat PLA (2)	2.47	/	1	/	/
PLA_CNC-Lauric5	2.28	0.09	0.92	/	/
PLA_CNC-Lauric10	2.24	0.1	0.91	/	/
PLA_neatCNC10	2.81	0.22	1.14	/	/

Table III. 3. Summarized oxygen permeability and water vapor permeability values for both neat PLA, PLA_CNC-PGMA-Br, PLA_CNC-Lauric and PLA_neatCNC nanocomposites

Regarding the results presented in the **Table III. 3** for neat PLA and PLA_CNC-PGMA-Br, it can be observed that the values of oxygen permeability of PLA_CNC-PGMA-Br decreased by increasing the nanofillers content from 2 wt% to 10 wt%. This decrease is hardly significant for low nanofillers contents (2 wt% and 5 wt%) but it could be confirmed for the PLA_CNC-PGMA-Br10 sample. Furthermore, the value obtained for the neat PLA as reference ($5.6 \pm 1 \text{ m}^3.\text{m}/\text{m}^2.\text{s}.\text{Pa}$) is very high compared to the values found in the literature, and interpretations taking this value into account must therefore be treated with caution. In **Figure III. 9 a)**, the P/P₀ ratio was plotted function of the CNC-PGMA-Br volumetric fraction (%vol). In the literature, several models have been proposed to predict the gas molecules permeability through a multiphasic polymer system, as recently synthesized in the review of Zid *et al.*⁵⁴. Among numerous models, that of Nielsen⁵⁵ was used in this study for PLA/CNC systems. This model is expressed as follows:

$$\frac{P}{P_0} = \frac{1 - \phi}{1 + \left(\frac{L}{2D}\right) \times \phi}$$

Equation III. 4. Calculation P/P₀ ratio according to Nielsen model^{55,56}

where ϕ is the volumetric fraction of nanofillers in the polymeric matrix and, L and D are respectively the average length and diameter of nanofillers. It is important to mention that this model considers the presence of ribbons nanofillers, which may not be the most suitable model for nanocomposites (for example, Maxwell's model for spherical particles could have been chosen). This inadequacy in the model could explain the difficult following interpretations. The **Equation III. 4** was used to plot the predicted oxygen permeability evolution function of the CNC-PGMA-Br (taking $L=600 \text{ nm}$ and $D=50$

nm for CNC-PGMA-Br, according to previous results presented in **Chapter II.1**) and of the neat CNCs (taking $L=110$ nm and $D=4$ nm for neat CNC) volumetric contents. In **Figure III. 9 a**), it is observed that P/P_0 ratios of PLA_CNC-PGMA-Br samples decreased by increasing the amount of CNC-PGMA-Br. Moreover, the results are relatively close to the Nielsen model plotted for CNC-PGMA-Br as fillers (grey solid line), whereas the P/P_0 ratio is far from the predicted model for unmodified CNCs (dashed line). It emphasizes the poor and heterogeneous dispersion of the unmodified CNCs in the matrix compared to that of CNC-PGMA-Br, inducing a positive effect on the oxygen barrier. It is thus possible to assume that the CNC-PGMA-Br network induces a tortuous pathway of oxygen gas molecules through the nanocomposites, and that this effect is reinforced at high CNC-PGMA-Br content (10 wt%). This notion of tortuosity has been widely used in the nanocomposites research field^{51,57,58}.

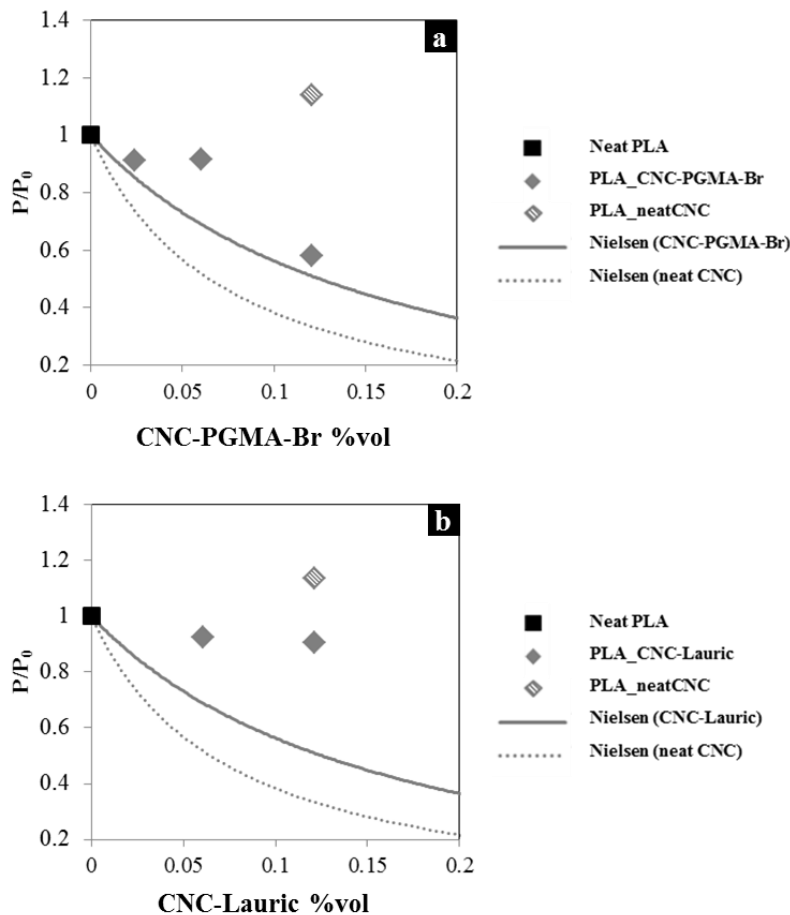


Figure III. 9. Evolution of the oxygen permeability P of PLA-based nanocomposites function of the a) CNC-PGMA-Br and b) CNC-Lauric volume fraction

By regarding the PLA_CNC-Lauric oxygen permeability results (taking into account “neat PLA (2)” sample as a new reference), the influence of the CNC-Lauric is not significant, contrary to that of the CNC-PGMA-Br. In fact, the P/P_0 ratio only shows a slight decrease, smaller than experimental uncertainty. In **Figure III. 9 b**), the values of P/P_0 ratios are far above the predicted Nielsen model (taking $L=350$ nm and $D=30$ nm for CNC-Lauric, according to the previous results presented in the

Chapter II.2.2). This behavior was surprising, taking into consideration the well dispersion of the CNC-Lauric in the PLA matrix previously discussed. However, these results are consistent with the values found in literature. Indeed, in their publication, Espino-Pérez *et al.*²² concluded about the slight effect of the well dispersed CNCs in the PLA matrix on the oxygen permeability. However, other studies, like that of Sung *et al.*⁵⁷, proved that the introduction of even a low amount of CNC in a PLA matrix can largely improve this oxygen permeability. It is confirmed by Fortunati *et al.*⁵⁹ who quantified an OTR reduction around 50% after having introduced 5 wt% of CNC in a PLA matrix. Nevertheless, this result was surprising and could also be attributed to the presence of iron particles or the reference permeability. Such unexpected results for PLA_CNC-Lauric – although encouraging CNC dispersion was previously discussed – can find explanation in the interface between the PLA and the CNC-Lauric, which can differ from that between the PLA and the CNC-PGMA-Br. Indeed, it has been previously discussed that the epoxy groups from the surface of the CNC-PGMA-Br could react with the PLA chains, inducing a strong network inside the nanocomposite. This could largely influence the gas – and especially oxygen – permeation through the material. In this sense, it would be interesting to further investigate both PLA/CNC-Lauric and PLA/CNC-PGMA-Br interfaces, and confirm the effect of the CNC-PGMA-Br using a reference closer to the values found in the literature.

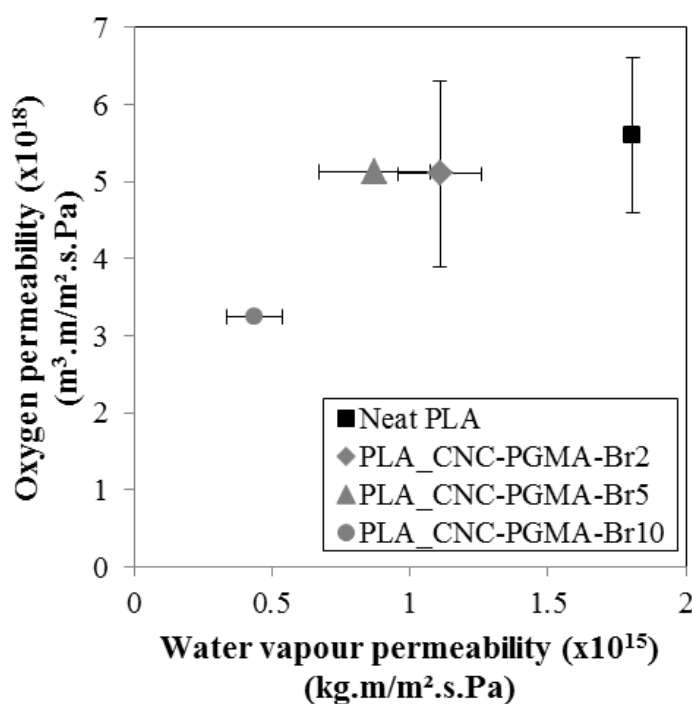


Figure III. 10. Water vapor and oxygen permeabilities of both neat PLA casted film and PLA_CNC-PGMA-Br nanocomposites

To deeply investigate the barrier properties of the prepared nanocomposites, the water vapor permeability of neat PLA and PLA_CNC-PGMA-Br samples was measured, and the results are presented in **Figure III. 10**, and are plotted function of oxygen permeability values previously described. All these water vapor permeability are presented in **Table III. 3**. According to **Figure III.**

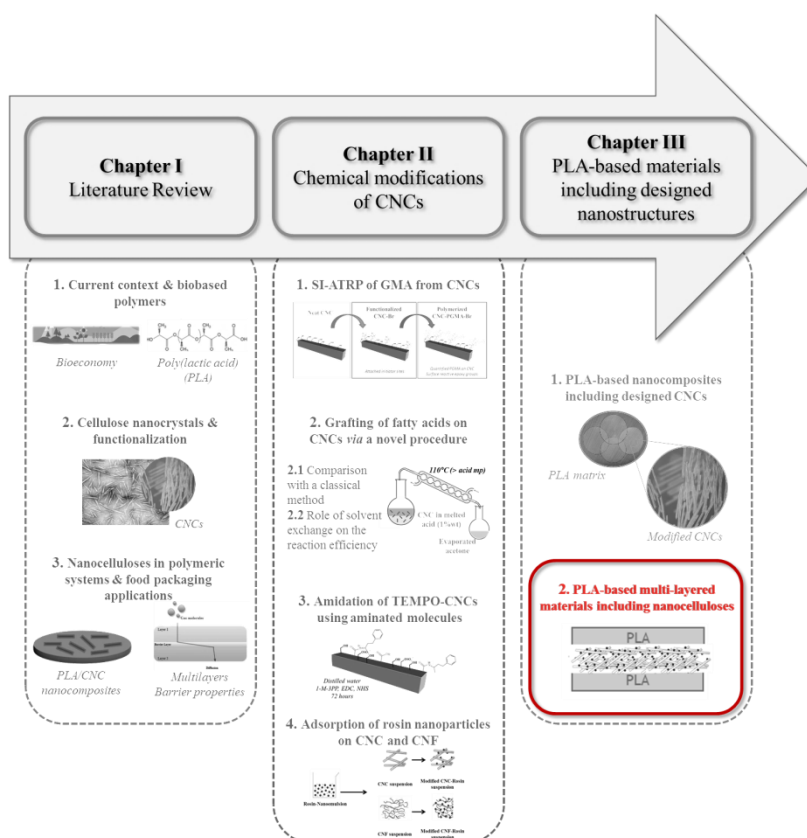
10, it is difficult to conclude about the influence of nanofillers on the nanocomposites water vapor permeability at low content of CNC-PGMA-Br, although these values are consistent with values found in literature for neat PLA⁵⁹. Furthermore, when a higher amount of CNC-PGMA-Br was introduced (i.e., 10 wt%), a significant decrease of 80% of water vapor permeability was measured. However, several studies showed that water vapor permeability of similar nanocomposites systems decreased by increasing the amount of nanofillers. In fact, Fortunati *et al.*⁵⁹ modified CNCs by adsorbing a surfactant (Beycostat A B09) on their surface, and proved that by introducing only 1 wt% of these modified CNCs, the water vapor permeability decreased by 34%, whereas 5% of modified CNCs induced a decrease of only 15%. Follain *et al.*⁵⁸ confirmed this result by showing that the water vapor barrier was negatively affected by increasing the amount of CNC from 3 wt% to 12 wt% in a poly(ϵ -caprolactone) matrix. It was explained by the hydrophilic behavior of CNCs, leading to a better affinity of nanofillers to water molecules. This increase in water vapor permeability was limited when the CNCs were surface modified, although no improvement was observed. The affinity between hydrophilic CNCs and water molecules was also investigated by Espino-Pérez *et al.*⁶⁰ who evidenced the increase in water vapour permeability according to the increasing content of neat CNC (increase of 21.3%, 42.4%, and 195.8% for CNC contents equal to 2.5 wt%, 7.5 wt%, and 15 wt%, respectively). More recently, Espino-Pérez *et al.*²² confirmed this result, and proved that the surface hydrophobization of CNCs led to the improvement of the water vapour permeability of the related PLA/CNC nanocomposites. In our study, CNC-PGMA-Br were covered at their surface by hydrophobic PGMA chains, explaining the different trend observed by increasing nanofillers amount in the PLA matrix. Moreover, it confirms the previously assumption, assuming that the CNC-PGMA-Br introduced in the PLA matrix created a strong network, inducing a possible tortuosity through the material.

4. Conclusion

Two different surface modifications were performed on the surface of CNCs. The first one, consisting in the surface-initiated radical polymerization of glycidyl methacrylate (GMA), led to polymerized CNC-PGMA-Br bearing functional epoxy groups on their surface. The second one consisted in the surface esterification of CNCs using long fatty acid (especially lauric acid), and led to modified CNC-Lauric exhibiting a hydrophobic behavior. The introduction of both CNC-PGMA-Br and CNC-Lauric in a hydrophobic amorphous PLA matrix has been successfully carried out by the solvent casting method. Unmodified CNCs were also introduced in a PLA matrix, as a negative reference. In accordance with what can be found in the literature, the PLA_neatCNC nanocomposites prepared with 10 wt% of neat CNC exhibited clear micrometric aggregates and a poor adhesion between the nanofillers and the polymeric matrix. However, both PLA_CNC-PGMA-Br and PLA_CNC-Lauric nanocomposites showed a clearly enhanced compatibilization. In fact, according to SEM and TEM observations of these nanocomposites cross-sections, the dispersion of both CNC-PGMA-Br and CNC-Lauric in PLA seemed to be improved, since no micrometric aggregates were distinguished, although the CNC-PGMA-Br were more aggregated at nanoscale than the CNC-Lauric. In case of CNC-PGMA-Br, their enhanced interface with the PLA can be attributed to cross-linking reaction between the highly reactive epoxy groups at their surface and the hydroxyl groups present at the end of the polymeric PLA chains. This reaction would occur during the nanocomposites preparation, and especially during the heat-pressing step. The hydrophobicity of CNC-Lauric was clearly evidenced by their enhanced dispersion in the PLA matrix. Regarding the barrier properties of the nanocomposites, and despite some surprising values obtained for the PLA references, the oxygen permeability was improved in both cases, although the influence of the CNC-PGMA-Br was more clearly distinguished than that of the CNC-Lauric, which could be explained by the formation of a strong network in PLA_CNC-PGMA-Br. These results are encouraging, especially in a scientific context, in which the development of bio-nanocomposites is currently challenging. In fact, although the preparation of CNC-PGMA-Br is more time-consuming and leads to small amount of materials, that of CNC-Lauric could be conceivable at a larger scale. It thus paves the way for the development of new bio-based nanocomposites with interesting properties, particularly for food packaging applications. In this perspective, it would be interesting to carry out further barrier properties towards other gases and organic molecules, in order to confirm their interest for specific food packaging applications.

2. Two distinct methods for the elaboration of multi-layered materials based on poly(lactic acid) and active cellulosic nanostructures

The second part of this section is adapted from « M. Le Gars, B. Dhuiège, A. Delvart, P. Roger, M. N. Belgacem, K. Missoum, J. Bras – High barrier antioxidant PLA/nanocellulose multi-layered materials for packaging », submitted and under revisions in ACS Omega in April 2020.



Abstract

In order to combine the outstanding properties of nanocellulosic materials (sustainability, crystallinity, high tensile strength, large specific surface area, low density, O₂-barrier properties) with those of biobased poly(lactic acid) (transparency, stiffness, biodegradability), three-phase multi-layered materials (TML) were built up *via* two different methods. Indeed, two kinds of multi-layered materials were produced (i) by depositing in wet state a thin layer of nanocellulose from an aqueous suspension, or (ii) by introducing a thicker dry nanocellulosic film, both between two PLA sheets, and using a heat-pressing process. Furthermore, after having proved the efficiency of the two procedures, barrier properties of the materials towards both oxygen and water vapor were investigated, and results were highly encouraging. Indeed, even a very thin layer of cellulose nanocrystals inside the PLA-based material induced a reduction in oxygen and water vapor permeability of around 90% and 50%, respectively. Moreover, effect of the surface pre modification of the nanocelluloses with different active molecules (1-methyl-3-phenylpropylamine and natural rosins) was investigated. It was proved that the introduction of rosin-based nanoparticles inside the materials was responsible for their antioxidant activity. In a more general way, the presence of various amounts of nanocellulose as an inner layer between two PLA films led to an enhancement of the barrier and active properties of the final multi-layered materials. Owing to the simplicity and efficiency of the two proposed methods, this study opens the way to the elaboration of hybrid multi-materials which could be highly interesting, especially for food packaging applications.

Keywords:

Cellulose nanofibrils — Cellulose nanocrystals — Poly(lactic acid) — Multi-layered materials — Barrier properties — Antioxidant properties

1. Introduction

Cellulose is a highly abundant biopolymer on earth, extracted most of the time from wood or annual plants. The cellulose fibers are composed of several fibrils, which were first isolated by Turbak *et al.*⁶¹ in 1983, are currently presented as microfibrillated cellulose (MFC), nanofibrillated cellulose (NFC) or cellulose nanofibrils (CNFs), and are obtained after mechanical disintegration, generally preceded by an enzymatic or a chemical pretreatment. Such pretreatments aim to weaken the cellulosic fibers, and thus, to reduce the energy consumed during the mechanical step of their production⁶²⁻⁶⁴. Biobased CNFs materials are highly studied, and their production, as well as, their applications, were reported in several books and reviews^{10,65-67}. Since the early 2010's, CNF development has demonstrated exponential interest in scientific field, as well as, in industrial one, and there are currently nearly 60 industrial producers all over the world. In 2016, CNFs were identified as the second bio-economy priority in Europe, thanks to their outstanding properties. Indeed, CNFs display high mechanical resistance and excellent barrier level, in addition to being biodegradable and biocompatible. All these properties make this bio-based material a prime candidate for many applications, such as packaging⁶⁸, paper and board⁶⁹, composites³³, printed electronics⁷⁰, biomedical devices⁷¹, etc. Another class of nanomaterials can be extracted from cellulosic biomass, by applying this time a chemical treatment. In fact, by subjecting biomass to a sulfuric acid hydrolysis, and thus by removing most of the amorphous parts of cellulose, cellulose nanocrystals (CNC) can be obtained. Their extraction was first reported by Ranby *et al.*^{72,73}, and their production has been widely studied and optimized since last decades. Currently, the CNC annual production capacity is approximately close to 400 tons, and around 13 companies already produce and market CNCs^{74,75}. Like CNFs, CNCs exhibit outstanding mechanical and barrier properties^{76,77} and can find applications in similar fields, like among others, biomedical^{78,79}, electronics^{70,80,81}, coatings⁸² and composites^{82,83}. Therefore, both CNFs and CNCs, owing to their exceptional intrinsic properties (morphology, crystallinity, large specific surface area, etc.), are nano-sized renewable materials that can be used for many applications.

Although nano-scale cellulosic materials present a wide range of applications and applied researches, composites field – and especially that of nanocomposites – is one of the most important targeted application in current ecological context. In fact, with consumer awareness of the use of biodegradable and synthetic plastic-free materials, packaging industry – and especially that of food packaging – has been constantly evolving for several years. Among biobased and biodegradable materials, poly(lactic acid) (PLA) is highly interesting because of its production from natural resources, as well as, its transparency, mechanical properties, and printability, making it a polymer of choice for replacing fossil-based plastics generally used in food packaging industry^{4,84}. However, thermal and barrier properties of PLA are generally not sufficient for food packaging applications. In fact, its glass transition temperature is around 60 °C, and PLA is highly permeable to water vapor and oxygen, comparing to other food packaging traditional polymers. Inserting cellulosic nanostructures in PLA-

based packaging makes it possible by combining their respective intrinsic properties, and thus, to produce packaging that is still biodegradable and more efficient in terms of mechanical and/or barrier properties. The elaboration of such multi-phasic materials has already been studied in literature, and the main type of process is based on the elaboration of nanocomposites. However, it is highly challenging, as the compatibilization between the hydrophilic nanocelluloses and the generally hydrophobic polymeric matrix needs to be highly improved, and numerous research groups proposed various procedures in order to enhance this compatibilization^{22,33,36,85}. Another strategy consists in the incorporation of one or multiple layer(s) to improve final barrier and mechanical properties of the multi-layered system.

The elaboration of multi-layered materials can be processed *via* different methods (like among others, layer by layer deposition, electrodynamic processing, microlayer co-extrusion, coating)³⁸ which all aim to deposit a layer of a specific material on a polymeric substrate. As suggested, a multi-layered material is composed of at least two layers, but the thinnest layer is generally covered with another polymeric layer, different or not from the initial one. The compatibility between the layers is generally challenging, and that explains the common use of adhesive layers, especially in packaging industry. Regarding the literature, only few studies deal with the preparation of such PLA-based multi-layers materials. In 2013, Aulin *et al.*⁸⁶ were among the firsts to perform the layer-by-layer deposition of CNFs combined with cationic polyethyleneimine (PEI) on a PLA substrate. They concluded about the efficient deposition of the nanocellulose/PEI mixture onto the PLA substrate, and highlighted the improvement of both oxygen and water vapor barrier properties of the final coated materials by 94% and 50%, respectively. This promising study was confirmed by the work of Meriçer *et al.*⁸⁷ who produced multi-layered PLA-based materials including MFC by casting evaporation of both layer with improved mechanical- (increase in Young's modulus by 60%) and barrier properties (decrease in oxygen permeability of one order of magnitude). Similarly, Hosseini *et al.*⁸⁸ prepared multi-layered films based on PLA and fish gelatin by successive solvent casting procedures with enhanced oxygen and water vapor barrier properties compared to pristine PLA, by 87% and 91%, respectively.

Furthermore, specific active compounds can be added to the food packaging to improve specificities of the packaging, like for example antibacterial, antimicrobial or antioxidant properties. This point was summarized in a recent review of Yildirim *et al.*⁸⁹, describing the various active compounds generally used in food packaging and emphasizing the clear distinction between absorbers (scavenging systems) and emitter (releasing systems) compounds. In case of multi-layered materials, such active compounds are generally inserted inside the multi-layered structure, in order to be released through the packaging or to scavenge some specific molecules from food products. In a multi-layer strategy, the presence of both nanocelluloses and active compounds inside the active layer can help for their entrapment and/or their possible release. In the literature CNC have been mixed with silver nanoparticles⁵² or with carvacrol⁹⁰ to confer them antibacterial or antioxidant properties, respectively.

Throughout this study, multi-layered materials based on PLA and nanocelluloses, including active molecules or not, were prepared following two different strategies. The first one consists in the wet deposition of a modified-CNC suspension on a PLA film, following by the heat-pressing with another PLA sheet above. Note that CNC were previously oxidized and covalently bound to aromatic molecules (1-methyl-3-phenyl-propylamine, or 1-M-3-PP) by an amidation procedure (previously detailed in **Chapter II.3**), leading to a low amount of 1-M-3-PP molecules on their surface. The 1-M-3-PP molecule was chosen because of its aromatic rings, which are expected to bring sorption properties to the modified CNCs. The second strategy consists in the complexing of two PLA sheets with an inner layer consisting in a CNF or CNC casted film including adsorbed rosin nanoparticles (previously described in **Chapter II.4**). After processes optimization, all materials were characterized, and their structural, mechanical, barrier, and antioxidant properties were investigated.

2. Materials and methods

2.1. Materials

Spray-dried cellulose nanocrystals (CNC) extracted from wood pulp were supplied from Canadian company Celluforce®. Cellulose nanofibrils (CNF) aqueous suspension (2 wt%) was provided by INOFIB (Saint-Martin d'Hères, France). 2,2,6,6-Tetramethyl-1-piperidinyloxy (TEMPO, 98%), sodium bromide (NaBr, BioXtra, >99.0%), sodium hydroxide (NaOH, BioXtra, >98%, pellets), hydrochloric acid (HCl, ACS reagent, 37%), N-(3-Dimethylaminopropyl)-N'-ethylcarbodiimide (EDC, >97%), N-Hydroxysuccinimide (NHS, 98%), 1-methyl-3-phenylpropylamine (98%), Tetradecyltrimethylammonium Bromide (TTAB), Gum rosin (natural resin), Chloroform (>99%), and 2,2-diphenyl-1-picrylhydrazyl (DPPH) were supplied by Sigma-Aldrich Chimie (France). Sodium hypochlorite solution (NaClO, 12% Cl) was provided by Carl Roth (France). Ethanol (95%) was purchased from Revol (France). Two different types of Earthfirst® PLA films (Indegeo™) were supplied by Sidaplast (France) company. PLA film used in the section 3.1 exhibits a theoretical thickness equal to 75 µm, and that used in the section 3.2 exhibits a theoretical thickness equal to 25 µm.

2.2. Elaboration of multi-layered materials by the wet way

2.2.1. Modification of CNC via an amidation procedure using 1-M-3-PP molecules

The grafting of 1-M-3-PP molecules on the surface of CNC was performed *via* a two-step procedure, previously described in **Chapter II.3**. Briefly, CNC were first TEMPO-mediated oxidized, and carboxylic groups were thus introduced on the surface of TEMPO-CNC. The amidation of 1-M-3-PP molecules on TEMPO-CNC was catalyzed by EDC/NHS reagents, and recovered CNC-1-M-3-PP were successfully surface modified, as detailed in **Chapter II.3**.

2.2.2. Coating of the CNC suspension on a PLA substrate

Before being coated, the PLA film was surface treated by corona effect, using a SG2 Generator (Société de Transfert Technologique, France), which was equipped with an ozone filter. By applying an electric discharge on the polymer surface, the corona treatment aims to create new polar carbonyl and hydroxyl groups, in order to increase the tension surface and the wettability of the film and thus, to facilitate the coating. Corona treatment was performed on the PLA film in motion at a speed equal to 2.5 m/min, and an intensity of 245 mA, with different number of passes under the generator.

Once corona treated, the PLA film was coated using a bar coater device (LGP2, France). TEMPO-CNC or CNC-1-M-3-PP suspension at 5 wt%, with a certain amount of isopropanol (5, 10 or 15

wt/wt) was deposited on the PLA substrate, with a coating speed equal to 3.5 m/min. Coated film was then dried at 40 °C, for 10 min in an oven. For each sample, two layers of CNC suspension were successively deposited in order to ensure a total recovering of the PLA film with the coating sauce.

2.2.3. Heat-pressing of the coated PLA

The multilayers materials were prepared by superposing previously coated PLA-TEMPO-CNC or PLA-CNC-1-M-3-PP films with another neat PLA film. The system was then heat-pressed (heat press device, Saint-Eloi Mécanique Outillage, France) between two metallic plates and two protective non-adhesive paper sheets under 0.5 MPa pressure for 30 min at 110 °C.

2.3. Elaboration of multi-layered materials by complexing

2.3.1. Preparation of rosin-based nano-emulsion

The rosin-based nano-emulsion was prepared by the INOFIB startup, following a patented protocol⁹¹. This confidential protocol was previously described in **Chapter II.4**.

2.3.2. Elaboration of neat and modified CNF and CNC films

The neat and rosin-modified CNF and CNC films were prepared according to the procedure previously described in **Chapter II.4**. Briefly, a proper amount of the rosin nano-emulsion was added to an aqueous suspension of CNF (2 wt%) or of CNC (1 wt%) in order to respect a rosin/nanocellulose weight ratio equal to 0.11. Thirty minutes of magnetic stirring at room temperature was performed to adsorb rosin nano-emulsion onto the nanocellulose surface. The films were prepared by filtration and solvent casting in the case of CNF and CNC, respectively, and called CNF-Rosin and CNC-Rosin, respectively.

2.3.3. Complexing of multi-layered materials by heat-pressing

The multi-layered materials were prepared by incorporating one neat or modified CNC or CNF film between two PLA sheets. The 3-layer sandwich system was then heat-pressed, according to the same protocol as previously described in **part 2.2.3**, under 0.5 MPa pressure, for 10 min at 170 °C.

2.4. Characterization methods

2.4.1. Contact angle and surface energy

Contact angle measurements were carried out by depositing 5 µL-water droplets at the surface of the substrate at room temperature. OCA20 DataPhysics (DataPhysics Instrument) system equipped with a CCD camera was used to record the angles between the solvent and the substrate. The acquisition of contact angle and drop volume was collected for the first 60 s after deposition. At least five measurements were performed for each sample. The substrates surface energy was determined in

accordance with the Owens-Wendt model, and using four different solvents (water, ethylene glycol, glycerol and diiodomethane). Briefly, by decomposing the surface energy into a dispersive and polar parts, γ^d and γ^p , respectively, it is possible to express the total surface energy of the substrate s and a liquid l through $\gamma_s = \gamma_s^d + \gamma_s^p$ and $\gamma_l = \gamma_l^d + \gamma_l^p$, respectively. These two surface energies are linked by the

Equation III. 5. By plotting $\gamma_l \times \frac{(1+\cos\theta)}{2\sqrt{\gamma_l^d}}$ as a function of $\sqrt{\gamma_s^p \gamma_l^p}$ with values obtained with the four

different solvents, the curve slope can directly be linked to the substrate surface energy γ_s value.

$$\gamma_l \times (1 + \cos \theta) = 2\sqrt{\gamma_s^d \gamma_l^d} + 2\sqrt{\gamma_s^p \gamma_l^p}$$

Equation III. 5. Owens-Wendt model for the determination of the substrate surface energy

2.4.2. Surface tension

The surface tensions of the different coating suspensions were measured using an Attension Sigma 700 (Biolin Scientific) force tensiometer. Briefly, a platinum ring was tared and immersed in the suspension to be analyzed. The surface tension values were recorded and processed using OneAttension software. At least 5 measurements were performed for each sample.

2.4.3. Oxygen permeability

The oxygen permeability of the materials was investigated at 23 °C and 0% RH or 50% RH, using a Systech Illinois (USA) M8001 Oxygen Permeation Analyzer. Data were processed according to the ASTM-F 1927 standard. For each sample, masks with a specific exchange surface of 6.2 cm² were prepared and placed in the device chamber. Pure oxygen was used for the measurement. The final value of the oxygen transmission rate (*OTR*) was determined when a plateau was reached. The oxygen permeability coefficient (*OP*) was obtained from **Equation III. 6**, where *l* is the average thickness of the sample in mm.

$$OP = OTR \times l$$

Equation III. 6. General relation between oxygen permeability coefficient (*OP*) and oxygen transmission rate (*OTR*) according to ASTM-F 1927 standard

Because of the large error of measurement, all experiments should be at least duplicated, as much as possible (limited number of samples).

2.4.4. Water vapor permeability

Water vapor permeability of the materials was determined at 23 °C and 50% RH, according to the T448 om-09 TAPPI standard. For each sample, masks with a specific exchange surface of 6.2 cm² were prepared and mounted on specific test dishes filled with dried CaCl₂ as desiccant material. A regular weighing of the whole system was performed, and the water vapor transmission rate (*WVTR*) in g/(m².day) was determined from **Equation III. 7**:

$$WVTR = \frac{24x}{Ay}$$

Equation III. 7. General equation for the calculation of the water vapor transmission rate (*WVTR*) according to T 448 om-09 TAPPI standard

where *x* is the gain, in grams for the period *y*, in hours, and *A* is the exposed area of the sample (6.2 cm² in our study). The water vapor permeability coefficient (*WVP*) was determined from **Equation III. 8**:

$$WVP = WVTR \times l$$

Equation III. 8. General relation between water vapor permeability coefficient (*WVP*) and water vapor transmission rate (*WVTR*)

where *l* is the average thickness of the sample, in mm. Each experiment has been at least duplicated.

2.4.5. Test on food product

The influence of the multi-layered materials as packaging materials on the evolution of food product's shelf-life was investigated. The protocol was inspired by the work of Bideau *et al.*⁹³. Banana was selected as a food product reference because of its fast and colored degradation. Briefly, banana slices (~ 10 g) were freshly cut and placed in a sachet composed of the multi-layered, and hermetically closed with aluminum tape. The samples were stored for 72 h at 23 °C and 50% RH. Qualitative observations were performed on each sample.

2.4.6. Scanning electron microscopy (SEM)

SEM images were obtained from PLA films and multi-layered materials sections obtained by cryofracture, using a Quanta200 device. The working distance during the acquisition was between 9.8 and 10.1 mm, with a voltage of 10 kV and at a magnification of x1000.

2.4.7. Tensile tests

Mechanical properties of the films were determined under specific conditions (23 °C, 50% RH) using an Instron Universal Testing Machine Model 4507 (Instron Engineering Corporation, Canton, MA) equipped with pneumatic. After its average thickness was measured, each sample (100 mm x 15 mm) endured a tensile cross-head speed of 10 mm/min, according to the French standard NF Q 03-004 (July 1986). The samples were preconditioned at 23 °C and 50% RH at least one day before the experiment. At least five tests were carried out for each sample.

2.4.8. UV-visible spectrophotometric direct transmission analysis

Three samples of each film were prepared with dimensions equal to 15 mm x 50 mm. Direct transmittance, at a wavelength of 550 nm (*T*_{550nm}), was measured at least three times for each sample, using a UV-vis spectrophotometer (UV-1800, Shimadzu).

2.4.9. Antioxidant activity characterization

The DPPH assay (free radical 2,2-diphenyl-1-picrylhydrazyl DPPH[•]) was performed to determine the radical scavenging activity (RSA) of the samples. The method was adapted from the one recently proposed by Crouvisier-Urien *et al.*⁹⁴. Samples of 100 mg of material previously prepared and placed in a closed vial containing 10 mL of a 50 mg/L solution of DPPH in ethanol, and were left under magnetic stirring in the dark and at room temperature. Aliquots of the medium solutions were collected at regular time intervals, and absorbance at 515 nm was measured (A_{sample}), using a UV-vis spectrophotometer (UV-1800, Shimadzu). Note that in ethanol, DPPH[•] is purple and turns yellowish when it is in direct contact with an antioxidant molecule. The collected solutions were returned to the corresponding vial after each measurement. Absorbance measurement of the DPPH solution (A_{DPPH}) in ethanol was performed at the same time, in order to correct for the auto-degradation of the DPPH[•] radical. From experimental data, the radical scavenging activity (RSA) at time t of each sample can be calculated from **Equation III. 9**:

$$\text{RSA}(t) = 100 - \frac{A_{\text{DPPH}}(t) - A_{\text{sample}}(t)}{A_{\text{DPPH}}(t)} \times 100$$

Equation III. 9. General equation for the calculation of the radical scavenging activity (RSA) of a material sample

For each sample, the measurements of the RSA (in %) were duplicated and plotted as a function of the reaction time until a plateau was visible.

3. Results and discussions

3.1. Coating of wet CNC suspension for the elaboration of PLA-based multi-layered materials

In this study, multi-layered materials based on two commercial poly(lactic acid) polymeric self-standing films and an inner nanocellulose-based layer were performed *via* two different routes, as previously presented in parts 02.2 and 2.3. The first method consists, in a first step, in the deposition, *via* a coating procedure, of a CNC suspension on the surface of one of the PLA sheets. This step has been carefully optimized in order to ensure a homogenous deposition of the nanomaterials on the substrate. In this sense, four different single- or multi-layered materials were studied : a commercial PLA film (75 μm thick), a PLA-PLA film (160 μm thick) prepared by the heat-pressing of two single commercial PLA films, and two multi-layered PLA-CNC-PLA materials prepared by the coating of oxidized TEMPO-CNC or modified CNC-1-M-3-PP on one of the PLA film as an inner layer, and referenced as PLA-TEMPO-CNC (166 μm thick) and PLA-CNC-1-M-3-PP-PLA (177 μm thick), respectively. The theoretical and experimental thicknesses of all these materials are summarized in the **Table III. 4**.

Sample	Theoretical thickness (μm)	Experimental thickness (μm)
PLA	75	77
PLA-PLA (thermopressed)	150	156
PLA-TEMPO-CNC(coated)-PLA	150+coated layer thickness	156
PLA-CNC-1-M-3-PP(coated)-PLA	150+coatd layer thickness	157

Table III. 4. Theoretical and experimental thicknesses of each sample prepared following the wet multi-layer preparation

3.1.1. Optimization of the coating step

In the literature, only few publications deal with the coating of a CNC suspension on a PLA substrate. Indeed, due to intrinsic hydrophobic character of PLA, poor adhesion between aqueous polar coating sauce and PLA is generally observed. At both industrial- and lab-scales, corona treatment is frequently performed on the substrate in order to chemically modify its surface, especially by introducing polar functional groups at its surface. This chemical surface modification of PLA aims to improve its adhesion by enhancing its surface tension and polarity. Rocca-Smith *et al.*⁹⁵ carried out a complete study on the effect of such a corona treatment on PLA sheet properties. They clearly proved the chemical modification of the PLA film after corona treatment, as well as, the increase in the surface energy of the film. In our study, in order to optimize corona treatment performed on our commercial film of PLA, its surface energy was determined after the film endured different corona treatments, and

results are presented in **Figure III. 11**. Note that the different corona treatments were quantified by the number of times the PLA film passed under the electrodes constituting the discharge generator.

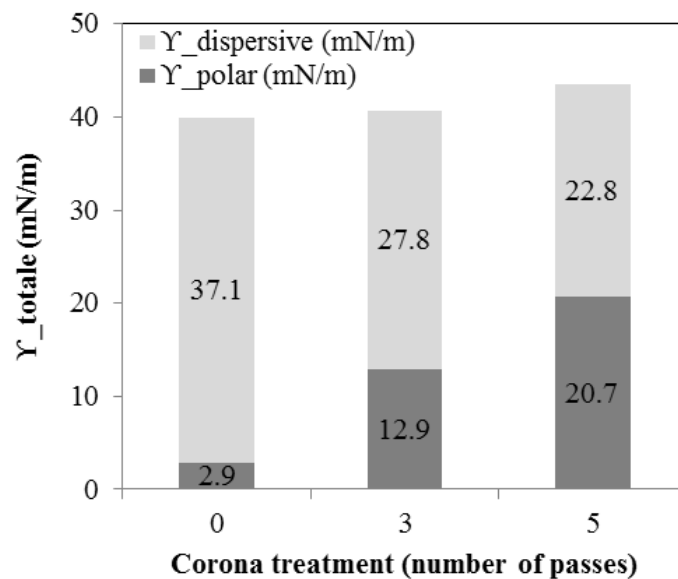


Figure III. 11. Dispersive and polar contributions of surface energies related to PLA films subjected to different corona treatments

As expected, the total surface energy of PLA film does not change significantly by increasing the number of passes under the corona system. Indeed, as shown in **Figure III. 11**, this surface energy increased from 40 mN/m to 40.7 mN/m and 43.5 mN/m for 3 and 5 passes, respectively. However, the polar contribution increased from 2.9 mN/m to 12.9 mN/m and 20.7 mN/m for 3 and 5 passes, respectively. It clearly confirms the creation of polar groups on the PLA surface induced by the corona treatment.

In order to investigate the behavior of the deposited coating sauces on the surface of the corona-treated PLA films, surface tensions of various aqueous CNC suspensions were determined. As described in part **2.2.2**, different amount of isopropanol were added to the water TEMPO-CNC suspension, the latter being studied as a reference suspension. Indeed, taking into account the low amount of grafted molecules on the surface of modified CNC-1-M-3-PP (previously proved in Chapter **II.3**), it was assumed that the behavior of both TEMPO-CNC and CNC-1-M-3-PP aqueous suspensions was almost similar. Isopropanol was selected because of its common use in industry - especially in coating and printing industry - to reduce the surface tension of dampening solutions. Evolution of the TEMPO-CNC suspension surface tension following the weight amount of isopropanol added to the suspension is plotted in **Figure III. 12**.

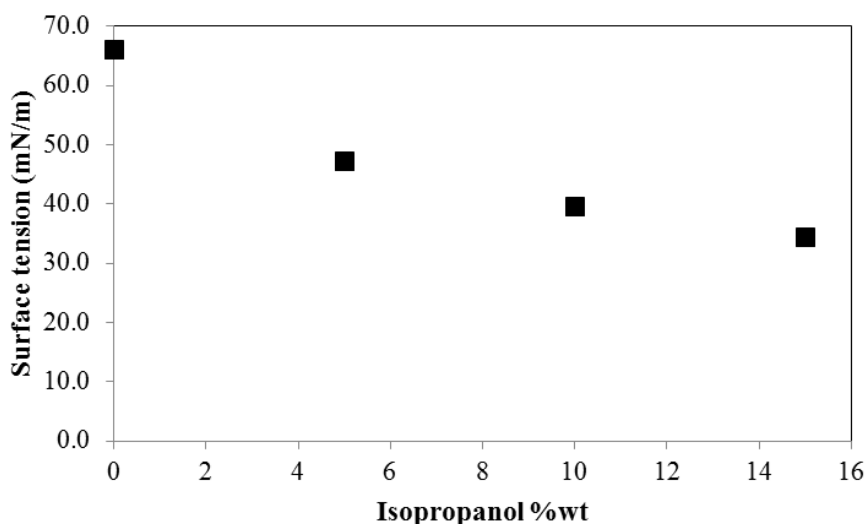


Figure III. 12. Surface tension of aqueous TEMPO-CNC suspensions prepared with various amount of isopropanol

According to **Figure III. 12**, a clear decrease in TEMPO-CNC suspensions' surface tension is observed by increasing the amount of isopropanol in the suspension, as expected. Indeed, due to its low surface tension, even a low amount of isopropanol can lead to a large decrease in the total surface tension of the suspension. As shown in **Figure III. 12**, by adding 15% (wt/wt) of isopropanol in the suspension, the surface tension decreases from 66.2 mN/m to 34.5 mN, or a decrease of almost 50%. These results are summarized in **Table III. 5**. Moreover, in order to concretely study the behavior of the suspensions deposited on PLA substrates, the adhesion work W_A^T was calculated in each case, according to **Equation III. 10**:

$$W_A^T = \gamma_l \times (1 + \cos \theta)$$

Equation III. 10. General equation for the calculation of the adhesion work between a substrate and a liquid

where γ_l is the surface energy of the liquid and θ the contact angle between the liquid and the substrate, more precisely between the TEMPO-CNC suspension with a certain amount of isopropanol and the corona-treated PLA. Measured contact angles and calculated adhesion work values are presented in **Table III. 5**. According to these results, the effect of corona treatment on the contact angle between the suspension and the PLA film is clearly visible. In fact, for a given suspension, the contact angle decreases by increasing the number of passes under the corona device. Moreover, by increasing the amount of isopropanol in the suspension, this contact angle decreases for a given number of passes under the corona device. By regarding calculated adhesion works, their values decrease by increasing the amount of isopropanol, but for a given suspension, the increasing of passes under corona led to an increase in adhesion work value.

Suspension 1 wt% TEMPO- CNC	Surface tension (mN/m)	Contact angle (°)			Adhesion work (J)		
		PLA	PLA+ Corona*3	PLA+ Corona*5	PLA	PLA+ Corona*3	PLA+ Corona*5
+0 wt% isopropanol	66.2 ± 0.2	77 ± 2	51 ± 3	50 ± 1	81.1 ± 0.03	107.9 ± 0.06	108.8 ± 0.02
+5 wt% isopropanol	47.3 ± 0.0	65 ± 1	44 ± 2	44 ± 1	67.3 ± 0.02	81.3 ± 0.05	81.3 ± 0.02
+10 wt% isopropanol	39.6 ± 0.1	57 ± 1	33 ± 3	33 ± 2	61.2 ± 0.02	72.8 ± 0.09	72.8 ± 0.06
+15 wt% isopropanol	34.5 ± 0.1	44 ± 1	28 ± 2	27 ± 1	59.3 ± 0.03	65.0 ± 0.07	65.2 ± 0.04

Table III. 5. Surface tensions of TEMPO-CNC suspensions prepared with various amount of isopropanol, contact angles of PLA substrates subjected to different corona treatments, and resulted calculated adhesion works between different previous substrates and suspensions

All these results allowed the optimization of the coating process of a TEMPO-CNC suspension on a PLA substrate. In fact, after numerous trials and after having taken into account the visual aspects of the different coatings performed, it was assumed that the most homogeneous coating was achieved with a TEMPO-CNC suspension containing 15% (wt/wt) of isopropanol and a PLA substrate subjected to 5 passes under the corona generator. In a second step, the heat-pressing step was optimized too, and different parameters, like the temperature, pressure, and time, were tested. It was assumed that the best multi-layered materials were obtained at 110 °C and 0.5 MPa, with a contact time equal to 30 min. Materials previously presented in **Table III. 4** were prepared following this optimized protocol.

3.1.2. Barrier properties of multi-layered materials prepared by wet deposition of a CNC suspension

The optimized protocol was applied to both TEMPO-CNC and CNC-1-M-3-PP aqueous suspension containing 15% (wt/wt) of isopropanol. Resulting PLA-TEMPO-CNC-PLA and PLA-CNC-1-M-3-PP-PLA multi-layered materials were then characterized, as well as, a neat PLA film and a heat-pressed PLA-PLA material without any inner coated layer, as reference. Investigation of the thickness of the coated layer was performed by different techniques (AFM, MEB) without success. In fact, due to the very low amount of deposited CNC, this investigation has proved highly difficult. However, regarding the literature, Li *et al.*⁹⁶ performed the coating of CNC on plastic substrates (poly(ethylene terephthalate, polypropylene, polyamide) using an automatic bar-coater, and the deposited CNC film thickness was determined equal to 600 nm. In our study, it is thus possible to similarly assume that the deposited layer thickness was around 500 nm, leading to a very low amount of CNC in the final material.

The barrier properties – especially towards oxygen and water vapor – of the prepared multi-layered materials were investigated. The oxygen and water vapor permeability values measured at 23 °C and 50% RH are presented in **Figure III. 13**. Commercial PLA film exhibits an oxygen and water vapor permeability equal to $3.9 \times 10^{18} \pm 0.3 \times 10^{18} \text{ m}^3 \cdot \text{m}/\text{m}^2 \cdot \text{s} \cdot \text{Pa}$ and $2.3 \times 10^{16} \pm 0.3 \times 10^{16} \text{ kg} \cdot \text{m}/\text{m}^2 \cdot \text{s} \cdot \text{Pa}$, respectively, which are consistent with values found in the literature^{4,6}, although water vapor permeability values are much higher in our study. This significant difference can be attributed to the PLA degradation since its purchase, leading to a decrease of its barrier property. Moreover, by comparing the values obtained for single PLA with that of the heat-pressed PLA-PLA reference, it can be observed that oxygen permeability is slightly improved (equal to $2.4 \times 10^{18} \pm 0.01 \times 10^{18} \text{ m}^3 \cdot \text{m}/\text{m}^2 \cdot \text{s} \cdot \text{Pa}$), whereas water vapor permeability value increases until $5.9 \times 10^{16} \pm 0.9 \times 10^{16} \text{ kg} \cdot \text{m}/\text{m}^2 \cdot \text{s} \cdot \text{Pa}$. It can be attributed to the fact that both corona treatment and heat-pressing could degrade the structure of the PLA and thus create some holes inside the films, leading to a preferential path for gas molecules.

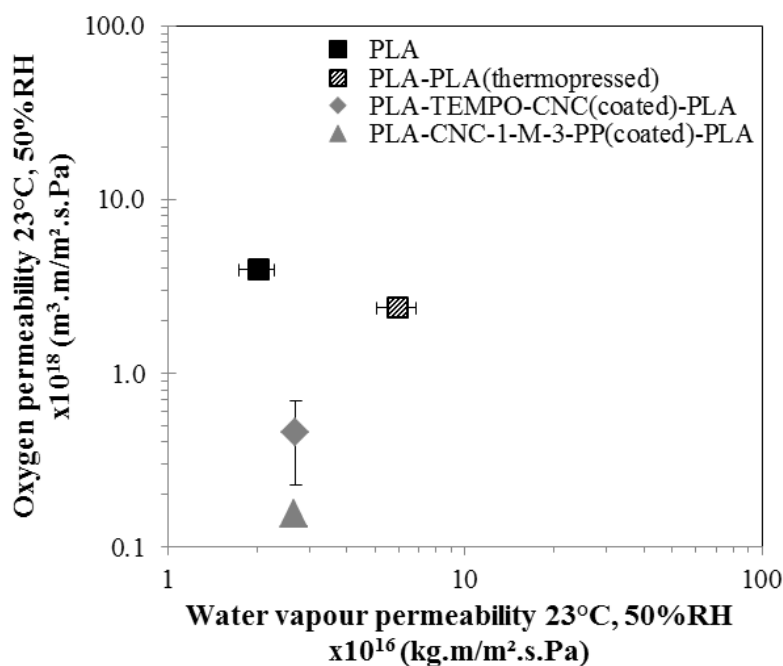


Figure III. 13. Oxygen and water vapor permeability of neat commercial PLA film, PLA-PLA reference, PLA-TEMPO-CNC-PLA, and PLA-CNC-1-M-3-PP-PLA multi-layered materials

However, according to **Figure III. 13**, it can clearly be assumed that the presence of an inner TEMPO-CNC layer between the two PLA films highly improves the barrier towards oxygen of the corresponding PLA-TEMPO-CNC-PLA sample, which exhibits an oxygen permeability value equal to $0.45 \times 10^{18} \pm 0.2 \times 10^{18} \text{ m}^3 \cdot \text{m}/\text{m}^2 \cdot \text{s} \cdot \text{Pa}$, or a decrease of almost 80% in regard to the PLA-PLA reference. Similar behavior is observed for PLA-CNC-1-M-3-PP-PLA sample, which exhibit an oxygen permeability equal to $0.15 \times 10^{18} \text{ m}^3 \cdot \text{m}/\text{m}^2 \cdot \text{s} \cdot \text{Pa}$, or a decrease of almost 94%. Note that for the PLA-TEMPO-CNC-PLA sample, no standard variation was obtained, and it is thus difficult to conclude about the specific influence of the 1-M-3-PP molecules grafted on CNC on the oxygen

permeability. Regarding the water vapor permeability, the values are equal to 2.7×10^{16} kg.m/m².s.Pa for either PLA-TEMPO-CNC-PLA and PLA-CNC-1-M-3-PP-PLA samples, or a reduction of almost 54% compared to the PLA-PLA reference. This reduction was less significant than the reduction of the oxygen permeability and it can be related to the hydrophilic character of CNC, which have the ability to retain water. This phenomenon was observed by Fortunati *et al.*⁵⁹ who prepared CNC/PLA nanocomposites by solvent casting, and observed that an increase in the amount of CNC led to a less important decrease in water vapor permeability. Similarly, Sanchez-Garcia *et al.*⁹⁷ produced PLA-based nanocomposites including cellulosic microfibers and observed that only 1 wt% of microfibers in the PLA matrix had an effect on water vapor permeability, higher amounts increasing this permeability. They assumed that poor dispersion of the fillers were responsible for lower tortuosity of water vapor molecules through the material. In our case, creation of cracks in the material during the heat-pressing can also be responsible for this increase in water vapor permeability. However, the highly significant decrease in oxygen permeability contradicts this assumption.

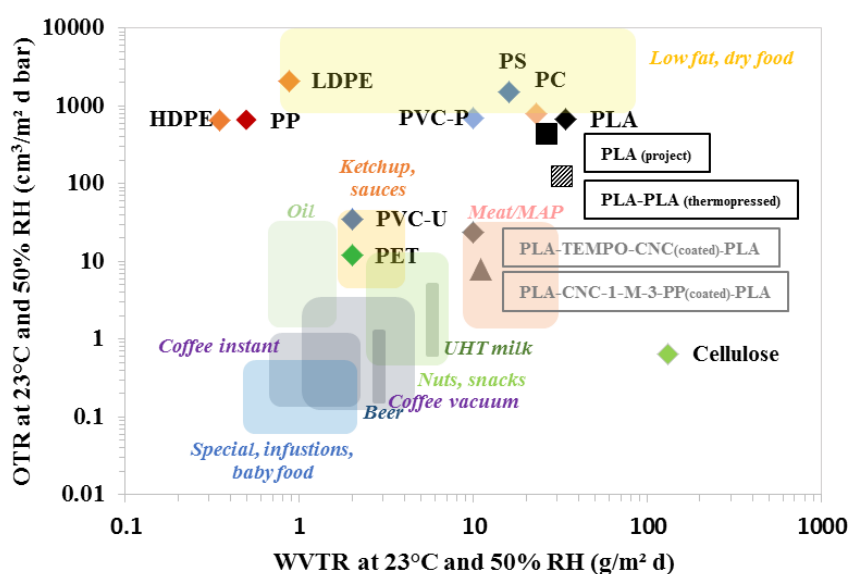


Figure III. 14. Oxygen and water vapor permeability values required for food packaging materials according to specific foodstuffs and multi-layered materials (PLA-PLA, PLA-TEMPO-CNC-PLA, and PLA-CNC-1-M-3-PP-PLA) positioning (adapted from⁹⁸)

Figure III. 14 shows the different oxygen and water vapor permeability values required for materials used for specific food packaging applications, and these values are compared to those determined from the materials studied and prepared in this work. According to **Figure III. 14**, it is confirmed that commercial PLA film is not enough barrier towards oxygen and water vapor for most of food packaging applications. Similar conclusions can be drawn for the PLA-PLA multi-layered reference material. However, by depositing even a very low amount of TEMPO-CNC or modified CNC-1-M-3-PP between the two PLA sheets, corresponding multi-layered materials are clearly usable in food packaging, especially for meat products packaging applications. **Figure III. 14** is highly interesting

since it exhibits the huge potential of such multi-layered materials including a very thin layer composed of nanocellulosic materials for food packaging applications.

In order to simulate the influence of such a multi-layered material on the evolution of the shelf-life of a food product, small bags prepared from commercial polyethylene (PE) film, commercial PLA film and multi-layered material PLA-CNC-1-M-3-PP-PLA, containing banana slices were prepared and hermetically closed in order to avoid any opening to the external environment. In each case, visual aspect of the banana slice was qualitatively evaluated, and corresponded pictures are presented in **Figure III. 15**.

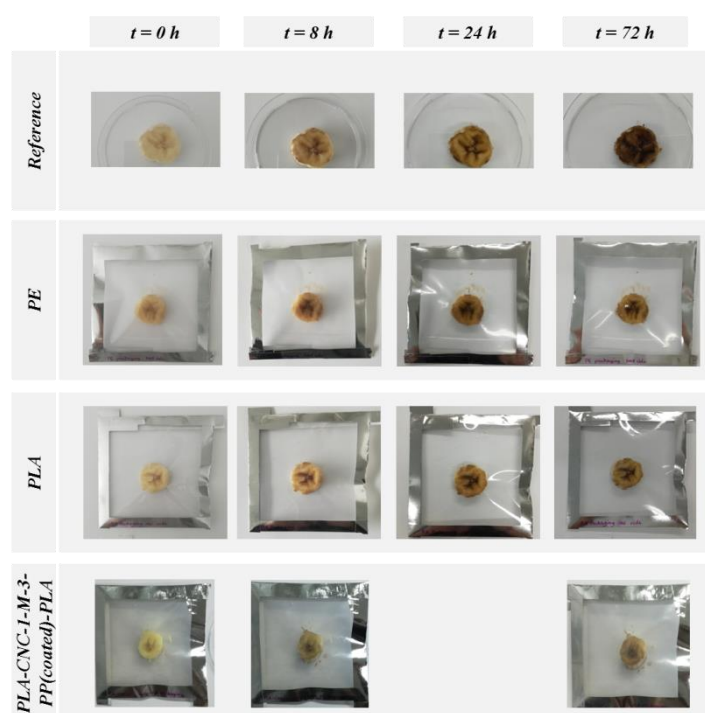


Figure III. 15. Comparison on a banana slice shelf-life evolution with different materials simulating its packaging: polyethylene (PE), poly(lactic acid) (PLA), and multi-layered PLA-CNC-1-M-3-PP-PLA, at 23 °C and 50% RH

In this study, banana was chosen as food product because of its rapid and visual degradation. In the literature, Bideau *et al.*⁹³ performed similar experiment using TEMPO-CNC combined with polypyrrole films to investigate banana preservation, related particularly to barrier and antioxidant properties of the films. In another study, Bideau *et al.*⁹² carried out antibacterial meat tests on pork liver in order to study the activity by contact of similar materials. In our case, even if test on meat product would have been interesting too, only banana products were tested. In **Figure III. 15**, the first line corresponds to the degradation of a banana at 23 °C and 50% RH without any packaging (negative reference). The second line corresponds to the evolution of a banana packaged in a polyethylene (PE) material, taken as positive reference, since PE is commonly used in food packaging industry. In the third line, banana slice was packaged in the commercial PLA material used in this study part, and no significant difference is observed between the PLA package and the PE one. However, by comparing

these pictures with the ones related to a packaging composed of PLA-CNC-1-M-3-PP-PLA materials (fourth line), it is possible to see a slight difference in terms of banana coloration. In fact, after 72 h in the PLA-CNC-1-M-3-PP-PLA packaging, the food product seems to be less brown colored. This could highlight the slower degradation of the banana induced by the package. However, at this stage, it is difficult to conclude about the role of the grafting of the 1-M-3-PP molecules at the surface of CNC, although the positive influence of CNC inside the package is confirmed once again. It is important to note that to investigate the role of the grafting of 1-M-3-PP aromatic molecules on the CNCs, sorption measures could have been performed. Indeed, in their study, Espino-Pérez *et al.*⁹⁹ proved that the presence of even a low amount of similar aromatic molecules on the CNC surface leads to the sorption of aromatic compounds such as anisole and, to a lesser extent, cyclohexane.

At this stage of the study, it is possible to conclude about the positive influence of a highly thin inner layer of nanocellulosic materials inside a PLA packaging on the barrier properties of the multi-layered materials. However, it is still difficult to clearly prove the role of the grafted 1-M-3-PP molecules on the material properties, and further experiments should be performed in this sense.

3.2. Multi-layered materials prepared by complexing

In this second part, multi-layered materials (TML) based on both PLA and nanocellulose were built up *via* the complexing of three dry films: two commercial PLA films (different from the commercial PLA used in the first part) and a single neat or modified CNC or CNF self-standing film in between. As previously described in part **2.3.2**, neat (or modified) CNC (or CNC-Rosin) and CNF (or CNF-Rosin) self-standing films were prepared by solvent casting or filtration processes, respectively, and were then heat-pressed between two PLA films (25 μm thick each) (see part **2.3.3**), leading to TML-CNC (or TML-CNC-Rosin) and TML-CNF (or TML-CNF-Rosin) multi-layered materials. After several trials, the optimal conditions for the protocol of heat-pressing of multi-layered materials were determined. Indeed, it was observed that at a temperature lower than 150 $^{\circ}\text{C}$, a delamination between the three layers occurred, and at 180 $^{\circ}\text{C}$, a yellowing of the material was observed. It was found that setting the temperature at 170 $^{\circ}\text{C}$ allowed the preparation of homogenous and uncolored samples. Note that this process temperature was higher than the temperature used for the elaboration of multi-layered materials in the previous part (wet coating). It is due to the fact that CNC or CNF films are thicker (\sim several tens of μm) than the CNC layer deposited by coating (\sim 500 nm), and the temperature needs to be higher than the melting temperature of the PLA (approximately 150 $^{\circ}\text{C}$) to permit the creep of the semi-crystalline polymer throughout the multi-layered system and to ensure good adhesion and sealing between the three layers. **Table III. 6** summarizes all the samples with their respective references, as well as, their determined basis weight (in g/m^2), and their theoretical and experimental thicknesses (in μm).

Sample		Basis weight (g/m ²)	Theoretical thickness (μm)	Experimental thickness (μm)
Single films	PLA	30	25	25
	CNC	67	40	40
	CNC-Rosin	61	40	44
	CNF	29	30	35
	CNF-Rosin	32	30	38
Heat-pressed multi-layered (TML) materials	TML-PLA	90	75	86
	TML-CNC	100	90	82
	TML-CNC-Rosin	121	94	94
	TML-CNF	90	85	78
	TML-CNF-Rosin	93	88	75

Table III. 6. Samples references with corresponding basis weights (in g/m²), and theoretical and experimental thicknesses

By comparing theoretical and experimental thicknesses presented in **Table III. 6** for multilayers (TML) prepared with an inner layer composed of CNC or CNF, it is worth noting that the experimental thicknesses are lower than the theoretical ones (except for TML-CNC-Rosin sample). This discrepancy can be explained by the potential impregnation of the melted PLA through the CNF or CNC nanoporous films during the heat-compression process, leading to a decrease in the total thickness of the material.

3.2.1. Structural and mechanical properties of complexed multi-layered materials

In order to confirm the assumption made about the impregnation of the PLA layers within the cellulosic layer, the structure of the multi-layered (TML) materials was investigated using SEM imaging. The cross-sectional images are presented in **Figure III. 16**.

In **Figure III. 16 a)** and **b)**, the cross-sections of the commercial PLA film built up in the same heat-pressing conditions as multi-layered materials and of the TML-PLA multi-layered system are respectively presented. Some defects can be observed on the PLA cross-section in **Figure III. 16 a)**, that might have been generated by the heat-pressing process. The corresponding multi-layered TML-PLA material (**Figure III. 16 b)**), composed of three heat-pressed PLA films, seems to be homogenous, and no separation between the three layers can be observed. However, some defects and cracks also appear, indicating that heat-pressing can affect the structure of the PLA-based materials. **Figure III. 16 c)** shows the cross-section of the TML-CNF. The inner CNF layer can be distinctly observed, although it seems to be impregnated with the top PLA layer. The boundary between the CNF and the lower PLA layer can be clearly distinguished, showing the poor compatibility between neat CNF and PLA. A similar boundary can be observed in the cross-section of the TML-CNC presented in **Figure III. 16 d)**. The top PLA layer seems to be impregnated in the inner CNC layer, whereas the boundary between the CNC and the lower PLA layer is visible.

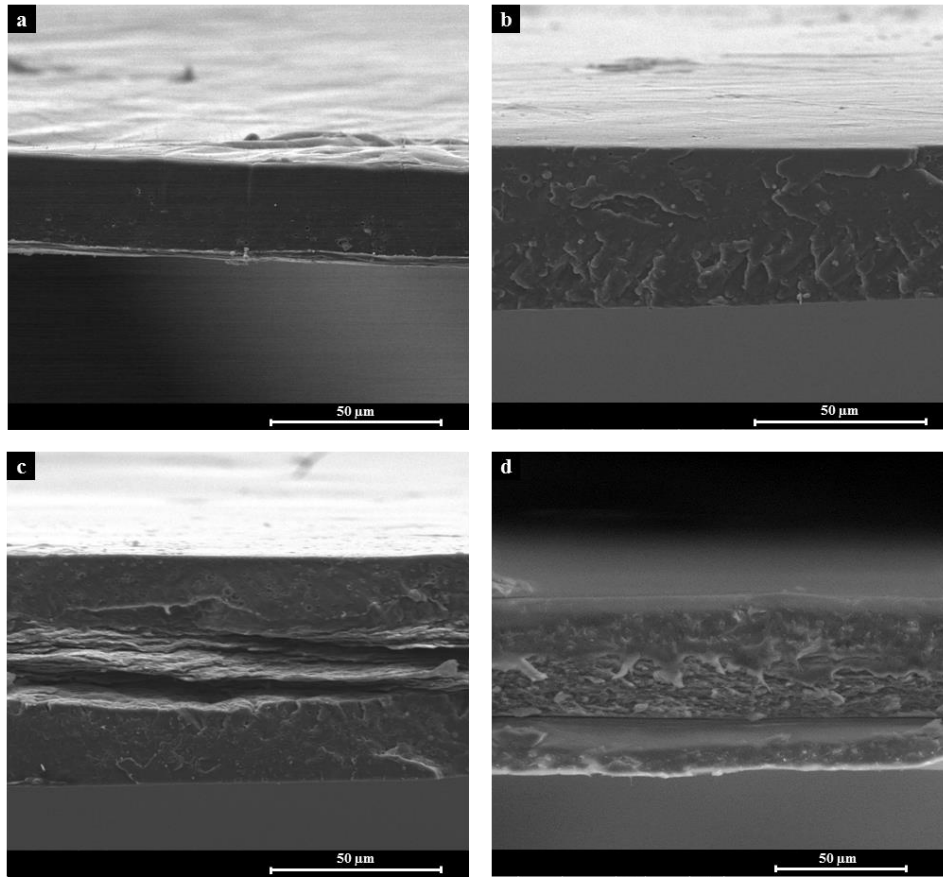


Figure III. 16. SEM images of **a)** commercial PLA heat-pressed film, **b)** reference TML-PLA multi-layered material, and multi-layered prepared with **c)** a CNF film, and **d)** a CNC film as the inner layer

Figure III. 16 a) and **b)** are interesting since they allow the conclusion about the efficiency of the heat-pressing method to complex several PLA sheets together. The process is not entirely homogeneous, probably because of a difference in temperature and pressure in the heat-press device, and it requires further optimization. However, both TML-CNF and TML-CNC materials are self-standing and uniform, without delamination between the layers. In their study, Sanyang *et al.*¹⁰⁰ prepared starch/PLA bi-layered materials using a casting procedure and observed, by SEM analysis, the interface between the two layers, probably due to the poor compatibility between the two components. However, they found the enhancement in mechanical and barrier properties in their bi-layered materials.

Regarding the transparencies of the different materials studied in this work, their transmittances were measured at the wavelength of 550 nm, corresponding to the visible light wavelength, and show the values in **Figure III. 17 c)**. The commercial film of PLA exhibits a transmittance at 550 nm equal to 91%, which is consistent with values found in the literature¹⁰¹. CNC and modified CNC-Rosin films have transmittances of 61% and 82%, respectively. The value obtained for neat CNC is consistent with the literature, although this value is highly dependent on the dispersion state and chirality of the CNC inside the film^{102,103}. The transmittances of CNF and CNF-Rosin films are equal to 15% and 11%, respectively, and highlight the fact that CNF-based films are less transparent than CNC films. These

values are consistent with values found in the literature¹⁰⁴ for similar CNF. In both cases, the presence of rosin nanoparticles in the film does not significantly influence the optical transparency of the CNC or CNF film.

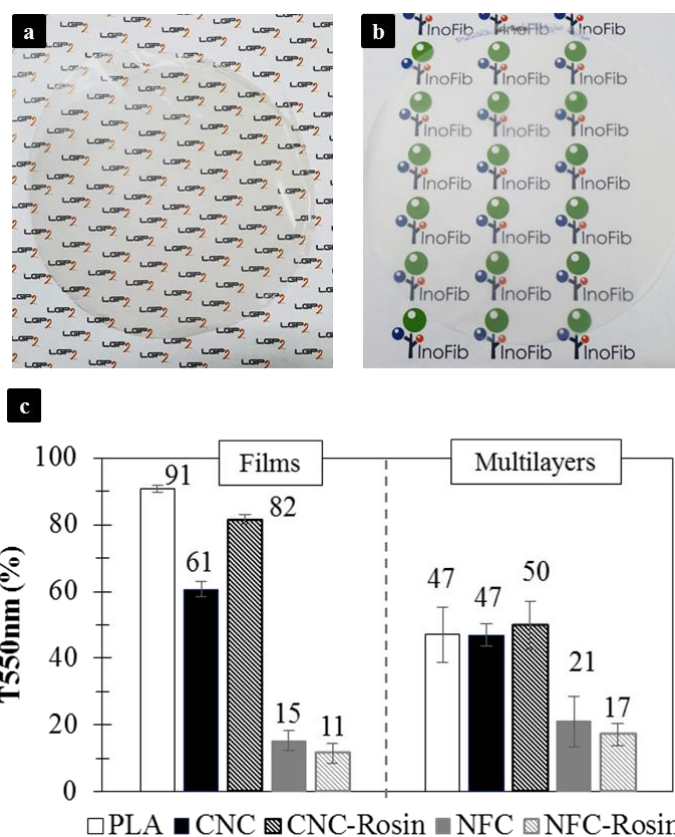


Figure III. 17. Photographs of films prepared by **a)** solvent-casting of a suspension of modified CNC-Rosin, and **b)** filtration of a suspension of a modified CNF-Rosin suspension, and **c)** Transmittance values of single films (PLA, CNC, CNC-Rosin, CNF, CNF-Rosin) and corresponding multi-layered materials

Figure III. 17 shows photographs of prepared films of modified CNC-Rosin (**Figure III. 17 a)**) and modified CNF-Rosin (**Figure III. 17 b)**) and highlights their self-standing and transparency properties. The transmittance values of multi-layers indicate that their transparency decreases by incorporating a PLA, CNC or CNC-Rosin layer between two PLA films. The transmittances of TML-PLA, TML-CNC and TML-CNC-Rosin are very close and equal to 47%, 47%, and 50%, respectively. Despite the lower transmittance values of CNC-based films compared to pure PLA film, the incorporation of the nanocellulosic films does not influence the entire multi-layered material transmittance. However, by incorporating a CNF or CNF-Rosin layer in the multi-layered system, transmittance slightly increases up to 21% and 17%, respectively. This result could be explained by the fact that the pores present in both CNF and CNF-Rosin films are closed and covered by transparent PLA during the heat-pressing procedure, leading to an increase in the transparency. Meriçer *et al.*⁸⁷ combined one layer of PLA with a top layer of CNF through a casting procedure, and reported a similar trend in the transmittance values. For food packaging applications, transparency of materials is essential for aesthetic, marketing, and consumer satisfaction, as often mentioned in the literature related to this topic^{37,38}.

The mechanical properties of both single- and multi-layered materials were also investigated. The values of Young's modulus E are presented in **Figure III. 18**.

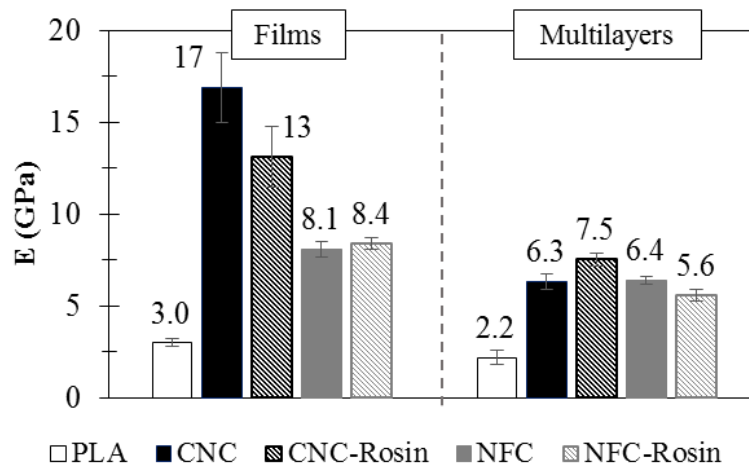


Figure III. 18. Young's modulus values measured on single films (PLA, CNC, CNC-Rosin, CNF, CNF-Rosin) and corresponding multi-layered materials

According to these values, commercial PLA film exhibits a Young's modulus equal to 3.0 GPa. Although this value is highly dependent on the type of PLA and its processing, it is consistent with the literature values^{4,5}. Young's modulus of CNC and CNF films is not affected by the presence of adsorbed rosin nanoparticles at the nanocelluloses surface. In fact, from the values presented in **Figure III. 18**, Young's modulus of CNC and CNC-Rosin is equal to 17 GPa and 13 GPa, respectively, and CNF and CNF-Rosin have the modulus equal to 8.1 GPa and 8.4 GPa, respectively. These values are consistent with the values found in the literature for CNF films, although the values obtained for the CNC films are somewhat higher^{10,105-107}. Note that these values are highly linked to the nature of the nanocelluloses, as well as to their dispersion and orientation. Nevertheless, Young's modulus values of multi-layered materials are lower than those of corresponding single films, probably due to the heat-pressing process inducing some defects in the material structure and thus a relative fragility, as suggested by SEM images in **Figure III. 16**. However, the presence of nanocellulosic film between the two PLA sheets clearly improves the final mechanical properties. In fact, in each case, Young's modulus of the multi-layered material (TML-CNC, TML-CNC-Rosin, TML-CNF or TML-CNF-Rosin) is at least 2.5 times higher than the modulus of the TML-PLA sample. It can be explained by the higher Young's modulus of the inner nanocellulosic layer compared to the pure PLA film, or by the relatively good adhesion between the three layers.

The evaluation of the mechanical properties is crucial when thinking about packaging applications, and especially food packaging, since one of the purposes of the food packaging material is to protect the product during its transportation and handling, while ensuring its mechanical integrity until it reaches the consumer^{88,108}.

3.2.2. Barrier and antioxidant properties

Still focusing on food packaging applications, barrier properties of the multi-layered materials (TML), as well as, those of the commercial PLA film, were investigated. Values of oxygen and water vapor permeability are presented in **Figure III. 19**. As expected, CNC and CNF films have a high barrier against oxygen (with values equal to 0.02 and $0.01 \times 10^{18} \text{ m}^3.\text{m}/\text{m}^2.\text{s}.\text{Pa}$, respectively) but low barrier towards water vapor (with values equal to 8.9 ± 0.3 and $14.3 \pm 0.2 \times 10^{16} \text{ kg}.\text{m}/\text{m}^2.\text{s}.\text{Pa}$, for CNC and CNF films, respectively). These values are expected for such nanocelluloses. In fact, the dense and entangled network of nanomaterials created in the dry films causes their high oxygen barrier properties, whereas their hydrophilic behavior explains their high water vapor transmission rate. Furthermore, a commercial single PLA film - different from the one used in the preparation strategy for wet multi-layered materials - exhibits an oxygen and water vapor permeability equal to $1.8 \times 10^{18} \text{ m}^3.\text{m}/\text{m}^2.\text{s}.\text{Pa}$ and $3.7 \pm 0.4 \times 10^{16} \text{ kg}.\text{m}/\text{m}^2.\text{s}.\text{Pa}$, respectively, which is consistent with values found in literature^{4,6}. The water vapor permeability value is still much higher in this study, which can be linked to the degradation of the commercial PLA in ambient conditions since its purchase (two years ago).

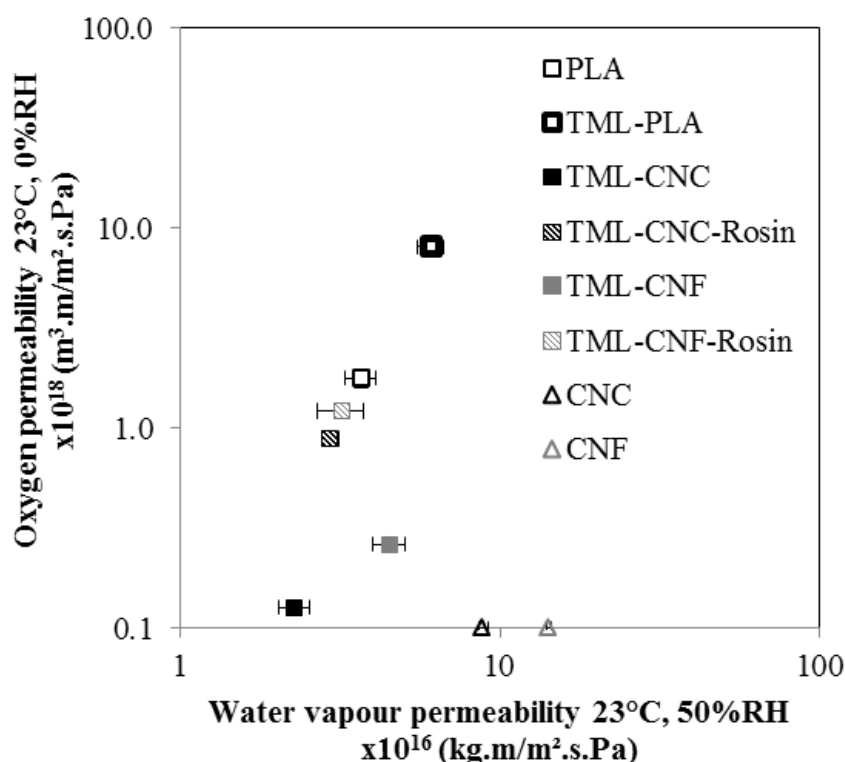


Figure III. 19. Oxygen and water vapor permeability of neat commercial PLA film, and multi-layered materials with PLA, CNC, CNC-Rosin, CNF, and CNF-Rosin films as inner layers (TML-PLA, TML-CNC, TML-CNC-Rosin, TML-CNF, and TML-CNF-Rosin, respectively)

As seen in **Figure III. 19**, oxygen and water vapor permeability values of multi-layered TML-PLA material increased to $8.1 \times 10^{18} \text{ m}^3.\text{m}/\text{m}^2.\text{s}.\text{Pa}$ and $6.1 \times \pm 0.6 \times 10^{16} \text{ kg}.\text{m}/\text{m}^2.\text{s}.\text{Pa}$, respectively. This increase is attributed to the heat-pressing process, during which some cracks or pores are created in the materials, inducing a preferential path for both oxygen and water vapor molecules. PLA crystallinity

might also be influenced by the heat-pressing step. The presence of a nanocellulosic layer between the two PLA films clearly decreases the oxygen permeability of the multi-layered materials. Indeed, TML-CNC and TML-CNF exhibit an oxygen permeability equal to $0.1 \times 10^{18} \text{ m}^3 \cdot \text{m} / \text{m}^2 \cdot \text{s} \cdot \text{Pa}$ and $0.3 \times 10^{18} \text{ m}^3 \cdot \text{m} / \text{m}^2 \cdot \text{s} \cdot \text{Pa}$, respectively. The oxygen permeability is thus reduced by 80 and 27 times, respectively, which is highly promising. However, the presence of rosin on the nanocellulose surface seems to increase these values up to $0.9 \times 10^{18} \text{ m}^3 \cdot \text{m} / \text{m}^2 \cdot \text{s} \cdot \text{Pa}$ and $1.2 \times 10^{18} \text{ m}^3 \cdot \text{m} / \text{m}^2 \cdot \text{s} \cdot \text{Pa}$, for TML-CNC-Rosin and TML-CNF-Rosin, respectively. This increase in oxygen permeability after the adsorption of rosin onto nanocellulosic materials could screen the hydrogen interactions, resulting in the spacing of the nanocrystals or the nanofibrils away from each other, and thus inducing a more porous cellulosic structure. The values obtained for water vapor permeability are equal to 2.3 ± 0.2 , 2.9 ± 0.2 , 4.5 ± 0.5 , and $3.2 \pm 0.5 \times 10^{16} \text{ kg} \cdot \text{m} / \text{m}^2 \cdot \text{s} \cdot \text{Pa}$, for TML-CNC, TML-CNC-Rosin, TML-CNF, and TML-CNF-Rosin, respectively. Water vapor permeability is enhanced in both cases with the introduction of nanocelluloses in the materials, compared to TML-PLA material, although any trend can be drawn for the presence of rosin in the sample. In addition, as the molecules composing the gum rosin mixture (previously detailed in **Chapter II.4**) are hydrophilic, their presence in both TML-CNC-Rosin and TML-CNF-Rosin should not positively influence the barrier properties against water vapor.

However, it is interesting to position the multi-layered materials prepared in this study in relation to the polymers classically used in food packaging industry, as shown in **Figure III. 20**. Note that in **Figure III. 20**, neither oxygen and nor water vapor permeability values are normalized with respect to their thickness, unlike what has been done for values presented in **Figure III. 19**. These are not permeability but transmission rate. Moreover, values of oxygen permeability were measured at 0% RH, whereas all other materials in **Figure III. 20** were characterized at 50% RH. However, since only a general trend is required here, this does not affect the conclusions made from this **Figure III. 20**. As expected and observed in the previous part (see **Figure III. 14**), the commercial PLA film used in this part is not a strong enough barrier against oxygen and water vapor to compete with the other synthetic polymers, in terms of the food packaging applications requirements.

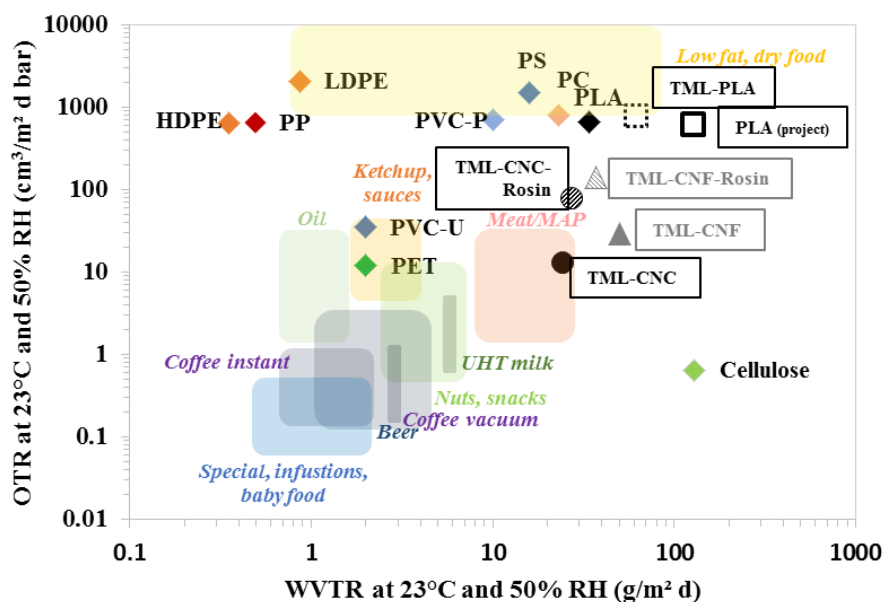


Figure III. 20. Oxygen and water vapor permeability values required for food packaging materials according to specific foodstuffs and TML multi-layered materials (TML-PLA, TML-CNC, TML-CNC-Rosin, TML-CNF, and TML-CNF-Rosin) positioning (adapted from ⁹⁸)

Moreover, the multi-layered TML-PLA material — prepared with an inner PLA layer — exhibits somewhat interesting properties which are, in fact, close to those required for a packaging of low fat and dry food. The multi-layered materials prepared with a nanocellulosic inner layer come closer, in terms of barrier properties, to meat packaging materials. However, only the material containing a neat CNC casted film (TML-CNC) could be used as such a meat packaging material. Other materials (TML-CNC-Rosin, TML-CNF, and TML-CNF-Rosin) are not a strong enough barrier towards oxygen and water vapor, although they could also be used as materials for low fat and dry food packaging. In addition, it could be highly interesting to investigate the sorption properties of the materials containing rosins in relation to aromatic compounds. Indeed, the presence of aromatic groups brought by rosin molecules could interact with aromatic rings of volatile compounds⁹⁹, and so enhance some specific sorption properties, interesting for special food packaging applications, as already studied in the literature¹⁰⁹.

In addition to their antimicrobial properties, widely demonstrated in the literature^{110,111}, antioxidant properties of natural rosins was investigated. Indeed, oxidation is one of the main degradation processes occurring during food degradation. Several methods exist to characterize this antioxidant activity, as presented in the review of Gomez-Estaca *et al.*¹¹². Among these methods, the DPPH assay is classically used to determine the efficiency of antioxidant-active materials, as previously detailed in part 2.4.9. Crouvisier-Urion *et al.*⁹⁴ performed the DPPH assay on chitosan/lignin composites films. Lignin is a known antioxidant compound, and the authors investigated the kinetics of the radical scavenging activity (RSA) of the films. They found that, for any antioxidant compound, RSA kinetics always decreases and generally reaches a plateau, with the value of this plateau a characteristic of the

antioxidant. In our study, a similar protocol as that proposed by Crouvisier-Urion *et al.*⁹⁴ was performed on commercial rosins, for the first time. In **Figure III. 21**, the RSA evolution of the rosins is plotted as a function of time, reaching a plateau leading to up to 90% decrease in the DPPH radical. It highlights the high antioxidant capacity of the rosin mixture.

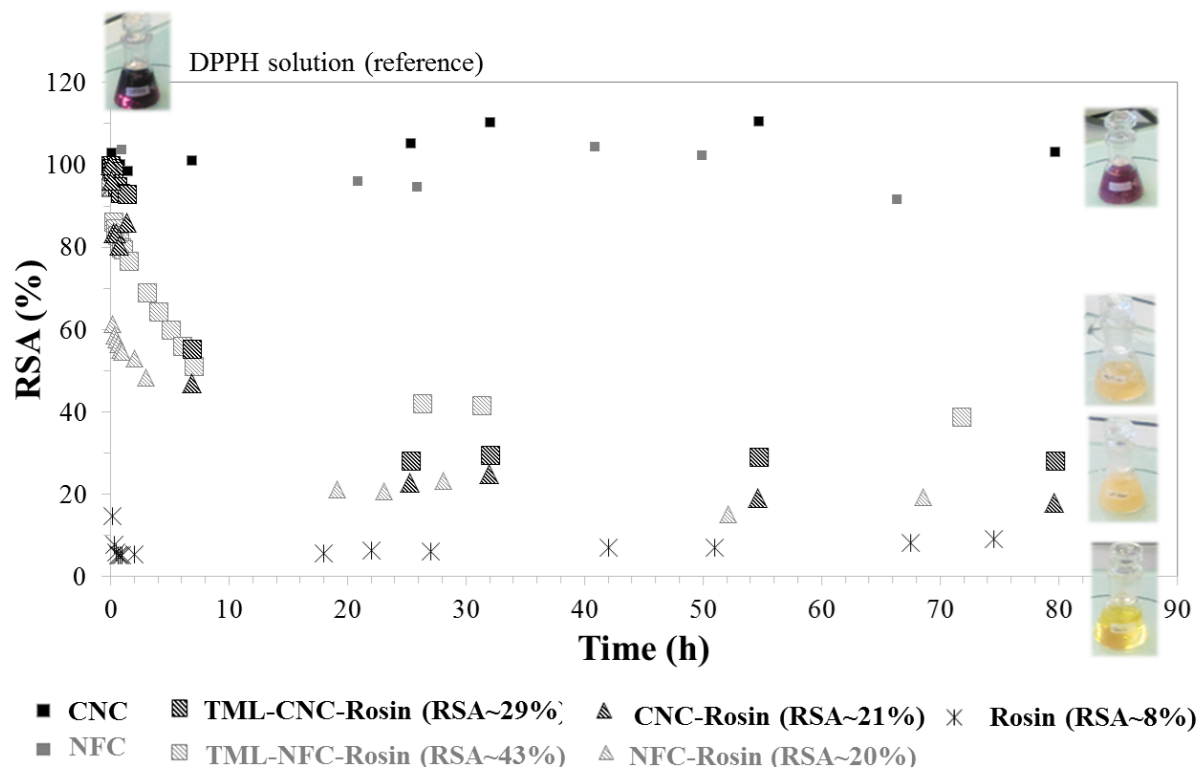


Figure III. 21. Evolution of the radical scavenging activity (RSA) as a function of time for different samples: neat CNC and CNF films, CNC-Rosin and CNF-Rosins films, TML-CNC-Rosin and TML-CNF-Rosin, and a rosin mixture

Moreover, the DPPH test was then performed on neat CNC, neat CNF, modified CNC-Rosin, and modified CNF-Rosin films, as well as, on TML-CNC-Rosin and TML-CNF-Rosin multi-layered materials. The resulted RSA kinetics are plotted as a function of time in **Figure III. 21**. The antioxidant capacity of CNC-Rosin and CNF-Rosin films is clearly observed, with the RSA value at the plateau equal to 21% and 20%, respectively. The CNC and CNF films were studied as a negative reference, and the observed unstable values can be directly linked to the fact that nanocellulose films were slightly disintegrated in the ethanol medium. However, it is noteworthy that neither CNC nor CNF exhibit any antioxidant capacity, as expected. In this sense, it is assumed that rosin nano-emulsion present in CNC-Rosin and CNF-Rosin films are still active against oxidation. Multi-layered materials TML-CNC-Rosin and TML-CNF-Rosin were also analyzed through the DPPH test. This experiment may be controversial and need some further explanations. Indeed, in DPPH assay, antioxidant compounds need to be in direct contact with radicals. An additional DPPH test was performed on samples fully sealed (no direct contact between the inner layer and the DPPH solution), and no significant decrease in RSA was observed. In this experiment, the inner cellulosic layer of the multi-layered materials is in direct contact with the DPPH solution, leading to the RSA values at the

plateau equal to 29% and 43% for TML-CNC-Rosin and TML-CNF-Rosin samples, respectively. These results highlight the activity of the rosin nanoparticles inside the multi-layered materials. However, it is difficult to deduce anything about the possible migration of the rosin nanoparticles through the films. Future release experiments should be performed on TML-CNC-Rosin and TML-CNF-Rosin samples, as well as on CNC-Rosin and CNF-Rosin films, to determine whether the antioxidant properties are due to the surface activity of the films or not. Moreover, according to the type of application, different antioxidant phenomena can be envisaged. Nevertheless, at this stage of the study, it can be assumed that TML-CNC-Rosin and TML-CNF-Rosin films are antioxidants by direct contact with the inner layer, which emphasizes the role of rosin nanoparticles in the films. Although they do not significantly influence the barrier properties against oxygen and water vapor molecules, they bring the antioxidant behavior to the prepared films, which is highly sought after for many food packaging applications. In addition, to go further in the characterization of all the multi-layered materials presented in this study, it would be interesting to investigate the possible phenomena of release and migrations of molecules from the materials, which are very critical for the elaboration of food packaging materials.

4. Conclusion

This study highlights two different effective methods for the development of PLA-based multi-layered materials containing different amounts of cellulosic nanostructures. The first method, consisting of the wet deposition of a modified CNC aqueous suspension on a PLA substrate, and following by the heat-pressing with another PLA film, allows concluding on the positive influence of even a very thin layer of CNC inside the material on the final barrier properties towards both oxygen and water vapor. The second method, consisting of the complexing of a dry CNC or CNF self-standing film modified with natural rosins by heat-pressing between two PLA sheets, clearly shows a significant improvement in oxygen barrier properties of the multi-layered materials. Moreover, presence of rosin nanoparticles in the inner cellulosic layer provides antioxidant properties to the materials. These two procedures make it possible to incorporate nanocelluloses – modified or not – into a PLA matrix quickly and easily, which opens the way to the development of hybrid-materials containing nanostructures and active compounds for, among others, food packaging applications.

Conclusions of Chapter III

The aim of the **Chapter III** was the elaboration of poly(lactic acid)-based materials including designed nanocelluloses (previously described in the Chapter II) for final food packaging applications. Two main different strategies were thus developed, and related materials were characterized.

- In the first section **III.1**, nanocomposites were produced at laboratory scale by introducing, at different charge contents, the modified CNC-PGMA-Br (described in Chapter II.1) and CNC-Lauric (described in Chapter II.2.2) in a PLA matrix, by solvent casting method. As detailed in the Chapter I, the dispersion of CNCs in a hydrophobic polymeric matrix is still a huge challenge. In this sense, the morphology of the PLA_CNC-PGMA-Br and PLA_CNC-Lauric nanocomposite materials was investigated by SEM and TEM. In both cases, the dispersion of nanofillers was enhanced, although the two samples exhibited different morphologies. In the case of PLA_CNC-PGMA-Br, a distinct network was clearly observed and related to the possible reaction between still reactive epoxy groups on polymerized CNC-PGMA-Br and hydroxyl groups present at the ends of PLA chains. On the other hand, hydrophobic behavior of CNC-Lauric seemed to clearly better enhance their dispersion in the PLA matrix. Furthermore, all the nanocomposites exhibited an improvement in the barrier properties towards oxygen and water vapor, with , respectively, the best reached decreasing equal to 40% and 80%, respectively, for the PLA_CNC-PGMA-Br (with 10 wt% of charge content). These barrier properties are encouraging, especially for what the development of biobased food packaging materials concerns.

- In the section **III.2**, another strategy was proposed for the preparation of materials based on both nanocelluloses and PLA. In fact, multi-layered materials were produced, with an inner layer composed of nanocelluloses — namely CNC-1-M-3-PP (described in Chapter II.3) and CNC-Rosin or CNF-Rosin (described in Chapter II.4) — previously modified with active molecules. Two routes were exposed for the introduction of the cellulosic layer: by coating (leading to a thin layer) or by complexing with a thicker dried film of nanocellulose. In both cases, final materials exhibited a decrease in oxygen permeability close to 90% (compared to the multi-layered PLA-PLA-PLA as reference). The decreasing in water vapor permeability of 50% was lower but also significant, and these barrier properties are highly encouraging. Moreover, the introduction of active molecules was carried out *via* their attachment (covalent or not) to the nanocelluloses. In fact, the antioxidant properties of rosins adsorbed on the CNC-Rosin or CNF-Rosin was found in the final multi-layered materials. Finally, the proposed multi-layered strategy allows the introduction of a huge panel of active molecules, and thus opens the way to the production of barrier and active food packaging materials.

The **Table III. 7** summarizes the different materials prepared and presented in the **Chapter III**, as well as, their processing method, and the decrease in both oxygen and water vapor permeability determined for each samples.

Chapter	Strategy	Method	Designed nanostructures	Barrier properties	
				Decrease in oxygen permeability (%)	Decrease in water vapor permeability (%)
III.1	PLA-based nanocomposites	Solvent Casting	CNC-PGMA-Br_1h (Section II.1)	10% or 40% (charge content: 5 or 10 wt%)	50% or 80% (charge content: 5 or 10 wt%)
			CNC-Lauric (Section II.2.2)	10% (charge content: 5 wt% or 10 wt%)	/
III.2	PLA-based multi-layered materials	Coating + Heat-pressing	CNC-1-M-3-PP (Section II.3)	90%	50%
		Dried films + Heat-pressing	CNF-Rosin and CNC-Rosin (Section II.4)	90% (for both CNC-Rosin and CNF-Rosin)	50% (for both CNC-Rosin and CNF-Rosin)

Table III. 7. Summary of the different final PLA-based materials presented in the Chapter III, and corresponding oxygen and water vapor barrier properties improvement

References – Chapter III

1. Kelly, A. Composites in context. *Composites Science and Technology* **23**, 171–199 (1985).
2. Thostenson, E. T., Li, C. & Chou, T.-W. Nanocomposites in context. *Composites Science and Technology* **65**, 491–516 (2005).
3. Winey, K. I. & Vaia, R. A. Polymer Nanocomposites. *MRS Bulletin* **32**, 314–322 (2007).
4. Castro-Aguirre, E., Iñiguez-Franco, F., Samsudin, H., Fang, X. & Auras, R. Poly(lactic acid)—Mass production, processing, industrial applications, and end of life. *Advanced Drug Delivery Reviews* **107**, 333–366 (2016).
5. Garlotta, D. A Literature Review of Poly(Lactic Acid). *Journal of Polymers and the Environment* **9**, 63–84 (2001).
6. Colomines, G., Ducruet, V., Courgneau, C., Guinault, A. & Domenek, S. Barrier properties of poly(lactic acid) and its morphological changes induced by aroma compound sorption. *Polymer International* **59**, 818–826 (2010).
7. Cabedo, L., Feijoo, J. L., Villanueva, M. P., Lagarón, J. M. & Giménez, E. Optimization of Biodegradable Nanocomposites Based on aPLA/PCL Blends for Food Packaging Applications. *Macromolecular Symposia* **233**, 191–197 (2006).
8. Thellen, C. *et al.* Influence of montmorillonite layered silicate on plasticized poly(l-lactide) blown films. *Polymer* **46**, 11716–11727 (2005).
9. Bouakaz, B. S., Pillin, I., Habi, A. & Grohens, Y. Synergy between fillers in organomontmorillonite/graphene–PLA nanocomposites. *Applied Clay Science* **116–117**, 69–77 (2015).
10. Dufresne, A. *Nanocellulose: from nature to high performance tailored materials*. (Walter de Gruyter GmbH & Co KG, 2017).
11. Scaffaro, R., Botta, L., Lopresti, F., Maio, A. & Sutera, F. Polysaccharide nanocrystals as fillers for PLA based nanocomposites. *Cellulose* **24**, 447–478 (2017).
12. Kargarzadeh, H. *et al.* Recent developments on nanocellulose reinforced polymer nanocomposites: A review. *Polymer* **132**, 368–393 (2017).
13. Kargarzadeh, H. *et al.* Recent developments in nanocellulose-based biodegradable polymers, thermoplastic polymers, and porous nanocomposites. *Progress in Polymer Science* **87**, 197–227 (2018).
14. Pracella, M., Haque, Md. M.-U. & Puglia, D. Morphology and properties tuning of PLA/cellulose nanocrystals bio-nanocomposites by means of reactive functionalization and blending with PVAc. *Polymer* **55**, 3720–3728 (2014).
15. Yang, W., Dominici, F., Fortunati, E., M. Kenny, J. & Puglia, D. Melt free radical grafting of glycidyl methacrylate (GMA) onto fully biodegradable poly(lactic) acid films: effect of cellulose nanocrystals and a masterbatch process. *RSC Advances* **5**, 32350–32357 (2015).
16. Bondeson, D. & Oksman, K. Dispersion and characteristics of surfactant modified cellulose whiskers nanocomposites. *Composite Interfaces* **14**, 617–630 (2007).
17. Mariano, M. *et al.* Preparation of Cellulose Nanocrystal-Reinforced Poly(lactic acid) Nanocomposites through Noncovalent Modification with PLLA-Based Surfactants. *ACS Omega* **2**, 2678–2688 (2017).
18. Xu, C. *et al.* Polylactide/acetylated nanocrystalline cellulose composites prepared by a continuous route: A phase interface-property relation study. *Carbohydrate Polymers* **146**, 58–66 (2016).
19. Bitinis, N. *et al.* Poly(lactic acid)/natural rubber/cellulose nanocrystal bionanocomposites Part I. Processing and morphology. *Carbohydrate Polymers* **96**, 611–620 (2013).

20. Zhou, C. *et al.* Electrospun Bio-Nanocomposite Scaffolds for Bone Tissue Engineering by Cellulose Nanocrystals Reinforcing Maleic Anhydride Grafted PLA. *ACS Appl. Mater. Interfaces* **5**, 3847–3854 (2013).
21. Robles, E., Urruzola, I., Labidi, J. & Serrano, L. Surface-modified nano-cellulose as reinforcement in poly(lactic acid) to conform new composites. *Industrial Crops and Products* **71**, 44–53 (2015).
22. Espino-Pérez, E. *et al.* Designed cellulose nanocrystal surface properties for improving barrier properties in polylactide nanocomposites. *Carbohydrate Polymers* **183**, 267–277 (2018).
23. Spinella, S. *et al.* Polylactide/cellulose nanocrystal nanocomposites: Efficient routes for nanofiber modification and effects of nanofiber chemistry on PLA reinforcement. *Polymer* **65**, 9–17 (2015).
24. Freire, C. S. R., Silvestre, A. J. D., Neto, C. P., Belgacem, M. N. & Gandini, A. Controlled heterogeneous modification of cellulose fibers with fatty acids: Effect of reaction conditions on the extent of esterification and fiber properties. *Journal of Applied Polymer Science* **100**, 1093–1102 (2006).
25. Habibi, Y., Aouadi, S., Raquez, J.-M. & Dubois, P. Effects of interfacial stereocomplexation in cellulose nanocrystal-filled polylactide nanocomposites. *Cellulose* **20**, 2877–2885 (2013).
26. Lizundia, E. *et al.* PLLA-grafted cellulose nanocrystals: Role of the CNC content and grafting on the PLA bionanocomposite film properties. *Carbohydrate Polymers* **142**, 105–113 (2016).
27. Miao, C. & Hamad, W. Y. In-situ polymerized cellulose nanocrystals (CNC)-poly(l-lactide) (PLLA) nanomaterials and applications in nanocomposite processing. *Carbohydrate Polymers* **153**, 549–558 (2016).
28. Lin, N., Chen, G., Huang, J., Dufresne, A. & Chang, P. R. Effects of polymer-grafted natural nanocrystals on the structure and mechanical properties of poly(lactic acid): A case of cellulose whisker-graft-polycaprolactone. *Journal of Applied Polymer Science* **113**, 3417–3425 (2009).
29. Sun, S., Zhang, M., Zhang, H. & Zhang, X. Polylactide toughening with epoxy-functionalized grafted acrylonitrile–butadiene–styrene particles. *Journal of Applied Polymer Science* **122**, 2992–2999 (2011).
30. Juntuek, P., Ruksakulpiwat, C., Chumsamrong, P. & Ruksakulpiwat, Y. Effect of glycidyl methacrylate-grafted natural rubber on physical properties of polylactic acid and natural rubber blends. *Journal of Applied Polymer Science* **125**, 745–754 (2012).
31. Yang, W., Fortunati, E., Dominici, F., Kenny, J. M. & Puglia, D. Effect of processing conditions and lignin content on thermal, mechanical and degradative behavior of lignin nanoparticles/polylactic (acid) bionanocomposites prepared by melt extrusion and solvent casting. *European Polymer Journal* **71**, 126–139 (2015).
32. Fortunati, E. *et al.* Lignocellulosic nanostructures as reinforcement in extruded and solvent casted polymeric nanocomposites: an overview. *European Polymer Journal* **80**, 295–316 (2016).
33. Oksman, K. *et al.* Review of the recent developments in cellulose nanocomposite processing. *Composites Part A: Applied Science and Manufacturing* **83**, 2–18 (2016).
34. Yang, W. *et al.* Synergic effect of cellulose and lignin nanostructures in PLA based systems for food antibacterial packaging. *European Polymer Journal* **79**, 1–12 (2016).
35. Fortunati, E. *et al.* Processing of PLA nanocomposites with cellulose nanocrystals extracted from *Posidonia oceanica* waste: Innovative reuse of coastal plant. *Industrial Crops and Products* **67**, 439–447 (2015).
36. Chi, K. & Catchmark, J. M. Enhanced dispersion and interface compatibilization of crystalline nanocellulose in polylactide by surfactant adsorption. *Cellulose* **24**, 4845–4860 (2017).
37. Arrieta, M. P., Samper, M. D., Aldas, M. & López, J. On the Use of PLA-PHB Blends for Sustainable Food Packaging Applications. *Materials* **10**, 1008 (2017).

38. Cerqueira, M. A. P. R., Lagaron, J. M., Castro, L. M. P. & de Oliveira Soares, A. A. M. *Nanomaterials for food packaging: materials, processing technologies and safety issues*. (Elsevier, **2018**).
39. Sullivan, E. M., Moon, R. J. & Kalaitzidou, K. Processing and Characterization of Cellulose Nanocrystals/Poly(lactic acid) Nanocomposite Films. *Materials* **8**, 8106–8116 (**2015**).
40. Wang, Y., Chen, K., Xu, C. & Chen, Y. Supertoughened Biobased Poly(lactic acid)–Epoxidized Natural Rubber Thermoplastic Vulcanizates: Fabrication, Co-continuous Phase Structure, Interfacial in Situ Compatibilization, and Toughening Mechanism. *J. Phys. Chem. B* **119**, 12138–12146 (**2015**).
41. Rigotti, D. *et al.* Poly(lactic acid)-lauryl functionalized nanocellulose nanocomposites: Microstructural, thermo-mechanical and gas transport properties. *Express Polym. Lett.* **13**, 858–876 (**2019**).
42. Dong, F., Yan, M., Jin, C. & Li, S. Characterization of Type-II Acetylated Cellulose Nanocrystals with Various Degree of Substitution and Its Compatibility in PLA Films. *Polymers* **9**, 346 (**2017**).
43. Shojaeiarani, J., Bajwa, D. S. & Stark, N. M. Green esterification: A new approach to improve thermal and mechanical properties of poly(lactic acid) composites reinforced by cellulose nanocrystals. *Journal of Applied Polymer Science* **135**, 46468 (**2018**).
44. Bagheriasl, D., Carreau, P. J., Riedl, B., Dubois, C. & Hamad, W. Y. Shear rheology of poly(lactide) (PLA)–cellulose nanocrystal (CNC) nanocomposites. *Cellulose* **23**, 1885–1897 (**2016**).
45. Xu, S., Girouard, N., Schueneman, G., Shofner, M. L. & Meredith, J. C. Mechanical and thermal properties of waterborne epoxy composites containing cellulose nanocrystals. *Polymer* **54**, 6589–6598 (**2013**).
46. Kaboorani, A., Auclair, N., Riedl, B. & Landry, V. Physical and morphological properties of UV-cured cellulose nanocrystal (CNC) based nanocomposite coatings for wood furniture. *Progress in Organic Coatings* **93**, 17–22 (**2016**).
47. Kamal, M. R. & Khoshkava, V. Effect of cellulose nanocrystals (CNC) on rheological and mechanical properties and crystallization behavior of PLA/CNC nanocomposites. *Carbohydrate Polymers* **123**, 105–114 (**2015**).
48. Azizi Samir, M. A. S., Alloin, F. & Dufresne, A. Review of Recent Research into Cellulosic Whiskers, Their Properties and Their Application in Nanocomposite Field. *Biomacromolecules* **6**, 612–626 (**2005**).
49. Jonoobi, M., Harun, J., Mathew, A. P. & Oksman, K. Mechanical properties of cellulose nanofiber (CNF) reinforced poly(lactic acid) (PLA) prepared by twin screw extrusion. *Composites Science and Technology* **70**, 1742–1747 (**2010**).
50. Miao, C. & Hamad, W. Y. Cellulose reinforced polymer composites and nanocomposites: a critical review. *Cellulose* **20**, 2221–2262 (**2013**).
51. Ferreira, F. V. *et al.* How do cellulose nanocrystals affect the overall properties of biodegradable polymer nanocomposites: A comprehensive review. *European Polymer Journal* **108**, 274–285 (**2018**).
52. Fortunati, E. *et al.* Multifunctional bionanocomposite films of poly(lactic acid), cellulose nanocrystals and silver nanoparticles. *Carbohydrate Polymers* **87**, 1596–1605 (**2012**).
53. Guinault, A., Sollogoub, C., Domenek, S., Grandmontagne, A. & Ducruet, V. Influence of crystallinity on gas barrier and mechanical properties of PLA food packaging films. *Int J Mater Form* **3**, 603–606 (**2010**).

54. Zid, S., Zinet, M. & Espuche, E. Modeling diffusion mass transport in multiphase polymer systems for gas barrier applications: A review. *J. Polym. Sci. Part B: Polym. Phys.* **56**, 621–639 (2018).
55. Nielsen, L. E. Models for the Permeability of Filled Polymer Systems. *Journal of Macromolecular Science: Part A - Chemistry* 929–942 (1967).
56. Duan, Z., Thomas, N. L. & Huang, W. Water vapour permeability of poly(lactic acid) nanocomposites. *Journal of Membrane Science* **445**, 112–118 (2013).
57. Sung, S. H., Chang, Y. & Han, J. Development of polylactic acid nanocomposite films reinforced with cellulose nanocrystals derived from coffee silverskin. *Carbohydrate Polymers* **169**, 495–503 (2017).
58. Follain, N. *et al.* Water transport properties of bio-nanocomposites reinforced by *Luffa cylindrica* cellulose nanocrystals. *Journal of Membrane Science* **427**, 218–229 (2013).
59. Fortunati, E. *et al.* Effects of modified cellulose nanocrystals on the barrier and migration properties of PLA nano-biocomposites. *Carbohydrate Polymers* **90**, 948–956 (2012).
60. Espino-Pérez, E. *et al.* Influence of chemical surface modification of cellulose nanowhiskers on thermal, mechanical, and barrier properties of poly(lactide) based bionanocomposites. *European Polymer Journal* **49**, 3144–3154 (2013).
61. Turbak, A. F., Snyder, F. W. & Sandberg, K. R. Microfibrillated cellulose, a new cellulose product: properties, uses, and commercial potential. *J. Appl. Polym. Sci.: Appl. Polym. Symp.; (United States)* **37**, (1983).
62. Pääkkö, M. *et al.* Enzymatic Hydrolysis Combined with Mechanical Shearing and High-Pressure Homogenization for Nanoscale Cellulose Fibrils and Strong Gels. *Biomacromolecules* **8**, 1934–1941 (2007).
63. Josset, S. *et al.* Energy consumption of the nanofibrillation of bleached pulp, wheat straw and recycled newspaper through a grinding process. *Nordic Pulp & Paper Research Journal* **29**, 167–175 (2014).
64. Rol, F., Belgacem, M. N., Gandini, A. & Bras, J. Recent advances in surface-modified cellulose nanofibrils. *Progress in Polymer Science* **88**, 241–264 (2019).
65. Nechyporchuk, O., Belgacem, M. N. & Bras, J. Production of cellulose nanofibrils: A review of recent advances. *Industrial Crops and Products* **93**, 2–25 (2016).
66. Klemm, D. *et al.* Nanocelluloses: A New Family of Nature-Based Materials. *Angewandte Chemie International Edition* **50**, 5438–5466 (2011).
67. Abdul Khalil, H. P. S. *et al.* Production and modification of nanofibrillated cellulose using various mechanical processes: A review. *Carbohydrate Polymers* **99**, 649–665 (2014).
68. Lavoine, N., Desloges, I., Dufresne, A. & Bras, J. Microfibrillated cellulose – Its barrier properties and applications in cellulosic materials: A review. *Carbohydrate Polymers* **90**, 735–764 (2012).
69. Brodin, F. W., Gregersen, Ø. W. & Syverud, K. Cellulose nanofibrils: Challenges and possibilities as a paper additive or coating material – A review. *Nordic Pulp & Paper Research Journal* **29**, 156–166 (2014).
70. Hoeng, F., Denneulin, A. & Bras, J. Use of nanocellulose in printed electronics: a review. *Nanoscale* **8**, 13131–13154 (2016).
71. Jorfi, M. & Foster, E. J. Recent advances in nanocellulose for biomedical applications. *Journal of Applied Polymer Science* **132**, 41719–41738 (2015).
72. Ranby, B. G. Fibrous macromolecular systems. Cellulose and muscle. The colloidal properties of cellulose micelles. *Discuss. Faraday Soc.* **11**, 158–164 (1951).
73. Ranby, B. G. & Ribí, E. Über den feinbau der zellulose. *Experientia* **6**, 12–14 (1950).

74. ISO/TC 6/TG 1 - Cellulose Nanomaterials. *Summary of International Activities on Cellulose Nanomaterials* (2017).
75. Cranston, E. Overview of Canada. In *TAPPI Nano Division Conference* (Chiba, Japan, 2019).
76. Habibi, Y., Lucia, L. A. & Rojas, O. J. Cellulose Nanocrystals: Chemistry, Self-Assembly, and Applications. *Chemical Reviews* **110**, 3479–3500 (2010).
77. Natterodt, J. C., Petri-Fink, A., Weder, C. & Zoppe, J. O. Cellulose Nanocrystals: Surface Modification, Applications and Opportunities at Interfaces. *CHIMIA International Journal for Chemistry* **71**, 376–383 (2017).
78. Domingues, R. M. A., Gomes, M. E. & Reis, R. L. The Potential of Cellulose Nanocrystals in Tissue Engineering Strategies. *Biomacromolecules* **15**, 2327–2346 (2014).
79. Lin, N. & Dufresne, A. Nanocellulose in biomedicine: Current status and future prospect. *European Polymer Journal* **59**, 302–325 (2014).
80. Csoka, L. *et al.* Piezoelectric Effect of Cellulose Nanocrystals Thin Films. *ACS Macro Lett.* **1**, 867–870 (2012).
81. Gaspar, D. *et al.* Nanocrystalline cellulose applied simultaneously as the gate dielectric and the substrate in flexible field effect transistors. *Nanotechnology* **25**, 094008 (2014).
82. Hubbe, M. A. *et al.* Nanocellulose in Thin Films, Coatings, and Plies for Packaging Applications: A Review. *BioResources* **12**, 2143–2233 (2017).
83. Mariano, M., Kissi, N. E. & Dufresne, A. Cellulose nanocrystals and related nanocomposites: Review of some properties and challenges. *Journal of Polymer Science Part B: Polymer Physics* **52**, 791–806 (2014).
84. Fiori, S. *Industrial Uses of PLA*. In: *Polymer Chemistry Series* (eds. Jiménez, A., Peltzer, M. & Ruseckaite, R.) (Royal Society of Chemistry, 2014).
85. Lin, N. & Dufresne, A. Physical and/or Chemical Compatibilization of Extruded Cellulose Nanocrystal Reinforced Polystyrene Nanocomposites. *Macromolecules* **46**, 5570–5583 (2013).
86. Aulin, C., Karabulut, E., Tran, A., Wågberg, L. & Lindström, T. Transparent Nanocellulosic Multilayer Thin Films on Polylactic Acid with Tunable Gas Barrier Properties. *ACS Appl. Mater. Interfaces* **5**, 7352–7359 (2013).
87. Meriçer, Ç. *et al.* Atmospheric plasma assisted PLA/microfibrillated cellulose (MFC) multilayer biocomposite for sustainable barrier application. *Industrial Crops and Products* **93**, 235–243 (2016).
88. Hosseini, S. F., Javidi, Z. & Rezaei, M. Efficient gas barrier properties of multi-layer films based on poly(lactic acid) and fish gelatin. *International Journal of Biological Macromolecules* **92**, 1205–1214 (2016).
89. Yildirim, S. *et al.* Active Packaging Applications for Food. *Comprehensive Reviews in Food Science and Food Safety* **17**, 165–199 (2018).
90. Luzi, F. *et al.* Cellulose nanocrystals from *Actinidia deliciosa* pruning residues combined with carvacrol in PVA_CH films with antioxidant/antimicrobial properties for packaging applications. *International Journal of Biological Macromolecules* **104**, 43–55 (2017).
91. Missoum, K., Bras, J. & Belgacem, N. Method for forming a hydrophobic layer. *U.S. Patent Application No. 14/907, 326* (2016).
92. Bideau, B., Bras, J., Saini, S., Daneault, C. & Loranger, E. Mechanical and antibacterial properties of a nanocellulose-polypyrrole multilayer composite. *Materials Science and Engineering: C* **69**, 977–984 (2016).
93. Bideau, B., Bras, J., Adoui, N., Loranger, E. & Daneault, C. Polypyrrole/nanocellulose composite for food preservation: Barrier and antioxidant characterization. *Food Packaging and Shelf Life* **12**, 1–8 (2017).

94. Crouvisier-Urien, K. *et al.* Biobased Composite Films from Chitosan and Lignin: Antioxidant Activity Related to Structure and Moisture. *ACS Sustainable Chemistry & Engineering* **4**, 6371–6381 (2016).
95. Rocca-Smith, J. R. *et al.* Impact of corona treatment on PLA film properties. *Polymer Degradation and Stability* **132**, 109–116 (2016).
96. Li, F., Biagioni, P., Bollani, M., Maccagnan, A. & Piergiovanni, L. Multi-functional coating of cellulose nanocrystals for flexible packaging applications. *Cellulose* **20**, 2491–2504 (2013).
97. Sanchez-Garcia, M. D., Gimenez, E. & Lagaron, J. M. Morphology and barrier properties of solvent cast composites of thermoplastic biopolymers and purified cellulose fibers. *Carbohydrate Polymers* **71**, 235–244 (2008).
98. Schmid, M. *et al.* Properties of Whey-Protein-Coated Films and Laminates as Novel Recyclable Food Packaging Materials with Excellent Barrier Properties. *International Journal of Polymer Science* **2012**, 1–7 (2012).
99. Espino-Pérez, E. *et al.* Cellulose nanocrystal surface functionalization for the controlled sorption of water and organic vapours. *Cellulose* **23**, 2955–2970 (2016).
100. Sanyang, M. L., Sapuan, S. M., Jawaid, M., Ishak, M. R. & Sahari, J. Development and characterization of sugar palm starch and poly(lactic acid) bilayer films. *Carbohydrate Polymers* **146**, 36–45 (2016).
101. Pinto, A. M., Cabral, J., Tanaka, D. A. P., Mendes, A. M. & Magalhães, F. D. Effect of incorporation of graphene oxide and graphene nanoplatelets on mechanical and gas permeability properties of poly(lactic acid) films: Incorporation of GO and GNP in PLA films. *Polym. Int.* **62**, 33–40 (2013).
102. Beck, S., Bouchard, J., Chauve, G. & Berry, R. Controlled production of patterns in iridescent solid films of cellulose nanocrystals. *Cellulose* **20**, 1401–1411 (2013).
103. Lizundia, E., Urruchi, A., Vilas, J. L. & León, L. M. Increased functional properties and thermal stability of flexible cellulose nanocrystal/ZnO films. *Carbohydrate Polymers* **136**, 250–258 (2016).
104. Xiong, R. *et al.* Flexible, highly transparent and iridescent all-cellulose hybrid nanopaper with enhanced mechanical strength and writable surface. *Carbohydrate Polymers* **113**, 264–271 (2014).
105. Hänninen, A. *et al.* Nanocellulose and chitosan based films as low cost, green piezoelectric materials. *Carbohydrate Polymers* **202**, 418–424 (2018).
106. Reising, A. B., Moon, R. J. & Youngblood, J. P. Effect of particle Alignment on mechanical properties of neat cellulose nanocrystal films. *Journal of Science & Technology for Forest Products and Processes* **2**, 32–41 (2012).
107. Bras, J., Viet, D., Bruzzese, C. & Dufresne, A. Correlation between stiffness of sheets prepared from cellulose whiskers and nanoparticles dimensions. *Carbohydrate Polymers* **84**, 211–215 (2011).
108. Arora, A. & Padua, G. W. Review: Nanocomposites in Food Packaging. *Journal of Food Science* **75**, R43–R49 (2010).
109. Auras, R., Harte, B. & Selke, S. Sorption of ethyl acetate and d-limonene in poly(lactide) polymers. *Journal of the Science of Food and Agriculture* **86**, 648–656 (2006).
110. de Castro, D. O., Bras, J., Gandini, A. & Belgacem, N. Surface grafting of cellulose nanocrystals with natural antimicrobial rosin mixture using a green process. *Carbohydrate Polymers* **137**, 1–8 (2016).
111. Niu, X., Liu, Y., Song, Y., Han, J. & Pan, H. Rosin modified cellulose nanofiber as a reinforcing and co-antimicrobial agents in polylactic acid /chitosan composite film for food packaging. *Carbohydrate Polymers* **183**, 102–109 (2018).

112. Gómez-Estaca, J., López-de-Dicastillo, C., Hernández-Muñoz, P., Catalá, R. & Gavara, R. Advances in antioxidant active food packaging. *Trends in Food Science & Technology* **35**, 42–51 (2014).

General conclusions and perspectives

General conclusions and perspectives

This PhD project focused on the surface modification of cellulose nanocrystals (CNCs), in order to enhance their compatibilization with a hydrophobic poly(lactic acid) (PLA) matrix. The main targeted application was the development of PLA-based materials for food packaging applications. The barrier and/or active properties of the final materials were thus the intended and targeted properties.

The **Chapter I** presented, in a complete manner, the general context of this study, namely the desire for a transition from fossil-based plastic materials to biobased and/or biodegradable ones. Knowing that food packaging is one of the most demanding sectors in plastic materials, the Chapter I mainly focused on this field. To date, no ideal solution has been developed to replace packaging petroleum-based materials, but a biobased material has stood out from the others for several years: the poly(lactic acid), also known as PLA. Furthermore, the use of nanocelluloses — cellulose nanocrystals (CNCs) or nanofibrils (CNFs) — to enhance the PLA properties has been the subject of numerous researches in the last decades, as presented in the Chapter I. Furthermore, the compatibilization of hydrophilic nanocelluloses, and especially CNCs, with the hydrophobic PLA remains a huge challenge.

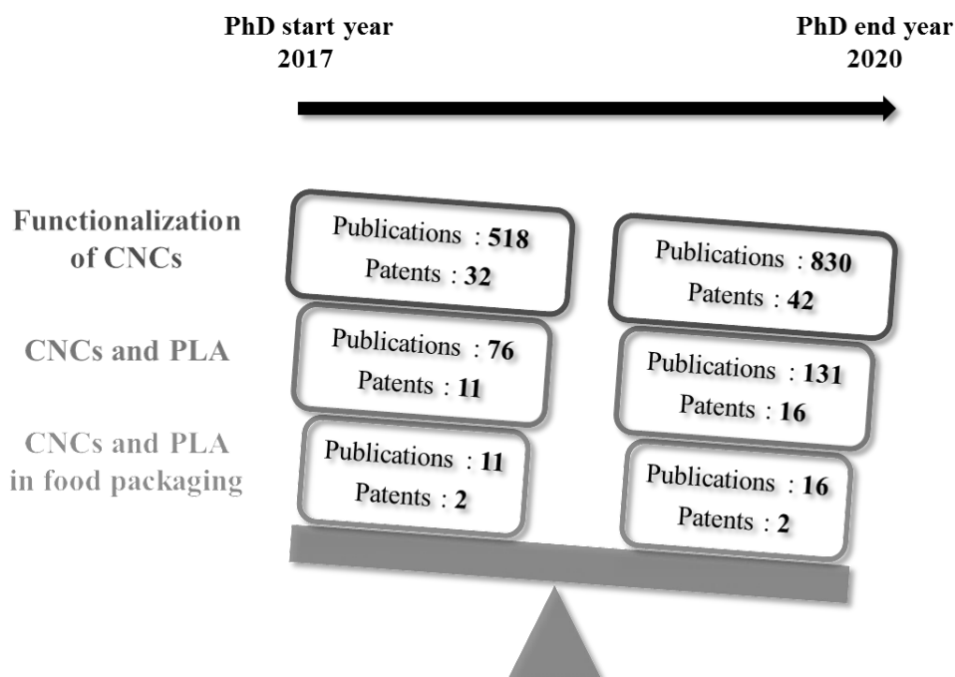


Figure 1. Main evolution in the number of publications and patents dealing with the main topics of the project (Functionalization of CNCs — CNCs and PLA — CNCs and PLA for food packaging applications) during the timeline of the project (Jan. 2017 – Jan. 2020)

The Chapter I synthesized the different chemical modifications of CNCs presented in the literature, as well as, the different routes for the preparation of PLA-based materials including the modified or not CNCs. The literature review also confirmed the recent CNCs use for food packaging applications. In fact, over this PhD project timeline (2017-2020), the number of publications and patents linked to the main PhD topics has largely increased, proving the innovativeness, as presented in **Figure 1**.

It is therefore fluidly that this PhD project was divided into two main complementary parts. In the **Chapter II**, CNCs were modified *via* different routes, with the aim of effectively grafting various molecules or polymers onto their surfaces, and keeping in mind a more environmentally friendly chemistry. The question of feasibility on an industrial scale was also an important point in the progress of this project. Then, in a second step (**Chapter III**), the interest of the different chemical modifications of the CNCs has been studied, with the development of materials based on both PLA and modified CNCs, for food packaging purposes.

This multi-disciplinary PhD project has allowed for a variety of experiments to be carried out, from chemical modifications and characterization of cellulose nanocrystals, to the development of final materials, including the investigation of their barrier properties. In order to have an overview of the work presented throughout this PhD manuscript, the main results obtained in the Chapters II and III are summarized in the **Table 1** and **Table 2**, respectively, as well as, the main related perspectives.

The **Chapter II** proposed different routes for the surface modification of cellulose nanocrystals, with a panel of four modification methods, resulting in the efficient production of CNCs decorated with the poly(glycidyl methacrylate) (PGMA) polymer (**II.1**), fatty acids (lauric and stearic acids) (**II.2.2**), aromatic 1-methyl-3-phenylpropylamine molecule (**II.3**), or rosin-nanoparticles (in a short additional part) (**II.4**). These modifications were efficiently performed after having optimized the reaction conditions, and led to interesting modified CNCs.

First, the PGMA chains polymerized from the pre-functionalized CNC-Br *via* a controlled SI-ATRP procedure induced the presence of highly reactive groups at their surface. Two different times of polymerization led to different amount of polymer at the surface of the CNCs (50% w/w and 80% w/w, for 1h and 24h of polymerization, respectively). These results are encouraging since these epoxy groups could lead to the improvement of their compatibilization with a polymer matrix. Nevertheless, the SI-ATRP method induced the use of metallic salts during the polymerization, and a perspective would be the carrying of another novel polymerization (like the ARGET ATRP or another metal-free ATRP) in order to simplify the washing steps. Moreover, by controlling the grafting densities of the BIB initiator on the CNCs, it would be interesting to control the density of the PGMA chains on the CNC. Furthermore, another perspective would be to take advantage of the epoxy groups by reacting them with PLA chains or other compatibilizing agents, for example, and thus obtain multi-branch

structures, with a huge range of possibilities. However, this strategy only allows very small quantities of CNCs to be grafted, which will remain a barrier to their use in further applications.

The novel procedure for the esterification of CNCs with long aliphatic chains (using both lauric and stearic acids) is highly encouraging, since by avoiding the use of organic toxic chemicals, satisfying grafting densities were achieved, and the hydrophobic behavior of modified CNCs was clearly evidenced. In perspective, this esterification route could be more optimized and performed at larger scale. To do this, the washing step would no longer have to be carried out by centrifugation (time-consuming), but by filtration. This would make it possible to produce CNCs on a large scale, and would considerably expand the possible applications.

Finally, the two-steps procedure, involving a well-known TEMPO-mediated oxidation followed by an amidation reaction (catalysed by EDC/NHS compounds) was also efficiently performed. The presence of aromatic grafted molecules on the CNCs surface was clearly highlighted and is encouraging for what sorption properties concerns, especially towards aromatic compounds. Moreover, the amidation procedure using the DMTMM (4-(4,6-dimethoxy-1,3,5-triazin-2-yl)-4-methyl-morpholinium chloride) reagent through a one-step activation would be highly interesting in a spirit of time and chemicals reducing. Furthermore, the adsorption of the 1-methyl-3-phenylpropylamine on the CNCs was evidenced, although the washing step performed during the adsorption experiment (QCM-d) was not similar to that of the grafting procedure. The investigation of the adsorption of 1-M-3-PP on CNCs should therefore be further conducted. For this adsorption at higher scale, no toxic chemicals or long and tedious washing steps would be necessary, which are often two limiting steps in the up-scaling.

	Scientific issue	Key results	Main perspectives
Chapter II	New routes for the efficient chemical surface modifications of cellulose nanocrystals	<p style="text-align: center;">Chapter II.1</p> <ul style="list-style-type: none"> ▪ Efficient SI-ATRP of GMA onto the CNCs surface ▪ Controlled polymerization ▪ Presence of reactive epoxy groups on the polymerized CNCs 	<ul style="list-style-type: none"> ▪ Polymerization of the PGMA <i>via</i> novel atom transfer radical polymerizations like ARGET ATRP or metal-free ATRP ▪ Different grafting densities of the grafted BIB initiator on CNC-Br for a more controlled and optimized amount of PGMA polymer on CNCs ▪ Functionalization of highly reactive epoxy groups bearing by CNC-PGMA-Br with poly(lactic acid) chains or other compatibilizing agents (multi-branch structure)
		<p style="text-align: center;">Chapter II.2</p> <ul style="list-style-type: none"> ▪ Novel process for the efficient esterification of CNCs with long aliphatic carboxylic acids (lauric and stearic acids) ▪ Clear positive influence of the solvent exchange of CNCs suspension from water to acetone ▪ No toxic chemicals ▪ Hydrophobicity of modified CNCs 	<ul style="list-style-type: none"> ▪ Optimization of the reaction conditions (i.e., initial CNCs concentration in acetone, amount of carboxylic acids) ▪ Pilot-scale tests for the efficient grafting on a large amount of CNCs
		<p style="text-align: center;">Chapter II.3</p> <ul style="list-style-type: none"> ▪ Optimized two-steps immobilization of aromatic 1-methyl-3-phenyl-propylamine on CNCs (TEMPO-mediated oxidation and EDC/NHS catalysed amidation) 	<ul style="list-style-type: none"> ▪ Optimization of the reaction conditions (i.e., amine and EDC/NHS amounts, reaction time) ▪ Aromatic molecules sorption capacity of grafted CNCs ▪ Comparison with other amidation procedure, like that involving DMTMM (4-(4,6-dimethoxy-1,3,5-triazin-2-yl)-4-methyl-morpholinium chloride) common reagent ▪ Adsorption of the 1-methyl-3-phenylpropylamine on a large amount of CNCs (pilot-scale)

Table 1. Main results and perspectives of the chemical modifications of CNCs performed in this PhD project (Chapter II)

In order to investigate the behavior of the various modified CNCs in final materials, two types of PLA-based materials were prepared, and corresponding results were reported in the **Chapter III**, and summarized in the **Table 2**.

The first strategy for the elaboration of final materials was that of nanocomposites, involving PLA as the polymeric matrix, and the modified CNCs as nanofillers. Polymerized CNCs with PGMA chains on their surface, as well as, esterified CNC with lauric acid were thus introduced in the PLA by the solvent casting method, and in both cases, an improvement in their dispersion, compared to that of unmodified CNCs, was clearly observed. Moreover, a significant improvement of the barrier properties towards oxygen and water vapor was highlighted, confirming the well-dispersion state of the nanofillers in the matrix. In perspective, it would be interesting to explore more in detail the different interfaces between the fillers and the PLA, and also understand the visible network created by the introduction of polymerized CNC-PGMA-Br in the PLA. Finally, since a well dispersion of the CNCs was reached thanks to their surface modification, the increasing of their content in the matrix (higher than 10 wt%) could significantly enhance the final thermomechanical and barrier properties of the nanocomposites.

The second strategy provided a proof of concept of the elaboration of multi-layered materials composed of two outer layers of PLA and one inner thin (deposited by coating) or thick (dried CNC or CNF film) layer of nanocelluloses previously modified by amidation or adsorption. Once the process was optimized, encouraging barrier properties were evidenced. This multi-layer strategy opened the way to a wide panel of materials, composed of various active molecules. In a further work, the structure of the multi-layered materials could be deeply understood, as well as, their active properties. Moreover, the elaboration of a demonstrator, in which the film would serve as a lid or a seal, could be an efficient tool to clearly highlight the barrier and/or antioxidant properties of the films.

The question of the biodegradability of and/or recyclability of multi-phase materials remains a key issue. Indeed, after being modified, the biodegradability of the modified-CNC is not always maintained, and it is therefore essential to investigate their behavior to ensure the biodegradability or recyclability of the final materials.

	Scientific issue	Key results	Main perspectives
Chapter III	Poly(lactic acid)-based materials including designed nanostructures with enhanced barrier and/or active properties	Chapter III.1	
		<ul style="list-style-type: none"> ▪ Improved dispersion of CNCs (previously modified in chapters II.1 and II.2) in PLA (solvent casting method) ▪ Decrease in oxygen and water vapor transmission rates of final nanocomposites 	<ul style="list-style-type: none"> ▪ Further investigation of the interfaces between both modified CNC-PGMA-Br or CNC-Lauric and the PLA matrix ▪ Highlighting the probable reaction between epoxy groups from CNC-PGMA-Br and the –OH groups from the end-chains of the PLA ▪ Introduce higher amount of modified CNCs in the PLA matrix (>10 wt%)
		Chapter III.2	
		<ul style="list-style-type: none"> ▪ Elaboration of PLA-based multi-layered materials with an inner nanocellulosic layer (CNCs or CNFs previously modified in chapters II.3 and II.4) ▪ Barrier and antioxidant properties of multi-layered materials 	<ul style="list-style-type: none"> ▪ Better understanding of the multi-layered structures ▪ Investigation of the sorption capacity towards organic molecules of multi-layered including modified CNC-1-M-3-PP (section I.3) ▪ Further food testing (for example, elaboration of a biobased food tray with the multi-layered as a sealed lid)

Table 2. Main results and perspectives of the PLA-based materials including modified CNCs performed in this PhD project (Chapter III)

To conclude, the works provides new results regarding the surface modification of cellulose nanocrystals *via* novel routes. Once CNCs are introduced into a PLA matrix or inside a PLA-based multi-layered structure, their enhanced dispersion, as well as, the interesting barrier properties of the materials are encouraging for further investigations on this topic. Although PLA was selected for this PhD project, the study could also be transposed to other biobased polymers, which would open the way to a huge panel of possible materials.

This study may is certainly useful for future work dealing with the surface modification of cellulose nanocrystals, and especially for their use in food packaging applications based on PLA or other biobased polymers.

Extended French Abstract

Résumé en français

Extended French abstract – Résumé en français

Il est aujourd'hui courant d'entendre parler de pollution, de développement durable, de recyclage, ainsi que de nombreux autres termes étroitement liés à des questions environnementales majeures. Ces dernières ne sont pourtant que le résultat logique d'une accumulation croissante de déchets – entre autres, plastiques – au fil des années, parallèlement à leur production qui n'a cessé de croître depuis des décennies. Toutefois, depuis quelques années maintenant, une prise de conscience environnementale est apparue, aussi bien dans les sphères citoyennes que politiques, avec notamment la mise en place, par la Commission Européenne, d'une stratégie de la Bioéconomie circulaire, visant à développer l'utilisation durable des ressources renouvelables pour relever les défis environnementaux mondiaux et locaux.

C'est dans ce contexte que les scientifiques et les industriels se tournent aujourd'hui vers des matériaux biosourcés, biodégradables et plus durables. Parmi eux, **l'acide polylactique, ou PLA**, a beaucoup fait parler de lui. En effet, le PLA (**Figure 1**) est produit à partir de ressources agricoles, telles que l'amidon de maïs, et présente des propriétés intéressantes (par exemple, sa rigidité, transparence, imprimabilité, ainsi que sa facilité de mise en forme). Bien que l'utilisation du PLA soit souvent controversée – notamment par le fait qu'il ne soit biocompostable qu'en milieu industriel, et qu'aujourd'hui, aucune filière ne permette son recyclage –, il reste à ce jour l'une des meilleures solutions en termes de plastiques biosourcés. Toutefois, son utilisation dans le secteur de l'emballage (qui est actuellement l'un des secteurs les plus demandeurs en termes de matières plastiques) reste limitée, du fait des propriétés thermiques et barrières souvent insuffisantes du PLA.



Figure 1. a) Structure chimique de l'acide polylactique (PLA), b) Billes de PLA utilisées pour la mise en forme de produits finaux c)

Afin d'améliorer les propriétés de ce polymère, l'introduction de charges (organiques ou non) pour l'élaboration de matériaux composites a été sujet à de nombreuses recherches. Plus récemment, l'introduction de charges de tailles nanométriques dans une matrice PLA pour la préparation de **nanocomposites** a montré des résultats particulièrement intéressants, notamment en termes de propriétés barrières (à l'oxygène et à la vapeur d'eau). D'autre part, avec l'intérêt croissant des matériaux biosourcés, des nano-charges issues de la cellulose sont produites et étudiées depuis plusieurs décennies, et représentent une excellente solution pour l'élaboration de nanocomposites.

Ces nanomatériaux cellulosiques — les **nanocelluloses** — peuvent être extraits à partir de différentes sources de biomasse (comme le bois, le coton, le tunicier, le lin, etc.), et par différents procédés, comme représenté sur la **Figure 2**. Selon le procédé subi par les fibres de celluloses, différents types de nanocelluloses sont obtenus. Les nanofibrilles de cellulose (NFC) sont obtenues par traitement mécanique, et s'apparentent à de longs filaments flexibles, alors que les nanocristaux de cellulose (NCC), semblables à des bâtonnets rigides, sont obtenus à partir de l'hydrolyse acide de la biomasse.

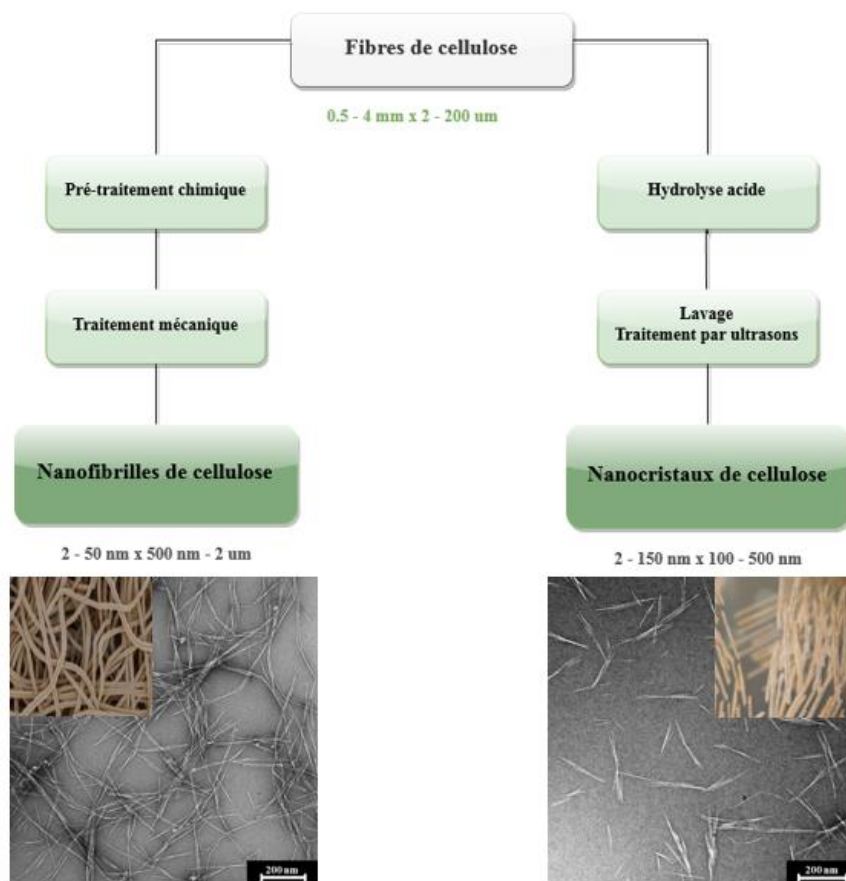


Figure 2. Schématisation de l'extraction des nanocelluloses (nanofibrilles (NFC) et nanocristaux (NCC)) à partir de fibres cellulosiques

Outre leur caractère biosourcé et biodégradable, les nanocelluloses présentent des propriétés exceptionnelles, comme entre autres, une surface très réactive, un aspect de forme élevé, et de très bonnes propriétés mécaniques. Ces propriétés en font des matériaux uniques et intéressants pour une large gamme d'applications, comme le papier et l'emballage, la formulation d'encre et de peintures, la cosmétique, le bâtiment, le biomédical, ou encore, comme précédemment mentionné, les nanocomposites.

C'est à cette dernière application que s'intéresse ce projet de thèse. En effet, afin de produire des matériaux à partir d'acide polylactique pour des applications d'emballage alimentaire, il peut être intéressant d'inclure des nano-charges cellulosiques, hydrophiles, préalablement modifiées afin d'améliorer leur compatibilité avec la matrice polymère hydrophobe. C'est autour de cette idée que, en

2017, s'est établi un consortium composé de plusieurs partenaires académiques et industriels, et qu'une collaboration est née au sein du projet GASP, financé par l'Agence Nationale de la Recherche (ANR-16-CE08-0040), et qui débuta en janvier 2017. Les travaux de thèse présentés dans ce manuscrit ont été réalisés dans le cadre de ce projet GASP, et se sont attachés à approfondir les points suivants :

1. La modification de surface des nanocristaux de cellulose par des voies innovantes et se rapprochant le plus possible des principes de la chimie verte
2. L'étude de l'influence des modifications de surface des nanocristaux de cellulose sur leur adhésion avec une matrice polymère basée sur le PLA
3. Le développement de matériaux actifs et biosourcés, basés sur le PLA et incluant des nanocelluloses, pour des applications d'emballages alimentaires

Ce travail de thèse a été mené dans un contexte dynamique, et de nombreux échanges ont eu lieu entre les différents partenaires du projet, aux champs de compétences variés et complémentaires. La **Figure 3** présente l'organisation de la thèse telle qu'elle est présentée dans ce manuscrit.

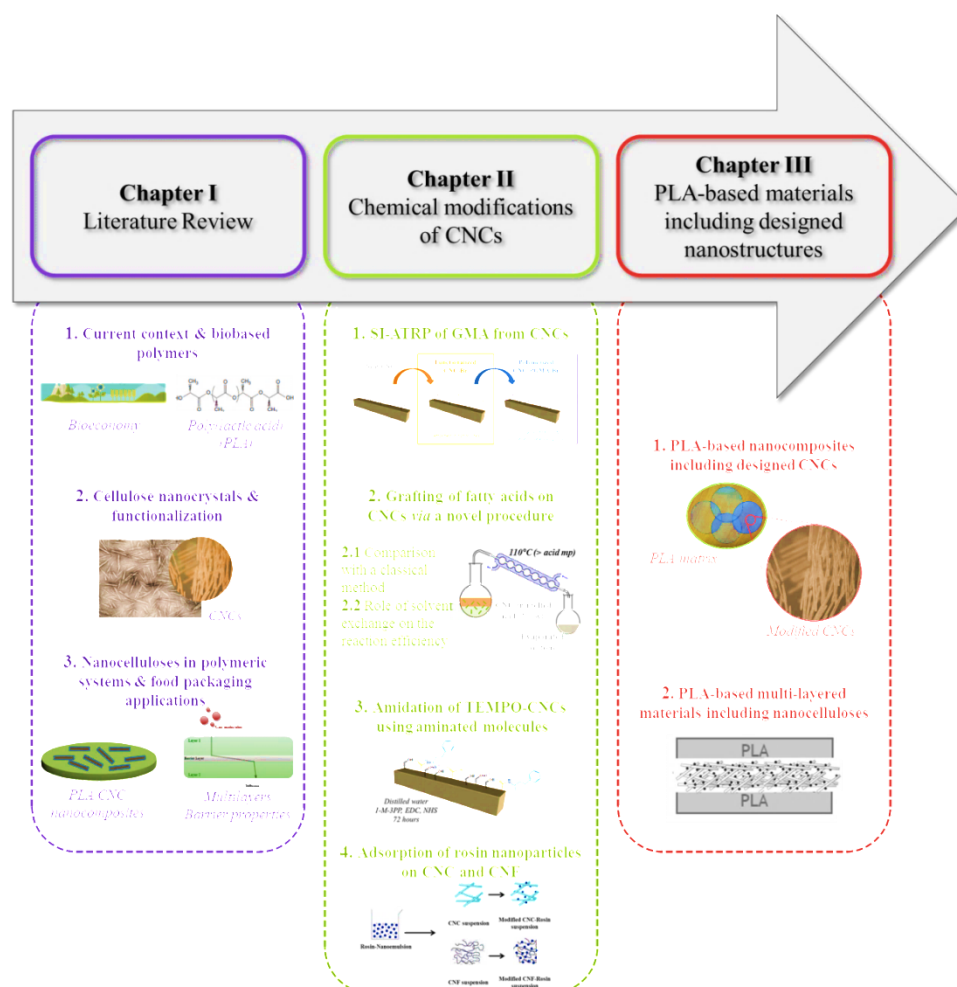


Figure 3. Schéma récapitulatif de l'organisation du manuscrit

Le **Chapitre I** s'applique à décrire, de la façon la plus complète possible, le contexte général de cette étude, avec une attention toute particulière portée sur l'acide polylactique (PLA), sur les nanocristaux de cellulose et leur modification de surface, ainsi que sur l'élaboration de matériaux biosourcés et multiphasiques pour l'emballage alimentaire.

Le **Chapitre II** propose quatre différentes voies pour la modification chimique des nanocristaux de cellulose. Du fait de la pluridisciplinarité du projet GASP et des différentes attentes propres à chacun des partenaires, ce chapitre est organisé autour de stratégies conduisant à des quantités croissantes de NCC modifiés. Dans le **Chapitre III**, les différents NCC modifiés sont introduits dans des matériaux PLA au travers de deux méthodes différentes, et les propriétés barrières des matériaux finis sont présentées.

Ainsi, dans une première stratégie, des NCC ont été fonctionnalisés, puis polymérisés depuis leur surface avec le poly(glycidyl methacrylate) (PGMA). Ces NCC polymérisés ont alors été introduits, à différents taux d'inclusion, dans une matrice de PLA par une méthode de moulage/évaporation, et l'observation des nanocomposites produits a permis de conclure quant à l'efficacité du greffage sur la dispersion des NCC dans le PLA (**Figure 4**). D'autre part, des résultats encourageants en termes de propriétés barrières à l'oxygène et à la vapeur d'eau ont été obtenus.

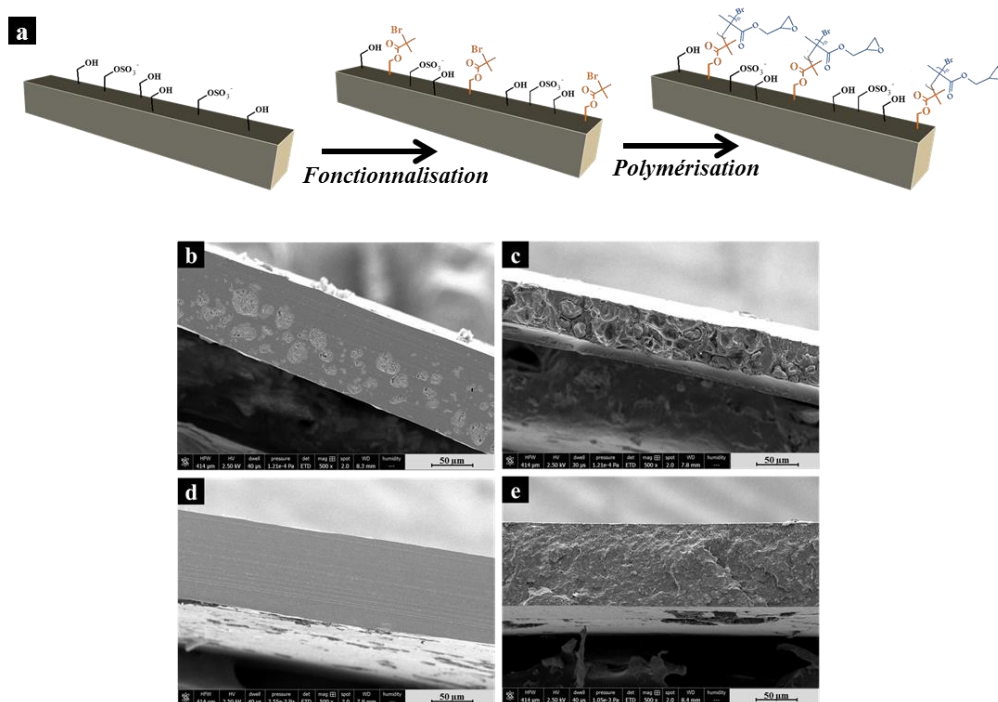


Figure 4. Stratégie de polymérisation du PGMA sur les nanocristaux de cellulose (NCC) (Chapitre I.1) et leur introduction dans une matrice PLA (Chapitre II.1)

a) Schématisation de la réaction en deux étapes de la polymérisation du PGMA sur les NCC préalablement modifiés avec un amorceur de la polymérisation radicalaire, et observations au microscope électronique à balayage des coupes des nanocomposites préparés avec des NCC non modifiés (b) et (c) et avec des NCC polymérisés avec le PGMA (d) et (e))

Dans une seconde stratégie visant à modifier les NCC à plus grande échelle, une méthode innovante d'estérification a été mise en place pour le greffage d'acides carboxyliques à longues chaînes aliphatiques — l'acide laurique (12 carbones) et stéarique (18 carbones) — sur des NCC, tout en limitant l'utilisation de produits chimiques toxiques et polluants. Cette méthode de greffage efficace a donc conduit à des NCC modifiés hydrophobes, qui ont également pu être introduits dans une matrice PLA pour la préparation de matériaux nanocomposites. L'amélioration flagrante de la dispersion des NCC dans le PLA après leur modification est l'un des résultats clé de cette stratégie (**Figure 5**), induisant une amélioration des propriétés barrières à l'oxygène et à la vapeur d'eau des nanocomposites.

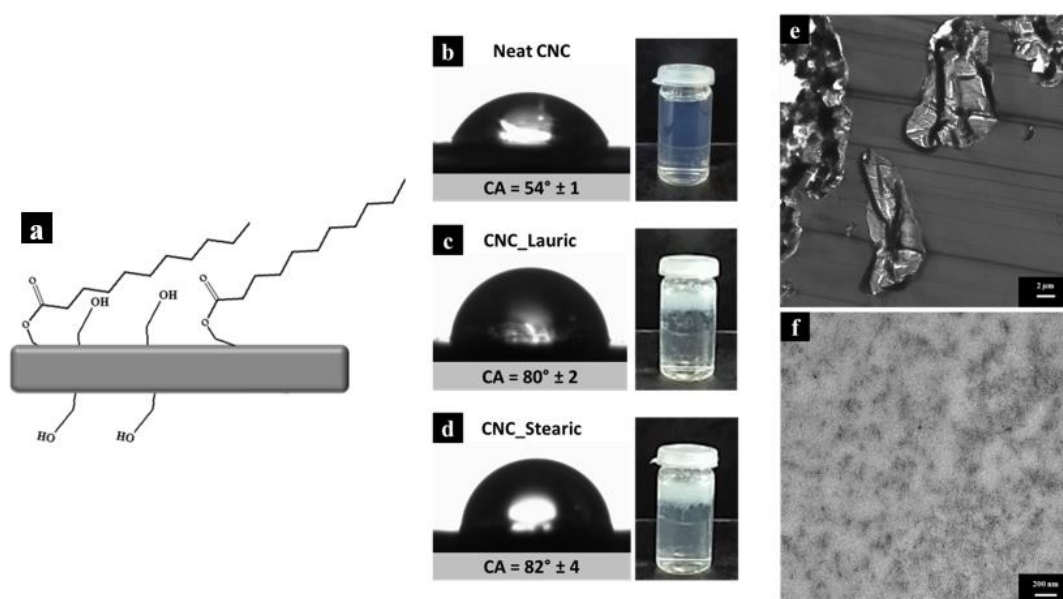


Figure 5. Stratégie de greffage d'acides gras (acide laurique et stéarique) sur les NCC (Chapitre I.2.2) et leur introduction dans une matrice PLA (Chapitre II.1)

a) Schéma d'un NCC modifié à sa surface avec un acide gras, angles de contacts d'une goutte d'eau sur des NCC non modifiés (b) et modifiés avec les acides gras (c) et (d)) ainsi que leur introduction dans l'eau, et images obtenues par microscopie électronique en transmission des coupes de nanocomposites préparées avec des NCC non modifiés (e) et modifiés (f))

Outre son efficacité, l'intérêt de cette méthode de greffage repose sur le possible recyclage des réactifs à la fin de la réaction, ainsi que sur la possibilité d'envisager ce greffage à une échelle plus large (échelle pilote).

Une réaction d'amidation en conditions aqueuses, précédée d'une oxydation des NCC (**Figure 6**), a également été réalisée, et l'efficacité du greffage d'une molécule aromatique (1-méthyl-3-phenylpropylamine) a été prouvée. D'autre part, l'adsorption de ces molécules sur les NCC oxydés a également été mise en évidence, laissant envisager une possible adsorption de ces molécules sur une quantité bien plus large de NCC. L'intérêt d'un tel greffage repose sur l'utilisation limitée de produits chimiques organiques et toxiques, ainsi que sur la présence de groupements aromatiques à la surface des NCC greffés. En effet, il a déjà été montré que de tels cycles pouvaient induire une capacité de

sorption des NCC modifiés, notamment pour ce qui concerne l'adsorption des molécules aromatiques (par exemple l'anisole, le cyclohexane). De plus, cette stratégie ouvre la voie vers d'innombrables greffages de molécules aminées sur des NCC.

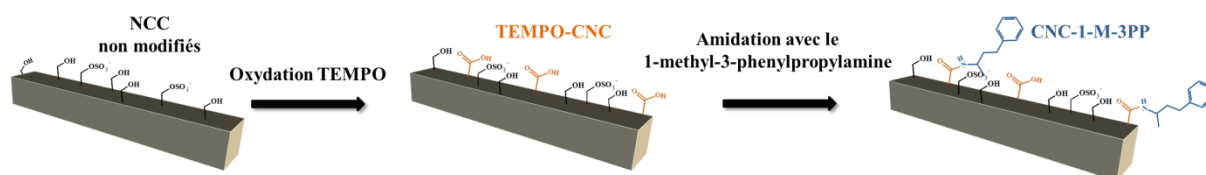


Figure 6. Réaction en deux étapes effectuée lors du greffage du 1-méthyl-3-phenylpropylamine sur les NCC (Chapitre I.3)

Ces NCC modifiés ont ensuite pu être introduits dans des structures multicouches PLA, *via* le couchage de leur suspension aqueuse sur des films commerciaux de PLA. Après optimisation du procédé de thermopressage appliqué sur le PLA couché avec un second film de PLA, des matériaux multicouches aux propriétés barrières considérablement améliorées ont été obtenus et caractérisés.

Cette stratégie a été transposée à l'élaboration de matériaux multiphasiques (TML) incluant, cette fois, des films secs de NCC ou NFC, préalablement adsorbés avec des nanoparticules de collophane naturelles (**Figure 7**). Ces matériaux, présentant une couche interne de NCC ou NFC plus épaisse que dans le cas précédent, présentent également des propriétés très intéressantes en termes de barrières à l'oxygène ou à la vapeur d'eau, de même qu'une activité antioxydante apportée par le collophane. Ces résultats ouvrent ainsi la voie vers des matériaux multicouches totalement biosourcés pour des applications d'emballages alimentaires spécifiques. En effet, *via* ce procédé, de nombreuses molécules, actives par exemple, peuvent être introduites dans les matériaux après avoir été immobilisées sur les nanocelluloses.

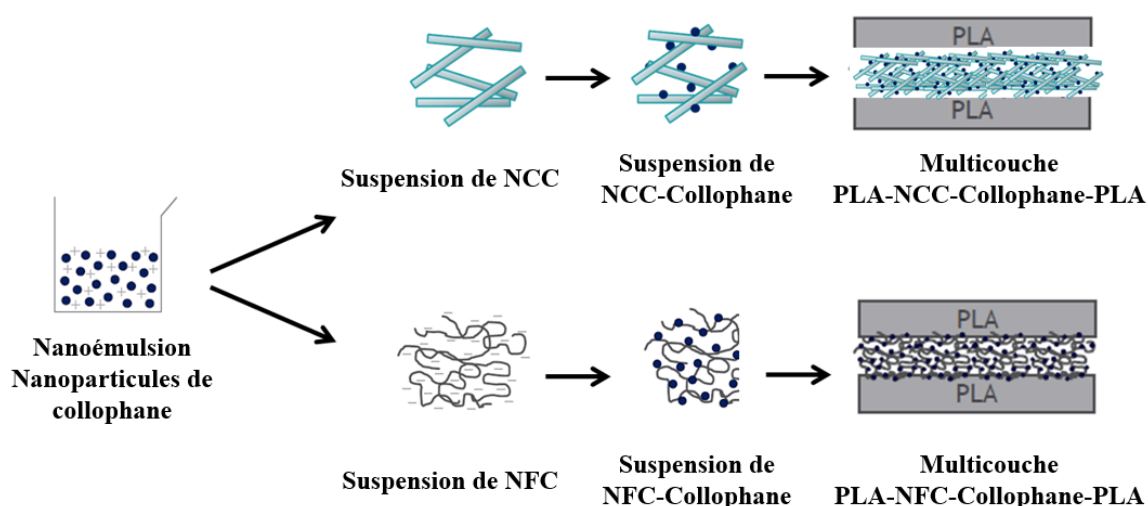


Figure 7. Stratégie de l'élaboration de matériaux PLA multicouches incluant une couche interne composée de NCC ou NFC préalablement adsorbés avec des nanoparticules de collophane (Chapitres I.4 et II.2)

L'étude des propriétés barrières à l'oxygène et à la vapeur d'eau des matériaux multicouches (TML) présentés dans la **Figure 7** a été réalisée, et des résultats intéressants et encourageants ont été obtenus. En effet, la présence d'une couche interne de nanocellulose (NCC ou NFC) entre les deux films de PLA a conduit à diviser la perméabilité à l'oxygène d'un facteur 80 ou 27 par rapport à une référence PLA-PLA, et à maintenir celle à la vapeur d'eau. La **Figure 8** situe les différentes perméabilités à l'oxygène et à la vapeur d'eau requises pour l'emballage d'aliments spécifiques. Les valeurs obtenues pour les matériaux multicouches produits dans cette étude ont été ajoutées, et permettent de conclure quant à l'intérêt de tels matériaux incluant des nanostructures celluloses pour une application d'emballage alimentaire, et plus particulièrement celui de produits carnés.

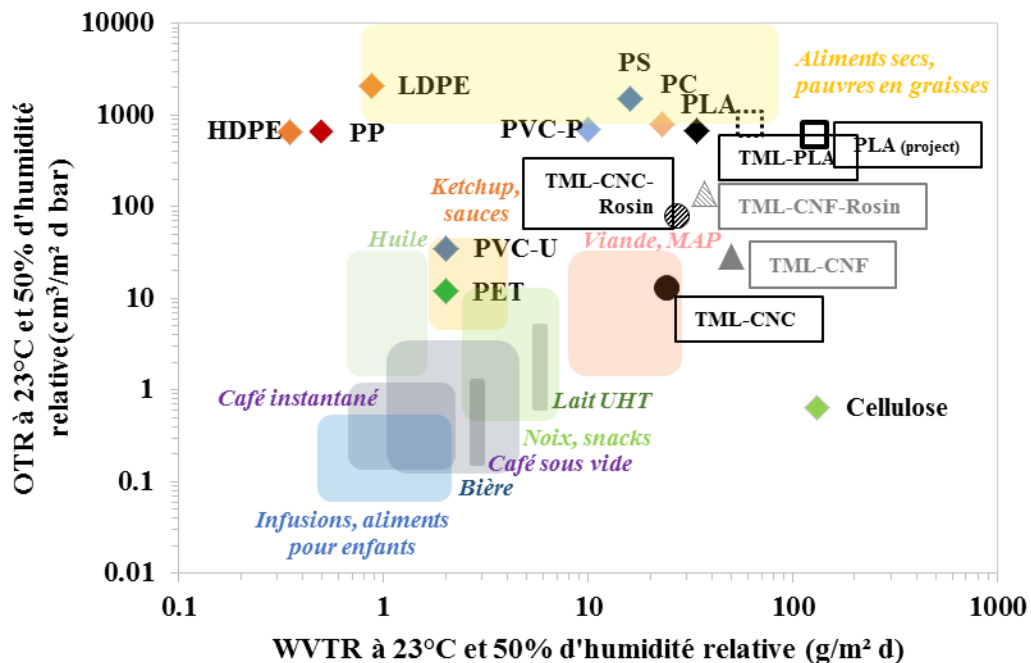


Figure 8. Perméabilités à l'oxygène et à la vapeur d'eau requises pour des applications spécifiques d'emballage alimentaire et positionnement des valeurs obtenues pour les matériaux multicouches élaborés au Chapitre III.2 (TML-PLA, TML-CNC, TML-CNC-Rosin, TML-CNF et TML-CNF-Rosin)

En conclusion, ce projet s'intéresse à la modification chimique de nanocristaux de cellulose pour leur utilisation dans des matériaux basés sur l'acide polylactique, pour des applications d'emballage alimentaire. Différentes méthodes de modification chimique, plus ou moins innovantes, des NCC sont présentées. Elles permettent toutes de venir greffer des molécules spécifiques à la surface des NCC, et sur différentes quantités. D'autre part, des matériaux — nanocomposites et multicouches — ont pu être efficacement mis en œuvre, et des résultats intéressants, notamment en termes de dispersion des nanocelluloses dans la matrice composée de PLA, ont pu être présentés.

Ces travaux de thèse viennent ainsi étayer les possibilités de modifications chimiques des NCC en vue de leur application dans des matériaux biosourcés, à des fins d'emballage alimentaire. Ils confirment l'intérêt de tels nanomatériaux celluloses dans le développement de matériaux innovants et actifs.

English abstract – Résumé en anglais

The purpose of this project is to develop new surface chemical modifications of cellulose nanocrystals (CNCs), in order to enhance their compatibility with biobased poly(lactic acid) (PLA) polymer, and to combine their respective outstanding intrinsic properties. Biobased PLA-based multi-phase materials, including the designed nanostructures, are produced. Furthermore, the final materials are expected to be used in food packaging sector, and the improvement of the barrier properties of the PLA, especially towards oxygen and water vapour, is a key point in the characterization of the materials. In this project, different routes are proposed for the grafting of various compounds — polymers or single molecules — on the surface of the CNCs. Their grafting efficiency has been confirmed and carefully characterized. The modified CNCs are then introduced in PLA-based materials *via* two different strategies. Indeed, they are either used as nanofillers in a PLA matrix with inclusion rates comprised between 2 and 10 wt%, or as an inner layer of PLA-based multi-layered materials. In both cases, final PLA-based materials including various designed cellulosic nanomaterials exhibit enhanced and highly encouraging properties in terms of homogeneity, transparency, and barrier towards oxygen and water vapour, in accordance with required properties for food packaging materials.

Keywords: *nanocellulose, cellulose nanocrystals, surface functionalization, nanocomposites, barrier properties*

Résumé en français – French abstract

Ce projet vise à développer de nouvelles modifications chimiques de surface des nanocristaux de cellulose (NCC), afin d'améliorer leur compatibilité avec le polymère biosourcé qu'est l'acide polylactique (PLA), afin de combiner leurs propriétés intrinsèques respectives. Ainsi, des matériaux multiphasiques ont été produits à partir du PLA en y incluant des nanomatériaux cellulosiques. L'application visée est celle de l'emballage alimentaire, et l'amélioration des propriétés barrières du PLA, notamment vis-à-vis de l'oxygène et de la vapeur d'eau, est alors un point clé dans la caractérisation des produits finis. Plus précisément, dans ce projet, différentes voies sont proposées pour le greffage de divers composés — polymères ou molécules — à la surface des nanocristaux de cellulose. Le succès de ces greffages a été confirmé et quantifié via diverses techniques de caractérisation. Les NCC ainsi modifiés sont ensuite introduits dans un matériau PLA à travers deux stratégies différentes : soit en tant que nanocharges dans une matrice PLA, avec des taux d'inclusion compris entre 2 et 10% massique, soit en tant que couche interne dans des matériaux multicouches de PLA. Dans les deux cas, les matériaux finaux, préparés à partir de PLA et de nanomatériaux cellulosiques modifiés, présentent des propriétés intéressantes et encourageantes en termes d'homogénéité, de transparence, et de barrière à l'oxygène et la vapeur d'eau, conformément aux propriétés requises pour les matériaux de conditionnement alimentaire.

Mots-clés : *nanocellulose, nanocristaux de cellulose, fonctionnalisation de surface, nanocomposites, propriétés barrières*